THE VOLCANIC-PLUTONIC RELATIONSHIP AT THREE CONTRASTING RIO-GRANDE-RIFT-FAULTED CALDERAS

By
Matthew J. Zimmerer

Submitted as partial fulfillment of the
Requirements for the Degree of
Doctor of Philosophy in Earth and Environmental Science
with Dissertation in Geochemistry
September 9, 2011

Department of Earth and Environmental Science
New Mexico Institute of Mining and Technology
Socorro, New Mexico

ABSTRACT

The temporal, spatial, and chemical relationships of volcanic and plutonic rocks of the Questa (NM), Mt. Aetna (CO), and Organ caldera (NM) complexes were investigated to help establish the origin of these caldera-related silicic magmas. Rio Grande Rift faulting and erosion at these systems has exposed both intracaldera sequences and subvolcanic plutons. Ar/Ar and U/Pb ages reveal the timing of volcanic activity and pluton emplacement and cooling. We observe a link between ignimbrite compositional zoning patterns and the temporal-chemical relationship of volcanic and plutonic rocks.

The Questa caldera erupted the Amalia Tuff, a high-SiO_2 peralkaline rhyolite, at 25.39 ± 0.04 Ma. Volumetrically minor phases of two resurgent plutons and a ring dike are compositionally similar to the Amalia Tuff. K-feldspar in the ring dike yields an Ar/Ar age of 25.38 ± 0.04 Ma, which is indistinguishable to the Amalia Tuff eruption age. Because of similarities in age and geochemistry, the peralkaline intrusions are interpreted to be nonerupted Amalia Tuff. U/Pb and Ar/Ar dating indicate that the remaining exposed plutons were emplaced 100 ka to 6.1 Ma after the Questa caldera eruption. These plutons are too young to be the less differentiated residual crystal mush from the Amalia Tuff magma chamber. Multiple diffusion domain (MDD) modeling of the plutonic K-feldspar indicates numerous reheating events related to protracted postcaldera magmatism.

The Mt. Princeton batholith and nested Mt. Aetna caldera are interpreted to be the sources for the 37.25 ± 0.08 Ma, low-SiO_2 rhyolitic Wall Mountain Tuff and the 34.26 ± 0.06 Ma, dacitic Badger Creek Tuff. U/Pb zircon ages of Mt. Princeton batholith range from 36.4 to 35.1 Ma, indicating that it was emplaced during the interval between the Wall Mountain Tuff and Badger Creek Tuff eruptions. Eight biotite ages of the Mt. Princeton batholith range from 35.8 to 35.2 Ma, indicating that the intrusion rapidly cooled to below ~300°C following emplacement. Dating of the Mt. Princeton batholith indicates that any Wall-Mountain-Tuff-age intrusions are now eroded. During the eruption of the Badger Creek Tuff, the fully crystallized Mt. Princeton batholith collapsed into the Mt. Aetna caldera. Intrusions along the margins of the Mt. Aetna caldera are compositionally identical to the Badger Creek Tuff and contain zircons 100 to 500 ka older than the tuff, suggesting that the Badger Creek Tuff magma chamber was incrementally assembled prior to the caldera eruption. Several post-Mt.-Aetna-caldera luecogranite plutons were emplaced at ~31 Ma. K-feldspar MDD thermal modeling of the Mt. Princeton batholith and Mt. Aetna caldera margin intrusions indicate the luecogranites caused widespread reheating of the intrusive suite.

The Organ caldera complex erupted a zoned ignimbrite sequence. The basal 36.45 ± 0.08 Ma Cueva Tuff is a high-SiO_2 rhyolite. The middle 36.23 ± 0.14 Ma Achenback Park Tuff is an intermediate-SiO_2 rhyolite. The upper 36.03 ± 0.16 Ma Squaw Mountain Tuff is zoned from an intermediate to a low-SiO_2 rhyolite. The intracaldera sequence is intruded by the Organ Needle pluton. U/Pb zircon and Ar/Ar biotite ages of the Organ Needle pluton range from 36.4 to 35.9 Ma, indicating that the intrusion was emplaced and cooled soon after eruption of the ignimbrites. The intrusion is vertically zoned from

an alkali feldspar granite phase at the top to intermediate syenite and monzodiorite phases at the base. The geochronology and geochemical zonation suggests that the Organ Needle pluton is the nonerupted silicic cap and the residual crystal mush of the Organ magma chamber. Three postcaldera plutons were emplaced between 36.0 and 34.3 Ma. MDD modeling suggests reheating events related to postcaldera magmatism at 34 Ma, 30-32 Ma, and as young as 26 Ma.

Primary conclusions are: 1) all three systems contain small-volume intrusions that are similar in age and composition to their coeval ignimbrite and are interpreted to be the nonerupted silicic cap, 2) the Organ caldera complex is the only studied system with a large-volume intrusion interpreted as residual crystal mush of the ignimbrite magma chamber, 3) the majority of plutons at the Questa and Mt. Aetna systems are either too old or too young to be nonerupted residual crystal mush of the magma chamber, and 4) postcaldera magmatism continued for several Ma at each caldera system. We propose that the Organ zoned ignimbrite sequence originated via in-situ differentiation and partial eruption of a zoned shallow magma chamber, whereas the Questa and Mt. Aetna non- to weakly zoned ignimbrite magma chambers were derived from a lower crustal sources and were nearly completely emptied by their ignimbrite eruptions.

TABLE OF CONTENTS

LIST OF FIGURES

LIST OF TABLES

LIST OF APPENDICES

INTRODUCTION

This Ph.D. dissertation research is focused on using the temporal, spatial, and chemical relationships of volcanic and plutonic rocks of contrasting caldera systems to examine the origin of silicic magmas and magma chamber processes. Three mid-Tertiary-Rio-Grande-rift-faulted caldera systems were selected as ideal field areas for this project because of the exceptional exposures of their subcaldera intrusive suites. An intrusive suite is here defined as a group of intrusions that are temporally, chemically, and/or spatially related. Accordingly, for each field area all of the exposed intrusions are interpreted to be part of the subcaldera intrusive suite. All Ar/Ar and LA-ICP-MS U/Pb zircon ages were obtained by Zimmerer. CA-TIMS U/Pb zircon dating was conducted by collaborators at the University of North Carolina at Chapel Hill. Results from each caldera complex are presented in separate chapters. Each chapter has been or will be submitted to a peer-reviewed journal. Chapter one discusses magmatism at the Questa caldera, northern New Mexico. This chapter was submitted to the Geological Society of America Bulletin in Spring 2011 and is currently under review. Chapter two discusses the relationship of volcanic and plutonic rocks exposed at the Mt. Aetna caldera complex, central-Colorado. Chapter three explains the volcanic-plutonic relationship at the Organ caldera complex and also provides a comparison of all three caldera systems. Chapters two and three will be submitted for publication shortly after the completion of Zimmerer's Ph.D.

CHAPTER 1: THE AR/AR GEO- AND THERMOCHRONOLOGY OF THE LATIR VOLCANIC FIELD AND ASSOCIATED INTRUSION: UNDERSTANDING CALDERA MAGMATIC PROCESSES AND THE VOLCANIC-PLUTONIC RELATIONSHIP

1.1. Abstract

Volcanic and plutonic rocks exposed in the Latir volcanic field, northern New Mexico, provide an opportunity to study caldera-related magmatism and understand the spatial and temporal relationship between cogenetic volcanism and plutonism. Fifty-four mineral separates were dated using the Ar/Ar method. The volcanic geochronology provides point-in-time information about magmatism whereas the ages of plutonic rocks establishes emplacement ages and cooling histories. Volcanism began at 28.5 Ma and ended at 22.7 Ma, climaxing with the eruption of the high-SiO_2 peralkaline Amalia Tuff from the Questa caldera at 25.39 ± 0.04 Ma. Following caldera collapse, four resurgent plutons were emplaced between 25.4 and 25.0 Ma. Each resurgent pluton cooled rapidly following emplacement. Using geochemistry, previous research indicated that the peralkaline phases of two resurgent plutons and a peralkaline ring dike were nonerupted Amalia Tuff. K-feldspar from the ring dike yielded a plateau age of 25.38 ± 0.04 Ma, supporting the previous conclusion. Ar/Ar analyses indicate that five plutons, located along the southern caldera margin and south of the caldera, were emplaced between 24.9 and 19.3 Ma. Multiple diffusion domain modeling of these plutonic K-feldspar indicates variable thermal histories related to incremental pluton emplacement. With the exception

of the small-volume peralkaline intrusions, the remaining exposed plutons at the Questa caldera are too young to be the residual crystal mush of the Amalia Tuff magma chamber. The plutons record emplacement of a caldera magma chamber, near complete emptying of the magma chamber during caldera collapse, and the emplacement of a postcaldera batholith during the waning stages of magmatism.

1.2. Introduction

The nature of magmatism beneath calderas has long been a focus of research interest (Hamilton and Myers, 1967; Smith, 1979; Lipman, 1984; Bartley et al., 2005; Lipman, 2007; Glazner et al., 2008). Using recent advances in geochronological and geochemical techniques, previous studies have developed numerous models to explain the origin of caldera-related magmas (Johnson et al., 1989; Jellinek and DePaulo, 2003; Bachmann and Bergantz, 2004; Glazner et al., 2004; Hildreth, 2004; Bartley et al., 2005; Annen et al., 2006; Lipman, 2007; Bryan et al., 2008; Annen, 2009). Classic caldera magmatism models, based largely on the study of volcanic rocks, suggest that rhyolites represent erupted silicic caps produced via in-situ differentiation in upper crustal magma chambers (Smith, 1979; Bachmann and Bergantz, 2004; Hildreth, 2004). According to this model, the nonerupted silicic cap and less-differentiated residual crystal-mush in the caldera-forming magma chamber are preserved in the plutonic record (Johnson et al., 1989, Bachmann et al., 2007a, de Silva and Gosnold, 2007). The nonerupted residual-mush may remain unchanged or may be thermally and chemically modified during postcaldera magmatism (Lipman, 2007; Miller et al., 2007; Walker et al., 2007).

Contrasting studies suggest that many plutonic rocks do not represent the residual crystal mush of a magma chamber (Glazner et al., 2008; Michel et al., 2008). Studies of the Mesozoic Tuolumne Intrusive Suite in the Sierra Nevada have suggested that these subvolcanic batholiths formed by the incremental emplacement of plutons over durations as long as 10 Ma, during which individual plutons may not have contained melt fractions sufficient for differentiation or a voluminous eruption (Mahan et al., 2003; Coleman et al., 2004; Glazner et al., 2004). Additionally, Ulmer et al. (2007) and Mills et al. (2008) showed that plutonic rocks share similar major and trace element chemistries to volcanic rocks, rather than the expected residual mush and extracted melt complimentary geochemistry.

As an alternative to upper crustal differentiation, silicic magmas have been proposed to originate in the lower crust (Coleman et al., 2004; Glazner et al., 2004; Glazner et al., 2008; Quick et al., 2009). Differentiation of mantle-derived basaltic magmas in the lower crust, combined with partial melting and magma mixing can generate silicic magma (Dufek and Bergantz, 2005; Annen et al., 2006). These silicic magmas are then emplaced into the upper crust, undergo limited chemical differentiation, and are either erupted or crystallize to form plutons. According to this model, caldera-forming ignimbrites are generated during high-flux magmatic periods, whereas most plutonic rocks are emplaced and preserved during the waxing and waning stages of magmatism (Glazner et al., 2004; Annen, 2009). If silicic magmas are generated at depth, the caldera-forming ignimbrite and shallow, coeval plutons representing the nonerupted magma chamber are expected to be compositionally similar.

Hence, a problem arises. Many studies of volcanic rocks suggest upper crustal differentiation, but studies of some plutonic rocks suggest lower crustal differentiation. Solving this contradiction is difficult, because few caldera systems have sufficient exposures of both volcanic and subcaldera plutonic rocks.

The volcanic and plutonic rocks of the Latir volcanic field in northern New Mexico (Figure 1.1) provide special insights into caldera-related silicic magmatism. Rio-Grande-rift-related faulting and erosion has exposed substantial parts the subcaldera intrusive suite. Unlike other Oligocene large silicic volcanic fields in which multiple calderas spatially and temporally overlap (McIntosh et al., 1992; Lipman, 2007), the Latir field contains only one caldera, Questa (Lipman et al., 1986), from which the Amalia Tuff erupted at 25.4 Ma (Smith et al., 2002; this study). As a result, the volcanic record in the Latir field has not been complicated by eruptions from other volcanic centers, nor has the geo- and thermochronology of the exposed plutons been complicated by magmatism associated with younger caldera cycles.

This paper presents new Ar/Ar ages of volcanic and plutonic rocks from the Latir volcanic field. Dating of the volcanic rocks is important because it determines the timing and duration of the volcanism and constrains the temporal-geochemical trends observed from inception to cessation of the volcanic field. The timing of volcanism is intrinsically related to the emplacement of magma into the crust that may not be preserved by plutons, either because they are not exposed or were completely erupted. Ar/Ar ages of intrusive rocks are compared to recently determined CA-TIMS U/Pb zircon ages (Tappa et al., in review) to assess the emplacement and cooling histories of plutons. In the absence of U/Pb ages for some intrusions, the thermochronology of the plutons is used to understand

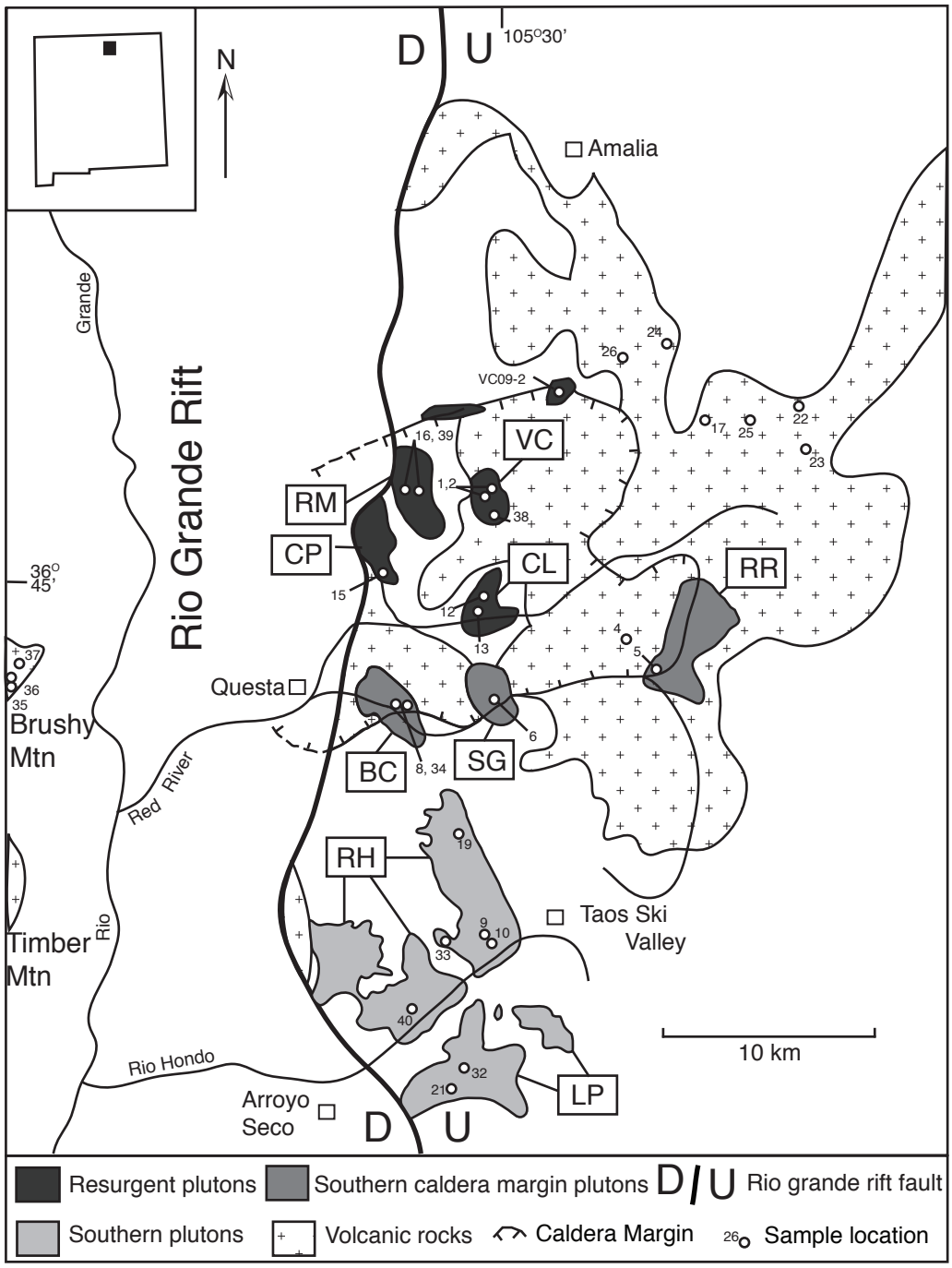

Figure 1.1. Generalized geologic map of the Questa caldera showing the distribution of the volcanic rocks and plutons, after Lipman et al. (1986) and Czamanske et al (1990). Map also contains the MZQ samples localities (samples along the western margin of the Rio Grande Rift are not shown). Plutons are grouped into three categories (resurgent, southern caldera margin, and south plutons) and the corresponding abbreviations for each pluton are: VC, Virgin Canyon; RM, Rito del Medio; CP, Canada Pinabete; CL, Cabresto Lake; BC, Bear Canyon; SG, Sulfur Gulch; RR, Red River; RH, Rio Hondo; LP, Lucero Peak.

how subcaldera plutons are constructed, cool, and are thermally modified by protracted magmatism. Thermal histories are affected by the depth of emplacement, changing geothermal gradients, and thermal perturbations resulting from multi-stage melt emplacement. Reheating by protracted magmatism is further investigated using multiple diffusion domain (MDD) thermal modeling of plutonic K-feldspars, a method proven useful in deciphering the 300-150°C thermal histories of plutons (Lovera et al., 1989; Richter et al., 1991; Dalrymple et al., 1999).

1.3. Geologic Framework of the Questa caldera

The Latir volcanic field is located in the Sangre de Cristo Mountains of northern New Mexico (Figure 1.1). The Latir field is part of the larger Southern Rocky Mountain volcanic field (Lipman, 2007), thought to be the consequence of flat-slab subduction of the Farallon plate beneath the North America (Lipman et al., 1972; Coney et al., 1977; Dickenson et al., 1978). By 45 Ma the rate of convergence had slowed, the subducted slab began to 'roll-back' beneath the western margin of North America, and back-arc crustal stresses began to transition from compression to extension (Chapin et al., 2004; Lawton et al., 1999). Extension across the southwestern North American plate allowed large volumes of silicic magma to intrude into the upper crust, leading to caldera volcanism. Extension has continued to the present, transitioning from ductile to brittle deformation and forming the present Rio Grande rift (Baldridge and Olsen, 1989; Baldrigde et al., 1995; Chapin et al., 2004).

Exposed rocks in the Latir field cover an area of approximately 1200 km^2 and are the erosional remnants of a much larger field (Lipman et al., 1986). Like many caldera

systems, compositionally intermediate eruptions characterized volcanism prior to caldera formation (Colucci et al, 1991; Chapin et al., 2004; Lipman, 2007). Basaltic andesite and dacite are the most voluminous precaldera volcanic rocks in the field, though small volumes of precaldera rhyolitic tuffs and lava flows were also erupted. Previous work has suggested that the earliest precaldera volcanism was calc-alkaline and that prior to caldera formation volcanism transitioned to alkaline composition magmas (Lipman et al., 1986; Johnson and Lipman, 1988). Volcanism climaxed with the formation of the Questa caldera during the eruption of the ~500 km^3 high-SiO_2 peralkaline Amalia Tuff (Lipman et al., 1986). Most of postcaldera volcanic rocks are absent from the field because of uplift and subsequent erosion. However, some postcaldera volcanic rocks are exposed on the intrarift horst blocks of Brushy and Timber Mountains, as well as clasts in sedimentary units. Similar to precaldera volcanism, postcaldera volcanism is characterized by intermediate and silicic eruptions (Lipman et al., 1986; Thompson et al., 1986).

Structural uplift, erosion, and Rio Grande rift faulting have exposed nine Tertiary granitic plutons in the Latir field (Lipman, 1988). A large Bouguer gravity low, centered on the caldera and continuing to the south, suggests that the intracaldera plutons may connect at depth to form a composite subvolcanic batholith (Cordell et al., 1986; Lipman, 1988). The plutons are grouped into three categories: resurgent, southern caldera margin, and southern plutons, based on similarities in geographic location, age, and structural position with respect to the subvolcanic batholith (Figure 1.1).

The resurgent plutons (Virgin Canyon, Canada Pinabete, Rito del Medio, Cabresto Lake plutons) are located within the subsided caldera block. Both the Virgin

Canyon and Canada Pinabete plutons contain peralkaline and metaluminous phases. The upper peralkaline phases have been interpreted to be nonerupted Amalia Tuff, whereas the lower metaluminous phases have been interpreted to represent the late stages of emplacement of these plutons (Lipman et al., 1986; Johnson and Lipman, 1988). Discontinuous peralkaline intrusions along the northern caldera margin are interpreted to be a partially exposed ring dike (Lipman et al., 1986; Johnson et al., 1989). Miarolitic cavities within the granitic Rito del Medio indicate shallow emplacement, consistent with resurgence. The Cabresto Lake pluton is the most mafic resurgent pluton and was emplaced at the structurally deepest levels. This pluton may represent a transition between the highly evolved peralkaline and metaluminous intrusions and the lesser-evolved plutons located in the south (Lipman et al., 1986; Johnson et al., 1989).

The southern caldera margin plutons, from west to east, are: Bear Canyon, Sulfur Gulch, and Red River. The plutons are characterized by varying degrees of hydrothermal and quartz-sericite-pyrite alteration and molybdenum mineralization (Leonardson, 1983; Lipman et al., 1986; Czamanske et al., 1990). The Bear Canyon and Sulfur Gulch plutons are relatively homogenous granites that contain minor aplite dikes. In contrast, the Red River pluton consists of granite, quartz monzonite, and numerous dikes of various compositions.

The two southern plutons, Rio Hondo and Lucero Peak, are exposed as far as 20 km south of the caldera margin. The Rio Hondo pluton is porphyritic granodiorite that grades into a thin granitic roof zone beneath Precambrian rocks (Lipman, 1988; Johnson et al., 1989; Czamanske et al., 1990). Mafic enclaves and deformed mafic dikes are present in deep exposures. Hundreds of northwest-trending dikes of felsic and mafic

composition intrude the pluton and overlying roof rocks (Lipman and Reed, 1989). Unlike the Rio Hondo pluton, the Lucero Peak pluton is a homogenous megacrystic granite, intruded by a few dikes in its eastern section. The Lucero Peak pluton is interpreted to be the youngest magmatic event in the Latir field (Lipman et al., 1986; Czamanske et al., 1990).

Though several geochronological studies have examined the timing of Latir magmatism (Pillmore et al., 1973; Lipman et al., 1986; Czamanske et al., 1990; Miggins et al., 2002; Smith et al., 2002), no published comprehensive study has used high-resolution methods. K-Ar and fission-track dating (Lipman et al., 1986) combined with detailed mapping (Lipman and Reed, 1989) provided the first thorough framework for the geochronology for the Latir field. Despite lack of precision and other complications with the earlier dating methods, these studies developed a volcanic stratigraphy and recognized an overall younging of plutonism towards the south. Czamanske et al. (1990) used Ar/Ar incremental-heating techniques to determine a more precise timing of the intrusions, but because neither analytical data nor age spectra were reported, the quality and geologic significance of these ages are difficult to assess. Smith et al. (2002) provided the only single-crystal laser-fusion Ar/Ar dates and determined the age of the Amalia Tuff to be 25.43 ± 0.1 Ma (recalculated relative to FC-2 = 28.201 Ma; Kuiper et al., 2008).

1.4. Methods

Sixty-seven samples were collected from the Latir volcanic field and surrounding areas during this study. In addition, Peter Lipman provided seven samples from the

Lipman et al. (1986) study and Ren Thompson of the USGS provided one. From this suite, 54 mineral separates from thirty-two samples were analyzed using the Ar/Ar dating method (Table 1.1).

Volcanic rocks were mostly collected from the northeastern region of the field to avoid hydrothermal alteration in the southern caldera region. Volcanic rocks were also collected from the intrarift horst (Brushy Mountain) and distal outflow Amalia Tuff in the Tusas Mountains. Intrusive rocks were collected from within the caldera, along the southern margin, and south of the caldera. At least two samples were collected from each pluton to better characterize the emplacement and thermal histories. Weathered or altered outcrops were avoided whenever possible.

Sample preparation techniques included crushing, grinding, sieving, ultrasonic cleaning in deionized water and 15% hydrofluoric solution (volcanic samples only), magnetic separation, and heavy liquid techniques. Minerals were then optically inspected using a binocular microscope and handpicked to obtain monomineralic separates. Samples to be dated were analyzed using a Cameca SX-100 electron microprobe at the New Mexico Bureau of Geology and Mineral Resources to accomplish two goals. First, BSE images obtained from the electron microprobe insure the highest quality of mineral separation. Second, geochemical characterization of samples prior to Ar/Ar analysis allows for recognition of any geochemical variation within the samples, which may be the result of alteration or geochemical contamination that would degrade the quality of geochronology results.

Samples were placed in 20-hole aluminum disks and irradiated with the interlabratory standard FC-2 (28.201 Ma; Kuiper et al., 2008) in a known geometry. In

addition to unknowns and monitors, CaF_2 and K-glass were irradiated to determine calcium and potassium correction factors. Samples were analyzed at the New Mexico Geochronology Research Laboratory between 2006 and 2010. Sanidine separates were heated using the single-crystal laser-fusion method. Biotite, hornblende, K-feldspar, and groundmass concentrate were step-heated in a double-vacuum Mo resistance furnace. Gas was then cleaned in an all-metal extraction line and analyzed using a MAP 215-50 mass spectrometer. Appendix 1.1 contains a more detailed description of the analytical procedures and parameters for this study.

1.5. Results

Table 1.1 summarizes all the Ar/Ar results from this study. All data tables and corresponding ideograms and age spectra are in Appendix 1.2. For completeness, results in Table 1.1 are presented with and without error in the ^{40}K decay constant. Uncertainty in the decay constant should be propagated through the error calculation because this study compares Ar/Ar ages to U/Pb ages (Tappa et al., in review). The ^{40}K decay constant of Min et al. (2000) is considered to be the most accurate value. However, propagation of the decay constant uncertainty results in highly imprecise ages. In subsequent sections we will only discuss ages and corresponding errors that exclude errors in the decay constant.

1.5.1. Sanidine laser-fusion analyses of volcanic rocks

Fifteen sanidine separates (8 collected for this study, 7 reanalyzed from the study by Lipman et al.1986) were dated using the laser-fusion method. Results are plotted as apparent ages versus relative probability (Deino and Potts, 1992). Also included with age probability diagrams are K/Ca and $\%^{40}Ar^*$ (radiogenic yield) auxiliary plots. Six

TABLE 1.1. Ages of the Questa caldera samples

Caldera Stage	Sample	Unit	Mineral*	Age Calc. Method †	Age§ (Ma)	Internal Error# (2σ)	External Error** (2σ)
Precaldera volcanism	MZQ-23	Commanche Creek Andesite	hbl	plateau	28.50	0.19	1.13
	MZQ-17	Tetilla Peak	san	ideogram	28.22	0.05	1.11
	MZQ-24	Dacite	bt	plateau	27.94	0.10	1.10
	83L-8	Cordova Creek Rhyolite	san	ideogram	25.57	0.04	1.00
	MZQ-26	Cordova Creek Rhyolite	san	ideogram	25.57	0.04	1.00
Caldera Collapse	MZQ-4	Intracaldera Amalia	san	ideogram	25.49	0.13	1.01
	MZQ-25	Rheomorphic Rhyolite	san	ideogram	25.49	0.07	1.00
	82L-42H	Outflow Amalia Tuff	san	ideogram	25.46	0.05	1.00
	82L-37	Outflow Amalia Tuff	san	ideogram	25.43	0.09	1.00
	82L-38	Outflow Amalia Tuff	san	ideogram	25.43	0.06	1.00
	82L-31	Outflow Amalia Tuff	san	ideogram	25.34	0.08	1.00
	TPS04	Outflow Amalia Tuff	san	ideogram	25.34	0.06	1.00
	MZQ-7	Outflow Amalia Tuff	san	ideogram	25.36	0.04	1.00
	78L-183	Rheomorphic Amalia	san	ideogram	25.29	0.08	0.99
Postcaldera volcanism	MZQ-22	Commanche Point Rhyolite	san	ideogram	25.28	0.04	0.99
	79L-64	Commanche Pt. Rhyolite	san	ideogram	25.26	0.04	0.99
	MZQ-35	Brushy Mountain Rhyolite	san	ideogram	25.17	0.04	0.99
	MZQ-36	Brushy Mtn. Andesite	gmc	plateau	22.69	0.08	0.89
	MZQ-37	Brushy Mtn. Dacite	hbl	n/a	exc;alt	n/a	n/a
Resurgent Plutonism	VC09-2	Peralkaline Northern Ring Dike	kspar	plateau	25.38	0.04	1.00
	MZQ-15	Metaluminous Canada Pinabete	bt	isochron	25.38	0.09	1.00
	MZQ-16	Granite Rito del Medio	Kspar	isochron	24.94	0.09	1.00
	MZQ-16	Granite Rito del Medio	bt	plateau	25.19	0.06	0.99
	MZQ-39	Granite Rito del Medio	bt	plateau	24.82	0.17	0.99
	MZQ-39	Granite Rito del Medio	Kspar	plateau	24.80	0.09	0.98
	MZQ-13	Granite Cabresto Lake	Kspar	plateau	25.02	0.15	0.99
	MZQ-13	Granite Cabresto Lake	bt	plateau	24.84	0.11	0.98
	MZQ-12	Granite Cabresto Lake	bt	plateau	24.81	0.13	0.99
	MZQ-12	Granite Cabresto Lake	Kspar	isochron	24.88	0.09	0.98
	MZQ-1	Peralkaline Virgin Canyon	Kspar	n/a	exc	n/a	n/a
	MZQ-2	Metaluminous Virgin Canyon	Kspar	n/a	exc	n/a	n/a
	MZQ-38	Peralkaline Virgin Canyon	Kspar	n/a	exc	n/a	n/a
	MZQ-15	Metaluminous Canada Pinabete	Kspar	n/a	exc	n/a	n/a
Southern Caldera Margin Plutonism	MZQ-6	Granite Sulfur Gulch	Kspar	n/a	exc;a.l	n/a	n/a
	MZQ-5	Granite Red River	bt	plateau	24.94	0.06	0.98
	MZQ-5	Granite Red River	Kspar	n/a	a.l.	n/a	n/a
	MZQ-6	Granite Sulfur Gulch	bt	plateau	24.73	0.14	0.98
	AR-171	Granite Sulfur Gulch	bt	plateau	24.64	0.10	0.97
	MZQ-8	Granite Bear Canyon	bt	plateau	24.54	0.12	0.97
	MZQ-34	Granite Bear Canyon	bt	plateau	24.37	0.11	0.96
	MZQ-8	Granite Bear Canyon	Kspar	plateau	23.79	0.17	0.95
	MZQ-34	Granite Bear Canyon	Kspar	plateau	22.33	0.11	0.88
Southern Plutonism	MZQ-19	Granodiorite Rio Hondo	bt	integrated	21.51	0.09	0.85
	MZQ-9	Granodiorite Rio Hondo	bt	plateau	21.22	0.10	0.84
	MZQ-21	Granite Lucero Peak	bt	plateau	19.34	0.08	0.76
	MZQ-32	Granite Lucero Peak	bt	plateau	19.14	0.10	0.76
	MZQ-10	Rhyolite Dike in Rio Hondo	Kspar	plateau	16.60	0.16	0.67
	MZQ-9	Granodiorite Rio Hondo	hbl	n/a	exc;alt	n/a	n/a
	MZQ-19	Granodiorite Rio Hondo	hbl	n/a	exc;alt	n/a	n/a
	MZQ-9	Granite Rio Hondo	Kspar	n/a	a.l.	n/a	n/a
	MZQ-33	Granite Rio Hondo	Kspar	n/a	a.l.	n/a	n/a
	MZQ-19	Granodiorite Rio Hondo	Kspar	n/a	a.l.	n/a	n/a
	MZQ-21	Granite Lucero Peak	Kspar	n/a	a.l.	n/a	n/a
	MZQ-32	Granite Lucero Peak	Kspar	n/a	a.l.	n/a	n/a

* - Groundmass concentrate (gmc), hornblende (hbl), biotite (bt), sanidine (san), K-feldspar (kspar)

† - n/a (not applicable); discordant age spectrum because of various reasons, see below

§ - Age determined using Fish Canyon (FC-2) = 28.201 Ma (Kuiper et al., 2008); exc (excess argon), alt (alteration), a.l. (argon loss via slow cooling or reheating)

- Includes error in J and irradiation parameter

**- Uncertainty includes error in K decay constant $(5.463\pm0.214)\times10^{-10}yr^{-1}$ (Min et al., 2000)

representative ideograms are in shown in Figure 1.2. Seven to 35 crystal aliquots from each sample were analyzed to determine the age. At least 15 single crystals were analyzed for all the MZQ samples. Some of the Lipman et al. (1986) samples were originally run as single crystals, but the small size of the crystals (≤250 μm) resulted in small, imprecise ^{39}Ar signals. To increase precision, the samples were reanalyzed again as multiple-crystal (~5-20 crystals per set) laser-fusion analyses.

Several criteria were used to determine which analyses were included in the age calculation. Analyses with small or imprecise ^{39}Ar mol measurements, low radiogenic yield, and high or low K/Ca values compared to the bulk values were excluded from the age calculation. Analyses of xenocrysts were also excluded.

Overall, the age probability plots display single age populations without large age variations between individual ages. Of the fifteen samples analyzed, ten ages used all the crystal analyses for the mean age calculation (e.g., Tetilla Peak Tuff, Figure 1.2F). For the remainder of the ages, 1 to 10 analyses were omitted because of: anomalously low radiogenic yields (MZQ-4 and 82L-37), young apparent ages due to alteration (MZQ-4, Figure 1.2E), small ^{39}Ar signals (79L-64) or possible xenocrystic contamination (MZQ-25, 82L-37, 78L-183)

Because the Lipman sanidines were analyzed as multiple crystals, there was the possibility of xenocrystic contamination. To assess contamination, two samples, the postcaldera rhyolite of Commanche Point (Figure 1.2B) and the precaldera Cordova Creek rhyolite (Figure 1.2D) were recollected and analyzed using the sanidine single-crystal laser-fusion method (SCLF). For both samples, the SCLF analyses (Figure 1.2B

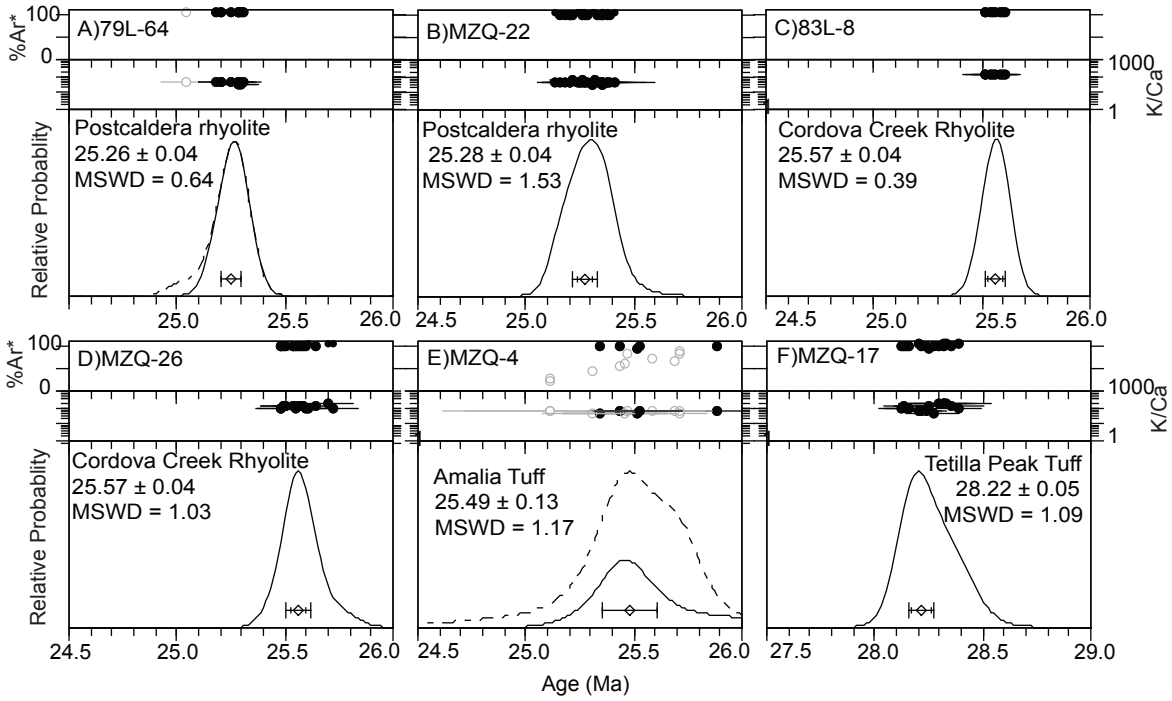

Figure 1.2. Representative ideograms of the Questa caldera sanidine single-crystal laser-fusion analyses. Auxiliary plots include K/Ca and radiogenic yield (%^{40}Ar*). All errors are reported at 2σ and do not include error in decay constant.

and D) display a normal distribution (i.e., MSWD ~1) without outliers and are indistinguishable in age the multiple-crystal analyses (Figure 1.2A and C).

For Amalia Tuff sample MZQ-4 (Figure 1.2E), 10 of the 15 analyses had radiogenic yields <95%. This sample was collected from the hydrothermally altered southern caldera margin region. The low radiogenic yields measured for this sample reflects mild hydrothermal alteration of the sanidine. BSE microprobe images indicated minor amounts of clay within fractures. Clay commonly has high atmospheric contents and thus is the preferred reason for the overall low radiogenic yields observed in the sample.

Thirteen laser-fusion analyses of the Amalia Tuff (Figure 1.3) range from 25.29 ± 0.11 to 25.49 ± 0.13 Ma and yield a mean of age 25.39 ± 0.04 Ma (MSWD = 0.80). This age calculation includes four SCLF analyses of samples collected during this study, five reanalyzed samples from Lipman et al. (1986), and four SLCF analyses from Smith et al. (2002). Smith et al. (2002) used a FC-2 age of 27.84 Ma; accordingly, these ages were adjusted relative to FC-2 =28.201 Ma (Kuiper et al., 2008). The new weighted mean age for the Amalia Tuff is in close agreement with the previously published age of 25.43 ± 0.1 Ma (Smith et al., 2002; corrected for FC-2 = 28.201 Ma). This age represents the eruption age of the Amalia Tuff and the formation of the Questa caldera.

1.5.2. Biotite, hornblende, and groundmass analyses

Representative biotite, hornblende, and groundmass age spectra are shown in Figure 1.4. Ages were determined using integrated or plateau methods. A plateau is here defined as three contiguous steps that comprise 50% or more of the $^{39}Ar_K$ released and have ages overlapping within two-sigma error (Fleck et al., 1977). Fifteen biotite, four

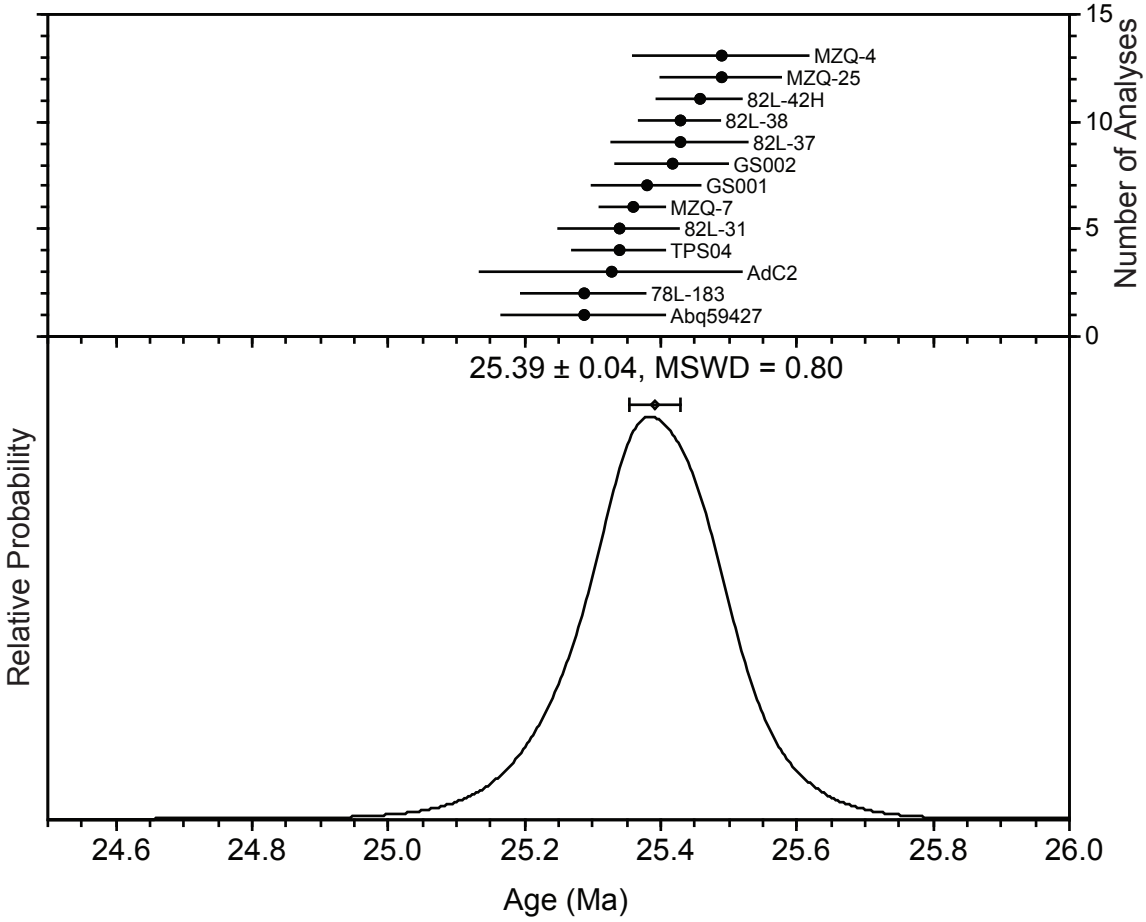

Figure 1.3. Ideogram displaying the thirteen ages for the Amalia tuff. Samples Abq59427, AdC2, GS001, and GS002 are sanidine single-crystal laser-fusion analyses from Smith et al., (2002) recalculated relative to FC-2 = 28.201 (Kuiper et al., 2008).

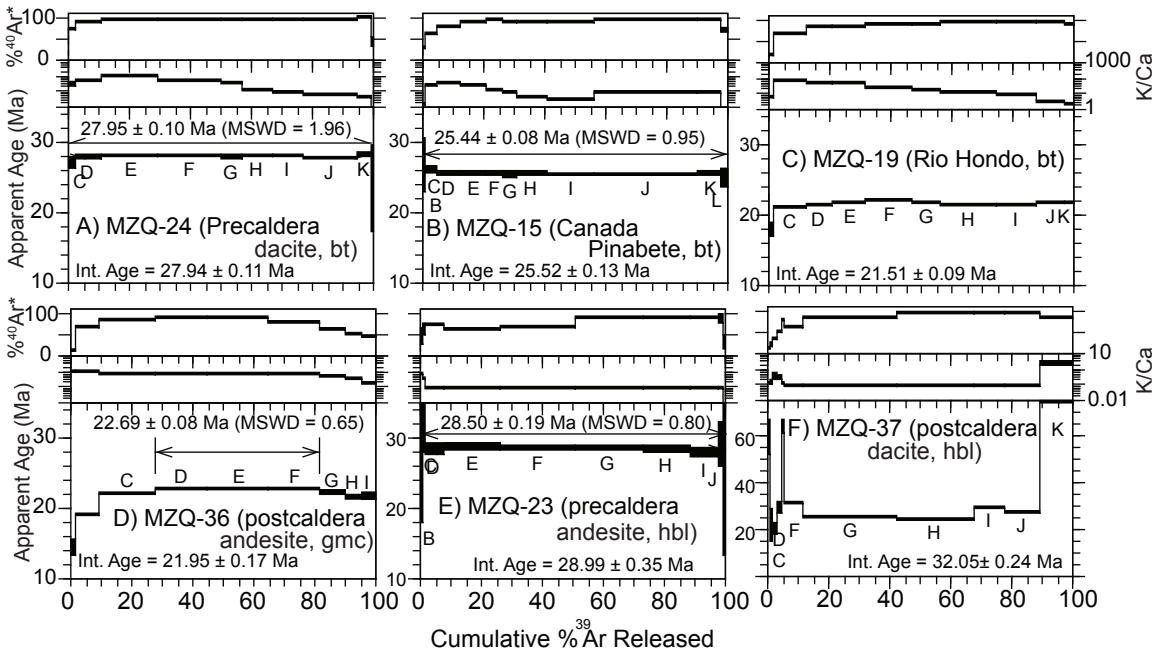

Figure 1.4. Representative age spectra for the Questa caldera biotite (bt), hornblende (hbl), and groundmass concentrate (gmc) analyses. Auxiliary plots included K/Ca and radiogenic yield (%^{40}Ar*). All errors are reported at 2σ and do not include error in decay constant.

hornblende, and one groundmass concentrate separates were step-heated. Separates from volcanic rocks were analyzed to determine an eruption age. Hornblende and biotite ages from plutonic rocks indicate timing at which the sample cooled to 550-500°C and 350-300°C, respectively (Harrison, 1981; Hodges, 1991).

K/Ca values are similar for all the biotite samples. Initial values are ~100 and values decrease during heating. This trend is common in biotites and records the progressive degassing of high Ca apatite inclusions at higher temperatures (Lo and Onstott, 1989). Radiogenic yields are initially ~25% and in all samples increase to values nearing 100% during the analysis. The initially low $^{40}Ar^*$ values are due to atmospheric argon degassing at low temperatures. The combination of high radiogenic yields and 8-10 wt% K_2O indicate pristine, unaltered biotites. Although some inverse isochron plots for the biotite, hornblende, and groundmass samples do not have $^{40}Ar/^{36}Ar$ intercepts of 295.5 within 2σ error, the inverse isochron ages are within 2σ error of that calculated from the age spectrum.

In general, biotite age spectra are not complex and ages were determined using the plateau method (e.g., Figure 1.4A and B). For the spectra with a plateau, plateaus comprise between ~80% to 97% of the ^{39}Ar released. Of these spectra, the first one or two steps were anomalously older or younger, have large errors, and low radiogenic yields. Small signals are the cause of imprecise ages. Small amounts of excess argon or alteration at the grains surface would produce old or young apparent ages, respectively. The small percentage of the total ^{39}Ar released in fusion step indicates complete ^{39}Ar degassing of the biotite separates.

MZQ-19 (Figure 1.4C) is the only biotite analysis that did not yield a plateau. Ages of the first several steps are ~17 Ma, then they increase to 22 Ma, then decrease to 21 Ma and finally increase 22 Ma. Lo and Onstott (1989) concluded that geologically meaningful ages could be obtained from disturbed biotite spectra using the total gas age. During irradiation, neutrons interacting with ^{39}K atoms can recoil the newly formed ^{39}Ar atoms into the adjacent chloritized layers or in severe cases of alteration completely eject ^{39}Ar from the biotite grains. For MZQ-19, wt% K_2O is 8.61, which is the expected range for pristine biotite (McDougall and Harrison, 1999), suggesting that any alteration is in negligible amounts. The preferred age is 21.51 ± 0.09 Ma, calculated from the total gas released.

A groundmass separate from a postcaldera andesite on Brushy Mountain yielded a plateau age of 22.69 ± 0.08 (MSWD = 0.65) (Figure 1.4D). The initial 30% of the $^{39}Ar_K$ released (steps A-C) displays a monotonic increase in ages, from 14.3 to 21.9 Ma, a plateau consisting of steps D-F, and the last 20% of the spectrum decreases in age to 21.6 Ma. Argon loss in glass is the most likely explanation for the initial age gradient within the sample. Though the last three steps display decreasing ages, the addition of those steps to the age calculation only changes the plateau age from 22.69 ± 0.08 to 22.6 ± 0.3 Ma. The plateau age is interpreted to represent the eruption age of the andesite on Brushy Mountain.

Only one of the four hornblende analyses yielded statistically robust results. The plateau for the MZQ-23 (Figure 1.4E) analysis is comprised of steps B through K corresponding to ~98% of the spectrum. K/Ca values of 0.1 and radiogenic yields

approaching 100% are typical of pristine hornblendes. The age of 28.50 ± 0.19 (MSWD = 0.80) from the hornblende-bearing andesite is interpreted as an accurate eruption age.

MZQ-9, MZQ-19, and MZQ-37 hornblende age spectra displayed extreme discordance (e.g., MZQ-37, Figure 1.4F) throughout the spectra. The age spectra of the hornblende, though disturbed, are remarkably similar. The overall "saddle" shape of the age spectra is common to samples containing excess ^{40}Ar (Kelly, 2002). Inverse isochrons for the analyses do not display clear trends, so if excess ^{40}Ar is responsible for spectra discordance, it is not homogeneously distributed. The most likely cause of scatter in the age spectra is small amounts of chloritic alteration, coupled with excess ^{40}Ar and/or ^{39}Ar recoil.

1.5.3. K-feldspar age spectra and MDD thermal histories of plutons

Twenty plutonic K-feldspars were step-heated to determine the 300-150ºC cooling history of the plutons. Nine representative K-feldspar age spectra are shown in Figure 1.5. K-feldspar analyses were modeled using the multiple diffusion domain (MDD) thermal modeling method of Lovera et al., (1989, 1991). Supplementary MDD plots (Arrhenius diagram, Log r/r_o) are in Appendix 1.3. The MDD thermal modeling method of K-feldspar Ar/Ar analysis is within Appendix RD2 of Sanders et al. (2006). Two thermal histories were produced for each K-feldspar analysis that was modeled using the MDD theory. Monotonic cooling models (Figure 1.6) only allow for cooling from high temperatures, whereas unconstrained models (Figure 1.7) allow for reheating events.

Radiogenic yields and K/Ca auxiliary plots provide guidance for evaluating the K-feldspar age spectra. Radiogenic yields for the analyzed samples have similar trends.

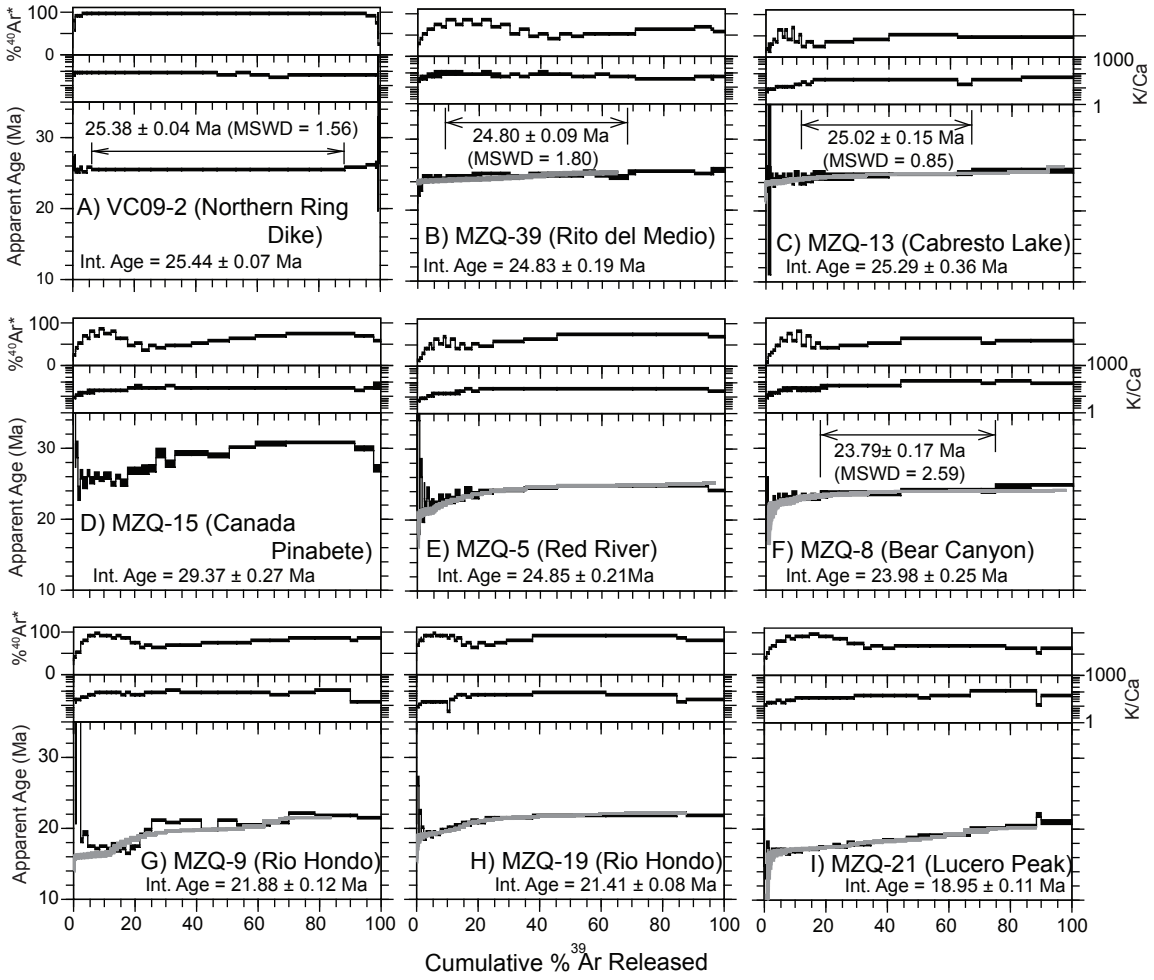

Figure 1.5. Representative age spectra for the Questa caldera plutonic K-feldspar. Auxiliary plots include K/Ca and radiogenic yield (%^{40}Ar*). All errors are reported at 2σ and do not include error in decay constant. Modeled age spectra that result from MDD cooling histories are shown in gray.

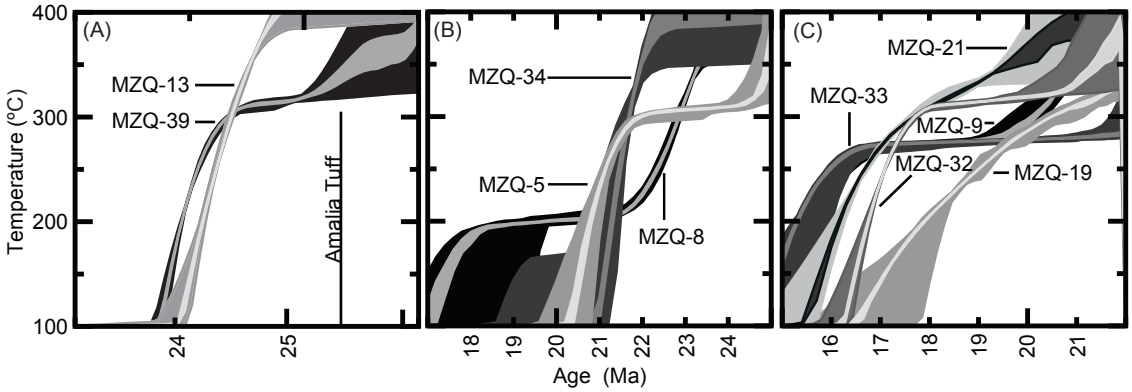

Figure 1.6. MDD Monotonic cooling histories from the exposed Questa caldera plutons. The ages on the x-axis are different for the three subdivisions of plutons. A) Resurgent plutons. MZQ-39 is from Rito del Medio and MZQ-13 is from Cabresto Lake. The line labeled Amalia tuff corresponds the age reported in this study of 25.39 ± 0.04 Ma. B) Southern caldera margin plutons. MZQ-8 and 34 are from the Bear Canyon pluton and MZQ-5 is from the Red River pluton. C) Southern plutons. MZQ-9, 19, and 33 are from the Rio Hondo pluton and MZQ-21 and 32 are from Lucero Peak. MZQ-9 and 33 follow the same cooling trend from 19 to 15 Ma and a portion of the cooling history of MZQ-9 is obscured by that of MZQ-33.

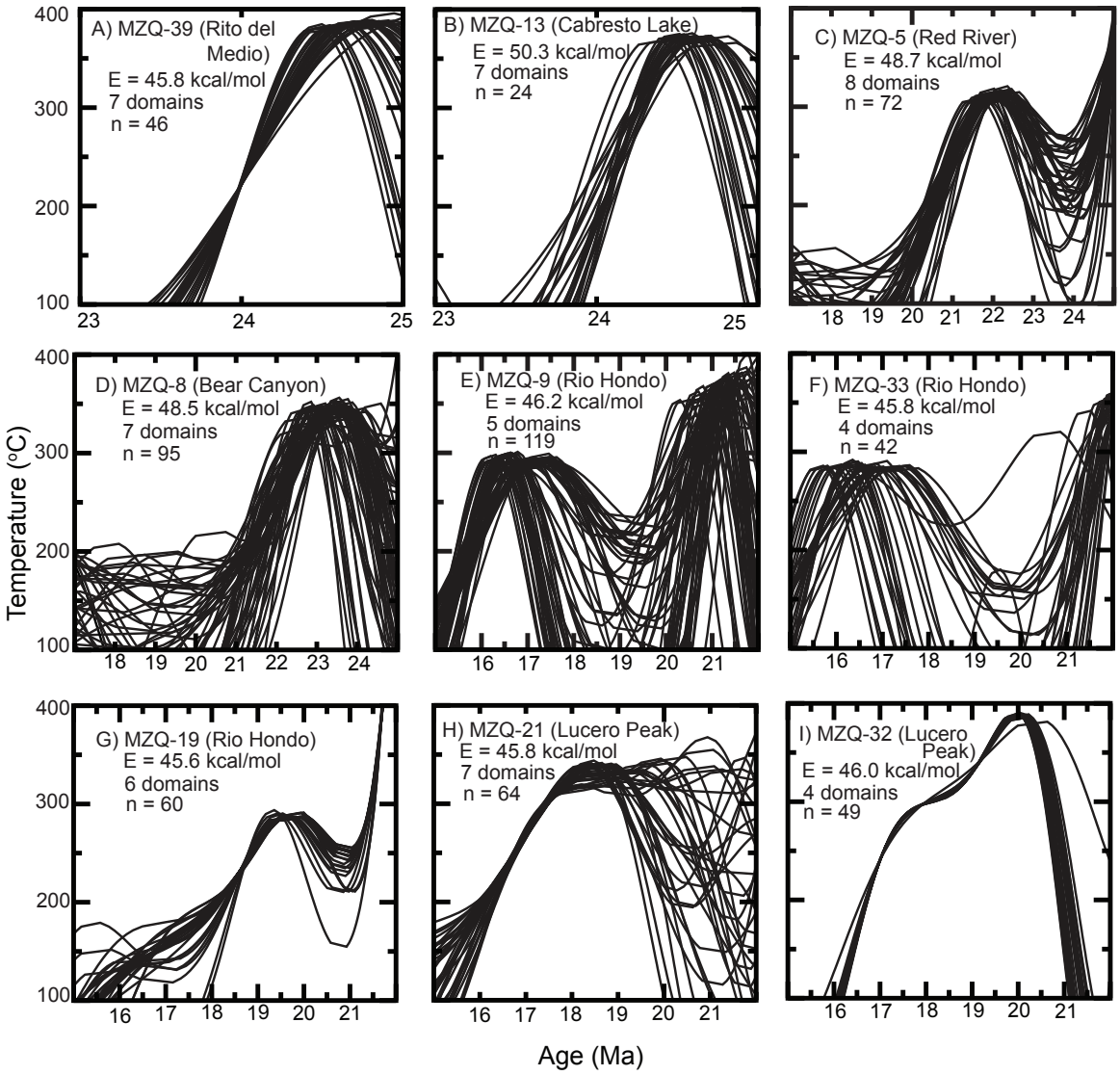

Figure 1.7. MDD unconstrained thermal histories from the exposed Questa caldera plutons. Note the scale along the x-axis changes amongst samples. Activation energy and number of domains are the same for corresponding monotonic cooling histories. n = number of solutions.

Within the initial 10-30% ^{39}Ar released radiogenic yields begin at approximately 50%, climb to values nearing 90-100%, then decrease to values of 40-60% $^{40}Ar^{*}$. Following this initial peak, radiogenic yields steadily increase, ending in values of 90-100%. The saw-tooth oscillation observed in the radiogenic yield, as well as the K/Ca in some samples, is a result of isothermal duplicate step heating technique that was used to degas the K-feldspar. The first step decrepitates fluid inclusions, which host excess argon. The second duplicate step is more characteristic of volume diffusion from K-feldspar crystal (Harrison et al., 1994). The reason radiogenic yields of some samples are so low is not completely understood. Fluid inclusions are known to host excess argon (Kelley, 2002), and perhaps pluton emplacement into a shallow crustal environment incorporates atmospheric argon into the fluid inclusions as well. Accordingly, all cooling histories were modeled using the second of the isothermal duplicate steps to avoid erroneous results.

Overall, the K-feldspar age spectra display a variety of complexities resulting from excess argon and thermal histories. The age spectra are of the ring dike and resurgent plutons, southern caldera margin, intrusions, and southern plutons are discussed separately below because K-feldspar analyses from each these three groups display similarities in age and thermal histories. Though some age spectra are discordant and not useful for interpreting the geologic history, the age spectra are briefly discussed.

1.5.3.1. Resurgent plutons and northern ring dike

K-feldspar age spectra from the resurgent plutons and ring dike display evidence for rapid cooling or are discordant due to alteration and/or excess argon. Five K-feldspars yielded geologically meaningful results. K-feldspar from sample VC09-2

(Figure 1.5A), the peralkaline intrusion along the northern caldera margin, yielded a plateau age of 25.38 ± 0.04 Ma (MSWD = 1.56). The plateau is comprised of ~80% of the total ^{39}Ar released. This was the only K-feldspar that did not display the previously discussed radiogenic yield pattern. Because of the lack of an age gradient observed in the age spectrum, the sample is interpreted to have cooled quickly from magmatic temperature following caldera collapse at 25.4 Ma.

Samples from the Rito del Medio and Cabresto Lake pluton provide information concerning the 300-150ºC cooling history of the resurgent plutons. K-feldspar from the Rito del Medio pluton (e.g., MZQ-39; Figure 1.5B) are characterized by monotonically increasing steps from ~22 to 24 Ma during the initial 5% of the spectrum, followed by a plateau comprised of the next 60 to 70% of the ^{39}Ar released, and finally ending in an increase in ages over the last 20-30% of the spectrum. For sample MZQ-39, the plateau age is age 24.80 ± 0.09 Ma (MSWD = 1.80), whereas the plateau age of MZQ-16 is 25.41 ± 0.15 (MSWD = 1.19). However, the plateau age of MZQ-16 is older than the corresponding biotite age (25.2 Ma). The inverse isochron yields a ^{40}Ar/^{36}Ar intercept of 301.4 ± 1.8, indicative of slight excess argon. The preferred age is inverse isochron age, 24.94 ± 0.09 Ma. Monotonic cooling models of MZQ-39 indicate rapid cooling histories between 24 and 25 Ma (Figure 1.6A), whereas unconstrained thermal models allow reheating at ~25 Ma, followed by rapid cooling (Figure 1.7A) similar to the monotonic model.

K-feldspar spectra from the Cabresto Lake pluton (MZQ-12 and 13; e.g., Figure 1.5C) are similar to the Rito del Medio K-feldspar. Plateau ages are 25.31 ± 0.12 Ma (MSWD = 2.81) and 25.02 ± 0.15 (MSWD = 0.85) for MZQ-12 and 13, respectively. The

inverse isochron for MZQ-12 has a $^{40}Ar/^{36}Ar$ intercept of 317 ± 6, suggesting excess argon contamination. The preferred age is 24.88 ± 0.09 Ma, calculated from inverse isochron regression. This age is preferred because it agrees with the MZQ-12 biotite age of 24.81 ± 0.13 Ma and K-feldspar plateau age from MZQ-13. The MDD thermal history of MZQ-13 indicates rapid cooling (400ºC/Ma) between 24 and 25 Ma (Figure 1.6A and 1.7B).

The Virgin Canyon and Canada Pinabete plutonic K-feldspar (MZQ-1, 2, 38, and 15), yielded geologically meaningless results (e.g., MZQ-15; Figure 1.5D). Both analyses from the metaluminous phases of the Virgin Canyon pluton (MZQ 2, 38) have plateau ages (26.8 and 25.9 Ma, respectively) significantly older than the age of the caldera (25.4 Ma). Samples from the peralkaline region of the Virgin Canyon and Canada Pinabete (MZQ-1 and MZQ-15, respectively) did not yield plateaus and most steps are also older than the Amalia Tuff. Anomalously old ages observed in K-feldspar age spectra, typically from gas released at higher temperature, are interpreted to be the result of excess argon trapped during cooling within the largest domains (Foster et al., 1990).

1.5.3.2. Southern caldera-margin plutons

K-feldspar age spectra from the southern caldera-margin plutons are more complex than those of the resurgent plutons. MDD thermal models display trends that suggest changes in cooling rates from 300 to150ºC. (Figure 1.6B) and/or reheating events (Figure 1.7C and D). Ages and cooling histories vary among individual plutons and within individual plutons.

K-feldspar analysis from the Red River pluton yielded monotonically increasing ages throughout the analysis (Figure 1.5E). Ages of the first steps increase from 16 to 22

Ma within the first 5% of the spectrum. The steep age gradient and large errors associated with the low temperature steps makes modeling the cooling history from the smallest domains of the K-feldspar difficult. This is reflected in the large errors at ~150ºC in the cooling history of the Red River Pluton (Figure 1.6B). Following the initially steep age profile, ages of steps gradually increase in age from 22.5 to 25 Ma. The monotonic cooling models indicate cooling to 300ºC by 24 Ma. Between 24 and 22 Ma monotonic models suggest the sampled remained at ~300ºC. At 22 Ma, cooling rates increase to 100ºC/Ma, though the exact cooling rate is uncertain due to the large errors associated with the smallest domains. Alternatively, unconstrained models (Figure 1.7C) allow for rapid cooling at ~ 25 Ma and subsequent reheating to 300ºC at ~22 Ma.

K-feldspar age spectra from the Bear Canyon pluton, MZQ-8 (Figure 1.5F) and 34, yield plateau ages of 23.79 ± 0.17 Ma (MSWD = 2.59) and 22.33 ± 0.11 Ma (MSWD = 2.15), respectively. In addition to plateau segments, both age spectra display small age gradients at the beginning of the analysis. Monotonic cooling model results (Figure 1.6B) are variable with respect to timing and trend of cooling, though the two samples are separated by less than two kilometers. MZQ-34 cooled through the K-feldspar closure temperature in roughly 1 Ma, although errors associated with closure of the smallest domains allow for the possibility of a range of ages between 19.5 and 17 Ma at 150ºC. MZQ-8 monotonic thermal models indicate that cooling from 300 to 200ºC occured between 23 and 21.5 Ma and require a period of prolonged temperatures of 200ºC, until 20 Ma. The timing of cooling between 200 and 150ºC is highly uncertain. The unconstrained model of MZQ-8 (Figure 1.7D) allows for possible reheating to 300ºC between 22 and 24 Ma and rapid cooling thereafter. Numerous unconstrained models

permit thermal perturbations up to 200ºC, as young as 17 Ma. The prolonged cooling and numerous thermal events younger than 22 Ma corresponds to the initial ~10% of the spectrum and this segment of the cooling history may be inaccurate because of large uncertainties.

The K-feldspar separate of the Sulfur Gulch pluton, MZQ-6, produced anomalous results. Like the Virgin Canyon and Canada Pinabete K-feldspar, the age spectra exhibits monotonically increasing ages from 21 Ma to 26.5 Ma during the first 30% of the spectrum and ends with a plateau older than the age of the caldera, which is geologically unsupported.

1.5.3.3. Southern plutons

Age spectra and MDD cooling models of the Rio Hondo and Lucero Peak plutons suggest long, complex thermal histories (Figures 1.5G-I, 1.6C, and 1.7F-J). In general, age spectra are complex because of excess argon, protracted cooling, and/or reheating events. Samples from the deepest exposed section of the Rio Hondo pluton (MZQ-9; Figure 1.5G) and upper granite (MZQ-33) are the most complex and disturbed. Excess argon is present through the majority of age spectra, indicated by the oscillation of the ages resulting from isothermal duplicate step heating. Excess argon degassed at the low temperature steps complicates determining the ages of the smallest domains. Both samples show climbing ages until 20% ^{39}Ar released. At this point during both analyses, ages of steps increase abruptly and the remaining age spectrum is characterized by discordant steps that generally decrease in age.

For both samples, age spectra were modeled using a straight line through the 'hump' portion of the spectrum. Monotonic cooling models (Figure 1.6C) agree and

show good correlation between 19 Ma and 16 Ma, depicting isothermal conditions at ~260ºC. At temperatures between 250 and 150ºC both samples have the same cooling trends but errors are larger. Unconstrained thermal models (Figure 1.7E and F) are also similar to one another, depicting rapid cooling to ≤150ºC at ~20 to 21 Ma followed by reheating to 300ºC between 16 to 18 Ma.

Sample MZQ-10 is from a rhyolitic dike that intruded into the main granodiorite phase of the Rio Hondo pluton. The age spectrum is characterized by an initial age gradient from 15 to 17 Ma, followed by a plateau age of 16.60 ± 0.16 Ma (MSWD = 1.24) composed of ~70% of the ^{39}Ar released. Radiogenic yields are enigmatic. During the analysis, radiogenic yields are as low as 10% and do not exceed 50%. The radiogenic yield does not have the typical oscillation pattern of isothermal duplicate step heating that characterizes excess argon degassing from fluid inclusions. An inverse isochron plot of the sample indicates a ^{40}Ar/^{36}Ar intercept of 297 ± 1, consistent with an absence of excess argon. Weight percent K_2O from microprobe analyses averaged 14.4 wt% (n=9) and BSE images do not indicate alteration, but shows a large population of fluid inclusions. The low radiogenic yields are probably because of atmospheric-argon-bearing, excess-argon-lacking fluid inclusions that degassed throughout the most of the analysis.

Age spectra from the upper region of the main granodiorite phase of the Rio Hondo pluton (MZQ-19; Figure 1.5H) and the Lucero Peak pluton (MZQ-21; Figure 1.5I and MZQ-32) also suggest slow cooling or reheating. All three analyses exhibit age gradients throughout the spectra. Also observed are short, flat segments containing between 10-30% of the spectrum (e.g. from 20-40% ^{39}Ar released for sample MZQ-19). The monotonic cooling history of MZQ-19 (Figure 1.6C) indicates a nearly constant

cooling rate from 21.5 to 16 Ma. Lucero Peak monotonic cooling models (Figure 1.6C) are similar to each other. From 21 to 18 Ma, cooling rates are slow, between 33ºC/Ma to near isothermal conditions. Between 17 and 18 Ma, cooling rates change to as fast as 100°C/Ma, though the change in cooling is more pronounced in MZQ-32. Though there is considerable agreement between the samples, models indicate that MZQ-32 may have cooled through the smallest domain closure temperatures as much as 1 Ma prior to MZQ-21.

Unconstrained thermal models for these three samples are variable. MZQ-19 unconstrained models (Figure 1.7G) allow for cooling to between 150 and 250ºC at ~21 Ma, reheating to 290ºC between 19 and 20 Ma, and variable cooling rates between 19 and 15 Ma. Unconstrained thermal models of MZQ-21 (Figure 1.7H) did not generate common cooling trends between 22 and 20 Ma, but allow for various amounts of cooling and subsequent reheating. All models converge at 300 to 325ºC at 19 Ma. Similar cooling styles and rates occur between 300 and 150°C. All MZQ-32 unconstrained thermal models (Figure 1.7I) indicate reheating to 375ºC between 21 and 20 Ma and suggest cooling without reheating until 16 Ma.

1.6. Magmatic history of the Questa caldera

Ar/Ar geochronology and thermochronology of the Questa magmatic system, summarized in Table 1.1 and Figure 1.8, provide insight into the volcanic-plutonic relationship related to shallow crustal (≤ 5km) caldera-related magmatism. Figure 1.9 is a schematic illustration of the Questa caldera magmatism. Age determinations from this study, along with previous work, support the inference that caldera related magmatism is

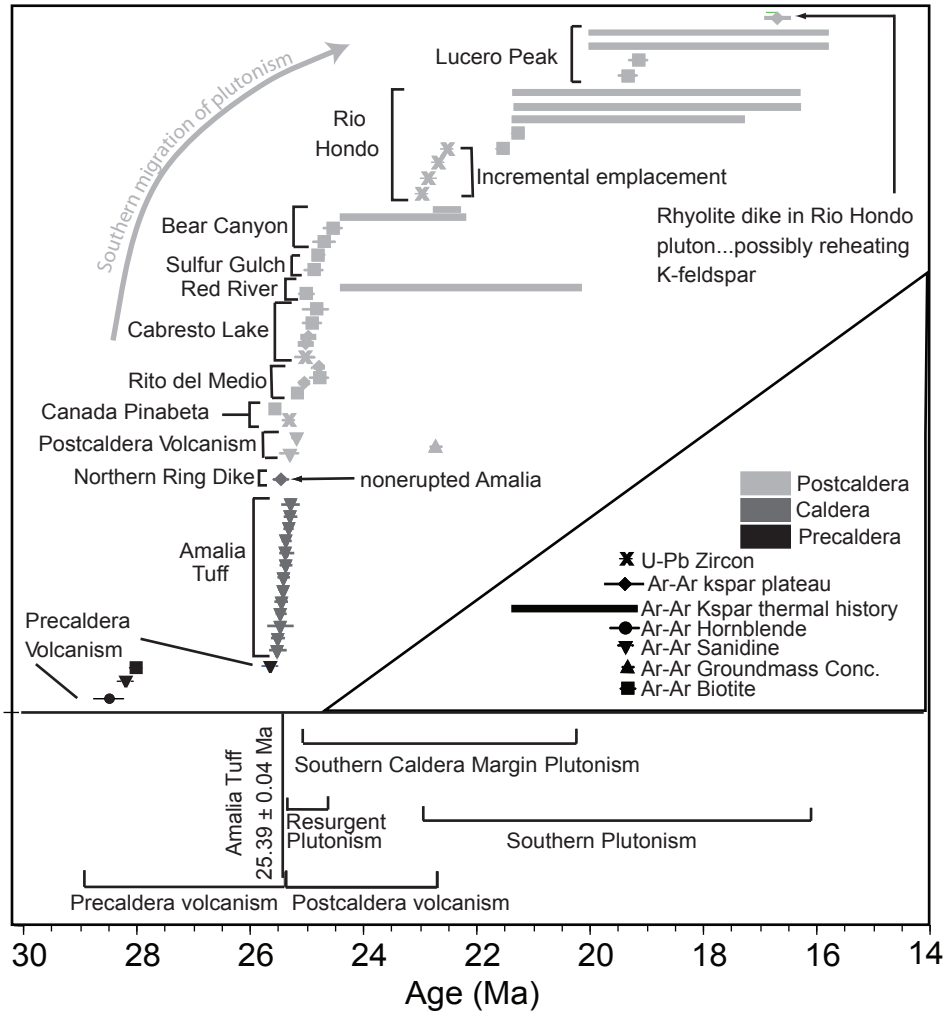

Figure 1.8. Questa caldera geochronology summary. Ages are reported at 2σ error. Different minerals are indicated by different symbols. Zircon ages are from Tappa et al. (in review). K-feldspar with long, bold horizontal lines correspond to time represented in MDD cooling histories (Fig. 6 and 7). The bottom panel shows a generalized interpretation of the magmatic history of the Questa caldera based on the geochronology summary.

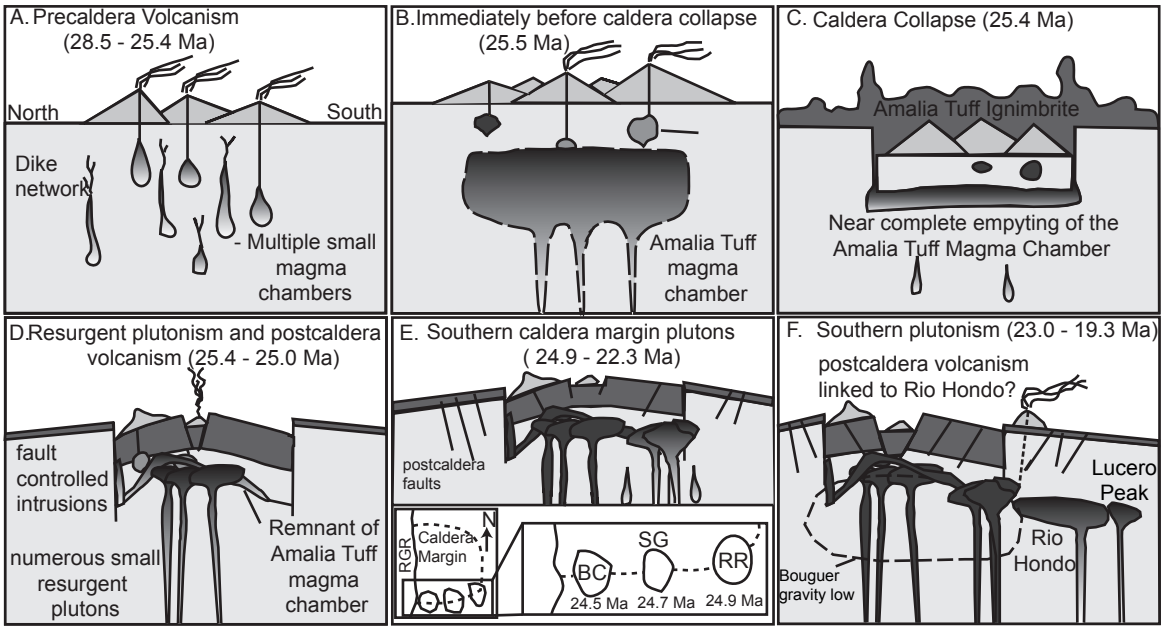

Figure 1.9. Simplified schematic diagram illustrating the magmatic evolution of the Questa caldera. Crystallized magma chambers shown in dark gray. Active magma chambers are indicated by a gray gradient. Diagram is not to scale. See text for discussion of each panel.

a dynamic process, characterized by repeated intrusions of melt over long (> 9.2 Ma for Questa caldera) periods, and document emplacement of a short-lived caldera-forming magma chamber accompanied and followed by the incremental assembly of a postcaldera batholith. The volcanic rocks provide point-in-time information regarding the spatial-temporal-compositional changes in the Latir magmatic system, whereas the plutonic record provides a more continuous record of the waning stages of magmatism.

Because of the low closure temperatures of the minerals used for argon dating (hornblende, 550-500°C; biotite, 350-300°C; K-feldspar, 300-150°C) compared to the emplacement temperature of granites, the Ar/Ar dates are cooling ages, not emplacement ages. However, cooling is inherently related to emplacement and in cases of rapid cooling (e.g., resurgent plutons, pluton margins, dikes), may constitute a good approximation of the emplacement age.

1.6.1. Precaldera volcanism (28.5 - 25.4 Ma)

Ar/Ar age determinations of precaldera volcanic rocks suggest that the earliest caldera magmatism was characterized by emplacement of numerous, short-lived, compositionally diverse, small magma chambers (Figure 1.9A). Ages are interpreted as the timing of eruption and provide important constraints on the temporal-spatial evolution of initial caldera-related magmatism.

Precaldera volcanism began in the Latir volcanic field at 28.50 ± 0.19 Ma, with the eruption of a calc-alkaline hornblende-bearing andesite (MZQ-25). At 28.22 ± 0.05 Ma the calc-alkaline rhyolite tuff of Tetilla Peak (MZQ-17) erupted, now preserved as discontinuous outcrops throughout the northern and eastern region of the field. Beginning at 27.94 ± 0.10 Ma, large volumes of dacite were erupted as lava flows and

emplaced as small-volume shallow intrusions into northeastern parts of the field. Between the emplacement of the voluminous dacite and the eruption of the Amalia Tuff at 25.39 ± 0.04 Ma, intermediate composition volcanic rocks were erupted. The majority of the volcanic rocks erupted during this interval, including alkaline units that were previously interpreted to have erupted just prior to caldera formation, have not yet been dated largely because of alteration. The youngest dated volcanic eruption prior to the Amalia Tuff is the calc-alkaline rhyolite of Cordova Creek at 25.57 ± 0.04 Ma, which is now preserved as faulted remnants of three rhyolitic domes northeast and east of the caldera. The total duration of precaldera volcanism was 3.11 ± 0.23 Ma.

Determining the duration of precaldera volcanism provides constraints for the physical and compositional changes to the crust prior to a caldera eruption (Lipman, 2007). Geothermal gradients are low at the onset of magmatism, the crust is brittle, and magma is emplaced primarily as small dikes, sills, and stocks. Geothermal gradients increase with continued magmatism, fracture networks develop, and wall rock metamorphism occurs. Each of these processes decreases the effective viscosity of the country rocks and allows magma to accumulate in the crust without an immediate eruption (Jellinek and DePaolo; 2003). Magma chambers increase in size and a caldera eruption may occur. Additionally, extension can provide room in the crust for magma to accumulate, culminating in the formation of caldera. Because the previous geochronology of the Latir volcanic field suggested a total duration of ~5 Ma for precaldera magmatism (Lipman et al., 1986; Lipman, 2007), the new age determinations indicate more rapid rates for physical and compositional changes of the crust prior to caldera eruption.

The timing of compositional changes during precaldera volcanism provides information relating the temporal-spatial assembly of magma prior to caldera eruption. The previous studies suggested the earliest magma erupted was calc-alkaline, then compositions transitioned to alkaline, climaxing with the eruption of the peralkaline Amalia Tuff (Lipman, 1984; Lipman et al., 1986; Johnson and Lipman, 1988). The compositional evolution could be explained by a single source evolving though time. Periodic 'tapping' of this source produced the compositional evolution of the precaldera volcanism. However, at 25.57 ± 0.04 Ma the calc-alkaline rhyolite of Cordova Creek erupted and at 25.39 ± 0.04 Ma the peralkaline Amalia Tuff erupted. Because the timing of alkalic intermediate composition precaldera volcanism has not been determined, the implications of the age of the Cordova Creek rhyolite are not fully established. If the Cordova Creek rhyolite is younger than the period of alkaline volcanism, this suggests rapid, oscillating changes from alkaline to calc-alkaline to peralkaline magmatism that could be explained by the presence of multiple, compositionally different magma chambers (Figure 1.9A and B). If the Cordova Creek rhyolite predates the alkalic precaldera volcanism, this suggests a rapid transition from calc-alkaline to alkaline volcanism in ~200 ka.

1.6.2. Eruption of the Amalia Tuff and emplacement of the northern ring dike (25.4 Ma)

The Questa caldera formed at 25.39 ± 0.04 Ma during the eruption of the Amalia Tuff (Figure 1.9C). The eruption created a depression approximately 15 km in diameter inferred by northern ring-fault intrusions and the geometry of the intracaldera fill (Lipman et al., 1986; Lipman and Reed, 1989; Meyer and Foland, 1991). The erupted

volume is approximately 500 km^3 (Lipman et al., 1986) and outflow sheets are preserved as much as 60 km west of the caldera margin in the Tusas Mountains (Lipman et al., 1986). The overlapping errors and the normal distribution of the Amalia Tuff sanidine ages indicate that the Amalia Tuff is the only ignimbrite associated with the formation of the Questa caldera. Zircon from the Amalia Tuff yielded an U/Pb age of 25.52 ± 0.06 Ma (Tappa et al., in review). Though the absolute U/Pb age of the zircon is older than the eruption age, ages are indistinguishable when uncertainty in the ^{238}U and ^{40}K decay constant are propagated through the error calculation. Alternatively, the discrepancy between U/Pb and Ar/Ar age of the Amalia Tuff may be related to zircon residence in the caldera-forming magma chamber.

Small, discontinuous peralkaline intrusions are located along the northern caldera margin (Lipman et al., 1986; Johnson et al., 1989). K-feldspar from the largest northern peralkaline intrusion yielded an age of 25.38 ± 0.04 Ma, indistinguishable to the eruptive age of the Amalia Tuff. This age confirms prior conclusions that the northern ring dike is nonerupted Amalia Tuff (Lipman et al., 1986; Johnson et al., 1989) and may represent a vent for the Amalia Tuff eruption.

1.6.3. Postcaldera magmatism: Resurgent plutonism and coeval volcanism (25.4 – 25.0 Ma)

Immediately following the eruption of the Amalia Tuff and formation of the Questa caldera at 25.4 Ma, four resurgent plutons were emplaced within ~ 400 ka (Figure 1.9D). Marginal peralkaline phases of the Virgin Canyon and Canada Pinabete are chemically similar to the Amalia Tuff. The Rito del Medio and Cabresto Lake plutons

are younger than the Amalia Tuff and record changing magma compositions. Postcaldera volcanism began and continued throughout resurgent plutonism.

Similar to the ring dike, the peralkaline margins of the Virgin Canyon and Canada Pinabete pluton to the Amalia Tuff led previous workers to suggest these plutons were the quenched remnants of the tuff (Lipman et al., 1986; Johnson and Lipman, 1988; Johnson et al., 1989). A statistically robust age could not be determined for the peralkaline phases of the Virgin Canyon or Canada Pinabete pluton because age spectra are discordant. However, because of the similar composition to the Amalia Tuff and newly dated ring dike, the peralkaline phases of the Virgin Canyon and Canada Pinabete plutons may well be contemporaneous with the Amalia Tuff.

The metaluminous phase of the Canada Pinabete pluton is interpreted to have been emplaced after the eruption of the Amalia Tuff. Zircon from metaluminous Canada Pinabete yielded an U/Pb age of 25.29 ± 0.05 Ma (Tappa et al., in review), which is statistically younger from the Amalia Tuff eruption age. A biotite analysis from the metaluminous phase of the Canada Pinabete pluton (Figure 1.4B) yielded a plateau age of 25.44 ± 0.08 Ma, however, the $^{40}Ar/^{36}Ar$ intercept of the biotite analysis intercept is slightly elevated compared to atmospheric values (304±4 vs. 295.5), indicating some excess argon is present. The inverse isochron age of the biotite, 25.38 ± 0.09 Ma, is indistinguishable to the both U/Pb zircon age of the metaluminous Canada Pinabete and the Amalia Tuff eruption age. The U/Pb age is the preferred emplacement age of the metaluminous Canada Pinabete, which agrees with previous mapping and paleomagnetic studies that suggested these intrusions were emplaced after the peralkaline phases (Hagstrum and Lipman, 1986; Lipman et al., 1986). Because the zircon and biotite age

are statistically similar, the intrusion is interpreted to have rapidly cooling following emplacement.

Following the emplacement of the Virgin Canyon and Canada Pinabete plutons, magmatism continued with the emplacement of the Rito del Medio pluton. Ar/Ar analyses yielded ages that range from 25.2 to 24.8 Ma. Overlapping biotite and K-feldspar ages, characteristic of both samples, indicates rapid cooling. Because of the small size of the pluton and proximity of the samples to one another, the age variation is not interpreted to be the result of differential cooling, but rather suggests rapid cooling of an incrementally emplaced pluton.

Contrastingly, the Cabresto Lake pluton, which is a similar size to the Rito del Medio pluton, was emplaced during a single episode. Four Ar/Ar age determinations, two biotite and two K-feldspar, are statistically similar ranging from to 25.02 ± 0.15 to 24.81 ± 0.13 Ma. U/Pb zircon ages are 25.07 ± 0.07 Ma and 25.02 ± 0.04 Ma (Tappa et al., in review), similar to the Ar/Ar ages. Emplacement ages and thermal histories of the Cabresto Lake pluton are consistent with rapid cooling following emplacement.

Though the postcaldera volcanic record is fragmentary, the ages from this study indicate postcaldera volcanism occurred during the emplacement and cooling of the resurgent plutons. Volcanism began within ~100 ka of caldera formation with the eruption of rhyolitic lavas and tuffs. A hypabyssal rhyolite intrusion at Comanche Point is 25.28 ± 0.04 Ma, similar to the U/Pb age from the metaluminous phase of the Canada Pinabete pluton. A rhyolite tuff at the base of the Brushy Mountain horst block is 25.17 ± 0.04 Ma, similar to the emplacement ages of the Rito del Medio and Cabresto Lake pluton. Comparing the geochemistry of the postcaldera volcanic rocks to the resurgent

plutons will be important for linking small-volume volcanic eruptions to plutons and determining the relationship between the two processes.

1.6.4. Postcaldera magmatism: Southern caldera-margin plutonism (24.9 – 22.3 Ma)

Three plutons were emplaced along the southern caldera margin following the emplacement of the resurgent plutons (Figure 1.9E). The plutons, which appear to be the cupolas of a larger, semi-continuous intrusion based on gravity data (Cordell et al., 1986; Lipman et al., 1986), have younging east to west Ar/Ar ages, possibly suggesting incremental emplacement during a ~400 ka period. Unlike the resurgent plutons that cooled rapidly, MDD modeling of southern caldera margin K-feldspar indicate the thermal histories from 300 to 150ºC was variable, possibly involving reheating events.

The oldest southern caldera margin pluton is the Red River pluton. The biotite age indicates cooling to ~350ºC at 24.94 ± 0.06 Ma, which is the best estimate for the age of emplacement. The K-feldspar age spectra are indicative of slow cooling and/or reheating. Monotonic MDD thermal models indicate that the pluton remained at 300°C between 24 and 21 Ma, which could be explained by a prolonged, locally elevated geothermal gradient. However, the preferred thermal history is the unconstrained model, which suggests rapid cooling at 24 Ma and reheating at 22 Ma. This model is preferred because 1) numerous dikes and smaller intrusive bodies, though not yet dated, are present in the pluton, 2) the pluton is the oldest part of a larger, incrementally emplaced intrusion (Cordell et al., 1986; Lipman et al., 1986), and 3) the Rio Hondo Pluton to the south has U/Pb ages between 22 and 23 Ma, similar to the age of reheating event.

Ages from two biotite analyses from the Sulfur Gulch pluton are 24.73 ± 0.14 and 24.64 ± 0.10 Ma, suggesting that the pluton was emplaced and cooled as a single

intrusive unit, after the emplacement of the Red River pluton. K-feldspar did not yield geologically meaningful ages. Because of the lack of U/Pb ages, the biotite ages are the best approximation for the emplacement age.

The Bear Canyon pluton is the youngest and has the most complicated thermal history of the southern caldera margin plutons. Two samples collected less than 2 km away from each other along the northern margin of the pluton have similar biotite plateau ages, 24.54 ± 0.12 and 24.37 ± 0.11 Ma, but the ages and thermal histories of the K-feldspars are radically different. The similar ages for the two biotites indicate that the pluton experienced a similar cooling history to 350ºC, followed by heterogeneous cooling at lower temperatures. The close proximity of the two samples to each other would suggest that difference in age between the two samples is not related to different geothermal gradients of the country rock. The similar biotite ages, combined with the absence of changes in texture or composition within the pluton, suggest the difference in K-feldspar cooling histories is the not result of incremental emplacement. The preferred explanation is reheating to, but not exceeding 350ºC. Small-scale dikes could result in localized partial argon degassing to produce the younger ages, but the absence of dikes in the pluton or the host rock makes this an unlikely possibility. Thus the reheating event is not completely understood at this time.

1.6.5. Postcaldera magmatism: Southern plutons and coeval volcanism (23.0 – 19.3 Ma)

The Rio Hondo and Lucero Peak plutons are the youngest plutons in the Latir field and have the most protracted thermal histories (Figure 1.8 and 9F). U/Pb ages suggest rapid incremental assembly of the Rio Hondo pluton and Ar/Ar

thermochronology of both plutons indicates protracted thermal histories. Unconstrained MDD cooling histories for the deepest exposed section of the Rio Hondo pluton indicate a thermal perturbation at 16.5 Ma, which potentially corresponds to a 16.6 Ma rhyolitic dike within the Rio Hondo pluton. The Lucero Peak pluton also has a prolonged thermal history with the possibility of younger, but unidentified, reheating events.

U/Pb zircon ages indicate the Rio Hondo pluton was incrementally emplaced during a 500 ka period (Tappa et al., in review). U/Pb ages from the main granodiorite body are 22.8, 22.7, and 22.6 Ma and the upper granitic unit is 23.0 Ma. A biotite age from the structurally highest exposed granodiorite body is 21.51 ± 0.09 and a biotite from a structurally low exposure of the granodiorite body is 21.22 ± 0.10 Ma.

Particularly interesting in the cooling history of the Rio Hondo pluton is the divergence of the thermal histories recorded by the K-feldspars. MDD monotonic cooling histories from the deepest exposed sections of the Rio Hondo pluton suggest isothermal residence at 275°C between 21 and 16.6 Ma (Figure 1.6D). However, this is more likely to be the result of later reheating caused by dike emplacement at 16.6 Ma (Figure 1.7E and 1.8). The cooling history of MZQ-19 from the upper part of the Rio Hondo granodiorite is significantly different. The extended thermal history is thought to be the result of a younger reheating based on interpretation of the other Rio Hondo pluton samples. The unconstrained cooling history suggests a thermal perturbation between 19 and 20 Ma, which may reflect another period of Rio Hondo-related dike emplacement.

The last known volcanic event in the Latir volcanic field was an eruption of a pyroxene andesite at 22.69 ± 0.08 Ma on Brushy Mountain. This age is important for two reasons. First, it constrains the duration of postcaldera volcanism to 2.70 ± 0.12 Ma,

shorter than the previous conclusions of Lipman et al. (1986), which determined postcaldera volcanism lasted from 26 to 22 Ma. Recall that the duration of precaldera volcanism was 3.11 ± 0.23 Ma, which suggests that in some 'simple' one-caldera systems the durations of pre- and postcaldera volcanism may be similar in duration. Second, though the andesite of Brushy Mountain has not been geochemically linked to the Rio Hondo pluton, it indicates postcaldera volcanism occurred during some of the postcaldera pluton emplacement. One of the cruxes regarding linking plutonism to volcanism, with respect to incremental emplacement, is that if a pluton is assembled at a slow rate, there may not be enough melt available for a caldera eruption. It is interesting that the andesite of Brushy Mountain, and possibly the overlying dacite, is a similar age to the younger Rio Hondo pluton increments. Volcanism coeval with the Rio Hondo pluton indicates that incremental emplacement over ~ 500 ka may be able to sustain volcanic activity. A melt-rich magma chamber may form shortly after a period of prolonged incremental emplacement, when conditions exist for a magma chamber to be thermally sustained (Hansen and Glazner, 1995; Glazner et al., 2004, Matzel et al., 2006).

For the two Lucero Peak pluton samples, biotite ages and K-feldspar cooling histories are similar, though one sample is from the margin and the other is from the interior. Biotite ages from these samples are 19.14 ± 0.10 (margin) and 19.34 ± 0.08 (interior). K-feldspar monotonic cooling models are very similar, both indicating a period of slow cooling, followed by a more rapid cooling. During classic batch emplacement of plutons, the margins of the pluton cool first and more rapidly than the later, slowly cooled interior (Glazner et al., 2004). However, the results from the Lucero Peak pluton are not supportive of this model and instead invoke a more complicated intrusive history.

Dalrymple et al. (1999) suggested that spatially disorganized assembly of a pluton could cause resetting to produce results that do not match cooling of a single magma chamber. It is possible that younger, unexposed plutons are located beneath the Lucero Peak pluton, as well as beneath the Rio Hondo pluton. The emplacement and cooling history is interpreted to be more complex than can be explained by batch emplacement.

1.7. Implications for caldera magmatism and the volcanic-plutonic relationship

Two contrasting processes have been proposed for generating silicic magmas. Each process predicts different temporal-chemical-spatial relationships for caldera-related volcanic and plutonic rocks. Shallow differentiation predicts that a large-volume (3 to 10:1 intrusive:extrusive ratio; White et al., 2006) of the intrusions will be coeval with the ignimbrite eruption and these intrusions will geochemically represent the less-differentiated residual crystal mush (Bachmann et al., 2007a, de Silva et al., 2007, Bachmann and Bergantz, 2008). Alternatively, deep differentiation and/or partial melting of the lower crust predict that small-volumes of the intrusive suite will be coeval with the ignimbrite and that these intrusions will be compositionally identical to the ignimbrite (Glazner et al., 2004).

Plutons exposed at the Questa caldera include small-volume intrusions interpreted to be nonerupted Amalia Tuff (i.e., nonerupted silicic cap) and much larger volumes of postcaldera plutons. Only the northern ring dike and marginal peralkaline phases of the Virgin Canyon and Canada Pinabete plutons are geochemically (Lipman et al., 1986; Johnson et al., 1989) and geochronologically similar to the Amalia Tuff. These intrusions represent remnants of the Amalia Tuff magma that did not erupt. The ring dike and peralkaline phases of the Virgin Canyon and Canada Pinabete plutons are not interpreted

to be the residual crystal mush from which the Amalia Tuff differentiated. The total volume of these intrusions, though difficult to accurately determine, is very small compared to the estimated eruptive volume of the Amalia Tuff (~500km^3; Lipman et al., 1986) and total volume of exposed plutonic rocks. This suggests that some caldera-forming eruptions may efficiently evacuate most of the source magma chamber. The peralkaline phases of the Virgin Canyon and Canada Pinabete plutons were not successfully dated. However, the marginal peralkaline phases are interpreted to be the same age as the Amalia Tuff because these phases are compositionally identical to the ring dike (Lipman et al., 1986; Johnson et al., 1991) and the ring dike is temporally indistinguishable from the Amalia Tuff.

The remaining intrusions (metaluminous phases of the Virgin Canyon and Canada Pinabete, Rito del Medio, Cabresto Lake, southern caldera margin, and southern plutons) are younger than the Amalia Tuff, by ~100 ka to ~6 Ma. These plutons represent magmatism that continued after the Questa caldera eruption and record the growth of a postcaldera batholith. The postcaldera plutons are not interpreted to be the nonerupted residual crystal mush that differentiated to produce the Amalia Tuff magma.

The results of this study indicate that a complementary residual crystal mush for the Amalia Tuff is not preserved as an exposed pluton. Because of the limited exposure of the Questa-caldera related plutons there exists the possibility that the residual crystal mush is located beneath current crustal exposure levels. The Bouguer gravity anomaly of Cordell et al., (1986) indicate crystalline material, which could be residual crystal mush, is located beneath the Questa caldera. The only plutons that are temporally and chemically similar to the Amalia Tuff (i.e. northern ring dike, peralkaline phases of the

Virgin Canyon and Canada Pinabete plutons) are located at the structurally highest part of the intrusive suite. If a less-differentiated, more-mafic residual crystal mush exists, shallow differentiation models predict it should be preserved as an intrusion in contact with plutons that represent nonerupted Amalia Tuff (i.e., the peralkaline intrusions or nonerupted silicic cap). However, the exposed plutons emplaced beneath the peralkaline intrusions at deeper structural levels (~3-5 km; The Rito del Medio and Cabresto Lake, the southern caldera margin, and the southern plutons) are younger than the Amalia Tuff (this study; Tappa et al., in review). Because the ages of the exposed plutons indicate that the shallow plutons were emplaced first and deeper plutons were emplaced later, we speculate that the nonexposed plutons, as indicated by the gravity anomaly, are younger than the exposed intracaldera plutons and that these plutons were also emplaced during the waning stage of postcaldera batholith emplacement.

The geochronology of the Questa caldera-related plutonic rocks suggests that nearly all the intrusions represent waning stages of magmatism. There is no upper crustal evidence for the residual crystal-mush from which the Amalia Tuff differentiated. The lack of geochronologic evidence to support upper crustal differentiation suggests that these intermediate and silicic magmas were generated at deeper levels in the mid- to lower crust (Sisson et al., 2005; Annen et al., 2006; Bryan et al., 2008; Quick et al., 2009). Silicic magma ascended through the crust via a network of dikes (Petford et al., 2000). Limited differentiation and magma mixing occurred during emplacement and storage in the upper crust. During high magmatic rates (i.e., formation and eruption of the Amalia Tuff magma chamber), most magma was erupted and some magma, though very limited in volume, was preserved in the plutonic record as a ring dike and thin capping

phases of two resurgent plutons. Contrastingly, large volumes of compositionally diverse magma were preserved as plutons during the waning stages of magmatism.

1.8. Conclusions

Hornblende, biotite, plutonic K-feldspar and volcanic sanidine Ar/Ar analyses provide an accurate and precise timing of magmatism associated with the Latir volcanic field. The ages of volcanic rocks were used to modify the pre-existing stratigraphy and understand the volcanic evolution of the field. Precaldera volcanism began at 28.5 Ma and continued for ~3.1 Ma. The Questa caldera formed during the eruption of the 25.4 Ma Amalia Tuff. Postcaldera volcanism began shortly after the eruption of the Amalia Tuff and postcaldera eruptions occurred as much as ~2.7 Ma after caldera collapse. The Ar/Ar ages of the plutonic rocks provide a relatively continuous postcaldera intrusive and thermal history of the Latir volcanic field. Ar/Ar thermochronology suggests that most plutons had extended thermal histories caused by repeated reheating events during protracted emplacement of the postcaldera batholith. Ar/Ar ages suggest a ~ 9.2 Ma period of magmatism (28.5 – 19.3 Ma) associated with the Latir volcanic field and that some magmatism occurred as much as ~8.8 Ma (i.e., 16.6 Ma rhyolitic dike in the Rio Hondo) after the caldera forming event.

Comparing the ages of the Questa caldera volcanic rocks to the plutonic rocks established the volcanic-plutonic relationship, which was then exploited to understand caldera-related magmatism. The exposed plutons at Questa represent either nonerupted Amalia Tuff or postcaldera plutons emplaced during the waning stages of magmatism. Intrusions that represent nonerupted Amalia Tuff include a discontinuous ring dike and

marginal phases of two resurgent plutons, which represent a very small volume of exposed intrusive suite. The remaining plutons are too young to be the residual mush for the Amalia Tuff. This suggests that the Questa caldera silicic magmas were generated in a lower crustal source, that the Amalia Tuff magma chamber nearly completely emptied during the caldera eruption, and that most of the Questa caldera-related plutons were emplaced during the waning stages of magmatism.

CHAPTER 2: CALDERA ERUPTIONS AND THE EMPLACEMENT OF PRE-, SYN-, AND POSTCALDERA INTRUSIONS AT THE MT. AETNA CALDERA COMPLEX

2.1. Abstract

The temporal and chemical relationships of volcanic and plutonic rocks exposed at the Mt. Aetna caldera complex, central Colorado, provide insight into the emplacement history and assembly rates of pre-, syn-, and postcaldera plutons and the origin of caldera-related silicic magmas. Ar/Ar sanidine ages indicate the low-SiO_2 rhyolitic Wall Mountain Tuff erupted at 37.25 ± 0.08 Ma. LA-ICP-MS U/Pb ages of the compositionally zoned Mt. Princeton batholith, which has been interpreted by several previous studies to be the nonerupted residual crystal mush of the Wall Mountain Tuff magma chamber, indicate that it was emplaced between 36.38 ± 0.40 and 35.06 ± 0.48 Ma. The U/Pb ages suggest that the Mt. Princeton batholith was incrementally emplaced as a series of downward stacking intrusions during post-Wall Mountain Tuff magmatism. The emplacement rate of the Mt. Princeton batholith was 9.9 x 10^{-4} km^3/yr, which is too slow to sustain a magma chamber capable of differentiation. Instead, the compositional zoning of the Mt. Princeton batholith represents emplacement of chemically diverse magma originating from a lower crustal source. Nested within the Mt. Princeton batholith is the Mt. Aetna caldera. The Badger Creek Tuff erupted at 34.26 ± 0.06 Ma during Mt. Aetna caldera collapse. The Badger Creek Tuff is deposited on some of the Mt. Princeton

intrusive units, demonstrating that the Wall Mountain Tuff caldera and any Wall Mountain Tuff age plutons were eradicated during exhumation and erosion prior to 34.3 Ma. Following Mt. Aetna caldera collapse, the intracaldera ignimbrite and caldera ring faults were intruded by magma that is compositionally identical to the Badger Creek Tuff, but contains zircons as much as 500 ka older than caldera-forming event. The Badger Creek Tuff magma chamber was apparently incrementally emplaced during a 500 ka period prior to Mt. Aetna caldera collapse. Numerous postcaldera luecogranites were emplaced at ~31 Ma, which caused localized thermal resetting of biotite and K-feldspar in older, adjacent intrusions.

2.2. Introduction

Caldera-related magmatism is a societally important geologic phenomenon. Caldera forming eruptions are arguably the most catastrophic geologic hazard (Francis and Oppenheimer, 2004; Self and Blake, 2008; Miller and Wark, 2008). Caldera systems are also potential sources of geothermal energy and ore deposits (Meyer and Foland, 1990; Hilton et al., 1996; Stimac et al., 2004; Klemm et al., 2009). Because of both the possible harm and potential benefit to society, caldera magmatism has been the focus of numerous studies. Understanding the rates and timescales of magma emplacement, the patterns of magma assembly, and eruption of subcaldera magmas is necessary for evaluating hazards at currently active caldera systems, assessing the geothermal potential of calderas, and developing genetic models to explain caldera-hosted ore deposits.

Many caldera-oriented studies have used the volcanic record to construct caldera evolution models and to infer the origin of silicic magmas (Smith, 1979; Hildreth, 1981;

Lipman et al., 1978; Bachmann et al., 2002). By nature, the volcanic rocks represent a fragmental record of entire magmatic history. Because of this, other studies have used plutonic rocks to understand the nature of silicic magmatism (Johnson and Lipman 1988; Weibe, 1994; Verplank et al., 1999; Glazner et al., 2004). Processes such as magma emplacement, rejuvenation and modification of existing magma chambers, dike and sill emplacement, upwelling of magma during resurgence, and the duration of the waning stages of magmatism can be explored using the plutonic record. However, connecting plutonic processes to volcanic processes is difficult in the absence of the volcanic record.

Extensive erosion and faulting related to the Rio Grande rift has exposed volcanic and plutonic rocks at the Mt. Aetna caldera complex (Figure 2.1), Sawatch Range, central Colorado (Epis and Chapin, 1975; Shannon, 1988), providing an opportunity to test contrasting caldera magmatism models. The specific goals of this work include: understanding emplacement patterns of pre-, syn-, and postcaldera plutons, establishing the volume and composition of material that remains in the caldera-forming-magma-chamber after the collapse event, and determining the depth of silicic melt generation. By comparing the temporal and chemical relationship of caldera-related plutonic and volcanic rocks of the same caldera system, models for caldera magmatism can be assessed and modified.

This paper presents new Ar/Ar and U/Pb ages of volcanic and plutonic rocks exposed at the Mt. Aetna caldera complex. Ar/Ar dating constrains the timing of volcanic events and thermal evolution of the subcaldera batholith, and in absence of U/Pb ages, provides a minimum age of pluton emplacement. Laser ablation-inductively coupled plasma-mass spectrometry (LA-ICP-MS) U/Pb zircon dating establishes the emplacement

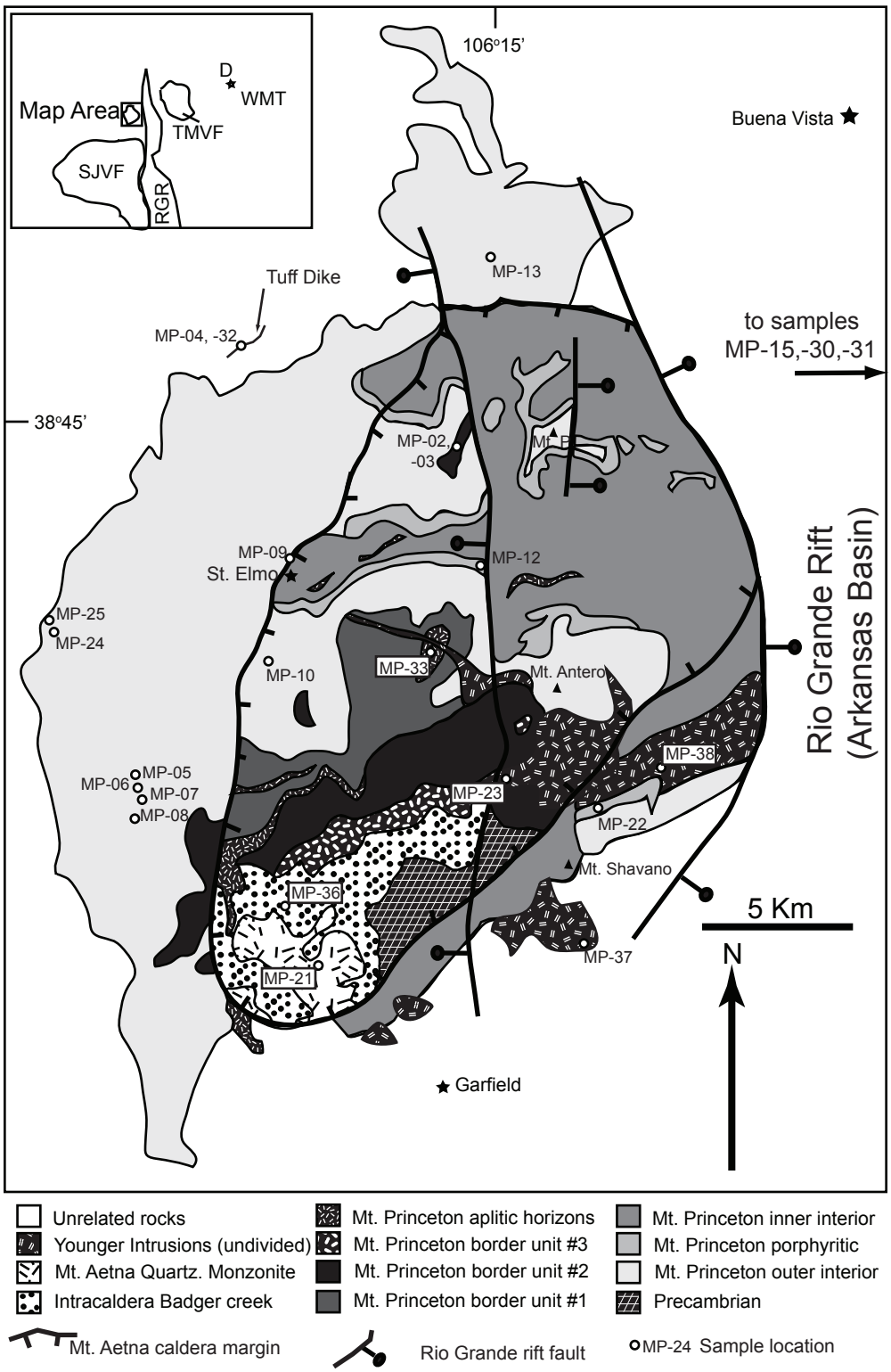

Figure 2.1. Simplified geologic map of the Mt. Aetna caldera complex modified from Shannon (1988). Samples MP-15, 30, and 31 (not shown) are located in paleovalleys to the east. Unrelated rocks include Proterozoic granitoid and sedimentary rocks. SJVF – San Juan Volcanic Field, RGR – Rio Grande Rift, TMVF – Thirtynine Mile Volcanic Field, D – Denver. Star indicates most eastern outcrop of Wall Mountain Tuff (WMT).

history of the exposed intrusive suite. Additionally, the in-situ LA-ICP-MS technique allows for assessing inherited zircon cores. This paper also presents CA-TIMS U/Pb dating results, conducted by University of North Carolina collaborators, which provide high-precision zircon crystallization ages.

In general, Ar/Ar and U/Pb ages of the Mt. Aetna caldera complex volcanic and plutonic rocks suggest that 1) some postcaldera plutons are emplaced from the top-down, 2) only a very small-volume of exposed intrusions are temporally, spatially, and compositionally related to syncaldera magmatism, 3) some caldera-forming magma chambers are incrementally emplaced into the upper crust prior to caldera collapse, and 4) magmatism at the Mt. Aetna caldera complex continued for an extended duration following caldera collapse.

2.3. Unresolved aspects of caldera magmatism

The origin of silicic caldera magmas remains controversial (Glazner et al., 2004; Bachmann et al., 2007a; Lipman, 2007). During caldera collapse, a large volume (10^2-10^4 km^3) of silicic magma is erupted from upper crustal magma chambers (Hildreth, 2004; Bachmann and Bergantz, 2008; Miller and Wark, 2008). Contrastingly, most studies suggest that the primary melt extracted from the upper mantle is basalt (Davies and Stevens, 1992; Ulmer, 2001; Wood, 2004). Petrologic, geochemical, and experimental studies suggest two possible processes for generating silicic melts from basaltic magmas: in-situ differentiation and partial melting of the crust (Dufek and Bergantz, 2005; Annen et al., 2006; Walker et al., 2007; Bachmann and Bergantz, 2008). Though both processes

undoubtedly occur, disagreement exists regarding which process is dominant and the depth of differentiation.

Several models propose that silicic melts are generated via in-situ differentiation of a magma chamber in the upper crust (Smith, 1967; Johnson, 1991; Lipman, 2007; Bachmann et al., 2007a; Walker et al., 2007). Early models suggested that basaltic to rhyolite differentiation occurred in the upper crust (Smith, 1979). Opponents of this early model cite problems with emplacing large volumes of dense basalt into the less-dense upper crust (Glazner, 1994; Dufek and Bergantz, 2005). Additionally, basalt magma emplaced into the relatively cold shallow crust rapidly crystallizes before differentiating and generating silicic magmas. Recent studies have suggested that at least some differentiation of basalt occurs in the lower crust and that intermediate magmas are emplaced into the upper crust (Annen et al., 2006), where they undergo further differentiation to silicic compositions (Miller and Miller, 2002, Ulmer et al., 2007; Bachmann et al., 2007a). According to this model, large-volume caldera magma chambers differentiate into a silica-rich cap and a silica-poor residual crystal mush (Smith, 1979, Bachmann and Bergantz, 2004). Most of the cap is erupted during caldera collapse and the residual crystal mush and the nonerupted silicic cap are preserved as plutons (Buddington, 1959; Shannon, 1988; Hildreth, 2004; Bachmann et al., 2007a; de Silva and Gosnold, 2007; Lipman, 2007; Walker et al., 2007). This model implies that a significant volume of caldera-related plutonic rocks should be coeval with and geochemically complimentary to the associated ignimbrite (Smith et al., 1979, Bachmann et al., 2007a, de Silva and Gosnold, 2007).

Other studies suggest that silicic magmas are generated in the lower crust. Emplacement of mafic magma into the lower crust causes partial melting of the country rocks. Differentiated melts derived from basalt fractionation mix with partial melts of the lower crust and the hybrid, silicic magmas are emplaced into the upper crust (Annen et al. 2006, Dufek and Bergantz, 2005; Quick et al., 2009). Some additional shallow differentiation may occur, but the degree of upper crustal differentiation is minor compared to that which occurs in the lower crust. During caldera eruption, magma chambers can nearly completely drain because the residual crystal mush, if any, is located in the lower crust (Coleman et al., 2004; Glazner et al., 2004; Annen et al., 2006). According to this model, nonerupted remnants of the caldera forming magma chamber will represent only a small percentage of the total intrusive suite and these coeval intrusions will have a similar geochemistry to the caldera-forming ignimbrite (Glazner et al., 2007; Mills et al., 2008). Caldera magma chambers are ephemeral features emplaced during high-magmatic-input events (Glazner et al., 2004; Annen, 2009). Most plutons represent pre- or postcaldera magmatism when magmatic input is relatively low compared to during syncaldera magmatism (Lipman, 1984; Jellinek and DePaolo, 2003; Glazer et al., 2004).

2.4. Geology and previous studies of the Mt. Aetna caldera complex

Rocks exposed at the Mt. Aetna caldera complex (Figure 2.1) and in adjacent paleovalleys represent the initiation of ignimbrite volcanism in the Southern Rocky Mountain Volcanic Field (McIntosh and Chapin, 2004; Lipman, 2007). During the Laramide flat-slab subduction of the Farallon plate, magmatism and volcanism migrated

>1000 km to the east of the subduction trench. Following the decoupling of the Farallon plate from beneath the North America plate, the ignimbrite flare-up began in the western United States (Coney and Reynolds, 1977; Lawton and McMillan, 1999; Chapin et al., 2004). One of the largest erosional remnants of the ignimbrite flare-up is the Southern Rocky Mountain Volcanic Field, which includes over 30 calderas and corresponding ignimbrites (Lipman, 2007). Volcanism in the southern Rocky Mountains began in central Colorado and migrated to southwestern Colorado between 38 and 23 Ma (McIntosh and Chapin, 2004; Lipman, 2007; Lipman and McIntosh, 2008). Following the cessation of magmatism, large-scale faulting commenced during the initiation of the Rio Grande rift (Baldridge and Olsen, 1989). Faulting, uplift, and erosion related to the rift exposed the volcanic and plutonic rocks at the Mt. Aetna caldera complex (Shannon, 1988).

The magmatic evolution at the Mt. Aetna caldera complex consists of three temporally distinct stages. The Mt. Princeton batholith represents the oldest exposed magmatic event. Nested within the Mt. Princeton batholith is the younger Mt. Aetna caldera, the source of the Badger Creek Tuff. The youngest intrusions include numerous, small-volume luecogranites that cross cut many of the older intrusions.

The Mt. Princeton batholith has been suggested to be the nonerupted, residual crystal mush for the crystal-rich, low-SiO_2, rhyolitic, >1000 km^3 Wall Mountain Tuff (Epis and Chapin, 1975; Shannon, 1988; Toulmin and Hammarstrom, 1990; Fridrich et al., 1998). The Mt. Princeton batholith is the largest mid-Tertiary intrusion in Colorado (875 km^2; Tweto, 1979; Shannon, 1988; McIntosh and Chapin, 2004). The batholith is composed of relatively homogeneous interior units (structurally lowest units; referred to

as the Mt. Princeton quartz monzonite in some previous studies) consisting of granite and quartz monzonite and the structurally highest, texturally diverse, more mafic border units (Shannon, 1988; Toulmin and Hammarstrom, 1990). Based on compositional zoning, continuous textural and compositional layers, and lack of cross cutting relationships, Shannon (1988) suggested the batholith was emplaced as a single magma chamber that differentiated following emplacement. Numerous previous studies inferred that the Mt. Princeton batholith was the source of the Wall Mountain Tuff because 1) shallow differentiation models predict that large volumes of nonerupted mafic to intermediate residual mush (i.e., granodiorite) remain in magma chambers after eruption and are preserved as plutons (Smith, 1967; Toulmin and Hammarstrom, 1990; Bachmann and Bergantz, 2004, 2008; Bachmann et al., 2007a), 2) paleovalleys that converge toward the Mt. Princeton batholith contain thick (~5-150 m) deposits of the Wall Mountain Tuff (Epis and Chapin, 1975; McIntosh and Chapin, 2004), and 3) the Wall Mountain Tuff and Mt. Princeton batholith have been reported to be similar in age (Shannon, 1998, Toulmin and Hammarstrom, 1990; Fridrich et al., 1998). Shannon (1988) highlighted the potential genetic relationship between the border units and the Wall Mountain Tuff, largely because of the presence of clinopyroxene in both units.

Several studies have investigated the temporal and chemical relationship between the Wall Mountain Tuff and Mt. Princeton batholith. Using the sanidine single-crystal laser-fusion technique, McIntosh and Chapin (2004) dated five samples of the Wall Mountain Tuff to obtain an age of 37.16 ± 0.09 Ma (all Ar/Ar ages reported from previous studies are recalculated using FC-2=28.201 Ma; Kuiper et al., 2008). Toulmin and Hammarstrom (1990) report a $^{208}Pb/^{232}Th$ date of 36.6 Ma from the Mt. Princeton

quartz monzonite, though the analytical errors are not provided. This study also reported hornblende Ar/Ar incremental heating ages of 36.3 and 37.1 Ma. Neither analysis yielded a plateau; the ages are from the highest temperature steps and the authors speculate that excess ^{40}Ar may be present. Biotite Ar/Ar ages of the Mt. Princeton interior units are between 35.0 and 34.7 Ma (n=4) (McIntosh and Chapin, 2004). Differences in whole-rock, trace-element, and REE geochemistry led Campbell (1994) to suggest that the Mt. Princeton quartz monzonite is not the source for the Wall Mountain Tuff. The lack of U/Pb zircon ages, the large range in ages from previous studies, incomplete sampling, and absence of any caldera features have prevented establishing a definitive relationship for the Wall Mountain Tuff and Mt. Princeton batholith.

Following emplacement of the Mt. Princeton batholith, the crystal-rich, dacitic, >250 km^3 Badger Creek Tuff erupted from the Mt. Aetna caldera. Evidence for the nested caldera includes the intracaldera Badger Creek Tuff, ring faults and shear zones, and a discontinuous ring dike that grades into a more massive quartz monzonite pluton. The caldera formed during trap-door style collapse (Shannon et al., 1987; Toulmin and Hammarstrom, 1990). The greatest subsidence of the caldera floor occurred in the south, which is the only remaining location of remaining intracaldera Badger Creek Tuff. At present erosional levels the majority of rocks within the Aetna ring faults are Mt. Princeton intrusive units that represent the eroded floor of the caldera. A quartz monzonite stock, which intrudes the intracaldera tuff, has been interpreted as a resurgent pluton (Shannon, 1988; Toulmin and Hammarstrom, 1990). Based on similarities in geochemistry, mineralogy, and ages (constrained by fission-track and K/Ar ages), Shannon (1987) and Campbell (1994) concluded that the ring dike and Mt. Aetna quartz

monzonite pluton represent nonerupted Badger Creek magma that intruded into the intracaldera sequence shortly after caldera collapse. The Calico Mountain volcanic units and possibly several intrusive tuff dikes are the only record of pre-Mt. Aetna caldera volcanism (Shannon et al., 1987; Shannon 1988).

The age relationships of the Calico Mountain volcanic units, resurgent pluton, ring dike, Badger Creek Tuff, and intrusive tuff dikes remains uncertain. Sanidine single-crystal laser-fusion analyses of the Badger Creek Tuff yielded an age of 34.25 ± 0.11 Ma. Hornblende and biotite Ar/Ar analyses of the Mt. Aetna quartz monzonite yielded a weighted mean age of 34.51 ± 0.90 Ma. K-feldspar from the ring dike yielded an age of 34.57 ± 0.18 Ma, slightly older than the Badger Creek Tuff eruption age (McIntosh and Chapin, 2004). Fission-track ages of the intrusive tuff dikes are 33.4 and 33.7 Ma, but the associated errors are large and do not provide a definitive relationship to the Badger Creek Tuff (Shannon et al., 1987). Timing of Calico Mountain volcanism has not been determined, largely because of widespread alteration (Toulmin and Hammarstrom, 1990).

Following the Badger Creek Tuff eruption, numerous luecogranites were emplaced into the upper crust in the Mt. Aetna area (Shannon, 1998). The three largest luecogranitic intrusions are the Mt. Antero, California, and North Fork intrusions. Crosscutting relationships indicate that these intrusions represent the last stages of magmatism. Geochemistry indicates that these plutons are the most evolved melts in the complex (Campbell, 1994; Zimmerer et al., 2010) and are possibly related to Rio Grande rift bimodal magmatism (Shannon, 1988). Biotite and muscovite from the Mt. Antero granite yielded a weighted mean Ar/Ar age of 29.97 ± 0.13 Ma (McIntosh and Chapin, 2004).

2.5. Methods

Thirty-four volcanic and plutonic samples were collected as part of this study (samples MP-02 to MP-38; see Appendix 2.1 for the location of dated samples). Four additional sanidine separates of the Wall Mountain Tuff were re-dated from McIntosh and Chapin (2004). From this suite, 38 mineral separates were dated using the Ar/Ar method (8 sanidine, 18 biotite, and 12 K-feldspar separates) and 14 zircon separates were dated using the laser ablation–inductively coupled plasma–mass spectrometry (LA-ICP-MS) U/Pb technique.

Samples were collected from a variety of locations and units in order to obtain a representative sample suite of the caldera complex. Samples were taken of both the Mt. Princeton interior and border units. Sample MP-03 is especially important because it is the only Mt. Princeton intrusion that contains clinopyroxene, a mineral that is also present in the Wall Mountain Tuff. Samples of the Mt. Princeton interior units were collected from both within and outside the Mt. Aetna ring dikes and faults to examine if caldera collapse affected the thermal history of the Mt. Princeton batholith. Alteration is pervasive throughout the field area. Only the most pristine samples were collected. Because intracaldera Wall Mountain Tuff is apparently completely eroded away, samples of outflow tuff were collected from paleovalleys to the east of the Sawatch Range. Both intracaldera and outflow facies of the Badger Creek Tuff, as well as two samples of the tuff dike in the northwestern region of the field were also collected and dated.

Mineral separates were obtained using standard separating techniques. Following jaw crushing and disk milling, samples for Ar/Ar analysis were processed using a frantz magnetic separator and density liquids. Volcanic sanidine crystals were treated in HF

acid to remove adhering glass. Samples intended for U/Pb zircon dating were processed using a Wilfley table to isolate dense minerals. Zircon separates were then processed using a frantz magnetic separator and placed into lithium metatungstate and then methylene idodine heavy liquids to obtain zircon concentrates. Mineral concentrates were finally hand picked using a binocular microscope to obtain monomineralic separates.

LA-ICP-MS U/Pb zircon analyses were conducted at the Arizona Laserchron Center. Zircon separates and the 564 Ma Sri Lanka zircon standard were placed into pucks and imaged using a cathodluminesense (CL) microscope. CL images were used to identify oscillatory zoning indicative of magmatic growth, potential inherited cores, and mineral inclusions. An excimer laser with a spot size of 30-35μm was used to ablate the zircons. Zircon inheritance was assessed by comparing the ages of rims and cores. For each sample, at least 20 spots were analyzed. Isotopic ratios were measured using a GVI Isoprobe mass spectrometer. Gehrels et al. (2008) provides a comprehensive description of analytical procedures at the Arizona Laserchron Center. Data was reduced using the in-house program "Agecalc". $^{206}Pb/^{238}U$ analyses were used to calculate ages, as recommended by Gehrels et al. (2008). Weighted mean ages were calculated using Isoplot v3.7 (Ludwig, 2009). Analyses that yielded $^{206}Pb/^{238}U$ ages with >10% uncertainty or >30% discordance were excluded from age calculations.

Ar/Ar analyses were performed at the New Mexico Geochronology Research Laboratory. Unknowns and the interlaboratory standard FC-2 (28.201 Ma; Kuiper et al., 2008) where placed into aluminum disks and irradiated in a known geometry. Argon was liberated from single crystals of sanidine using a CO_2 laser, whereas a double-vacuum Mo resistance furnace was used to incrementally heat plutonic K-feldspar and biotite.

Following heating, sample gas was expanded into an all-metal extraction line and cleaned using SAES getter pumps. Isotopic ratios were measured using a MAP 215-50 noble gas mass spectrometer. A comprehensive description of operating and analytical procedures is provided in McIntosh et al. (2003).

2.6. Results

2.6.1. U/Pb Geochronology

Zircon separates from 14 samples were dated using the LA-ICP-MS technique. A summary of $^{206}Pb/^{238}U$ weighted mean ages is provided in Table 2.1. U/Pb zircon data tables and weighted average plots are located in Appendix 2.2. The range of U/Pb weighted mean ages for the suite of zircons is from 37.01 ± 0.27 to 30.75 ± 0.24 Ma. The average precision for an individual analysis is between 1 and 3%. The precision for the weighted mean ages is between 0.7 and 1.4% (values quoted at 2σ). Some zircons contained Proterozoic cores. Ages obtained from xenocrystic cores were not used in the age calculations. MSWD (mean standard weighted deviates) values for the calculated U/Pb ages range from 1.5 to 10.5. An MSWD of ~1 indicates that the scatter in the data is predicted by the analytical errors (Mahon, 1996). Elevated MSWD values of zircon ages have been attributed to the presence of antecrysts, which are zircons that grew from an earlier episode of magmatism and recycled during later stages of magmatism (Miller et al., 2007). The elevated MSWD values for some Mt. Aetna zircons is not interpreted to be related to antecrysts because there is no distinction between the ages of rims and cores nor is there a correlation between age, spot location, and U/Th ratios. Instead, elevated

TABLE 2.1 – Summary of the LA-ICP-MS U/Pb ages of the Mt. Aetna caldera complex

Sample	Unit	Age (Ma)[$]	Internal Error[†]	External Error[††]	MSWD*	Comments
Mt. Princeton Units						
MP-15	Wall Mountain Tuff	37.01	0.27	0.49	1.8	Indistinguisable from sanidine age
MP-33	Mt. Princeton Border Unit2	36.38	0.40	0.65	2.8	Structrally highest sample
MP-03	Mt. Princeton Border Unit2	36.21	0.28	0.49	1.5	Most mafic border unit
MP-07	Mt. Princeton inner interior	35.92	0.25	0.76	1.6	Outside of Aetna caldera margin
MP-25	Mt. Princeton inner interior	35.56	0.21	0.57	2.5	Located at PreCambrian contact
MP-10	Mt. Princeton inner interior	35.20	0.50	0.84	10.5	Structurally lowest sample
MP-08	Mt. Princeton inner interior	35.12	0.30	0.67	1.5	Outside of Aetna caldera margin
MP-05	Mt. Princeton inner interior	35.08	0.41	0.67	2.7	Outside of Aetna caldera margin
MP-06	Mt. Princeton inner interior	35.06	0.48	0.64	4.0	Outside of Aetna caldera margin
Mt. Aetna Units						
MP-21	Mt. Aetna Qtz. Monz.	36.40	0.35	0.53	7.3	Anomalously old
MP-09	Mt. Aetna Ring Dike	35.01	0.41	0.75	10.0	
MP-30	Badger Creek Tuff	34.69	0.33	0.62	6.5	Indistinguishable from sanidine age
Younger Plutons						
MP-37	North Fork Luecogranite	31.29	0.29	0.72	2.7	
MP-38	California Leucogranite	30.75	0.24	0.52	2.4	Youngest exposed pluton

$ - Age calculated relative to Sri Lanka Zircon (564±4 Ma), ^{238}U and ^{235}U decay constants equal to 9.8485×10^{-10} and 1.55125×10^{-10} yr-1, and $^{238}U/^{235}U$ equal to 137.88.

† - Internal errors include analytical measurements

†† - External errors include decay constants, age of standard, fractionation factor, and common Pb correction

* - Mean Standard Weighted Deviants

MSWD values are attributed to slight Pb-loss or ablating zircon domains that contained inclusions.

Of the 14 zircon separates, 13 samples yielded U/Pb ages that are interpreted to accurately date zircon crystallization. Zircons from the Wall Mountain Tuff yielded an age of 37.01±0.27 Ma. Unlike many of the zircons from the Mt. Aetna complex, which contained sparse inherited Precambrian cores, a large population of the Wall Mountain Tuff zircons contained 1.4 Ga cores. The U/Pb ages of the Mt. Princeton batholith samples range from 36.38 ± 0.40 to 35.06 ± 0.48 Ma. These ages are interpreted to be the age of pluton emplacement. Ages of the compositionally identical Mt. Aetna ring dike and Badger Creek Tuff (Shannon, 1988; Campbell, 1994) are 35.01 ± 0.41 and 34.69 ± 0.33 Ma, respectively. Zircons from the North Fork Luecogranite yielded an U/Pb age of 31.29 ± 0.29 Ma. Zircons from the California Luecogranite yielded a slightly younger U/Pb age of 30.75 ± 0.24

Zircons from sample MP-21, the Mt. Aetna quartz monzonite, yielded an anomalously old U/Pb age. Thirty-four spots were analyzed from which 33 analyses were used to calculate a weighted mean age of 36.40 ± 0.35 Ma, which is ~2 Ma older than the 34.3 Ma intracaldera Badger Creek Tuff that it intrudes. The MSWD for this sample is 7.3. Inheritance cannot readily explain the anomalous age and elevated MSWD because the oldest ages of the population do not correspond to cores. Because the ring dike and Mt. Aetna quartz monzonite are mapped as a single, composite intrusion (Shannon, 1988; Toulmin and Hammarstrom, 1990) and the two are compositionally similar (Shannon et al., 1987; Campbell, 1994), the U/Pb age of the ring dike is considered to be the best

estimate for the age of zircon crystallization in the Mt. Aetna quartz monzonite (see discussion for further explanation).

2.6.2. Ar/Ar Geochronology and Thermochronology

Thirty-eight mineral separates (8 sanidine, 18 biotite, and 12 K-feldspar) were dated using the Ar/Ar technique. Table 2.2 summarizes the Ar/Ar results. Ages were calculated using FC-2 = 28.201 (Kuiper et al., 2008) and $^{40}K\ \lambda_{total} = 5.463x10^{-10}\ yr^{-1}$ (Min et al., 2000). For each sample, the error is reported with and without propagating the uncertainty of the ^{40}K decay constant. Propagation of decay constant uncertainty into the error calculation greatly increases the errors. Ages and internal errors only are used for discussing the results because magmatic events cannot be distinguished with large external errors associated with the decay constant. All Ar/Ar data tables and associated plots are located in Appendix 2.3.

2.6.2.1. Ar/Ar Sanidine

Eight sanidine separates were dated using the single-crystal laser-fusion (SCLF) analysis technique. For each sample, 15-30 crystals were analyzed. Analyses of xenocrystic sanidine or plagioclase grains were not used in the age calculations. Analyses with radiogenic yields <95% or anomalously large errors were also excluded from the age calculation. MSWD values for the SCLF analyses range from 0.95 to 6.76. The high MSWD values for some samples indicate scatter in the data that is not attributed solely to analytical error.

Five samples were dated from the Wall Mountain Tuff. Sample ages range from 37.10 ± 0.10 to 37.34 ± 0.06 Ma and yield a weighted mean age of 37.25 ± 0.08 Ma (MSWD = 1.26) (Figure 2.2). This age is interpreted as an accurate eruption age for this

TABLE 2.2. Summary of the Ar/Ar ages for the Mt. Aetna caldera complex

Caldera Stage	Sample	Unit	Mineral†	Age calc. method††	Age (Ma)*	Internal Error$	External Error$$
Wall Mountain Tuff							
	MP-15	Wall Mountain Tuff	san	ideo.	37.34	0.06	1.46
	MP-15-HF	Wall Mountain Tuff	bt	plt.	37.24	0.11	1.46
	MP-15	Wall Mountain Tuff	bt	plt.	37.51	0.09	1.48
	NM-1152	Wall Mountain Tuff	san	ideo.	37.24	0.08	1.46
	NM-1307	Wall Mountain Tuff	san	ideo.	37.23	0.12	1.46
	NM-531	Wall Mountain Tuff	san	ideo.	37.20	0.07	1.46
	NM-1416	Wall Mountain Tuff	san	ideo.	37.10	0.10	1.46
Mt. Princeton border unit plutonism							
	MP-03	Mt. Princeton Border Unit 2	bt	plt.	35.78	0.11	1.40
	MP-02	Mt. Princeton Border Unit 2	bt	int. (rcl.)	35.72	0.16	1.40
Mt. Princeton interior unit plutonism							
	MP-24	Mt. Princeton outer interior	bt	plt.	35.56	0.11	1.40
	MP-24	Mt. Princeton outer interior	kspar	plt.	35.27	0.11	1.38
	MP-05	Mt. Princeton outer interior	bt	int.	35.54	0.16	1.40
	MP-05	Mt. Princeton outer interior	kspar	int. (alt.)	35.06	0.34	1.42
	MP-25	Mt. Princeton outer interior	bt	int. (rcl.)	35.46	0.16	1.40
	MP-25	Mt. Princeton outer interior	kspar	plt.	35.10	0.08	1.38
	MP-10	Mt. Princeton outer interior	bt	int. (rcl.)	35.33	0.16	1.40
	MP-10	Mt. Princeton outer interior	kspar	plt. (a.l)	33.33	0.11	1.32
	MP-08	Mt. Princeton outer interior	bt	int. (rcl.)	35.28	0.19	1.40
	MP-08	Mt. Princeton outer interior	kspar	plt.	35.57	0.19	1.40
	MP-07	Mt. Princeton outer interior	bt	plt.	35.23	0.09	1.38
	MP-13	Mt. Princeton outer interior	bt	int. (rcl.)	34.37	0.18	1.36
	MP-13	Mt. Princeton outer interior	kspar	int. (a.l)	34.23	0.17	0.68
	MP-12	Mt. Princeton porphyritic	bt	int. (rcl)	31.49	0.18	1.24
	MP-12	Mt. Princeton porphyritic	kspar	int. (a.l.)	27.99	0.14	1.10
	MP-22	Mt. Princeton porphyritic	bt	int. (rcl.)	30.80	0.09	1.22
Pre-Aetna caldera volcanism							
	MP-04	Tuff dike	bt	int. (xc.)	37.54	0.17	1.48
	MP-32	Tuff dike	bt	int. (xc.)	62.37	0.17	2.64
	MP-32	Tuff dike	bt	ideo.	34.53	0.12	1.36
Badger Creek Tuff							
	MP-30	Badger Creek Tuff	san	ideo.	34.26	0.06	1.34
	MP-30	Badger Creek Tuff	bt	int. (alt; xc.)	38.55	0.43	1.58
	MP-31	Badger Creek Tuff	san	ideo.	34.26	0.06	1.34
	MP-31	Badger Creek Tuff	bt	int. (alt, xc.)	35.01	0.49	1.46
	MP-36	Badger Creek Tuff	san	ideo.	34.24	0.05	1.34
Mt. Aetna intrusions							
	MP-21	Mt. Aetna Qtz. Monz.	kspar	int. (a.l.)	33.93	0.09	1.34
	MP-09	Ring Dike	kspar	int. (exc., xc)	40.02	0.18	1.58
Younger Plutonism							
	MP-38	California Luecogranite	bt	plt.	30.07	0.08	1.18
	MP-38	California Luecogranite	kspar	int. (a.l.)	26.45	0.12	1.04
	MP-37	North Fork Luecogranite	bt	int.	29.65	0.09	1.16
	MP-37	North Fork Luecogranite	kspar	int. (a.l.)	29.02	0.13	1.14
	MP-23	Mt. Antero Luecogranite	kspar	int. (a.l.)	28.18	0.13	1.12

† - san (sanidine); bt (biotite); kspar(K-feldspar)

†† - ideo. (ideogram); plt. (plateau); int. (Integrated); rcl. (recoil); alt. (alteration); a.l. (argon loss via reheating); xc. (xenocrysts); exc. (excess argon)

* - Age calculated relative to FC-2 equal to 28.201 Ma (Kuiper et al., 2008)

$ - Error (2σ) includes uncertainty in J and irradiation parameters

$$ - Error (2σ) includes uncertainty in ^{40}K decay constant $(5.462\pm0.214)x10^{-10}$ yr^{-1} (Min et al., 2000)

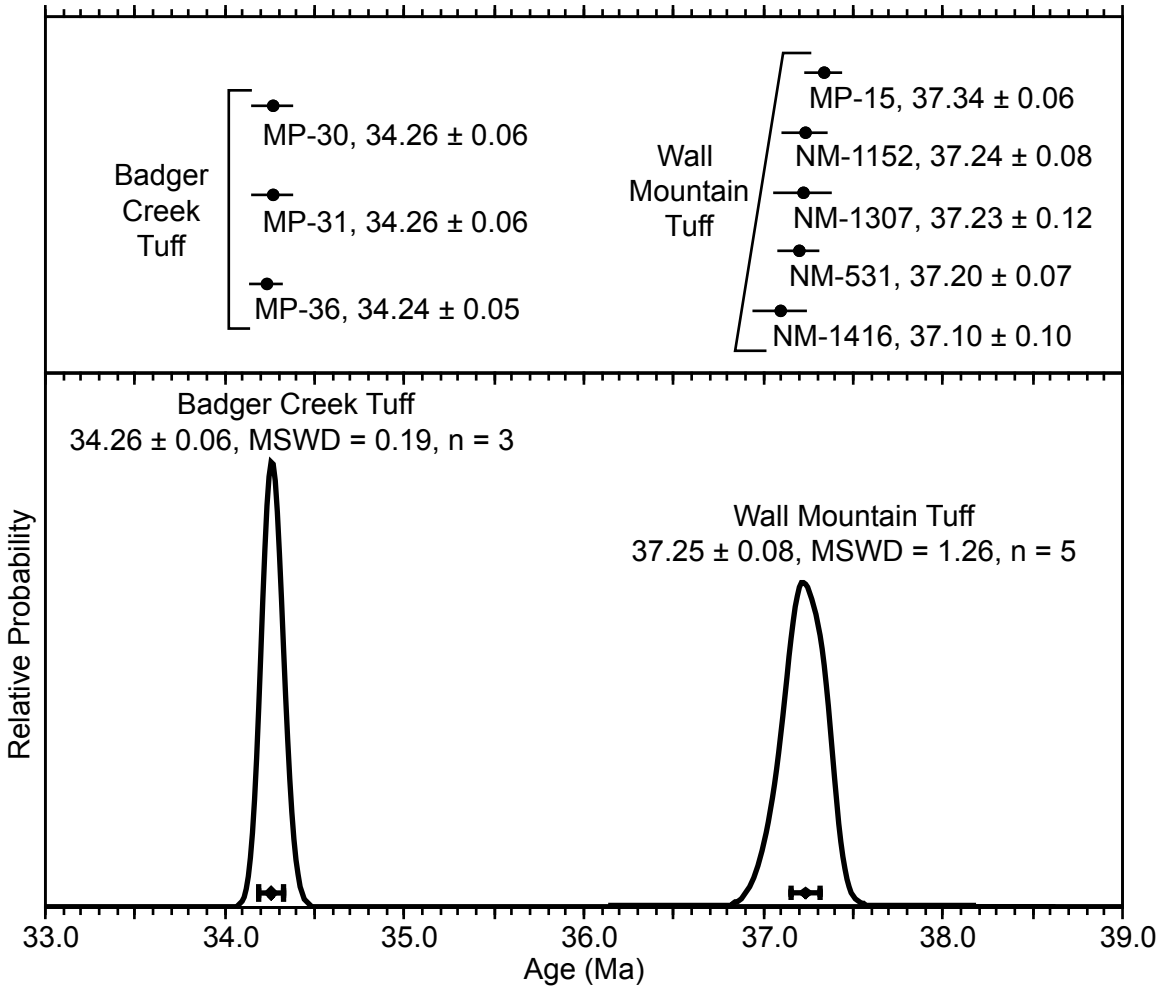

Figure 2.2. Summary ideogram of Wall Mountain and Badger Creek Tuff sanidine separates dated as part of this study. Each data point represents the weighted mean age calculated from sanidine single-crystal laser-fusion analyses. All errors are reported at 2σ and do not included error in the ^{40}K decay constant.

ignimbrite. The MSWD of ~1 indicates a near Gaussian distribution of ages. Two Wall Mountain Tuff samples contained xenocrysts. Sample NM-1416 contained abundant xenocrysts with ages ranging from 38 to 375 Ma. Sample MP-15 contained two 37.7 Ma xenocrysts. Xenocrysts were probably incorporated from vent walls or entrained into the ignimbrite as it flowed. The weighted mean age of the Wall Mountain Tuff is indistinguishable to the published age of 37.16 ± 0.09 Ma (McIntosh and Chapin, 2004).

Three sanidine samples were dated to obtain an age for the Badger Creek Tuff. Ages range from 34.24 ± 0.05 to 34.28 ± 0.06 and yield a weighted mean age of 34.26 ± 0.06 Ma (MSWD = 0.19) (Figure 2.2). The weighted mean age is interpreted to be the eruption age of the ignimbrite and the timing of Mt. Aetna caldera collapse. The low MSWD value is interpreted as an artifact of the small number of samples used to calculate the weighted mean age rather than an overestimation of errors. Though the newly calculated age is indistinguishable to the published age for the Badger Creek Tuff, 34.25 ± 0.11 Ma (McIntosh and Chapin, 2004), the error is slightly more precise.

2.6.2.2. Ar/Ar Biotite

Eighteen biotite separates were dated to determine the timing of volcanic eruptions and plutons thermal histories. Six representative age spectra are shown in Figure 2.3. The total range in ages is 62.37 ± 0.17 to 29.65 ± 0.09 Ma. For age spectra that contained a plateau, the age was calculated by weighting each step of the plateau by the inverse variance. A plateau is defined as three consecutive steps that overlap in error at 2σ and contain ≥ 50% of the ^{39}Ar released (Fleck et al., 1977). For analyses that did not yield a plateau, the age was calculated by using the integrated age of all the steps.

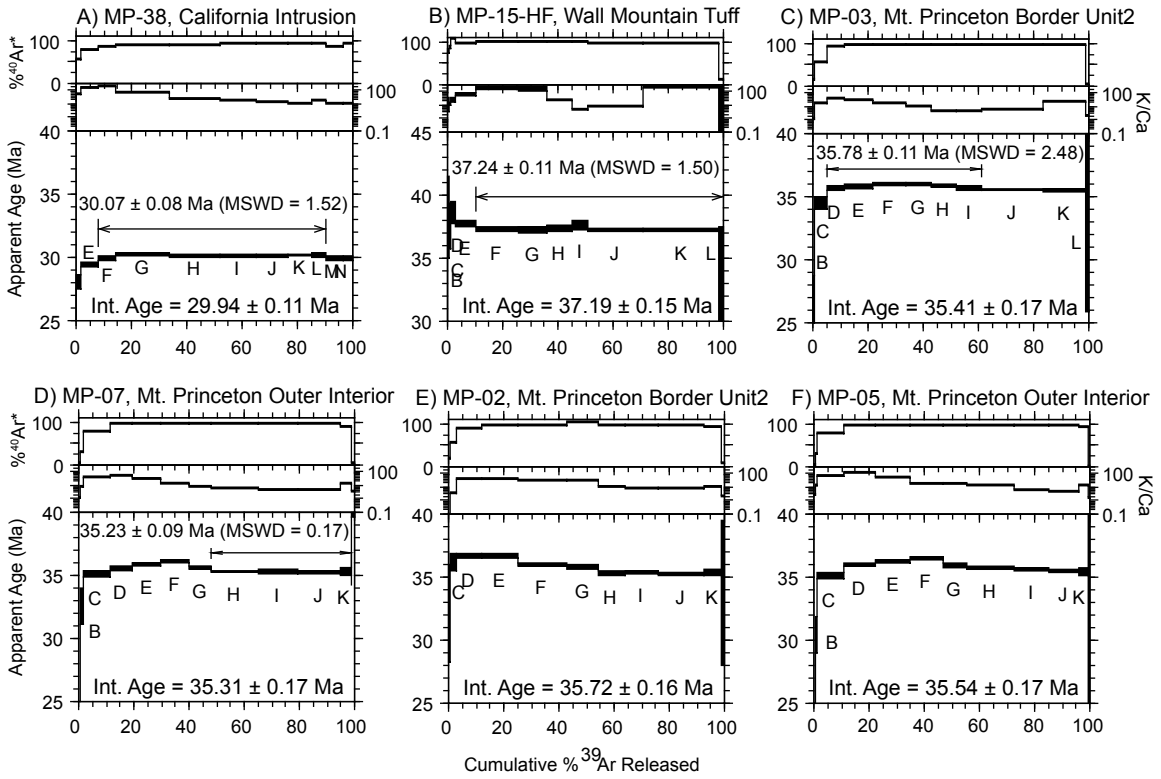

Figure 2.3. Six representative age spectra for the Mt. Aetna caldera complex biotite separates. Auxiliary plots include K/Ca and radiogenic yield (%^{40}Ar*). All errors are reported at 2σ and do not included error in the ^{40}K decay constant.

Biotite age spectra display a variety of complexity related to the degree of alteration, recoil, and/or possible xenocrystic contamination. Six out of eighteen biotite analyses yielded a plateau. For these six samples, the plateau comprises ~50 to 100% of the total ^{39}Ar released (e.g., Figures 2.3A-D). For intrusive samples, the biotite plateau age determines the timing of cooling to ~350°C (Hodges, 1991). The only volcanic biotite analyses that yielded a plateau were from the Wall Mountain Tuff. Two aliquots of the Wall Mountain Tuff biotite were analyzed, one sample pretreated in HF and the other untreated. The untreated biotite yielded a plateau of 37.51 ± 0.09, which is statistically older than the corresponding sanidine age of 37.34 ± 0.06. The HF treated biotite from the Wall Mountain Tuff yielded an age of 37.24 ± 0.11 (Figure 2.3B), which is statistically indistinguishable to the corresponding sanidine age. HF treatment likely removed adhering glass or inclusions that contain minor amounts of excess ^{40}Ar.

Twelve biotite analyses did not yield a plateau. For most of these samples, the ages of steps gradually increase during the first 40% of ^{39}Ar released and then subsequently decrease (e.g., Figures 2.3E and F). The overall ^{39}Ar release pattern is characteristic of ^{39}Ar recoil in some altered samples (Lo and Onstott, 1989). Typical K_2O values for pristine biotite are 8-10% (McDougall and Harrison, 1999). K_2O values for the disturbed biotite spectra are 5-6%, which suggests alteration and probable ^{39}Ar recoil. For these samples, the integrated age is interpreted to be the most accurate age (Heizler, 1988; Lo and Onstott, 1989). Though the age spectra for samples MP-30 and MP-31 (i.e., Badger Creek outflow sheet) have a broad hump shape, the integrated age is 1-3 Ma older than the corresponding sanidine age. This suggests that some ^{39}Ar may have been

recoiled out of the sample, thereby increasing the age. Alternatively, some of the biotite crystals that were dated in the bulk analysis may be xenocrysts.

Two biotite separates (MP-04 and MP-32, Figure 2.4), both from the northwestern intrusive tuff dike, were dated to determine the eruption age of the tuff and potentially to correlate it to the Badger Creek Tuff. The bulk separates were incrementally heated, one using the resistance furnace and the other with a defocused CO_2 laser (Figure 2.4A). Though both samples display initially old steps that gradually decrease in age during the experiment, the pattern is far more pronounced for sample MP-32. To assess xenocrystic contamination, 15 aliquots of 5-10 crystals were fused using the CO_2 laser. The multiple-crystal laser-fusion analysis yielded a weighted mean age of 34.53 ± 0.12 Ma (MSWD=2.07, Figure 2.4B). No aliquots were anomalously old, which suggests that xenocrysts, if present, constitute a very small percentage (e.g., <1%) of the total population. The laser-fusion weighted mean age is interpreted to be an accurate emplacement age for the tuff dike.

2.6.2.3. Ar/Ar K-feldspar and MDD thermal histories

Twelve plutonic K-feldspar separates were dated to constrain the 300-150°C thermal history of the intrusive units (Lovera et al., 1989). Age spectra are plotted in Figure 2.5 and ages are reported in Table 2.2. Step-heating schedules included isothermal duplicates steps to assess excess ^{40}Ar in fluid inclusions (Harrison et al., 1994). Seven samples were modeled in accordance to the multiple diffusion domain (MDD) theory (Lovera et al., 1991; 1997) using the methods of Sanders and Heizler (2005). Samples that yielded flat ^{39}Ar release profiles were not modeled because the geometry of the spectra indicates rapid cooling through the K-feldspar closure temperature. Likewise,

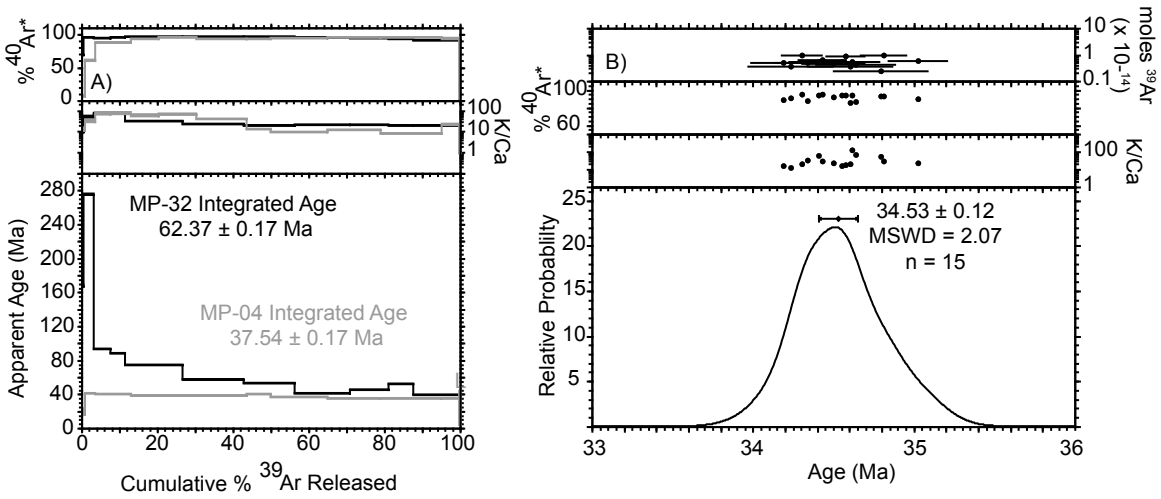

Figure 2.4. Ar/Ar analyses of biotite from the intrusive tuff dike. A) Age spectra of the incrementally-heated biotite separates. MP-04 was step-heated using the double-vacuum Mo resistance furnace, whereas MP-32 was step-heated using the CO2 laser. B) Ideogram of the multiple-crystal laser-fusion analysis of MP-32 biotite. Each fusion step analysis consisted of 5-10 crystals of biotite.

samples that yielded anomalous results were not modeled. For age spectra that contained argon loss profiles, two thermal histories were generated. Monotonic cooling histories (Figure 2.6) only allow for cooling from initially high temperatures, where as unconstrained thermal histories (Figure 2.7) allow for reheating events. Supplementary MDD figures are provided in Appendix 2.4.

Four of the twelve samples yielded nearly flat age spectra (MP-05, -08, -24, -25; Figures2.5 A, B, I, and J). The initial 10-25% of the age spectra is characterized by discordant contiguous steps. This portion of the age spectra also contains oscillating radiogenic yields and K/Ca values. The initial discordance is probably related to fluid inclusions that contain excess and/or atmospheric argon (Harrison et al., 1994). The plateau segment for these samples indicates the timing of cooling. One sample, MP-05 (Figure 2.5A), did not yield a plateau, but the age spectrum is nearly flat. For this sample, the integrated age is interpreted to be the timing of cooling.

Seven K-feldspar age spectra are characterized by argon loss profiles indicative of slow cooling and/or reheating events (Lovera et al., 1989; Gillespie, 1982). The age gradients observed in the K-feldspar age spectra range from ~1-2 Ma to as much as 8-10 Ma. Sample MP-13 (Figure 2.5F) has the smallest age gradient. Both the monotonic and unconstrained thermal histories indicate rapid cooling between 34 and 32 Ma (Figures 2.6C and 2.7C). Using Al-in-hornblende geobarometry, Hammarstrom and Zen (1986) concluded the Mt. Princeton batholith was emplaced at 1 kbar or ~3km. Based on the depth of emplacement, the large age gradients observed in the remainder of the K-feldspar spectra are not interpreted to be the result of protracted cooling in the very

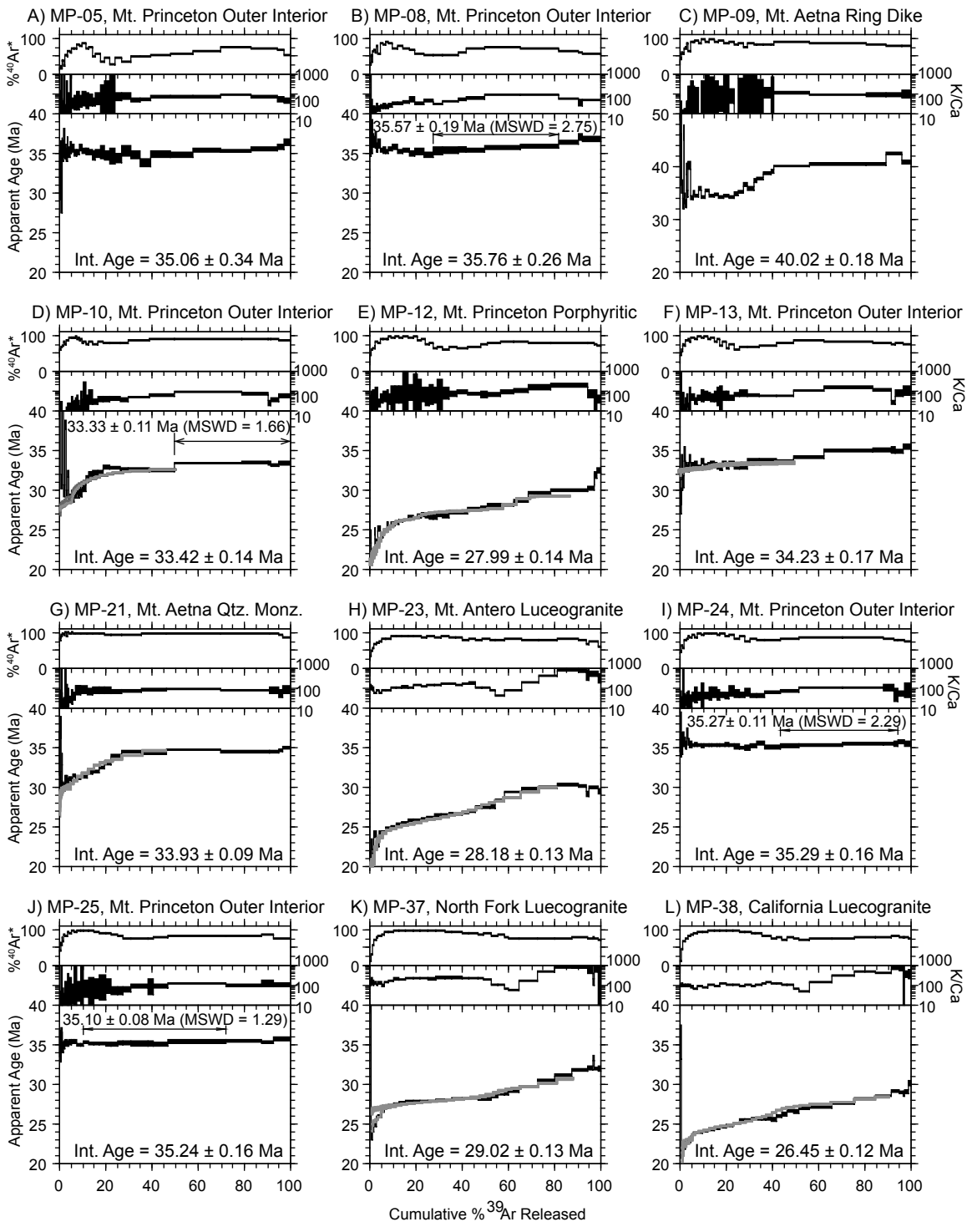

Figure 2.5. Age spectra for the Mt. Aetna plutonic K-feldspar analyses. Auxiliary plots include K/Ca and radiogenic yield (%^{40}Ar*). All errors are reported at 2σ and do not included error in the ^{40}K decay constant. The gray age spectra represent the modeled age spectra that were used to generate the MDD thermal histories.

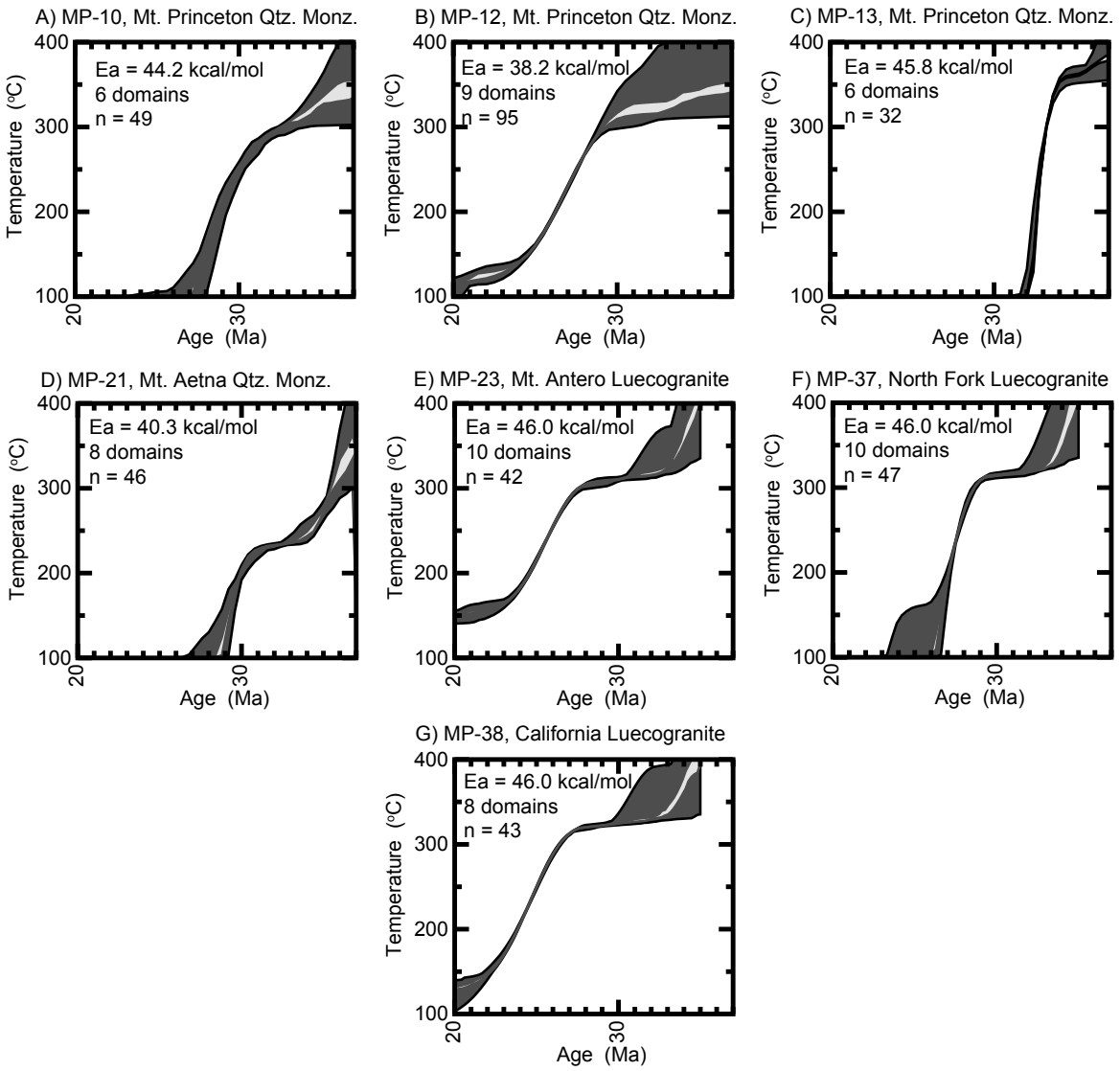

Figure 2.6. Monotonic MDD cooling histories generated for the Mt. Aetna K-feldspar. The dark gray band is 90% confidence interval of the entire distribution, whereas the light gray band is 90% confidence interval of the mean. Activation energy, number of domains, and number of solutions are also provided.

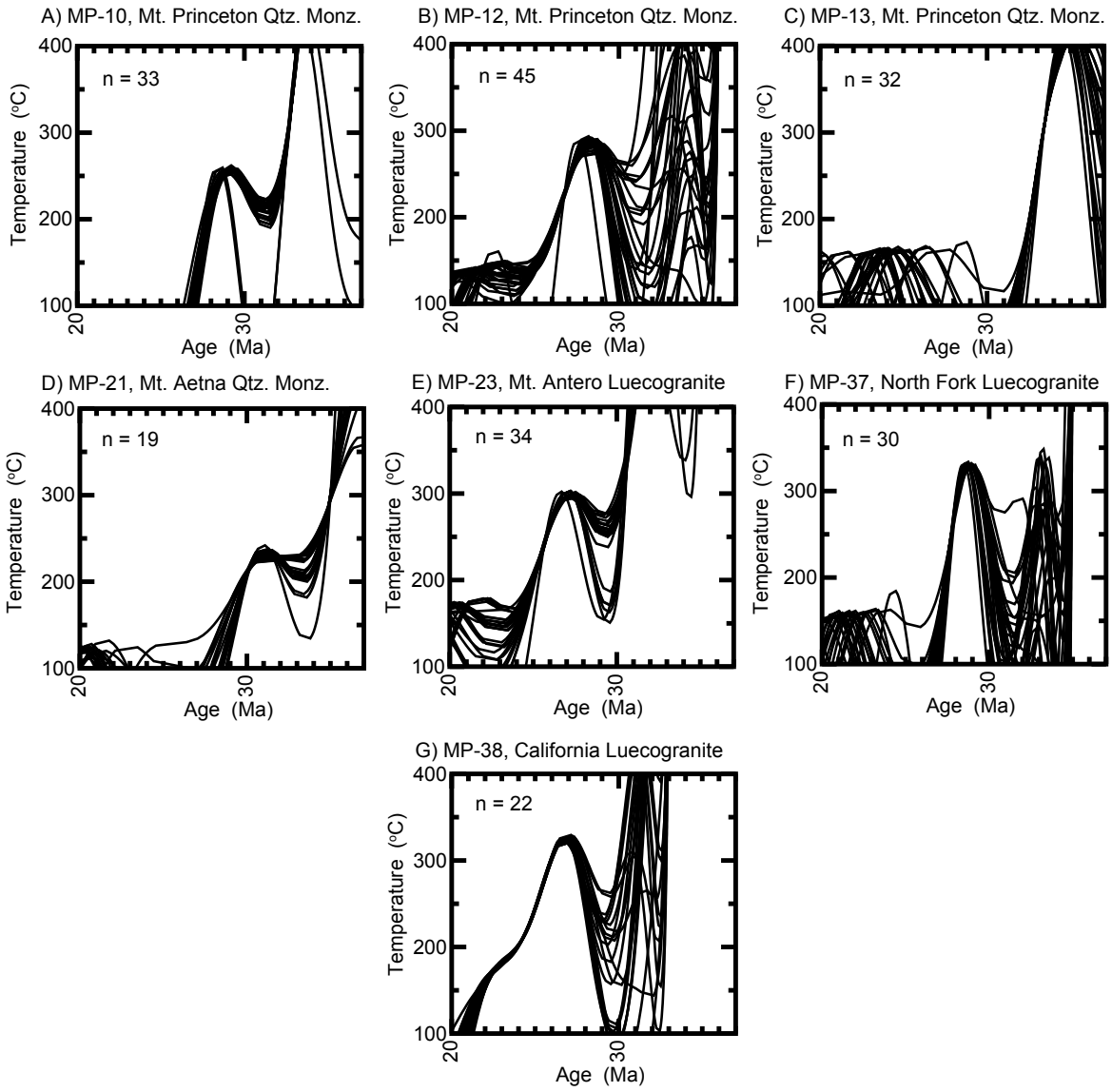

Figure 2.7. Unconstrained MDD thermal histories generated for the Mt. Aetna K-feldspar. Each thermal history corresponds to a unique solution to the diffusion parameters. Activation energy and number of domains are the same as those reported in Figure 2.6.

shallow upper crust. Instead, the argon loss profiles are attributed to reheating events during protracted magmatism (see discussion for more detail).

The K-feldspar from the Mt. Aetna ring dike, MP-09 (Figure 2.5C), yielded anomalous results. The initial part of the age spectrum is characterized by oscillating ages of isothermal duplicate steps, which are indicative of excess argon. At ~20% ^{39}Ar released, the ages of steps gradually climb to ~40 Ma, which is ~6 Ma older than the intracaldera Badger Creek Tuff that the unit intrudes. The anomalous results may be related to excess argon in the largest domains (Foster et al., 1990) or xenocrystic contamination.

2.7. Magmatic evolution of the Mt. Aetna caldera complex

U/Pb and Ar/Ar geo- and thermochronology of volcanic and plutonic rocks from the Mt. Aetna caldera complex record the emplacement, eruption, preservation, and thermal history of caldera-related silicic magmas. Figure 2.8 summarizes the Mt. Aetna geochronology and thermochronology. Figure 2.9 is a schematic diagram that illustrates the magmatic evolution of the caldera complex. U/Pb and Ar/Ar geochronology indicate protracted magmatism between 37.3 and 30.8 Ma. None of the exposed plutons are interpreted to be the residual mush for either caldera forming ignimbrite. Currently exposed parts of the Mt. Princeton batholith were emplaced between 36.4 and 35.1 Ma. The batholith is interpreted to represent both post-Wall Mountain Tuff and pre-Badger Creek Tuff magmatism. The source caldera for the 37.3 Wall Mountain Tuff is interpreted to have been in the same geographic location as the Mt. Princeton batholith, but all evidence for the caldera and the associated magma chamber (i.e., intracaldera tuff

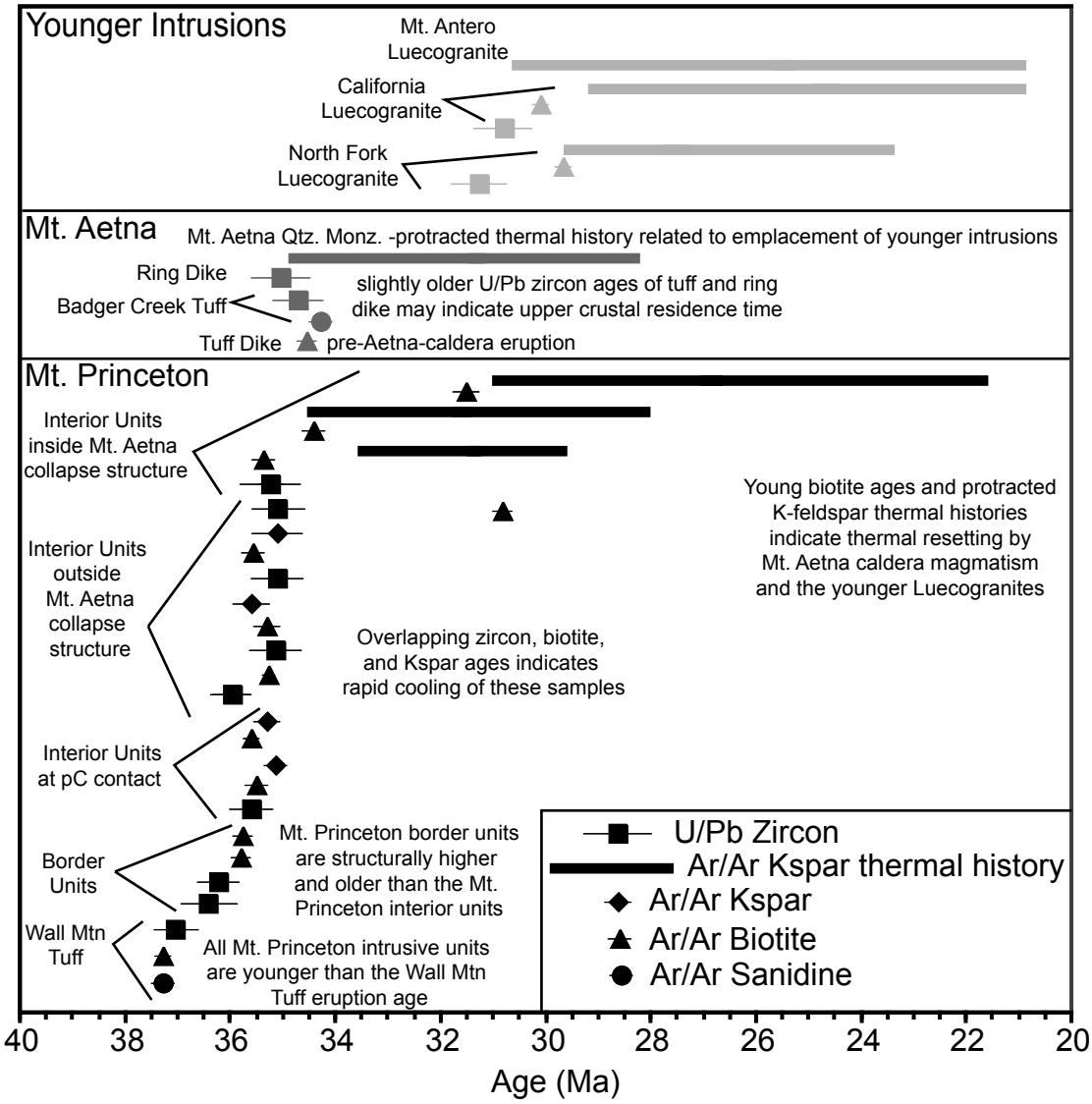

Figure 2.8. Summary of the geochronology and thermochronology of the Mt. Aetna caldera complex. All errors are reported at 2σ. Uncertainties associated with U/Pb and Ar/Ar ages include only systematic errors. Bold horizontal lines represent the range of ages observed in K-feldspar age spectra.

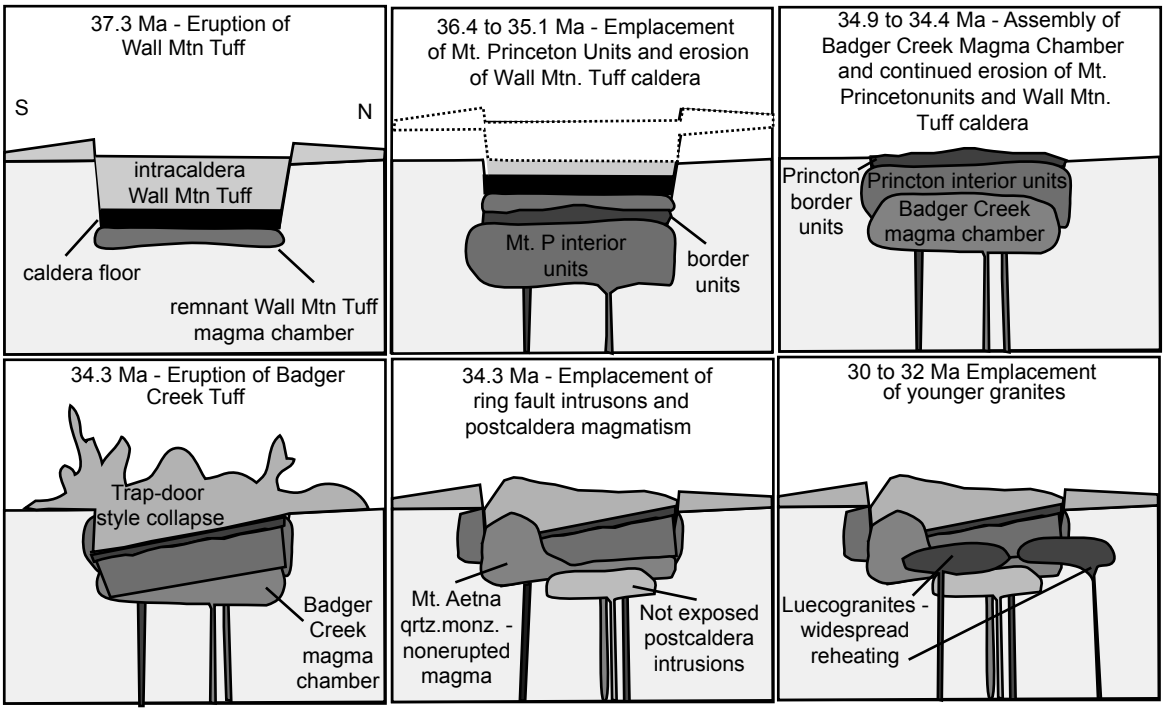

Figure 2.9. Schematic diagram illustrating the magmatic evolution of the Mt. Aetna caldera complex. Diagram is not to scale. See text for discussion of each panel.

and nonerupted magma) has eroded away. Based on the chemical and temporal similarity, the ring dike and Mt. Aetna quartz monzonite are interpreted to be nonerupted Badger Creek Tuff. The youngest intrusions were emplaced at ~31 Ma and are the most evolved melts. The youngest intrusions caused widespread reheating and thermal resetting of biotite and K-feldspar in many of the older intrusions.

2.7.1. Wall Mountain Tuff and Mt. Princeton batholith relationship

The crystal-rich, low-SiO_2 Wall Mountain Tuff erupted at 37.25 ± 0.08 Ma (Figure 2.9A). The U/Pb zircon age of the tuff, 37.01 ± 0.27 Ma, is slightly younger, but analytically indistinguishable. Based on location of outcrops within paleovalleys and up to 140 km to the east of the Mt. Princeton batholith, the outflow covered a minimum area of 10,400 km^2 (Epis and Chapin, 1975; Shannon, 1988). The total volume of the Wall Mountain Tuff is estimated to be ~1000km^3 (Lipman, 2007). Because the Wall Mountain Tuff was deposited directly onto the late Eocene erosional surface (Epis and Chapin, 1975), the age of the tuff provides a minimum estimate for the age of this erosional horizon.

Ages of zircon cores and radiogenic isotope values indicate a significant crustal component in the Wall Mountain Tuff. LA-ICP-MS U/Pb zircon dating identified numerous 1.4 Ga xenocrystic cores. Though only 7 of 41 analyses targeted cores, CL images indicate that approximately one-third of the imaged zircons contain inherited cores. The initial $^{87}Sr/^{86}Sr$ value of the tuff is 0.709377 and the ε_{Nd} value is -10.66 (Zimmerer et al., 2010). The crustal component of the Wall Mountain Tuff, preserved in the radiogenic isotopic signature and as xenocrystic cores in zircons, indicates that these

caldera-related silicic magmas were generated in part by partial melting and/or assimilation of 1.4 Ga crust.

The Mt. Princeton batholith was incrementally emplaced into the upper crust (Figure 2.9B). U/Pb zircon ages of the Mt. Princeton batholith are between 36.38 ± 0.40 and 35.06 ± 0.48 Ma. Shannon (1988) suggested that the Mt. Princeton batholith was emplaced as a single magma body, which differentiated to produce the numerous compositionally diverse phases. Magma chambers must contain volumetrically significant melt volumes (i.e., > 60%) in order to differentiate and erupt (Smith, 1967; Bachmann and Bergantz, 2004, Annen, 2009). Large magma chambers can only be sustained if magma emplacement rates exceed 10^{-2}-10^{-3} km^3/yr (Schmitz and Bowring, 2001, Charlier et al., 2005; Annen, 2009). Based on U/Pb zircon ages, the Mt. Princeton batholith was emplaced over a duration of 1.32 ± 0.88 Ma. Considering that the exposure of the Mt. Princeton batholith covers an area of ~875 km^2 (Tweto, 1979; Shannon, 1988; Lipman, 2007) and the total of relief of the exposed intrusion is ~1.5 km, the estimated volume of the Mt. Princeton batholith is ~1312.5 km^3. This yields emplacement rates between $3.0x10^{-3}$ km^3/yr and $6.0x10^{-4}$ km^3/yr. The average emplacement rate of the Mt. Princeton batholith, 9.9×10^{-4} km^3/yr, is too slow to have sustained a large enough magma chamber that could have differentiated (Annen, 2009). Instead, the compositional variation within the Mt. Princeton batholith was acquired at greater depths well below the current exposure of the batholith. This is consistent with several studies that have suggested silicic melts can be generated in the lower crust (Glazner et al., 2004; Dufek and Bergantz, 2005; Annen et al., 2006).

The Mt. Princeton batholith was most likely emplaced as a series of downward stacking sills following the eruption of the Wall Mountain Tuff. The oldest units of the Mt. Princeton batholith are the structurally highest border units, which have U/Pb zircon crystallization ages of 36.38 ± 0.40 and 36.21 ± 0.28 Ma. Shannon (1988) suggested that border units that contain clinopyroxene (e.g., MP-03) represent nonerupted Wall Mountain Tuff. However, the U/Pb age of that unit is 36.21 ± 0.28 Ma. The statistically significantly younger U/Pb age compared to the eruption age precludes a correlation. The interior units have zircon crystallization ages that range from 35.92 ± 0.25 to 35.06 ± 0.48 Ma. Numerous studies have suggested that some upper crustal plutons and laccoliths are emplaced as a series of downward staking sills or tabular bodies (Hirt, 2007; Coleman et al., 2008; Michel et al., 2008; Morgan et al., 2008; Farina et al., 2010; Tappa et al., in review). Though the ages of some Mt. Princeton interior units are indistinguishable to the border units, many of the interior units are younger than the oldest border unit, which suggests the Mt. Princeton batholith was also emplaced by a series of downward stacking intrusions. This interpretation is consistent with geologic mapping, which has shown that the Mt. Princeton batholith is composed of numerous, near-horizontal compositional horizons (Shannon, 1988).

Though previous studies suggested that the Mt. Princeton batholith was the source for the Wall Mountain Tuff, new U/Pb and Ar/Ar ages of the Mt. Princeton batholith indicate that the batholith is too young to be the crystallized source magma chamber. This conclusion supports the geochemical investigation of Campbell (1994), who suggested the interior Mt. Princeton quartz monzonite and Wall Mountain Tuff were not cogenetic. We propose that the source caldera and magma chamber for the Wall Mountain Tuff was

located in the same geographic area as the Mt. Princeton batholith, but at a structurally higher level, and was completely eroded away shortly after the caldera forming eruption (Figure 2.9B and C). In this framework, the Mt. Princeton batholith represents both post-Wall Mountain Tuff and pre-Badger Creek Tuff magmatism.

High erosion and exhumation rates characterized central Colorado during the late Eocene/early Oligocene. Paleovalleys in central Colorado were repeatedly filled by outflow of regional ignimbrites. Continued erosion re-incised the valleys, which acted as pathways for pyroclastic deposits during subsequent volcanism (Epis and Chapin, 1975; McIntosh and Chapin, 2004). The Mt. Princeton batholith was emplaced at ~3 km depth (Hammarstrom and Zen, 1986), but was exposed at the surface prior to the 34.3 Ma eruption of the Badger Creek Tuff. Using the oldest U/Pb age of the Mt. Princeton batholith, this implies an average uplift rate of 1.4 mm/yr, which is similar to exhumation rates of the Himalayans (Theide et al., 2004). Erosion and high exhumation rates apparently obliterated the caldera for the Wall Mountain Tuff.

Erosion and exhumation rates slowed following the eruption of the 34.3 Ma Badger Creek Tuff. A ~0.5 km thick deposit of intracaldera Badger Creek Tuff is preserved along the southern margin of the Mt. Aetna caldera. Because of erosion, the original, maximum thickness of the intracaldera tuff is unknown. However, mapping of highly faulted calderas indicates the thickness of intracaldera ignimbrites typically ranges from 3 to 5 km thick (Lipman et al., 1986; Seager and McCurry, 1988; Lipman, 1997; John et al., 2008). This suggests that 2.5 to 4.5 km of intracaldera Badger Creek Tuff has been removed by erosion. If the calculated average exhumation and erosion rates that existed between the emplacement of the Mt. Princeton batholith and the eruption Badger

Creek Tuff continued after formation of the Mt. Aetna caldera, the current surface would have been exposed in 1.8 to 3.2 Ma. The preservation of some intracaldera Badger Creek Tuff indicates exhumation and erosional rates must have slowed prior to or after 31.1 or 32.5 Ma.

Another line of reasoning that suggests the Mt. Princeton batholith represents post-Wall Mountain Tuff magmatism is that similar studies of intrusions from simple, single caldera systems indicate that plutons typically represent syn- or postcaldera magmatism (Lipman, 1984; Lipman et al., 1986; Seager and McCurry, 1988; Tappa et al., in review; Zimmerer and McIntosh, in review). Volumetrically significant precaldera intrusions are rare. During precaldera magmatism the crust is cold and overpressure created by magmatism fractures the country rock, which causes dike propagation. Early magma emplacement results in eruptions that may efficiently drain the chamber rather than storing and preserving the magma as plutons. However, after continued precaldera magmatism, the effective wall-rock rheology may change from an elastic regime to a viscous regime, which is more likely to store magma rather than erupt magma (Jellinek and DePaulo, 2003). If the source caldera for the Wall Mountain Tuff was not in the same geographic location as the Mt. Princeton batholith, then the Mt. Princeton batholith is a rare example of a volumetrically significant precaldera intrusion. However, if the Mt. Princeton batholith is interpreted in the framework of a two-caldera system, than the Mt. Princeton batholith represents both post-Wall Mountain Tuff and pre-Badger Creek Tuff magmatism. Following the Wall Mountain Tuff eruption the crust was warm and the mid- to upper crustal effective rheology was likely in the viscous regime, which favored

magma storage rather than eruption. Extension in the upper crust during this period may have also promoted magma storage (Petford et al., 2000).

The volume and composition of the nonerupted material in the Wall Mountain Tuff source magma chamber is impossible to constrain because the record has been removed by erosion. Several studies have proposed that some caldera forming magma chambers may nearly completely drain during caldera collapse (Roche and Druitt, 2001; Glazner et al., 2004; Tappa et al., in review; Zimmerer and McIntosh, in review), leaving behind small-volume intrusions that are compositionally similar to the caldera forming ignimbrite. In situ differentiation predicts a 3 to 10:1 intrusive:extrusive ratio (White et al., 2006). For the Wall Mountain Tuff, this corresponds to 3,000 to 10,000 km^3 of nonerupted material. If the Wall Mountain Tuff magma chamber had a similar area to the current exposure of the Mt. Princeton batholith (875 km^2) the nonerupted residual crystal mush would be between 3.4 and 11.4 km thick. Eradication of plutons of that size would require exceptionally high erosion and exhumation rates that are not indicated by the data presented in this study. We speculate that the Wall Mountain Tuff magma was generated in a lower crustal source, these magmas were rapidly emplaced into the upper crust, and the magma chamber efficiently drained during the eruption leaving behind very little intrusive material, which was later eroded away (Figure 2.9C).

Ar/Ar thermochronology indicates that the thermal history of the Mt. Princeton batholith was influenced by the emplacement history and proximity to country rock and younger intrusions. Biotite separates from the outer, border units (MP-02, -03) are the oldest, consistent with U/Pb ages that indicate these phases were emplaced first. In general, biotite, K-feldspar, and zircon ages from Mt. Princeton interior units outside the

Mt. Aetna collapse structure have a narrow age range from 35.6 to 35.1 Ma. Zircon, biotite, and K-feldspar ages of many samples are statistically indistinguishable indicating rapid cooling. This is consistent with shallow emplacement depths and rapid exhumation rates. Contrastingly, Mt. Princeton intrusive units within the Mt. Aetna collapse structure and adjacent to younger intrusions display a prolonged thermal history. For example, sample MP-22 is located < 500 m from the 30.8 Ma California Intrusion. Biotite from MP-22 yielded an age 30.80 ± 0.12 Ma, indistinguishable to the 30.8 Ma emplacement age of adjacent California intrusion. MDD unconstrained thermal models of sample MP-10 and 12 (Figure 2.7 A and B, respectively) indicate reheating events at ~30 Ma, which corresponds to emplacement of the younger luecogranites. MDD models of MP-12 K-feldspar also show evidence for reheating events as young as ~22 Ma. Although there are no exposures of ~22 Ma igneous rocks in the immediate vicinity (McIntosh and Chapin, 2004), this does not preclude the possibility for unexposed intrusions of this age at this time. Although young ages observed in some age spectra (Figure 2.5E) may be related to hydrothermal alteration and recrystallization of the smallest K-feldspar domains, the age spectra are not chaotic and are thus not likely related to recrystallization (Lovera et al., 2002).

One sample that did not yield indistinguishable biotite and K-feldspar ages is MP-10 (Figure 2.5D), a Mt. Princeton interior unit. Biotite from this sample yielded an integrated age of 35.33 ± 0.16 Ma, indicating cooling to ~350°C at this time. The oldest ages observed in the MP-10 K-feldspar age spectrum are from the highest temperature steps, which yielded a plateau age of 33.33 ± 0.11 Ma. MDD unconstrained thermal histories of MP-10 K-feldspar indicate a ~400°C reheating event at 33.3 Ma (Figure

2.7A). However, a ~400°C reheating event at 33.3 Ma should have reset the biotite crystals as well. The ~2 Ma age discrepancy between the biotite and K-feldspar ages could be related to extremely slow cooling from ~350°C (biotite closure temperature) to 300°C (closure temperature of the largest K-feldspar domains) between 35.3 and 33.3 Ma. This latter scenario seems unlikely considering the shallow depth of emplacement and the exhumation rates previously discussed. The steps that define the K-feldspar plateau were generated during high-temperature analyses. The high-temperature steps correlated to degassing of the largest domains. The largest domains of K-feldspar are commonly contaminated with excess ^{40}Ar (Foster et al., 1990). Because of this, the anomalous K-feldspar plateau age is interpreted to be related to excess argon and is thus, not geologically significant. The youngest ages observed in the K-feldspar age spectrum are ~30 Ma, which likely correlates reheating events related to the emplacement of the ~30 Ma young luecogranites.

2.7.2. Mt. Aetna caldera, Badger Creek Tuff, and associated intrusions

Following the eruption of the Wall Mountain Tuff, erosion of the source caldera, and the emplacement and exhumation of the Mt. Princeton batholith, the Badger Creek Tuff erupted at 34.26 ± 0.06 Ma (Figure 2.9D). During the eruption of the Badger Creek Tuff the Mt. Aetna caldera collapsed in a trap-door style. The greatest subsidence occurred in the southern portion of the caldera (Shannon et al., 1987; Toulmin and Hammarstrom, 1990). Numerous studies have correlated the intracaldera and outflow Badger Creek Tuff using geochemical, paleomagnetic, and geochronologic techniques (Shannon, 1988; Campbell, 1994; McIntosh and Chapin, 2004). The ages of intracaldera (MP-36) and outflow (MP-31 and -31) Badger Creek Tuff are analytically

indistinguishable, which supports the correlation of the previous studies. The geochemistry of numerous intracaldera and outflow Badger Creek Tuff samples are similar, indicating that the dacitic, crystal-rich Badger Creek Tuff is not zoned (Shannon et al, 1987; Campbell, 1994).

U/Pb zircon ages of the Badger Creek Tuff outflow sheet are significantly older than Ar/Ar sanidine ages. LA-ICP-MS zircon analyses yielded an U/Pb age of 34.69 ± 0.33 (± 0.62 if systematic errors are included). Mills et al. (2010) reported a statically indistinguishable, but more precise CA-TIMS age of 34.46 ± 0.06 Ma. The slightly older U/Pb age of the Badger Creek Tuff may be related to an inaccurate intercalibration of the U/Pb and K/Ar systems (Bachmann et al., 2007b; Kuiper et al., 2008; Renne et al., 2010). If uncertainties in the U and K decay constant are propagated through the error calculation, the two ages overlap at 2σ. Alternatively, the older U/Pb age may indicate pre-eruption zircon residence in Badger Creek Tuff magma chamber.

During or shortly after caldera collapse, magma that is compositionally identical to the Badger Creek Tuff intruded into the ring faults, caldera vents, and intracaldera deposits (Figure 2.9E). The LA-ICP-MS U/Pb zircon age of the ring dike is 35.01 ± 0.41 Ma. Mills et al. (2010) reported a CA-TIMS age of 34.95 ± 0.04 Ma for the Mt. Aetna quartz monzonite intrusion. The compositional similarity of the two intrusions and the analytically indistinguishable U/Pb ages suggest that the Mt. Aetna ring dike and quartz monzonite pluton are closely related.

Though the U/Pb ages of the Mt. Aetna ring dike and quartz monzonite pluton are older than the intracaldera tuff, field relationships and textures indicate that these units intruded into the intracaldera sequence. The interior of the quartz monzonite intrusion is

coarsely porphyritic, containing ~5cm long megacrysts of K-feldspar and plagioclase. However, within ~20 cm of the contact with the intracaldera tuff, the quartz monzonite is appreciably finer-grained and lacking megacrysts. This texture is characteristic of chilled margins in some plutons (Hubbert and Sparks, 1989; Winter, 2001). The ignimbrite is densely welded and contains eutaxitic textures at the contact with the pluton. The base of an ignimbrite is commonly identified by nonwelded textures, a vitrophyre zone, or pyroclastic fall deposits (Fisher and Schmincke, 1984; Branney and Kokelaar, 2002). Lack of these facies at the tuff-pluton contact suggests that the tuff was not deposited on the intrusion. The lack of any unconsolidated sediment anywhere between the contact of the quartz monzonite and tuff also suggests that the pluton was not exposed prior to the caldera eruption. Finally, the Mt. Aetna quartz monzonite cross cuts some megabreccia units that were deposited during syn-caldera collapse (Toulmin and Hammarstrom, 1990; Shannon, 1988).

The Badger Creek Tuff magma chamber was apparently assembled during a >500 ka period prior to the Mt. Aetna caldera collapse (Figure 2.9C). Caldera-related intrusions that are compositionally identical to the caldera-forming ignimbrite are commonly interpreted to be the nonerupted equivalent of the ignimbrite (Lipman et al., 1986; Johnson et al., 1989; Seager and McMurry, 1988; Lipman, 2007; John et al., 2008). The compositional similarity of the ring dike, Mt. Aetna quartz monzonite, and Badger Creek Tuff suggests that the units are genetically related (Shannon et al., 1987; Campbell, 1994). Zircons in the ring dike and Mt. Aetna quartz monzonite are as much as ~600 ka older than the eruption age of the Badger Creek Tuff, which implies that magma similar in composition to the Badger Creek Tuff was accumulating in the upper crust prior to the

caldera formation. Contrastingly, zircons in the Badger Creek Tuff outflow are only 100-200 ka older than the eruption age. This suggests that the Badger Creek Tuff magma chamber was incrementally emplaced during a >500 ka period prior to eruption, rather than as a single pulse at 34.9 Ma. During caldera eruption, the youngest (and possibly the warmest and least viscous) portions of the magma chamber erupted, whereas the oldest (and possibly the coldest and most viscous) portions of the magma chamber did not erupt. Instead, these older, but compositionally identical portions of the magma chamber were intruded into the ring faults, vents, and intracaldera tuff (Figure 2.9E).

The abundant K-feldspar megacrysts in the coarsely porphyritic quartz monzonite are additional evidence for incremental emplacement of the Badger Creek magma chamber. The Mt. Aetna quartz monzonite is unlike many intracaldera plutons, which are typically fine-grained to slightly porphyritic (Fridrich and Mahood, 1984; Lipman et al., 1986; John et al., 2008). Johnson and Glazner (2010) hypothesized that K-feldspar megacrysts grow via textural coarsening during thermal cycling of incrementally emplaced granite and granodiorite plutons. The oldest portion of the Badger Creek magma chamber, now preserved as the Mt. Aetna quartz monzonite, likely experienced the most thermal cycles during incremental assembly of the magma chamber. During thermal cycling, this region of the magma chamber texturally evolved into a porphyritic quartz monzonite.

The relationship of U/Pb zircon ages of the Mt. Aetna quartz monzonite and ring dike to the U/Pb zircon age of the Badger Creek Tuff provide a framework to speculate on the assembly pattern of the Badger Creek Tuff magma chamber. Caldera forming eruptions are interpreted to drain the magma chamber from the top-down (Smith, 1979;

Hildreth, 1981; Seager and McCurry, 1988; Bachmann and Bergantz, 2008). The outflow Badger Creek Tuff, presumably erupted during the initial stages of caldera collapse, contains zircons 100-200 ka older than the tuff. The Mt. Aetna quartz monzonite and ring dike, the nonerupted part of the magma chamber, contain zircons ~500 ka older than the tuff. Accordingly, the youngest magma in the chamber at the time of caldera collapse was located near the top of the chamber and that the older parts of the magma chamber were near the bottom or sides. This indicates the Badger Creek Tuff magma chamber may have been assembled from the bottom-up, which is different than the top-down assembly pattern of the Mt. Princeton batholith. This may illustrate fundamental differences in assembly patterns of postcaldera plutons compared to caldera magma chambers.

Evidence for prolonged assembly of upper crustal magma chambers has been observed at other caldera systems. The Fish Canyon Tuff, which is lithologically very similar to the Badger Creek Tuff (i.e., crystal-rich, nonzoned, and dacitic), contains zircons that are ~600 ka older than the eruption age (Bachmann et al., 2007b). U/Pb SHRIMP dating of zircons from the compositionally zoned Whakamaru ignimbrite group erupted from the Taupo volcanic center have rims and cores that differ in age by as much as 250 ka, indicating prolonged upper crustal residence (Brown and Fletcher, 1999). These studies relied on using pre-eruptive zircon growth of the erupted material to assess magma chamber assembly. However, evidence for prolonged Badger Creek Tuff magma chamber assembly stems mostly from U/Pb dating of a compositionally identical intrusion. This study demonstrates that some caldera-related plutons can be used to infer caldera-forming magma chamber processes.

The Badger Creek eruption was preceded by numerous, small-volume eruptions. The Calico Mountain volcanic units consist of intermediate to silicic lavas, tuffs, and breccias. Because of pervasive alteration no attempt was made to date these rocks. The only dated pre-Badger Creek Tuff volcanic rock is an intrusive tuff dike (MP-32) located in the northwest region of the complex (Figure 2.1). The age of this unit is 34.53 ± 0.12 Ma (Figure 2.4B). The intrusive tuff dike was originally interpreted as a vent for the Badger Creek Tuff because of similarities in location, mineralogy, and whole-rock geochemistry. The new age of the tuff dike precludes it being a vent for the Badger Creek eruption. However, the geochemical similarity of the two units may indicate that the tuff dike represents a small-volume eruption from the Badger Creek Tuff magma chamber that was being incrementally assembled at that time.

Current exposures of the Mt. Aetna caldera provide a limited view of subcaldera intrusions. Only the caldera floor, intracaldera ignimbrite, ring structures and dikes, and the structurally highest intrusions of the subcaldera batholith are exposed. Because deeper portions of the Badger Creek Tuff magma chamber are not exposed, we could not directly assess whether the dacitic Badger Creek Tuff differentiated from a more mafic magma in the upper crust or was generated at deeper crustal levels. The lack of mineralogical and chemical zoning in the tuff, intrusive tuff dike, and intracaldera intrusions (Shannon et al., 1987; Campbell, 1994) suggests that in-situ differentiation in the upper crust was minor or absent. This may be because the melt content was high enough to allow convection to homogenize the magma chamber or that the melt fraction was too low and melt-crystal separation could not occur (Bachmann and Bergantz, 2004; 2008). The source of the Mt. Aetna caldera-related magmas was capable of generating

compositionally uniform magmas for an extended duration, considering that the Mt. Aetna quartz monzonite and Badger Creek Tuff are chemically identical, yet were emplaced at different episodes >500 ka apart. Campbell (1994) noted the compositional similarities between the Mt. Aetna caldera intrusive and extrusive rocks and Mt. Princeton interior quartz monzonite, which suggests that the source may have been compositionally uniform for an even longer duration. Similar to the Wall Mountain Tuff, none of the exposed plutons are interpreted to represent the less differentiated portion of the Badger Creek Tuff magma chamber.

The thermal history of the Mt. Aetna quartz monzonite, like that of the Mt. Princeton batholith, was influenced by proximity to the younger intrusions. The age spectrum of the quartz monzonite K-feldspar is characterized by monotonically increasing steps from 30 to 34 Ma (Figure 2.5G). The unconstrained MDD models indicate a reheating event that reaches a maximum temperature of ~250°C at ~31 Ma (Figure 2.7D), consistent with reheating by younger intrusions. K-feldspar from the ring dike yielded a disturbed plateau (Figure 2.5C). Accordingly, the age spectrum was not modeled using the MDD theory.

2.7.3. Young Luecogranites

The youngest magmatic events in the Mt. Aetna caldera complex were the emplacement of numerous luecogranites. All exposures of the luecogranites are located in the southeastern portion of the caldera complex. U/Pb zircon ages of the North Fork and California intrusions are 31.29 ± 0.29 and 30.75 ± 0.24 Ma, respectively. Ar/Ar thermochronology of western and northern outcrops of the Mt. Princeton batholith do not

display evidence for reheating events at ~31 Ma, suggesting that emplacement of luecogranites was limited to the immediate vicinity of the mapped outcrops.

Ar/Ar thermochronology of the luecogranites indicate rapid cooling from magmatic temperatures followed by a protracted thermal history at low temperatures. Biotite ages of the North Fork and California intrusion are 29.65 ± 0.09 and 30.07 ± 0.08 Ma. If U/Pb systematic errors are included, the biotite and zircon ages of the North Fork intrusion are indistinguishable and the biotite and zircon ages of the California intrusion nearly overlap. K-feldspar age spectra from the luecogranites samples indicate a protracted thermal history (Figure 2.5 H, K, and L). For all three samples, the oldest ages in the spectrum are approximately the same age as the timing of emplacement. However, the youngest ages in the age spectra are between 20 and 24 Ma. Because of the shallow depth of emplacement, slow cooling through the K-feldspar closure temperature is not likely. MDD unconstrained models of the three samples (Figure 2.7E-G) indicate a major reheating event between 27 and 29 Ma and numerous, low-temperature reheating events as young as ~20 Ma. These reheating events are not correlated to known magmatic events. Thus, the youngest ages observed in the age spectra maybe related to reheating events due to the emplacement of unexposed intrusions or possibly K-feldspar recrystallization (Lovera et al., 2002).

2.8. Conclusions

U/Pb and Ar/Ar ages of volcanic and plutonic rocks exposed at the Mt. Aetna caldera complex provide insight into the duration and rates of caldera-related magmatism and the emplacement history of a subcaldera batholith. Sanidine single-crystal laser-

fusion analyses constrain the timing of caldera eruptions. The ages of the Wall Mountain Tuff and Badger Creek Tuff are 37.25 ± 0.08 and 34.26 ± 0.06 Ma, respectively. LA-ICP-MS U/Pb zircon ages of the exposed plutons range from 36.38 ± 0.40 to 30.75 ± 0.24 Ma. The Ar/Ar ages of volcanic rocks and the U/Pb ages of pluton rocks indicate that magmatism at the Mt. Aetna complex spanned a minimum duration of 6.5 Ma. During the evolution of the caldera complex magmatic rates varied from periods of low magmatic flux, which resulted in the emplacement of plutons, to high magmatic flux, which resulted in caldera eruptions.

With the exception of the Mt. Aetna quartz monzonite and ring dike, all the caldera-related intrusions apparently represent pre- and/or postcaldera caldera magmatism. Though the Wall Mountain Tuff and Mt. Princeton batholith connection has been previously interpreted as a classic example of the volcanic-plutonic rock pair produced by in-situ differentiation of a large-volume magma chamber in the upper crust (Shannon, 1988; Lipman, 2007), the batholith is in fact too young to be the source for the tuff. Additionally, the U/Pb ages suggest the batholith was emplaced as downward stacking sheets. Though emplacement of the Mt. Princeton batholith may have been punctuated by periods of high intrusive rates, the average emplacement rate of the exposed Mt. Princeton intrusion was too slow to have sustained a large magma chamber capable of differentiation or a large-volume eruption. This suggests that the numerous phases of the Mt. Princeton batholith acquired chemical characteristics at deeper levels in the crust. During postcaldera incremental emplacement of the Mt. Princeton batholith, the Wall Mountain Tuff caldera and any nonerupted magma chamber intrusions were eroded away. This work challenges the hypothesis that caldera-forming rhyolitic ignimbrites

represent a silicic cap that differentiated from a large volume of crystal mush. The absence of a coeval residual mush for the Wall Mountain Tuff suggests that these silicic magmas were generated in a deep crustal source. Though in situ differentiation in the upper crust certainly occurs, the assumption that granodiorite plutons spatially associated with calderas necessarily represent the residual crystal mush is incorrect. Our research illustrates the importance of establishing both geochemical and temporal relationships of caldera-related plutons and ignimbrites.

The Mt. Aetna quartz monzonite and ring dike are the only intrusions that are interpreted to represent nonerupted magma from the Badger Creek Tuff magma chamber. Both intrusions are compositionally similar to the Badger Creek Tuff, but contain zircons ~500 ka older than the Ar/Ar sanidine eruption age. This suggests that the Badger Creek Tuff magma chamber was incrementally assembled in the upper crust and was a long-lived feature. Prior to eruption, the caldera magma chamber was compositionally uniform but chronologically heterogeneous. Though the ring dike and Mt. Aetna quartz monzonite are interpreted to have been part of the Badger Creek magma chamber, the intrusive units are not interpreted as a residual crystal mush.

CHAPTER 3: MAGMATIC HISTORY OF THE ORGAN CALDERA COMPLEX AND COMPARISON TO THE RIO GRANDE RIFT FAULTED QUESTA AND MT. AETNA CALDERA COMPLEXES

3.1. Abstract

The combination of new Ar/Ar and U/Pb ages and published geochemistry of the volcanic and plutonic rocks of the Organ caldera complex provides a framework for understanding the origin of these silicic magmas. The Organ caldera complex erupted three ignimbrites: the 36.45 ± 0.08 Ma Cueva Tuff, the 36.23 ± 0.14 Ma Achenback Park Tuff, and the 36.03 ± 0.16 Ma Squaw Mountain Tuff. The ignimbrite sequence is zoned from a crystal-poor, high-SiO_2 rhyolite at the base to a crystal-rich, low-SiO_2 rhyolite at the top. The ignimbrite sequence is intruded by the zoned Organ Needle pluton, which has previously been interpreted to be the nonerupted silicic cap and less differentiated residual crystal mush of the caldera forming magma chamber. U/Pb and Ar/Ar dating of the various phases of the Organ Needle pluton indicate that these silicic magmas were generated via shallow crustal in-situ differentiation. U/Pb zircon and many Ar/Ar biotite ages of the different phases of the Organ Needle pluton are temporally indistinguishable from the Squaw Mountain Tuff eruption age, indicating that this pluton was emplaced and rapidly cooled during or shortly after the youngest caldera eruption. Volcanism continued after caldera eruptions until at least 35.7 Ma. Three silicic postcaldera plutons were emplaced between 36.0 and 34.3 Ma. Multiple diffusion domain thermal modeling of plutonic K-feldspar suggest reheating events related to postcaldera magmatism at 34

Ma, 30-32 Ma, and as young as 26 Ma. The temporal-chemical relationship of volcanic and plutonic rocks of the Organ caldera complex contrasts with the volcanic-plutonic relationship at the Questa and Mt. Aetna caldera complexes, two recently examined Rio-Grande-Rift faulted caldera systems, where silicic magmas were not apparently generated by shallow differentiation.

3.2. Introduction

Determining the genesis of caldera-related silicic magmas and the origin of compositional zonation patterns of ignimbrites is central to our understanding of caldera-forming magma chambers (Smith, 1979; Hildreth, 1981; Lipman, 1984; Bachmann and Bergantz, 2004; Lipman, 2007; Quick et al., 2009). Though the hazards associated with calderas are understood (Francis and Oppenheimer, 2004; Miller and Wark, 2008; Self and Blake, 2008), caldera eruptions are infrequent and have not been directly observed. Because of this, most caldera magmatism models are developed using extinct caldera systems. Previous studies have shown that ignimbrites display variations in mineral modality, phenocryst contents, and major- and trace-element geochemistry (Eichelberger, 2000; Hildreth and Wilson, 2007; Bachmann and Bergantz, 2008). Some large-volume caldera-forming ignimbrites are compositionally zoned and others are nonzoned (Bacon and Druitt, 1988; Seager and McCurry, 1988; Dunbar et al., 1989; Bachmann et al., 2002; Hildreth, 2004; Lipman, 2007). Despite decades of research, the origin of the 10^2-10^4 km^3 of silicic magma erupted during caldera collapse and the processes that occur within caldera-forming magma chambers remain controversial (Glazner et al., 2004; Annen et

al., 2006; Eichelberger et al., 2006; Bachmann et al., 2007a; Kennedy and Stix, 2007; Knelsel and Duffield, 2007).

The compositional zonation patterns observed in ignimbrites are generally interpreted to represent varying degrees in-situ differentiation of magma in the upper crust (Smith, 1979; Hildreth, 2004; Bachmann and Bergantz, 2008). By this model, when the crystal content of a magma chamber is low, convective mixing can efficiently homogenize compositional variations (Jellinek et al., 1999; Bachmann and Bergantz, 2008). However, as a magma chamber cools and crystal percentages increase to 40-60%, mixing via convection eventually ceases. The quasi-rigid framework of crystals begins to compact and silica-rich melt is extracted from the more-mafic, crystal-rich region of the magma chamber (Bachmann et al., 2002; Miller and Miller, 2002; Bachmann and Bergantz, 2004; Walker Jr. et al., 2007). This process compositionally and mineralogically stratifies the caldera-forming magma chamber. Silica-rich, crystal-poor magma accumulates at the top of the magma chamber, leaving behind crystal-rich, silica-poor residual crystal mush. Previous studies have suggested that 1) compositionally zoned ignimbrites represent the eruption of both the silica-rich cap and some volume of silica-poor residual mush, 2) nonzoned rhyolitic ignimbrites represent the eruption of only the silicic cap, and 3) crystal-rich dacites represents eruption of the crystal-mush before liquid-residual extraction occurs Bacon and Druitt, 1988; Halliday et al., 1991; Bachmann et al., 2002, Bachmann and Bergantz, 2004; Hildreth, 2004; Bachmann and Bergantz, 2008). Accordingly, the nonerupted, less-differentiated, residual crystal mush is preserved in the plutonic record (Bachmann et al., 2007; de Silva and Gosnold, 2007).

Although the proposed hypothesis discussed above is accepted by many, recent studies have questioned whether this is the only mechanism that can generate caldera-related silicic magmas (Coleman et al., 2004; Glazner et al., 2004; Annen, 2006; Knessel and Duffield, 2007; Glazner et al., 2008; Tappa et al., in press). Models that suggest voluminous silicic magmas originate via in-situ differentiation were largely developed using only the volcanic record (Smith, 1979; Hildreth, 1981; Bacon and Druitt, 1988; Lipman et al., 1996; Bachmann and Bergantz, 2004). However, volcanic rocks represent a limited view of the entire magmatic plumbing system. Processes that generate silicic melts are also recorded in plutonic rocks. Many studies of the intrusive record have shown that plutons are incrementally emplaced into the upper crust and do not represent the crystal-rich regions of magma chambers where melt was extracted to feed voluminous silicic eruptions (Coleman et al., 2004; Glazner et al.,2004; Michel et al., 2008, Annen, 2009). Studies have also shown that many plutons are emplaced after the caldera-forming event and are not related to the caldera-forming magma chamber (Lipman, 1984; Lipman et al., 1986; Lipman, 2007; Tappa et al., in review; Zimmerer and McIntosh, in review).

An alternative approach to developing caldera magmatism models is to determine the connection between the volcanic and plutonic records. Establishing the temporal and chemical relationship of caldera-related volcanic and plutonic rocks provides a framework for understanding caldera-related magmatism and testing hypotheses that explain the origin of caldera-related silicic magma. However, this approach requires sufficient exposures of both volcanic and plutonic rocks of the same caldera system, which is rare in the geologic record.

Faulting, uplift, and erosion along the flanks of the Rio Grande rift have exposed the intracaldera sequence and numerous subvolcanic intrusions at three caldera systems. These systems include: the Organ caldera (south-central NM), the Questa caldera (north-central NM), and the Mt. Aetna (central CO). In addition to the exceptional exposures, the ignimbrites display different compositional zonation patterns. The Organ caldera erupted a zoned ignimbrite sequence, whereas both the Questa and Mt. Aetna caldera complexes erupted non- to weakly zoned rhyolitic and dacitic ignimbrites (Lipman et al., 1986; Seager and McCurry, 1988; Shannon, 1988; McIntosh and Chapin, 2004; Lipman, 2007). The compositional diversity of the ignimbrites and subvolcanic intrusions provide an opportunity to understand the origin of silicic magmas and compositional zoning patterns.

There are two goals of this paper. The first goal is to present new Ar/Ar and U/Pb ages of the volcanic and plutonic rocks of the Organ caldera complex. The geochronology results of the Organ caldera support the published geochemistry, which suggests that the zoned Organ caldera complex ignimbrites originated via upper crustal in-situ differentiation. The results also establish the timing of postcaldera volcanism and plutonism at the Organ caldera. Plutonic K-feldspar age spectra were modeled using the multiple diffusion domain (MDD) theory to establish thermal histories of the intrusive complex and detect reheating events by emplacement of postcaldera plutons that are not exposed. The second goal is to compare and contrast the volcanic-plutonic connection at Organ caldera complex to the recently investigated Questa and Mt. Aetna caldera systems in order to asses magmatic processes at different caldera systems.

3.3. Geologic background and previous studies of the Organ caldera complex

The Organ caldera complex (Figure 3.1) is exposed in the Organ Mountains, south-central New Mexico, at the eastern margin of the 40,000 km^2 Mogollon-Datil volcanic field (Dunham, 1935; Seager and McCurry, 1988; McIntosh; 1992). The Mogollon-Datil volcanic field is an erosional remnant of a discontinuous mid-Tertiary volcanic belt that extends from central Colorado to central Mexico (Chapin et al., 2004). Mid-Tertiary silicic caldera volcanism (i.e., the ignimbrite-flare up) of southwestern North America is attributed to slab foundering following Laramide flat-slab subduction of the Farallon plate beneath the North American plate, which allowed hot asthenosphere to contact the hydrated North American lithosphere and induce widespread magmatism (Humphreys et al., 2003; Chapin et al., 2004). Following the cessation of caldera magmatism, regional extension eventually led to the formation of Rio Grande rift (Baldridge et al., 1995). Rio-Grande-rift-related faulting exposes both intracaldera volcanic units and the subcaldera batholith at the Organ Caldera complex (Seager, 1981; Seager and McCurry, 1988), similar to the Questa and Mt. Aetna caldera systems (Lipman et al., 1986; Meyer and Foland, 1991; Shannon, 1988).

The volcanic rocks exposed at the Organ caldera complex consist of incomplete pre- and postcaldera volcanic records and a relatively well-exposed intracaldera ignimbrite sequence. Similar to most caldera systems, catastrophic caldera collapse eruptions were preceded by intermediate composition volcanism (Seager and McCurry, 1988; Colucci et al., 1991). Precaldera volcanic rocks were erupted onto the mid-Tertiary surface, which includes Paleozoic sediments and Precambrian granites and metamorphic rocks. The precaldera volcanic deposits, named the Orejon Andesite (Dunham, 1935),

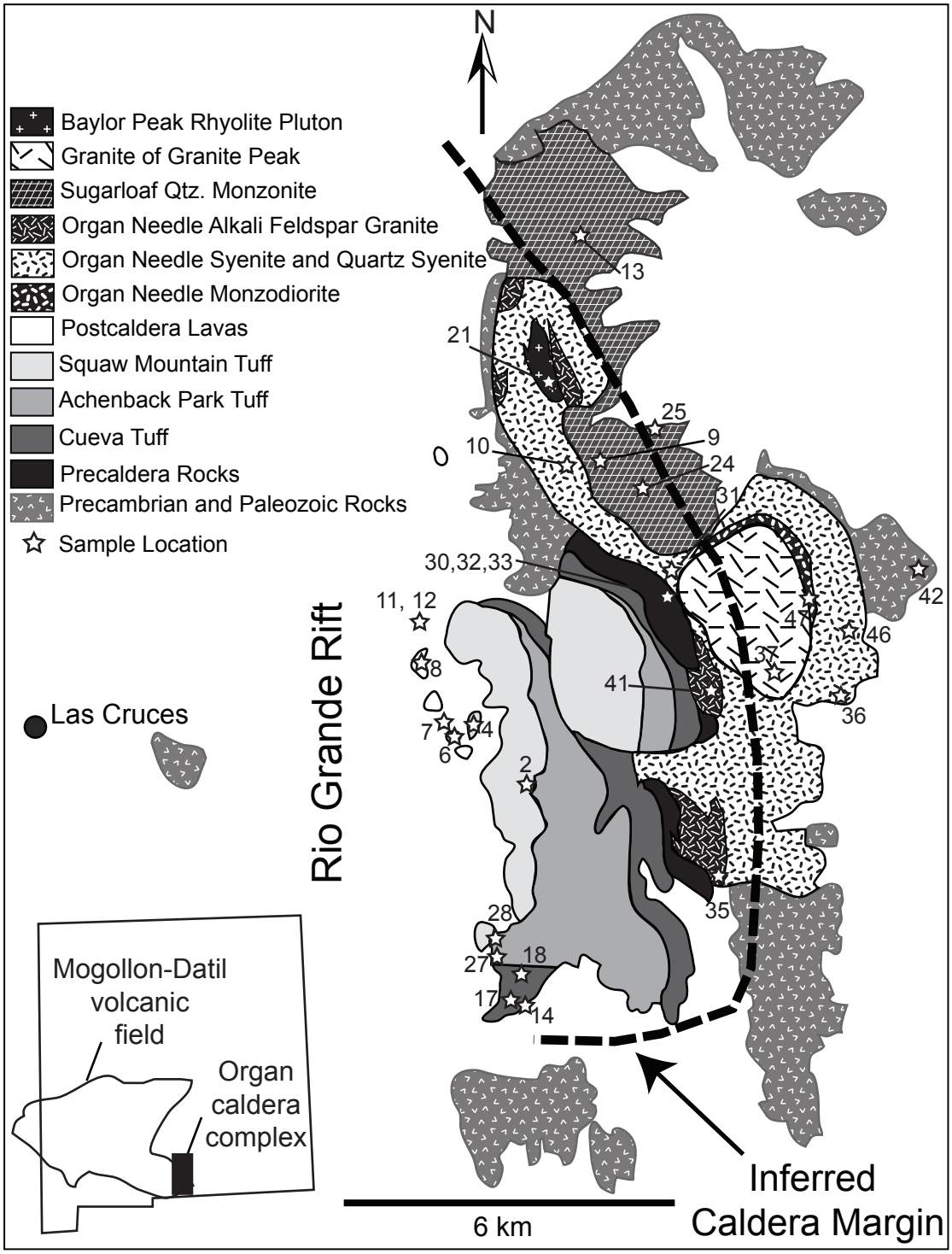

Figure 3.1. Simplified geologic map of the Organ caldera complex modified from Seager (1980) and Verplanck et al. (1999). Precambrian rocks consist of granites and foliated metamorphic rocks and Paleozoic rocks include lithologically diverse sedimentary rocks.

consist of highly altered lavas, lahar breccias, and small-volume pyroclastic deposits. Postcaldera volcanism was characterized by numerous eruptions of rhyolitic and dacitic lavas. Seager (1981) named the postcaldera volcanic rocks the 'west-side lavas' because exposures are limited to isolated outcrops located in the western foothills of the Organ Mountains.

Three caldera-collapse-related ignimbrites are located at the Organ caldera complex. From oldest to youngest the units are: the Cueva Tuff, the Achenback Tuff, and Squaw Mountain Tuff. The total volume of the ignimbrites is estimated to be between 500 and 1,000 km^3. Deposits of epiclastic rocks are interlayered between each unit indicating that each ignimbrite was emplaced during temporally distinct eruptions. The ignimbrite sequence thins from 3.3 km in the west to only several hundred meters along the contact with the Organ Needle pluton. The geometry of the intracaldera deposits led Seager (1981) and Seager and McCurry (1988) to suggest that the Organ caldera formed during trap-door style collapse. The western margin of the caldera, which presumably had the greatest fault offset, is now buried beneath Rio Grande rift sediments. The intracaldera ignimbrite sequence, as a whole, is zoned from a crystal-poor, high-SiO_2 rhyolite at the base (i.e., Cueva Tuff) to a crystal-rich, low-SiO_2 rhyolite at the top (i.e., Squaw Mountain Tuff). The zonation pattern of the caldera-collapse-ignimbrite sequence has been interpreted to represent episodic eruptions from a zoned pre-caldera-collapse magma chamber (Seager, 1981; Seager and McCurry, 1988).

Each Organ caldera complex ignimbrite displays different compositional zonation patterns. The Cueva Tuff is a lithic-rich, compound ignimbrite, consisting of multiple cooling units that are interlayered with minor amounts pyroclastic fall deposits. The

composition of the lithics is dominated by rhyolite, but sparse granite, gneiss, and andesites fragments are also common. The Cueva Tuff is generally crystal poor (< 1% phenocrysts). However, there are two crystal-rich (10-20% phenocrysts) intervals in the middle of the unit. The Cueva Tuff has a SiO_2 content of ~77% and is the most silicic of the three caldera collapse ignimbrites. The Achenback Park Tuff is less-silicic and displays only slightly more compositional variation than the Cueva Tuff. The SiO_2 content of the Achenback Park Tuff varies from 74% at the top to 75% at the base. The Achenback Park Tuff is also crystal-poor, but unlike the Cueva Tuff it contains very few lithic fragments. The last ignimbrite erupted from the Organ caldera complex was the Squaw Mountain Tuff, which is the least silicic and displays the most major and trace-element variation of the three caldera-related ignimbrites. The SiO_2 content of the tuff ranges from 72% at the base to 68% at the top of the unit. Chemical zonation correlates with an increase in phenocryst content, from 1-5% at the base to as much as 20% at the top (Seager, 1981; Seager and McCurry, 1988).

Though previous research of the Organ caldera established the volcanic stratigraphy (Dunham, 1935; Seager, 1981), a comprehensive geochronology of the eruptive history did not exist. Sanidine incremental-heating analysis of the Cueva Tuff and Squaw Mountain Tuff yielded ages (all ages reported in this study are calculated relative to the Fish Canyon Tuff sanidine standard FC-2 = 28.201 Ma; Kuiper et al. 2008) of 36.68 ± 0.13 and 36.22 ± 0.12 Ma, respectively (McIntosh et al., 1992). The timing of pre- and postcaldera volcanism, as well as the age of the Achenback Tuff had not been determined.

The Organ Needle pluton, the largest exposed intrusion at the Organ caldera complex, has been interpreted to record the differentiation and crystallization of an upper crustal magma chamber (Seager and McCurry, 1988; Verplanck et al., 1995; 1999). The Organ Needle pluton crops out along the eastern margin of the caldera complex and probably intruded along caldera ring-faults. The Organ Needle pluton is compositionally zoned from a monzodiorite at the base to an equigranular syenite in the interior and inequigranular syenite phases located at the margins of the intrusions. Cupolas of alkali feldspar granite are located at the top of the intrusion. The contact between the alkali feldspar granite and the underlying syenite is gradational. Geochemical studies indicate that the equigranular syenite has higher ε_{Nd} and lower $^{87}Sr/^{86}Sr$ values (-2 and 0.7060, respectively) than the monzodiorite, inequigranular syenite, and alkali feldspar granite (-5 and 0.7085, respectively; Verplanck et al., 1995; 1999). Previously proposed models suggest that the equigranular syenite formed during closed-system fractionation of a mafic source, whereas, the inequigranular syenite formed later from a crustal-contaminated mafic source (i.e., the monzodiorite), migrated along the walls of the chamber and finally differentiated into the alkali feldspar granite near the roof (Seager and McCurry, 1988, Yanicak, 1992; Verplanck et al., 1995; 1999). The geochemical similarities between the Squaw Mountain Tuff and alkali feldspar granite suggest that the granite may be the nonerupted intrusive equivalent of the tuff (Seager and McCurry, 1988; Verplanck et al., 1995, 1999).

Numerous postcaldera silicic intrusions cross-cut the Organ Needle pluton. The largest postcaldera intrusion is the Sugarloaf Peak quartz monzonite pluton. The Sugarloaf Peak pluton is compositionally homogenous, but contains abundant aplitic

dikes at high structural levels and mafic enclaves swarms at the deepest structural levels. The contact between the Sugarloaf Peak and Organ Needle pluton is sharp, indicating that the latter was cool during emplacement of the Sugarloaf Peak pluton. The Granite of the Granite Peak is a cylindrical intrusion that cross cuts the monzodiorite and equigranular syenite phases of the Organ Needle pluton. Similar to the Sugarloaf Peak pluton, contacts with the Organ Needle pluton are sharp, indicating a large thermal difference between the two intrusions during emplacement. The smallest postcaldera intrusion is the Baylor Peak rhyolite porphyry, which is exposed in the northern region of the Organ caldera complex (Seager and McCurry, 1988).

The timing of pluton emplacement at the Organ caldera complex is not well constrained. The geochemical similarity between the Squaw Mountain Tuff and Organ Needle pluton, as well as the gradational contacts of the Organ Needle phases, suggest that all the phases of the Organ Needle Pluton are temporally similar to the Squaw Mountain Tuff. The relative ages of the plutons indicate the Organ Needle pluton is the oldest pluton. There are no cross cutting relationships between any of the postcaldera plutons. K/Ar ages of the Sugarloaf Peak pluton and dikes that cross-cut the intrusion suggest it was emplaced between 34.4 and 32.1 Ma (Loring and Loring; 1980).

3.4. Methods

Forty-eight volcanic and plutonic rock samples were collected as part of this study. Appendix 3.1 contains the sample names, lithologic unit, and UTM coordinates. Pre-, syn-, and postcaldera volcanic rocks were sampled to obtain a representative suite for the volcanic record. Multiple samples of the various phases of the Organ Needle

pluton and two or more samples of each postcaldera pluton were collected. Additionally, one sample of the Precambrian porphyritic granite was collected. From this suite, 32 samples were selected for U/Pb and/or Ar/Ar analyses. Mineral separates were prepared using standard rock crushing, acid, magnetic, and mineral density techniques. Optical picking assured pure separates. Seven zircon separates were dated using the laser ablation multicollection inductively coupled plasma mass spectrometry (LA-MC-ICP-MS) U/Pb method. Forty-seven mineral separates (8 sanidine, 17 biotite, 1 plagioclase, 5 hornblende, 4 groundmass concentrates, and 12 plutonic K-feldspar) were dated using the Ar/Ar technique.

LA-MC-ICP-MS U/Pb zircon dating was conducted at the Arizona Laserchron Center. Zircon mineral separates and the Sri Lanka zircon standard were mounted in 1-inch epoxy disks. Prior to U/Pb dating, the polished pucks were CL imaged. CL images were used to identify xenocrystic cores, mineral and melt inclusions, and magmatic textures. A 193 nm wavelength excimer laser operating with a spot diameter of 30 μm was used to ablate zircons domains. If CL imaging indicated possible xenocrystic cores, inheritance was assessed by ablating both the rim and core of individual zircons. For each sample, 30 to 40 spots were analyzed. Isotopic ratios were measured on a NU Plasma MC-ICP mass spectrometer. The precision of $^{206}Pb/^{238}U$ ages for individual analyses ranged from < 2 to > 30% (1σ level). The low precision of some analyses is attributed to the electrostatic analyzer on the NU mass spectrometer, which can filter up to 40% of the ion beam (Mark Pecha, personal communication, March 2011). Data was reduced using "Agecalc", an excel macro developed by the Arizona Laserchron Center. Because of the large errors associated with some individual analyses, the nominal cutoff of 10%

$^{206}Pb/^{238}U$ error for acceptable data was increased to as much as 30% to provide a large enough population for statistical calculations. Only the $^{206}Pb/^{238}U$ ages were used to calculate an age (Gehrels et al., 2008). Zircon crystallization ages were determined using the *TuffZirc* algorithm (Ludwig and Mundil, 2002) of Isoplot v3.7 (Ludwig, 2009). The asymmetric *TuffZirc* errors are useful in describing the source(s) of age dispersion. A large positive uncertainty suggests more complexity related to xenocrystic or antecrystic contamination, whereas a large negative uncertainty suggests more complexity related to Pb-loss (Ludwig, 2009). Gehrels et al. (2008) and Johnston et al., (2010) provide comprehensive information about the LA-MC-ICP-MS method. Additional information can be found on the Arizona Laserchron Center website (https://sites.google.com/a/laserchron.org/laserchron/home/).

Ar/Ar dating was performed at the New Mexico Geochronology Research Laboratory located at the New Mexico Institute of Mining and Technology. Mineral separates were irradiated with the interlaboratory FC-2 sanidine standard (28.201±0.046 Ma; Kuiper et al., 2008) in a known geometry. Single crystals of sanidine were fused using a focused CO_2 laser. Six crystals from each monitor position in an irradiation tray were analyzed to calculate the neutron flux. Fifteen crystals of each Organ sanidine separate were analyzed to calculate a weighted mean age. Biotite, plagioclase, hornblende, and groundmass concentrate separates were step-heated using a defocused CO_2 laser. Plutonic K-feldspar separates were incrementally heated in a double-vacuum Mo resistance furnace. Heating schedules for K-feldspar separates used the isothermal duplicate heating technique, which is useful for assessing excess ^{40}Ar hosted within fluid inclusions (Harrison et al., 1994). Gas from the heated samples was exposed to SAES

getters in an all-metal, fully automated extraction line to remove reactive gases. Cleaned gas was then expanded into a MAP 215-50 mass spectrometer for isotope ratio measurements. McIntosh et al. (2003) provides additional information for the typical operating procedures at the New Mexico Geochronology Research Laboratory.

3.5. Results

3.5.1. U/Pb geochronology

U/Pb ages are summarized in Table 3.1. The corresponding analytical data tables and *TuffZirc* plots are located in Appendix 3.2. U/Pb ages ranged from $36.48^{+0.48}_{-0.46}$ to $34.28^{+0.54}_{-0.51}$ Ma. Uncertainties of the U/Pb ages ranged from 0.6 to 3.7%. Systematic errors during the U/Pb dating session ranged from 1.0 to 1.1 %. Zircon ages are geologically consistent with relative ages of the intrusions constrained by cross cutting relationships. Zircon ages are interpreted to represent the timing of zircon crystallization during pluton emplacement.

Zircon crystallization ages from the Organ Needle Pluton ranged from $36.48^{+0.48}_{-0.46}$ to $34.93^{+0.89}_{-1.29}$ Ma. U/Pb ages from the structurally highest, lowest, and margins of the Organ Needle pluton (ORGAN-41, -45, and -46, respectively) are statistically indistinguishable from each other. The U/Pb age of the Organ Needle pluton equigranular syenite (ORGAN-10) yielded an age of $34.93^{+0.89}_{-1.29}$ Ma. Gradational contacts between the alkali feldspar granite and the equigranular syenite indicate that the two phases are coeval. The large negative uncertainty of the equigranular syenite may indicate that the slightly younger age is related to Pb-loss.

Table 3.1. Summary of Organ caldera LA-ICP-MS U/Pb zircon ages

Sample	Unit	Age (Ma)[§]	Internal Error[†]	External Error[††]	Comments
Organ Needle pluton					
ORGAN-41	ONP alkali feldspar granite	36.48	+0.48/-0.46	+0.62/-0.61	structurally highest
ORGAN-45	ONP monzodiorite	36.13	+0.55/-0.23	+0.66/-0.43	structurally lowest
ORGAN-46	Inequigranular ONP syenite	35.53	+0.53/-0.38	+0.64/-0.52	
ORGAN-10	Equigranular ONP syenite	34.93	+0.89/-1.29	+0.97/-1.35	Pb-loss
Postcaldera plutons					
ORGAN-37	Granite of Granite Peak	35.24	+0.68/-0.30	+0.77/-0.46	intrudes ONP monzodiorite
ORGAN-13	Sugarloaf Peak qtz. Monz.	35.31	+0.43/-0.39	+0.58/-0.55	youngest intrusion
ORGAN-9	Sugarloaf Peak qtz. Monz.	34.28	+0.54/0.51	+0.66/-0.64	youngest intrusion

§ - Ages and errors calculated using the TuffZirc algorithms described in Ludwig (2003). Ages calculated relative to Sri Lanka Zircon (564±4 Ma), ^{238}U and ^{235}U decay constants equal to 9.8485×10^{-10} and 1.55125×10^{-10} yr-1, and $^{238}U/^{235}U$ equal to 137.88.

† - Internal errors include analytical measurements

†† - External errors include decay constants, age of standard, fractionation factor, and common Pb correction

Two postcaldera plutons were dated using the LA-ICP-MS U/PB zircon dating technique. Zircons from one sample of the Granite of Granite Peak pluton yielded an U/Pb age of $35.24^{+0.68}_{-0.30}$ Ma. Zircons from two samples of the Sugarloaf Peak pluton yielded statistically distinguishable ages of $35.31^{+0.43}_{-0.39}$ and $34.28^{+0.54}_{-0.51}$ Ma.

Zircons in Organ-caldera-related intrusions lack evidence for significant Precambrian xenocrystic inheritance. Verplanck et al. (1995; 1999) suggested that compositional zoning of the Organ Needle pluton was generated by sidewall crystallization and fractionation of a parental magma combined with assimilation and partial melting of 1.4-1.7 Ga Precambrian granite. The absence of Precambrian zircon cores suggests inherited zircons dissolved following incorporation into the magma chamber (Watson and Harrison, 1983). Only one zircon core in ORGAN-41, the alkali feldspar granite, yielded a statistically different age from the bulk population. The analysis of this core yielded an age of ~262 Ma. This analysis may represent a mixing age between a Precambrian zircon core and mid-Tertiary zircon rim. Alternatively, the age of this core may indicate that some Permian sedimentary rocks, which crop out in the southern Organ Mountains, were assimilated into the Organ Needle pluton.

3.5.2. Ar/Ar geochronology and thermochronology

Forty-seven volcanic and plutonic K-bearing mineral separates were dated using the Ar/Ar technique. Table 3.2 summarizes the Ar/Ar results. Ages were calculated using FC-2 = 28.201 (Kuiper et al., 2008) and $^{40}K\ \lambda_{total} = 5.463x10^{-10}\ yr^{-1}$ (Min et al., 2000). The error is reported with and without propagating the uncertainty of the ^{40}K decay constant. Propagation of decay constant uncertainty into the error calculation greatly increases the errors. Ages and corresponding errors will be discussed excluding decay

Table 3.2. Summary of the Ar/Ar ages for the Organ caldera complex

Caldera Stage	Sample	Unit	Mineral[1]	Age calculation method[2]	Age[3]	Internal Error[4]	External Error[5]
Precaldera volcanism							
		Orejon Andesite		could not determine age			
Caldera-forming ignimbrites							
	ORGAN-18	Cueva Tuff	san	SCLF	36.46	0.05	1.43
	ORGAN-14	Cueva Tuff	san	SCLF	36.45	0.10	1.43
	ORGAN-17	Cueva Tuff	san	SCLF	36.43	0.09	1.43
			unit weighted mean		*36.45*	*0.08*	
	ORGAN-28	Achenback Park Tuff	san	SCLF	36.26	0.09	1.42
	ORGAN-27	Achenback Park Tuff	san	SCLF	36.17	0.12	1.42
			unit weighted mean		*36.23*	*0.14*	
	ORGAN-4	Squaw Mountain Tuff	san	SCLF	36.12	0.10	1.42
	ORGAN-2	Squaw Mountain Tuff	san	SCLF	35.96	0.09	1.41
			unit weighted mean		*36.03*	*0.16*	
Syn-caldera intrusion (Organ Needle Pluton)							
	ORGAN-41	alkali feldspar granite	bt	plt.	36.25	0.12	1.43
		"	kspar	int.; a.l.	34.13	0.22	1.38
	ORGAN-35	"	bt	plt.	36.17	0.12	1.42
	ORGAN-36	equigranular syenite	bt	plt.	35.98	0.14	1.42
	ORGAN-10	"	kspar	int.; a.l.	34.28	0.17	1.40
	ORGAN-46	inequigranular syenite	bt	plt.	35.77	0.14	1.41
	ORGAN-31	equigranular qtz. syenite	bt	plt.	35.19	0.10	1.38
		"	kspar	int.; a.l.	35.04	0.22	1.41
	ORGAN-47	monzodiorite	bt	plt.	35.94	0.13	1.41
	ORGAN-43	"	bt	plt.	35.42	0.12	1.39
	ORGAN-45	"	bt	int.	34.63	0.16	1.35
Precambrian country rock							
	ORGAN-42	porphyritic granite	bt	plt.	36.16	0.15	1.43
Post caldera volcanism							
	ORGAN-6	rhyolitic west-side lava	san	SCLF	35.79	0.09	1.41
	ORGAN-7	dacitic west-side lava	bt	plt.	35.68	0.09	1.40
		"	hbl	plt.	36.13	0.30	1.45
	ORGAN-8	dacitic west-side lava	bt	plt.	35.77	0.08	1.40
		"	hbl	plt.	36.28	0.23	1.44
		"	plag	plt.	36.19	0.21	1.43
	ORGAN-11	dacitic west-side lava	gmc	int.	36.10	0.21	1.42
	ORGAN-12	rhyolitic west-side lava	bt	plt.	35.78	0.09	1.42
Postcaldera intrusions							
	ORGAN-37	Granite of granite peak	bt	plt.	35.41	0.13	1.39
			kspar	int.; a.l.	34.31	0.22	1.34
	ORGAN-24	Sugarloaf Peak pluton	bt	plt.	34.66	0.06	1.36
	ORGAN-9	"	bt	plt	33.60	0.15	1.33
	ORGAN-13	"	bt	plt.	33.48	0.07	1.31
	ORGAN-25	Sugarloaf enclave	bt	plt.	33.46	0.19	1.33
	ORGAN-22	aplite dike in Sugarloaf	kspar	int.; a.l.	31.46	0.24	1.27
	ORGAN-21	Baylor Peak porphyry	kspar	int.; a.l.	34.13	0.10	1.34

1- san (sanidine), bt (biotite), kspar (plutonic K-feldspar), hbl (hornblende), plag (plagioclase), gmc (groundmass concentrate
2- SCLF (single crystal laser fusion; weighted mean), plt. (plateau), int. (integrated age), a.l. (argon loss via reheating)
3 - Age calculated relative to FC-2 equal to 28.201 Ma (Kuiper et al., 2008)
4 - Error (2σ) includes uncertainty in J and irradiation parameters
5 - Error (2σ) includes uncertainty in 40K decay constant $(5.462\pm0.214)\times10^{-10}$ yr^{-1} (Min et al., 2000)

constant error. All Ar/Ar data tables, ideograms, and age spectra are located in Appendix 3.3.

3.5.2.1. Ar/Ar sanidine single-crystal laser-fusion (SCLF)

Samples of the Cueva, Achenback, and Squaw Mountain Tuffs as well as one postcaldera lava flow were dated using the sanidine SCLF technique. Sanidine SCLF ages ranged from 36.46 ± 0.05 to 35.79 ± 0.09 Ma. Figure 3.2 contains the ideograms for the caldera-collapse ignimbrites. Sanidine weighted mean ages are interpreted to accurately represent the timing of eruption. Between two to three samples of each caldera-forming ignimbrite was dated. Results indicate that xenocrystic sanidine and phenocrysts of plagioclase were not dated. Numerous crystals from the Cueva Tuff and Squaw Mountain Tuff had low radiogenic ^{40}Ar yields (i.e., > 95% $^{40}Ar^*$ is a common cutoff for acceptable radiogenic yields). Many of the low radiogenic crystals yielded ages that statistically overlapped with ages from high radiogenic yield crystals. Exclusions of these low radiogenic yield analyses from the age calculation commonly increased the MSWD value. Only crystals with extremely low radiogenic yields (i.e., < 80% $^{40}Ar^*$) were excluded from the age calculation.

3.5.2.2. Ar/Ar laser step-heating

Biotite, plagioclase, hornblende separates, and groundmass concentrates were step-heated using a defocused CO_2 laser. Six representative age spectra are shown in Figure 3.3. Ages were calculated using the plateau or the integrated age calculation methods. A plateau is defined as three or more contiguous steps that contain 50% or more of the ^{39}Ar released from the sample and the ages of those steps are indistinguishable within 2σ limits (Fleck et al., 1977). For samples that did not yield a plateau, the

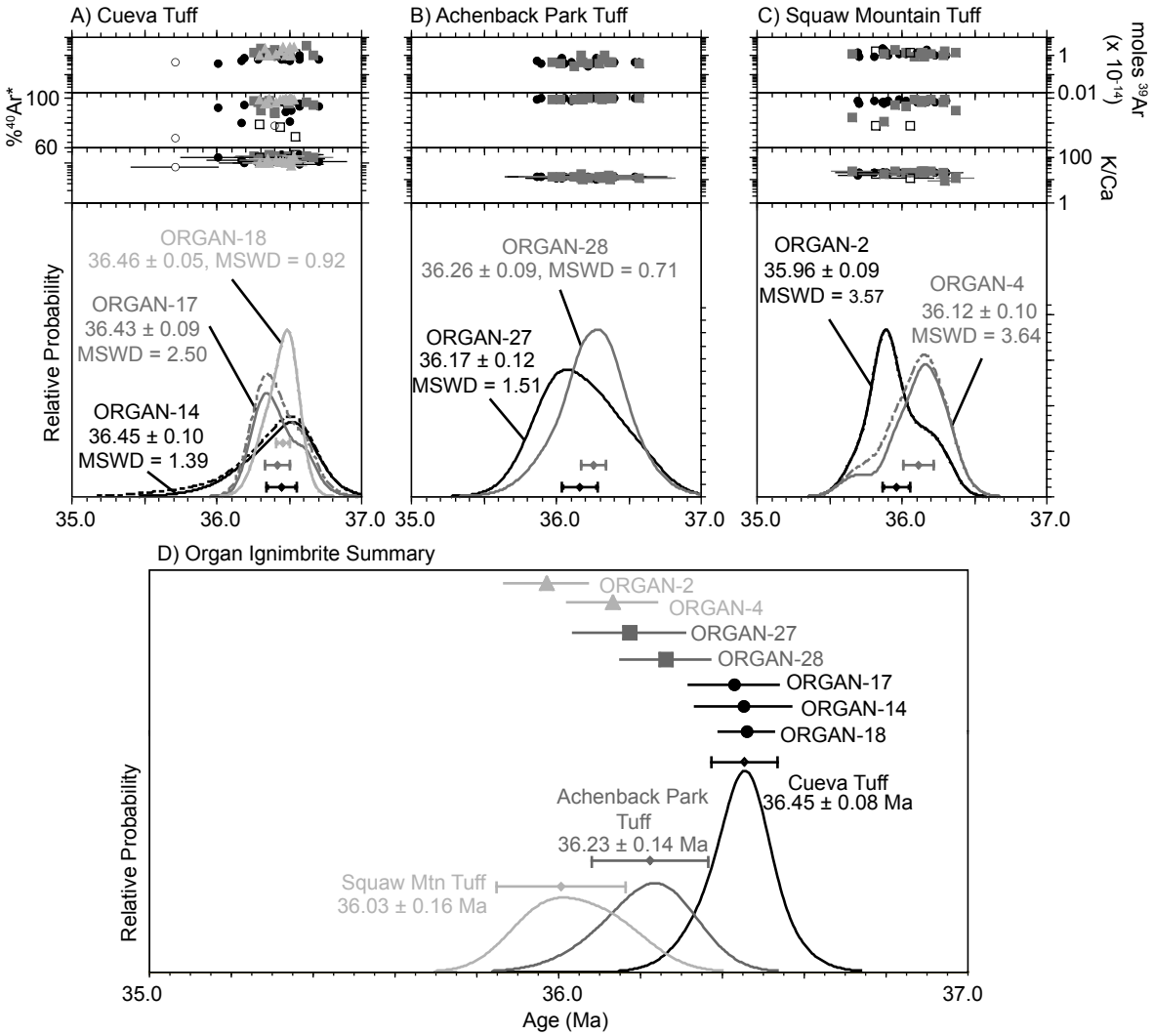

Figure 3.2. Ideograms of the Organ caldera ignimbrites. A) Cueva Tuff, B) Achenback Park Tuff, and C) Squaw Mountain Tuff. D) Summary ideogram for the caldera-forming ignimbrites. All errors are reported at 2σ and do not included error in the ^{40}K decay constant. Auxiliary plots include K/Ca, radiogenic yield (%$^{40}Ar^*$), and moles of ^{39}Ar.

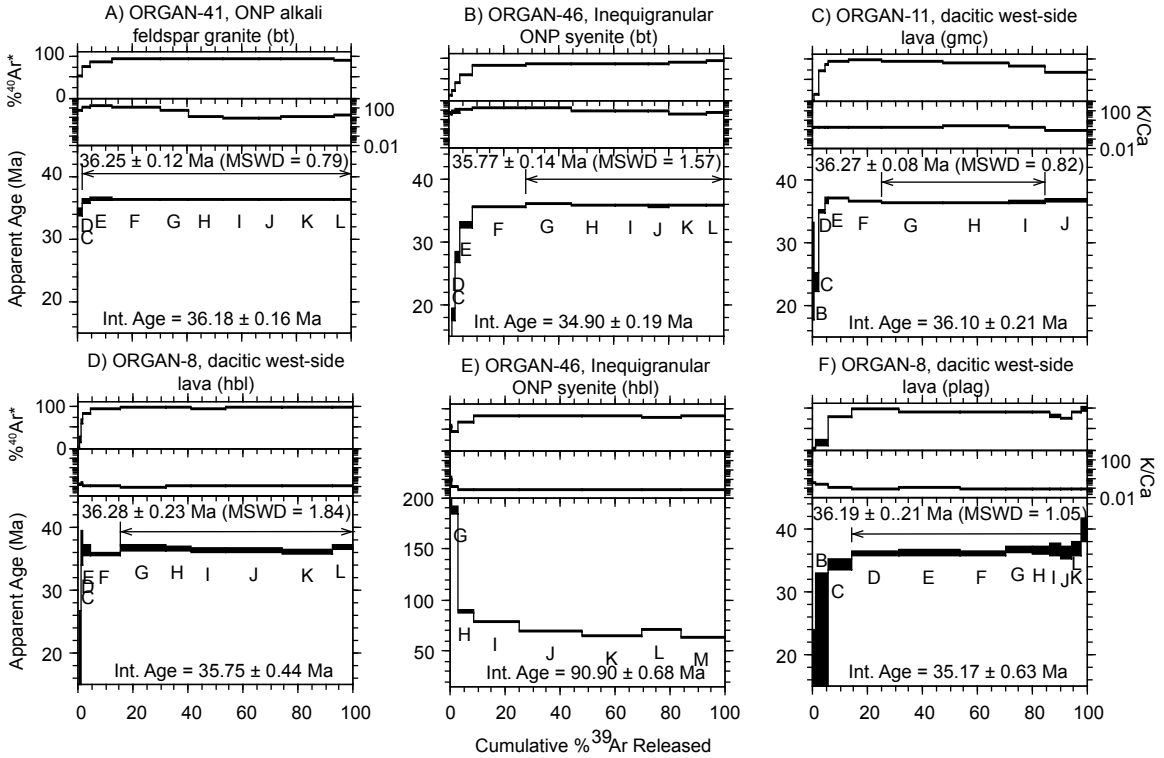

Figure 3.3. Representative age spectra for the Organ caldera biotite (bt), plagioclase (plag), hornblende (hbl), and groundmass concentrate (gmc) analyses. Auxiliary plots include K/Ca and radiogenic yield (%^{40}Ar*).

integrated age of all the steps was used only if it was geologically consistent with field relationships.

Seventeen biotite separates (3 volcanic and 14 plutonic) were step-heated. The ages of volcanic biotite separates are interpreted as the eruption ages, whereas the ages of plutonic biotites are interpreted to represent cooling to 350-300°C (Hodges et al., 1994; McDougall and Harrison, 1999). Sixteen separates yielded a plateau segment. Plateau ages ranged from 36.25 ± 0.12 to 33.46 ± 0.19 Ma. Some of the biotite age spectra contained >95% of the ^{39}Ar released, with only minor discordance between the first one or two steps and the plateau segment (e.g., Figure 3.3A). However, numerous biotite age spectra are characterized by monotonically increasing ages in the initial 10-30% of the ^{39}Ar released, which is then followed by the plateau (e.g., Figure 3.3B). The initial age gradient observed in these biotite analyses is interpreted to represent degassing from slightly altered regions of the biotite crystal during the low power steps.

Only one biotite analysis, ORGAN-45 (see Appendix 3.3), did not yield a plateau. The ages of the steps monotonically increase from ~16 to 36 Ma during the step-heating experiment. The K_2O value for this biotite is 6.1%, which is slightly lower than the 8-10% K_2O content expected for a pristine biotite (McDougall and Harrison, 1999). The integrated age of this sample, 34.63 ± 0.16 Ma, is interpreted to represent the timing of biotite closure.

Four volcanic groundmass concentrated separates were dated to help determine the eruptive history of pre- and postcaldera volcanism. Only one of the four groundmass concentrate sampled yielded geologically reasonable results. Sample ORGAN-11, a dacitic west-side lava, yielded a plateau age of 36.27 ± 0.08 Ma (Figure 3.3C). However,

because this sample is stratigraphically located above the Squaw Mountain Tuff, the plateau age is inconsistent with field relationship. The age spectrum exhibits some characteristics of samples that have experienced ^{39}Ar recoil (Heizler, 1988; Lo and Onstott, 1989). Because some ^{39}Ar was likely recoiled during irradiation, the integrated age, 36.10 ± 0.21 Ma, is used as the eruption age.

Three groundmass separates from the precaldera Orejon andesite yielded disturbed age spectra. Age spectra are characterized by either old steps at the beginning of the spectrum that decrease in age during the ^{39}Ar released and yield integrated ages that are too old to be part of the caldera cycle (e.g., 41-44 Ma) or age spectra with initially young steps that increase in age and yield integrated ages that younger than the overlying units. Age spectra discordance is likely related to alteration by hydrothermal fluid circulation during the emplacement of the Organ Needle pluton (Seager, 1981)

Five hornblende separates, two from volcanic samples and three from plutonic samples, were dated during this study. Both volcanic hornblende age spectra, ORGAN-7 and -8, contained plateau segments (e.g. Figure 3.3D), but are older than the corresponding biotite plateau ages and inconsistent with stratigraphic position. Inaccurate, old ages observed in some Ar/Ar analyses are commonly attributed to excess ^{40}Ar. The ^{40}Ar/^{36}Ar intercept for these two samples do not suggest excess argon. The biotite ages for these two samples are the preferred eruption age.

Three-plutonic hornblende separates yielded discordant age spectra (e.g. Figure 3.3E). Integrated ages for these three samples do not agree with corresponding U/Pb ages or field relationships. Inverse isochron plots have ^{40}Ar/^{36}Ar intercepts greater than atmosphere (i.e., ^{40}Ar/^{36}Ar = 295.5), but the elevated MSWD values suggest that if excess

^{40}Ar is present it is not homogenously distributed. An accurate age could not be determined for these samples.

A plagioclase separate from sample ORGAN-8, a west-side lava, yielded a plateau age of 36.19 ± 0.21 Ma (Figure 3.3F). Similar to the plateau age of the hornblende separate from this sample, the plagioclase plateau age is older than underlying units. The integrated age is 35.17 ± 0.63 Ma, which agrees with field relationships but is imprecise. The corresponding biotite age of this sample is 35.77 ± 0.08 Ma and is preferred eruption age.

3.5.2.3. Ar/Ar K-feldspar analyses and MDD cooling histories

Twelve plutonic K-feldspar separates were dated to determine the low-temperature thermal history of the caldera-related intrusions. Six K-feldspar analyses yielded geologically meaningful results (Figure 3.4). For these six samples, two thermal histories were generated using the multiple domain diffusion technique (Lovera et al., 1989; 1991). Monotonic cooling histories (Figure 3.5 A-F) only allow for cooling from an initially high temperature, whereas unconstrained thermal histories (Figure 3.5 G-L) allow for multiple reheating events. Some age spectra contain contiguous steps that oscillate with respect to age. This is an artifact of the isothermal duplicate step-heating method. The first isothermal duplicate step releases excess ^{40}Ar from fluid inclusions and the second isothermal duplicate step releases gas from the K-feldspar lattice. MDD thermal histories were generated using synthetic age spectra that did not include the first-isothermal duplicate step.

MDD thermal histories provide information on the cooling history of the intrusive suite and indicate protracted postcaldera magmatism. MDD monotonic models indicate

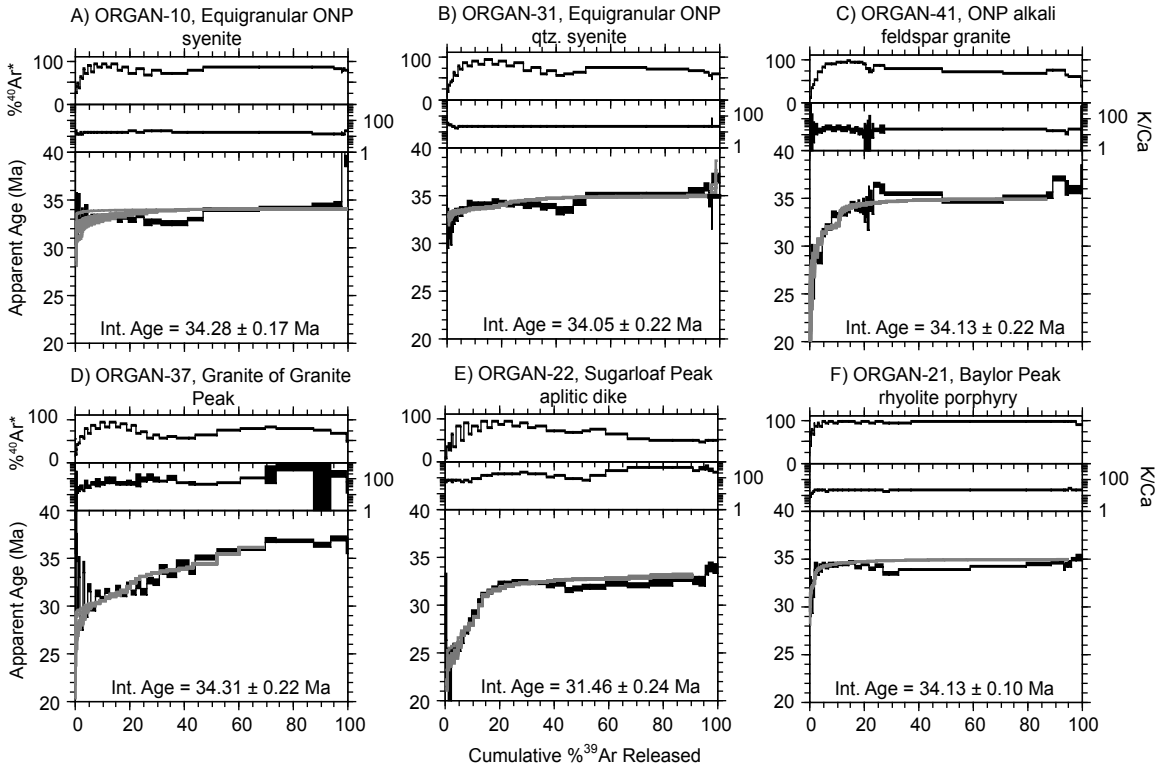

Figure 3.4. Selected age spectra for Organ caldera plutonic K-feldspar. Auxiliary plots include K/Ca and radiogenic yield (%^{40}Ar*). Modeled age spectra used to generated MDD thermal histories are shown in gray.

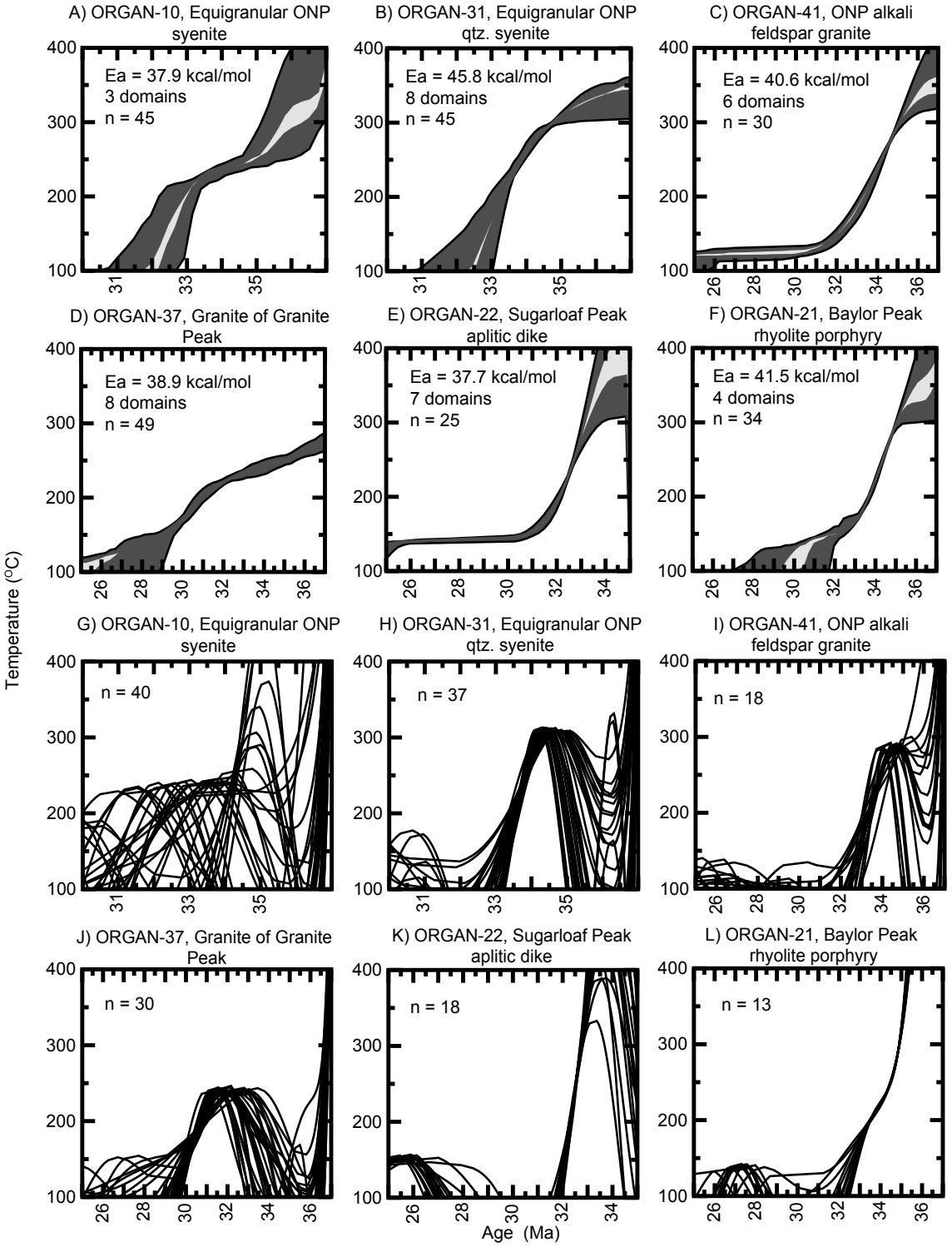

Figure 3.5. MDD thermal models of the Organ caldera plutonic K-feldspar.
A-F) Monotonic MDD cooling histories. The dark gray band is the 90% confidence interval of the entire distribution. The light gray band is the 90% confidence interval of the mean. G-L) Unconstrained MDD thermal histories. Activation energy, number of domains, and the number of thermal histories used to generate each cooling history are also provided.

variable cooling rates for the intrusions. For example, ORGAN-10 (Figure 3.5A) indicates rapid cooling between 36 and 35 Ma, slower cooling between 35 and 33 Ma, and rapid cooling between 33 and 32. K-feldspar from the alkali feldspar granite and an aplitic dike in the Sugarloaf Peak pluton (Figure 3.5C and E, respectively) indicate initially rapid cooling followed by prolonged periods of isothermal conditions. Contrastingly, K-feldspar in ORGAN-31, -37, and -21 (Figure 3.5 B, D, and F, respectively) indicate nearly constant cooling rates through the K-feldspar closure temperatures. Alternatively, unconstrained cooling models suggest that the argon loss observed in the age spectra is related reheating events between 34 and 35 Ma (Figures 3.5 G-I), 30-32 Ma (Figure 3.5 J), and as young as 25-28 Ma (Figures 3.5K and L).

Six K-feldspar analyses were not modeled using the MDD technique. Age spectra for these samples contained abundant medium to high-temperature steps that were older than corresponding Ar/Ar biotite and U/Pb zircon ages or any known magmatic events at the Organ Caldera. Similar results have been observed in other plutonic K-feldspars (Lovera et al., 2002). Anomalously old steps that correspond to high-temperature heating are commonly attributed to excess ^{40}Ar within the largest domains (Foster et al., 1990).

3.6. Magmatic history of the Organ Caldera complex

Volcanic and plutonic rocks exposed at the Organ caldera complex provide an opportunity to study the origin of compositionally zoned caldera-related magmas and assess existing geochemical models for the magmatic evolution of this particular caldera system. Published geochemistry suggests that the Organ Needle pluton represents the emplacement and differentiation of a caldera magma chamber (Seager, 1981; Seager and

McCurry, 1988; Verplanck 1995; 1999). Following differentiation of a more-mafic parental magma, the majority of the silicic cap evacuated the magma chamber during eruption of the 36.0 Ma Squaw Mountain Tuff. Cupolas of the nonerupted silicic cap and residual crystal mush are preserved as the compositionally zoned Organ Needle pluton (Seager and McCurry, 1988; Verplanck et al., 1995; 1999). New U/Pb and Ar/Ar ages (Figure 3.6) support this proposed genetic model. The Ar/Ar age of the Squaw Mountain Tuff, 36.03 ± 0.16 Ma, and U/Pb zircon and most Ar/Ar biotite ages of the various phases of the Organ Needle pluton are statistically indistinguishable. Ar/Ar and U/Pb ages also show that postcaldera volcanism and plutonism commenced shortly after the eruption of the Squaw Mountain Tuff. Postcaldera pluton emplacement continued until at least 34.3 Ma. MDD modeling of multiple plutonic K-feldspar samples indicate reheating events at 34, 30, and as young as 26 Ma. Reheating events are evidence for postcaldera intrusions that are either not exposed or have been eroded.

3.6.1. Precaldera magmatism

Compositionally diverse magmas were erupted prior to the formation of the Organ caldera. The most volumetrically significant precaldera unit is the Orejon Andesite (Dunham, 1935; Seager, 1981; Seager and McCurry, 1988), a sequence of variably altered intermediate composition lava flows, breccias, and minor pyroclastic units. Though the Orejon Andesite is the only precaldera volcanic unit preserved in outcrop, abundant rhyolitic lithic fragments in the basal section of the Cueva Tuff suggests that voluminous rhyolitic magmatism also occurred prior to caldera collapse. Several samples of the Orejon Andesite were collected and dated by the Ar/Ar methods, but age spectra are discordant and do not provide robust ages for the timing of pre-Organ-caldera

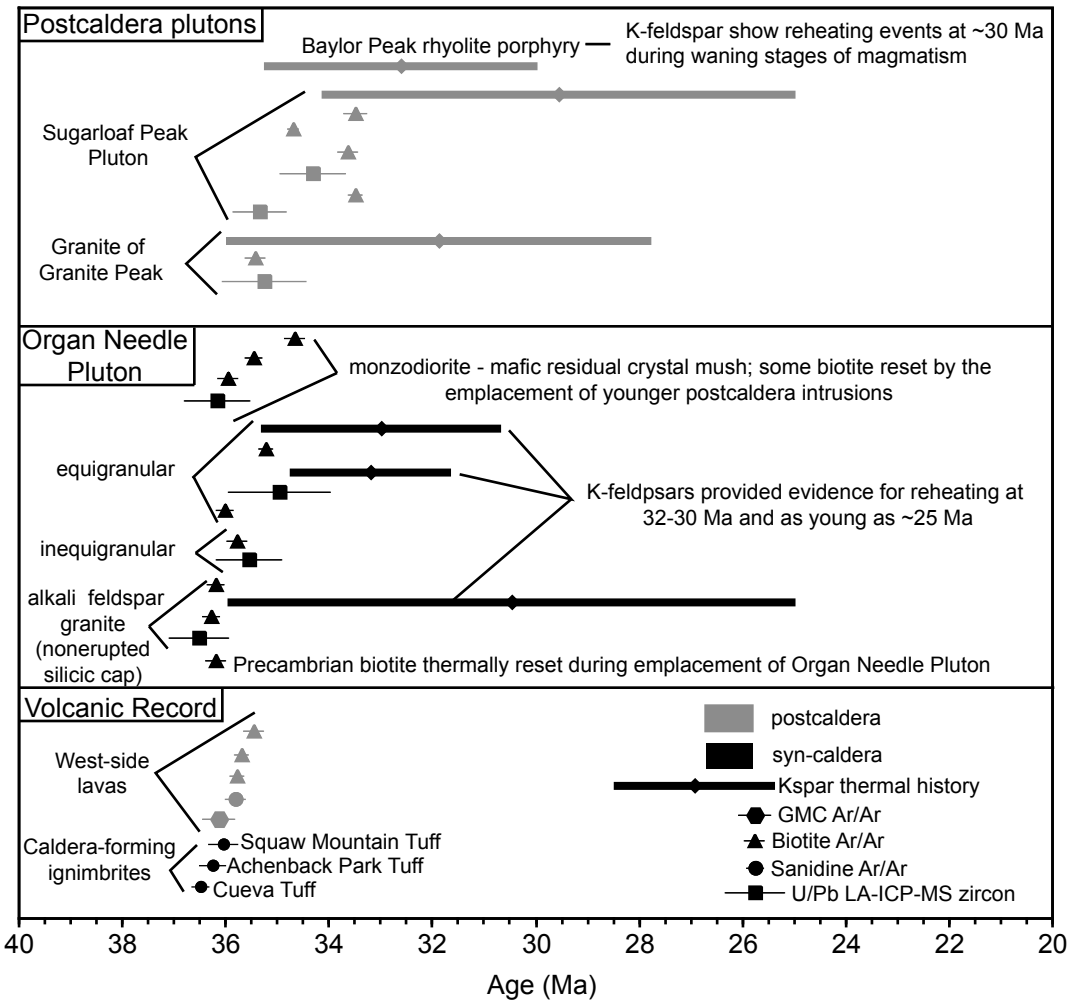

Figure 3.6. Summary of the Organ caldera complex geochronology. U/Pb and Ar/Ar ages are reported at 2σ and do not included error in the associated decay constant. Bold horizontal lines represent the range of ages observed in K-feldspar age spectra that were modeled using the MDD theory.

volcanism. The Orejon Andesite is stratigraphically located beneath the Cueva Tuff, which indicates that precaldera volcanism ended prior to 36.45 ± 0.08 Ma. Studies of precaldera volcanism at similar caldera systems suggest that precaldera volcanism at the Organ Caldera complex probably occurred for several hundred ka to several Ma before eruption of the Cueva Tuff (Jellinek and Depaolo, 2003; Hildreth, 2004; du Bray et al., 2004; Lipman, 2007).

3.6.2. The caldera collapse ignimbrites

The Organ caldera complex ignimbrites were erupted during three distinct collapse events between 36.45 ± 0.08 Ma and 36.03 ± 0.16 Ma (Figure 3.2D). The oldest caldera-forming ignimbrite is the Cueva Tuff. Sanidine SCLF analyses of the Cueva Tuff (n = 3 samples) yield a unit weighted mean age of 36.45 ± 0.08 Ma. Because of the limited exposure, very little evidence exists for the associated caldera structure. The ignimbrite is several hundred meters thick in the southern Organ Mountains and it contains abundant micro- and mesobreccias. These characteristics are common features of many intracaldera tuffs (Lipman; 1976; Cole et al., 2005). Following a period of volcanic quiescence, the Achenback Park Tuff (n = 2 samples) erupted at 36.23 ± 0.14 Ma. Similar to the Cueva Tuff, evidence that the Achenback Park Tuff is intracaldera facies is limited to the exceptional thickness of the unit (~1 km) as well as volumetrically minor microbreccias included in the tuff. The final caldera collapse event erupted the Squaw Mountain Tuff at 36.03 ± 0.16 Ma (n = 2 samples). The Squaw Mountain Tuff is ~1.4 km thick at its maximum. Epiclastic rocks are interlayered between each of the ignimbrites indicate periods of volcanic quiescence following the each of caldera-collapse events (Seager, 1981; Seager and McCurry, 1988).

The geometry of the intracaldera ignimbrite deposits suggests each caldera eruption occurred in a trap-door style collapse. All three ignimbrites display the same eastward-thinning geometry. Exposures of the three caldera-collapse ignimbrites are the thickest in the west outcrops and dramatically thin to only several hundred meters at the contact with the Organ Needle pluton in the east. The greatest offset of the caldera floor occurred along the western caldera margin, which is now buried beneath the Rio Grande rift basin. Trap-door style caldera collapse occurred during the eruption of the Cueva Tuff and each subsequent caldera collapse event probably occurred along existing, structurally weakened, caldera margin faults, producing a nested caldera complex.

The compositional zonation pattern of the intracaldera ignimbrite sequence led Seager and McCurry (1988) to suggest that the Cueva, Achenback, and Squaw Mountain Tuff represent episodic eruptions from a single compositionally zoned magma chamber. The ignimbrite sequence is linearly zoned from a crystal-poor, high-SiO_2 rhyolite at the base to a crystal-rich, low-SiO_2 rhyolite at the top. The increase in phenocrysts and decrease in SiO_2 content from the bottom to the top of the ignimbrite sequence correlates to an increase trace elements (e.g., Sr, Ba, La, and Y). Accordingly, the Cueva Tuff represents the most differentiated magma in the source chamber, whereas the Achenback Park Tuff and Squaw Mountain Tuff represent a transitional composition between the most silicic melt (i.e., Cueva Tuff) and the more-mafic residual crystal mush (Organ Needle pluton). Seager and McCurry (1988) noted slight compositional discontinuities between each ignimbrite, suggesting that after each eruption the magma chamber was slightly modified by in situ (i.e., fractionation and differentiation) and/or open-system (i.e., assimilation and magma recharge) processes.

The established compositional zonation pattern of the Organ caldera ignimbrites, combined with Ar/Ar SCLF dating of the Organ caldera ignimbrites indicates that a large-volume magma chamber resided in the upper crust for ~400 ka, between 36.45 ± 0.08 Ma and 36.03 ± 0.16 Ma. The magma chamber differentiated to generate compositionally diverse magmas and erupted large-volume, caldera-forming ignimbrites. The magma chamber may not have remained above the solidus for the entire eruptive history and likely would have waxed and waned with respect to crystallinity.

Magma residence times have been determined at numerous caldera systems and provide a framework for comparison to the Organ caldera complex ignimbrite sequence. Some published studies indicate that many caldera-forming magma chambers resided in the upper crust for up to several 100 ka prior to eruption. High-precision U/Pb dating of zircons in the 5,000 km^3 dacitic Fish Canyon Tuff indicate ~600 ka of zircon growth prior to the 28.2 Ma caldera eruption (Bachmann et al., 2007b). Likewise, some high-silica rhyolitic ignimbrites yield zircons that are as much as ~300 ka older than the eruption age (Reid et al., 1997; Brown and Fletcher, 1999). In contrast, dating of some other caldera-forming ignimbrites suggest very short magma residence time. Simon et al. (2007) compared U/Pb and U/Th zircon ages to eruption ages for multiple, large-volume silicic eruptions from around the world and determined a median residence time of only 70 ka. Dating of a single sample from earliest erupted material from the compositionally zoned Bishop Tuff yielded an U/Pb zircon age that is indistinguishable from the Ar/Ar sanidine eruption age (770.4±3.9 ka), indicating that the zircons grew very shortly before the eruption (Crowley and Bowring, 2007). The zircon crystallization histories of the less-silicic, late-erupted products were not investigated and thus the magma chamber

residence history for the entire ignimbrite remains unknown. However, numerous small-volume precaldera eruptions that are compositionally linked to the Bishop Tuff occurred for ~ 400 ka prior to the Bishop Tuff eruption, apparently recording assembly of the Bishop Tuff magma chamber during this period (Hildreth, 2004). Some of these results are consistent with the Ar/Ar dating of the Organ caldera ignimbrites, which suggest a minimum ~400 ka lifetime for the compositionally evolving magma chamber.

3.6.3. The Organ Needle Pluton

Following the final episode of caldera collapse during the eruption of the Squaw Mountain Tuff, the Organ Needle pluton intruded into the eastern caldera margin and intracaldera sequence. The compositionally zoned Organ Needle pluton has been previously interpreted to represent both the nonerupted silicic cap and more-mafic, less-differentiated residual crystal mush of the Organ caldera-forming magma chamber (Seager and McMurry, 1988; Verplanck et al., 1995; 1999). U/Pb and Ar/Ar ages of the Organ Needle pluton indicate that 1) this intrusion is coeval with the Squaw Mountain Tuff, the youngest of three caldera-forming ignimbrites, 2) the intrusion represents the nonerupted remnants of a shallow, compositionally zoned caldera-forming magma chamber, and 3) the intrusion rapidly cooled following caldera collapse, then several parts of the intrusion were later reheated during postcaldera magmatism.

U/Pb zircon and some Ar/Ar biotite ages of the Organ Needle pluton are indistinguishable from the 36.03 ± 0.16 Ma eruption age of the Squaw Mountain Tuff. The alkali-feldspar granite is the most silicic and structurally highest phase of the Organ Needle pluton. The U/Pb zircon age of this unit is $36.48^{+0.48}_{-0.46}$ Ma and Ar/Ar biotite ages at two locations are 36.25 ± 0.12 and 36.17 ± 0.12 Ma, respectively. The alkali feldspar

granite has a gradational contact with an equigranular syenite and quartz syenite phase of the Organ Needle pluton. Though the U/Pb zircon age of this phase, $34.93^{+0.89}_{-1.29}$ Ma, is statistically younger than the Squaw Mountain Tuff, the ages agree if the ^{238}U and ^{40}K decay constant error uncertainty is propagated through the error calculation. Alternatively, the large negative uncertainty of the equigranular syenite may indicate Pb-loss. Though biotite from this sample of the equigranular syenite was too altered to date, biotite from a compositionally similar sample, ORGAN-36, yielded an age of 35.98 ± 0.14 Ma, indicating that the intrusion was emplaced at or prior to 36.0 Ma. The monzodiorite phase is the most mafic phase of the Organ Needle pluton. A single U/Pb age of this sample is $36.13^{+0.55}_{-0.23}$ Ma, which is statistically indistinguishable the sanidine Ar/Ar age of the Squaw Mountain Tuff. Only one of three Ar/Ar biotite analyses of the monzodiorite yielded an age similar to the Squaw Mountain Tuff, 35.94 ± 0.13 Ma. The remaining biotite ages are 35.4 and 34.6 Ma and were likely reset during emplacement of the Granite of Granite Peak and/or Sugarloaf peak pluton. The inequigranular syenite, which is exposed as a thin (e.g., ~1-10 m) phase along the eastern constant of the Organ Needle pluton, yielded U/Pb zircon and Ar/Ar biotite ages of $35.53^{+0.53}_{-0.38}$ and 35.77 ± 0.14 Ma, respectively, indicating that the phase was emplaced and cooling shortly after the Squaw Mountain Tuff eruption.

Ar/Ar dating of reheated minerals in the 1.4-1.7 Ga Precambrian porphyritic granite country rocks also indicates that the Organ Needle pluton is temporally indistinguishable to the Squaw Mountain Tuff. Biotite from the Precambrian yielded an age of 36.16 ± 0.15 Ma indicating a resetting event at this time. The biotite age of the

Precambrian granite is indistinguishable with the U/Pb zircon crystallization ages of the Organ Needle plutonic units.

U/Pb zircon and Ar/Ar biotite ages of the Organ Needle pluton establish the emplacement history and provide an opportunity to assess the preexisting geochemical models for the evolution of this intrusive unit. Verplanck et al., (1995; 1999) determined that the top (alkali feldspar granite), side (inequigranular syenite), and bottom (monzodiorite) phases of the Organ Needle pluton have a more crustal radiogenic isotopic signature than the main equigranular syenite phases located with the interior of the intrusion (ε_{Nd} = -5 and $^{87}Sr/^{86}Sr$ = 0.7085 vs. ε_{Nd} = -2 and $^{87}Sr/^{86}Sr$ = 0.7060, respectively). Based on these geochemical differences, Verplanck et al., (1995; 1999) suggested that the alkali feldspar granite, inequigranular syenite, and monzodiorite phases of the Organ Needle pluton evolved separately from the interior equigranular syenite and quartz syenite phases (see fig. 14 of Verplanck et al., 1999 for a more detailed explanation). The interior phases were emplaced first and the minor compositional variations within this phase originated from closed system differentiation. During differentiation of the interior phases, the monzodiorite phase was emplaced at the base of the interior phases. Fractional crystallization and differentiation of the monzodiorite, coupled with wall-rock assimilation of Precambrian granite, generated the inequigranular syenite. The inequigranular syenite further differentiated during sidewall crystallization and the alkali feldspar granite accumulated at the top of the intrusion and was erupted as Squaw Mountain Tuff. The U/Pb and Ar/Ar ages produced as part of this study did not measure any temporal difference, within analytical uncertainty, between the Squaw Mountain Tuff and all of the various phases of the Organ Needle pluton. Though the

U/Pb and Ar/Ar ages of the Organ Needle pluton do not disagree with this previously proposed model, the ages do not require that the interior equigranular syenite and quartz syenite were emplaced first and that the monzodiorite, inequigranular syenite, and alkali feldpsar granite were emplaced and chemically evolved during a later event. Instead, the entire Organ Needle pluton may have been emplaced during a single event and, following emplacement, differentiated to various compositions. The compositional and radiogenic isotopic variation may reflect the degree of differentiation and assimilation of wall rock.

3.6.4. Postcaldera magmatism

Records of postcaldera magmatism include several silicic intrusions that cross cut the Organ Needle pluton and small, isolated outcrops of lava flows located in the western Organ Mountain foothills. Ar/Ar dating of the postcaldera volcanic rocks indicate that volcanism commenced soon after the eruption of the Squaw Mountain Tuff at 36.0 Ma and continued until at least 35.7 Ma. U/Pb dating of the postcaldera plutons indicate pluton emplacement between 35.4 and 34.3 Ma. MDD thermal modeling of K-feldspar from the Organ Needle and postcaldera plutons indicate numerous reheating events at 34 Ma, 32 to 30 Ma, and possibly also 26 Ma, suggesting protracted postcaldera magmatism.

Five lithologically diverse west-side postcaldera lava flows were dated to determine the timing of postcaldera volcanic activity. The eruptive ages of the west-side lavas range from 36.10 ± 0.21 to 35.68 ± 0.09 Ma. The compositional zonation pattern that is preserved in the caldera-forming ignimbrite sequence does not continue into the postcaldera lavas. Instead, postcaldera west-side lava flows display discontinuous flow-to-flow variations in major and trace elements, and crystal and vesicle content (Seager, 1981). Considering the relatively rapid eruption rate constrained by this work, the

discontinuous compositional variation suggests either a single, rapidly evolving source or multiple sources for the postcaldera lavas.

Three silicic plutons were emplaced following the eruption of the Squaw Mountain Tuff and crystallization of the Organ Needle pluton. A U/Pb zircon age of the Granite of Granite Peak indicates emplacement at $35.24^{+0.68}_{-0.30}$ Ma and the corresponding biotite age, 35.41 ± 0.13 Ma, suggests rapid cooling following emplacement. Two zircon separates from the Sugarloaf Peak pluton yielded U/Pb ages of $35.31^{+0.43}_{-0.39}$ and $34.28^{+0.54}_{-0.51}$ Ma, indicating the pluton was incrementally emplaced. Biotite ages of four Sugarloaf Peak pluton samples range from 34.66 ± 0.06 to 33.46 ± 0.19 Ma. This suggests that some parts of the Sugarloaf Peak pluton rapidly cooled following emplacement, whereas other parts of the pluton were later reheated by younger magmatism. Zircons separates were not analyzed from the Baylor Peak rhyolitic porphyry. However, the emplacement age of this intrusion is constrained to be between ~36.0 Ma, the age of the Squaw Mountain Tuff and Organ Needle pluton, and ~34.5 Ma, the oldest ages observed in the K-feldspar age spectrum. MDD unconstrained models of an aplitic dike in the Sugarloaf Peak pluton, located ~1 km south of the Baylor Peak porphyry, shows a reheating event at 34 Ma. Thermal resetting of this sample may be related to emplacement of the Baylor Peak rhyolitic porphyry.

MDD K-feldspar modeling of the Organ caldera complex intrusions provides evidence for protracted magmatism related to postcaldera magmatic activity. Organ Needle plutonic K-feldspar from samples of the equigranular syenite, quartz syenite, and alkali feldspar granite indicate reheating events at ~34 Ma, corresponding to the 35.4-34.3 Ma emplacement of the Sugarloaf Peak pluton and Baylor Peak rhyolitic porphyry.

MDD modeling also indicates reheating events between ~32 and 30 Ma. K-feldspar from the Baylor Peak rhyolitic porphyry and a nearby aplitic rhyolite dike in the Sugarloaf Peak pluton both indicate reheating events as young as 26-28 Ma, suggesting localized magma emplacement into this part of Organ caldera complex ~8 Ma after the caldera forming event. Alternatively, the youngest reheating events may be related to hydrothermal fluid circulation and K-feldspar recrystallization, rather than reheating.

3.7. Comparison of the Organ caldera to other calderas with exposed plutons

An outstanding problem related to caldera magmatism is determining the origin of silicic magmas. A controversial aspect of silicic magmatism is whether differentiation occurs in the upper or lower crust (e.g., Glazner et al., 2004; Bachmann et al., 2007a). According to the shallow differentiation hypothesis, intermediate to mafic magmas are emplaced into the upper crust and differentiate into a silicic cap and residual crystal mush (Smith, 1979; Hildreth, 1981; Bachmann and Bergantz, 2004, 2008; Lipman, 2007). During caldera collapse, most of the silicic cap is erupted and the nonerupted silicic cap and less-differentiated, more-mafic residual mush are preserved in the plutonic record (Bachmann et al., 2007a; de Silva et al., 2007). Alternatively, some other workers have hypothesized that some silicic magmas originate at deep (>25 km) crustal levels (Eichelberger, 2000; Petford, 2000; Coleman et al., 2004; Glazner et al., 2004; Knessel and Duffield, 2007; Quick et al., 2009). Mantle-derived basaltic magmas accumulate at the base of the crust. Differentiation of these basalts, combined with partial melting of the lower crust, generates silicic melts (Dufek and Bergantz, 2005; Annen et al., 2006). Silicic melts that are generated in the lower crust and erupt from shallow magma

chambers will not have a complementary upper crustal residual crystal mush. Instead, nonerupted material in the magma chamber that crystallizes to form intrusions will be temporally and compositionally similar to their ignimbrite.

The origin of silicic magmas remains controversial, in part, because most studies have focused on either volcanic rocks (Eichelberger et al., 2006; Hildreth and Wilson, 2007; Knessel and Duffield, 2007; Hora et al., 2009) or plutonic rocks (Wiebe, 1994; Coleman et al., 2004; Glazner et al., 2004; Paterson, 2009) to determine the processes that generate silicic melts. Few studies have investigated the spatial, temporal, and chemical relationship of volcanic and plutonic rocks of the same caldera system. However, studying both volcanic and plutonic rocks is a useful approach for understanding caldera magma chambers (Lipman et al., 1986; Johnson and Lipman, 1988; Seager and McCurry, 1988; Shannon, 1988; Lipman et al., 1990; Bachmann et al., 2007; John et al., 2008). As previously discussed in this study, the volcanic-plutonic relationship at the Organ caldera indicates that these silicic magmas were generated via in-situ differentiation in the upper crust.

The purpose of this section is to assess whether the magmatic processes inferred at the Organ caldera have also occurred at different caldera systems with similar exposures of the subcaldera intrusions. The spatial and temporal relationships of volcanic and plutonic rocks at the Questa (northern NM) and Mt. Aetna caldera (central CO) have recently been examined (Zimmerer et al., 2010; Mill et al., 2010; Tappa et al., in review; Zimmerer and McIntosh, in review). Similar to the Organ caldera complex, these two caldera systems are located on the flanks of the Rio Grande Rift and have exceptional exposures the intracaldera sequence and subvolcanic intrusions. In addition to these Rio

Grande Rift faulted calderas, the volcanic-plutonic relationship of the Caetano, Chegem, and Turkey Creek calderas have been investigated (Table 3.3)(Lipman et al., 1993; duBray et al., 2004; John et al., 2008). The subvolcanic batholiths at these systems are not as well exposed as the Rio Grande rift calderas. However, the temporal-chemical relationships of their ignimbrites and the small-volumes of the exposed intrusive suite exhibit similarities and differences with the Organ, Questa, and Mt. Aetna systems. Intrusions are exposed at numerous other caldera systems (e.g., Lake City (CO) - Lipman et al., 1973; Platoro (CO) – Lipman, 1975; Grizzly Peak (CO) – Fridrick et al., 1991; Stein (NM) – Elston, 1984; Marysvale volcanic field (UT) – Steven et al., 1984). However, caldera ignimbrite-pluton pairs at these localities have not been investigated in detail using modern geochemical and geochronologic techniques.

A condensed geochronologic summary of the Organ, Questa, and Mt. Aetna systems is displayed in Figure 3.7. All three caldera systems have some evidence for pre- and postcaldera volcanism. However, the preservation, alteration, and the quality of ages for the pre- and postcaldera volcanic records are different at each location. We choose to focus on the temporal-chemical relationship of the caldera-forming ignimbrites and exposed intrusions.

3.7.1. The Organ, Questa, and Mt. Aetna calderas and their associated ignimbrites

The Organ caldera complex erupted three ignimbrites. The basal ignimbrite, the 36.45±0.08 Ma Cueva Tuff, is a crystal-poor, high-SiO_2 (>77% SiO_2) rhyolite. The middle ignimbrite, the 36.23±0.14 Ma Achenback Park Tuff, is a crystal-poor, intermediate-SiO_2 (74-75% SiO_2) rhyolite. The upper ignimbrite, the 36.03±0.16 Ma

Table 3.3. Comparison of calderas with dated exposed plutons

Caldera (location)	Ignimbrite/ Compsition	Ignimbrite age (Ar/Ar)	Exposed plutons/ composition	Age of plutons (dating method)	Comments; study
Questa (New Mexico)	Amalia Tuff - 500 km^3 , crystal-poor, high-SiO_2 peralkaline rhyolite	25.39±0.04 (Ma)	peralkaline ring dike and phases of resurgent plutons postcaldera plutons	25.38±0.04 (Ar/Ar) 25.3 – 19.3 Ma (Ar/Ar; U/Pb)	Plutons exposed from 3-5 km depth (Lipman et al., 1986); Zimmerer and Mcintosh, in review
Mt. Aetna (Colorado)	Badger Creek Tuff - ~250 km^3 xstal-rich dacite	34.26±0.06 Ma	Precaldera Mt. Princeton batholith compositionally similar ring dike and intrusion luecrogranite postcaldera plutons	36.5 to 35.0 Ma (Ar/Ar; U/Pb) 34.4 to 34.9 Ma (U/Pb) ~31 Ma (Ar/Ar; U/Pb)	Only top of intrusive suite exposed; Mills et al., 2010 and Zimmerer et al., 2010
Organ (New Mexico)	Cueva Tuff - crystal-poor high SiO_2 rhyolite Achenback Park - crystal-poor low-SiO_2 rhyolite Squaw Mountain Tuff - zoned from crystal-poor low silica rhyolite to crystal-rich low SiO_2 rhyolite	36.45±0.08 Ma 36.23±0.14 Ma 36.03±0.16 Ma	Organ Needle pluton –vertically zoned from alkali feldspar granite at top to interior syenite to monzodiorite at base postcaldera silicic intrusions	36.4 to 36.0 Ma (Ar/Ar; U/Pb) 36.0 to 34.3 Ma (Ar/Ar; U/Pb)	Plutons exposed from 3-6 km depth (Seager, 1981); This study
Caetano (Nevada)	Caetano Tuff - 850 km^3 zoned from a high SiO_2 to low SiO_2 rhyolite	33.79±0.05 Ma	Carico lake resurgent pluton – similar in composition to late phase Caetano Tuff	33.78±0.05 Ma (Ar/Ar)	Only top of intrusive suite exposed; John et al., 2008
Turkey Creek (Arizona)	Rhyolite Canyon Tuff – 500 km^3 high SiO_2 rhyolite	26.96±0.06 Ma	Resurgent pluton - dacitic	26.90±0.04 (Ar/Ar)	Only top of intrusive suite exposed; du Bray et al., 2004
Chegem (Russia)	Chegem Tuff - 500km^3 zoned from rhyolite to dacite	2.84±0.03 Ma	resurgent granidiorite pluton Eldjurta Granite	2.84±0.03 (Ar/Ar) 2.8 - 0.8 Ma (Ar/Ar)	Only top of intrusive suite exposed; Lipman et al., 1993

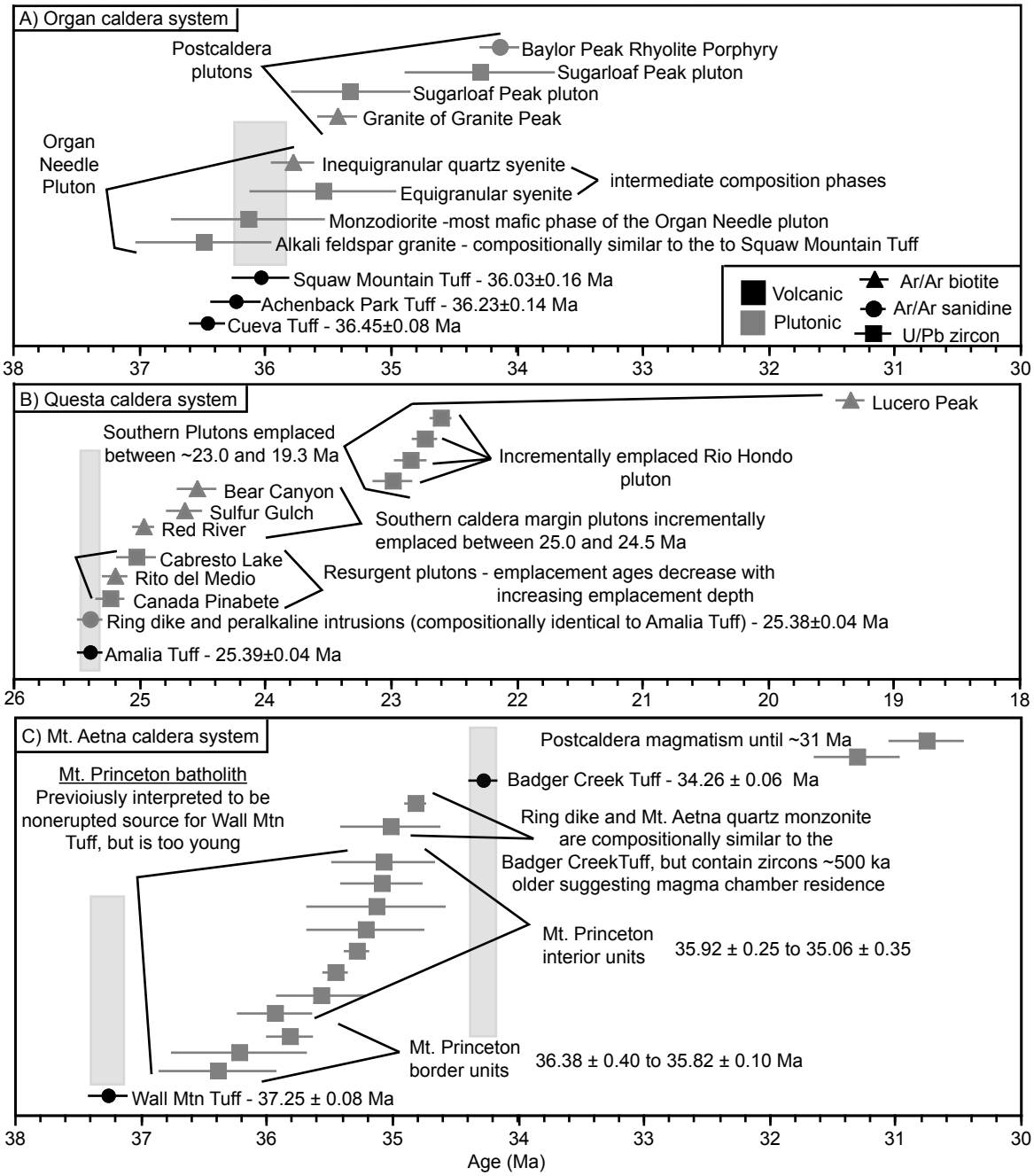

Figure 3.7. Condensed geochronologic summaries for the A) Organ, B) Questa, and C) Mt. Aetna caldera systems. U/Pb and Ar/Ar ages reported at 2σ and do not included error in the corresponding decay constants. Vertical gray bars represent the age and associated uncertainty of the caldera forming ignimbrite(s). Pluton emplacement ages determined by CA-TIMS or LA-ICP-MS U/Pb zircon ages and, in the absence of robust U/Pb zircon ages, the age of the oldest biotite, or integrated age of the K-feldspar (i.e., Baylor Peak rhyolitic porphyry).

Squaw Mountain Tuff, is zoned from a crystal-poor, low-SiO_2 (72% SiO_2) rhyolite at the base, to a crystal-rich, lower-SiO_2 (68% SiO_2) rhyolite at the base. Though zoning is nearly absent in the two basal ignimbrites, the ~500-1000 km^3 ignimbrite sequence, as a whole, is zoned from a crystal-poor, high-SiO_2 at the base to a crystal-rich, low-SiO_2 at the top (Seager, 1981; Seager and McCurry, 1988). The maximum thickness of the Organ ignimbrite sequence is 3.3 km. (Seager, 1981; Seager and McCurry, 1988). Because of Rio Grande Rift faulting and basin development, evidence for the caldera structure is sparse. Ring faults have not been mapped. However, the crescent-shaped outcrop geometry of the exposed intrusions suggests that they have been emplaced along the eastern caldera margin.

The Questa caldera complex erupted a single ignimbrite, the 500 km^3, 25.38±0.04 Ma Amalia Tuff (Lipman et al., 1986; Zimmerer and McIntosh; in review). The Amalia Tuff is a crystal-poor, high-SiO_2 (>77% SiO_2), peralkaline rhyolite (Lipman et al., 1986; Johnson and Lipman, 1988). Lack of volcaniclastic intervals or cooling breaks within the Amalia Tuff indicate that it was emplaced during a single event. Diagnostic caldera features include ring faults, a discontinuous ring dike, thick (>2 km) intracaldera tuff, exposed caldera floor, and caldera-collapse breccias (Lipman et al., 1986).

Two ignimbrites erupted from the highly eroded Mt. Aetna caldera complex. The 37.25 ± 0.08 Ma Wall Mountain Tuff is a crystal-rich rhyolite (74% SiO_2). The Mt. Princeton batholith, the largest exposed intrusion at the complex, has previously been interpreted to be the nonerupted source for the Wall Mountain Tuff (Shannon, 1988; Toulmin and Hammarstrom, 1990; Lipman, 2007). Linking the Mt. Princeton batholith to the Wall Mountain Tuff has been difficult, largely because caldera features have

apparently been eroded. Following erosion of the Wall Mountain Tuff caldera, the fully crystallized Mt. Princeton batholith collapsed into the Mt. Aetna caldera during the eruption of the ~250 km^3 dacitic 34.26±0.06 Ma Badger Creek and Antero Tuffs (Shannon, 1988; McIntosh and Chapin, 2004; Lipman, 2007; Zimmerer et al., 2010). Evidence for the Mt. Aetna caldera includes ring faults, ring dikes, highly eroded intracaldera Badger Creek Tuff, and megabreccias (Shannon, 1988; Toulmin and Hammarstrom, 1990). Using Ar/Ar dating and paleomagnetic techniques, McIntosh and Chapin (2004) determined that the Antero Tuff and Badger Creek Tuff were both erupted from the Mt. Aetna caldera. Unlike the Amalia Tuff, which was emplaced as a single unit, the Badger Creek/Antero Tuff consists of multiple, interlayered nonwelded ignimbrite and volcaniclastic deposits, indicating that the caldera eruption was not continuous and had several periods of repose (Epis and Chapin; 1975; Shannon, 1988; McIntosh and Chapin, 2004). Though both the Organ caldera ignimbrites and the Badger Creek/Antero Tuffs are interlayered with volcaniclastics indicating periods of volcanic quiescence, any age difference of the Badger Creek/Antero Tuffs has not been resolved (McIntosh and Chapin, 2004).

3.7.2. Exposed subvolcanic intrusions

Four plutons are exposed at the Organ caldera complex. The largest intrusion is the Organ Needle pluton, which is vertically zoned from an alkali feldspar granite at the top to an interior syenite and a monzodiorite at the base. The Organ Needle pluton has been interpreted to be the nonerupted silicic cap and the residual crystal mush of the Squaw Mountain Tuff (Seager and McCurry, 1988; Verplanck et al., 1995; 1999). Three

younger silicic intrusions, the Sugarloaf Peak pluton, the Granite of Granite Peak, and the Baylor Peak rhyolitic porphyry intrude the Organ Needle pluton (Seager, 1981).

Nine plutons and a ring dike are exposed at the Questa caldera. Four plutons are exposed in the core of the resurgent dome near the center of the caldera. The ring dike and capping phases of the Virgin Canyon and Canada Pinabete resurgent plutons are peralkaline granites that are similar in composition to the Amalia Tuff. Metaluminous phases of the Virgin Canyon and Canada Pinabete plutons and the Rito del Medio and Cabresto Lake resurgent plutons, which are all located beneath the peralkaline intrusions, are interpreted to represent a progressive younging sequence (Johnson et al., 1989). The Cabresto Lake quartz monzonite pluton, the structurally deepest and most mafic resurgent intrusion, has been interpreted a less differentiated part of the magma system (Lipman et al., 1986; Johnson et al., 1988). Three plutons are located along the caldera margin and two plutons are located 1-20 km south of the caldera margin (Lipman et al., 1986).

Three genetically distinct intrusions are exposed at the Mt. Aetna caldera. The compositionally zoned Mt. Princeton batholith is the oldest and largest exposed intrusion at the complex. Ring dikes and a quartz monzonite pluton were emplaced into the Mt. Aetna caldera margin. These intrusions are similar in composition to the Badger Creek Tuff (Shannon, 1988; Toulmin and Hammarstrom, 1990; Lipman, 2007). Volumetrically minor luecogranites cross cut the Mt. Princeton batholith and Mt. Aetna caldera.

3.7.2.1. Coeval plutons

Each complex contains intrusions that are temporally similar to their caldera-forming ignimbrite. However, the volume and composition of these intrusions varies at each system.

U/Pb zircon and Ar/Ar biotite ages indicate that the Organ Needle pluton is coeval with the 36.03 ± 0.16 Ma Squaw Mountain Tuff. The alkali feldspar granite phase of the Organ Needle pluton, which is compositionally similar to the Squaw Mountain Tuff, crops out in small-volume cupolas located along the roof zone of the Organ Needle pluton. The U/Pb zircon age alkali feldspar granite is $36.48^{+0.48}_{-0.46}$ Ma and biotite ages are 36.25 ± 0.12 and 36.17 ± 0.12 Ma. The syenite and monzodiorite phases, which were interpreted to be the residual mush for the Squaw Mountain Tuff, yield U/Pb zircon ages of $35.53^{+0.53}_{-0.38}$ and $36.13^{+0.55}_{-0.23}$ Ma, respectively. Biotite from these units are range from 36.0 to 34.6 Ma indicating that some parts of the Organ Needle pluton cooled rapidly after emplacement and other regions where reheated during postcaldera magmatism.

Small volumes of the Questa caldera-related intrusions are temporally indistinguishable to the 25.39±0.04 Ma peralkaline Amalia Tuff. The peralkaline ring dike yields a K-feldspar plateau age of 25.38 ± 0.04 Ma. Samples of the peralkaline phases of the Virgin Canyon and Canada Pinabete resurgent plutons did not yield robust ages. However, the compositional similarity between the ring dike and the peralkaline phases of these two resurgent plutons suggest that they are also temporally similar to the Amalia Tuff. The peralkaline intrusions are interpreted to represent nonerupted Amalia Tuff (Tappa et al., in review; Zimmerer and McIntosh, in review).

Similar to the Questa system, only small-volumes of the exposed intrusions at the Mt. Aetna caldera complex are coeval with the 34.26 ± 0.06 Ma Badger Creek Tuff. The ring dike, quartz monzonite intrusion, and Badger Creek Tuff are compositionally similar. All three units have zircons that are 100-500 ka older than the eruption age of the Badger Creek Tuff. We propose that the Badger Creek Tuff magma chamber was

incrementally assembled during a 500 ka period prior to eruption. During the Mt. Aetna caldera eruption, magma that was older, yet compositionally similar to the Badger Creek Tuff was remobilized from within the incrementally assembled caldera-forming magma chamber and intruded into ring faults and/or caldera vents (Mills et al., 2010; Zimmerer et al., 2010).

Similar to these three caldera systems, the Caetano, Turkey Creek, and Chegem calderas (Table 3.3) have exposed intrusions that are temporally similar their associated ignimbrites. Like the faulted Rio Grande rift calderas, these plutons are the structurally highest plutons of the intrusive suite and in particular are located within the eroded and faulted resurgent domes. At the Caetano and Chegem calderas, resurgent intrusions are compositionally similar to the latest erupted phase of their coeval ignimbrites. Both of these intrusions have also been interpreted to represent the nonerupted intrusive equivalent to the caldera-forming ignimbrite (Lipman et al., 1993; John et al., 2008). At the Turkey Creek caldera, the high-SiO_2 rhyolitic 26.9 Ma Rhyolite Canyon Tuff was intruded by a dacitic intrusion interpreted to be the residual crystal mush (du Bray et al., 2004). Both the caldera-forming rhyolite and the dacitic intrusion yield ages of 26.9 Ma, which supports the idea that the dacitic intrusion is the less-differentiated residual of the caldera magma chamber.

3.7.2.2. Postcaldera plutons

In addition to plutons that are coeval with their ignimbrite, each system contains intrusions that are significantly younger than the caldera forming eruption. These intrusions are interpreted to be postcaldera plutons that record the waning stages of caldera magmatism.

Dating of exposed postcaldera plutons indicates that magmatism continued for at least 1.7 Ma following the last eruption of the Organ caldera at 36.0 Ma. U/Pb zircon and Ar/Ar biotite ages of the exposed postcaldera intrusions indicate emplacement between 35.4 and 34.3 Ma. Outcrops of these intrusions are volumetrically minor and more silicic than to the Organ Needle pluton. MDD modeling of plutonic K-feldspar suggests that postcaldera magmatism may have continued until at least ~30 Ma.

The majority of plutons at the Questa caldera have U/Pb and Ar/Ar ages that are younger than the 25.4 Ma Amalia Tuff. The oldest postcaldera plutons are the metaluminous phases of the Virgin Canyon and Canada Pinabete intrusion. The metaluminous phase of Canada Pinabete pluton yields an U/Pb zircon age 25.29 ± 0.05 Ma (Tappa et al., in review). U/Pb zircon and Ar/Ar biotite and K-feldspar ages of the Cabresto Lake pluton are indistinguishable in age at 25.0 Ma, indicating rapid cooling after emplacement. Following resurgent plutonism, the southern caldera margin plutons were emplaced between 24.9 and 24.5 Ma. Four U/Pb zircon ages of the Rio Hondo indicate that it was incrementally emplaced between 23.0 and 22.5 Ma. The oldest biotite age from the most southern pluton, Lucero Peak, is 19.3 Ma and provides the best estimate for the emplacement age (Tappa, in review; Zimmerer and McIntosh, in review).

Similar to the Questa caldera, the majority of the exposed intrusions at the Mt. Aetna caldera complex are postcaldera plutons. The compositionally zoned Mt. Princeton batholith, which has been previously interpreted to be the crystallized remnants of the 37.3 Ma Wall Mountain Tuff magma chamber (Chapin and Epis, 1975; Shannon, 1988; McIntosh and Chapin, 2004; Lipman, 2007), was in fact emplaced between 36.4 and 35.1 Ma, 0.9 to 2.2 Ma after the eruption of the Wall Mountain Tuff. Some Ar/Ar biotite and

K-feldspar ages of the Mt. Princeton batholith are within error of U/Pb zircon ages indicating rapid cooling following emplacement. Results suggest that 1) the Mt. Princeton batholith was incrementally emplaced from the top down during the interval between the eruptions of the 37.3 Ma Wall Mountain Tuff and 34.3 Ma Badger Creek Tuff, 2) the Mt. Princeton batholith is too young to be the source of Wall Mountain Tuff, and 3) the Mt. Princeton batholith represents post-Wall Mountain Tuff magmatism and pre-Badger Creek Tuff magmatism. Evidence for post-Mt. Aetna caldera magmatism is limited to the ~31 Ma luecogranites. Some K-feldspar age spectra indicate an argon loss event as young as ~20 Ma, which is related either to fluid-flow or to a reheating event not related to the Mt. Aetna caldera complex.

3.7.3. The origin of the Organ, Questa, and Mt. Aetna silicic magmas

A major goal of this study is to use both the volcanic and plutonic record to determine if silicic magmas originate via upper crustal differentiation or from differentiation and partial melting in a lower crustal source. Because both processes predict that some volume of the intrusions may be compositionally similar to the coeval ignimbrite, the crux of determining if deep or shallow differentiation has occurred requires sufficient exposures of the subcaldera intrusions in order to assess whether coeval plutonic rocks resemble the residual crystal mush.

Each caldera complex contains coeval intrusions that are compositionally similar to their ignimbrite. In general, these plutons are small-volume, occur along ring faults or are phases of intracaldera intrusions, are located at or near the top of the intrusive suite, are the same age or slightly older than the coeval ignimbrite, and cooled rapidly

following emplacement. Because of the similarity in age and composition to the ignimbrites that they intrude, the intrusions are interpreted to represent nonerupted ignimbrite magmas.

By using the volcanic-plutonic relationship of these three contrasting caldera systems, we propose that silicic caldera-forming magmas can be in either the upper or lower crust. Models of upper crustal-differentiation predict that residual crystal mush should be located directly beneath the nonerupted silicic cap. Only the Organ Needle pluton at the Organ caldera is temporally and chemically compatible with a residual crystal mush. Both the Questa and Mt. Aetna caldera complexes have exposed plutons that, based on the published geochemistry (Questa – Lipman et al., 1986; Johnson and Lipman, 1988; Johnson et al., 1989; Mt. Aetna – Shannon, 1988; Toulmin and Hammarstrom; 1990), might represent the more-mafic, less-differentiated parts of the caldera magma chamber. However, these intrusions have U/Pb and Ar/Ar ages that indicate they were emplaced during postcaldera magmatism. None of the exposed plutons at the Questa and Mt. Aetna caldera complexes are interpreted to be the residual crystal mush. The lack of evidence for a residual crystal mush below the Questa and Mt. Aetna calderas implies that these silicic magmas were generated in a deeper source (i.e., the mid- to lower crust) and not via in-situ upper crustal differentiation.

3.7.4. Links between ignimbrite zoning patterns, silicic magma differentiation, and the volcanic-plutonic relationship

We also observe a link between ignimbrite zoning patterns and the volume and composition of nonerupted material in the caldera-forming magma chamber. The Organ

caldera complex zoned ignimbrite sequence originated via upper crustal in-situ differentiation. Like the many zoned ignimbrites, the youngest ignimbrite eruption terminated with crystal-rich magmas, apparently because magma withdrawal intersected the viscosity barrier between the eruptible cap and crystal-rich residual mush (Bacon and Druitt, 1988; Bachmann et al., 2002; Hildreth, 2004). The crystal-rich residual mush is preserved as the Organ Needle pluton. The volume ratio of the nonerupted magma to the volume of the ignimbrite is impossible to accurately determine because of erosion and current exposures. However, models of upper crustal differentiation predict a 3 to 10:1 intrusive:extrusive ratio (White et al., 2006).

The non- to weakly zoned Questa and Mt. Aetna ignimbrites were apparently generated in the lower crust. Despite exceptional exposures, only small-volume intrusions that are compositionally similar to their caldera forming ignimbrite are temporally linked to the caldera magma chamber. Without major viscosity barriers related to zoning, most of the magma chamber drained during the caldera-forming eruption.

We doubt that this observed link between ignimbrite zoning patterns, the depth of differentiation, and the volume and composition of the nonerupted magma is ubiquitous at all caldera systems. We speculate that some nonzoned ignimbrites may be generated in the upper crust. For example, the Turkey Creek caldera (Table 3.3) erupted a nonzoned rhyolite and the intracaldera sequence was intruded by the dacitic residual mush. However, in light of the volcanic-plutonic relationships at the Questa, Mt. Aetna, and Organ caldera complexes, we emphasize that caldera-forming silicic magmas should be investigated in the framework of both upper and lower crustal differentiation and not one or the other.

3.8. Concluding remarks

The temporal-chemical relationship of volcanic and plutonic rocks has been used to understand the origin of silicic magmas at the Organ, Questa, and Mt. Aetna caldera complexes. Results suggest that caldera magmatism is a dynamic process characterized by emplacement of compositionally diverse magmas over prolonged periods. Results also show that silicic magmas can be generated in either the upper or lower crustal sources. Caldera-forming magma chambers vary in volume and composition and during ignimbrite eruptions the caldera-forming magma chamber may nearly completely empty or only a small volume of the chamber may be erupted.

Continued caldera-related research should focus on comparing the relationship of pre- and postcaldera volcanism to pre- and postcaldera plutonism, establishing the volcanic-plutonic relationship at caldera systems from various tectonic settings, understanding zircon crystallization histories and geochemistry in zoned and nonzoned ignimbrites and plutons, and intercalibrating the Ar/Ar and U/Pb methods. Finally, continued collaborations between volcano-oriented and pluton-oriented investigators will undoubtedly further our understanding of caldera-related magmatism.

REFERENCES

Annen, C., 2009, From plutons to magma chambers: Thermal constraints on the accumulation of eruptible silicic magma in the upper crust: Earth and Planetary Science Letters, v. 284, p. 409-416.

Annen C., Blundy, J. D., and Sparks, R.S.J, 2006, The genesis of intermediate and silicic magmas in deep crustal hot zones: Journal of Petrology, v. 47, p. 505-539.

Bachmann, O., Dungan, M., and Lipman, P. W., 2002, The Fish Canyon Magma Body, San Juan volcanic field, Colorado: Rejuvenation and eruption of an upper-crustal batholith: Journal of Petrology, v. 43, p. 1369-1503.

Bachmann, O., and Bergantz, G., 2004, On the origin of crystal-poor rhyolites: Extracted from batholith crystal mushes: Journal of Petrology, v. 45, p. 1565-1582.

Bachmann, O., Miller, C. F., and de Silva, S. L., 2007a, The volcanic-plutonic connection as a stage for understanding crustal magmatism: Journal of Volcanology and Geothermal Research, v. 167, p. 1-23.

Bachmann, O., Oberlie, F., Dungan, M. A., Meier, M. Mundil, R., and Fischer, H., 2007b, $^{40}Ar/^{39}Ar$ and U/Pb dating of the Fish Canyon magmatic system, San Juan volcanic field, Colorado; evidence for an extended crystallization history: Chemical Geology,v. 236, p. 134-166.

Bachmann, O., and Bergantz, G. W., 2008, Deciphering magma chamber dynamics from styles of compositional zoning in large silicic ash flow sheets, Reviews in Mineralogy and Geochemistry, v. 69, p. 651-674.

Bacon, C. R., and Druitt, T. H., 1988, Compositional evolution of the zoned calcalkaline magma chamber of Mount Mazama, Crater Lake, Oregon: Contributions to Mineralogy and Petrology, v. 98, p. 224-256.

Baldridge, W. S., and Olsen, K. H., 1989, The Rio Grande rift: American Scientist, v. 77, p. 240-247.

Baldridge, W. S., Keller, G. R., Haak, V., Wendlandt, E., Jiracek, G. R., and Olsen, K. H., 1995, The Rio Grande rift in Olsen, K. H. ed. Continental rifts: evolution, structure, and tectonics: Developments in geotectonics, v. 25, Elsevier, Amsterdam, p. 233-276.

Bartley, J.M., Glazner, A.F., and Coleman, D.S., 2005, Do large silicic eruptions leave behind even larger plutons?: Eos (Transactions, American Geophysical Union), v. 86, no. 18, p. 58.

Branney, M. J., and Kokelaaar, B. P., 2002, Pyroclastic denistry currents and the sedimentation of ignimbrites: Geological Society of London, Memoir 27, 152 p.

Bryan, S. E., Ferrari, L., Reiners, P. W., Allen, C. M., Petrone, C. M., Rosique, A. D., and Campbell I. H., 2008, New Insights into crustal contributions to large-volume Rhyolite Generation in the Mid-Tertiary Sierra Madre Occidental Province, Mexico, Revealed by U-Pb Geochronology: Journal of Petrology, v. 49, p. 47-77.

Brown. S. J. A, and Fletcher, I. R., 1999, SHRIMP U-Pb dating of the preeruptive growth history of zircons from the 340 ka Whakamaru Ignimbrite, New Zealand: Evidence for >250 k.y. magma residence times: Geology, v. 27, p. 1035-1038.

Buddington, A. F., 1959, Granite emplacement with special reference to North America: Geological Society of America Bulletin, v. 70, p. 671-748.

Campbell, S. K., 1994, A geochemical and strontium isotopic investigation of Laramide and younger igneous rocks in central Colorado, with emphasis on the petrogenesis of the Thirtynine Mile volcanic field. Ph.D. diss., Florida State University, Tallahassee, FL, United States (USA).

Chapin, C. E, Wilks, M., and McIntosh, W. C., 2004, Space-time patters of Late Cretaceous to present magmatism in New Mexico-comparison with Andean volcanism and potential for future volcanism: New Mexico Bureau of Geology and Mineral Resources, Bulletin 160, p. 13-40.

Cole, J. W., Milner, D. M., and Spinks, K. D., 2005, Calderas and caldera structures: a review: Earth-Science Reviews, v. 69, p. 1-26.

Coleman, D. S., Gray, W., and Glazner, A. F., 2004, Rethinking the emplacement and evolution of zoned plutons: geochronological evidence for incremental assembly of the Tuolumne Intrusive Suite, California: Geology, v. 32, p. 433-436.

Coleman, D. S., Davis, J. W., Bartley, J. M., Glazner, A. F., 2008, Downward-stacking laccoliths: LASI III Conference, Elba Island, Abstracts with Program, p. 33-35.

Colucci, M.T., Dungan, M. A., and Ferguson, K. M., 1991, Precaldera lavas of the southeast San Juan volcanic field: Parent magmas and crustal interactions: Journal of Geophysical Research, v. 96, p. 13,413-13,434.

Coney, P. J., and Reynolds, S. J., 1977, Cordilleran Benioff zones: Nature, v. 270, p. 403-407.

Cordell, L., Long, C. L., and Jones, D. W., 1986, Geophysical expression of the batholith beneath Questa caldera, New Mexico: Journal of Geophysical Research, v. 90, p. 11,263-11,274.

Crowley, J. L., Schoene, B., and Bowring, S. A., 2007, U-Pb dating of zircon in the Bishop Tuff at the millennial scale: Geology, v. 35, p. 1123-1126.

Czamanske, G.K., Foland, K.A., Hubacher, F.A., and Allen, J.C., 1990, The $^{40}Ar/^{39}Ar$ chronology of caldera formation, intrusive activity and Mo-Ore near Questa, New

Mexico: New Mexico Geological Society, Field Conference, 41st Guidebook, p. 355-358.

Davis, J. H., and Stevenson, D. J., 1992, Physical model of source region of subduction zone volcanics: Journal of Geophysical Research, v. 97, p. 2037-2070.

de Silva, S., and Gosnold, W., 2007, Episodic construction of batholiths: Insights from the spatiotemporal development of an ignimbrite flare-up: Journal of Volcanology and Geothermal Research, v. 167, p. 320-335.

Deino, A., and Potts, R., 1992, Age-probability spectra for examination of single-crystal $^{40}Ar/^{39}Ar$ dating results: Examples from Olorgesailie, Southern Kenya Rift: Quaternary International, v. 13-14, p. 47-53.

Dickenson, W. R., and Snyder, W. S., 1978, Plate tectonics of the Laramide orogeny: Geological Society of America, Memoir 151, p. 355-366.

du Bray, E. A., Snee, L. W., and Pallister, J. S., 2004, Geochemistry and geochronology of middle Tertiary volcanic rocks of the central Chiricahua Mountains, Southeast Arizona, U.S. Geological Survey Professional Paper 1684, 57p.

Dufek, J., and Bergantz, G. W., 2005, Lower crustal magma genesis and preservation: a stochastic framework for the evaluation of basalt-crust interations: Journal of Petrology, v. 46, p. 2167-2195.

Dunbar, N. W., Kyle, P. R., and Wilson, C. J. N., 1989, Evidence for limited zonation in silicic magma systems, Taupo Volcanic Zone, New Zealand: Geology, 17, p. 234-236.

Dunham, K. C., The geology of the Organ Mountains: New Mexico Bureau of Mines and Mineral Resources Bulletin, v.11, 272 p.

Fleck, R. J., Sutter, J. F., and Elliot, D. H., 1977, Interpretation of discordant $^{40}Ar/^{39}Ar$ age-spectra of Mesozoic tholeiites from Antarctica, Geochimica Cosmochimica Acta, v. 41, p. 15-32.

Eichelberger, J. C., Chertoff, D. G., Dreher, S. T., and Nye, C. J., 2000, Magmas in collision: Rethinking chemical zonation in silicic magmas: Geology, v. 28, p. 603-606.

Eichelberger J. C., Izbekov, P. E., and Browne, B. L., 2006, Bulk chemical trends at arc volcanoes are not liquid lines of descent; Mantle to magma; lithospheric and volcanic processes in western North America: Lithos, v. 87, p. 135-154.

Elston, W. E., 1984; Mid-Tertiary ash flow tuff cauldrons, southwestern New Mexico: Journal of Geophysical Research, v. 89, p. 8733-8750.

Epis, R. C., and Chapin, C. E., 1975, Geomorphic and tectonic implications of the post-Laramide, late Eocene erosion surface in the Southern Rocky Mountains, in Curtis, B. F. (ed.), Cenozoic history of the southern Rocky Mountains: Geological Society of America, Memior 144, p. 45-74.

Farina, F., Dini, A., Innocenti, F., Rocchi, S., and Westerman, S. D., 2010, Rapid incremental assembly of the Monte Capanne pluton (Elba Islan, Tuscany) by downward stacking of magma sheets: Geological Society of America Bulletin, v. 122, p. 1463-1479.

Foster, D. A., Harrison, T. M., Copeland, P., and Heizler, M. T., 1990, Effects of excess argon within large diffusion domains on K-feldspar age: Geochimica Cosmochimica Acta, v. 54, p. 1699-1708

Francis, P., and Oppenheimer, C., 2004, Volcanoes. Oxford Univesiety Press, Oxford, 521 pp.

Fisher, R. V., and Schmincke, H. U., 1984, Pyroclastic Rocks, New York: Springer-Verlag.

Fridrich, C. J., and Mahood, G. A., 1984, Reverse zoning in the resurgent intrusions of the Grizzley Peak cauldron, Sawatch Range, Colorado: Geological Society of America Bulletin, v. 95, p. 779-787.

Fridrich, C. J., DeWitt, E., Bryant, B., Steve, R., and Smith, R. P., 1998, Geologic map of the Collegiate Peaks Wilderness Area and the Grizzley Peak caldera, Sawatch Range, central Colorado: U. S. Geological Survey, Miscellaneous Investigations Series map I-2565, scale 1:5000, 29 p.

Gehrels, G. E., Valencia, V. A., and Ruiz, J, 2008, Enhanced precision, accuracy, efficiency, and spatial resolution of U-Pb ages by laser ablation-multicollector-inductively coupled plasma-mass spectrometry: Geochemistry Geophysics Geosystems, v. 9, p. 1-13.

Gillespie, A. R., Huneke, J. C., and Wasserburg, G. J., 1982, An assessment of $^{40}Ar/^{39}Ar$ dating of incompletely degassed xenoliths: Journal of Geophysical Research Letters, v. 87, p. 9247-9257.

Glazner, A. F.,Bartley, J. M., Coleman, D. S., Gray, W. M. and Taylor, R. Z., 2004, Are plutons assembled over millions of years by amalgamation from small magma chambers?: Geological Society of America Today, v. 14, no. 4/5, p. 4-11.

Glazner, A. F., Coleman, D. S., and Bartley, J. M., 2008, The tenuous connection between high- silica rhyolites and granodiorite plutons: Geology, v. 36, p. 183-186.

Hagstrum, J. T., and Lipman, P. W., 1986, Paleomagnetism of the structurally deformed Latir volcanic field, northern New Mexico: relations to formation of the Questa

caldera and development of the Rio Grande rift: Journal of Geophysical Research, v. 91, p. 7383-7402.

Halliday, A. N., Davidson, J. P., Hildreth, W., Holden, P., 1991, Modeling the petrogenesis of high Rb/Sr silicic magmas: Chemical geology, v. 92, p. 107-114.

Hamilton, W.B., and Myers, W.B., 1967, The nature of batholiths: USGS Professional Paper 554-C, 30 p.

Hammarstrom, J. M., and Zen, E., 1986, Aluminum in hornblende: An empirical igneous geobarometer: American Mineralogist, v. 71, p. 1297-1313.

Hanson, R. B., and Glazner, A. F., 1995, Thermal requirements for extensional emplacement of granitoids: Geology, v. 23, p. 213-216.

Harrison, T. M., 1981, Diffusion of ^{40}Ar in Hornblende: Contributions to Mineralogy and Petrology, v. 78, p. 324-331.

Harrison, T. M., Heizler, M. T., Lovera, O. M., Wenji, C., and Grove, M., 1994, A chlorine disinfectant for excess argon released from K-feldspar during step heating: Earth and Planetary Science Letters, v. 123, p. 95-104.

Heizler, M. T., Lux, D. R., and Decker, E. R., 1988, The age and cooling history of The Chain of Ponds and Big Island plutons and the Spider Lake Granite, west-central Maine and Quebec: American Journal of Science, v. 288, p. 925-952.

Heizler, M. T., 2001, ^{39}Ar recoil distance and implantation efficiency: Eos Transactions, AGU, Fall meeting supplementary abstracts, abstract v22C-1060.

Hildreth, W. 1981, Gradients in silicic magma chambers: Implications for lithospheric magmatism: Journal of Geophysical Research, v. 86, p. 10153-10192.

Hildreth, W., 2004, Volcanological perspectives on Long Valley, Mammoth Mountain, and Mono Craters: several contiguous but discrete systems: Journal of Volcanology and Geothermal Research, v. 136, p. 169–198.

Hildreth, W., and Wilson, C. J. N., 2007, Compostional zoning of the Bishop Tuff: Journal of Petrology, v. 48, p. 1-49.

Hilton, D. R., 1996, The helium and carbon isotope systematics of a continental geothermal system: results from monitoring studies at the Long Valley caldera (California, U.S.A.): Chemical Geology, v. 127, p. 269-295.

Hirt, W. J., 2007, Petrology of the Mount Whitney Intrusive Suite, eastern Sierra Nevada, California: Implications for the emplacement and differentiation of composite felsic intrusions: Geological Society of America Bulletin, v. 119, p. 1185-1200.

Hodges, K. V., 1991, Pressure-temperature-time paths: Annual Reviews Earth and Planetary Science Letters, v. 19, p. 207-236.

Hodges, K. V., Hames, W. E., and Bowring, S. A., 1994, $^{40}Ar/^{39}Ar$ age gradients in micas from a high-temperature-low-pressure metamorphic terrain: Evidence for very slow cooling and implications for the interprettion of age spectra: Geology, v. 22, p. 55-58.

Horra, J. M., Singer, B. S., Worner, G., Beard, B. L., Jicha, B. R., and Johnson, C. M., 2009, Shallow and deep crustal control on differentiation of calc-alkaline and tholeiitic magma: Earth and Planetary Science Letters, v. 285, p. 75-86.

Hubbert, H. E., and Sparks, R. S. J., 1989, Chilled margins in igneous rocks: Earth and Planetary Science Letters, v. 92, p. 397-405.

Jellinek, A. M., and Kerr, R. C., 1999, Mixing and compostional stratification producted by natural convection: 2. Applications to the differentiation of basaltic and silcic magma chambers and komatiite lava flows: Journal of Geophysical Research, v. 104, p. 7203-7218.

Jellinek, A. M., and DePaolo, D. J., 2003, A model for the origin of large silicic magma chambers: Precursors of caldera-forming eruptions: Bulletin of Volcanology, v. 65, p. 363–381.

John, D. A., Henry, C. D., and Colgan, J. P., 2008, Magmatic and tectonic evolution of the Caetano caldera, noerth-central Nevada: A tilted, mid-Tertiary eruptive center and source of the Caetano Tuff: Geosphere, v. 4., 75-106.

Johnson, B. R., and Glazner, A. F., 2010, Formation of K-feldspar megacrysts in granodioritic plutons by thermal cycling and late-stage textural coarsening: Contributions to Mineralogy and Petrology, v. 159, p. 599-619.

Johnson, C. M., and Lipman, P. W., 1988, Origin of metaluminous and alkaline volcanic rocks of the Latir volcanic field, northern Rio Grande Rift, New Mexico: Contributions to Mineralogy and Petrology, v. 100, p. 107-128.

Johnson, C. M., Czamanske, G. K., and Lipman, P. W., 1989, Geochemistry of intrusive rocks associated with the Latir volcanic field, New Mexico, and contrasts between evolution of plutonic and volcanic rocks: Contributions to Mineralogy and Petrology, v. 103, p. 90-109.

Johnson, C. M., 1991, Large-scale crustal formation and lithosphere modification beneath middle to late Cenozoic calderas and volcanic fields, western North America: Journal of Geophysical Research, v. 96, p. 13,485-13,507.

Johnston, S., Gehrels, G., Valencia, V., and Ruiz, J., 2010, Small-volume U-Pb zircon geochronology by laser ablations-multicollector-ICP-MS: Chemical Geology, v. 259, p. 218-229.

Kelley, S, 2002, Excess argon in K-Ar and Ar-Ar geochronology, Chemical Geology, v. 188, p. 1-22.

Kennedy, B., and Stix, J., 2007, Magmatic processes associated with caldera collapse at Ossipee ring dyke, New Hampshire: Geological Society of America Bulletin, v. 119, p. 3.

Klemm, L.M., Pettke, T., and Heinrich, C.A., 2008, Fluid and source magma evolution of the Questa porphyry Mo deposit, New Mexico, USA: Miner Deposita, v. 43, p. 533-552.

Knesel, K. M., and Duffield, W. A., 2007, Gradients in silicic eruptions caused by rapid inputs from above and below rather than protracted chamber differentiation: Journal of Volcanology and Geothermal Research, v. 167, p. 181-197.

Kuiper, K. F., Deino, A., Hilgen, F. J., Krijgsman, W., Renne, P. R., and Wijbrans, J. R., 2008, Synchronizing rock clocks of earth history: Science, v. 320, p. 500-504.

Lawton, T. F., and McMillan, N. J., 1999, Arc abandonment as a cause for passive continental rifting: Comparison of the Jurassic Mexican Borderland rift and the Cenozoic Rio Grande Rift: Geology, v. 27, p. 779-782.

Leonardson, R. W., Dunlop, G., Starquist, V. L., Bratton, G. P., Meyer, J. W., and Osborne, L.W. Jr., 1983, Preliminary geology and molybdenum deposits at Questa, New Mexico; in Babcock, J. W., The genesis of Rocky Mountain ore deposits; changes with time and tectonics: Denver Region Exploration Geologists Society, p. 151-155.

Lipman, P. W., 1975, Evolution of the Platoro caldera complex and related volcanic rocks, southeastern San Juan Mountains, Colorado: U.S. Geological Survey Professional Paper 852, 128 p.

Lipman, P. W., 1984, The roots of ash flow calderas in western North America: Windows into the tops of granitic batholiths: Journal of Geophysical Research, v. 89, p. 8801-8841.

Lipman, P. W., 1988, Evolution of silicic magma in the upper crust: The mid-Tertiary Latir volcanic field and its cogenetic granitic batholith, northern New Mexico, USA: Transactions of the Royal Society of Edinburgh, v. 79, p. 265-288.

Lipman, P. W., 1997, Subsidence of ash-flow calderas: relation to caldera size and magma-chamber geometry: Bulletin of Volcanology, v. 59, p. 198-218.

Lipman, P. W. 2007, Incremental assembly and prolonged consolidation of Cordilleran magma chambers: evidence from the Southern Rocky Mountain volcanic field: Geosphere, v. 3, p. 42-70.

Lipman, P. W., Prostka, H. J., and Christiansen, R. L., 1971, Evolving subduction zones in the Western United States, as interpreted from igneous rocks: Science, v. 174, p. 821-825.

Lipman, P. W., Doe, B. R., Hedge, C. E., and Steven, T. A., 1978, Petrologic evolution of the San Juan volcanic field, southwestern Colorado: Pb and St isotope evidence: Geological Society of America Bulletin, v. 89, p. 59-82.

Lipman, P. W., Mehnert, H. H., Naeser, C. W., and Keller, G. R., 1986, Evolution of the Latir volcanic field, northern New Mexico, and its relation to the Rio Grande Rift, as indicated by potassium-argon and fission track dating: Journal of Geophysical Research, v. 91, p. 6329-6345.

Lipman, P. W., Bogatikov, O. A., Tsvetkov, A. A., Gazis, C., Gurbanov, A. G., Hon, K., Koronovsky, N. V., Kavalenko,V. I., and Marchev, P., 1993, 2.8-Ma ash-flow caldera at Chegem River in the northern Caucasus Mountains (Russia), contemporaneous granites, and associated ore deposits: Journal of Volcanology and Geothermal Research, v. 57, p. 85-124.

Lipman, P. W., and Reed, J.C. Jr., 1989, Geologic map of the Latir volcanic field and adjacent areas, northern New Mexico: U.S. Geological Survey, Miscellaneous Map 1907, scale 1:48,000.

Lipman, P. W., and McIntosh, W. C., 2008, Eruptive and noneruptive calderas, northeastern San Juan Mountains, Colorado: Where did the ignimbrites come from?: Geological Society of America Bulletin, v. 120, p. 771-795.

Ludwig, K., and Mundil, R., 2002, Extracting reliable U-Pb ages and errors from complex populations of zircons from Phanerozoic tuffs: Journal confernce abstracts 12th Goldschmidt conference 2002.

Ludwig, K., 2009, User's Manual for Isoplot 3.70 A geochronological toolkit for Microsoft Excel: Berkeley Geochronology Center Special Publication No. 4

Lo, C., and Onstott, T. C., 1989, ^{39}Ar recoil artifacts in chloritized biotite: Geochimica Cosmochimica Acta, v.53, p. 2967-2711.

Loring, A. K., and Loring, R. B., K/Ar ages of middle Tertiary igneous rocks from southern New Mexico: New Mexico Bureau of Mines and Mineral Resources Isochron/West: v. 28, p. 17-19.

Lovera, O. M., Richter, F. M., and Harrison, T. M., 1989, ^{40}Ar/^{39}Ar thermochronology for slowly cooled samples having a distribution of domain sizes: Journal of Geophysical Research, v.94, p. 17,917-17,935.

Lovera, O. M., Richter, F. M., and Harrision, T. M., 1991, Diffusion domains determined by ^{39}Ar released during step heating, Journal of Geophysical Research., v. 96, p. 2057-2069.

Lovera, O. M., Grove, M., Harrison, T. M., and Mahon, K. I., 1997, Systematic analysis of K-feldspar ^{40}Ar/^{39}Ar step heating results I: Significance of activation energy determinations: Geochemicica et Cosmochimica Acta, v. 61, p. 3171-3192.

Lovera, O. M., Grove, M., and Harrison, T. M., 2002, Systematic analysis of K-feldspar ^{40}Ar/^{39}Ar step heating results II: Relevance of laboratory argon diffusion properties to nature: Geochemicica et Cosmochimica Acta, v. 66, p. 1237-1255.

Mahan, K. H., Bartley, J. M., Coleman, D. S., Glazner, A. F., and Carl, B. S., 2003, Sheet intrusion of the synkinematic McDoogle pluton, Sierra Nevada, California: Geological Society of America Bulletin, v. 115, p 1570-1582.

Mahon, K. I., 1996, The new "York" regression: Application of an improved statistical method to geochemistry. International Geology Review, v.38, p. 293-303.

Matzel, J.E.P., Bowring, S.A., and Miller, R.B., 2006, Time scales of pluton construction at differing crustal levels: Examples from the Mount Stuart and Tenpeak Intrusions, North Cascades, Washington: Geological Society of America Bulletin, v. 118, p. 1412–1430.

McDougall, I., and Harrison, T. M., 1999, Geochronology and thermochronology by the $^{40}Ar/^{39}Ar$ method: New York, Oxford University Press, p. 269.

McIntosh, W. C., Sutter, J. F., Chapin, C. E., and Kedzie, L. L., 1990, High-precision $^{40}Ar/^{39}Ar$ sanidine geochronology of ignimbrites in the Mogollon-Datil volcanic field, southwestern New Mexico: Bulletin of Volcanology, v. 52, p. 584-601.

McIntosh, W. C., Chapin, C. E., Ratte, J. C., and Sutter, J. F., 1992, Time-stratigraphic framework of the Eocene-Oligocene Mogollon-Datil volcanic field, southwest New Mexico: Geological Society of America Bulletin, v. 104, p. 851-871.

McIntosh, W. C., Heizler, M., Peters, L., and Esser, R., 2003, 40Ar/39Ar Geochronology at the New Mexico Bureau of Geology and Mineral Resources: New Mexico Bureau of Geology and Mineral Resources, Open file report OF-Ar-1, p.10.

Meyer, J., and Foland, K.A., 1991, Magmatic-tectonic interaction during early Rio Grande rift extension at Questa, New Mexico: Geological Society of America Bulletin, v. 103, p. 993-1006.

Michel, J., Baumgartner, L., Putlitz, B., Schaltegger, U., and Ovtcharova, M., 2008, Incremental growth of the Patagonian Torres del Paine laccolith over 90 k.y.: Geology, v. 36, p. 459-462.

Miggins, D. P., 2002, Geochronology, geochemical, and isotopic framework of the igneous rocks within the Raton Basin and the adjacent Rio Grande rift, south-central Colorado and northern New Mexico [M.S. thesis]: Boulder, University of Colorado at Boulder, 438 pp.

Miller, C. F. and Miller, J. S., 2002, Contrasting stratified plutons exposed in tilt blocks, Eldorado Mountains, Colorado River Rift, NV, USA: Lithos, v. 61, p. 209-224.

Miller, J. S., Matzel, J. E. P., Miller, C. F., Burgess, S. D., and Miller, R. B., 2007, Zircon growth and recycling during assembly of large composite arc plutons: Journal of Volcanology and Geothermal research, v. 167, p. 282-299.

Miller, C. F., and Wark, D. A., 2008, Supervolcanoes and their explosive supereruptions: Elements, v. 4, p. 11-16.

McIntosh, W. C., and Chapin, C. E., 2004, Geochronology of the central Colorado

volcanic field: New Mexico Bureau of Geology & Mineral Resources, Bulletin 160, p. 205-238.

Meyer, J., and Foland, K. A., 1991, Magmatic-tectonic interaction during early Rio Grande rift extension at Questa, New Mexico: Geological Society of America Bulletin, v. 103, p. 993-1006.

Michel, J., Baumgartner, L., Putlitz, B., Schaltegger, U., and Ovtcharova, M., 2008, Incremental growth of the Patagonian Torres del Paine laccolith over 90 k.y.: Geology, v. 36, p. 459-462.

Min, K., Mundil, R., Renne, P. L., and Ludwig, K. R., 2000, A test for systematic errors in $^{40}Ar/^{39}Ar$ geochronology through comparison with U/Pb analysis of a 1.1-Ga rhyolite: Geochimica et Cosmochimica Acta, v. 64, p. 73-98.

Mills, R. D., Glazner, A. F., and Coleman, D. S. 2008, Comparing the compositional patterns of volcanic and plutonic rocks using the NAVDAT database: Geochimica et Cosmochimica Acta, v. 72.

Mills, R. D., Zimmerer, M. J., Coleman, D. S., McIntosh, W. C., Samperton, K. M., and Tympel, J. F., 2010, High-precision geochronology of ignimbrites and associated plutons of two caldera systems in central Colorado and northern New Mexico: Geological Society of America Abstracts with Programs, v. 42, p. 618.

Morgan, S., Stanik, A., Horsman, E., Tikoff, B., Blanquat, M., and Habert, G., 2008, Emplacement of multiple magma sheets and wall rock deformation: Trachyte Mesa intrusion, Henry Mountains, Utah: Journal of Structural Geology, v. 30, p. 491-512.

Paterson, S. R., Magmatic tubes, pipes, troughs, diapers, and plumes: Late-stage convection instabilities resulting in compositional diversity and permeable networks in crystal-rich magmas of the Tuolumne batholith, Sierra Nevada, California: Geosphere, v. 5, p. 496-527.

Petford, N, Cruden, A. R., McCaffrey, K. J. W., and Vigneresse J. L., 2000, Granite magma formation, transport, and emplacement in the Earth's crust: Nature, v. 408, p. 669-673.

Pillmore, C. L., Obradovich, J. D., Landreth, J. O., and Pugh, L. E., 1973, Mid-Tertiary volcanism in the Sangre de Cristo Mountains of northern New Mexico: Geological Society of America Abstracts with Programs, v. 5, p. 502.

Quick, J.E., Sinigoi, S., Peressini, G., Demarchi, G., Wooden, J.L., and Sbisa, A., 2009, Magmatic plumbing of a large Permian caldera exposed to a depth of 25 km: Geological Society of America Bulletin, v. 37, p. 603-606.

Reid, M. R., Coath, C. D., Harrison, T. M., and McKeegan, K. D., 1997, Protracted residence times for the youngest rhyolites associated with Long Valley Caldera: ^{230}Th-^{238}U ion microprobe dating of young zircon: Earth and Planetary Science Letters, v. 150, p. 27-39.

Renne, P. R., Mundil, R., Balco, G., Min, K., and Ludwig, K. R., 2010, Joint determination of ^{40}K decay constand and $^{40}Ar^*/^{40}K$ for the Fish Canyon sanidine standard, and improved accuracy for $^{40}Ar/^{39}Ar$ geochronology: Geochimica et Cosmochimica Acta, v. 74, p. 5349-5367.

Richter, F.M., Lovera, O.M., Harrison, T.M., and Copeland, P., 1991, Tibetan tectonics from $^{40}Ar/^{39}Ar$ analysis of a single K-feldspar sample, Earth and Planetary Science, v.105, p. 266-278.

Sanders, R. E, and Heizler, M. T., 2005, Extraction of MDD thermal histories from $^{40}Ar/^{39}Ar$ K-feldspar step heating data: New Mexico Bureau of Geology and Mineral Resources Open-File Report OF-AR 26, p. 11.

Schmitz, M. D., and Bowring, S. A., 2001, U-Pb zircon and titanite systematics of the Fish Canyon Tuff; an assessment of high-precision U-Pb geochronology and its application to young volcanic rocks: Geochimica et Cosmochimica Acta, v. 65, p. 2571-2587.

Seager, W. R., 1981, Geology of the Organ Mountains and southern San Andres Mountains, New Mexico: New Mexico Bureau of Mines and Mineral Resources Memoir 36, 97 p.

Seager, W. R. and McCurry, M., 1988, The cogenetic Organ cauldron and batholith, south-central New Mexico: evolution of a large-volume ash flow cauldron and its source magma chamber: Journal of Geophysical Research, v. 93, p. 4421-4433.

Self, S., and Blake, S., 2008, Consequences of explosive supereruptions: Elements, v. 4, p. 41-46.

Simon, J. I., Renne, P. R., Mudnil, R., 2008, Implications of pre-eruptive magmatic histories of zircons for U/Pb geolchronology of silcic extrusions: Earth and Planetary Science Letters, v. 266. P. 182-194.

Sisson, T.W., Ratajeski, K., Hankins, W.B., Glazner, A.F., 2005, Voluminous granitic magmas from common basaltic sources: Contributions to Mineralogy and Petrology 148 (6), p. 635–661.

Shannon, J. R., 1988, Geology of the Mount Aetna cauldron complex, Sawatch Range: Colorado. Ph.D. dissertation, Colorado School of Mines, Golden, CO, United States (USA), 439p.

Shannon, J. R., Epis, R. C., Naeser, C. W., and Obradovich, J. D., 1987, Correlation of intracaldera and outflow and an intrusive tuff dike related to the Oligocene Mount Aetna cauldron, central Colorado, in Drexler J. W., and Larson, E. E. (eds.), Cenozoic volcanism in the Southern Rocky Mountains revisited: Colorado School of Mines, Quarterly, v. 82, p. 65-80.

Smith, R. L., 1979, Ash-flow magmatism: Geological Society of America Bulletin, v. 71, p. 795- 842.

Smith, G. A., Moore, J. D., and McIntosh, W. C., 2002, Assessing roles of volcanism and basin subsidence in causing Oligocene-lower Miocene sedimentation in the northern Rio Grande rift, New Mexico, USA.: Journal of Sedimentary Research, v. 72, p. 836-848.

Stacey, J., and Kramers, J., 1975, Approximation of terrestrial lead isotope evolution by a two-stage model: Earth and Planetary Science Letters, v. 26, p. 207-221.

Steven, T. A., Cunningham, C. G., Naeser, C. W., and Mehnert, H. H., 1979, Revised stratigraphy and radiometric ages of volcanic rocks in the Marysvale area, west-central Utah: U.S. Geological Survey Bulletin 1469, 40 p.

Stimac, J. A., Goff, F., Counce, D., Larocque, A.C.L., Hilton, D.R. and Morgenstern, U., 2004, The crater lake and hydrothermal system of Mount Pinatubo, Phillippines; evolution in the decade after eruption: Bulletin of Volcanology, v. 66, p. 149-167.

Tappa, M. J., Coleman, D. S., Mills, R. D., and Samperton, K. M., (in review), The plutonic record of a silicic ignimbrite from the Latir volcanic field, New Mexico.

Theide, R. C., Bookhagan, B., Arrowsmith, J., R., Sobel, E. R., and Strecker, M. R., 2004, Climatic control on reapid exhumation along the southern Himalayan Front: Earth and Planetary Science Letters, v. 222, p. 791-806.

Thompson, R. A., Dungan, M. A., and Lipman, P. W., 1986, Multiple differentiation processes in the early-rift calc-alkaline volcanics, northern Rio Grande rift, New Mexico: Journal of Geophysical Research, v. 91, p. 6046-6058.

Toulmin, P., and Hammarstrom, J. M., 1990, Geology of the Mount Aetna volcanic center, Chaffee and Gunnison Counties, Colorado: U.S. Geological Seruvey, Bulletin 1864, 44p.

Tweto, O., 1979, The Rio Grande rift system in Colorado, in Riecker, R. E. (ed.) Rio Grande rift: Tectonics and magmatism: Washington D.C., American Geophysical Union, p. 35-36.

Ulmer, P., 2001, Partial melting of the mantle wedge-the role of H2O in the genesis of mantle-derivd ‘arc-related’ magmas: Physics of the Earth and Planetary Interiors, v. 127, p. 215-232.

Ulmer, P., Müntener, O., Kägi, R., Alonzo Pérez, R. and Villiger, S., 2007, Where do primitive arc magmas differentiate and acquire major and trace element composition? An assessment based on field, geochemical and experimental data: SOTA-State of the Arc.

Verplanck, P. L., Farmer, G L., McCurry, M., Mertzman, S., and Snee, L. W., 1995, Isotopic evidence on the origin of compositional layering in an epizonal magma body: Earth and Planetary Science Letters, v. 136, p. 31-41.s

Verplanck, P. L., Farmer, G. L., McCurry, M. and Mertzman, S. A, 1999, The chemical and isotopic differentiation of an epizonal magma body: Organ Needle Pluton, New Mexico: Journal of Petrology, v. 40, p. 653-678.

Walker, B. A., Miller. C. F., Claiborne, L. L., Wooden, J. L., and Miller J. S., 2007,

Geology and geochronology of the Spirit Mountain batholith southern Nevada: Implications for timescales and physical processes of batholith construction: Journal of Volcanology and Geophysical Research, v. 167, p. 239-262.

Watson, E. B., and Harrison, T. M., 1983, Zircon saturation revisited: temperature and composition effects in a variety of crustal magma types: Earth and Planetary Science Letters, v. 64, p. 295-304.s

White, S.M., Crisp, J.A. and Spera, F.J., 2006, Long-term volumetric eruption rates and magma budgets: Geochemistry Geophysics Geosystems, v. 7, p. 1-20.

Wiebe, R. A., 1994, Silicic magma chambers as traps for basaltic magmas: The Cadillac Mountain Intrusive Complex, Mount Desert Island, Maine: The Journal of Geology, v. 102, p. 423-437.

Winter, J. D., 1995, An introduction to igneous and metamorphic petrology, New Jersey: Prentice Hall.

Wood, B. J., 2004, Melting of the fertile peridotite with variable amounts of H_2O, In: Sparks, R. S. J. and Hawkesworth, C. J. (eds) The state of the planet: Frontiers and Challenges in Geophysics. Washington D.C: American Geophysical Union, pp. 69-80.

Yanicak, S., 1992, Petrology and major and trace element geochemistry of the quartz syenite faces of the Organ Needle pluton, New Mexico [M.S. Thesis]: New Mexico State Univeristy, 165 p.

Zimmerer, M. J., Mills, R. D., Coleman, D. S., McIntosh, W. C., and Hughes, S., 2010, Using the intrusive record to understand caldera magmatism: The geochronology and geochemistry of the Mt. Aetna caldera complex, central Colorado: Geological Society of America Abstracts with Programs, v. 42, p. 655.

Zimmerer, M. J., and McIntosh, W. C., in review, The Ar/Ar geo- and thermochronology of the Questa caldera and associated intrusions: Understanding caldera magmatic processes using the volcanic-plutonic relationship.

APPENDIX 1.1.

ANALYTICAL PROCEDURES

Sample Preparation

Table 1.1.1 lists the samples and UTM coordinates of the dated samples. Seven previously prepared minerals separates were provided by Peter Lipman (XXL-XX) and one by Ren Thompson (TPS04) of the USGS. From this sample suite, 54 mineral separates were analyzed.

Samples were prepared using standard mineral separation techniques. Rock samples were crushed in a standard disk mill, sieved to between 200 to 850 μm, and washed in deionized water to remove any dust created by the crushing procedure. Volcanic samples received an additional cleaning in a 15% HF solution for 5-15 minutes to remove any glass and/or quartz adhered to the grains. All samples were then prepared by Frantz magnetic separation, density separated with lithium metatungstate heavy liquid, rinsed and dried. Samples were then handpicked to obtain monomineralic separates. Samples to be dated were analyzed using Cameca SX-100 electron microprobe at the New Mexico Bureau of Geology and Mineral Resources to accomplish two goals. First, BSE images obtained from the electron microprobe insure the highest quality of mineral separation. Second, geochemical characterization of samples prior to $^{40}Ar/^{39}Ar$ analysis allows for recognition of any geochemical variation within the samples, which may be

the result of alteration or geochemical contamination that would degrade the quality of geochronology results.

Irradiations and Correction Factors

Between 20 and 35 mg of the samples selected for dating were placed into 20-hole machined aluminum disks. To monitor neutron fluxes, the interlabratory standard FC-2 = 28.201 Ma (Kuiper et al., 2008) was placed in every other hole. In addition to unknowns and monitors, CaF_2 and K-glass were irradiated to determine calcium and potassium correction factors. Samples were irradiated at either the USGS Triga reactor in the NM-202H position for 6 hrs or the Nuclear Science reactor at the Texas A & M University in the NM-192A and B position for 7 hrs, the NM-196K,L, and M position for 8.85 hrs, the NM-203H position for 7.03 hrs, or the NM-208 K,L, and M position for 7 hrs. Following irradiation, J-values were determined by fusing 5 to 6 single grains of FC-2 from each hole for each tray. J-values were then calculated by assigning mean ages for each hole, fitting a sine curve to the values, and then extrapolating the J-values to the unknowns. Potassium and calcium correction factors were determined by fusing 4 to 5 grains of the CaF_2 and K-glass and the weighted mean averages are: NM-192: $(^{36}Ar/^{37}Ar)_{Ca} = 0.00028\pm0.00001$; $(^{39}Ar/^{37}Ar)_{Ca} = 0.0007\pm0.00002$; $(^{38}Ar/^{39}Ar)_{K} = 0.126\pm4.00e\text{-}4$; $(^{40}Ar/^{39}Ar)_{K} = 0.00\pm4.00e\text{-}4$; NM-196: $(^{36}Ar/^{37}Ar)_{Ca} = 0.000277\pm2.00e\text{-}6$; $(^{39}Ar/^{37}Ar)_{Ca} = 0.000676\pm4.00e\text{-}6$; $(^{38}Ar/^{39}Ar)_{K} = 0.013\pm.0005$; $(^{40}Ar/^{39}Ar)_{K} = 0.00\pm4.00e\text{-}4$; NM-202: $(^{36}Ar/^{37}Ar)_{Ca} = 0.00028\pm0.00002$; $(^{39}Ar/^{37}Ar)_{Ca} = 0.0007\pm0.00005$; $(^{38}Ar/^{39}Ar)_{K} = 0.013\pm0.001$; $(^{40}Ar/^{39}Ar)_{K} = 0.01\pm0.002$; NM-203:

$(^{36}Ar/^{37}Ar)_{Ca}$ = 0.00028±0.00001; $(^{39}Ar/^{37}Ar)_{Ca}$ = 0.00068±0.00002; $(^{38}Ar/^{39}Ar)_{K}$ = 0.0.013±0.001; $(^{40}Ar/^{39}Ar)_{K}$ = 0.00±4.00e-4; NM-208: $(^{36}Ar/^{37}Ar)_{Ca}$ = 0.00028±0.00001; $(^{39}Ar/^{37}Ar)_{Ca}$ = 0.00068±0.00002; $(^{38}Ar/^{39}Ar)_{K}$ = 0.013±0.0005; $(^{40}Ar/^{39}Ar)_{K}$ = 0.00±4.00e-4.

Extraction line and mass spectrometer

All $^{40}Ar/^{39}Ar$ dating was performed at New Mexico Institute of Mining and Technology in the New Mexico Geochronology Research Laboratory. Samples were either incrementally heated using a double-vacuum Molybdenum resistance furnace (hornblende, biotite, K-Feldspar) or fused using a Synrad 50W CO_2 laser (sanidine). Temperature control on the furnace was accomplished by melting Cu-foil for calibration. Following furnace-step heating, gas was expanded into a two-stage extraction line. The first stage contains a SAES GP-50 getter pump, operated at 450°C, where the gas was cleaned before being expanded into the second stage and isolated from the first stage. The second stage contains two SAES GP-50 getter pumps, one operated at room temperature and the other at 450°C, as well as a tungsten filament operated at 2000°C. Clean gas is then expanded into the mass spectrometer and isolated from the second stage. Extracted gas from the laser chamber is expanded into the second stage, but first cleaned using a cold-finger operated at -140°C. Once in the second stage, the gas is treated similarly to the furnace gas as described above.

Isotopic ratios were measured on a MAP-215 50 mass spectrometer with an extended geometry and an effective radius of 30 cm. The mass spectrometer was equipped with a Nier type ion source and used both a Johnston electron multiplier and Faraday collectors, with the electron multiplier operating at 2.2 kV and a gain of

approximately 10,000 over the Faraday. Resolution for mass 40 was approximately 600 during the analysis. Air pipette analysis were conducted to determine the mass discrimination, which were 1.00297±0.00095 to 1.00323±0.00095 for NM-192, 0.99582±0.00086 to 0.99720±0.00084 for NM-196, 1.00141±0.00070 to 1.00216±0.00065 for NM-202, 1.00141±0.00070 for NM-203, and 1.00449±0.00058 for NM-208. Sensitivities (mol/pA) of the furnace and laser, respectively, during the course of this project were: 2.5100 e^{-16} to 2.6500 e^{-16} and 1.4400 e^{-16} to1.5200 e-16 for NM-192, 1.2299 e^{-16} to 1.2700 e^{-16} and 7.0600 e^{-17} to 7.9200 e^{-17} for NM-196, 8.7329 e^{-17} to 8.9676 e^{-17} and 5.0100 e^{-17} to 5.1500 e^{-17} for NM-202, 8.9676 e^{-17} and 5.15 e^{-17} for NM-203, and 8.7771 e^{-17} and 6.4200 e^{-17} for NM-208.

Single-Crystal Laser-Fusion

Single crystals of the monitors and unknown sanidine were loaded into a 221-hole laser tray and were fused by the CO_2 laser. The laser power was between 1.8-3.3 watts for 15 to 30 seconds. After examination of peak regression to determine if any cycles should be removed, blanks and background calculated by taking the average ± standard deviation. Blanks and background for the CO_2 laser averaged 330, 8.10, 1.41, 4.29, 5.52, 29 x 10^{-18} at masses 40, 39, 38, 37, and 36 respectively for the duration of this study.

Furnace Step-Heating

Unknowns to be heated in the furnace were weighed and wrapped in high purity copper foil packets. Sample weights varied as follows: 5.4 to 9.8 mg for biotite, 12.75 to 15.15 mg for hornblende, and 9.03 to 19.2 mg for K-feldspar. Heating schedules varied for each phase. Biotite samples were heated using 11 steps, beginning at 650°C, increasing in 50 to 100°C step intervals, and ending with total fusion. Hornblende

samples were also step heated using 11 increments, but began at higher temperature and had 20-30°C intervals for the bulk of the heating schedule. K-feldspars were heated using isothermal duplicate steps designed to decrepitate fluid inclusions known to host excess argon. In order to extract maximum $^{39}Ar_K$ prior to melting, heating schedules began at lower temperatures, involved isothermal duplicate steps throughout the entire analysis, contain as many as four 1100°C steps, and the time at temperature varied from as little as ten minutes to as much as 2 hours. A similar process of peak regression handling used for laser samples was applied to furnace samples.

Blanks were analyzed during sample step-heating schedules and between samples. Blanks for biotite and hornblende were measured every three to four heating steps and in the case in which numerous samples were ran continuously, blanks corrects were calculated using average ± standard deviation. K-feldspar contained no blanks during the analysis, in an attempt to keep the furnace at temperature, and thus bracketing or preceding blanks were used. Total blanks + backgrounds for the furnace averaged 1290, 20.7, 3.63, 9.68, 7.29 x 10^{-18} at masses 40, 39, 38, 37, and 36 respectively during the course of this study.

Age assignments

Ages were calculated using the FC-2 flux monitor with an assigned age of 28.201 Ma (Kuiper et al., 1998) and a total ^{40}K decay constant of 5.463x10^{-10} derived by Min et al., (2000). Samples heated in the furnace are plotted on age spectra as % ^{39}Ar released vs. apparent age. Additionally, the age spectra are plotted along with auxiliary K/Ca and radiogenic yield plots. A plateau age was assigned to samples that yielded three or more contiguous step that comprise 50% of more the spectrum and overlap at two sigma. The

plateau age is calculated by weighting each of the steps by the inverse of the variance. For analyses not yielding a plateau, the total gas was used to approximate the age. The total gas age was calculated by summing all gas fractions from the steps. Because several of the K-feldspar age spectra yield complex, monotonically increasing ages without a plateau, no weighted mean age was assigned to these spectra.

Laser heated samples are plotted on age probability diagram as apparent age vs. the summation of the normal probability distribution of the individual analysis (Deino and Potts, 1992). Radiogenic yields and K/Ca auxiliary plots are included with the age probability diagrams. After removal of any xenocrystic or problematic ages, the age was calculated by using the inverse variance of the age for each analysis. Errors for both the furnace and laser analysis were calculated using the methods of Taylor (1982). Isochron ages, MSWD, and errors where the MSWD values are ≤ 1 are calculated using method of York (1969). When the MSWD is > 1, the error is multiplied by the square root of the MSWD.

APPENDIX 1.2.

AR/AR DATA TABLES, AGE SPECTRA, AND IDEOGRAMS FOR THE QUESTA CALDERA SAMPLES

Appendix 1.2 contains the data tables, age spectra, and ideograms for all the analyses of this study. Table 1.2.1 contains the single-crystal laser-fusion analyses, table 1.2.2 contains the biotite, hornblende, and groundmass concentrate analyses, and table 1.2.3 contains the K-feldspar analyses. Figure 1.2.1 contains the sanidine ideograms, figure 1.2.2 contains the biotite, hornblende, and groundmass concentrate age spectra, and figure 1.2.3 contains the Kspar analyses.

Table 1.2.1. Questa sanidine laser-fusion $^{40}Ar/^{39}Ar$ analytical data.

	ID	$^{40}Ar/^{39}Ar$	$^{37}Ar/^{39}Ar$	$^{36}Ar/^{39}Ar$ (x 10^{-3})	$^{39}Ar_K$ (x 10^{-15} mol)	K/Ca	$^{40}Ar^*$ (%)	Age (Ma)	±1σ (Ma)
	79L-64, Sanidine, J=0.0007325±0.05%, D=1.003±0.001, NM-192A, Lab#=55916								
X	22	18.97	0.0137	0.5696	3.799	37.2	99.1	25.05	0.08
	16	19.01	0.0138	0.3301	8.642	37.0	99.5	25.18	0.05
	18	18.97	0.0134	0.1428	7.582	38.1	99.8	25.21	0.06
	25	19.05	0.0152	0.3965	8.107	33.7	99.4	25.21	0.06
	23	19.02	0.0143	0.2063	10.165	35.6	99.7	25.25	0.04
	20	19.08	0.0168	0.3154	5.615	30.4	99.5	25.28	0.06
	19	19.09	0.0141	0.3327	10.212	36.1	99.5	25.29	0.05
	21	19.04	0.0144	0.1550	7.151	35.5	99.8	25.29	0.06
	24	19.08	0.0161	0.2715	6.060	31.6	99.6	25.30	0.06
	17	19.12	0.0133	0.3743	6.379	38.3	99.4	25.31	0.06
	Mean age ± 2σ	n=9		MSWD=0.64		35.2 ±5.5		25.26	0.04
	83L-8, Sanidine, J=0.0007313±0.04%, D=1.003±0.001, NM-192A, Lab#=55915								
	18	19.24	0.0047	0.1408	7.790	108.9	99.8	25.53	0.06
	21	19.23	0.0052	0.1047	10.218	97.6	99.8	25.53	0.05
	16	19.24	0.0051	0.1044	7.530	100.5	99.8	25.54	0.06
	23	19.26	0.0046	0.1290	8.402	111.5	99.8	25.55	0.05
	17	19.38	0.0050	0.4987	5.825	103.1	99.2	25.57	0.07
	22	19.28	0.0051	0.1136	7.502	99.2	99.8	25.59	0.06
	20	19.28	0.0051	0.0779	8.743	100.2	99.9	25.60	0.05
	19	19.27	0.0050	0.0219	12.718	103.0	100.0	25.61	0.05
	Mean age ± 2σ	n=8		MSWD=0.39		103.0 ±9.7		25.57	0.04
	82L-42H, Sanidine, J=0.0007304±0.04%, D=1.003±0.001, NM-192A, Lab#=55914								
	23	19.12	0.0099	0.1102	7.351	51.6	99.8	25.34	0.06
	24	19.17	0.0106	0.1160	11.610	48.0	99.8	25.41	0.05
	18	19.18	0.0104	0.0927	11.251	48.8	99.9	25.43	0.05
	17	19.19	0.0099	0.1366	9.240	51.6	99.8	25.43	0.05
	20	19.23	0.0108	0.2095	9.449	47.3	99.7	25.45	0.05
	16	19.22	0.0107	0.0986	9.416	47.7	99.9	25.48	0.06
	21	19.27	0.0108	0.2666	10.898	47.3	99.6	25.49	0.05
	22	19.34	0.0101	0.2749	7.772	50.4	99.6	25.57	0.07
	19	19.30	0.0098	0.0026	8.260	51.9	100.0	25.63	0.06
	Mean age ± 2σ	n=9		MSWD=1.95		49.4 ±3.9		25.46	0.05
	82L-31, Sanidine, J=0.00073±0.04%, D=1.003±0.001, NM-192A, Lab#=55913								
	17	19.77	0.0123	2.817	3.512	41.6	95.8	25.14	0.09
	20	19.13	0.0119	0.5329	3.802	42.8	99.2	25.19	0.09
	16	19.14	0.0133	0.1813	5.532	38.5	99.7	25.33	0.07
	21	19.36	0.0140	0.8500	3.541	36.4	98.7	25.37	0.09
	22	19.43	0.0128	1.033	5.737	39.8	98.4	25.39	0.07
	18	19.23	0.0122	0.3131	5.435	41.8	99.5	25.40	0.06
	19	19.30	0.0135	0.4503	4.317	37.9	99.3	25.44	0.08
	Mean age ± 2σ	n=7		MSWD=1.82		39.8 ±4.7		25.34	0.08
	82L-38, Sanidine, J=0.0007318±0.05%, D=1.003±0.001, NM-192A, Lab#=55911								
	18	19.31	0.0121	1.195	4.101	42.0	98.2	25.22	0.08
	22	19.48	0.0129	1.507	6.135	39.4	97.7	25.32	0.08
	24	19.48	0.0124	1.337	5.146	41.3	98.0	25.39	0.07
	17	19.36	0.0125	0.9208	5.916	40.9	98.6	25.40	0.07
	20	19.51	0.0129	1.350	4.045	39.6	98.0	25.43	0.08
	23	19.28	0.0122	0.5015	6.476	41.7	99.2	25.45	0.06

	25	19.40	0.0130	0.9054	7.060	39.1	98.6	25.45	0.07
	21	19.29	0.0134	0.5082	5.657	38.2	99.2	25.46	0.06
	19	19.33	0.0121	0.5751	5.309	42.3	99.1	25.49	0.07
	16	19.37	0.0121	0.6445	7.418	42.0	99.0	25.51	0.06
	Mean age ± 2σ	n=10	MSWD=1.33			40.6 ±2.9		25.43	0.06
	82L-37, Sanidine, J=0.0007306±0.04%, D=1.003±0.001, NM-192A, Lab#=55912								
	17	20.32	0.0109	4.056	4.725	46.8	94.1	25.40	0.08
	21	20.68	0.0133	5.133	4.592	38.5	92.7	25.45	0.10
	25	20.63	0.0118	4.942	5.113	43.2	92.9	25.45	0.09
	20	20.01	0.0118	2.866	3.388	43.3	95.8	25.46	0.10
x	22	22.84	0.0114	12.38	2.879	44.8	84.0	25.48	0.12
x	19	20.66	0.0132	4.644	6.462	38.8	93.4	25.62	0.07
x	24	20.37	0.0138	3.568	2.759	36.9	94.8	25.65	0.12
x	23	20.17	0.0124	2.881	3.551	41.1	95.8	25.66	0.09
x	16	21.11	0.0111	6.025	6.037	46.0	91.6	25.67	0.08
x	18	20.80	0.0136	4.415	4.543	37.4	93.7	25.89	0.08
	Mean age ± 2σ	n=4	MSWD=0.12			42.9 ±6.8		25.43	0.09
	78L-183, Sanidine, J=0.000733±0.04%, D=1.003±0.001, NM-192A, Lab#=55910								
	24	18.94	0.0031	0.4213	2.724	163.8	99.3	25.07	0.11
	18	18.93	0.0031	0.1172	3.424	165.1	99.8	25.18	0.09
	16	19.08	0.0028	0.6076	3.602	184.1	99.1	25.19	0.09
	21	19.05	0.0050	0.3055	3.257	102.1	99.5	25.27	0.09
	25	19.17	0.0043	0.6228	3.442	118.3	99.0	25.30	0.09
	22	19.12	0.0054	0.3946	2.911	94.6	99.4	25.33	0.10
	19	19.17	0.0033	0.4083	4.337	152.3	99.4	25.38	0.08
	20	19.10	0.0037	0.1838	3.014	136.7	99.7	25.39	0.10
	17	19.18	0.0052	0.2873	3.418	97.2	99.6	25.44	0.09
x	23	19.26	0.0033	-0.1042	4.215	155.7	100.2	25.71	0.08
	Mean age ± 2σ	n=9	MSWD=1.53			134.9 ±66.6		25.29	0.08
	TPS04, Sanidine, J=0.0008937±0.04%, D=1.002±0.001, NM-196K, Lab#=56274								
	09	15.66	0.0035	0.6321	10.089	146.3	98.8	25.13	0.07
	04	15.85	0.0033	1.010	4.169	154.7	98.1	25.26	0.13
	14	15.62	0.0044	0.2464	7.304	116.8	99.5	25.27	0.08
	15	15.64	0.0055	0.2129	16.564	92.7	99.6	25.30	0.05
	02	15.95	0.0053	1.235	3.246	95.5	97.7	25.32	0.17
	07	15.68	0.0024	0.2871	6.487	210.6	99.5	25.34	0.09
	08	15.66	0.0029	0.2169	5.777	175.4	99.6	25.34	0.10
	03	15.87	0.0037	0.9111	5.835	137.1	98.3	25.35	0.10
	10	15.66	0.0028	0.1261	9.041	181.3	99.8	25.37	0.07
	05	15.69	0.0022	0.2018	6.486	230.7	99.6	25.40	0.09
	11	15.78	0.0023	0.4854	3.676	219.7	99.1	25.41	0.14
	01	15.82	0.0033	0.5885	3.852	152.6	98.9	25.41	0.14
	13	15.73	0.0025	0.1550	9.388	201.7	99.7	25.48	0.06
	12	15.85	0.0024	0.4987	3.495	215.7	99.1	25.50	0.15
	06	15.86	0.0038	0.4147	5.682	134.2	99.2	25.57	0.10
	Mean age ± 2σ	n=15	MSWD=1.74			164.3 ±90.1		25.34	0.06
	MZQ-7, Sanidine, J=0.0008934±0.05%, D=1.002±0.001, NM-196K, Lab#=56276								
	06	15.60	0.0031	0.3012	17.124	165.4	99.4	25.19	0.06
	03	15.70	0.0017	0.4638	13.698	293.1	99.1	25.28	0.06
	09	15.63	0.0027	0.2158	10.285	192.2	99.6	25.28	0.08
	12	15.68	0.0010	0.3604	13.101	531.3	99.3	25.29	0.07
	10	15.65	0.0018	0.2803	10.810	287.2	99.5	25.29	0.07
	05	16.04	0.0037	1.596	9.014	137.6	97.1	25.29	0.09
	07	15.67	0.0023	0.3018	13.613	223.5	99.4	25.30	0.06
	34	15.66	0.0036	0.2481	9.799	140.4	99.5	25.31	0.05
	22	15.68	0.0020	0.3333	18.804	250.7	99.4	25.31	0.04
	04	15.75	0.0073	0.5709	5.643	70.0	98.9	25.31	0.13

	24	15.62	0.0027	0.0906	11.767	188.9	99.8	25.32	0.04
	02	15.72	0.0024	0.4154	18.083	210.0	99.2	25.32	0.06
	25	15.68	0.0019	0.2809	5.593	268.6	99.5	25.32	0.06
	28	15.77	0.0032	0.5907	14.374	158.9	98.9	25.33	0.04
	30	15.66	0.0040	0.1929	10.519	126.6	99.6	25.35	0.05
	08	15.77	0.0024	0.5388	6.031	208.5	99.0	25.36	0.12
	15	15.70	0.0043	0.2577	6.345	118.6	99.5	25.37	0.12
	26	15.68	0.0034	0.1787	3.513	148.3	99.7	25.37	0.08
	13	15.68	0.0025	0.1638	6.348	200.9	99.7	25.38	0.11
	27	15.68	0.0028	0.1534	6.995	179.9	99.7	25.39	0.05
	11	15.85	0.0028	0.7350	7.659	179.8	98.6	25.40	0.10
	01	15.78	0.0032	0.4765	8.291	158.6	99.1	25.40	0.09
	29	15.73	0.0026	0.2838	7.631	196.8	99.5	25.41	0.05
	14	15.72	0.0025	0.1218	3.802	203.2	99.8	25.46	0.18
	35	16.04	0.0034	1.233	8.070	150.8	97.7	25.46	0.05
	23	15.79	0.0027	0.3445	6.263	188.9	99.4	25.47	0.06
	32	15.79	0.0010	0.3488	5.073	487.4	99.3	25.48	0.06
	31	15.90	0.0012	0.6498	7.476	421.4	98.8	25.51	0.05
	33	15.99	0.0015	0.8783	6.675	344.1	98.4	25.54	0.06
	Mean age ± 2σ	n=29	MSWD=1.95			221.8 ±213.8		25.36	0.04

MZQ-25, Sanidine, J=0.0008943±0.05%, D=1.002±0.001, NM-196K, Lab#=56279

	14	15.65	0.0058	0.0902	11.823	87.7	99.8	25.40	0.07
	11	15.74	0.0037	0.3880	7.283	139.7	99.3	25.40	0.10
	15	15.95	0.0031	0.9902	11.419	164.0	98.2	25.45	0.07
	04	15.76	0.0042	0.3436	10.299	120.2	99.4	25.46	0.08
	13	15.89	0.0046	0.7763	3.670	111.9	98.6	25.46	0.19
	01	16.00	0.0036	1.011	7.889	142.8	98.1	25.52	0.09
	05	16.60	0.0022	2.991	3.058	228.8	94.7	25.55	0.23
	12	15.75	0.0035	0.0252	4.318	146.6	100.0	25.59	0.16
	03	15.78	0.0037	0.1085	5.109	137.9	99.8	25.60	0.14
	08	15.77	0.0031	-0.0989	4.667	163.6	100.2	25.67	0.15
	09	15.87	0.0036	0.1360	4.291	139.9	99.7	25.73	0.16
	02	15.96	0.0041	0.3835	4.795	124.2	99.3	25.75	0.15
x	06	15.83	0.0021	-0.5526	1.863	248.7	101.0	25.99	0.36
x	10	15.77	0.0061	-0.7884	2.432	84.3	101.5	26.01	0.28
x	07	16.58	0.0004	0.6324	1.705	1152.7	98.9	26.64	0.40
	Mean age ± 2σ	n=12	MSWD=0.99			142.3 ±69.2		25.49	0.07

MZQ-4, Sanidine, J=0.0008934±0.04%, D=1.002±0.001, NM-196K, Lab#=56275

x	01	63.39	0.0112	162.2	14.975	45.6	24.4	25.11	0.36
x	13	76.50	0.0109	206.6	7.255	46.7	20.2	25.12	0.47
x	14	37.33	0.0154	73.59	11.590	33.2	41.8	25.32	0.20
	02	16.42	0.0115	2.746	3.994	44.3	95.1	25.35	0.14
x	03	28.74	0.0102	44.26	15.166	49.9	54.5	25.44	0.14
	06	15.85	0.0106	0.6221	6.769	48.1	98.8	25.44	0.09
x	12	27.59	0.0116	40.32	11.934	43.9	56.8	25.47	0.13
x	11	19.56	0.0112	13.13	6.617	45.7	80.2	25.47	0.11
	05	17.47	0.0132	5.927	4.970	38.8	90.0	25.52	0.12
	15	16.10	0.0109	1.272	3.032	46.9	97.7	25.53	0.17
x	08	22.31	0.0106	22.17	8.149	47.9	70.6	25.60	0.11
x	07	25.45	0.0113	32.57	7.131	45.1	62.2	25.70	0.15
x	09	20.17	0.0149	14.66	8.355	34.1	78.5	25.72	0.10
x	10	18.12	0.0101	7.725	8.134	50.7	87.4	25.72	0.09
	04	16.30	0.0102	1.201	2.430	50.0	97.8	25.89	0.22
	Mean age ± 2σ	n=5	MSWD=1.17			45.6 ±8.7		25.49	0.13

MZQ-17, Sanidine, J=0.0008936±0.05%, D=1.002±0.001, NM-196K, Lab#=56277

	12	18.39	0.0063	3.605	15.427	81.6	94.2	28.13	0.07
	04	17.65	0.0042	1.047	17.940	120.1	98.2	28.14	0.06
	13	17.91	0.0062	1.910	23.950	81.9	96.9	28.15	0.06

	09	17.85	0.0064	1.692	10.246	79.4	97.2	28.16	0.08
	01	17.53	0.0103	0.5023	24.063	49.6	99.2	28.21	0.05
	02	17.66	0.0083	0.9275	18.310	61.7	98.5	28.22	0.06
	03	18.04	0.0099	2.145	12.451	51.5	96.5	28.25	0.07
x	05	18.78	0.0050	4.635	6.323	102.8	92.7	28.26	0.12
	15	17.78	0.0132	1.193	10.225	38.6	98.0	28.28	0.08
	08	17.69	0.0037	0.8398	7.432	136.3	98.6	28.30	0.10
	07	17.51	0.0037	0.2021	7.114	136.8	99.7	28.32	0.10
	11	18.18	0.0037	2.454	5.869	138.3	96.0	28.33	0.12
	06	17.46	0.0032	-0.0016	4.048	159.0	100.0	28.34	0.18
	10	17.72	0.0049	0.8342	5.928	105.2	98.6	28.37	0.12
	14	17.54	0.0058	0.1732	9.481	88.7	99.7	28.39	0.08
	Mean age ± 2σ	n=14	MSWD=1.17		94.9	±76.5		28.22	0.05

MZQ-26, Sanidine, J=0.0008945±0.05%, D=1.002±0.001, NM-196K, Lab#=56280

	03	15.96	0.0062	0.9699	14.668	82.3	98.2	25.49	0.06
	09	16.40	0.0080	2.450	13.145	63.5	95.6	25.49	0.07
	14	16.00	0.0054	1.090	15.900	95.3	98.0	25.50	0.06
	13	16.15	0.0052	1.569	10.310	98.0	97.1	25.51	0.08
	10	16.05	0.0050	1.148	26.971	102.9	97.9	25.54	0.05
	07	16.25	0.0051	1.839	21.132	100.6	96.7	25.55	0.06
	05	16.30	0.0060	1.995	29.354	84.5	96.4	25.55	0.05
	12	16.05	0.0049	1.124	19.906	103.5	97.9	25.56	0.05
	11	16.10	0.0055	1.235	26.656	92.3	97.7	25.58	0.05
	08	16.48	0.0053	2.513	23.155	96.9	95.5	25.59	0.05
	04	16.08	0.0059	1.150	20.959	86.2	97.9	25.60	0.05
	06	15.86	0.0060	0.3570	7.961	84.9	99.3	25.62	0.10
	01	15.98	0.0049	0.7012	29.607	104.1	98.7	25.64	0.04
	15	15.91	0.0040	0.3509	7.333	128.0	99.4	25.70	0.10
	02	15.86	0.0061	0.1161	9.160	84.1	99.8	25.73	0.08
	Mean age ± 2σ	n=15	MSWD=1.03		93.8	±28.8		25.57	0.04

MZQ-22, Sanidine, J=0.0008939±0.05%, D=1.002±0.001, NM-196K, Lab#=56278

	18	15.59	0.0129	0.3852	10.692	39.6	99.3	25.14	0.05
	26	15.67	0.0125	0.6467	9.795	40.9	98.8	25.16	0.05
	07	15.80	0.0121	1.034	12.120	42.1	98.1	25.18	0.07
	08	15.68	0.0120	0.5753	23.417	42.4	98.9	25.21	0.05
	14	15.76	0.0115	0.8391	12.515	44.3	98.4	25.21	0.07
	04	15.83	0.0106	1.058	13.082	48.3	98.0	25.23	0.07
	02	15.65	0.0156	0.3902	9.232	32.8	99.3	25.25	0.08
	27	15.62	0.0140	0.2552	7.559	36.6	99.5	25.26	0.05
	05	15.62	0.0124	0.2631	7.899	41.3	99.5	25.26	0.09
	25	15.60	0.0112	0.1767	10.608	45.7	99.7	25.26	0.05
	17	15.76	0.0136	0.7113	8.067	37.7	98.7	25.27	0.05
	10	15.73	0.0142	0.6054	11.473	35.8	98.9	25.28	0.07
	15	15.62	0.0142	0.2285	11.456	35.8	99.6	25.28	0.07
	12	15.74	0.0132	0.5874	7.297	38.6	98.9	25.29	0.10
	01	15.63	0.0192	0.1884	13.625	26.5	99.7	25.32	0.06
	28	15.65	0.0101	0.2153	7.006	50.6	99.6	25.33	0.05
	16	15.83	0.0123	0.8334	3.636	41.3	98.5	25.33	0.09
	23	15.94	0.0123	1.138	9.355	41.5	97.9	25.35	0.04
	20	15.83	0.0149	0.7858	6.290	34.3	98.5	25.35	0.06
	22	15.72	0.0123	0.4087	4.618	41.6	99.2	25.35	0.07
	13	15.68	0.0140	0.2533	7.679	36.4	99.5	25.36	0.09
	03	15.75	0.0123	0.4840	5.545	41.5	99.1	25.36	0.13
	24	15.87	0.0200	0.8861	8.622	25.6	98.4	25.36	0.05
	06	15.82	0.0134	0.6599	3.734	38.2	98.8	25.39	0.19
	21	15.73	0.0135	0.3553	7.233	37.8	99.3	25.39	0.06
	19	15.91	0.0118	0.9443	5.316	43.3	98.3	25.40	0.07
	09	15.70	0.0119	0.2105	5.933	43.0	99.6	25.41	0.12
	Mean age ± 2σ	n=27	MSWD=1.53		39.4	±11.2		25.28	0.04

MZQ-35, Sanidine, J=0.0007861±0.04%, D=1.0068±0.0015, NM-208L, Lab#=57184

14	17.64	0.0099	0.4045	2.764	51.7	99.3	25.04	0.06
13	17.72	0.0143	0.5639	1.753	35.6	99.1	25.09	0.09
05	17.61	0.0103	0.1784	6.975	49.4	99.7	25.10	0.05
06	17.72	0.0126	0.4100	1.891	40.5	99.3	25.15	0.08
07	17.66	0.0118	0.2131	2.862	43.1	99.6	25.15	0.06
12	17.73	0.0117	0.4382	2.284	43.8	99.3	25.16	0.07
09	17.87	0.0130	0.8449	2.372	39.3	98.6	25.18	0.07
17	17.69	0.0100	0.1956	2.791	51.0	99.7	25.20	0.06
10	17.84	0.0078	0.7047	2.252	65.4	98.8	25.20	0.07
16	17.72	0.0100	0.3026	2.333	51.0	99.5	25.20	0.07
08	17.74	0.0081	0.2932	2.548	63.1	99.5	25.23	0.07
15	17.72	0.0091	0.2094	2.650	56.2	99.7	25.23	0.07
11	17.73	0.0119	0.1137	4.142	42.9	99.8	25.30	0.06
Mean age ± 2σ	n=13	MSWD=1.21			48.7 ±18.0		25.17	0.04

Notes:

Isotopic ratios corrected for blank, radioactive decay, and mass discrimination, not corrected for interfering reactions.
Errors quoted for individual analyses include analytical error only, without interfering reaction or J uncertainties.
Mean age is weighted mean age of Taylor (1982). Mean age error is weighted error
of the mean (Taylor, 1982), multiplied by the root of the MSWD where MSWD>1, and also
incorporates uncertainty in J factors and irradiation correction uncertainties.
Decay constants and isotopic abundances after Min et al. (2000).
symbol preceding sample ID denotes analyses excluded from mean age calculations.
Ages calculated relative to FC-2 Fish Canyon Tuff sanidine interlaboratory standard at 28.201 Ma (Kuiper et al., 2008)
Decay Constant (LambdaK (total)) = 5.463e-10/a
Correction factors:
$(^{39}Ar/^{37}Ar)_{Ca}$ = 0.00068 ± 2e-05
$(^{36}Ar/^{37}Ar)_{Ca}$ = 0.00028 ± 1e-05
$(^{38}Ar/^{39}Ar)_{K}$ = 0.0125
$(^{40}Ar/^{39}Ar)_{K}$ = 0 ± 0.0004

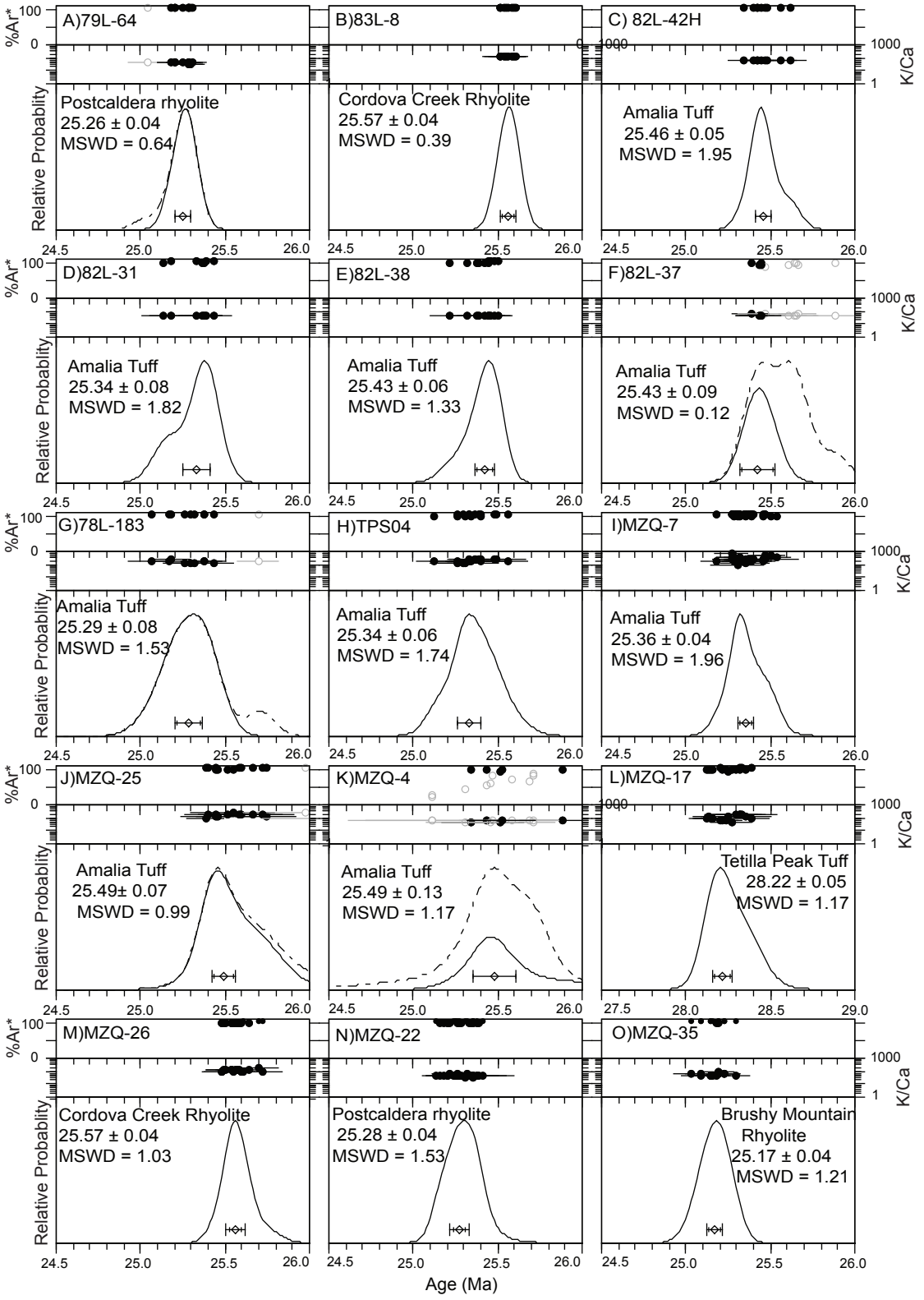

Figure 1.2.1. Ideograms of the Questa caldera sanidine laser-fusions analyses

Table 1.2.2. Questa biotite, hornblende, and groundmass concentrate $^{40}Ar/^{39}Ar$ analytical data.

	ID	Temp (°C)	$^{40}Ar/^{39}Ar$	$^{37}Ar/^{39}Ar$	$^{36}Ar/^{39}Ar$ (x 10^{-3})	$^{39}Ar_K$ (x 10^{-15} mol)	K/Ca	$^{40}Ar^*$ (%)	^{39}Ar (%)	Age (Ma)	±1σ (Ma)
	MZQ-24, Biotite, 7.33 mg, J=0.0013512±0.07%, D=1.002±0.001, NM-202H, Lab#=56745-01										
x	A	650	199.0	0.2005	621.4	0.343	2.5	7.8	0.3	37.80	4.30
	B	750	35.14	0.0473	84.22	0.321	10.8	29.2	0.6	25.17	3.44
	C	850	15.89	0.0164	16.55	2.75	31.2	69.2	3.0	26.99	0.42
	D	920	12.76	0.0106	4.672	9.88	48.2	89.2	11.5	27.92	0.13
	E	1000	11.88	0.0063	1.426	21.3	80.5	96.5	30.0	28.11	0.07
	F	1075	11.76	0.0088	1.306	23.3	57.7	96.7	50.2	27.90	0.07
	G	1110	11.80	0.0138	1.553	8.45	36.9	96.1	57.5	27.81	0.14
	H	1180	11.94	0.0461	1.845	11.12	11.1	95.5	67.2	27.97	0.11
	I	1210	11.78	0.0553	1.284	11.73	9.2	96.8	77.3	27.97	0.10
	J	1250	11.69	0.0714	1.155	20.1	7.1	97.1	94.8	27.84	0.07
	K	1300	11.81	0.1299	1.047	5.70	3.9	97.5	99.7	28.23	0.20
x	L	1720	21.87	19.02	47.50	0.352	0.027	43.0	100.0	23.42	3.09
	Integrated age ± 2σ			n=12	MSWD=2.27	115.3	5.4	K2O=4.47%		27.94	0.11
	Plateau ± 2σ	steps B-K		n=10	MSWD=1.96	114.6	37.8 ±51.9		99.4	27.95	0.10
	Isochron±2σ	steps A-L		n=12	MSWD=2.25		$^{40}Ar/^{36}Ar$=	299.5±5.4		27.94	0.08
	MZQ-15, Biotite, 6.96 mg, J=0.0013512±0.07%, D=1.002±0.001, NM-202H, Lab#=56743-01										
x	A	650	349.5	1.266	1114.2	0.249	0.40	5.8	0.4	49.70	6.40
	B	750	38.59	0.3260	94.00	0.618	1.6	28.1	1.4	26.60	1.88
	C	850	17.23	0.0242	22.42	4.29	21.1	61.5	7.9	26.02	0.29
	D	920	13.23	0.0179	9.716	7.47	28.6	78.3	18.6	25.43	0.17
	E	1000	11.44	0.0190	3.615	8.86	26.8	90.7	30.1	25.47	0.13
	F	1075	11.25	0.0435	2.961	5.71	11.7	92.3	37.0	25.46	0.20
	G	1110	11.37	0.0521	3.629	4.47	9.8	90.6	42.2	25.27	0.25
	H	1180	11.65	0.0984	4.320	9.73	5.2	89.1	52.6	25.47	0.12
	I	1210	11.47	0.1520	3.942	15.47	3.4	89.9	67.3	25.31	0.09
	J	1250	10.99	0.0613	2.135	34.6	8.3	94.3	93.8	25.45	0.05
	K	1300	11.04	0.0499	2.022	7.79	10.2	94.6	98.9	25.63	0.15
	L	1720	14.52	5.007	16.32	1.79	0.10	69.6	100.0	24.91	0.62
	Integrated age ± 2σ			n=12	MSWD=2.17	101.1	3.2	K2O=4.13%		25.52	0.13
	Plateau ± 2σ	steps B-L		n=11	MSWD=0.95	100.8	11.1 ±19.7		99.8	25.44	0.08
	Isochron±2σ	steps A-L		n=12	MSWD=0.82		$^{40}Ar/^{36}Ar$=	303.7±4.3		25.38	0.09
	MZQ-16, Biotite, 8.1 mg, J=0.000897±0.06%, D=1.002±0.001, NM-196M, Lab#=56294-01										
x	A	650	272.2	0.0460	881.1	0.607	11.1	4.3	0.5	19.34	2.64
x	B	750	44.74	0.0347	99.99	1.30	14.7	34.0	1.7	24.79	0.58
x	C	850	28.83	0.0110	46.23	5.40	46.2	52.6	6.5	24.74	0.19
x	D	920	21.40	0.0096	21.70	9.99	53.1	70.0	15.2	24.45	0.11
	E	1000	17.37	0.0100	6.479	11.3	51.1	89.0	24.8	25.20	0.06
	F	1075	16.65	0.0139	4.038	10.19	36.8	92.8	33.4	25.21	0.07
	G	1110	17.08	0.0037	5.303	9.23	136.4	90.8	41.0	25.29	0.07
	H	1180	16.59	0.0128	3.998	25.4	39.8	92.9	61.2	25.13	0.05
	I	1210	16.11	0.0041	2.267	30.1	124.7	95.8	84.1	25.18	0.04
	J	1720	16.40	0.0088	3.288	21.8	58.1	94.1	100.0	25.16	0.05
	Integrated age ± 2σ			n=10	MSWD=6.01	125.3	55.2	K2O=6.63%		25.07	0.11
	Plateau ± 2σ	steps E-J		n=6	MSWD=0.71	108.0	76.3 ±88.5		86.2	25.19	0.06
	Isochron±2σ	steps A-J		n=10	MSWD=3.63		$^{40}Ar/^{36}Ar$=	289.2±2.7		25.21	0.06
	MZQ-39, Biotite, 7.89 mg, J=0.0007667±0.07%, D=1.004±0.001, NM-208M, Lab#=57199-01										
x	A	650	347.5	0.0265	1158.2	0.749	19.3	1.5	1.3	7.43	3.82
x	B	750	56.65	0.0042	139.0	2.290	120.2	27.5	5.1	21.72	1.13
	C	850	25.63	0.0020	26.63	12.66	250.7	69.3	23.5	24.75	0.21
	D	920	25.14	0.0021	26.37	12.29	240.7	69.0	37.9	24.19	0.22

	E	1000	23.86	0.0030	21.79	9.31	168.8	73.0	47.0	24.28	0.27
	F	1075	21.06	0.0053	12.14	6.93	96.8	83.0	53.1	24.36	0.34
	G	1110	20.01	0.0045	7.568	7.15	112.5	88.8	58.7	24.77	0.33
	H	1180	20.56	0.0049	9.415	19.69	103.2	86.5	71.8	24.78	0.14
	I	1210	19.47	0.0163	5.453	18.82	31.2	91.7	81.8	24.89	0.14
	J	1250	18.86	0.0042	3.227	27.5	120.7	94.9	93.2	24.96	0.10
	K	1300	18.96	0.0015	3.268	17.41	336.7	94.9	99.1	25.07	0.14
	L	1650	20.48	0.1370	11.61	3.06	3.7	83.3	100.0	23.79	0.77
	Integrated age ± 2σ			n=12	MSWD=4.50	137.9	61.4		K2O=8.76%	24.60	0.17
	Plateau ± 2σ	steps C-L		n=10	MSWD=2.36	134.8	155.7	±206.8	97.8	24.82	0.17
	Isochron±2σ	steps A-L		n=12	MSWD=0.99		$^{40}Ar/^{36}Ar$=	282.7±4.2		24.98	0.13
	MZQ-12, Biotite, 8.97 mg, J=0.0007714±0.08%, D=1.004±0.001, NM-208M, Lab#=57195-01										
x	A	650	1083.5	0.0826	3656.0	1.110	6.2	0.3	1.6	4.42	7.10
x	B	750	89.11	0.0196	253.5	5.89	26.0	15.9	9.9	19.94	0.72
	C	850	22.56	0.0054	16.96	30.4	93.7	77.8	42.3	24.62	0.11
	D	920	19.52	0.0044	5.900	25.4	115.8	91.1	60.8	24.93	0.11
	E	1000	20.43	0.0073	9.684	18.65	69.5	86.0	71.4	24.64	0.14
	F	1075	21.28	0.0139	12.79	17.79	36.7	82.3	79.8	24.55	0.15
	G	1110	20.21	0.0188	8.464	12.84	27.1	87.6	85.0	24.83	0.20
	H	1180	19.74	0.0620	6.524	16.52	8.2	90.3	90.9	24.99	0.15
	I	1210	19.34	0.2380	5.104	15.46	2.1	92.3	95.8	25.04	0.16
	J	1250	19.05	0.5024	4.157	12.86	1.0	93.8	99.4	25.06	0.19
	K	1300	20.23	0.2139	7.751	1.924	2.4	88.8	99.9	25.19	1.21
	L	1650	61.92	3.181	144.2	0.278	0.16	31.6	100.0	27.49	8.64
	Integrated age ± 2σ			n=12	MSWD=6.11	159.1	6.0		K2O=8.83%	24.50	0.23
	Plateau ± 2σ	steps C-L		n=10	MSWD=1.55	152.1	54.4	±85.5	95.6	24.81	0.13
	Isochron±2σ	steps A-L		n=12	MSWD=2.44		$^{40}Ar/^{36}Ar$=	288.3±2.3		24.90	0.11
	MZQ-13, Biotite, 9.16 mg, J=0.0007705±0.07%, D=1.004±0.001, NM-208M, Lab#=57196-01										
x	A	650	671.9	0.1529	2270.7	0.988	3.3	0.1	1.5	1.23	4.79
x	B	750	96.46	0.0194	275.8	3.01	26.3	15.5	5.8	21.00	1.03
x	C	850	24.46	0.0059	24.33	16.86	86.8	70.6	26.6	24.20	0.17
	D	920	19.85	0.0038	7.215	25.1	134.7	89.3	49.4	24.82	0.11
	E	1000	20.87	0.0078	11.00	27.6	65.0	84.4	67.5	24.69	0.10
	F	1075	20.02	0.0190	7.400	20.48	26.9	89.1	77.8	24.98	0.13
	G	1110	18.93	0.0241	3.888	13.56	21.1	93.9	83.6	24.91	0.18
	H	1180	18.69	0.0629	3.096	16.41	8.1	95.1	89.7	24.91	0.15
	I	1210	18.32	0.1363	2.179	18.24	3.7	96.5	95.6	24.78	0.14
	J	1250	18.31	0.4015	1.754	13.54	1.3	97.4	99.4	24.98	0.18
	K	1300	19.13	0.2820	3.077	1.808	1.8	95.4	99.9	25.56	1.30
	L	1650	41.36	3.173	83.55	0.318	0.16	40.9	100.0	23.78	7.28
	Integrated age ± 2σ			n=12	MSWD=5.02	157.9	6.8		K2O=8.59%	24.57	0.18
	Plateau ± 2σ	steps D-L		n=9	MSWD=0.61	137.0	45.5	±89.3	86.8	24.84	0.11
	Isochron±2σ	steps A-L		n=12	MSWD=0.96		$^{40}Ar/^{36}Ar$=	286.8±2.6		24.89	0.11
	MZQ-5, Biotite, 5.4 mg, J=0.0008978±0.06%, D=1.002±0.001, NM-196L, Lab#=56290-01										
x	A	650	608.1	0.0491	2005.7	0.232	10.4	2.5	0.4	25.22	6.05
x	B	750	103.1	0.0056	290.4	0.836	90.9	16.7	1.7	28.10	1.07
	C	850	34.77	0.0036	65.05	3.89	141.0	44.7	7.7	25.37	0.26
	D	920	22.35	0.0016	24.14	5.47	319.7	68.1	16.1	24.84	0.15
	E	1000	18.13	0.0033	9.854	6.19	156.0	83.9	25.4	24.85	0.10
	F	1075	17.13	0.0032	6.119	6.31	158.9	89.4	34.8	25.02	0.10
	G	1110	17.54	0.0027	7.750	5.26	187.3	86.9	42.4	24.90	0.10
	H	1180	16.85	0.0064	5.322	15.0	80.2	90.7	63.3	24.94	0.06
	I	1210	16.03	0.0030	2.527	20.2	169.2	95.3	90.1	24.94	0.05
	J	1720	16.59	0.0345	4.426	7.79	14.8	92.1	100.0	24.96	0.07
	Integrated age ± 2σ			n=10	MSWD=1.54	71.1	70.0		K2O=5.63%	25.00	0.14
	Plateau ± 2σ	steps C-J		n=8	MSWD=0.73	70.0	142.5	±175.3	98.5	24.94	0.06
	Isochron±2σ	steps A-J		n=10	MSWD=1.12		$^{40}Ar/^{36}Ar$=	298.1±2.5		24.92	0.07

MZQ-6, Biotite, 7.5 mg, J=0.0008977±0.06%, D=1.002±0.001, NM-196L, Lab#=56291-01

x	A	650	458.8	0.1486	1516.5	0.777	3.4	2.3	0.8	17.53	4.17
x	B	750	40.61	0.0281	88.72	3.75	18.2	35.4	4.7	23.50	0.54
	C	850	23.94	0.0154	30.63	13.4	33.1	62.2	18.5	24.31	0.17
	D	920	19.04	0.0166	13.59	16.0	30.7	78.9	34.5	24.53	0.13
	E	1000	19.66	0.0300	15.07	15.7	17.0	77.4	49.6	24.82	0.14
	F	1075	17.00	0.0302	5.879	14.7	16.9	89.8	63.3	24.92	0.13
	G	1110	16.19	0.0291	3.278	15.1	17.5	94.0	76.9	24.84	0.13
	H	1180	15.80	0.2107	2.295	15.1	2.4	95.8	90.2	24.71	0.13
	I	1210	15.64	0.0864	1.532	9.74	5.9	97.2	98.5	24.80	0.19
	J	1720	19.96	0.2953	15.05	1.83	1.7	77.8	100.0	25.36	0.98
	Integrated age ± 2σ			n=10	MSWD=2.24	106.3	8.2		K2O=6.06%	24.63	0.19
	Plateau ± 2σ	steps C-J		n=8	MSWD=1.74	101.7	17.8 ±23.9		95.7	24.73	0.14
	Isochron±2σ	steps A-J		n=10	MSWD=1.15		$^{40}Ar/^{36}Ar$=	290.9±3.0		24.80	0.12

AR-171, Biotite, 8.24 mg, J=0.0007661±0.07%, D=1.004±0.001, NM-208M, Lab#=57200-01

x	A	650	169.2	0.0556	524.3	1.805	9.2	8.4	3.0	19.83	1.78
	B	750	51.79	0.0364	117.6	6.10	14.0	32.9	12.5	23.73	0.49
	C	850	20.69	0.0048	9.836	20.08	105.7	86.0	37.4	24.78	0.14
	D	920	18.81	0.0039	3.704	20.96	131.4	94.2	56.3	24.68	0.12
	E	1000	18.78	0.0183	3.869	9.31	27.8	93.9	63.1	24.57	0.26
	F	1075	19.71	0.1088	7.770	3.69	4.7	88.4	65.6	24.27	0.63
	G	1110	19.19	0.0962	6.486	3.06	5.3	90.1	67.6	24.08	0.76
	H	1180	19.08	0.1229	5.060	9.08	4.2	92.2	73.0	24.51	0.26
	I	1210	18.63	0.0894	3.189	37.9	5.7	95.0	90.7	24.65	0.08
	J	1250	18.28	0.0143	2.107	25.2	35.7	96.6	99.4	24.60	0.11
	K	1300	19.03	0.1384	6.928	1.092	3.7	89.3	99.7	23.68	2.11
	L	1650	38.73	0.5935	71.22	0.971	0.86	45.8	100.0	24.71	2.43
	Integrated age ± 2σ			n=12	MSWD=1.21	139.2	10.2		K2O=8.47%	24.52	0.17
	Plateau ± 2σ	steps B-L		n=11	MSWD=0.61	137.4	46.7 ±90.2		98.7	24.64	0.10
	Isochron±2σ	steps A-L		n=12	MSWD=0.36		$^{40}Ar/^{36}Ar$=	289.5±4.0		24.68	0.11

MZQ-8, Biotite, 9.85 mg, J=0.0007719±0.08%, D=1.004±0.001, NM-208M, Lab#=57194-01

x	A	650	177.1	0.4616	555.8	1.190	1.1	7.3	1.5	18.13	2.30
x	B	750	44.03	0.0294	84.40	3.28	17.3	43.4	5.6	26.79	0.80
	C	850	21.40	0.0075	11.74	14.23	68.2	83.8	21.3	25.16	0.18
	D	920	18.50	0.0091	3.343	20.10	55.9	94.7	39.1	24.58	0.15
	E	1000	18.28	0.0230	2.564	15.28	22.2	95.9	50.0	24.59	0.16
	F	1075	18.46	0.0460	2.938	10.54	11.1	95.3	56.6	24.70	0.23
	G	1110	18.38	0.0440	2.642	11.05	11.6	95.8	62.7	24.71	0.22
	H	1180	18.23	0.0652	2.886	28.9	7.8	95.4	76.1	24.40	0.09
	I	1210	17.91	0.1217	1.521	30.9	4.2	97.5	87.2	24.51	0.09
	J	1250	17.77	0.0232	1.160	38.6	22.0	98.1	98.0	24.46	0.08
	K	1300	18.31	0.0170	2.460	8.03	30.0	96.0	99.9	24.67	0.30
	L	1650	34.94	1.531	53.12	0.534	0.33	55.4	100.0	27.19	4.46
	Integrated age ± 2σ			n=12	MSWD=2.97	182.7	9.6		K2O=9.23%	24.59	0.13
	Plateau ± 2σ	steps C-L		n=10	MSWD=1.90	178.2	23.1 ±45.0		97.6	24.54	0.12
	Isochron±2σ	steps A-L		n=12	MSWD=3.23		$^{40}Ar/^{36}Ar$=	294.8±5.6		24.55	0.10

MZQ-34, Biotite, 8.62 mg, J=0.0007675±0.07%, D=1.004±0.001, NM-208M, Lab#=57198-01

	B	750	40.01	0.0161	77.83	2.71	31.6	42.5	4.4	23.74	0.91
	C	850	20.17	0.0038	8.594	19.35	132.7	87.4	30.2	24.60	0.14
	D	920	18.77	0.0041	4.419	16.54	125.4	93.0	46.8	24.38	0.15
	E	1000	18.62	0.0123	3.804	10.62	41.4	94.0	55.5	24.42	0.22
	F	1075	19.17	0.0203	5.861	7.81	25.2	91.0	61.2	24.34	0.30
	G	1110	18.71	0.0160	4.710	10.35	31.8	92.6	67.9	24.18	0.23
	H	1180	18.98	0.0326	5.138	27.3	15.7	92.0	82.3	24.37	0.10
	I	1210	18.25	0.0405	2.737	25.0	12.6	95.6	92.4	24.35	0.10
	J	1250	18.03	0.0111	2.126	18.69	45.9	96.5	98.6	24.29	0.13
	K	1300	18.51	0.0182	3.815	3.23	28.0	93.9	99.5	24.25	0.72

	L	1650	21.72	0.3575	19.46	1.552	1.4	73.7	100.0	22.35	1.47
	Integrated age ± 2σ			n=11	MSWD=0.65	143.1	21.7		K2O=8.31%	24.34	0.14
	Plateau ± 2σ	steps B-L		n=11	MSWD=0.65	143.1	51.6	±87.2	100.0	24.37	0.11
	Isochron±2σ	steps B-L		n=11	MSWD=0.68		$^{40}Ar/^{36}Ar$=	295.4±16.2		24.38	0.15
	MZQ-19, Biotite, 9.69 mg, J=0.0006961±0.04%, D=1.002±0.001, NM-203H, Lab#=56825-01										
X	A	650	606.9	-0.0050	1961.9	0.188	-	4.5	0.1	34.25	5.76
X	B	750	70.84	0.0919	192.2	2.25	5.6	19.8	1.5	17.83	0.46
X	C	850	25.17	0.0072	28.95	17.2	71.3	66.0	12.5	21.06	0.09
X	D	920	20.17	0.0091	10.79	13.09	56.0	84.2	20.9	21.51	0.07
X	E	1000	19.83	0.0110	8.689	16.3	46.2	87.1	31.3	21.86	0.06
X	F	1075	19.35	0.0227	6.959	24.0	22.5	89.4	46.9	21.90	0.05
X	G	1110	18.42	0.0307	4.422	13.25	16.6	92.9	55.5	21.68	0.05
X	H	1180	17.81	0.0353	3.195	29.4	14.5	94.7	74.8	21.36	0.04
X	I	1210	17.77	0.0628	2.881	19.6	8.1	95.2	87.9	21.43	0.05
X	J	1250	17.79	0.1382	2.623	14.54	3.7	95.7	97.6	21.57	0.05
X	K	1300	18.92	0.1961	6.244	3.64	2.6	90.3	100.0	21.65	0.14
	Integrated age ± 2σ			n=11	MSWD=21.32	153.5	11.9		K2O=8.74%	21.51	0.09
	Plateau ± 2σ	no plateau		n=0	MSWD=0.00	0.000	0.000±0.000		0.0	0.00	0.00
	Isochron±2σ	steps A-K		n=11	MSWD=20.77		$^{40}Ar/^{36}Ar$=	289.3±2.6		21.61	0.04
	MZQ-9, Biotite, 7.4 mg, J=0.0008972±0.06%, D=1.002±0.001, NM-196L, Lab#=56292-01										
x	A	650	216.6	0.3433	691.0	0.597	1.5	5.7	0.6	20.29	3.42
x	B	750	30.09	0.0380	61.03	5.18	13.4	40.1	5.8	19.70	0.37
x	C	850	15.33	0.0127	8.863	17.9	40.1	82.9	23.2	20.75	0.11
	D	920	13.55	0.0086	1.831	14.7	59.0	96.0	37.1	21.25	0.12
	E	1000	14.14	0.0196	3.643	17.6	26.0	92.4	53.2	21.33	0.11
	F	1075	13.52	0.0414	2.099	18.4	12.3	95.4	69.4	21.06	0.10
	G	1110	13.56	0.0593	2.053	12.9	8.6	95.6	80.4	21.16	0.14
	H	1180	13.38	0.1781	1.237	15.3	2.9	97.4	93.2	21.27	0.12
	I	1210	13.43	0.2858	1.139	6.83	1.8	97.7	98.7	21.42	0.25
	J	1250	13.95	0.6095	4.428	1.39	0.84	91.0	99.8	20.73	1.17
	K	1300	19.90	2.186	22.05	0.211	0.23	68.2	100.0	22.18	7.88
	Integrated age ± 2σ			n=11	MSWD=3.46	111.0	6.6		K2O=6.42%	21.08	0.13
	Plateau ± 2σ	steps D-K		n=8	MSWD=0.70	87.4	19.7	±40.3	78.7	21.22	0.10
	Isochron±2σ	steps A-K		n=11	MSWD=2.57		$^{40}Ar/^{36}Ar$=	288.3±4.8		21.18	0.10
	MZQ-21, Biotite, 9.8 mg, J=0.000897±0.07%, D=1.002±0.001, NM-196M, Lab#=56295-01										
x	A	650	351.1	0.0953	1154.0	2.40	5.4	2.9	1.6	16.45	2.59
x	B	750	29.29	0.0228	60.79	6.59	22.4	38.7	6.2	18.50	0.31
x	C	850	23.30	0.0152	40.00	15.5	33.6	49.3	16.8	18.76	0.16
	D	920	18.33	0.0116	22.34	22.9	44.0	64.0	32.4	19.17	0.11
	E	1000	16.51	0.0185	15.68	16.0	27.6	71.9	43.4	19.39	0.12
	F	1075	13.28	0.0181	5.042	24.2	28.2	88.8	60.0	19.27	0.08
	G	1110	12.85	0.0283	3.221	16.6	18.1	92.6	71.3	19.43	0.10
	H	1180	12.56	0.1531	2.360	22.9	3.3	94.5	87.0	19.40	0.08
	I	1210	12.30	0.0615	1.497	14.4	8.3	96.4	96.8	19.37	0.12
	J	1720	14.36	0.2127	6.936	4.61	2.4	85.8	100.0	20.14	0.36
	Integrated age ± 2σ			n=10	MSWD=3.44	146.1	10.0		K2O=6.38%	19.21	0.19
	Plateau ± 2σ	steps D-J		n=7	MSWD=1.67	121.6	21.7	±30.8	83.2	19.35	0.11
	Isochron±2σ	steps A-J		n=10	MSWD=2.25		$^{40}Ar/^{36}Ar$=	291.7±2.3		19.37	0.09
	MZQ-32, Biotite, 8.69 mg, J=0.0007685±0.07%, D=1.004±0.001, NM-208M, Lab#=57197-01										
x	A	650	273.9	0.0958	905.7	0.829	5.3	2.3	1.3	8.74	3.29
	B	750	37.35	0.0109	82.40	4.33	46.8	34.8	7.8	18.19	0.58
	C	850	17.92	0.0046	14.11	20.66	110.4	76.7	33.2	19.24	0.13
	D	920	16.16	0.0050	8.158	14.80	101.9	85.1	47.1	19.24	0.16
	E	1000	17.30	0.0086	11.92	14.26	59.0	79.6	58.0	19.28	0.17
	F	1075	17.18	0.0173	11.51	11.55	29.5	80.2	65.6	19.29	0.21
	G	1110	15.58	0.0166	6.354	16.00	30.7	88.0	74.6	19.18	0.15

	H	1180	15.32	0.0415	5.635	26.9	12.3	89.2	86.7	19.11	0.10
	I	1210	14.76	0.0788	3.995	19.68	6.5	92.0	93.8	19.02	0.12
	J	1250	14.47	0.0464	2.970	17.54	11.0	94.0	99.2	19.02	0.13
	K	1300	14.82	0.0332	4.985	2.237	15.4	90.1	99.9	18.69	1.00
	L	1650	24.53	1.205	44.30	0.493	0.42	47.0	100.0	16.18	4.40
	Integrated age ± 2σ			n=12	MSWD=1.57	149.3	15.1		K2O=8.59%	19.06	0.14
	Plateau ± 2σ	steps B-L		n=11	MSWD=0.73	148.4	42.8	±75.5	99.4	19.14	0.10
	Isochron±2σ	steps A-L		n=12	MSWD=0.81		$^{40}Ar/^{36}Ar$=	288.7±4.7		19.22	0.11

MZQ-36, Groundmass Concentrate, 24.01 mg, J=0.0007736±0.08%, D=1.0068±0.0015, NM-208K, Lab#=57182-01

x	A	3	66.22	0.5791	190.0	1.76	0.88	15.3	3.0	14.30	0.57
x	B	3	20.48	0.5559	23.65	7.36	0.92	66.1	14.8	19.08	0.10
x	C	4	18.89	0.6332	11.50	18.2	0.81	82.3	39.8	21.89	0.07
	D	4	18.30	0.5806	7.679	16.10	0.88	87.9	57.8	22.64	0.06
	E	5	18.01	0.5893	6.466	19.3	0.87	89.7	75.8	22.73	0.06
	F	6	19.71	0.6358	12.42	16.29	0.80	81.7	88.5	22.67	0.07
x	G	8	25.85	0.8988	34.43	8.08	0.57	60.9	94.1	22.19	0.14
x	H	10	29.84	1.342	49.88	4.70	0.38	51.0	97.3	21.43	0.19
x	I	25	33.46	2.907	62.31	4.30	0.18	45.7	100.0	21.57	0.22
	Integrated age ± 2σ			n=9	MSWD=165.88	96.1	0.66		K2O=1.99%	21.95	0.17
	Plateau ± 2σ	steps D-F		n=3	MSWD=0.65	51.7	0.85	±0.08	53.8	22.69	0.08
	Isochron±2σ	steps A-I		n=9	MSWD=130.55		$^{40}Ar/^{36}Ar$=	268.4±2.8		22.70	0.08

MZQ-23, Hornblende, 15.15 mg, J=0.0013513±0.07%, D=1.002±0.001, NM-202H, Lab#=56744-01

x	A	800	1165.1	5.916	3757.5	0.109	0.086	4.7	0.6	132.33	17.44
	B	900	28.08	0.8817	52.76	0.101	0.58	44.7	1.2	30.81	6.50
	C	1000	22.97	1.308	31.12	0.213	0.39	60.4	2.5	34.03	3.17
	D	1100	16.05	5.059	16.69	1.78	0.10	71.9	12.4	28.41	0.43
	E	1130	18.31	5.177	24.05	5.04	0.099	63.5	36.8	28.63	0.26
	F	1160	17.45	4.845	21.04	6.56	0.11	66.7	62.3	28.62	0.19
	G	1190	13.12	4.696	6.484	6.14	0.11	88.4	81.6	28.53	0.16
	H	1220	12.55	5.131	4.900	4.25	0.099	91.9	92.9	28.37	0.21
	I	1250	12.77	5.491	6.362	2.43	0.093	88.8	98.8	27.93	0.36
	J	1300	13.57	6.390	7.972	0.435	0.080	86.5	99.8	28.92	1.61
	K	1650	44.17	80.16	127.5	0.075	0.006	29.7	100.0	34.11	10.44
	Integrated age ± 2σ			n=11	MSWD=4.26	27.1	0.098		K2O=0.51%	28.99	0.35
	Plateau ± 2σ	steps B-K		n=10	MSWD=0.80	27.0	0.11	±0.35	99.6	28.50	0.19
	Isochron±2σ	steps A-K		n=11	MSWD=0.74		$^{40}Ar/^{36}Ar$=	306.3±3.8		28.22	0.21

MZQ-9, Hornblende, 14.4 mg, J=0.0008966±0.06%, D=1.002±0.001, NM-196L, Lab#=56293-01

X	A	800	165.3	0.4423	406.7	1.88	1.2	27.3	10.8	72.62	2.14
X	B	900	23.41	0.5744	39.48	1.50	0.89	50.4	19.2	19.26	1.10
X	C	1000	35.21	5.734	59.75	2.08	0.089	51.2	30.7	29.46	0.95
X	D	1030	29.47	8.981	39.62	2.65	0.057	62.8	44.8	30.29	0.76
X	E	1050	22.17	8.444	23.31	3.13	0.060	72.0	61.0	26.17	0.59
X	F	1070	21.47	7.447	24.53	2.10	0.069	69.1	71.6	24.31	0.83
X	G	1090	22.90	6.760	30.65	1.21	0.075	62.9	77.5	23.59	1.43
X	H	1120	26.02	6.229	45.75	0.585	0.082	50.0	80.4	21.32	2.81
X	I	1160	22.77	5.656	36.26	0.690	0.090	55.0	83.7	20.51	2.36
X	J	1250	28.77	8.896	37.65	2.15	0.057	63.9	94.0	30.09	0.91
X	K	1700	33.59	8.428	52.68	1.29	0.061	55.7	100.0	30.63	1.51
	Integrated age ± 2σ			n=11	MSWD=57.12	19.3	0.078		K2O=0.57%	31.17	0.77
	Plateau ± 2σ	no plateau		n=0	MSWD=0.00	0.000	0.000	±0.000	0.0	0.00	0.00
	Isochron±2σ	steps A-K		n=11	MSWD=9.25		$^{40}Ar/^{36}Ar$=	371.4±5.7		23.26	0.75

MZQ-19, Hornblende, 12.75 mg, J=0.0006951±0.04%, D=1.002±0.001, NM-203H, Lab#=56826-01

X	A	800	440.2	0.5957	1236.2	0.514	0.86	17.0	6.0	92.97	2.77
X	B	900	68.55	0.2875	168.4	0.715	1.8	27.4	13.9	23.77	0.69
X	C	1000	37.04	1.154	62.34	0.779	0.44	50.5	22.1	23.67	0.62
X	D	1100	62.60	10.17	124.7	3.78	0.050	42.5	55.5	33.77	0.36

X	E	1130	25.96	9.676	23.65	2.61	0.053	76.2	73.8	25.15	0.18
X	F	1160	31.14	7.601	42.69	0.636	0.067	61.5	77.8	24.33	0.63
X	G	1190	30.46	8.125	36.42	0.559	0.063	66.9	81.3	25.87	0.69
X	H	1220	31.08	11.29	34.82	0.835	0.045	69.9	86.2	27.65	0.49
X	I	1250	32.67	11.29	40.95	0.912	0.045	65.8	91.2	27.37	0.45
X	J	1300	38.18	12.05	57.09	0.919	0.042	58.4	96.1	28.40	0.45
X	K	1650	105.5	11.93	295.1	0.778	0.043	18.3	100.0	24.52	0.90
	Integrated age ± 2σ			n=11	MSWD=112.52	13.04	0.058	K2O=0.57%		30.71	0.55
	Plateau ± 2σ	no plateau		n=0	MSWD=0.00	0.000	0.000±0.000		0.0	0.00	0.00
	Isochron±2σ	steps A-K		n=11	MSWD=49.99		$^{40}Ar/^{36}Ar$=	330.9±3.0		24.48	0.34

MZQ-37, Hornblende, 16.75 mg, J=0.0007719±0.08%, D=1.002±0.001, NM-208M, Lab#=57193-01

X	A	800	380.6	4.722	1145.9	0.388	0.11	11.1	0.9	59.08	3.64
X	B	900	78.75	3.414	215.9	0.149	0.15	19.3	1.2	21.42	3.69
X	C	1000	41.73	1.498	94.43	0.385	0.34	33.4	2.1	19.62	1.30
X	D	1100	40.75	1.763	69.21	0.435	0.29	50.2	3.1	28.70	1.31
X	E	1130	58.68	4.129	45.80	0.353	0.12	77.5	3.9	63.35	1.48
X	F	1160	35.35	6.234	46.30	1.86	0.082	62.8	8.3	31.21	0.38
X	G	1190	21.76	6.286	14.55	8.9	0.081	82.6	32.6	25.34	0.10
X	H	1220	18.84	6.333	6.169	7.4	0.081	93.1	58.0	24.73	0.10
X	I	1250	22.03	6.003	7.138	2.96	0.085	92.7	69.7	28.74	0.20
X	J	1300	20.53	6.479	5.752	3.48	0.079	94.3	85.1	27.28	0.18
X	K	1650	61.98	0.2372	29.39	3.02	2.2	86.0	100.0	73.84	0.32
	Integrated age ± 2σ			n=11	MSWD=2349.57	29.4	0.093	K2O=0.87%		32.05	0.24
	Plateau ± 2σ	no plateau		n=0	MSWD=0.00	0.000	0.000±0.000		0.0	0.00	0.00
	Isochron±2σ	steps A-K		n=11	MSWD=1136.60		$^{40}Ar/^{36}Ar$=	752.3±13.7		21.59	0.23

Notes:

Isotopic ratios corrected for blank, radioactive decay, and mass discrimination, not corrected for interfering reactions.
Errors quoted for individual analyses include analytical error only, without interfering reaction or J uncertainties.
Integrated age calculated by summing isotopic measurements of all steps.
Integrated age error calculated by quadratically combining errors of isotopic measurements of all steps.
Plateau age is inverse-variance-weighted mean of selected steps.
Plateau age error is inverse-variance-weighted mean error (Taylor, 1982) times root MSWD where MSWD>1.
Plateau error is weighted error of Taylor (1982).
Decay constants and isotopic abundances after Min et al. (2000).
symbol preceding sample ID denotes analyses excluded from plateau age calculations.
Weight percent K_2O calculated from ^{39}Ar signal, sample weight, and instrument sensitivity.
Ages calculated relative to FC-2 Fish Canyon Tuff sanidine interlaboratory standard at 28.201 Ma (Kuiper et al., 2008)
Decay Constant (LambdaK (total)) = 5.463e-10/a
Correction factors:
$(^{39}Ar/^{37}Ar)_{Ca}$ = 0.00068 ± 2e-05
$(^{36}Ar/^{37}Ar)_{Ca}$ = 0.00028 ± 1e-05
$(^{38}Ar/^{39}Ar)_{K}$ = 0.0125
$(^{40}Ar/^{39}Ar)_{K}$ = 0 ± 0.0004

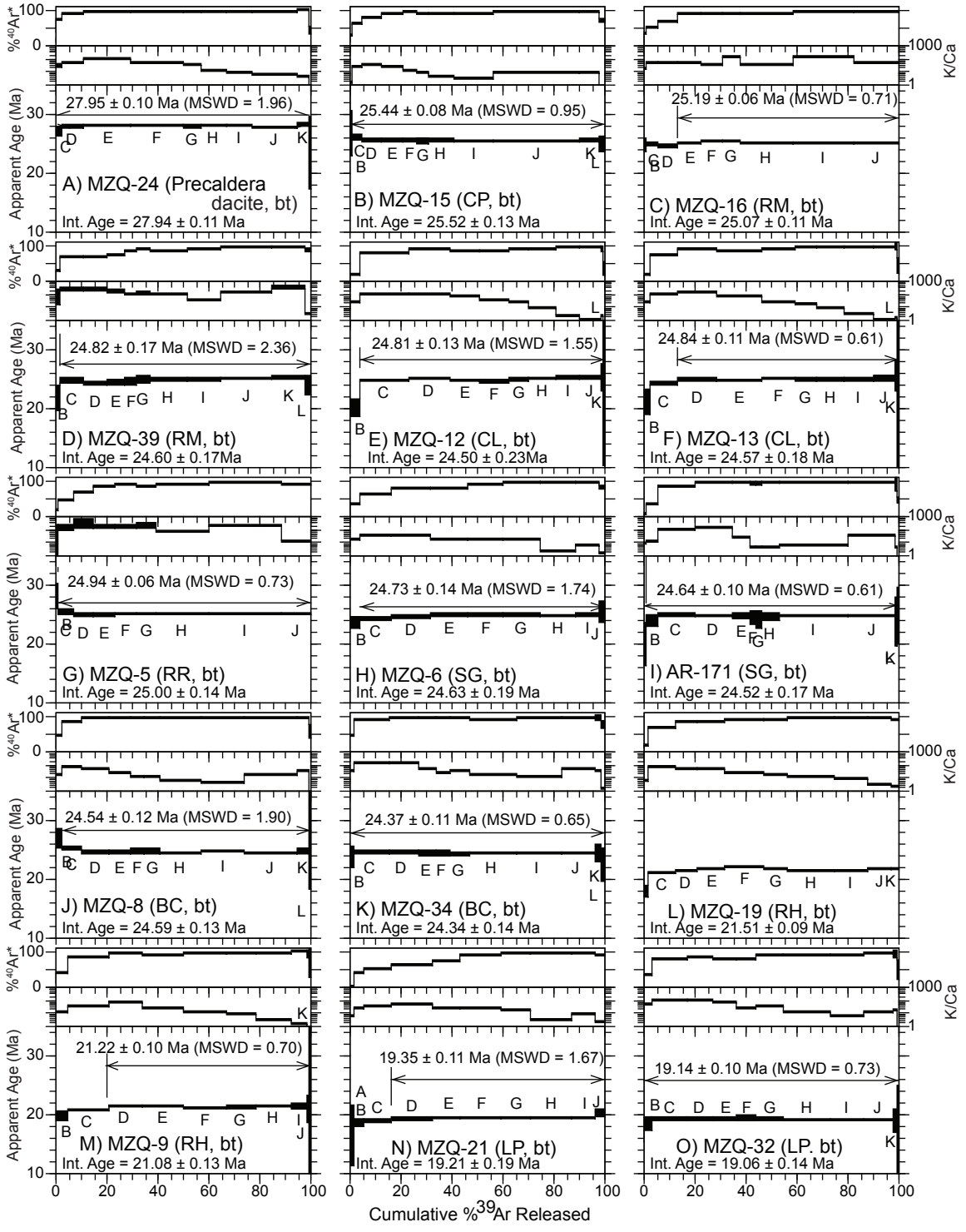

Figure 1.2.1. Age spectra for the Questa caldera biotite (bt), hornblende (hbl), and groundmass concentrate (gmc). Auxiliary plots include K/Ca and radiogenic yield (%^{40}Ar*). All errors are reported at 2 sigma.

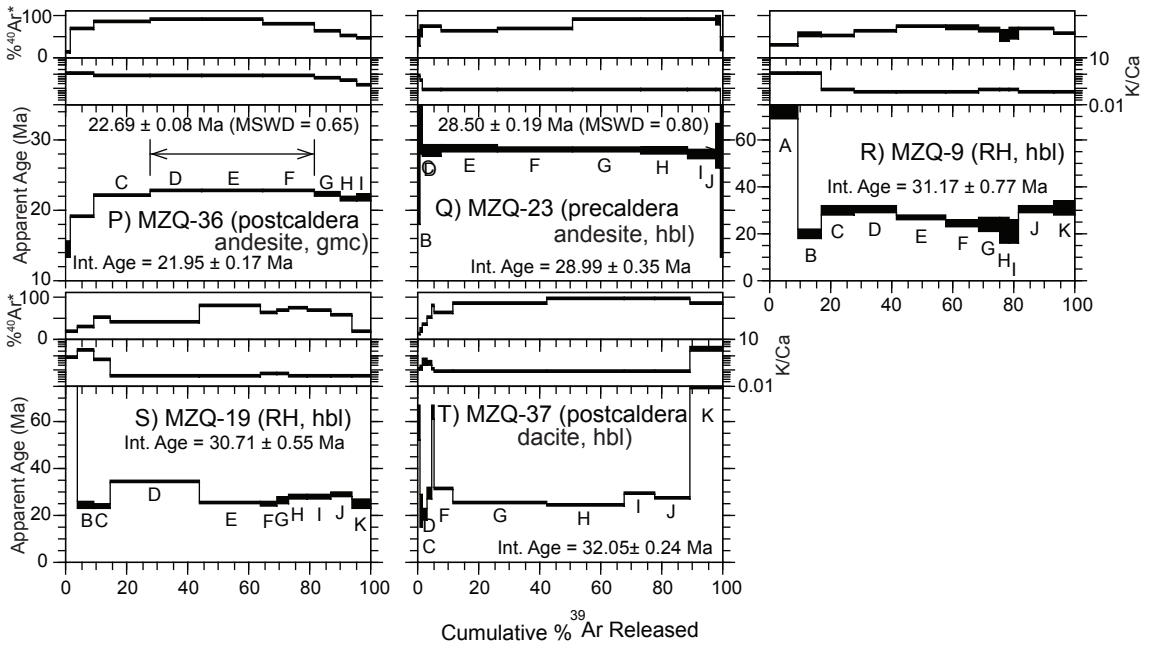

Figure 1.2.1. continued

Table 1.2.3. Questa K-feldspar $^{40}Ar/^{39}Ar$ analytical data.

	ID	Temp (°C)	$^{40}Ar/^{39}Ar$	$^{37}Ar/^{39}Ar$	$^{36}Ar/^{39}Ar$ (x 10^{-3})	$^{39}Ar_K$ (x 10^{-15} mol)	K/Ca	$^{40}Ar^*$ (%)	^{39}Ar (%)	Age (Ma)	±1σ (Ma)
	MZQ-1, K-Feldspar, 16.5 mg, J=0.0008946±0.05%, D=1.002±0.001, NM-196K, Lab#=56281-01										
X	B	500	1070.7	0.0117	3029.5	2.98	43.6	16.4	0.8	266.88	5.70
X	C	500	115.8	0.0151	322.8	1.118	33.7	17.6	1.0	33.08	1.27
X	D	550	214.3	0.0071	537.6	3.11	71.9	25.9	1.8	88.63	1.25
X	E	550	43.26	0.0105	86.74	2.65	48.5	40.8	2.5	28.65	0.36
X	F	600	106.4	0.0015	257.0	10.83	342.6	28.6	5.1	49.24	0.60
X	G	600	26.17	0.0028	34.54	5.77	181.9	61.0	6.5	25.95	0.20
X	H	650	46.18	0.0020	88.97	9.05	256.3	43.1	8.7	32.28	0.28
X	I	650	24.16	0.0024	28.98	5.98	209.3	64.6	10.1	25.37	0.15
X	J	700	67.06	0.0032	158.3	11.39	158.1	30.3	12.8	32.94	0.39
X	K	700	21.36	0.0009	18.94	6.55	574.0	73.8	14.3	25.63	0.16
X	L	750	48.46	0.0030	99.04	12.04	169.6	39.6	17.0	31.16	0.27
X	M	750	19.58	0.0020	13.04	7.21	258.4	80.3	18.6	25.58	0.12
X	N	800	32.61	0.0037	51.72	10.07	137.2	53.1	20.8	28.16	0.19
X	O	800	18.06	0.0033	9.703	6.66	154.0	84.1	22.3	24.71	0.10
X	P	850	20.86	0.0053	17.51	7.35	95.6	75.2	23.8	25.51	0.12
X	Q	850	17.63	0.0071	8.333	6.51	71.5	86.0	25.2	24.67	0.12
X	R	900	22.40	0.0037	23.09	8.57	136.5	69.5	27.0	25.34	0.13
X	S	900	19.20	0.0046	12.93	8.34	111.4	80.1	28.7	25.01	0.11
X	T	950	27.22	0.0025	34.98	14.02	204.7	62.0	31.5	27.44	0.13
X	U	950	23.45	0.0017	22.14	16.0	307.6	72.1	34.7	27.48	0.11
X	V	1000	26.51	0.0015	29.58	31.0	350.5	67.0	40.6	28.88	0.10
X	W	1000	22.70	0.0014	19.05	20.0	367.7	75.2	44.3	27.74	0.09
X	X	1050	23.60	0.0013	20.49	56.4	405.3	74.3	54.0	28.51	0.08
X	Y	1100	23.01	0.0011	19.25	87.6	477.9	75.3	67.7	28.15	0.07
X	Z	1150	23.08	0.0008	19.76	75.9	627.6	74.7	78.3	28.02	0.08
X	AA	1250	19.48	0.0005	9.384	151.4	954.0	85.8	96.6	27.15	0.05
X	AB	1300	24.15	0.0207	24.75	5.24	24.7	69.7	97.2	27.37	0.19
X	AC	1400	23.70	0.0182	22.18	10.83	28.0	72.4	98.4	27.86	0.13
X	AD	1700	23.21	0.0449	20.70	15.13	11.4	73.7	100.0	27.79	0.11
	Integrated age ± 2σ			n=29	MSWD=341.72	609.7	163.7	K2O=15.87%		29.76	0.24
	Plateau ± 2σ	no plateau		n=0	MSWD=0.00	0.000	0.000±0.000		0.0	0.00	0.00
	Isochron±2σ	steps B-AD		n=29	MSWD=106.09		$^{40}Ar/^{36}Ar$=	344.3±1.4		25.71	0.07
	MZQ-2, K-Feldspar, 14.4 mg, J=0.0008944±0.05%, D=1.002±0.001, NM-196K, Lab#=56282-01										
X	B	500	783.3	0.0173	2388.6	0.822	29.5	9.9	0.4	122.67	5.26
X	C	500	167.3	0.0384	508.3	0.484	13.3	10.2	0.6	27.82	2.39
X	D	550	147.3	0.0097	414.2	0.997	52.6	16.9	1.0	40.26	1.43
X	E	550	68.01	0.0124	179.5	1.158	41.2	22.0	1.5	24.34	0.89
X	F	600	89.26	0.0069	232.8	3.51	74.3	22.9	3.0	33.22	0.67
X	G	600	35.37	0.0045	65.77	2.31	113.4	45.1	4.0	25.90	0.40
X	H	650	39.77	0.0014	76.71	3.49	372.3	43.0	5.5	27.79	0.35
X	I	650	25.78	0.0037	35.09	3.00	139.4	59.8	6.8	25.06	0.28
X	J	700	39.80	0.0058	79.74	4.23	88.1	40.8	8.6	26.40	0.32
X	K	700	20.11	0.0036	15.65	3.90	141.2	77.0	10.2	25.18	0.20
X	L	750	34.21	0.0036	60.88	5.87	143.0	47.4	12.5	26.37	0.23
X	M	750	18.01	0.0053	8.184	4.88	96.5	86.6	14.5	25.34	0.14
X	N	800	25.57	0.0032	32.39	6.17	161.6	62.6	16.9	26.01	0.19
X	O	800	17.91	0.0026	8.517	4.45	197.2	85.9	18.7	25.03	0.17
X	P	850	26.51	0.0059	35.83	4.41	86.9	60.1	20.3	25.89	0.23
X	Q	850	20.58	0.0047	17.41	3.17	107.7	75.0	21.5	25.10	0.22
X	R	900	37.34	0.0028	73.13	4.13	181.3	42.1	23.1	25.57	0.31
X	S	900	27.61	0.0069	39.72	3.53	73.9	57.5	24.4	25.81	0.27
X	T	950	44.64	0.0036	94.71	7.46	141.8	37.3	27.1	27.06	0.29
X	U	950	33.99	0.0036	60.31	7.91	143.2	47.6	29.9	26.28	0.23
	V	1000	37.74	0.0020	71.16	17.4	251.4	44.3	35.9	27.16	0.21

	W	1000	30.73	0.0024	48.27	11.51	209.1	53.6	39.7	26.76	0.17
	X	1050	29.57	0.0023	44.29	34.7	222.9	55.7	50.6	26.79	0.14
	Y	1100	27.13	0.0018	35.90	66.4	291.1	60.9	68.8	26.85	0.11
	Z	1150	25.75	0.0019	31.34	47.6	265.0	64.0	80.2	26.79	0.10
	AA	1250	23.23	0.0048	22.76	35.9	107.4	71.1	88.0	26.83	0.09
	AB	1300	26.32	0.0135	32.70	17.4	37.7	63.3	91.6	27.08	0.14
	AC	1400	23.05	0.0060	22.32	31.0	84.4	71.4	97.7	26.74	0.09
X	AD	1700	21.22	0.0350	17.54	12.41	14.6	75.6	100.0	26.07	0.10
	Integrated age ± 2σ			n=29	MSWD=33.30	350.2	103.1	K2O=10.44%		26.99	0.24
	Plateau ± 2σ steps V-AC			n=8	MSWD=1.02	261.9	204.6	±188.1	74.8	26.84	0.09
	Isochron±2σ steps B-AD			n=29	MSWD=15.84		$^{40}Ar/^{36}Ar$=	311.7±1.6		25.62	0.11

MZQ-38, K-Feldspar, 18.15 mg, J=0.0007828±0.05%, D=1.004±0.001, NM-208L, Lab#=57191-01

X	B	570	344.6	0.0034	1004.7	2.48	148.8	13.8	1.7	67.11	1.99
X	C	570	56.66	0.0157	130.2	0.951	32.4	32.1	2.4	25.89	0.95
X	D	620	50.48	-0.0005	101.3	3.38	-	40.7	4.6	29.22	0.41
X	E	620	30.79	0.0011	44.58	1.614	454.4	57.2	5.7	25.07	0.54
X	F	670	31.11	0.0033	43.20	3.89	153.5	59.0	8.2	26.10	0.26
X	G	670	23.96	0.0066	22.71	2.082	77.6	72.0	9.5	24.56	0.35
X	H	670	24.07	0.0169	20.36	0.468	30.2	75.0	9.8	25.70	0.68
X	I	670	22.71	0.0035	16.93	1.471	145.3	78.0	10.7	25.19	0.22
X	J	720	22.39	-0.0001	15.27	3.05	-	79.9	12.5	25.45	0.19
X	K	720	21.05	0.0045	12.26	2.135	113.0	82.8	13.8	24.81	0.19
X	L	770	24.25	0.0040	21.03	5.65	128.4	74.4	17.1	25.67	0.15
X	M	770	19.86	0.0034	7.874	3.31	151.7	88.3	19.0	24.95	0.15
X	N	820	21.93	0.0020	13.61	6.85	249.4	81.7	22.7	25.48	0.11
X	O	820	19.25	0.0021	6.626	3.66	243.0	89.8	24.6	24.61	0.15
X	P	870	20.85	0.0008	11.24	5.29	653.5	84.1	27.3	24.94	0.11
X	Q	870	19.55	0.0037	7.168	3.49	136.6	89.2	29.0	24.80	0.14
X	R	920	21.77	0.0027	14.10	5.10	191.2	80.9	31.4	25.06	0.12
X	S	920	20.99	0.0024	12.07	2.67	215.2	83.0	32.7	24.80	0.20
X	T	970	25.87	0.0034	27.31	5.17	148.2	68.8	35.0	25.34	0.15
X	U	970	24.55	0.0036	23.61	3.43	141.1	71.6	36.5	25.00	0.18
X	V	1020	28.56	0.0003	33.86	8.92	######	65.0	40.3	26.39	0.12
	W	1020	25.51	0.0022	25.19	7.00	234.1	70.8	43.2	25.70	0.13
	X	1070	25.72	0.0015	25.16	18.57	341.1	71.1	50.2	26.02	0.10
	Y	1070	23.34	0.0014	17.74	11.38	365.9	77.5	54.1	25.76	0.10
	Z	1120	23.68	0.0024	18.26	33.4	211.6	77.2	64.4	26.01	0.07
	AA	1120	22.79	0.0003	15.36	20.89	######	80.1	70.0	25.97	0.09
	AB	1120	22.42	0.0017	14.38	24.8	299.4	81.0	75.9	25.86	0.07
	AC	1170	21.64	0.0016	11.27	88.0	324.3	84.6	92.6	26.04	0.05
	AD	1220	20.13	0.0031	6.714	9.59	166.7	90.1	94.1	25.81	0.08
	AE	1320	19.77	0.0010	5.225	36.1	488.3	92.2	99.3	25.94	0.05
	AF	1370	21.08	0.0011	8.784	1.349	454.3	87.7	99.4	26.30	0.35
X	AG	1470	24.99	-0.0076	16.33	0.306	-	80.7	99.5	28.66	1.25
X	AH	1770	24.28	0.0014	21.50	3.89	376.8	73.8	100.0	25.51	0.16
	Integrated age ± 2σ			n=33	MSWD=29.51	330.4	282.3	K2O=8.93%		26.19	0.14
	Plateau ± 2σ steps W-AF			n=10	MSWD=1.87	251.2	422.3	±763.9	76.0	25.94	0.07
	Isochron±2σ steps B-AH			n=33	MSWD=16.00		$^{40}Ar/^{36}Ar$=	317.5±2.3		25.33	0.07

MZQ-15, K-Feldspar, 15.56 mg, J=0.0007822±0.04%, D=1.004±0.001, NM-208L, Lab#=57187-01

X	B	570	3104.8	0.1172	9834.2	0.296	4.4	6.4	0.2	264.56	16.78
X	C	570	317.0	0.0748	984.0	0.838	6.8	8.3	0.9	37.26	2.73
X	D	620	196.6	0.0631	511.2	2.049	8.1	23.2	2.4	64.12	1.12
X	E	620	60.90	0.0483	137.3	1.286	10.6	33.4	3.3	28.88	0.83
X	F	670	50.79	0.0478	101.3	2.271	10.7	41.1	5.0	29.63	0.57
X	G	670	32.73	0.0403	54.68	1.942	12.7	50.6	6.3	23.59	0.48
X	H	720	35.69	0.0368	58.54	2.87	13.9	51.5	8.3	26.15	0.38
X	I	720	25.45	0.0329	26.66	2.71	15.5	69.1	10.2	24.99	0.34
X	J	770	30.90	0.0259	41.79	3.78	19.7	60.0	12.7	26.37	0.30
X	K	770	22.47	0.0269	16.02	4.07	19.0	78.9	15.3	25.22	0.22
X	L	820	26.13	0.0231	26.67	4.73	22.0	69.8	18.2	25.94	0.25

X	M	820	21.23	0.0206	11.40	5.38	24.8	84.1	21.4	25.40	0.17
X	N	870	25.70	0.0244	25.12	6.30	21.0	71.1	25.0	25.99	0.19
X	O	870	22.03	0.0244	15.25	4.65	20.9	79.6	27.6	24.92	0.20
X	P	920	28.85	0.0254	36.01	6.03	20.1	63.1	30.7	25.90	0.19
X	Q	920	29.25	0.0227	39.46	6.92	22.5	60.1	34.2	25.02	0.21
X	R	970	42.76	0.0169	81.19	7.08	30.1	43.9	37.6	26.68	0.29
X	S	970	37.21	0.0127	62.61	5.72	40.2	50.3	40.2	26.60	0.27
X	T	1020	52.70	0.0151	114.4	7.60	33.7	35.9	43.6	26.86	0.31
X	U	1020	43.29	0.0142	82.40	6.98	36.0	43.7	46.5	26.92	0.25
X	V	1070	51.17	0.0138	103.7	10.64	37.0	40.1	50.7	29.18	0.29
X	W	1070	41.53	0.0115	74.91	9.29	44.4	46.7	54.2	27.56	0.23
X	X	1120	42.39	0.0132	74.08	16.20	38.6	48.4	59.8	29.12	0.22
X	Y	1120	40.86	0.0143	68.92	16.10	35.7	50.2	64.9	29.11	0.20
X	Z	1170	35.86	0.0149	52.53	20.39	34.1	56.7	70.7	28.89	0.14
X	AA	1170	33.91	0.0142	43.17	26.7	36.0	62.4	77.4	30.05	0.13
X	AB	1220	30.77	0.0140	31.40	29.6	36.6	69.8	84.0	30.52	0.11
X	AC	1320	29.91	0.0128	27.93	69.8	39.9	72.4	96.5	30.75	0.09
X	AD	1370	31.02	0.0197	33.62	8.27	25.9	68.0	97.7	29.95	0.18
X	AE	1470	31.67	0.0154	36.10	10.71	33.1	66.3	99.3	29.83	0.15
X	AF	1770	34.90	0.0098	53.81	5.06	51.9	54.4	100.0	27.01	0.26
	Integrated age ± 2σ			n=31	MSWD=153.32	306.3	30.4		K2O=9.67%	29.37	0.27
	Plateau ± 2σ	no plateau		n=0	MSWD=0.00	0.000	0.000±0.000		0.0	0.00	0.00
	Isochron±2σ	steps B-AF		n=31	MSWD=125.35		$^{40}Ar/^{36}Ar$=	317.1±1.6		27.32	0.12

MZQ-16, K-Feldspar, 19.2 mg, J=0.0008971±0.05%, D=1.002±0.001, NM-196L, Lab#=56288-03

xi	B	500	2334.4	0.1257	7838.1	0.021	4.1	0.8	0.0	29.79	46.85
xi	C	500	93.12	0.0502	273.7	1.007	10.2	13.1	0.2	19.98	1.12
xi	D	550	41.89	0.0345	97.54	1.258	14.8	31.2	0.5	21.34	0.65
xi	E	550	19.51	0.0244	18.42	1.72	20.9	72.1	0.9	22.95	0.31
X	F	600	34.51	0.0215	63.96	4.34	23.7	45.2	1.9	25.45	0.33
xi	G	600	18.72	0.0164	13.67	3.62	31.1	78.4	2.7	23.95	0.19
X	H	650	24.64	0.0191	31.58	5.80	26.8	62.1	4.1	24.96	0.20
X	I	650	18.38	0.0136	10.38	5.31	37.6	83.3	5.3	24.97	0.14
X	J	700	21.79	0.0182	22.06	7.49	28.1	70.1	7.0	24.91	0.14
X	K	700	17.03	0.0085	5.780	7.45	59.9	90.0	8.7	24.99	0.17
X	L	750	23.13	0.0142	26.04	8.50	35.9	66.7	10.7	25.18	0.13
X	M	750	16.50	0.0111	4.115	9.43	46.2	92.6	12.9	24.93	0.09
X	N	800	21.30	0.0117	20.22	15.8	43.7	72.0	16.5	25.00	0.10
X	O	800	16.51	0.0095	4.210	13.17	53.8	92.5	19.5	24.91	0.08
X	P	850	21.53	0.0108	20.16	15.5	47.2	72.3	23.1	25.39	0.11
X	Q	850	17.73	0.0114	8.031	13.19	44.9	86.6	26.1	25.04	0.08
X	R	900	26.71	0.0139	37.98	15.31	36.7	58.0	29.6	25.27	0.14
X	S	900	22.01	0.0141	22.75	12.90	36.2	69.5	32.6	24.94	0.13
	T	950	38.23	0.0145	76.82	15.15	35.1	40.6	36.1	25.32	0.22
	U	950	29.63	0.0118	47.92	12.63	43.3	52.2	39.0	25.23	0.18
	V	1000	41.10	0.0102	85.76	17.6	50.0	38.3	43.0	25.69	0.23
	W	1000	31.19	0.0115	53.22	*10.29*	44.2	49.6	45.4	25.21	0.19
	X	1050	35.68	0.0115	67.85	23.9	44.5	43.8	50.9	25.50	0.18
	Y	1100	30.75	0.0137	51.87	44.4	37.2	50.2	61.1	25.15	0.15
	Z	1150	29.25	0.0158	46.31	47.6	32.4	53.2	72.0	25.39	0.14
	AA	1250	24.69	0.0157	30.61	55.2	32.5	63.4	84.7	25.52	0.10
	AB	1300	27.78	0.0257	40.83	7.08	19.8	56.6	86.3	25.64	0.20
X	AC	1400	28.04	0.0252	40.83	22.2	20.2	57.0	91.4	26.04	0.14
xi	AD	1700	26.05	0.0265	33.14	37.2	19.3	62.4	100.0	26.50	0.11
	Integrated age ± 2σ			n=29	MSWD=14.23	435.1	32.6		K2O=9.70%	25.38	0.21
	Plateau ± 2σ	steps T-AB		n=9	MSWD=1.19	223.6	36.8 ±18.1		51.4	25.41	0.12
	Isochron±2σ	steps F-AC		n=23	MSWD=2.70		$^{40}Ar/^{36}Ar$=	301.4±1.8		24.94	0.09

MZQ-39, K-Feldspar, 18.39 mg, J=0.0007846±0.05%, D=1.004±0.001, NM-208L, Lab#=57192-01

X	B	570	84.75	0.0176	241.4	1.717	29.0	15.8	1.2	19.18	0.83
X	C	620	53.51	0.0186	127.4	2.53	27.4	29.6	3.0	22.64	0.46
X	D	620	39.41	0.0136	78.18	2.70	37.4	41.4	4.9	23.28	0.36

X	E	670	34.44	0.0124	59.01	3.63	41.1	49.4	7.3	24.26	0.27
X	F	670	28.21	0.0096	37.62	4.29	53.4	60.6	10.1	24.39	0.22
X	G	720	26.90	0.0089	33.70	4.49	57.5	63.0	12.9	24.18	0.19
X	H	720	23.21	0.0063	20.49	5.61	81.5	73.9	16.3	24.47	0.14
X	I	770	24.40	0.0066	24.79	6.81	77.5	70.0	20.3	24.36	0.13
	J	770	20.63	0.0068	11.03	8.18	75.1	84.2	24.8	24.78	0.10
	K	820	22.99	0.0069	19.34	8.15	74.4	75.1	29.0	24.64	0.11
	L	820	19.99	0.0072	9.162	9.86	70.9	86.5	33.8	24.66	0.08
	M	870	23.86	0.0077	21.89	8.87	65.8	72.9	37.9	24.81	0.11
	N	870	20.68	0.0068	10.36	10.66	74.6	85.2	42.4	25.14	0.08
	O	920	26.45	0.0093	30.33	9.07	55.1	66.1	46.1	24.95	0.13
	P	920	22.87	0.0099	18.49	10.71	51.3	76.1	50.2	24.83	0.10
	Q	970	32.38	0.0076	51.20	8.83	67.3	53.3	53.4	24.61	0.18
	R	970	26.93	0.0105	32.59	10.63	48.4	64.2	57.0	24.68	0.12
	S	1020	38.80	0.0091	72.39	9.10	56.0	44.9	60.0	24.84	0.23
	T	1020	31.96	0.0070	49.46	11.51	72.4	54.3	63.5	24.74	0.14
	U	1070	40.26	0.0082	77.47	10.31	62.0	43.1	66.4	24.77	0.19
	V	1070	33.61	0.0081	54.87	13.04	63.0	51.8	70.0	24.82	0.16
	W	1120	37.50	0.0095	68.18	11.77	53.5	46.3	73.0	24.75	0.20
	X	1120	32.47	0.0093	50.51	13.91	54.7	54.0	76.3	25.03	0.17
	Y	1170	34.39	0.0094	57.87	12.77	54.5	50.3	79.2	24.67	0.15
	Z	1170	34.51	0.0121	58.44	19.50	42.2	50.0	83.3	24.60	0.16
X	AA	1220	33.64	0.0128	53.95	9.67	39.8	52.6	85.2	25.25	0.17
X	AB	1320	27.39	0.0126	32.86	59.4	40.4	64.6	95.5	25.22	0.09
X	AC	1370	24.85	0.0111	24.62	18.24	45.8	70.7	98.2	25.07	0.10
X	AD	1470	29.51	0.0114	39.53	3.31	44.9	60.4	98.6	25.43	0.25
X	AE	1770	32.02	0.0119	47.66	9.89	42.7	56.0	100.0	25.59	0.14
	Integrated age ± 2σ			n=30	MSWD=7.55	319.2	50.9		K2O=8.50%	24.83	0.19
	Plateau ± 2σ	steps J-Z		n=17	MSWD=1.80	186.9	59.8	±20.4	58.5	24.80	0.09
	Isochron±2σ	steps B-AE		n=30	MSWD=7.11		$^{40}Ar/^{36}Ar$=	292.5±1.8		24.96	0.10

MZQ-12, K-Feldspar, 17.59 mg, J=0.0007856±0.04%, D=1.004±0.001, NM-208L, Lab#=57185-01

X	B	570	50.36	-0.0569	104.6	0.164	-	38.6	0.0	27.77	3.04
xi	C	620	62.83	-0.0174	129.9	0.493	-	38.9	0.2	34.80	1.63
X	D	620	29.22	-0.0264	36.25	0.408	-	63.3	0.3	26.42	1.22
X	E	670	33.54	0.0157	49.53	0.878	32.4	56.4	0.5	26.99	0.61
X	F	670	23.75	-0.0284	18.83	0.588	-	76.6	0.7	25.96	0.80
X	G	720	23.72	0.0159	19.30	1.233	32.1	76.0	1.0	25.73	0.48
X	H	720	20.36	0.0034	8.596	1.450	148.2	87.5	1.4	25.45	0.37
X	I	770	20.23	0.0121	9.665	2.40	42.2	85.9	2.0	24.81	0.23
X	J	770	19.21	0.0078	6.042	2.261	65.3	90.7	2.7	24.89	0.23
X	K	820	18.87	0.0047	5.282	3.43	108.5	91.7	3.6	24.72	0.16
X	L	820	18.52	0.0079	4.021	3.37	64.2	93.6	4.5	24.75	0.15
X	M	870	18.72	0.0115	4.623	4.51	44.5	92.7	5.7	24.79	0.12
X	N	870	18.40	0.0075	3.225	4.56	68.2	94.8	6.9	24.92	0.13
X	O	920	18.67	0.0116	3.621	5.85	44.1	94.3	8.5	25.13	0.11
X	P	920	18.38	0.0091	3.618	5.96	56.3	94.2	10.1	24.72	0.11
X	Q	970	18.62	0.0106	3.812	6.92	48.0	94.0	12.0	24.98	0.09
X	R	970	18.47	0.0080	2.920	6.73	64.0	95.3	13.8	25.14	0.11
X	S	1020	19.17	0.0106	6.129	7.97	48.2	90.6	15.9	24.80	0.09
X	T	1020	18.65	0.0094	4.200	8.16	54.2	93.3	18.1	24.87	0.10
X	U	1070	19.98	0.0093	8.839	8.57	54.9	86.9	20.4	24.82	0.09
X	V	1070	19.27	0.0089	5.980	8.68	57.1	90.8	22.8	24.99	0.09
X	W	1120	21.37	0.0108	13.44	8.80	47.4	81.4	25.1	24.85	0.09
X	X	1120	20.53	0.0089	9.661	8.81	57.3	86.1	27.5	25.25	0.09
X	Y	1170	23.70	0.0104	20.92	12.93	49.2	73.9	31.0	25.02	0.11
	Z	1170	24.00	0.0105	21.46	16.81	48.5	73.6	35.5	25.22	0.09
	AA	1220	22.47	0.0109	16.41	24.3	46.7	78.4	42.1	25.16	0.08
	AB	1320	21.04	0.0108	10.98	126.3	47.2	84.6	76.1	25.41	0.05
	AC	1370	20.50	0.0095	9.498	27.4	53.8	86.3	83.4	25.27	0.07
X	AD	1470	21.57	0.0098	12.09	17.02	52.1	83.4	88.0	25.70	0.08
X	AE	1770	21.25	0.0108	11.44	44.5	47.5	84.1	100.0	25.52	0.06
	Integrated age ± 2σ			n=30	MSWD=9.10	371.4	50.5		K2O=10.32%	25.29	0.10

	Plateau ± 2σ steps Z-AC		n=4	MSWD=2.81	194.7	48.2 ±6.5		52.4	25.31	0.12
	Isochron±2σ steps B-AE		n=29	MSWD=6.05		$^{40}Ar/^{36}Ar$=	317.1±5.7		24.88	0.09
	MZQ-13, K-Feldspar, 18.5 mg, J=0.0008965±0.05%, D=1.002±0.001, NM-196L, Lab#=56287-01									
X	B	500	2674.8	0.2028	8651.7	0.154	2.5	4.4	0.0	184.38	21.89
X	C	500	477.6	0.1404	1556.2	0.311	3.6	3.7	0.1	28.88	4.89
X	D	550	684.4	0.0959	2217.0	0.529	5.3	4.3	0.2	47.45	5.88
X	E	550	247.2	0.0798	777.9	0.750	6.4	7.0	0.4	28.28	2.74
X	F	600	212.7	0.0495	661.1	2.35	10.3	8.1	1.0	28.17	1.68
X	G	600	92.22	0.0421	257.1	1.96	12.1	17.6	1.5	26.51	0.90
X	H	650	84.81	0.0422	229.8	3.43	12.1	19.9	2.3	27.55	7.88
X	I	650	58.31	0.0420	142.3	3.11	12.1	27.9	3.1	26.50	0.51
X	J	700	52.42	0.0413	125.0	4.47	12.3	29.5	4.2	25.23	0.43
X	K	700	33.88	0.0422	63.27	4.47	12.1	44.8	5.3	24.76	0.29
X	L	750	41.77	0.0380	88.96	6.28	13.4	37.1	6.7	25.23	0.31
X	M	750	23.17	0.0383	26.36	5.51	13.3	66.4	8.0	25.08	0.18
X	N	800	32.14	0.0355	56.31	7.34	14.4	48.2	9.8	25.26	0.22
X	O	800	22.63	0.0399	24.90	5.87	12.8	67.5	11.1	24.90	0.18
X	P	850	35.69	0.0323	68.81	7.04	15.8	43.0	12.7	25.04	0.25
X	Q	850	21.58	0.0355	21.93	5.69	14.4	70.0	14.0	24.61	0.17
X	R	900	45.80	0.0276	102.3	7.48	18.5	34.0	15.7	25.40	0.34
X	S	900	28.53	0.0266	45.30	6.28	19.2	53.1	17.1	24.69	0.23
	T	950	68.45	0.0190	180.3	9.74	26.9	22.2	19.2	24.72	0.44
	U	950	41.79	0.0197	90.07	8.15	25.9	36.3	20.9	24.74	0.29
	W	1000	46.10	0.0173	104.5	8.67	29.4	33.0	22.8	24.82	0.34
	X	1050	57.33	0.0141	142.0	24.0	36.2	26.8	27.7	25.08	0.34
	Y	1100	43.63	0.0143	96.14	54.7	35.6	34.9	38.3	24.81	0.23
	Z	1150	37.58	0.0136	75.56	70.1	37.6	40.6	50.7	24.86	0.19
	AA	1250	29.31	0.0140	47.07	140.6	36.5	52.5	72.1	25.10	0.12
	AB	1300	31.73	0.0249	54.95	30.3	20.5	48.8	76.2	25.26	0.16
X	AC	1400	33.64	0.0154	60.81	100.0	33.2	46.6	88.7	25.54	0.15
X	AD	1700	32.29	0.0088	56.07	102.0	57.7	48.7	100.0	25.62	0.14
	Integrated age ± 2σ			n=28	MSWD=4.69	621.3	30.2	K2O=14.39%		25.30	0.36
	Plateau ± 2σ steps T-AB			n=8	MSWD=0.85	346.3	34.5 ±12.6		55.7	25.02	0.15
	Isochron±2σ steps B-AD			n=28	MSWD=3.15		$^{40}Ar/^{36}Ar$=	299.5±1.3		24.73	0.16
	MZQ-5, K-Feldspar, 18.4 mg, J=0.000894±0.05%, D=1.002±0.001, NM-196K, Lab#=56283-01									
X	B	500	1597.4	0.0846	4841.2	0.474	6.0	10.4	0.2	254.57	10.21
X	C	500	326.1	0.0946	1045.2	0.247	5.4	5.3	0.3	27.99	5.07
X	D	550	395.3	0.0558	1217.2	0.498	9.1	9.0	0.4	57.33	3.62
X	E	550	157.8	0.0612	484.0	0.569	8.3	9.4	0.7	24.13	2.15
X	F	600	183.2	0.0534	537.3	1.89	9.6	13.3	1.3	39.52	1.42
X	G	600	68.82	0.0383	185.7	1.358	13.3	20.3	1.8	22.69	0.82
X	H	650	84.62	0.0401	225.9	2.40	12.7	21.1	2.7	29.02	0.67
X	I	650	42.08	0.0375	95.68	2.09	13.6	32.8	3.4	22.45	0.47
X	J	700	52.51	0.0390	124.6	3.05	13.1	29.9	4.5	25.50	0.51
X	K	700	31.22	0.0376	56.84	2.57	13.6	46.2	5.4	23.46	0.37
X	L	750	38.28	0.0308	77.97	3.88	16.6	39.8	6.8	24.77	0.36
X	M	750	24.96	0.0231	35.85	2.62	22.0	57.6	7.7	23.36	0.29
X	N	800	31.74	0.0240	58.87	3.55	21.2	45.2	8.9	23.33	0.31
X	O	800	21.20	0.0236	23.71	5.15	21.6	67.0	10.7	23.09	0.17
X	P	850	26.47	0.0195	39.96	5.83	26.2	55.4	12.6	23.84	0.21
X	Q	850	19.65	0.0195	18.00	5.02	26.2	72.9	14.3	23.31	0.15
X	R	900	30.16	0.0210	52.69	6.49	24.3	48.4	16.4	23.73	0.23
X	S	900	21.74	0.0198	24.71	5.45	25.8	66.4	18.2	23.48	0.16
X	T	950	37.24	0.0174	75.53	5.85	29.3	40.1	20.0	24.25	0.27
X	U	950	26.12	0.0156	39.78	7.25	32.8	55.0	22.3	23.37	0.17
X	V	1000	37.23	0.0126	75.25	10.92	40.6	40.3	25.6	24.38	0.23
X	W	1000	27.29	0.0146	42.53	7.38	35.0	54.0	27.8	23.94	0.16
X	X	1050	30.42	0.0140	52.61	20.5	36.5	48.9	33.8	24.18	0.16
X	Y	1100	25.80	0.0137	37.14	41.9	37.1	57.5	45.1	24.11	0.11
X	Z	1150	23.47	0.0152	28.53	47.0	33.5	64.1	56.6	24.44	0.09

X	AA	1250	20.15	0.0131	16.71	102.9	39.0	75.5	78.4	24.74	0.07
X	AB	1300	21.21	0.0152	19.90	34.0	33.5	72.3	84.7	24.93	0.08
X	AC	1400	20.57	0.0151	18.00	71.2	33.7	74.1	96.7	24.79	0.07
X	AD	1700	20.79	0.0219	19.83	20.9	23.3	71.8	100.0	24.28	0.09
	Integrated age ± 2σ			n=29	MSWD=40.00	423.0	31.0		K2O=9.88%	24.85	0.21
	Plateau ± 2σ	no plateau		n=0	MSWD=0.00	0.000	0.000±0.000		0.0	0.00	0.00
	Isochron±2σ	steps B-AD		n=29	MSWD=29.80		$^{40}Ar/^{36}Ar$=	306.0±1.3		23.92	0.09

MZQ-6, K-Feldspar, 16.7 mg, J=0.0008961±0.06%, D=1.002±0.001, NM-196L, Lab#=56284-01

X	B	500	1696.7	0.0459	4706.2	0.519	11.1	18.0	0.2	443.61	9.76
X	C	500	235.9	0.0359	750.9	0.395	14.2	5.9	0.3	22.83	3.07
X	D	550	275.4	0.0202	804.9	0.765	25.3	13.6	0.5	60.59	2.31
X	E	550	121.7	0.0301	359.9	1.013	16.9	12.6	0.9	24.94	1.42
X	F	600	131.0	0.0187	355.4	3.13	27.3	19.8	1.9	42.18	0.95
X	G	600	52.23	0.0115	127.7	2.45	44.2	27.8	2.6	23.64	0.51
X	H	650	47.95	0.0115	107.1	4.12	44.3	34.0	3.9	26.57	0.43
X	I	650	29.53	0.0076	53.45	3.66	67.1	46.5	5.1	22.39	0.28
X	J	700	29.56	0.0089	50.46	5.02	57.4	49.6	6.6	23.88	0.24
X	K	700	20.34	0.0060	22.83	4.73	85.2	66.8	8.1	22.16	0.18
X	L	750	23.55	0.0083	30.40	6.30	61.2	61.9	10.0	23.75	0.18
X	M	750	17.33	0.0060	12.02	5.55	85.6	79.5	11.6	22.47	0.15
X	N	800	22.43	0.0081	26.43	7.37	63.2	65.2	13.8	23.83	0.16
X	O	800	16.46	0.0066	8.580	5.94	77.7	84.6	15.5	22.70	0.13
X	P	850	22.24	0.0075	27.16	7.19	68.3	63.9	17.6	23.17	0.16
X	Q	850	17.17	0.0055	10.68	6.37	92.5	81.6	19.4	22.85	0.13
X	R	900	25.88	0.0076	38.48	8.79	66.8	56.1	21.8	23.65	0.17
X	S	900	20.67	0.0069	21.70	7.53	74.4	69.0	23.8	23.24	0.14
X	T	950	32.36	0.0053	58.24	10.39	96.0	46.8	26.6	24.69	0.20
X	U	950	26.12	0.0059	38.23	9.44	86.0	56.7	29.1	24.16	0.16
X	V	1000	36.70	0.0056	69.33	15.36	91.1	44.2	33.0	26.41	0.20
X	W	1000	29.77	0.0055	47.70	10.11	93.5	52.7	35.5	25.53	0.18
	X	1050	34.26	0.0051	59.76	26.5	100.6	48.5	41.9	27.04	0.17
	Y	1100	30.53	0.0056	47.15	52.4	91.6	54.4	53.5	27.03	0.13
	Z	1150	26.29	0.0072	33.36	83.7	70.6	62.5	70.0	26.76	0.10
	AA	1250	22.75	0.0050	21.60	111.6	102.0	72.0	88.6	26.66	0.07
	AB	1300	24.59	0.0089	27.66	18.6	57.4	66.8	91.4	26.73	0.10
	AC	1400	22.66	0.0053	20.89	39.2	96.8	72.8	97.1	26.85	0.09
X	AD	1700	21.55	0.0143	17.63	21.4	35.6	75.8	100.0	26.62	0.09
	Integrated age ± 2σ			n=29	MSWD=223.36	479.6	75.7		K2O=12.31%	26.78	0.22
	Plateau ± 2σ	steps X-AC		n=6	MSWD=1.90	332.0	89.2 ±36.5		69.2	26.79	0.12
	Isochron±2σ	steps B-AD		n=29	MSWD=147.62		$^{40}Ar/^{36}Ar$=	327.1±1.5		24.02	0.10

MZQ-8, K-Feldspar, 14.5 mg, J=0.0008959±0.06%, D=1.002±0.001, NM-196L, Lab#=56285-01

X	B	500	2222.4	0.1025	7288.4	0.342	5.0	3.1	0.1	109.34	15.98
X	C	500	316.2	0.1258	1007.5	0.236	4.1	5.8	0.2	30.06	4.56
X	D	550	293.6	0.0677	931.2	0.515	7.5	6.3	0.4	29.99	3.32
X	E	550	159.7	0.0336	502.3	0.640	15.2	7.1	0.6	18.37	1.82
X	F	600	170.9	0.0237	526.6	2.18	21.6	8.9	1.3	24.90	1.37
X	G	600	67.52	0.0242	184.2	1.59	21.1	19.4	1.8	21.35	0.72
X	H	650	57.00	0.0166	148.5	2.79	30.7	23.0	2.7	21.41	0.55
X	I	650	44.13	0.0132	102.3	2.50	38.7	31.5	3.5	22.66	0.47
X	J	700	39.91	0.0146	86.28	3.54	34.9	36.1	4.7	23.49	0.38
X	K	700	28.71	0.0142	49.24	3.46	35.9	49.3	5.8	23.08	0.24
X	L	750	31.80	0.0127	58.50	5.15	40.0	45.6	7.4	23.64	0.27
X	M	750	21.13	0.0093	23.61	4.82	54.7	67.0	8.9	23.07	0.17
X	N	800	25.73	0.0111	38.42	7.34	45.8	55.9	11.1	23.43	0.18
X	O	800	18.30	0.0089	13.02	5.88	57.2	79.0	12.9	23.54	0.12
X	P	850	25.06	0.0081	35.00	7.16	63.1	58.7	15.0	23.98	0.18
X	Q	850	18.05	0.0098	12.26	5.95	52.0	79.9	16.8	23.51	0.13
X	R	900	29.16	0.0109	49.87	7.94	46.8	49.5	19.1	23.50	0.19
X	S	900	20.79	0.0106	21.53	6.45	48.3	69.4	20.9	23.51	0.15
X	T	950	35.07	0.0111	69.76	8.46	46.1	41.2	23.3	23.55	0.24

X	U	950	26.18	0.0089	40.09	6.55	57.3	54.8	25.1	23.35	0.20
	V	1000	37.39	0.0080	77.28	10.04	64.0	38.9	27.8	23.72	0.25
	X	1050	35.23	0.0091	70.10	18.7	56.2	41.2	32.8	23.65	0.19
	Y	1100	29.82	0.0084	52.04	44.6	60.7	48.4	43.8	23.53	0.14
	Z	1150	26.95	0.0076	42.23	50.8	67.0	53.7	55.2	23.59	0.12
	AA	1250	22.59	0.0040	26.74	122.4	126.6	65.0	78.7	23.93	0.08
	AB	1300	28.21	0.0064	45.56	21.6	79.5	52.3	82.4	24.02	0.13
X	AC	1400	26.66	0.0049	39.21	51.6	104.6	56.5	90.6	24.55	0.12
X	AD	1700	25.38	0.0068	34.76	64.6	74.6	59.5	100.0	24.60	0.10
	Integrated age ± 2σ			n=28	MSWD=9.31	467.8	70.3	K2O=13.83%		23.98	0.25
	Plateau ± 2σ steps V-AB			n=6	MSWD=2.59	268.2	93.3 ±52.3		57.3	23.79	0.17
	Isochron±2σ steps B-AD			n=28	MSWD=9.24		$^{40}Ar/^{36}Ar$=	296.5±1.4		23.74	0.11

MZQ-34, K-Feldspar, 18.03 mg, J=0.0007812±0.05%, D=1.004±0.001, NM-208L, Lab#=57190-01

X	B	520	161.0	0.0304	480.1	0.315	16.8	11.9	0.2	27.09	2.91
X	C	570	153.2	0.0466	438.4	0.390	10.9	15.4	0.4	33.51	1.96
X	D	570	129.1	-7.3605	1530.8	0.032	-	-250.7	0.4	-530.73	1558.80
X	E	620	85.91	0.0187	232.4	1.435	27.4	20.1	1.1	24.51	0.86
X	F	620	32.40	0.0174	59.02	1.887	29.4	46.2	2.0	21.27	0.46
X	G	670	36.79	0.0151	72.06	2.146	33.8	42.1	3.1	22.03	0.43
X	H	670	23.68	0.0089	29.82	2.31	57.6	62.8	4.2	21.15	0.28
X	I	720	28.47	0.0126	43.52	2.36	40.6	54.8	5.4	22.19	0.32
X	J	720	21.27	0.0088	19.94	3.00	57.9	72.3	6.8	21.87	0.23
X	K	770	31.84	0.0114	53.62	2.86	44.9	50.2	8.1	22.73	0.33
X	L	770	19.35	0.0082	12.52	3.99	62.1	80.9	9.9	22.25	0.18
X	M	820	24.27	0.0073	28.32	3.72	70.2	65.5	11.6	22.61	0.25
X	N	820	19.24	0.0107	10.73	4.23	47.6	83.5	13.4	22.83	0.15
X	O	870	26.34	0.0125	34.46	3.76	40.8	61.3	15.1	22.96	0.22
X	P	870	19.52	0.0077	12.88	4.16	66.1	80.5	16.8	22.33	0.16
X	Q	920	31.25	0.0087	50.98	3.31	58.9	51.8	18.2	23.01	0.29
X	R	920	22.78	0.0106	22.14	4.08	48.3	71.3	19.8	23.07	0.19
X	S	970	38.60	0.0111	76.70	3.59	46.1	41.3	21.2	22.65	0.31
	T	970	26.31	0.0079	36.08	4.20	64.3	59.5	22.9	22.24	0.20
	U	1020	41.98	0.0081	88.17	5.07	63.0	37.9	24.8	22.63	0.30
	V	1020	30.20	0.0091	48.80	5.83	56.1	52.3	27.0	22.43	0.21
	W	1070	40.28	0.0069	82.87	7.28	73.9	39.2	29.6	22.44	0.27
	X	1070	32.08	0.0050	55.91	9.67	102.9	48.5	32.9	22.11	0.16
	Y	1120	36.43	0.0059	70.85	13.42	86.3	42.5	37.3	22.02	0.19
	Z	1120	31.07	0.0050	52.39	18.22	101.1	50.2	42.8	22.17	0.15
	AA	1170	30.56	0.0069	50.94	26.8	74.4	50.7	50.2	22.04	0.13
	AB	1170	26.66	0.0069	37.11	36.0	74.3	58.9	58.9	22.31	0.10
	AC	1170	22.63	0.0059	23.47	53.5	87.1	69.3	69.9	22.30	0.08
	AD	1170	21.23	0.0054	18.18	49.1	94.2	74.7	78.3	22.54	0.07
X	AE	1270	21.05	0.0036	17.27	39.7	141.4	75.8	84.2	22.67	0.07
X	AF	1320	21.43	0.0018	16.90	97.6	276.5	76.7	96.1	23.35	0.06
X	AG	1420	22.33	0.0030	19.82	16.83	168.9	73.8	97.8	23.41	0.10
X	AH	1770	23.35	0.0039	22.38	22.28	129.5	71.7	100.0	23.78	0.10
	Integrated age ± 2σ			n=33	MSWD=15.90	453.1	106.9	K2O=12.36%		22.68	0.17
	Plateau ± 2σ steps T-AD			n=11	MSWD=2.15	229.070	84.687±31.416		50.6	22.33	0.11
	Isochron±2σ steps B-AH			n=33	MSWD=15.29		$^{40}Ar/^{36}Ar$=	291.1±1.9		22.90	0.09

MZQ-9, K-Feldspar, 12.4 mg, J=0.0008961±0.05%, D=1.002±0.001, NM-196L, Lab#=56286-01

X	B	460	967.8	0.0236	2085.6	0.654	21.6	36.3	0.2	501.25	6.59
X	C	460	180.5	0.0826	510.0	0.151	6.2	16.5	0.3	48.16	3.80
X	D	510	152.6	0.0405	323.1	0.474	12.6	37.4	0.4	91.40	1.90
X	E	510	65.40	0.0347	157.6	0.486	14.7	28.8	0.6	30.64	1.24
X	F	560	119.2	0.0198	236.2	1.60	25.7	41.4	1.1	79.29	0.86
X	G	560	26.20	0.0337	44.53	1.34	15.2	49.8	1.5	21.26	0.41
X	H	610	50.33	0.0217	85.19	4.20	23.5	50.0	2.8	40.82	0.34
X	I	610	14.97	0.0178	13.18	2.98	28.6	74.0	3.7	18.07	0.17
X	J	660	15.14	0.0147	11.58	4.56	34.8	77.4	5.2	19.12	0.13
X	K	660	12.11	0.0114	5.004	4.40	44.6	87.8	6.5	17.35	0.11

X	L	710	11.81	0.0108	3.815	5.46	47.4	90.5	8.2	17.44	0.09
X	M	710	11.26	0.0077	2.662	5.67	66.3	93.0	10.0	17.09	0.09
X	N	760	11.63	0.0085	3.613	6.65	60.3	90.8	12.0	17.24	0.08
X	O	760	11.24	0.0072	2.957	6.15	70.8	92.2	13.9	16.93	0.09
X	P	810	12.58	0.0082	6.308	6.77	62.0	85.2	16.0	17.50	0.10
X	Q	810	11.34	0.0078	4.039	5.60	65.6	89.5	17.7	16.56	0.09
X	R	860	12.27	0.0096	6.437	5.07	53.0	84.5	19.3	16.93	0.11
X	S	860	11.87	0.0083	6.101	4.54	61.3	84.8	20.6	16.44	0.11
X	T	910	14.85	0.0117	14.77	4.93	43.5	70.6	22.1	17.12	0.14
X	U	910	14.15	0.0094	11.93	5.07	54.2	75.1	23.6	17.34	0.11
X	V	960	18.76	0.0106	24.16	6.90	48.0	62.0	25.7	18.97	0.13
X	W	960	17.74	0.0069	19.03	8.69	74.3	68.3	28.3	19.77	0.11
X	X	1010	20.50	0.0066	25.72	14.0	77.3	62.9	32.5	21.04	0.11
X	Y	1010	18.13	0.0058	18.57	17.4	87.2	69.7	37.6	20.63	0.09
X	Z	1060	19.28	0.0067	21.47	24.8	76.1	67.1	44.7	21.09	0.08
X	AA	1060	16.38	0.0064	14.34	20.0	79.3	74.1	50.4	19.81	0.07
X	AB	1110	17.34	0.0069	15.17	20.9	74.0	74.1	56.3	20.97	0.09
X	AC	1110	16.33	0.0079	13.04	16.9	64.2	76.4	61.0	20.36	0.07
X	AD	1110	15.57	0.0085	10.54	21.3	60.3	80.0	66.8	20.32	0.07
X	AE	1110	15.48	0.0092	9.475	22.7	55.7	81.9	73.0	20.68	0.06
X	AF	1210	16.11	0.0065	9.099	30.2	79.1	83.3	81.0	21.88	0.06
X	AG	1260	15.43	0.0054	7.074	40.3	94.1	86.5	91.5	21.75	0.06
X	AH	1360	16.40	0.0291	10.57	6.12	17.5	81.0	93.1	21.66	0.11
X	AI	1700	15.79	0.0309	9.393	27.2	16.5	82.4	100.0	21.22	0.06
	Integrated age ± 2σ			n=34	MSWD=855.96	354.2	49.9	K2O=12.24%		21.88	0.12
	Plateau ± 2σ	no plateau		n=0	MSWD=0.00	0.000	0.000±0.000		0.0	0.00	0.00
	Isochron±2σ	steps B-AI		n=34	MSWD=240.35		$^{40}Ar/^{36}Ar$=	445.8±2.5		17.38	0.06

MZQ-33, K-Feldspar, 16.69 mg, J=0.0007807±0.04%, D=1.004±0.001, NM-208L, Lab#=57189-01

X	B	520	546.8	0.0760	1382.5	0.339	6.7	25.3	0.2	187.63	4.01
X	C	520	172.5	0.0517	494.1	0.436	9.9	15.4	0.4	37.54	2.58
X	D	570	206.6	0.0345	438.3	1.219	14.8	37.3	1.1	106.96	1.41
X	E	570	54.11	0.0321	138.5	1.055	15.9	24.4	1.6	18.76	0.80
X	F	620	87.96	0.0158	165.9	3.11	32.3	44.3	3.3	54.82	0.53
X	G	620	24.93	0.0184	44.73	2.33	27.8	47.0	4.5	16.66	0.34
X	H	670	28.10	0.0123	41.49	4.04	41.3	56.4	6.6	22.50	0.26
X	I	670	17.88	0.0069	21.00	3.67	73.5	65.3	8.4	16.60	0.20
X	J	720	18.95	0.0070	19.66	4.64	73.3	69.4	10.7	18.69	0.17
X	K	720	15.34	0.0060	13.30	5.19	85.5	74.4	13.1	16.24	0.14
X	L	770	18.16	0.0066	16.62	6.86	77.6	73.0	16.3	18.84	0.14
X	M	770	14.24	0.0077	9.348	6.15	66.5	80.6	19.0	16.32	0.13
X	N	820	16.28	0.0049	12.11	6.34	105.1	78.0	21.7	18.06	0.14
X	O	820	14.58	0.0078	8.886	5.64	65.7	82.0	24.0	17.00	0.13
X	P	870	17.01	0.0039	13.80	5.89	131.2	76.0	26.4	18.39	0.13
X	Q	870	15.75	0.0096	13.46	4.38	53.4	74.8	28.1	16.75	0.18
X	R	920	18.39	0.0108	20.06	4.09	47.3	67.8	29.7	17.73	0.18
X	S	920	18.03	0.0100	19.67	3.70	50.9	67.8	31.1	17.38	0.20
X	T	970	25.22	0.0096	40.58	4.48	52.9	52.5	32.7	18.81	0.22
X	U	970	23.54	0.0071	34.49	5.16	71.4	56.7	34.5	18.98	0.19
X	V	1020	31.58	0.0068	53.15	7.72	75.0	50.3	37.2	22.54	0.18
X	W	1020	27.57	0.0066	41.01	9.75	77.2	56.0	40.5	21.94	0.16
X	X	1070	30.98	0.0055	47.03	16.30	92.5	55.1	45.5	24.25	0.15
X	Y	1070	24.89	0.0044	30.80	18.66	115.0	63.4	50.9	22.43	0.12
X	Z	1120	26.36	0.0052	33.06	28.3	98.8	62.9	58.3	23.56	0.11
X	AA	1120	21.39	0.0053	20.62	26.7	96.9	71.5	64.5	21.73	0.09
X	AB	1170	22.13	0.0064	21.16	36.1	79.8	71.7	71.9	22.55	0.08
X	AC	1170	19.95	0.0066	16.16	36.1	77.5	76.1	78.4	21.56	0.07
X	AD	1170	18.81	0.0056	13.66	38.5	91.9	78.5	84.5	20.99	0.06
X	AE	1170	19.26	0.0037	15.56	30.7	138.2	76.1	88.9	20.83	0.07
X	AF	1270	18.11	0.0046	8.992	19.95	111.9	85.3	91.5	21.96	0.07
X	AG	1320	18.73	0.0022	9.856	44.0	228.5	84.5	96.8	22.47	0.05
X	AH	1420	20.43	0.0048	14.52	12.27	107.0	79.0	98.1	22.92	0.11
X	AI	1770	20.40	0.0027	14.77	17.97	189.8	78.6	100.0	22.77	0.08

	Integrated age ± 2σ		n=34	MSWD=594.81	421.9	89.1	K2O=12.44%			22.09	0.13
	Plateau ± 2σ	no plateau	n=0	MSWD=0.00	0.000	0.000±0.000			0.0	0.00	0.00
	Isochron±2σ	steps B-AI	n=34	MSWD=268.27		$^{40}Ar/^{36}Ar$=	397.4±2.5			18.85	0.08
	MZQ-10, K-Feldspar, 18.85 mg, J=0.000784±0.04%, D=1.004±0.001, NM-208L, Lab#=57186-01										
X	B	570	567.1	0.0050	1870.9	5.89	101.6	2.5	3.2	20.30	3.36
X	C	570	100.5	0.0064	303.1	5.04	79.2	10.9	5.9	15.61	0.65
X	D	620	63.16	0.0040	175.3	9.47	127.3	18.0	10.7	16.24	0.42
X	E	620	50.32	0.0029	130.1	6.40	175.5	23.6	13.8	16.94	0.35
X	F	670	43.71	0.0034	107.9	7.87	152.3	27.1	17.4	16.89	0.28
X	G	670	38.17	0.0056	90.42	5.76	90.4	30.0	20.0	16.36	0.32
X	H	720	34.10	0.0012	76.13	6.07	433.6	34.0	22.6	16.57	0.26
X	I	720	30.48	0.0058	65.65	4.86	87.7	36.4	24.6	15.83	0.23
	J	770	29.08	0.0027	58.89	6.63	186.0	40.1	27.3	16.68	0.22
	K	770	24.96	0.0035	46.12	5.37	146.0	45.4	29.5	16.19	0.22
	L	820	26.12	0.0034	49.14	5.99	150.1	44.4	31.7	16.57	0.21
	M	820	25.06	0.0027	46.68	5.06	186.0	45.0	33.6	16.10	0.23
	N	870	40.47	0.0020	97.12	5.63	254.0	29.1	35.6	16.81	0.30
	O	870	46.59	0.0046	118.9	5.23	111.2	24.6	37.5	16.36	0.38
	P	920	107.1	0.0050	324.2	7.01	101.4	10.5	39.9	16.10	0.75
	Q	920	106.6	0.0053	321.5	7.22	96.6	10.9	42.2	16.54	0.70
	R	970	161.3	0.0037	504.8	11.48	136.1	7.5	45.9	17.30	0.93
	S	970	128.9	0.0018	395.2	11.64	288.0	9.4	49.3	17.30	0.77
	T	1020	143.4	0.0041	443.1	18.40	124.4	8.7	54.4	17.81	0.82
	U	1020	99.82	0.0045	298.2	15.11	114.5	11.7	58.4	16.74	0.60
	V	1070	102.7	0.0042	306.0	20.67	121.1	11.9	63.3	17.48	0.58
	W	1070	69.43	0.0052	195.6	14.64	98.1	16.8	66.6	16.63	0.41
	X	1120	76.30	0.0052	219.0	18.72	98.1	15.2	70.5	16.53	0.42
	Y	1120	56.90	0.0040	153.1	14.14	129.1	20.5	73.3	16.64	0.34
	Z	1170	52.73	0.0073	140.2	9.29	69.8	21.4	75.0	16.15	0.33
	AA	1170	50.86	0.0040	132.1	9.62	127.8	23.2	76.8	16.89	0.34
	AB	1220	55.92	0.0034	150.6	12.40	149.6	20.4	79.0	16.33	0.34
	AC	1320	44.65	0.0021	110.9	101.1	237.5	26.6	93.7	16.95	0.21
	AD	1370	47.21	0.0021	119.3	29.3	248.6	25.3	97.1	17.07	0.26
X	AE	1470	55.19	0.0048	144.5	7.57	105.2	22.6	98.0	17.84	0.35
X	AF	1770	50.66	0.0037	127.9	18.57	137.7	25.4	100.0	18.37	0.27
	Integrated age ± 2σ		n=31	MSWD=3.20	412.1	145.3	K2O=10.71%			16.97	0.73
	Plateau ± 2σ	steps J-AD	n=21	MSWD=1.24	334.6	175.8	±120.2		81.2	16.60	0.16
	Isochron±2σ	steps B-AF	n=31	MSWD=2.86		$^{40}Ar/^{36}Ar$=	297.1±1.1			16.41	0.21
	MZQ-19, K-Feldspar, 18.2 mg, J=0.0006972±0.03%, D=1.002±0.001, NM-203H, Lab#=56824-01										
X	C	550	80.98	0.0699	190.4	0.474	7.3	30.5	0.2	31.27	1.13
X	D	600	68.62	0.0651	101.7	0.873	7.8	56.2	0.5	48.57	0.61
X	E	600	26.27	0.0468	37.89	0.615	10.9	57.4	0.7	19.15	0.60
X	F	650	30.56	0.0571	32.92	1.235	8.9	68.2	1.2	26.40	0.35
X	G	650	19.55	0.0496	17.60	1.217	10.3	73.4	1.7	18.23	0.31
X	H	700	22.80	0.0371	18.07	2.09	13.7	76.6	2.4	22.15	0.20
X	I	700	17.19	0.0409	8.931	2.02	12.5	84.7	3.2	18.48	0.19
X	J	750	19.48	0.0323	12.46	3.33	15.8	81.1	4.4	20.05	0.13
X	K	750	16.27	0.0311	5.776	3.12	16.4	89.5	5.6	18.50	0.12
X	L	800	16.99	0.0291	5.951	4.36	17.5	89.7	7.1	19.34	0.09
X	M	800	16.10	0.0276	4.327	3.89	18.5	92.1	8.5	18.82	0.11
X	N	850	16.48	0.0304	3.863	4.84	16.8	93.1	10.3	19.48	0.09
X	O	850	16.19	0.0289	4.043	4.31	17.7	92.6	11.8	19.04	0.09
X	P	900	16.83	0.0269	4.973	4.99	19.0	91.3	13.5	19.50	0.09
X	Q	900	16.82	0.0250	4.439	4.37	20.4	92.2	15.0	19.68	0.10
X	R	950	18.27	0.1211	8.531	4.92	4.2	86.3	16.6	20.00	0.09
X	S	950	17.82	0.0193	6.871	4.49	26.4	88.6	18.1	20.04	0.10
X	T	1000	20.13	0.0161	13.69	5.05	31.7	79.9	19.8	20.42	0.10
X	U	1000	19.50	0.0126	11.46	5.14	40.6	82.6	21.5	20.45	0.09
X	V	1050	23.21	0.0115	24.05	6.42	44.2	69.4	23.5	20.44	0.12
X	W	1050	21.24	0.0123	17.30	6.54	41.4	75.9	25.6	20.47	0.10

X	X	1100	25.78	0.0109	31.55	9.47	46.7	63.8	28.5	20.88	0.12
X	Y	1100	21.98	0.0105	18.91	8.73	48.6	74.6	31.2	20.81	0.10
X	Z	1150	24.02	0.0112	24.55	14.12	45.4	69.8	35.3	21.28	0.08
X	AA	1150	22.87	0.0117	20.49	13.55	43.8	73.5	39.2	21.34	0.08
X	AB	1150	21.65	0.0114	16.30	35.1	44.8	77.8	48.6	21.36	0.06
X	AC	1250	19.45	0.0060	7.866	98.1	85.2	88.1	71.5	21.72	0.04
X	AD	1350	18.93	0.0092	5.875	96.7	55.3	90.8	90.0	21.82	0.04
X	AE	1450	19.84	0.0278	8.415	13.08	18.3	87.5	92.3	22.02	0.06
X	AF	1750	22.06	0.0205	16.80	47.5	24.8	77.5	100.0	21.69	0.06
	Integrated age ± 2σ			n=30	MSWD=237.51	410.6	34.5	K2O=12.43%		21.41	0.08
	Plateau ± 2σ	no plateau		n=0	MSWD=0.00	0.000	0.000±0.000		0.0	0.00	0.00
	Isochron±2σ	steps C-AF		n=30	MSWD=169.73		$^{40}Ar/^{36}Ar$=	369.3±4.0		20.15	0.06

MZQ-21, K-Feldspar, 17.4 mg, J=0.0008976±0.05%, D=1.002±0.001, NM-196L, Lab#=56289-01

X	B	460	379.2	0.1357	1072.0	0.227	3.8	16.5	0.1	99.85	4.80
X	C	460	67.89	0.1203	204.1	0.281	4.2	11.2	0.1	12.43	2.19
X	D	510	60.91	0.0579	141.0	0.698	8.8	31.6	0.3	31.36	1.05
X	E	510	29.72	0.0329	67.87	1.007	15.5	32.5	0.6	15.82	0.67
X	F	560	29.98	0.0325	60.23	2.10	15.7	40.7	1.1	19.92	0.36
X	G	560	20.80	0.0275	38.64	2.71	18.6	45.1	1.8	15.35	0.27
X	H	610	20.76	0.0239	32.42	5.72	21.4	53.9	3.3	18.28	0.18
X	I	610	15.28	0.0212	17.38	5.15	24.0	66.4	4.6	16.59	0.16
X	J	660	15.30	0.0214	16.22	7.76	23.9	68.7	6.5	17.18	0.11
X	K	660	12.60	0.0200	7.078	7.21	25.5	83.4	8.3	17.19	0.10
X	L	710	12.80	0.0217	7.577	9.18	23.5	82.5	10.6	17.27	0.09
X	M	710	11.41	0.0175	3.592	9.15	29.1	90.7	12.8	16.92	0.07
X	N	760	11.88	0.0169	4.885	12.00	30.1	87.9	15.6	17.07	0.06
X	O	760	11.07	0.0130	1.913	12.34	39.3	94.9	18.4	17.18	0.05
X	P	810	11.57	0.0134	3.270	14.78	37.9	91.7	21.8	17.33	0.05
X	Q	810	11.15	0.0134	1.782	14.32	38.0	95.3	24.9	17.38	0.05
X	R	860	11.98	0.0137	4.176	15.5	37.2	89.7	28.2	17.58	0.05
X	S	860	11.50	0.0131	2.716	15.01	38.9	93.0	31.4	17.50	0.05
X	T	910	12.85	0.0141	6.723	13.13	36.2	84.6	34.0	17.77	0.07
X	U	910	12.57	0.0119	5.995	15.26	43.0	85.9	37.1	17.66	0.06
X	V	960	14.99	0.0123	13.31	11.66	41.5	73.8	39.4	18.08	0.09
X	W	960	14.70	0.0104	12.87	16.0	49.2	74.1	42.4	17.82	0.07
X	X	1010	16.96	0.0101	20.01	17.8	50.5	65.1	45.7	18.06	0.09
X	Y	1010	16.19	0.0084	17.35	20.2	60.6	68.3	49.4	18.08	0.08
X	Z	1060	17.41	0.0088	20.73	22.2	57.9	64.8	53.3	18.44	0.09
X	AA	1060	16.00	0.0085	15.91	23.4	60.2	70.6	57.2	18.47	0.07
X	AB	1110	17.41	0.0087	19.66	21.2	58.8	66.6	60.7	18.96	0.09
X	AC	1110	16.92	0.0115	17.90	24.0	44.3	68.7	64.5	19.02	0.08
X	AD	1110	17.08	0.0104	18.38	35.6	48.9	68.2	69.9	19.05	0.07
X	AE	1110	17.69	0.0094	20.25	42.9	54.2	66.2	76.1	19.14	0.08
X	AF	1210	18.17	0.0053	19.92	66.8	95.5	67.6	85.0	20.08	0.07
X	AG	1260	19.48	0.0041	23.86	61.7	125.7	63.8	92.6	20.31	0.07
X	AH	1360	25.78	0.0394	41.06	9.23	12.9	52.9	93.7	22.29	0.15
X	AI	1700	20.74	0.0109	26.88	55.4	46.8	61.7	100.0	20.91	0.08
	Integrated age ± 2σ			n=34	MSWD=205.79	591.6	45.8	K2O=14.55%		18.95	0.11
	Plateau ± 2σ	no plateau		n=0	MSWD=0.00	0.000	0.000±0.000		0.0	0.00	0.00
	Isochron±2σ	steps B-AI		n=34	MSWD=54.50		$^{40}Ar/^{36}Ar$=	359.4±2.0		16.96	0.05

MZQ-32, K-Feldspar, 17.83 mg, J=0.0007811±0.04%, D=1.004±0.001, NM-208L, Lab#=57188-01

X	B	520	158.0	0.0271	372.1	1.411	18.8	30.4	0.6	67.41	1.16
X	C	520	25.61	0.0112	48.85	1.194	45.7	43.6	1.1	15.91	0.51
X	D	570	20.14	0.0087	25.28	3.10	58.6	62.9	2.5	18.03	0.27
X	E	570	15.79	0.0080	14.82	2.99	64.0	72.3	3.7	16.24	0.21
X	F	620	18.56	0.0081	15.53	6.20	62.9	75.3	6.3	19.87	0.14
X	G	620	14.01	0.0021	5.296	5.08	240.1	88.8	8.4	17.70	0.14
X	H	670	13.69	0.0065	4.997	7.81	78.8	89.2	11.4	17.38	0.09
X	I	670	13.28	0.0064	4.127	8.03	79.6	90.8	14.5	17.17	0.09
X	J	720	12.93	0.0055	2.769	10.14	92.9	93.7	18.2	17.23	0.07

X	K	720	13.01	0.0055	3.494	10.20	92.6	92.1	21.7	17.04	0.07
X	L	770	12.81	0.0053	2.233	12.94	96.4	94.9	26.0	17.29	0.06
X	M	770	12.87	0.0035	2.430	13.78	144.4	94.4	30.3	17.29	0.06
X	N	820	12.77	0.0035	1.848	14.57	145.3	95.7	34.5	17.39	0.05
X	O	820	13.14	0.0054	3.047	13.49	94.8	93.2	38.3	17.42	0.06
X	P	870	13.07	0.0046	2.611	12.82	112.0	94.1	41.7	17.50	0.06
X	Q	870	13.48	0.0047	3.932	12.00	109.5	91.4	44.7	17.52	0.06
X	R	920	13.90	0.0054	4.955	11.15	95.3	89.5	47.4	17.69	0.07
X	S	920	14.35	0.0043	6.389	10.40	119.0	86.8	49.8	17.73	0.08
X	T	970	15.24	0.0053	9.394	9.70	96.5	81.8	52.0	17.74	0.09
X	U	970	15.69	0.0050	10.55	10.08	102.1	80.1	54.1	17.89	0.07
X	V	1020	16.96	0.0033	13.92	10.55	152.7	75.7	56.3	18.27	0.08
X	W	1020	16.91	0.0041	13.71	11.80	125.9	76.0	58.7	18.30	0.07
X	X	1070	17.84	0.0043	15.95	12.96	119.1	73.6	61.2	18.67	0.10
X	Y	1070	17.17	0.0040	13.49	14.23	128.5	76.8	63.8	18.76	0.08
X	Z	1120	17.96	0.0046	15.32	15.59	112.0	74.8	66.6	19.11	0.08
X	AA	1120	17.25	0.0060	12.82	16.30	85.4	78.0	69.3	19.15	0.07
X	AB	1170	18.03	0.0053	14.35	13.95	95.8	76.5	71.5	19.61	0.09
X	AC	1170	17.88	0.0056	14.70	17.67	91.6	75.7	74.2	19.26	0.08
X	AD	1170	18.28	0.0048	15.28	28.0	107.3	75.3	78.2	19.58	0.08
X	AE	1170	19.16	0.0029	18.04	32.4	176.4	72.2	82.4	19.67	0.08
X	AF	1270	18.74	0.0023	14.17	30.3	222.3	77.6	86.1	20.69	0.07
X	AG	1320	19.02	0.0013	14.45	81.4	387.8	77.6	94.7	20.98	0.06
X	AH	1420	19.87	0.0015	17.20	26.5	330.8	74.4	97.1	21.03	0.08
X	AI	1770	20.79	0.0015	18.28	33.3	334.4	74.0	100.0	21.88	0.07
	Integrated age ± 2σ			n=34	MSWD=381.07	522.1	135.2	K2O=14.40%		19.39	0.09
	Plateau ± 2σ	no plateau		n=0	MSWD=0.00	0.000	0.000±0.000		0.0	0.00	0.00
	Isochron±2σ	steps B-AI		n=34	MSWD=66.05		$^{40}Ar/^{36}Ar$=	432.8±3.5		16.76	0.06

VC09-2, Kspar, 16.98 mg, J=0.0022593±0.05%, D=1.005±0.001, NM-227A, Lab#=59205-01

X	B	540	54.82	0.0204	163.4	1.84	25.0	11.9	0.3	26.75	1.66
X	C	540	10.71	0.0111	15.72	1.20	46.2	56.6	0.5	24.87	0.77
X	D	590	8.219	0.0091	6.297	2.05	55.9	77.3	0.8	26.07	0.50
X	E	590	12.19	0.0088	19.35	2.71	58.2	53.1	1.3	26.53	0.47
X	F	640	7.006	0.0076	2.989	3.95	66.9	87.4	2.0	25.11	0.24
X	G	640	6.763	0.0074	2.146	5.42	69.2	90.6	2.9	25.14	0.19
X	H	690	6.861	0.0083	2.233	6.91	61.7	90.4	4.0	25.43	0.14
X	I	690	6.476	0.0078	1.364	9.5	65.3	93.8	5.6	24.91	0.11
	J	740	6.431	0.0080	0.6827	10.6	64.0	96.9	7.3	25.55	0.10
	K	740	6.367	0.0077	0.7075	14.5	66.0	96.7	9.7	25.26	0.08
	L	790	6.352	0.0081	0.5409	14.8	63.0	97.5	12.1	25.39	0.08
	M	790	6.309	0.0082	0.4856	20.8	62.2	97.7	15.5	25.28	0.06
	N	840	6.284	0.0077	0.4419	20.3	66.0	97.9	18.8	25.23	0.06
	O	840	6.299	0.0077	0.3957	28.3	66.1	98.2	23.4	25.35	0.06
	P	890	6.306	0.0083	0.4460	25.6	61.5	97.9	27.5	25.32	0.06
	Q	890	6.304	0.0080	0.3683	36.0	64.1	98.3	33.2	25.41	0.05
	R	940	6.298	0.0080	0.3625	30.1	63.4	98.3	37.9	25.39	0.05
	S	940	6.309	0.0082	0.3369	41.3	62.3	98.4	44.4	25.47	0.05
	T	990	6.310	0.0082	0.3646	31.7	61.9	98.3	49.3	25.43	0.05
	U	990	6.305	0.0087	0.4044	42.3	58.9	98.1	55.8	25.37	0.05
	V	1040	6.320	0.0083	0.4167	30.2	61.8	98.1	60.4	25.41	0.05
	W	1040	6.331	0.0087	0.3931	38.7	58.9	98.2	66.2	25.48	0.06
	X	1090	6.309	0.0143	0.4405	40.2	35.8	98.0	72.2	25.34	0.05
	Y	1090	6.327	0.0113	0.4929	42.6	45.1	97.7	78.5	25.35	0.05
	Z	1140	6.430	0.0106	0.7622	27.1	48.4	96.5	82.4	25.45	0.06
	AA	1190	6.495	0.0100	0.9980	48.7	50.8	95.5	89.5	25.43	0.05
X	AB	1190	6.568	0.0095	1.135	46.2	53.7	94.9	96.1	25.56	0.05
X	AC	1190	6.948	0.0099	2.210	17.8	51.6	90.6	98.6	25.81	0.09
X	AD	1190	8.526	0.0093	7.496	5.35	54.7	74.0	99.4	25.88	0.22
X	AE	1190	8.071	-0.0293	6.697	0.250	-	75.4	99.4	24.97	2.70
X	AF	1290	8.069	-0.0015	3.087	0.523	-	88.7	99.5	29.32	1.40
X	AG	1340	9.561	-0.0238	8.099	0.440	-	74.9	99.6	29.36	1.74
X	AH	1390	15.00	0.0087	28.27	0.346	58.8	44.3	99.6	27.24	2.56

X	AI	1590	9.726	0.0087	10.76	2.41	58.8	67.3	99.9	26.84	0.43
X	AJ	1740	36.68	-0.0126	98.04	0.366	-	21.0	100.0	31.56	3.03
	Integrated age ± 2σ			n=35	MSWD=3.73	651.1	55.9	K2O=6.52%		25.44	0.07
	Plateau ± 2σ	steps J-AA		n=18	MSWD=1.56	543.9	57.3 ±16.7		83.5	25.38	0.04
	Isochron±2σ	steps B-AJ		n=35	MSWD=3.22		$^{40}Ar/^{36}Ar$=	304.6±4.1		25.38	0.04

Notes:

Isotopic ratios corrected for blank, radioactive decay, and mass discrimination, not corrected for interfering reactions.
Errors quoted for individual analyses include analytical error only, without interfering reaction or J uncertainties.
Integrated age calculated by summing isotopic measurements of all steps.
Integrated age error calculated by quadratically combining errors of isotopic measurements of all steps.
Plateau age is inverse-variance-weighted mean of selected steps.
Plateau age error is inverse-variance-weighted mean error (Taylor, 1982) times root MSWD where MSWD>1.
Plateau error is weighted error of Taylor (1982).
Decay constants and isotopic abundances after Min et al. (2000).
symbol preceding sample ID denotes analyses excluded from plateau age calculations.
Weight percent K_2O calculated from ^{39}Ar signal, sample weight, and instrument sensitivity.
Ages calculated relative to FC-2 Fish Canyon Tuff sanidine interlaboratory standard at 28.201 Ma (Kuiper et al., 2008)
Decay Constant (LambdaK (total)) = 5.463e-10/a
Correction factors:
$(^{39}Ar/^{37}Ar)_{Ca}$ = 0.0007 ± 5e-05
$(^{36}Ar/^{37}Ar)_{Ca}$ = 0.00028 ± 2e-05
$(^{38}Ar/^{39}Ar)_{K}$ = 0.013
$(^{40}Ar/^{39}Ar)_{K}$ = 0.01 ± 0.002

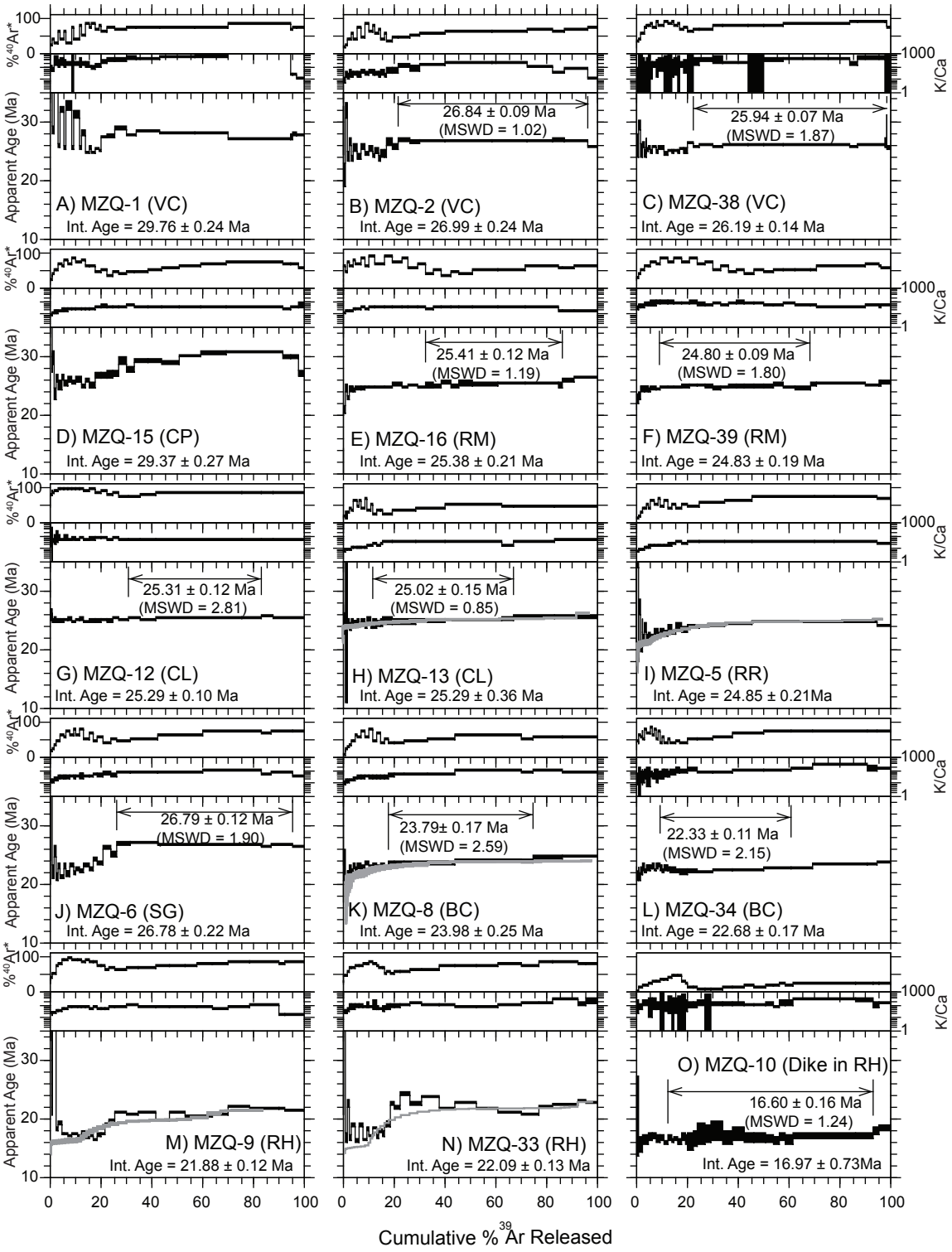

Figure 1.2.3. Age spectra for the Questa caldera plutonic K-feldspar. Auxiliary plots include K/Ca and radiogenic yield (%^{40}Ar*). All errors are reported at two sigma. Modeled age spectra used to model MDD coolinghistories are shown in gray.

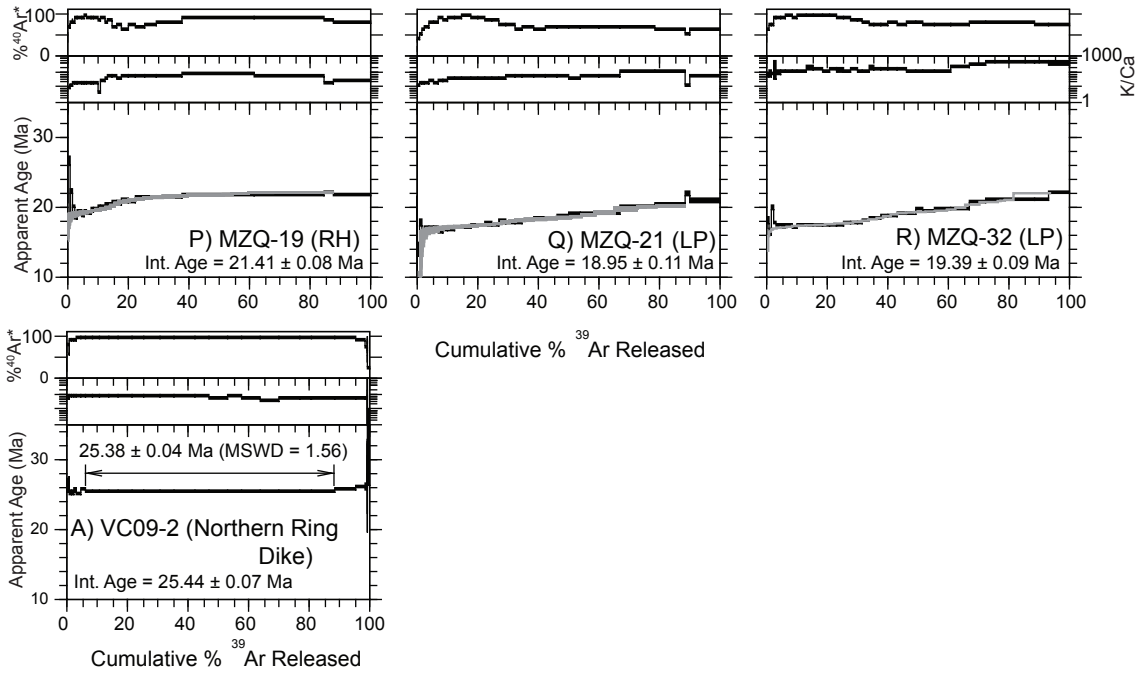

Figure 1.2.3. continued

APPENDIX 1.3.

SUPPLEMENTAL ARRHENIUS AND LOG (R/Ro) PLOTS FOR QUESTA CALDERA K-FELDSPAR MDD THERMAL HISTORIES

Appendix 1.3 contains Arrhenius and log (r/r_o) plots used for MDD thermal modeling of K-feldspars. Modeled age spectra and thermal histories, both monotonic and unconstrained, are located within the main body of the text. All MDD thermal histories were modeled using algorithms developed by Lovera et al., (1989, 1991). Arrhenius plots are constructed using the heating schedule and the fraction of $^{39}Ar_K$ released for each step. Log (r/r_o) plots are constructed by fitting an Arrhenius reference line (r_o) to the Arrhenius plot, calculating the deviation of the Arrhenius trend from r_o, and comparing that to the cumulative ^{39}Ar released. Black lines are the actual data and gray lines are the modeled data.

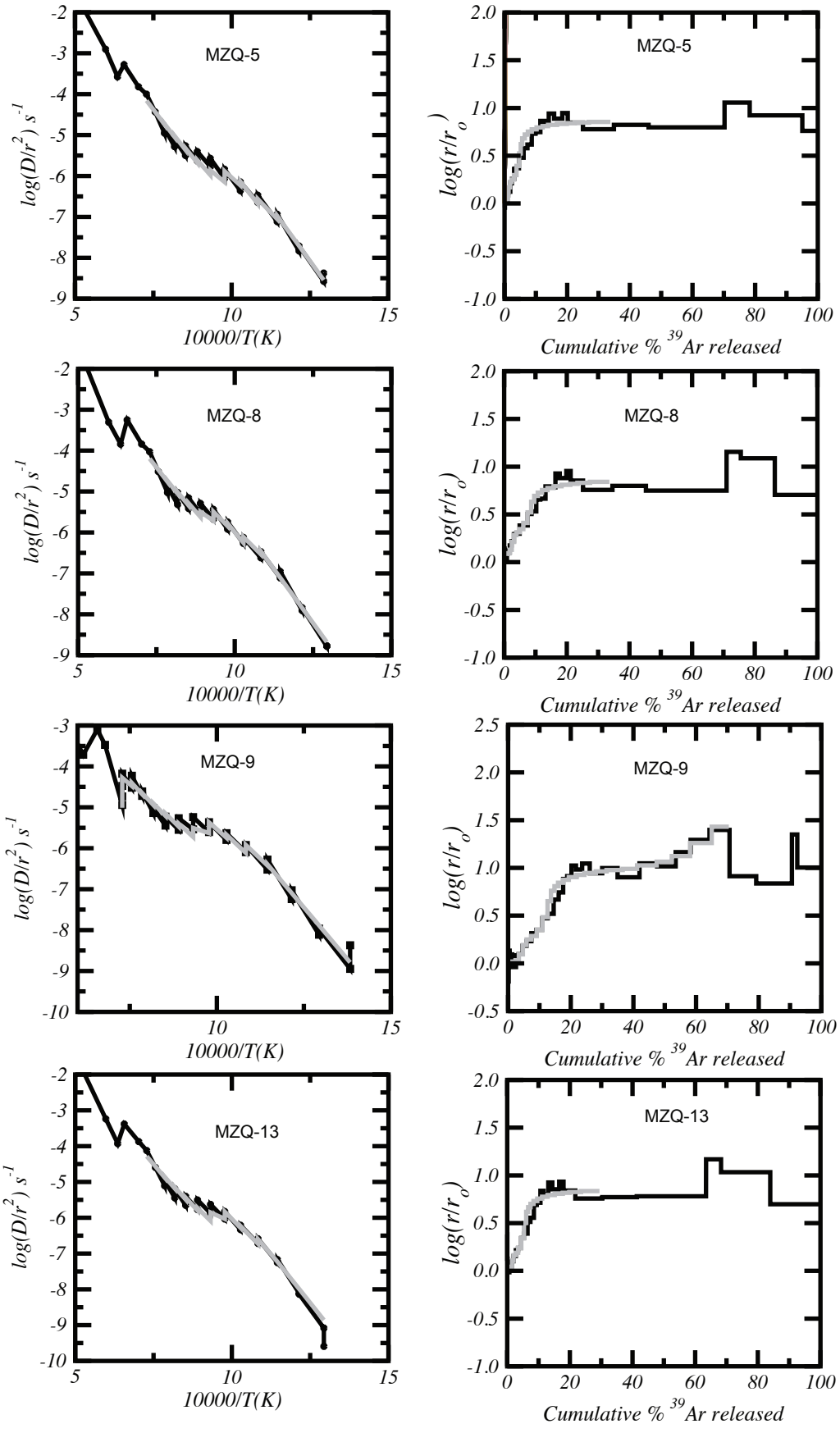
MZQ-5
log(D/r²) s⁻¹
10000/T(K)
log(r/r_o)
Cumulative % ³⁹Ar released
MZQ-8
log(D/r²) s⁻¹
10000/T(K)
log(r/r_o)
Cumulative % ³⁹Ar released
MZQ-9
log(D/r²) s⁻¹
10000/T(K)
log(r/r_o)
Cumulative % ³⁹Ar released
MZQ-13
log(D/r²) s⁻¹
10000/T(K)
log(r/r_o)
Cumulative % ³⁹Ar released

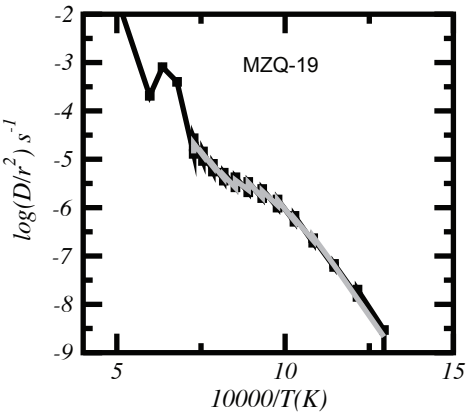
MZQ-19
log(D/r²) s⁻¹
10000/T(K)

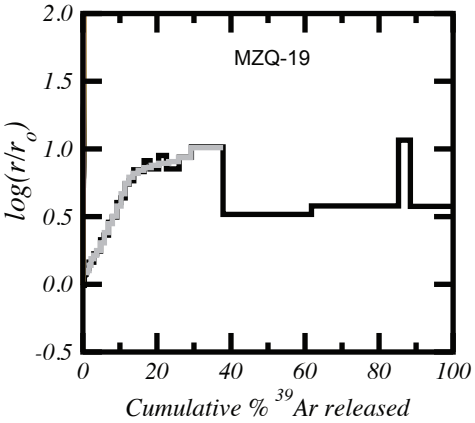
MZQ-19
log(r/r_o)
Cumulative % ³⁹Ar released

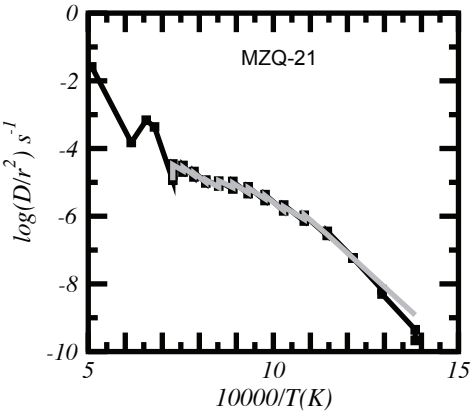
MZQ-21
log(D/r²) s⁻¹
10000/T(K)

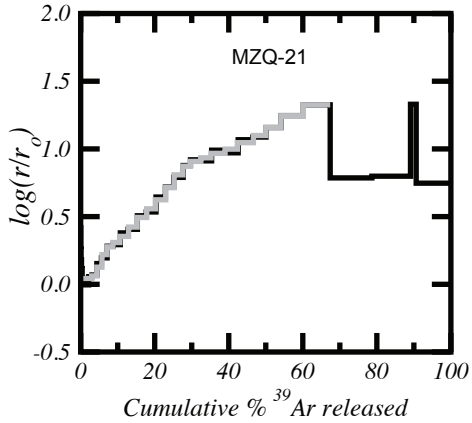
MZQ-21
log(r/r_o)
Cumulative % ³⁹Ar released

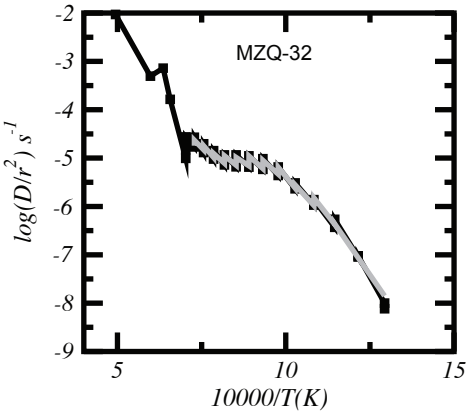
MZQ-32
log(D/r²) s⁻¹
10000/T(K)

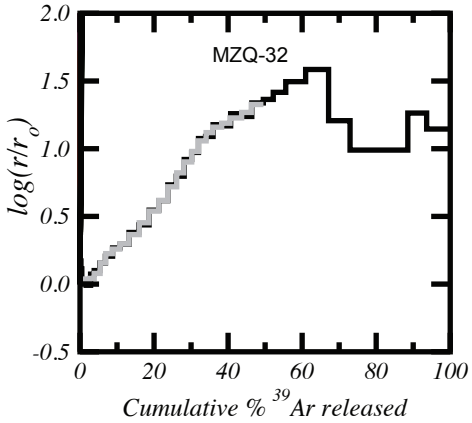
MZQ-32
log(r/r_o)
Cumulative % ³⁹Ar released

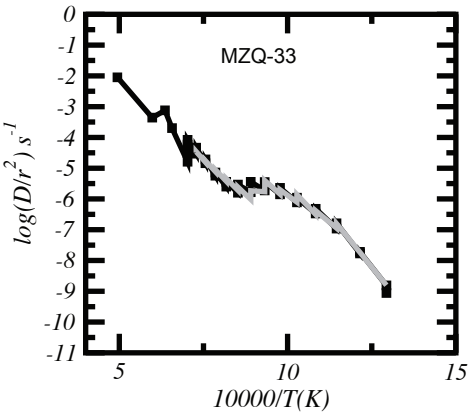
MZQ-33
log(D/r²) s⁻¹
10000/T(K)

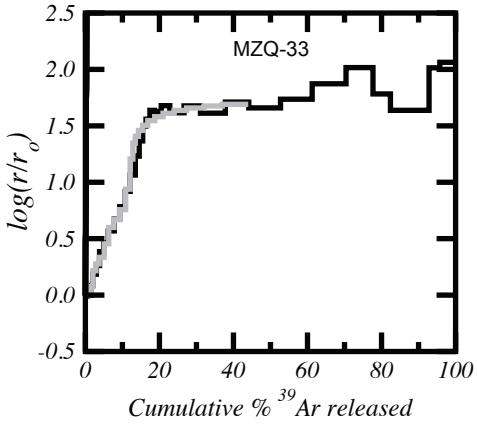
MZQ-33
log(r/r_o)
Cumulative % ³⁹Ar released

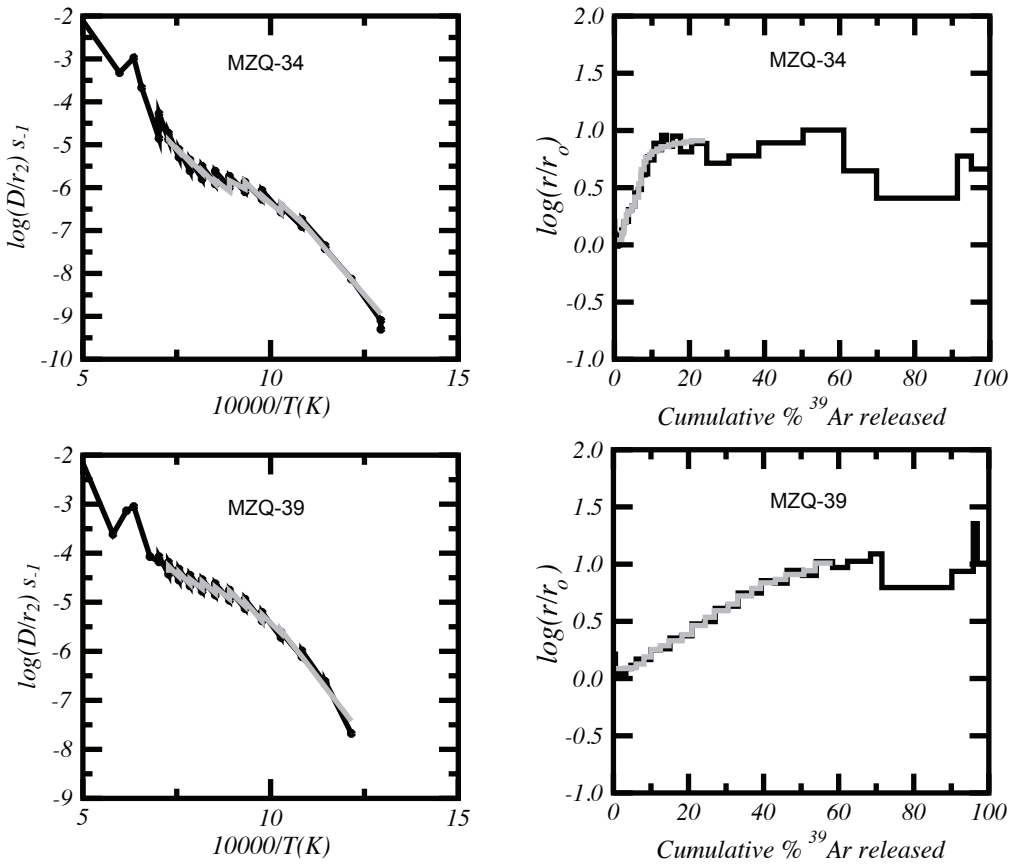
MZQ-34
log(D/r2) s-1
10000/T(K)
MZQ-34
log(r/ro)
Cumulative % 39Ar released
MZQ-39
log(D/r2) s-1
10000/T(K)
MZQ-39
log(r/ro)
Cumulative % 39Ar released

APPENDIX 2.1.

LOCATION OF THE DATED MT. AETNA CALDERA COMPLEX SAMPLES

Sample	Unit	Easting (Section 13S; NAD 27)	Northing (Section 13S; NAD 27)
MP-02	Mt. Princeton Border Unit 2	388877	4289681
MP-03	Mt. Princeton Border Unit 2	388877	4289681
MP-04	Tuff Dike	380061	4292398
MP-05	Mt. Princeton Outer Interior Qtz Monz.	377472	4278277
MP-06	Mt. Princeton Outer Interior Qtz Monz.	377514	4277352
MP-07	Mt. Princeton Outer Interior Qtz Monz.	377842	4276822
MP-08	Mt. Princeton Outer Interior Qtz Monz.	376899	4276285
MP-09	Mt. Aetna Ring Dike	382897	4285238
MP-10	Mt. Princeton Outer Interior Qtz Monz.	381394	4281494
MP-12	Mt. Princeton Porphyritic Qtz Monz.	390770	4285773
MP-13	Mt. Princeton Outer Interior Qtz Monz.	389990	4296079
MP-15	Wall Mountain Tuff Outflow Sheet	414721	4299549
MP-21	Mt. Aetna Qtz. Monz.	383745	4271437
MP-22	Mt. Princeton Porphyritic Qtz Monz.	393568	4277400
MP-24	Mt. Princeton Outer Interior Qtz Monz.	375718	4284932
MP-25	Mt. Princeton Outer Interior Qtz Monz.	375366	4285214
MP-30	Badger Creek Tuff Outflow Sheet	416691	4274214
MP-31	Badger Creek Tuff Outflow Sheet	425499	4285088
MP-32	Tuff Dike	380076	4292368
MP-33	Mt. Princeton Border Unit 2	387588	4281885
MP-36	Intracaldera Badger Creek	382557	4273339
MP-37	North Fork Luecogranite	390119	4272624
MP-38	California Luecogranite	396630	4279971
NM-531	Wall Mountain Tuff Outflow Sheet	428698	4281348
NM-1152	Wall Mountain Tuff Outflow Sheet	436788	4243828
NM-1307	Wall Mountain Tuff Outflow Sheet	410487	4292999
NM-1416	Wall Mountain Tuff Outflow Sheet	514171	4354374

APPENDIX 2.2.

MT. AETNA U/PB DATA TABLES AND WEIGHTED MEAN PLOTS

Appendix 2.2 contains the LA-ICP-MS U/Pb zircon data tables and weighted mean plots. Weighted mean ages were calculated from single grain ages using *Isoplot* (Ludwig, 2009). All uncertainties are reported at the 1-sigma level and include only analytical errors. Weighted mean plots contain uncertainties calculated only using internal and internal + external errors. U concentration and U/Th are calibrated relative to the Sri Lanka zircon standard and are accurate to ~20%. Common Pb correction is from ^{204}Pb, with composition interpreted from Stacey and Kramers (1975) and uncertainties of 1.0 for ^{206}Pb/ ^{204}Pb, 0.3 for ^{207}Pb/ ^{204}Pb, and 2.0 for ^{208}Pb/ ^{204}Pb. U/Pb ages and ^{206}Pb/ ^{207}Pb fractionation is calibrated relative to fragments of a large Sri Lanka zircon of 564±4 Ma (2σ). U decay constants and composition are as follows: ^{238}U = 9.8485 x 10 -10, ^{235}U = 1.55125 x 10 -10, ^{238}U/ ^{235}U = 137.88. For a more comprehensive description of LA-ICP-MS U-Pb zircon analytical procedures see Gehrels et al. (2008).

MP03 - Mt. Princeton Border Unit						Isotope ratios						Apparent ages (Ma)								
Analysis	U (ppm)	206Pb 204Pb	U/Th	206Pb* 207Pb*	± (%)	207Pb* 235U*	± (%)	206Pb* 238U	± (%)	error corr.	206Pb* 238U*	± (Ma)	207Pb* 235U	± (Ma)	206Pb* 207Pb*	± (Ma)	Best age (Ma)	± (Ma)	Conc (%)
MP03-11	153	1110	1.2	8.9233	119.9	-0.4749	119.9	-0.0307	0.5	0.00	-201.2	-1.0	-654.0	#NUM!	1833.2	119.5	-201.2	-1.0	-11.0
MP03-22	96	1110	1.3	31.6038	76.5	0.0227	76.6	0.0052	3.1	0.04	33.4	1.0	22.8	17.2	-998.1	2653.5	33.4	1.0	-3.3
MP03-30	108	1518	1.1	20.6782	55.0	0.0347	55.3	0.0052	5.2	0.09	33.4	1.7	34.6	18.8	116.9	1399.1	33.4	1.7	28.6
MP03-7	196	1752	1.0	18.6584	24.9	0.0384	25.2	0.0052	3.9	0.16	33.4	1.3	38.3	9.5	354.1	570.5	33.4	1.3	9.4
MP03-13	143	1800	1.1	30.4296	40.6	0.0237	41.0	0.0052	6.0	0.15	33.7	2.0	23.8	9.7	-887.3	1214.0	33.7	2.0	-3.8
MP03-10	147	1374	1.0	28.0178	36.9	0.0259	37.1	0.0053	4.0	0.11	33.8	1.4	26.0	9.5	-654.5	1042.9	33.8	1.4	-5.2
MP03-4	100	1122	1.1	23.1307	104.4	0.0322	104.4	0.0054	2.3	0.02	34.7	0.8	32.1	33.1	-154.2	1198.8	34.7	0.8	-22.5
MP03-6	161	1170	1.5	15.7420	65.2	0.0475	65.4	0.0054	5.9	0.09	34.9	2.0	47.1	30.1	725.8	1564.0	34.9	2.0	4.8
MP03-23	173	2412	1.0	20.4884	24.7	0.0365	25.0	0.0054	3.6	0.14	34.9	1.2	36.4	8.9	138.6	588.6	34.9	1.2	25.2
MP03-17	106	1500	1.2	26.6755	33.0	0.0284	33.1	0.0055	2.9	0.09	35.3	1.0	28.4	9.3	-521.4	903.2	35.3	1.0	-6.8
MP03-1	102	1380	1.2	27.2291	35.9	0.0278	35.9	0.0055	0.8	0.02	35.3	0.3	27.9	9.9	-576.6	996.8	35.3	0.3	-6.1
MP03-14	220	2166	0.8	21.1714	29.7	0.0360	29.8	0.0055	2.4	0.08	35.5	0.8	35.9	10.5	61.0	721.5	35.5	0.8	58.1
MP03-26	204	1596	0.9	16.6034	8.8	0.0460	9.3	0.0055	3.0	0.32	35.6	1.1	45.6	4.2	611.8	190.9	35.6	1.1	5.8
MP03-27	132	1710	0.9	24.2927	22.6	0.0315	22.7	0.0056	2.2	0.10	35.7	0.8	31.5	7.0	-277.4	581.4	35.7	0.8	-12.9
MP03-32	135	1488	0.9	24.2708	25.2	0.0316	25.4	0.0056	3.5	0.14	35.8	1.3	31.6	7.9	-275.1	648.8	35.8	1.3	-13.0
MP03-2	109	1020	1.0	13.0953	201.7	0.0589	201.7	0.0056	4.7	0.02	36.0	1.7	58.1	114.4	1104.6	857.6	36.0	1.7	3.3
MP03-31	129	1326	1.2	18.6265	28.8	0.0415	29.1	0.0056	3.4	0.12	36.0	1.2	41.3	11.7	357.9	663.7	36.0	1.2	10.1
MP03-20	236	2070	1.0	19.0527	21.7	0.0408	21.9	0.0056	2.4	0.11	36.3	0.9	40.6	8.7	306.7	500.2	36.3	0.9	11.8
MP03-25	141	1818	1.1	30.5252	41.1	0.0255	41.1	0.0057	0.8	0.02	36.3	0.3	25.6	10.4	-896.4	1231.5	36.3	0.3	-4.1
MP03-12	133	1722	1.2	27.2700	33.4	0.0286	33.6	0.0057	3.1	0.09	36.3	1.1	28.6	9.5	-580.7	925.8	36.3	1.1	-6.3
MP03-28	194	2268	0.9	21.0976	29.2	0.0370	29.2	0.0057	1.0	0.03	36.4	0.4	36.9	10.6	69.4	706.8	36.4	0.4	52.5
MP03-29	132	1848	1.3	30.6782	40.7	0.0255	40.9	0.0057	3.7	0.09	36.5	1.3	25.6	10.3	-910.9	1224.6	36.5	1.3	-4.0
MP03-9	427	4704	0.7	20.1971	7.3	0.0388	7.3	0.0057	0.5	0.07	36.5	0.2	38.6	2.8	172.1	170.2	36.5	0.2	21.2
MP03-24	124	1584	0.8	21.0805	39.6	0.0372	39.7	0.0057	3.0	0.08	36.6	1.1	37.1	14.5	71.3	975.2	36.6	1.1	51.4
MP03-5	182	2670	1.1	20.5385	20.2	0.0386	20.3	0.0057	2.0	0.10	36.9	0.7	38.4	7.6	132.9	478.5	36.9	0.7	27.8
MP03-35	116	1488	1.2	28.8201	44.3	0.0275	44.3	0.0058	1.6	0.04	37.0	0.6	27.6	12.1	-732.8	1291.2	37.0	0.6	-5.1
MP03-15	172	2178	1.3	20.6077	25.9	0.0387	26.0	0.0058	1.9	0.07	37.2	0.7	38.6	9.8	124.9	618.4	37.2	0.7	29.8
MP03-19	124	1704	0.9	29.2279	38.9	0.0274	39.0	0.0058	2.3	0.06	37.3	0.9	27.4	10.6	-772.2	1132.6	37.3	0.9	-4.8
MP03-21	94	1236	1.1	24.6064	27.7	0.0328	27.8	0.0059	3.0	0.11	37.7	1.1	32.8	9.0	-310.1	720.5	37.7	1.1	-12.1
MP03-16	102	1320	1.1	26.8843	36.5	0.0301	36.6	0.0059	3.1	0.08	37.7	1.2	30.1	10.9	-542.3	1007.2	37.7	1.2	-7.0
MP03-8	91	630	1.3	9.4700	13.0	0.0900	13.5	0.0062	3.8	0.28	39.7	1.5	87.5	11.4	1724.7	239.6	39.7	1.5	2.3

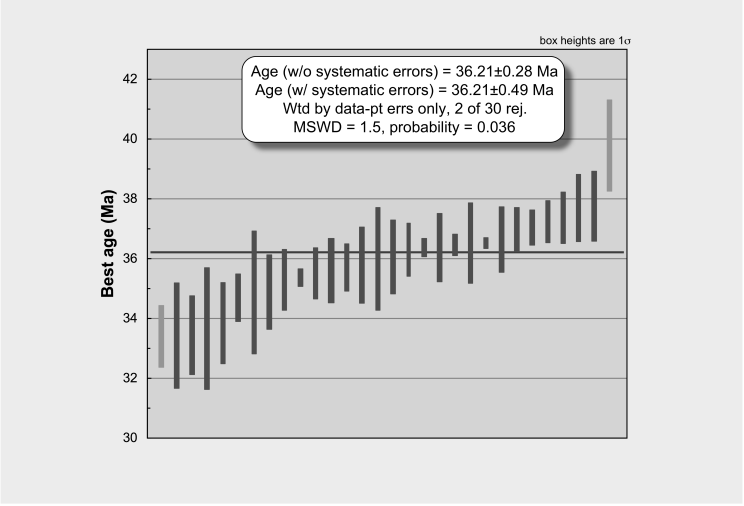

MP05 - Mt. Princeton Qtz. Monz.						Isotope ratios						Apparent ages (Ma)								
Analysis	U	206Pb	U/Th	206Pb*	±	207Pb*	±	206Pb*	±	error	206Pb*	±	207Pb*	±	206Pb*	±	Best age	±	Conc
	(ppm)	204Pb		207Pb*	(%)	235U*	(%)	238U	(%)	corr.	238U*	(Ma)	235U	(Ma)	207Pb*	(Ma)	(Ma)	(Ma)	(%)
MP05-13	333	1533	1.6	19.1521	23.2	0.0358	23.2	0.0050	1.7	0.07	32.0	0.5	35.7	8.2	294.8	535.0	32.0	0.5	10.9
MP05-9	370	2574	1.2	17.2547	18.5	0.0407	19.0	0.0051	4.4	0.23	32.7	1.4	40.5	7.5	528.1	407.8	32.7	1.4	6.2
MP05-5	430	2643	1.6	19.5290	14.2	0.0360	14.6	0.0051	3.4	0.23	32.8	1.1	35.9	5.1	250.1	327.6	32.8	1.1	13.1
MP05-15	210	1446	0.9	24.0757	37.9	0.0294	38.1	0.0051	3.0	0.08	33.1	1.0	29.5	11.1	-254.6	991.6	33.1	1.0	-13.0
MP05-23	377	2091	1.4	19.6526	37.3	0.0362	37.4	0.0052	2.3	0.06	33.1	0.7	36.1	13.2	235.6	888.7	33.1	0.7	14.1
MP05-20	305	2211	1.7	23.2703	23.7	0.0306	24.2	0.0052	5.0	0.21	33.2	1.7	30.6	7.3	-169.1	596.1	33.2	1.7	-19.6
MP05-33	339	2121	1.5	20.9140	21.6	0.0346	21.7	0.0053	1.9	0.09	33.8	0.6	34.6	7.4	90.1	517.0	33.8	0.6	37.5
MP05-27	378	2088	1.4	22.4102	31.4	0.0325	31.8	0.0053	4.8	0.15	34.0	1.6	32.5	10.2	-76.2	785.7	34.0	1.6	-44.6
MP05-1	380	1440	1.1	18.7829	21.1	0.0388	21.2	0.0053	2.5	0.12	34.0	0.8	38.7	8.0	339.0	481.7	34.0	0.8	10.0
MP05-18	355	2814	1.4	25.1785	23.3	0.0291	23.5	0.0053	3.4	0.14	34.1	1.1	29.1	6.7	-369.3	610.1	34.1	1.1	-9.2
MP05-4	351	2151	1.5	22.6319	20.3	0.0324	20.4	0.0053	1.8	0.09	34.2	0.6	32.4	6.5	-100.3	504.1	34.2	0.6	-34.1
MP05-14	409	2910	1.5	23.5857	20.7	0.0311	20.8	0.0053	1.9	0.09	34.2	0.6	31.1	6.4	-202.8	522.9	34.2	0.6	-16.9
MP05-10	377	2781	1.4	19.9182	22.6	0.0369	22.7	0.0053	2.2	0.10	34.3	0.8	36.8	8.2	204.5	530.0	34.3	0.8	16.8
MP05-24	361	2220	1.1	18.5671	19.4	0.0396	19.7	0.0053	3.4	0.17	34.3	1.2	39.5	7.6	365.1	441.8	34.3	1.2	9.4
MP05-12	328	3126	1.6	17.3213	17.9	0.0427	17.9	0.0054	1.6	0.09	34.5	0.5	42.5	7.5	519.6	395.1	34.5	0.5	6.6
MP05-22	416	3174	1.5	20.0171	23.1	0.0370	23.1	0.0054	0.8	0.04	34.6	0.3	36.9	8.4	193.0	543.9	34.6	0.3	17.9
MP05-29	413	2883	1.5	23.8327	24.7	0.0312	24.9	0.0054	3.1	0.12	34.6	1.1	31.2	7.6	-229.0	631.2	34.6	1.1	-15.1
MP05-21	360	2241	0.9	23.0345	20.4	0.0323	20.6	0.0054	2.6	0.13	34.7	0.9	32.3	6.6	-143.8	510.8	34.7	0.9	-24.1
MP05-34	355	1590	1.0	18.0389	31.0	0.0416	31.3	0.0054	4.0	0.13	35.0	1.4	41.4	12.7	429.8	706.8	35.0	1.4	8.1
MP05-17	506	3603	1.7	21.6991	12.1	0.0346	12.2	0.0054	1.7	0.14	35.0	0.6	34.5	4.2	2.1	292.6	35.0	0.6	1691.5
MP05-11	276	2295	1.1	21.8701	24.2	0.0345	24.3	0.0055	1.7	0.07	35.2	0.6	34.4	8.2	-16.9	592.6	35.2	0.6	-208.6
MP05-31	296	1869	0.9	27.1926	32.0	0.0278	32.2	0.0055	3.7	0.12	35.2	1.3	27.8	8.8	-573.0	883.0	35.2	1.3	-6.2
MP05-25	382	858	1.6	20.6265	24.8	0.0368	24.9	0.0055	1.8	0.07	35.4	0.6	36.7	9.0	122.8	592.2	35.4	0.6	28.8
MP05-30	341	3030	1.6	26.6724	44.1	0.0286	44.2	0.0055	2.8	0.06	35.5	1.0	28.6	12.5	-521.1	1229.0	35.5	1.0	-6.8
MP05-7	257	2115	1.5	31.2467	40.8	0.0245	40.8	0.0055	1.6	0.04	35.7	0.6	24.6	9.9	-964.6	1241.6	35.7	0.6	-3.7
MP05-26	326	2982	1.4	19.8412	36.6	0.0389	36.7	0.0056	2.5	0.07	36.0	0.9	38.8	14.0	213.5	874.5	36.0	0.9	16.9
MP05-8	476	2865	1.3	22.2742	25.0	0.0347	25.0	0.0056	1.4	0.05	36.0	0.5	34.6	8.5	-61.3	618.0	36.0	0.5	-58.8
MP05-2	325	2409	1.6	22.6244	24.0	0.0347	24.2	0.0057	3.1	0.13	36.6	1.1	34.6	8.2	-99.5	598.1	36.6	1.1	-36.7
MP05-3	227	1653	1.4	22.2956	48.7	0.0352	48.7	0.0057	1.2	0.02	36.6	0.4	35.1	16.8	-63.7	1255.8	36.6	0.4	-57.5
MP05-35	106	1050	1.0	28.3397	86.7	0.0278	87.2	0.0057	9.0	0.10	36.8	3.3	27.9	24.0	-686.0	3085.5	36.8	3.3	-5.4
MP05-28	437	2958	1.1	21.1896	16.6	0.0374	16.6	0.0057	1.3	0.08	37.0	0.5	37.3	6.1	59.0	397.5	37.0	0.5	62.6
MP05-32	348	855	1.6	11.1208	21.6	0.0716	21.6	0.0058	1.8	0.08	37.1	0.7	70.2	14.7	1423.9	416.8	37.1	0.7	2.6
MP05-6	209	55971	2.5	9.8865	1.2	3.4549	2.0	0.2477	1.6	0.80	1426.8	20.4	1517.0	15.6	1645.3	21.9	1645.3	21.9	86.7

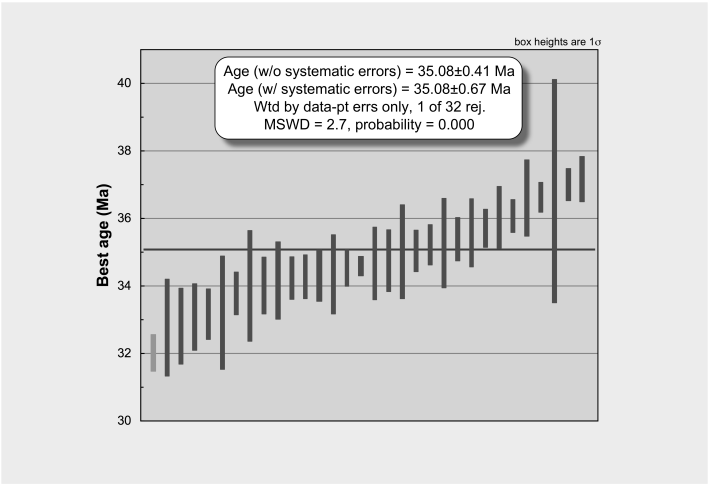

MP06 - Mt. Princeton Qtz. Monz.						Isotope ratios					Apparent ages (Ma)								
Analysis	U	206Pb	U/Th	206Pb*	±	207Pb*	±	206Pb*	±	error	206Pb*	±	207Pb*	±	206Pb*	±	Best age	±	Conc
	(ppm)	204Pb		207Pb*	(%)	235U*	(%)	238U	(%)	corr.	238U*	(Ma)	235U	(Ma)	207Pb*	(Ma)	(Ma)	(Ma)	(%)
MP6-11	339	1463	1.6	19.1846	32.2	0.0371	32.6	0.0052	5.0	0.15	33.2	1.7	36.9	11.8	290.9	752.9	33.2	1.7	11.4
MP6-8	405	2048	1.4	22.2950	17.8	0.0319	18.1	0.0052	3.3	0.18	33.2	1.1	31.9	5.7	-63.6	437.0	33.2	1.1	-52.2
MP6-7	335	1513	1.1	21.1798	37.0	0.0337	37.0	0.0052	1.8	0.05	33.3	0.6	33.7	12.3	60.1	908.1	33.3	0.6	55.4
MP6-20	311	1403	1.3	21.7505	35.2	0.0329	35.2	0.0052	1.0	0.03	33.4	0.3	32.9	11.4	-3.6	872.6	33.4	0.3	-923.0
MP6-23	334	1163	1.2	19.2259	24.2	0.0374	24.3	0.0052	2.1	0.08	33.5	0.7	37.3	8.9	286.0	560.9	33.5	0.7	11.7
MP6-6	327	1298	1.2	19.7713	25.5	0.0364	25.7	0.0052	3.1	0.12	33.6	1.0	36.3	9.2	221.6	598.7	33.6	1.0	15.1
MP6-22	320	1878	1.7	24.8283	28.1	0.0293	28.3	0.0053	3.3	0.12	33.9	1.1	29.3	8.2	-333.2	735.6	33.9	1.1	-10.2
MP6-5	416	2425	1.2	22.9880	19.7	0.0317	20.0	0.0053	2.9	0.15	34.0	1.0	31.7	6.2	-138.8	492.9	34.0	1.0	-24.5
MP6-19	272	1578	1.4	18.6447	48.6	0.0394	48.7	0.0053	3.9	0.08	34.3	1.3	39.2	18.8	355.7	1162.3	34.3	1.3	9.6
MP6-18	458	2648	1.1	18.2983	13.5	0.0402	13.6	0.0053	1.8	0.13	34.3	0.6	40.1	5.4	397.9	304.5	34.3	0.6	8.6
MP6-3	404	2020	1.5	24.2980	24.6	0.0303	24.8	0.0053	2.9	0.12	34.4	1.0	30.3	7.4	-277.9	635.1	34.4	1.0	-12.4
MP6-30	344	1713	1.1	24.9366	30.0	0.0297	30.5	0.0054	5.4	0.18	34.6	1.9	29.7	8.9	-344.4	788.6	34.6	1.9	-10.0
MP6-14	399	2293	1.2	29.6364	48.2	0.0251	48.3	0.0054	1.8	0.04	34.6	0.6	25.1	12.0	-811.6	1441.8	34.6	0.6	-4.3
MP6-10	526	2378	2.7	25.7710	21.2	0.0288	21.3	0.0054	1.8	0.09	34.7	0.6	28.9	6.1	-430.0	561.1	34.7	0.6	-8.1
MP6-15	279	320	1.2	10.8261	27.2	0.0689	28.3	0.0054	7.6	0.27	34.8	2.7	67.7	18.5	1475.0	525.9	34.8	2.7	2.4
MP6-29	606	2078	0.6	22.4728	9.2	0.0332	9.4	0.0054	1.8	0.19	34.8	0.6	33.2	3.1	-83.0	226.3	34.8	0.6	-41.9
MP6-17	259	1475	1.7	17.6738	17.6	0.0424	17.8	0.0054	2.7	0.15	35.0	0.9	42.2	7.4	475.2	392.1	35.0	0.9	7.4
MP6-27	420	1850	1.6	21.4749	18.8	0.0350	19.0	0.0054	2.7	0.14	35.0	0.9	34.9	6.5	27.0	454.3	35.0	0.9	129.6
MP6-12	413	1665	1.7	28.5839	43.7	0.0265	43.7	0.0055	2.0	0.04	35.3	0.7	26.6	11.5	-709.8	1266.4	35.3	0.7	-5.0
MP6-28	340	1400	1.5	34.2792	46.2	0.0221	46.2	0.0055	0.8	0.02	35.4	0.3	22.2	10.2	-1245.7	1511.3	35.4	0.3	-2.8
MP6-4	448	1905	1.5	19.6567	16.1	0.0387	16.1	0.0055	1.3	0.08	35.4	0.4	38.5	6.1	235.1	372.5	35.4	0.4	15.1
MP6-25	242	1425	1.7	18.2346	31.7	0.0418	31.9	0.0055	2.9	0.09	35.6	1.0	41.6	13.0	405.7	726.7	35.6	1.0	8.8
MP6-16	265	1248	1.2	30.0750	41.0	0.0257	41.2	0.0056	3.0	0.07	36.0	1.1	25.7	10.5	-853.5	1219.9	36.0	1.1	-4.2
MP6-13	416	2028	1.3	24.8844	19.3	0.0313	19.4	0.0057	1.4	0.07	36.3	0.5	31.3	6.0	-339.0	501.5	36.3	0.5	-10.7
MP6-2	424	2040	1.2	26.1231	34.5	0.0300	34.6	0.0057	2.1	0.06	36.5	0.8	30.0	10.2	-465.7	934.8	36.5	0.8	-7.8
MP6-9	369	1518	1.2	24.1030	22.4	0.0328	22.4	0.0057	0.9	0.04	36.8	0.3	32.8	7.2	-257.5	573.7	36.8	0.3	-14.3
MP6-1	280	453	1.2	9.5108	19.5	0.0833	20.0	0.0057	4.3	0.21	36.9	1.6	81.3	15.6	1716.8	362.8	36.9	1.6	2.2
MP6-21	190	1073	1.0	15.5873	21.1	0.0518	21.5	0.0059	4.2	0.20	37.6	1.6	51.3	10.7	746.7	449.7	37.6	1.6	5.0
MP6-24	331	1575	1.1	18.9019	22.9	0.0429	23.0	0.0059	2.1	0.09	37.8	0.8	42.6	9.6	324.7	526.6	37.8	0.8	11.6
MP6-26	420	1890	1.1	21.1598	26.8	0.0391	26.8	0.0060	1.7	0.06	38.6	0.6	39.0	10.3	62.4	648.4	38.6	0.6	61.9

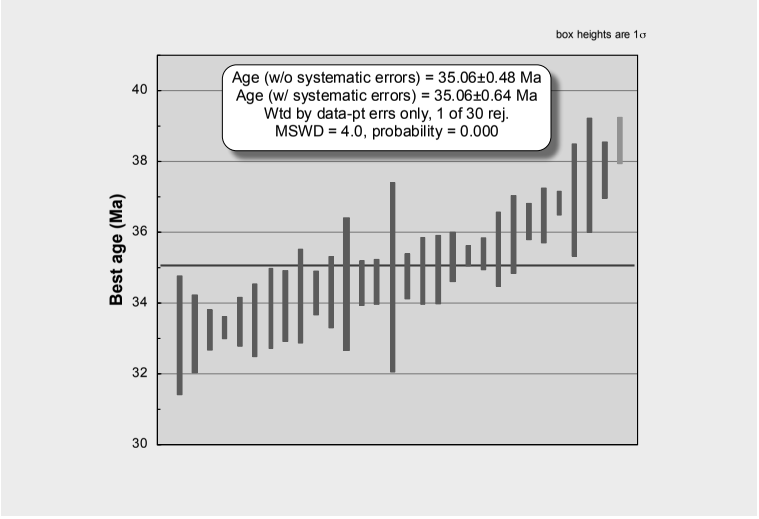

MP07 - Mt. Princeton Qtz. Monz.						Isotope ratios						Apparent ages (Ma)								
Analysis	U	206Pb	U/Th	206Pb*	±	207Pb*	±	206Pb*	±	error	206Pb*	±	207Pb*	±	206Pb*	±	Best age	±	Conc
	(ppm)	204Pb		207Pb*	(%)	235U*	(%)	238U	(%)	corr.	238U*	(Ma)	235U	(Ma)	207Pb*	(Ma)	(Ma)	(Ma)	(%)
MP7-2	253	3915	2.9	28.9840	83.8	0.0251	84.0	0.0053	5.3	0.06	33.9	1.8	25.2	20.9	-748.7	2925.4	33.9	1.8	-4.5
MP7-7	195	2830	2.6	20.8501	72.4	0.0356	72.4	0.0054	1.9	0.03	34.6	0.7	35.5	25.3	97.3	1995.8	34.6	0.7	35.5
MP7-5	1177	8370	1.6	20.2722	9.3	0.0368	10.0	0.0054	3.6	0.36	34.7	1.2	36.7	3.6	163.5	217.9	34.7	1.2	21.3
MP7-18	1349	7860	0.7	19.8357	8.7	0.0377	8.8	0.0054	1.5	0.17	34.8	0.5	37.6	3.3	214.2	201.6	34.8	0.5	16.3
MP7-10	505	4340	1.9	22.0852	14.6	0.0341	14.6	0.0055	1.5	0.10	35.1	0.5	34.0	4.9	-40.6	355.5	35.1	0.5	-86.4
MP7-20	271	3655	2.7	23.2443	31.3	0.0324	31.4	0.0055	2.9	0.09	35.1	1.0	32.4	10.0	-166.4	794.8	35.1	1.0	-21.1
MP7-1	494	7105	1.0	23.0375	13.7	0.0327	14.0	0.0055	2.8	0.20	35.1	1.0	32.6	4.5	-144.2	340.9	35.1	1.0	-24.3
MP7-4	562	5445	1.3	21.0568	8.3	0.0357	8.4	0.0055	1.4	0.17	35.1	0.5	35.7	2.9	74.0	197.1	35.1	0.5	47.5
MP7-13	483	5965	1.3	22.8146	14.5	0.0334	14.9	0.0055	3.1	0.21	35.5	1.1	33.3	4.9	-120.1	360.1	35.5	1.1	-29.6
MP7-15	444	6440	2.2	20.7036	42.1	0.0368	42.1	0.0055	0.8	0.02	35.6	0.3	36.7	15.2	114.0	1034.4	35.6	0.3	31.2
MP7-6	451	6905	2.1	21.9633	16.0	0.0348	16.0	0.0055	1.0	0.06	35.6	0.4	34.7	5.5	-27.2	388.7	35.6	0.4	-131.2
MP7-19	419	6750	2.3	18.4419	9.9	0.0417	10.1	0.0056	1.9	0.19	35.8	0.7	41.5	4.1	380.4	222.2	35.8	0.7	9.4
MP7-3	397	2570	1.1	15.8187	9.6	0.0486	10.3	0.0056	3.7	0.36	35.9	1.3	48.2	4.8	715.5	203.8	35.9	1.3	5.0
MP7-12	534	5655	2.4	20.3427	11.9	0.0380	12.0	0.0056	1.3	0.11	36.0	0.5	37.8	4.4	155.4	279.1	36.0	0.5	23.2
MP7-16	455	7350	1.6	23.8277	17.4	0.0325	17.6	0.0056	3.0	0.17	36.1	1.1	32.4	5.6	-228.4	440.2	36.1	1.1	-15.8
MP7-8	341	6380	1.4	23.3343	24.4	0.0332	24.5	0.0056	2.6	0.11	36.1	0.9	33.2	8.0	-176.0	615.9	36.1	0.9	-20.5
MP7-11	478	5170	2.0	21.5576	18.2	0.0360	18.2	0.0056	0.5	0.03	36.2	0.2	35.9	6.4	17.8	441.0	36.2	0.2	203.5
MP7-14	558	5840	1.8	20.6566	13.9	0.0376	13.9	0.0056	0.5	0.04	36.2	0.2	37.5	5.1	119.4	329.6	36.2	0.2	30.3
MP7-17	483	8080	1.8	22.2158	14.9	0.0354	15.0	0.0057	1.0	0.06	36.7	0.4	35.3	5.2	-54.9	365.1	36.7	0.4	-66.7
MP7-9	371	4410	1.1	20.8488	18.9	0.0384	18.9	0.0058	1.1	0.06	37.3	0.4	38.2	7.1	97.5	450.2	37.3	0.4	38.3

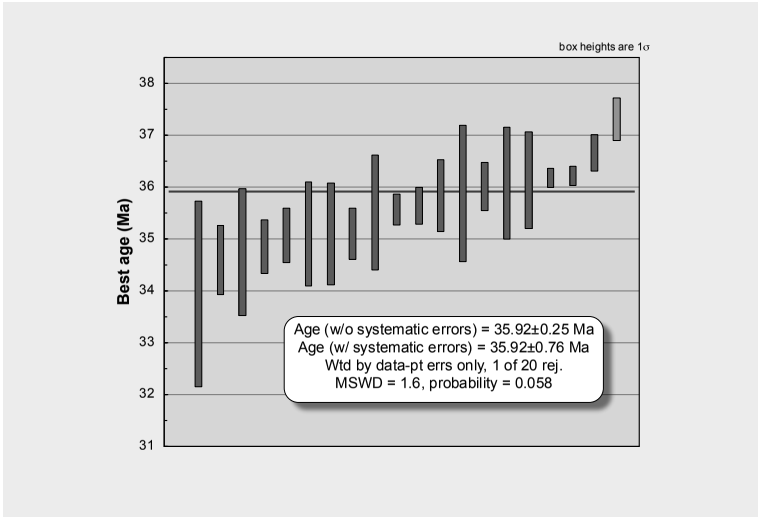

MP08 - Mt. Princeton Qtz. Monz.						Isotope ratios						Apparent ages (Ma)							
Analysis	U	206Pb	U/Th	206Pb*	±	207Pb*	±	206Pb*	±	error	206Pb*	±	207Pb*	±	206Pb*	±	Best age	±	Conc
	(ppm)	204Pb		207Pb*	(%)	235U*	(%)	238U	(%)	corr.	238U*	(Ma)	235U	(Ma)	207Pb*	(Ma)	(Ma)	(Ma)	(%)
MP8-26	206	1608	1.2	15.2107	23.9	0.0436	24.3	0.0048	4.6	0.19	30.9	1.4	43.3	10.3	798.2	507.8	30.9	1.4	3.9
MP8-19	191	1552	1.2	17.6276	181.4	0.0382	181.5	0.0049	5.3	0.03	31.4	1.7	38.1	67.9	481.0	1300.4	31.4	1.7	6.5
MP8-18	237	2280	0.8	21.6526	100.1	0.0320	100.3	0.0050	5.3	0.05	32.3	1.7	31.9	31.5	7.2	1026.1	32.3	1.7	447.8
MP8-10	233	1712	0.8	21.4703	44.5	0.0326	44.7	0.0051	4.5	0.10	32.6	1.5	32.6	14.3	27.6	1116.4	32.6	1.5	118.5
MP8-25	315	2544	1.2	22.8353	41.6	0.0311	41.7	0.0052	2.6	0.06	33.2	0.9	31.1	12.8	-122.4	1066.6	33.2	0.9	-27.1
MP8-22	412	4532	1.3	21.3470	26.2	0.0343	26.3	0.0053	2.6	0.10	34.1	0.9	34.2	8.9	41.4	636.4	34.1	0.9	82.5
MP8-8	203	2088	1.4	19.0693	154.1	0.0384	154.1	0.0053	2.0	0.01	34.1	0.7	38.2	57.9	304.7	1250.3	34.1	0.7	11.2
MP8-28	346	3164	1.3	19.0602	18.7	0.0387	18.9	0.0053	2.8	0.15	34.4	0.9	38.5	7.1	305.8	428.6	34.4	0.9	11.2
MP8-5	341	2684	1.4	19.1424	21.7	0.0385	21.8	0.0053	2.5	0.11	34.4	0.8	38.4	8.2	295.9	500.3	34.4	0.8	11.6
MP8-11	415	4120	1.2	22.8791	21.1	0.0324	21.2	0.0054	1.3	0.06	34.5	0.5	32.3	6.7	-127.1	527.2	34.5	0.5	-27.2
MP8-17	385	3332	1.2	26.1351	35.7	0.0283	35.8	0.0054	2.0	0.06	34.5	0.7	28.4	10.0	-467.0	970.3	34.5	0.7	-7.4
MP8-15	436	3500	1.1	25.5121	26.5	0.0290	26.7	0.0054	2.7	0.10	34.6	0.9	29.1	7.6	-403.6	702.4	34.6	0.9	-8.6
MP8-23	235	1892	0.8	20.0220	26.4	0.0371	26.7	0.0054	3.8	0.14	34.6	1.3	37.0	9.7	192.5	624.5	34.6	1.3	18.0
MP8-31	727	6556	1.7	20.7030	11.2	0.0361	11.2	0.0054	1.1	0.09	34.8	0.4	36.0	4.0	114.1	263.8	34.8	0.4	30.5
MP8-20	357	2528	1.2	17.2450	20.8	0.0433	20.9	0.0054	1.7	0.08	34.8	0.6	43.0	8.8	529.3	461.1	34.8	0.6	6.6
MP8-30	430	3220	1.4	21.8693	26.1	0.0342	26.2	0.0054	2.5	0.10	34.9	0.9	34.1	8.8	-16.8	639.2	34.9	0.9	-207.9
MP8-13	427	3180	1.4	22.1719	21.4	0.0338	21.5	0.0054	1.7	0.08	35.0	0.6	33.8	7.1	-50.1	526.5	35.0	0.6	-69.8
MP8-34	391	4208	1.3	25.3343	38.2	0.0297	38.3	0.0055	2.6	0.07	35.1	0.9	29.7	11.2	-385.4	1024.8	35.1	0.9	-9.1
MP8-27	324	1784	0.9	19.8562	26.5	0.0379	26.6	0.0055	2.8	0.10	35.1	1.0	37.8	9.9	211.7	623.2	35.1	1.0	16.6
MP8-6	360	2432	1.3	16.5651	22.1	0.0456	22.1	0.0055	1.6	0.07	35.2	0.5	45.3	9.8	616.8	481.7	35.2	0.5	5.7
MP8-16	720	6684	1.2	23.5247	15.7	0.0321	15.8	0.0055	1.6	0.10	35.2	0.6	32.1	5.0	-196.3	395.8	35.2	0.6	-17.9
MP8-33	701	5416	2.6	22.0744	15.0	0.0344	15.2	0.0055	2.6	0.17	35.4	0.9	34.3	5.1	-39.4	366.6	35.4	0.9	-89.7
MP8-35	411	3760	1.3	23.7613	32.2	0.0321	32.4	0.0055	3.8	0.12	35.6	1.3	32.1	10.2	-221.4	827.6	35.6	1.3	-16.1
MP8-1	482	3788	1.1	22.9705	16.1	0.0334	16.2	0.0056	2.0	0.12	35.8	0.7	33.4	5.3	-136.9	400.7	35.8	0.7	-26.1
MP8-14	456	4124	1.0	21.6378	23.7	0.0355	23.7	0.0056	0.7	0.03	35.8	0.2	35.4	8.3	8.9	578.0	35.8	0.2	402.5
MP8-32	278	2736	1.0	27.7176	69.8	0.0278	69.9	0.0056	3.9	0.06	36.0	1.4	27.9	19.2	-625.0	2163.6	36.0	1.4	-5.8
MP8-4	307	2296	1.5	20.4475	23.1	0.0378	23.2	0.0056	2.0	0.09	36.0	0.7	37.7	8.6	143.3	547.7	36.0	0.7	25.1
MP8-3	323	2184	1.1	18.7307	19.8	0.0414	19.9	0.0056	2.5	0.13	36.2	0.9	41.2	8.0	345.4	451.2	36.2	0.9	10.5
MP8-24	327	2704	1.3	29.8321	43.4	0.0261	43.5	0.0057	3.2	0.07	36.4	1.1	26.2	11.3	-830.3	1289.0	36.4	1.1	-4.4
MP8-29	255	2248	1.3	25.1649	30.9	0.0310	31.0	0.0057	2.8	0.09	36.4	1.0	31.0	9.5	-367.9	815.7	36.4	1.0	-9.9
MP8-2	338	1956	1.2	18.1268	16.1	0.0443	16.3	0.0058	1.9	0.12	37.4	0.7	44.0	7.0	419.0	362.6	37.4	0.7	8.9
MP8-7	272	1644	1.3	16.0845	15.1	0.0524	15.2	0.0061	1.5	0.10	39.3	0.6	51.9	7.7	680.0	324.6	39.3	0.6	5.8

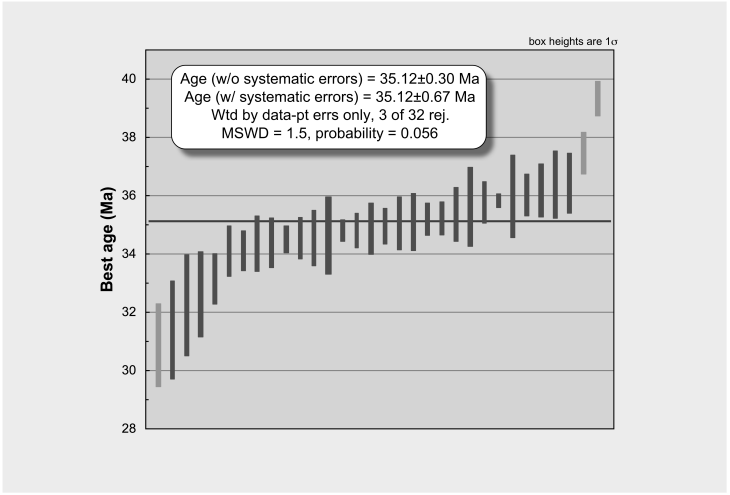

MP-09- Mt. Aetna Ring Dike						Isotope ratios						Apparent ages (Ma)								
Analysis	U	206Pb	U/Th	206Pb*	±	207Pb*	±	206Pb*	±	error	206Pb*	±	207Pb*	±	206Pb*	±	Best age	±	Conc
	(ppm)	204Pb		207Pb*	(%)	235U*	(%)	238U	(%)	corr.	238U*	(Ma)	235U	(Ma)	207Pb*	(Ma)	(Ma)	(Ma)	(%)
MP9-18	80	855	1.2	28.7154	79.5	0.0229	79.8	0.0048	6.9	0.09	30.7	2.1	23.0	18.1	-722.6	2661.4	30.7	2.1	-4.2
MP9-32	44	665	0.7	23.7534	107.4	0.0284	107.7	0.0049	8.1	0.07	31.5	2.5	28.5	30.2	-220.6	1285.2	31.5	2.5	-14.3
MP9-11	131	1100	1.1	27.2865	57.5	0.0249	57.8	0.0049	5.6	0.10	31.7	1.8	25.0	14.2	-582.3	1681.5	31.7	1.8	-5.4
MP9-19	271	1545	0.7	21.0201	16.3	0.0327	16.4	0.0050	2.3	0.14	32.0	0.7	32.6	5.3	78.1	388.2	32.0	0.7	41.0
MP9-30	191	910	0.6	24.6108	22.5	0.0289	22.5	0.0052	1.6	0.07	33.1	0.5	28.9	6.4	-310.6	581.8	33.1	0.5	-10.7
MP9-24	213	1685	0.8	29.1313	33.2	0.0245	33.2	0.0052	1.3	0.04	33.3	0.4	24.6	8.1	-762.9	954.6	33.3	0.4	-4.4
MP9-1	599	5715	1.1	21.9407	4.6	0.0326	4.7	0.0052	1.1	0.24	33.3	0.4	32.5	1.5	-24.7	111.0	33.3	0.4	-135.1
MP9-26	1339	3240	0.4	21.3200	3.3	0.0337	3.5	0.0052	1.1	0.32	33.5	0.4	33.6	1.2	44.4	79.6	33.5	0.4	75.4
MP9-28	238	1475	0.6	24.1572	18.2	0.0300	18.2	0.0052	1.2	0.06	33.7	0.4	30.0	5.4	-263.2	464.9	33.7	0.4	-12.8
MP9-5	844	9430	2.1	21.2158	4.9	0.0344	5.1	0.0053	1.2	0.23	34.0	0.4	34.3	1.7	56.1	117.5	34.0	0.4	60.7
MP9-13	1344	9150	2.4	21.9899	4.6	0.0332	4.8	0.0053	1.4	0.30	34.0	0.5	33.1	1.6	-30.1	110.6	34.0	0.5	-113.0
MP9-23	1490	16905	2.8	21.5101	2.3	0.0341	2.4	0.0053	0.9	0.36	34.2	0.3	34.0	0.8	23.1	54.1	34.2	0.3	147.7
MP9-22	830	8080	2.7	21.6894	5.7	0.0339	5.9	0.0053	1.4	0.23	34.3	0.5	33.8	2.0	3.1	138.3	34.3	0.5	1095.4
MP9-20	1361	6375	0.9	21.5924	2.4	0.0343	2.5	0.0054	0.5	0.20	34.6	0.2	34.3	0.8	13.9	57.8	34.6	0.2	248.4
MP9-27	1213	11285	3.3	21.5645	4.7	0.0344	5.1	0.0054	1.9	0.37	34.6	0.6	34.4	1.7	17.0	113.1	34.6	0.6	203.6
MP9-10	239	1920	0.8	24.6631	20.2	0.0301	20.2	0.0054	0.6	0.03	34.6	0.2	30.1	6.0	-316.0	522.7	34.6	0.2	-11.0
MP9-33	968	5385	0.8	21.8136	4.4	0.0342	4.5	0.0054	0.9	0.21	34.8	0.3	34.2	1.5	-10.6	106.0	34.8	0.3	-327.7
MP9-16	425	5490	3.5	23.7764	12.6	0.0314	12.7	0.0054	0.7	0.06	34.8	0.3	31.4	3.9	-223.0	319.1	34.8	0.3	-15.6
MP9-3	696	7720	2.3	22.4814	6.4	0.0333	6.5	0.0054	1.4	0.22	34.9	0.5	33.2	2.1	-84.0	156.5	34.9	0.5	-41.5
MP9-9	682	7750	1.3	21.6359	3.7	0.0346	3.9	0.0054	1.2	0.31	34.9	0.4	34.5	1.3	9.1	89.2	34.9	0.4	383.3
MP9-21	451	5840	1.9	20.9912	8.5	0.0361	8.5	0.0055	0.9	0.11	35.3	0.3	36.0	3.0	81.4	202.0	35.3	0.3	43.4
MP9-14	448	830	0.6	10.8951	6.7	0.0701	6.7	0.0055	0.8	0.12	35.6	0.3	68.8	4.5	1462.9	127.2	35.6	0.3	2.4
MP9-15	801	8355	1.8	22.1716	5.3	0.0345	5.4	0.0055	1.1	0.20	35.7	0.4	34.4	1.8	-50.1	129.8	35.7	0.4	-71.2
MP9-12	480	4715	1.3	22.3138	9.1	0.0347	9.2	0.0056	0.7	0.08	36.1	0.3	34.6	3.1	-65.7	223.5	36.1	0.3	-54.9
MP9-31	797	7925	1.7	22.0939	23.6	0.0350	23.7	0.0056	1.2	0.05	36.1	0.4	35.0	8.1	-41.5	580.8	36.1	0.4	-86.9
MP9-8	510	3810	1.1	21.7819	5.0	0.0360	5.0	0.0057	0.5	0.10	36.5	0.2	35.9	1.8	-7.1	119.7	36.5	0.2	-514.7
MP9-4	1110	12145	3.3	21.8132	3.8	0.0360	3.9	0.0057	0.7	0.19	36.7	0.3	36.0	1.4	-10.6	92.1	36.7	0.3	-346.9
MP9-25	572	6910	2.8	22.0956	6.0	0.0356	6.5	0.0057	2.5	0.39	36.7	0.9	35.5	2.3	-41.7	144.8	36.7	0.9	-87.9
MP9-2	580	3250	1.3	15.9871	15.8	0.0496	15.9	0.0057	1.5	0.09	36.9	0.6	49.1	7.6	693.0	339.4	36.9	0.6	5.3
MP9-6	465	137275	9.0	11.1360	1.2	3.0198	1.3	0.2439	0.6	0.46	1406.9	7.8	1412.6	10.2	1421.2	22.7	1421.2	22.7	99.0
MP9-7	586	230875	3.0	9.4817	1.3	4.2763	1.7	0.2941	1.1	0.64	1661.8	16.3	1688.8	14.3	1722.4	24.4	1722.4	24.4	96.5

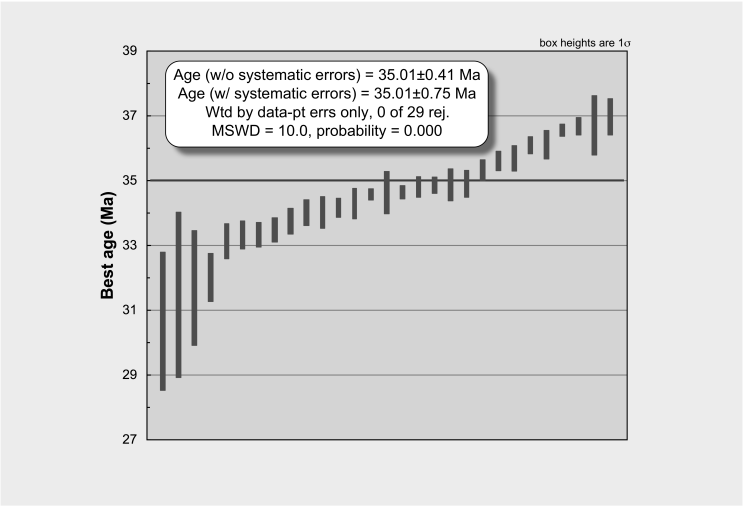

MP10 - Mt. Princeton Qtz. Monz.						Isotope ratios						Apparent ages (Ma)							
Analysis	U	206Pb	U/Th	206Pb*	±	207Pb*	±	206Pb*	±	error	206Pb*	±	207Pb*	±	206Pb*	±	Best age	±	Conc
	(ppm)	204Pb		207Pb*	(%)	235U*	(%)	238U	(%)	corr.	238U*	(Ma)	235U	(Ma)	207Pb*	(Ma)	(Ma)	(Ma)	(%)
MP10-20	179	2104	1.5	21.3819	15.4	0.0329	15.5	0.0051	1.9	0.12	32.8	0.6	32.9	5.0	37.4	370.3	32.8	0.6	87.8
MP10-5	385	2884	1.6	21.2201	13.2	0.0336	13.6	0.0052	3.3	0.24	33.2	1.1	33.5	4.5	55.6	315.6	33.2	1.1	59.8
MP10-19	392	3292	2.0	21.4475	9.8	0.0337	9.9	0.0052	1.1	0.11	33.7	0.4	33.6	3.3	30.1	235.5	33.7	0.4	112.1
MP10-3	345	2656	1.2	21.2873	10.5	0.0339	10.7	0.0052	1.9	0.17	33.7	0.6	33.9	3.6	48.0	251.6	33.7	0.6	70.2
MP10-8	359	1244	1.9	13.5869	20.9	0.0538	21.0	0.0053	1.2	0.05	34.1	0.4	53.2	10.9	1030.5	428.0	34.1	0.4	3.3
MP10-1	328	2572	1.8	22.9231	19.3	0.0321	19.3	0.0053	0.6	0.03	34.4	0.2	32.1	6.1	-131.8	480.5	34.4	0.2	-26.1
MP10-9	636	6580	1.9	22.5699	10.1	0.0328	10.1	0.0054	0.5	0.05	34.6	0.2	32.8	3.3	-93.6	248.6	34.6	0.2	-36.9
MP10-18	326	3324	1.8	21.5584	11.1	0.0346	11.2	0.0054	1.1	0.10	34.7	0.4	34.5	3.8	17.7	267.9	34.7	0.4	196.4
MP10-6	401	3844	2.0	19.8377	13.2	0.0377	13.2	0.0054	0.8	0.06	34.9	0.3	37.6	4.9	213.9	305.9	34.9	0.3	16.3
MP10-4	366	2628	1.7	19.1886	8.7	0.0394	8.8	0.0055	1.3	0.15	35.3	0.5	39.3	3.4	290.4	200.0	35.3	0.5	12.1
MP10-17	490	3912	1.5	21.8245	11.3	0.0348	11.3	0.0055	1.0	0.09	35.4	0.4	34.8	3.9	-11.8	273.3	35.4	0.4	-299.9
MP10-2	692	2268	1.0	18.8047	8.9	0.0407	8.9	0.0055	0.7	0.08	35.7	0.2	40.5	3.5	336.4	201.1	35.7	0.2	10.6
MP10-16	431	3524	1.7	21.2679	8.5	0.0365	8.5	0.0056	0.9	0.11	36.2	0.3	36.4	3.0	50.2	202.5	36.2	0.3	72.0
MP10-11	436	4128	1.9	22.8032	13.5	0.0341	13.5	0.0056	0.5	0.04	36.3	0.2	34.0	4.5	-118.9	334.2	36.3	0.2	-30.5
MP10-14	371	2852	1.8	22.5091	17.3	0.0346	17.4	0.0056	1.2	0.07	36.3	0.4	34.5	5.9	-87.0	426.9	36.3	0.4	-41.7
MP10-13	481	2012	1.4	19.8885	8.1	0.0391	8.2	0.0056	1.5	0.18	36.3	0.5	39.0	3.1	208.0	187.2	36.3	0.5	17.5
MP10-12	390	4368	1.8	21.4856	7.6	0.0369	7.7	0.0058	0.8	0.11	37.0	0.3	36.8	2.8	25.9	183.2	37.0	0.3	143.2
MP10-15	250	1780	2.3	19.5986	10.1	0.0409	10.5	0.0058	2.6	0.25	37.4	1.0	40.7	4.2	241.9	233.7	37.4	1.0	15.5

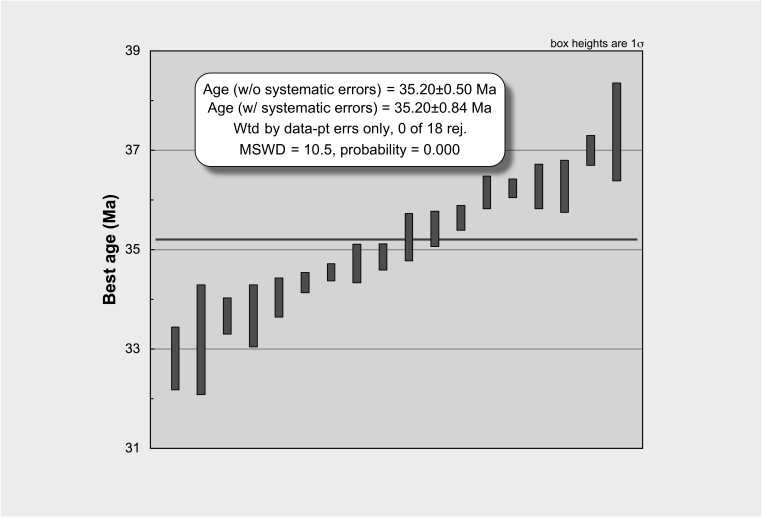

MP15 - Wall Mountain Tuff						Isotope ratios						Apparent ages (Ma)								
Analysis	U	206Pb	U/Th	206Pb*	±	207Pb*	±	206Pb*	±	error	206Pb*	±	207Pb*	±	206Pb*	±	Best age	±	Conc
	(ppm)	204Pb		207Pb*	(%)	235U*	(%)	238U	(%)	corr.	238U*	(Ma)	235U	(Ma)	207Pb*	(Ma)	(Ma)	(Ma)	(%)
MP15-19	78	2601	2.1	28.3884	87.1	0.0255	87.4	0.0053	7.0	0.08	33.8	2.4	25.6	22.1	-690.8	3115.4	33.8	2.4	-4.9
MP15-24	87	2214	1.2	28.5146	48.8	0.0254	48.9	0.0053	3.5	0.07	33.8	1.2	25.5	12.3	-703.1	1428.1	33.8	1.2	-4.8
MP15-16	143	2952	0.9	28.1024	40.6	0.0265	41.2	0.0054	6.7	0.16	34.7	2.3	26.6	10.8	-662.8	1158.8	34.7	2.3	-5.2
MP15-35	122	3051	1.0	28.6366	40.9	0.0261	41.0	0.0054	2.9	0.07	34.9	1.0	26.2	10.6	-715.0	1179.3	34.9	1.0	-4.9
MP15-6	81	1449	0.9	19.6432	76.5	0.0381	76.7	0.0054	6.3	0.08	34.9	2.2	38.0	28.6	236.7	2117.2	34.9	2.2	14.7
MP15-4	120	2070	1.0	17.2724	33.3	0.0437	33.5	0.0055	3.7	0.11	35.2	1.3	43.4	14.2	525.8	749.6	35.2	1.3	6.7
MP15-34	106	3375	1.2	24.0279	25.2	0.0314	26.2	0.0055	7.1	0.27	35.2	2.5	31.4	8.1	-249.6	646.1	35.2	2.5	-14.1
MP15-26	68	1908	1.0	33.5501	83.8	0.0226	84.0	0.0055	5.2	0.06	35.3	1.8	22.7	18.8	-1178.8	1346.4	35.3	1.8	-3.0
MP15-7	107	2376	0.8	14.4632	212.9	0.0525	212.9	0.0055	2.2	0.01	35.4	0.8	51.9	108.2	902.9	1110.3	35.4	0.8	3.9
MP15-32	119	2700	1.2	20.8034	40.5	0.0366	40.6	0.0055	3.0	0.07	35.5	1.1	36.5	14.5	102.6	994.5	35.5	1.1	34.5
MP15-5	137	2889	0.8	15.6543	161.8	0.0486	161.9	0.0055	3.8	0.02	35.5	1.3	48.2	76.4	737.6	922.9	35.5	1.3	4.8
MP15-15	149	3465	1.0	27.3836	36.4	0.0278	36.6	0.0055	4.1	0.11	35.5	1.5	27.9	10.1	-592.0	1014.2	35.5	1.5	-6.0
MP15-33	233	5256	1.1	19.9173	13.4	0.0388	13.5	0.0056	1.3	0.10	36.1	0.5	38.7	5.1	204.6	312.4	36.1	0.5	17.6
MP15-10	273	3942	1.0	20.6433	27.8	0.0377	27.8	0.0056	1.4	0.05	36.3	0.5	37.6	10.3	120.9	666.5	36.3	0.5	30.0
MP15-31	194	3681	1.0	18.8762	16.7	0.0413	17.0	0.0056	2.8	0.16	36.3	1.0	41.1	6.8	327.8	382.1	36.3	1.0	11.1
MP15-23	86	2421	1.4	16.7289	110.5	0.0466	110.5	0.0056	2.8	0.03	36.3	1.0	46.2	50.0	595.5	665.4	36.3	1.0	6.1
MP15-27	250	5517	1.1	19.6573	12.5	0.0397	12.6	0.0057	1.5	0.12	36.3	0.6	39.5	4.9	235.0	288.5	36.3	0.6	15.5
MP15-17	188	4986	1.2	21.0823	22.3	0.0370	22.3	0.0057	0.9	0.04	36.4	0.3	36.9	8.1	71.1	535.5	36.4	0.3	51.2
MP15-2	232	4446	1.1	18.8322	12.3	0.0415	12.4	0.0057	2.0	0.16	36.5	0.7	41.3	5.0	333.1	279.4	36.5	0.7	10.9
MP15-39	163	3546	1.0	18.8165	17.4	0.0418	17.5	0.0057	2.2	0.12	36.7	0.8	41.6	7.1	335.0	396.3	36.7	0.8	11.0
MP15-8	175	3654	1.1	18.0357	12.4	0.0438	12.4	0.0057	1.5	0.12	36.8	0.5	43.5	5.3	430.2	276.4	36.8	0.5	8.6
MP15-18	220	4140	1.3	19.9719	19.9	0.0396	19.9	0.0057	0.9	0.05	36.9	0.3	39.4	7.7	198.2	466.8	36.9	0.3	18.6
MP15-9	221	3969	1.1	21.4808	30.9	0.0369	30.9	0.0057	1.4	0.05	36.9	0.5	36.8	11.2	26.4	756.9	36.9	0.5	140.0
MP15-1	105	2601	1.1	23.0705	104.1	0.0344	104.1	0.0058	3.9	0.04	37.0	1.4	34.4	35.2	-147.7	1189.8	37.0	1.4	-25.1
MP15-20	104	2664	1.5	28.6799	29.9	0.0277	29.9	0.0058	1.1	0.04	37.0	0.4	27.7	8.2	-719.2	848.0	37.0	0.4	-5.1
MP15-30	140	3078	1.2	18.0437	18.3	0.0442	18.4	0.0058	1.9	0.10	37.1	0.7	43.9	7.9	429.2	410.3	37.1	0.7	8.7
MP15-36	208	4041	0.9	24.0140	40.6	0.0332	40.6	0.0058	1.4	0.04	37.2	0.5	33.2	13.3	-248.1	1064.4	37.2	0.5	-15.0
MP15-12	115	2898	0.9	15.3454	45.2	0.0524	45.3	0.0058	1.4	0.03	37.5	0.5	51.9	22.9	779.7	1002.2	37.5	0.5	4.8
MP15-37	192	3825	0.9	20.7242	27.8	0.0389	27.8	0.0058	1.1	0.04	37.6	0.4	38.7	10.6	111.7	666.7	37.6	0.4	33.6
MP15-40	400	6984	0.7	20.3391	11.2	0.0397	11.4	0.0059	2.2	0.19	37.7	0.8	39.6	4.4	155.8	263.4	37.7	0.8	24.2
MP15-25	177	4770	1.2	20.5673	20.6	0.0394	20.7	0.0059	2.1	0.10	37.8	0.8	39.2	8.0	129.6	489.8	37.8	0.8	29.1
MP15-22	196	4194	1.3	20.0166	20.4	0.0405	20.4	0.0059	0.5	0.02	37.8	0.2	40.3	8.1	193.1	478.9	37.8	0.2	19.6
MP15-28	79	2583	1.2	21.0551	45.7	0.0392	45.8	0.0060	2.8	0.06	38.4	1.1	39.0	17.5	74.2	1140.5	38.4	1.1	51.8
MP15-13	157	140508	1.0	11.1199	1.1	3.0073	1.2	0.2425	0.5	0.43	1399.9	6.7	1409.5	9.4	1424.0	21.2	1424.0	21.2	98.3
MP15-21	125	137853	2.2	11.1098	1.7	3.0610	1.8	0.2466	0.6	0.34	1421.1	7.9	1423.0	14.0	1425.7	32.9	1425.7	32.9	99.7
MP15-14	116	123345	2.1	11.0983	1.2	3.0815	1.4	0.2480	0.7	0.50	1428.4	8.8	1428.1	10.7	1427.7	23.1	1427.7	23.1	100.0
MP15-3	101	79560	1.9	11.0588	0.9	3.1200	1.2	0.2502	0.8	0.63	1439.7	9.7	1437.6	9.1	1434.5	17.6	1434.5	17.6	100.4
MP15-29	51	38664	1.4	10.9290	1.8	3.1617	1.9	0.2506	0.8	0.39	1441.6	9.7	1447.8	15.0	1457.0	34.0	1457.0	34.0	98.9
MP15-38	158	140607	2.3	10.9210	1.1	3.1645	1.7	0.2506	1.3	0.77	1441.8	17.3	1448.5	13.4	1458.4	20.9	1458.4	20.9	98.9
MP15-11	83	85086	1.6	10.8684	1.1	3.2026	1.2	0.2524	0.5	0.44	1451.1	7.0	1457.8	9.5	1467.6	20.9	1467.6	20.9	98.9

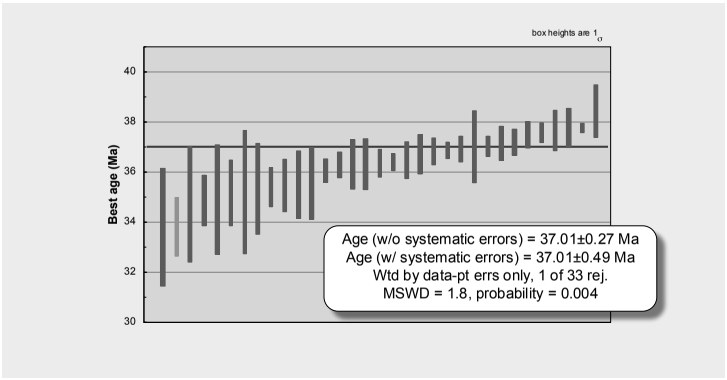

MP21 - Mt. Aetna Qtz. Monz.						Isotope ratios						Apparent ages (Ma)								
Analysis	U	206Pb	U/Th	206Pb*	±	207Pb*	±	206Pb*	±	error	206Pb*	±	207Pb*	±	206Pb*	±	Best age	±	Conc
	(ppm)	204Pb		207Pb*	(%)	235U*	(%)	238U	(%)	corr.	238U*	(Ma)	235U	(Ma)	207Pb*	(Ma)	(Ma)	(Ma)	(%)
MP21-11	169	1068	1.2	30.0512	37.5	0.0228	37.6	0.0050	2.6	0.07	31.9	0.8	22.9	8.5	-851.3	1107.7	31.9	0.8	-3.8
MP21-2	353	2513	1.6	17.6878	29.1	0.0391	29.5	0.0050	4.8	0.16	32.3	1.6	39.0	11.3	473.5	655.5	32.3	1.6	6.8
MP21-12	161	1040	0.8	24.7036	39.1	0.0286	39.5	0.0051	5.8	0.15	32.9	1.9	28.6	11.2	-320.2	1037.6	32.9	1.9	-10.3
MP21-15	102	644	1.5	17.7900	17.2	0.0409	17.4	0.0053	3.2	0.18	33.9	1.1	40.7	7.0	460.7	383.0	33.9	1.1	7.4
MP21-1	106	945	0.9	21.2909	95.0	0.0344	95.0	0.0053	1.4	0.02	34.2	0.5	34.4	32.1	47.6	946.1	34.2	0.5	71.8
MP21-3	178	1078	1.0	20.8329	19.6	0.0352	19.7	0.0053	0.9	0.05	34.2	0.3	35.1	6.8	99.3	468.3	34.2	0.3	34.4
MP21-19	442	1967	1.1	16.2360	33.3	0.0453	33.6	0.0053	4.3	0.13	34.3	1.5	45.0	14.8	659.9	732.6	34.3	1.5	5.2
MP21-20	377	2772	1.5	22.4382	13.0	0.0330	13.4	0.0054	3.5	0.26	34.6	1.2	33.0	4.4	-79.2	318.3	34.6	1.2	-43.6
MP21-14	95	662	1.1	30.1087	40.9	0.0248	41.0	0.0054	2.9	0.07	34.8	1.0	24.9	10.1	-856.8	1217.7	34.8	1.0	-4.1
MP21-13	441	2464	1.5	20.6586	7.0	0.0362	7.1	0.0054	1.2	0.16	34.9	0.4	36.1	2.5	119.2	164.7	34.9	0.4	29.3
MP21-4	407	2258	0.7	21.7756	12.7	0.0347	12.8	0.0055	0.9	0.07	35.2	0.3	34.6	4.3	-6.4	308.6	35.2	0.3	-550.5
MP21-31	414	2811	0.9	22.2204	13.1	0.0343	13.2	0.0055	1.4	0.11	35.5	0.5	34.2	4.4	-55.4	320.2	35.5	0.5	-64.1
MP21-9	967	6017	1.7	20.7971	2.8	0.0367	2.9	0.0055	1.0	0.33	35.6	0.3	36.6	1.1	103.4	65.8	35.6	0.3	34.4
MP21-17	1702	4260	0.5	20.5647	2.9	0.0373	3.0	0.0056	0.9	0.29	35.7	0.3	37.2	1.1	129.9	67.7	35.7	0.3	27.5
MP21-16	675	4498	2.2	20.8516	4.6	0.0368	4.9	0.0056	1.7	0.35	35.7	0.6	36.7	1.8	97.2	108.9	35.7	0.6	36.8
MP21-32	343	2489	1.2	21.7735	12.8	0.0354	12.9	0.0056	1.1	0.08	36.0	0.4	35.4	4.5	-6.2	310.3	36.0	0.4	-582.5
MP21-23	346	1908	1.3	21.6428	15.4	0.0357	15.4	0.0056	1.3	0.08	36.0	0.5	35.6	5.4	8.3	372.0	36.0	0.5	434.1
MP21-29	407	2412	0.9	20.3301	5.1	0.0380	5.1	0.0056	0.5	0.10	36.0	0.2	37.9	1.9	156.8	119.0	36.0	0.2	23.0
MP21-10	310	1782	1.0	20.5242	10.4	0.0377	10.5	0.0056	1.0	0.09	36.1	0.4	37.6	3.9	134.5	245.2	36.1	0.4	26.8
MP21-7	679	2468	0.4	20.1722	5.4	0.0385	5.6	0.0056	1.6	0.28	36.2	0.6	38.3	2.1	175.0	126.4	36.2	0.6	20.7
MP21-6	381	2037	1.2	20.7858	10.6	0.0374	10.9	0.0056	2.6	0.24	36.2	1.0	37.3	4.0	104.7	251.2	36.2	1.0	34.6
MP21-28	148	665	0.6	24.0109	21.1	0.0325	21.2	0.0057	1.7	0.08	36.4	0.6	32.5	6.8	-247.8	538.9	36.4	0.6	-14.7
MP21-26	132	837	1.2	21.2299	29.9	0.0368	30.0	0.0057	2.7	0.09	36.5	1.0	36.7	10.8	54.5	727.3	36.5	1.0	66.9
MP21-34	393	1768	1.1	20.3771	9.7	0.0386	10.2	0.0057	3.0	0.29	36.7	1.1	38.5	3.8	151.4	227.9	36.7	1.1	24.2
MP21-22	395	2349	1.3	21.9714	13.7	0.0359	13.7	0.0057	1.0	0.07	36.7	0.4	35.8	4.8	-28.1	332.4	36.7	0.4	-130.9
MP21-18	314	2247	1.4	21.2272	10.2	0.0372	10.3	0.0057	0.6	0.06	36.8	0.2	37.0	3.7	54.8	245.0	36.8	0.2	67.1
MP21-8	303	2125	1.1	21.1630	12.1	0.0374	12.2	0.0057	0.9	0.07	36.9	0.3	37.3	4.5	62.0	290.3	36.9	0.3	59.6
MP21-5	2062	8299	0.7	21.2555	3.2	0.0374	3.3	0.0058	0.8	0.23	37.1	0.3	37.3	1.2	51.6	76.7	37.1	0.3	71.9
MP21-21	469	2982	1.0	20.5267	5.0	0.0388	5.1	0.0058	1.1	0.22	37.1	0.4	38.6	1.9	134.2	116.7	37.1	0.4	27.6
MP21-24	375	1516	0.9	21.9609	33.1	0.0363	33.2	0.0058	3.1	0.09	37.2	1.2	36.3	11.8	-26.9	820.5	37.2	1.2	-138.3
MP21-33	836	5058	1.2	21.2472	5.2	0.0376	5.3	0.0058	1.2	0.22	37.2	0.4	37.5	1.9	52.5	123.1	37.2	0.4	70.9
MP21-25	662	4998	1.7	20.9062	3.6	0.0384	3.6	0.0058	0.5	0.15	37.4	0.2	38.2	1.4	91.0	85.3	37.4	0.2	41.1
MP21-35	477	3350	1.2	21.8744	12.8	0.0368	12.8	0.0058	0.6	0.04	37.5	0.2	36.7	4.6	-17.3	309.8	37.5	0.2	-216.3
MP21-27	420	3850	1.2	21.2607	6.8	0.0378	6.9	0.0058	0.7	0.10	37.5	0.3	37.7	2.5	51.0	163.6	37.5	0.3	73.5

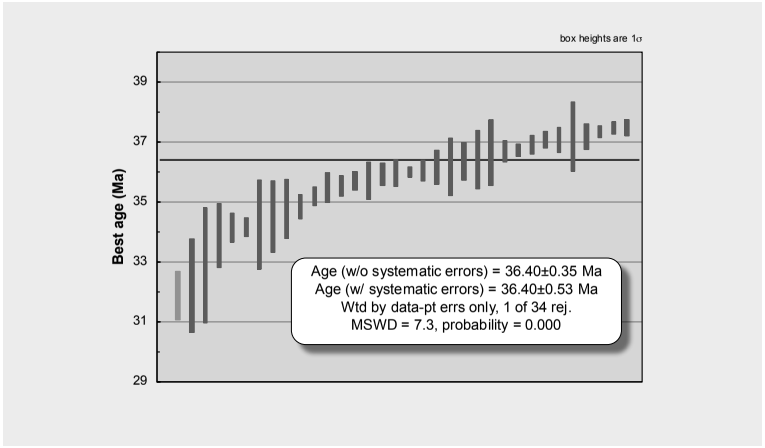

MP25 - Mt. Princeton Qtz. Monz.						Isotope ratios						Apparent ages (Ma)							
Analysis	U	206Pb	U/Th	206Pb*	±	207Pb*	±	206Pb*	±	error	206Pb*	±	207Pb*	±	206Pb*	±	Best age	±	Conc
	(ppm)	204Pb		207Pb*	(%)	235U*	(%)	238U	(%)	corr.	238U*	(Ma)	235U	(Ma)	207Pb*	(Ma)	(Ma)	(Ma)	(%)
MP25-3	339	2338	1.4	22.5393	16.3	0.0319	16.3	0.0052	1.2	0.07	33.6	0.4	31.9	5.1	-90.3	401.1	33.6	0.4	-37.2
MP25-4	518	3091	1.6	21.7024	11.0	0.0336	11.1	0.0053	1.3	0.12	34.0	0.4	33.6	3.7	1.7	266.3	34.0	0.4	2004.8
MP25-22	304	2482	1.2	31.2940	43.7	0.0234	43.7	0.0053	1.7	0.04	34.2	0.6	23.5	10.2	-969.0	1338.0	34.2	0.6	-3.5
MP25-7	312	1831	1.4	21.2000	12.5	0.0346	12.6	0.0053	1.3	0.10	34.3	0.4	34.6	4.3	57.8	298.7	34.3	0.4	59.2
MP25-14	444	2776	1.0	22.8212	16.8	0.0325	16.8	0.0054	0.9	0.05	34.6	0.3	32.5	5.4	-120.8	415.9	34.6	0.3	-28.6
MP25-17	245	1635	0.9	21.0630	15.3	0.0356	15.4	0.0054	1.6	0.11	35.0	0.6	35.5	5.4	73.2	365.3	35.0	0.6	47.8
MP25-16	198	1432	1.0	21.9758	21.1	0.0342	21.3	0.0055	2.9	0.14	35.1	1.0	34.2	7.2	-28.5	516.5	35.1	1.0	-122.9
MP25-18	409	1820	1.3	21.8907	21.1	0.0344	21.2	0.0055	1.0	0.05	35.1	0.4	34.4	7.2	-19.1	516.4	35.1	0.4	-183.6
MP25-21	276	1012	0.5	17.3053	24.4	0.0436	24.4	0.0055	1.1	0.05	35.2	0.4	43.3	10.4	521.6	542.5	35.2	0.4	6.7
MP25-20	508	3024	1.2	21.9213	11.3	0.0345	11.3	0.0055	1.0	0.09	35.2	0.4	34.4	3.8	-22.5	273.2	35.2	0.4	-156.4
MP25-10	460	3231	1.4	21.1459	7.4	0.0357	7.6	0.0055	1.6	0.20	35.2	0.5	35.7	2.7	63.9	176.6	35.2	0.5	55.1
MP25-6	285	2016	1.5	20.3627	8.5	0.0371	8.8	0.0055	2.2	0.24	35.2	0.8	37.0	3.2	153.0	199.8	35.2	0.8	23.0
MP25-31	486	2968	1.6	21.4029	9.9	0.0354	9.9	0.0055	1.3	0.13	35.3	0.5	35.3	3.4	35.1	236.5	35.3	0.5	100.7
MP25-13	1342	6017	0.8	21.2695	3.2	0.0356	3.3	0.0055	0.8	0.23	35.3	0.3	35.5	1.2	50.0	77.2	35.3	0.3	70.6
MP25-27	218	1019	0.9	18.2466	50.3	0.0415	50.5	0.0055	4.6	0.09	35.3	1.6	41.3	20.4	404.2	1199.7	35.3	1.6	8.7
MP25-2	439	2716	1.2	21.8323	11.7	0.0347	12.0	0.0055	2.4	0.20	35.4	0.8	34.7	4.1	-12.7	284.2	35.4	0.8	-278.9
MP25-19	846	3007	1.2	20.4487	6.6	0.0371	6.7	0.0055	0.7	0.10	35.4	0.2	37.0	2.4	143.2	155.8	35.4	0.2	24.7
MP25-1	498	1610	1.5	20.7998	11.3	0.0365	11.3	0.0055	0.7	0.07	35.4	0.3	36.4	4.1	103.1	268.4	35.4	0.3	34.4
MP25-9	540	2454	1.4	20.8259	12.4	0.0365	12.5	0.0055	1.6	0.13	35.5	0.6	36.5	4.5	100.1	294.3	35.5	0.6	35.4
MP25-12	436	3476	1.2	23.5416	15.9	0.0324	16.0	0.0055	0.9	0.05	35.5	0.3	32.3	5.1	-198.1	401.2	35.5	0.3	-17.9
MP25-34	451	2573	1.0	21.4519	10.0	0.0355	10.2	0.0055	2.0	0.19	35.5	0.7	35.4	3.5	29.6	239.6	35.5	0.7	120.0
MP25-24	373	2674	1.4	24.4188	33.0	0.0313	33.1	0.0055	1.5	0.04	35.6	0.5	31.3	10.2	-290.6	862.8	35.6	0.5	-12.2
MP25-29	573	1964	1.0	20.2584	7.3	0.0378	7.4	0.0056	1.0	0.13	35.7	0.3	37.6	2.7	165.0	171.8	35.7	0.3	21.6
MP25-23	573	3409	1.2	21.2542	7.5	0.0363	7.5	0.0056	0.5	0.07	36.0	0.2	36.2	2.7	51.7	179.8	36.0	0.2	69.5
MP25-15	317	1862	1.3	21.6604	15.2	0.0356	15.2	0.0056	0.8	0.05	36.0	0.3	35.6	5.3	6.4	366.7	36.0	0.3	566.6
MP25-35	492	2646	0.9	21.1143	9.2	0.0366	9.2	0.0056	0.8	0.08	36.0	0.3	36.5	3.3	67.5	219.1	36.0	0.3	53.4
MP25-33	216	1582	0.8	22.0166	19.3	0.0351	19.4	0.0056	1.3	0.07	36.1	0.5	35.1	6.7	-33.0	472.2	36.1	0.5	-109.2
MP25-28	340	2132	0.9	22.1142	16.5	0.0350	16.6	0.0056	1.4	0.09	36.1	0.5	34.9	5.7	-43.8	404.1	36.1	0.5	-82.4
MP25-30	684	2986	0.7	21.0422	7.5	0.0368	7.7	0.0056	1.8	0.23	36.1	0.6	36.7	2.8	75.6	177.6	36.1	0.6	47.8
MP25-25	209	1425	1.0	20.7277	13.3	0.0375	13.6	0.0056	2.8	0.21	36.2	1.0	37.4	5.0	111.3	314.4	36.2	1.0	32.6
MP25-26	418	2709	1.2	22.1242	12.7	0.0353	12.7	0.0057	1.0	0.08	36.4	0.4	35.2	4.4	-44.9	308.6	36.4	0.4	-81.1
MP25-5	386	1316	0.9	16.3502	28.0	0.0479	28.0	0.0057	0.7	0.03	36.5	0.3	47.5	13.0	644.9	613.4	36.5	0.3	5.7
MP25-32	543	3147	0.9	20.7551	6.5	0.0401	6.5	0.0060	0.5	0.08	38.8	0.2	39.9	2.6	108.2	154.2	38.8	0.2	35.9
MP25-11	221	37727	0.8	11.0235	0.9	3.0509	1.0	0.2439	0.6	0.54	1407.1	7.1	1420.5	8.0	1440.6	16.8	1440.6	16.8	97.7

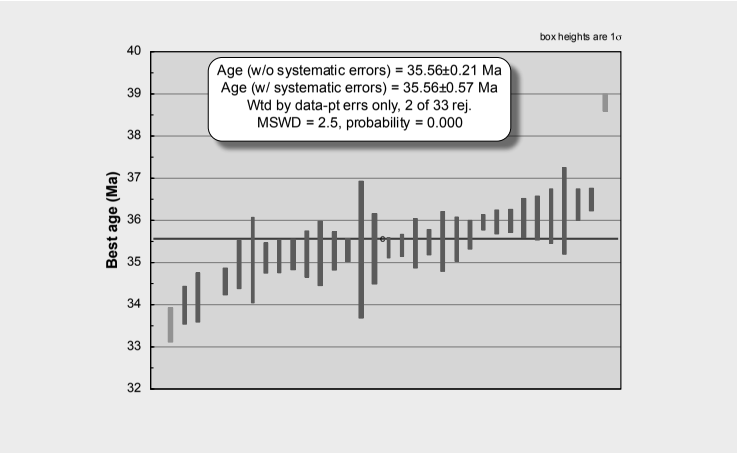

MP30 - Badger Creek Tuff						Isotope ratios						Apparent ages (Ma)								
Analysis	U (ppm)	206Pb 204Pb	U/Th	206Pb* 207Pb*	± (%)	207Pb* 235U*	± (%)	206Pb* 238U	± (%)	error corr.	206Pb* 238U*	± (Ma)	207Pb* 235U	± (Ma)	206Pb* 207Pb*	± (Ma)	Best age (Ma)	± (Ma)	Conc (%)
MP30-15	119	858	1.1	36.7139	43.9	0.0178	43.9	0.0047	1.5	0.03	30.4	0.4	17.9	7.8	-1466.2	1505.3	30.4	0.4	-2.1
MP30-29	276	1194	0.8	22.3845	19.0	0.0305	19.0	0.0049	1.2	0.06	31.8	0.4	30.5	5.7	-73.4	467.4	31.8	0.4	-43.3
MP30-10	148	741	0.9	21.3319	39.0	0.0321	40.2	0.0050	9.6	0.24	31.9	3.0	32.0	12.7	43.0	965.7	31.9	3.0	74.1
MP30-7	385	1146	0.7	20.5725	10.5	0.0345	10.6	0.0051	1.8	0.17	33.1	0.6	34.5	3.6	129.0	246.7	33.1	0.6	25.7
MP30-6	359	744	0.4	19.0147	11.2	0.0374	11.3	0.0052	0.8	0.07	33.1	0.3	37.2	4.1	311.2	256.5	33.1	0.3	10.6
MP30-35	429	1770	0.8	20.9947	7.6	0.0340	7.7	0.0052	1.2	0.16	33.2	0.4	33.9	2.6	81.0	181.8	33.2	0.4	41.1
MP30-4	619	1461	0.6	20.6878	6.6	0.0347	6.6	0.0052	0.6	0.09	33.5	0.2	34.7	2.3	115.9	156.0	33.5	0.2	28.9
MP30-2	1447	9900	3.6	22.0064	4.5	0.0331	4.5	0.0053	0.8	0.17	34.0	0.3	33.1	1.5	-31.9	108.1	34.0	0.3	-106.4
MP30-32	137	969	1.2	35.7366	43.2	0.0206	43.2	0.0053	1.2	0.03	34.3	0.4	20.7	8.8	-1378.2	1448.5	34.3	0.4	-2.5
MP30-13	401	2052	1.7	21.9441	11.4	0.0335	11.6	0.0053	1.9	0.16	34.3	0.7	33.5	3.8	-25.0	277.0	34.3	0.7	-137.0
MP30-1	666	5106	1.9	22.4771	8.2	0.0328	8.3	0.0053	1.0	0.13	34.4	0.4	32.8	2.7	-83.5	201.8	34.4	0.4	-41.2
MP30-22	416	2433	1.7	21.4233	8.5	0.0345	8.6	0.0054	1.5	0.18	34.4	0.5	34.4	2.9	32.8	203.2	34.4	0.5	105.0
MP30-24	799	2181	3.1	12.2317	47.8	0.0604	47.9	0.0054	4.1	0.09	34.5	1.4	59.6	27.7	1239.7	996.3	34.5	1.4	2.8
MP30-18	613	1407	0.4	20.5893	9.2	0.0360	9.2	0.0054	0.6	0.07	34.5	0.2	35.9	3.3	127.1	217.0	34.5	0.2	27.2
MP30-17	491	1677	0.5	21.8590	13.4	0.0339	13.5	0.0054	1.5	0.11	34.6	0.5	33.9	4.5	-15.6	326.3	34.6	0.5	-221.2
MP30-11	593	3603	2.4	22.3707	8.7	0.0332	8.8	0.0054	1.5	0.16	34.7	0.5	33.2	2.9	-71.9	212.4	34.7	0.5	-48.2
MP30-33	358	1938	0.9	22.4516	14.3	0.0331	14.4	0.0054	1.7	0.12	34.7	0.6	33.1	4.7	-80.7	350.8	34.7	0.6	-43.0
MP30-23	728	3744	0.8	21.1750	4.7	0.0353	4.8	0.0054	1.3	0.27	34.8	0.5	35.2	1.7	60.7	111.2	34.8	0.5	57.4
MP30-30	2507	4443	0.5	20.1784	4.9	0.0372	4.9	0.0054	0.5	0.10	35.0	0.2	37.0	1.8	174.3	113.8	35.0	0.2	20.1
MP30-19	395	846	0.6	16.9841	16.2	0.0442	16.2	0.0054	0.7	0.05	35.0	0.3	43.9	7.0	562.6	354.9	35.0	0.3	6.2
MP30-34	268	948	0.6	20.5990	14.9	0.0365	14.9	0.0054	0.8	0.05	35.0	0.3	36.4	5.3	126.0	351.6	35.0	0.3	27.8
MP30-12	1082	6021	2.8	22.5223	8.3	0.0336	8.3	0.0055	0.7	0.09	35.3	0.3	33.6	2.7	-88.4	202.6	35.3	0.3	-39.9
MP30-21	507	3519	1.4	23.1710	12.9	0.0329	13.0	0.0055	0.9	0.07	35.5	0.3	32.8	4.2	-158.5	322.5	35.5	0.3	-22.4
MP30-25	494	2094	0.7	21.2019	8.7	0.0359	8.9	0.0055	1.5	0.17	35.5	0.5	35.8	3.1	57.6	208.7	35.5	0.5	61.6
MP30-3	448	1866	0.8	20.6850	6.5	0.0369	6.7	0.0055	1.6	0.24	35.6	0.6	36.8	2.4	116.2	152.3	35.6	0.6	30.6
MP30-9	347	2040	0.9	22.2349	12.6	0.0344	12.6	0.0055	0.7	0.06	35.6	0.3	34.3	4.3	-57.0	308.3	35.6	0.3	-62.5
MP30-27	933	4734	1.5	21.7169	5.5	0.0352	5.5	0.0055	0.6	0.12	35.7	0.2	35.2	1.9	0.1	132.8	35.7	0.2	35677.5
MP30-26	213	951	0.8	31.1349	34.2	0.0247	34.3	0.0056	2.2	0.06	35.8	0.8	24.8	8.4	-954.1	1027.9	35.8	0.8	-3.8
MP30-20	370	1788	0.8	21.7009	12.5	0.0359	12.6	0.0056	1.5	0.12	36.3	0.6	35.8	4.4	1.8	303.3	36.3	0.6	1969.6
MP30-28	657	1884	1.6	19.9984	11.1	0.0391	11.2	0.0057	1.5	0.13	36.4	0.5	38.9	4.3	195.2	258.6	36.4	0.5	18.7
MP30-14	136	46323	3.8	11.1277	1.4	2.8941	2.3	0.2336	1.8	0.78	1353.2	22.0	1380.4	17.3	1422.7	27.1	1422.7	27.1	95.1

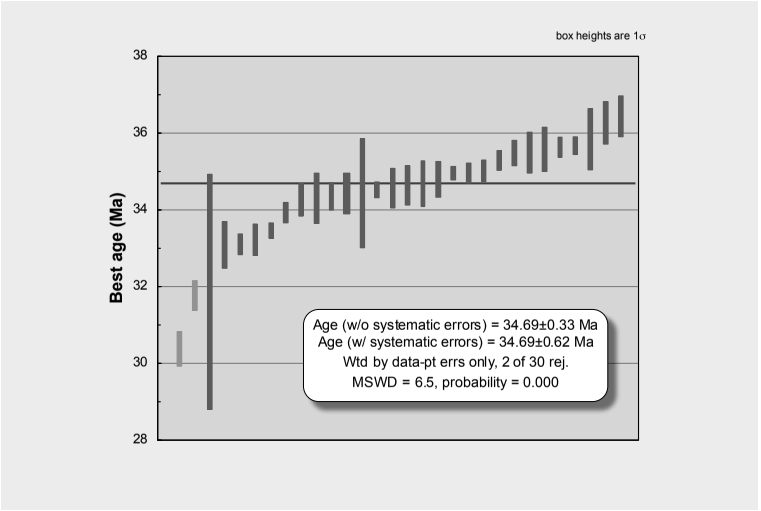

MP33 - Mt. Princeton Border Unit						Isotope ratios						Apparent ages (Ma)								
Analysis	U (ppm)	206Pb 204Pb	U/Th	206Pb* 207Pb*	± (%)	207Pb* 235U*	± (%)	206Pb* 238U	± (%)	error corr.	206Pb* 238U*	± (Ma)	207Pb* 235U	± (Ma)	206Pb* 207Pb*	± (Ma)	Best age (Ma)	± (Ma)	Conc (%)
MP33-32	113	1536	0.9	26.0863	31.4	0.0276	31.6	0.0052	3.2	0.10	33.6	1.1	27.7	8.6	-462.0	846.7	33.6	1.1	-7.3
MP33-21	155	1914	0.9	23.8315	19.3	0.0309	19.6	0.0053	2.9	0.15	34.3	1.0	30.9	5.9	-228.8	491.1	34.3	1.0	-15.0
MP33-15	132	1680	1.2	26.1044	40.6	0.0282	40.8	0.0053	3.5	0.09	34.3	1.2	28.2	11.4	-463.8	1112.0	34.3	1.2	-7.4
MP33-23	122	2208	1.2	33.0341	71.8	0.0223	71.9	0.0053	2.3	0.03	34.3	0.8	22.4	15.9	-1131.3	2497.1	34.3	0.8	-3.0
MP33-1	136	1584	1.0	23.1876	114.9	0.0319	114.9	0.0054	1.5	0.01	34.5	0.5	31.9	36.1	-160.3	1310.2	34.5	0.5	-21.6
MP33-33	122	1542	1.1	22.8880	41.2	0.0332	41.2	0.0055	1.7	0.04	35.4	0.6	33.1	13.4	-128.1	1056.6	35.4	0.6	-27.6
MP33-14	129	1878	1.3	22.1295	22.9	0.0344	23.0	0.0055	1.7	0.07	35.5	0.6	34.4	7.8	-45.5	563.2	35.5	0.6	-78.1
MP33-2	177	1242	0.7	12.8490	58.6	0.0593	58.8	0.0055	4.7	0.08	35.5	1.7	58.5	33.4	1142.5	1287.5	35.5	1.7	3.1
MP33-19	133	1758	0.8	25.9006	28.2	0.0295	28.3	0.0055	2.7	0.09	35.6	0.9	29.5	8.3	-443.2	754.9	35.6	0.9	-8.0
MP33-3	293	3000	0.9	22.6719	12.4	0.0337	12.4	0.0055	1.0	0.08	35.6	0.4	33.7	4.1	-104.7	305.7	35.6	0.4	-34.1
MP33-22	162	1884	1.0	24.3166	23.0	0.0315	23.0	0.0056	2.0	0.09	35.7	0.7	31.5	7.2	-279.9	590.9	35.7	0.7	-12.8
MP33-6	178	2328	0.8	25.0820	23.9	0.0308	24.0	0.0056	1.8	0.07	36.0	0.6	30.8	7.3	-359.4	626.7	36.0	0.6	-10.0
MP33-26	130	1866	0.9	29.4860	82.3	0.0262	82.3	0.0056	1.5	0.02	36.0	0.5	26.3	21.3	-797.1	2859.7	36.0	0.5	-4.5
MP33-8	138	1932	1.3	27.2333	32.2	0.0285	32.3	0.0056	3.2	0.10	36.1	1.2	28.5	9.1	-577.0	889.2	36.1	1.2	-6.3
MP33-11	132	2118	0.9	27.9322	40.4	0.0279	40.5	0.0057	3.2	0.08	36.3	1.1	27.9	11.2	-646.1	1147.9	36.3	1.1	-5.6
MP33-10	168	2640	0.8	22.3183	11.3	0.0350	11.6	0.0057	2.6	0.22	36.4	0.9	34.9	4.0	-66.2	277.0	36.4	0.9	-55.0
MP33-31	156	1464	1.0	14.1378	85.7	0.0553	85.8	0.0057	4.0	0.05	36.5	1.5	54.7	45.7	949.7	2350.2	36.5	1.5	3.8
MP33-7	95	984	1.2	28.8612	43.9	0.0271	44.1	0.0057	3.9	0.09	36.5	1.4	27.2	11.8	-736.8	1281.0	36.5	1.4	-5.0
MP33-5	101	1344	1.0	28.4523	65.0	0.0275	65.1	0.0057	3.4	0.05	36.5	1.2	27.6	17.7	-697.0	1998.8	36.5	1.2	-5.2
MP33-16	118	1344	0.9	34.8831	40.9	0.0225	40.9	0.0057	1.1	0.03	36.6	0.4	22.6	9.1	-1300.8	1342.4	36.6	0.4	-2.8
MP33-17	126	1356	1.0	30.5343	54.3	0.0258	54.3	0.0057	1.5	0.03	36.7	0.5	25.8	13.9	-897.2	1680.1	36.7	0.5	-4.1
MP33-30	103	1398	1.1	31.6918	48.5	0.0248	48.5	0.0057	1.9	0.04	36.7	0.7	24.9	11.9	-1006.4	1512.9	36.7	0.7	-3.6
MP33-12	169	1800	0.8	24.6183	23.6	0.0322	23.7	0.0057	1.4	0.06	36.9	0.5	32.1	7.5	-311.4	612.0	36.9	0.5	-11.9
MP33-25	101	1434	1.1	29.0598	63.1	0.0273	63.1	0.0057	2.8	0.04	36.9	1.0	27.3	17.0	-756.0	1948.8	36.9	1.0	-4.9
MP33-27	125	1794	1.3	25.1966	31.5	0.0316	31.7	0.0058	3.4	0.11	37.1	1.3	31.6	9.9	-371.2	834.5	37.1	1.3	-10.0
MP33-20	125	1752	1.1	24.3454	23.3	0.0327	23.4	0.0058	1.9	0.08	37.1	0.7	32.7	7.5	-282.9	601.4	37.1	0.7	-13.1
MP33-28	157	1932	1.1	23.5759	19.7	0.0340	19.7	0.0058	0.7	0.04	37.3	0.3	33.9	6.6	-201.7	496.7	37.3	0.3	-18.5
MP33-4	120	1566	0.8	29.7011	41.6	0.0270	41.7	0.0058	2.4	0.06	37.4	0.9	27.1	11.1	-817.8	1228.0	37.4	0.9	-4.6
MP33-13	141	1914	0.9	23.8919	30.2	0.0342	30.2	0.0059	1.2	0.04	38.1	0.4	34.2	10.1	-235.2	776.0	38.1	0.4	-16.2
MP33-9	134	1002	0.9	12.8374	25.7	0.0647	25.7	0.0060	0.9	0.03	38.7	0.3	63.6	15.9	1144.2	519.5	38.7	0.3	3.4
MP33-35	136	30444	1.4	11.6149	1.9	0.9120	7.4	0.0768	7.2	0.97	477.2	33.0	658.1	35.9	1340.3	36.0	477.2	33.0	35.6

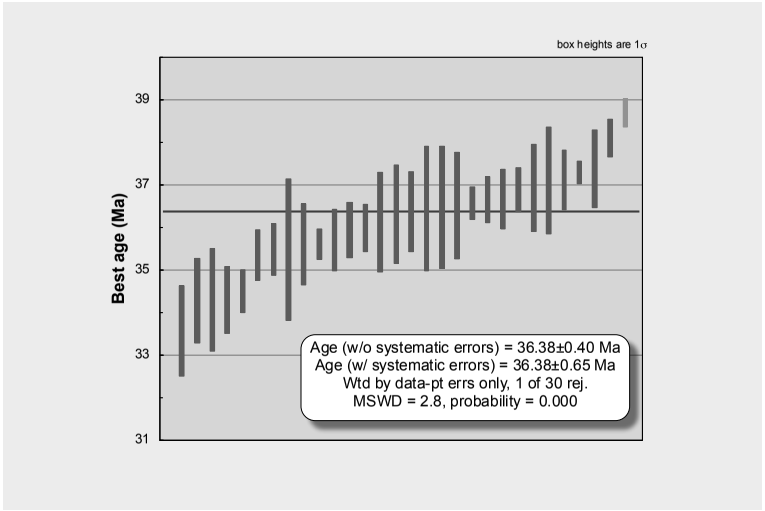

MP37 - North Fork Luecogranite						Isotope ratios						Apparent ages (Ma)							
Analysis	U	206Pb	U/Th	206Pb*	±	207Pb*	±	206Pb*	±	error	206Pb*	±	207Pb*	±	206Pb*	±	Best age	±	Conc
	(ppm)	204Pb		207Pb*	(%)	235U*	(%)	238U	(%)	corr.	238U*	(Ma)	235U	(Ma)	207Pb*	(Ma)	(Ma)	(Ma)	(%)
MP37-2	122	3480	1.6	32.1014	76.5	0.0178	76.5	0.0042	1.9	0.02	26.7	0.5	18.0	13.6	-1044.7	2677.5	26.7	0.5	-2.6
MP37-28	143	5220	1.3	22.5461	34.8	0.0273	35.7	0.0045	7.9	0.22	28.7	2.3	27.3	9.6	-91.0	877.1	28.7	2.3	-31.5
MP37-27	275	10600	1.3	20.6331	23.9	0.0303	23.9	0.0045	1.6	0.07	29.1	0.5	30.3	7.1	122.1	568.9	29.1	0.5	23.9
MP37-9	670	17280	1.0	21.4780	6.5	0.0297	6.8	0.0046	1.7	0.25	29.8	0.5	29.7	2.0	26.7	157.0	29.8	0.5	111.6
MP37-17	150	4840	1.4	27.8066	45.3	0.0232	45.3	0.0047	2.2	0.05	30.1	0.7	23.3	10.4	-633.7	1295.1	30.1	0.7	-4.7
MP37-10	3706	66540	3.3	20.5623	2.1	0.0314	2.9	0.0047	1.9	0.67	30.1	0.6	31.4	0.9	130.2	50.4	30.1	0.6	23.1
MP37-6	348	12940	1.5	24.1314	33.5	0.0268	33.9	0.0047	5.0	0.15	30.2	1.5	26.9	9.0	-260.4	871.1	30.2	1.5	-11.6
MP37-11	176	2120	1.5	10.0940	46.7	0.0645	47.3	0.0047	7.5	0.16	30.4	2.3	63.5	29.1	1606.6	926.5	30.4	2.3	1.9
MP37-33	490	13460	2.8	20.3600	15.2	0.0321	15.4	0.0047	2.4	0.15	30.4	0.7	32.0	4.8	153.3	357.4	30.4	0.7	19.8
MP37-12	281	11540	1.3	22.3495	14.2	0.0293	14.6	0.0047	3.8	0.26	30.5	1.1	29.3	4.2	-69.6	347.2	30.5	1.1	-43.9
MP37-19	168	4580	1.2	23.3792	43.2	0.0280	43.4	0.0047	4.0	0.09	30.5	1.2	28.0	12.0	-180.8	1125.8	30.5	1.2	-16.9
MP37-1	195	6900	1.6	29.2329	56.8	0.0224	56.9	0.0048	2.0	0.04	30.6	0.6	22.5	12.7	-772.7	1725.0	30.6	0.6	-4.0
MP37-34	2172	59860	4.7	21.0396	3.9	0.0313	4.2	0.0048	1.7	0.40	30.8	0.5	31.3	1.3	75.9	92.0	30.8	0.5	40.5
MP37-20	478	10040	0.9	21.0554	8.1	0.0314	8.1	0.0048	1.0	0.12	30.8	0.3	31.4	2.5	74.1	191.7	30.8	0.3	41.6
MP37-18	160	5640	1.0	18.8894	35.0	0.0352	35.1	0.0048	3.4	0.10	31.0	1.0	35.2	12.1	326.2	816.3	31.0	1.0	9.5
MP37-29	660	19180	1.4	21.9441	8.3	0.0305	8.3	0.0049	0.6	0.07	31.2	0.2	30.5	2.5	-25.0	200.6	31.2	0.2	-124.6
MP37-24	373	9180	0.9	23.8572	22.6	0.0281	22.7	0.0049	2.6	0.12	31.3	0.8	28.2	6.3	-231.6	575.6	31.3	0.8	-13.5
MP37-13	419	14640	1.0	30.4305	45.3	0.0220	45.3	0.0049	1.7	0.04	31.3	0.5	22.1	9.9	-887.4	1367.5	31.3	0.5	-3.5
MP37-23	490	11900	1.0	21.6284	11.4	0.0311	11.6	0.0049	2.3	0.19	31.3	0.7	31.1	3.6	9.9	275.4	31.3	0.7	316.7
MP37-8	546	15420	1.2	21.2153	6.6	0.0317	7.0	0.0049	2.2	0.31	31.4	0.7	31.7	2.2	56.1	158.3	31.4	0.7	55.9
MP37-15	262	7940	1.4	23.3731	22.5	0.0289	22.5	0.0049	1.3	0.06	31.5	0.4	28.9	6.4	-180.1	566.3	31.5	0.4	-17.5
MP37-4	844	23140	1.1	20.2805	5.7	0.0333	6.0	0.0049	1.7	0.29	31.5	0.5	33.2	1.9	162.5	133.5	31.5	0.5	19.4
MP37-5	1531	41860	1.2	21.3365	4.0	0.0316	4.3	0.0049	1.6	0.37	31.5	0.5	31.6	1.3	42.5	94.7	31.5	0.5	74.1
MP37-22	366	10380	1.6	21.3152	8.6	0.0317	9.1	0.0049	3.2	0.35	31.5	1.0	31.7	2.8	44.9	204.7	31.5	1.0	70.2
MP37-3	769	25760	1.7	20.5057	7.0	0.0331	7.1	0.0049	1.5	0.20	31.6	0.5	33.0	2.3	136.6	164.0	31.6	0.5	23.2
MP37-21	79	2540	1.9	34.3455	64.3	0.0198	64.4	0.0049	2.5	0.04	31.7	0.8	19.9	12.7	-1251.8	2222.4	31.7	0.8	-2.5
MP37-7	1586	40620	1.8	21.4345	2.7	0.0318	3.5	0.0049	2.1	0.61	31.7	0.7	31.7	1.1	31.6	65.5	31.7	0.7	100.6
MP37-16	494	18600	1.6	21.4753	11.7	0.0317	11.8	0.0049	1.4	0.12	31.8	0.4	31.7	3.7	27.0	280.8	31.8	0.4	117.8
MP37-25	547	12820	1.0	20.1631	8.2	0.0338	8.3	0.0049	1.0	0.12	31.8	0.3	33.8	2.7	176.1	191.5	31.8	0.3	18.1
MP37-32	456	11380	1.0	21.5507	15.5	0.0320	16.1	0.0050	4.6	0.28	32.2	1.5	32.0	5.1	18.6	373.3	32.2	1.5	173.0
MP37-26	3364	70380	1.7	21.5859	2.7	0.0321	2.9	0.0050	0.9	0.30	32.3	0.3	32.1	0.9	14.6	65.6	32.3	0.3	221.1
MP37-35	297	9840	1.5	21.8772	24.4	0.0318	24.5	0.0050	2.1	0.08	32.4	0.7	31.8	7.7	-17.7	597.5	32.4	0.7	-183.8
MP37-14	388	7820	1.0	17.0133	22.7	0.0418	22.8	0.0052	2.0	0.09	33.2	0.7	41.6	9.3	558.8	501.0	33.2	0.7	5.9
MP37-31	207	6440	1.0	18.9503	21.9	0.0378	22.0	0.0052	2.1	0.10	33.4	0.7	37.7	8.1	318.9	502.3	33.4	0.7	10.5

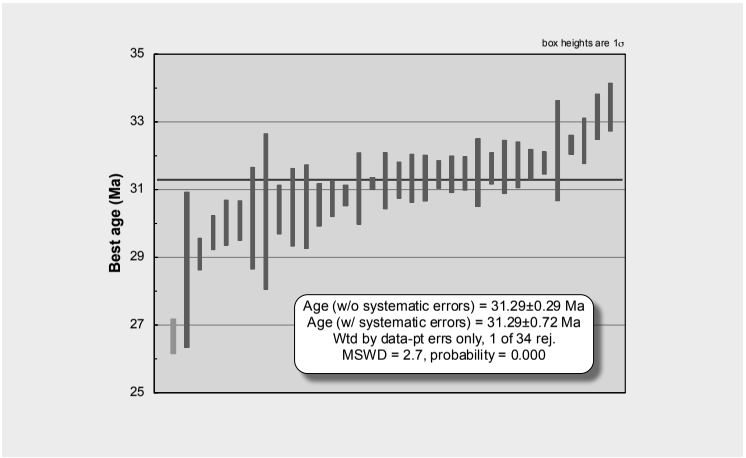

MP38 - California Luecogranite						Isotope ratios						Apparent ages (Ma)								
Analysis	U	206Pb	U/Th	206Pb*	±	207Pb*	±	206Pb*	±	error	206Pb*	±	207Pb*	±	206Pb*	±	Best age	±	Conc
	(ppm)	204Pb		207Pb*	(%)	235U*	(%)	238U	(%)	corr.	238U*	(Ma)	235U	(Ma)	207Pb*	(Ma)	(Ma)	(Ma)	(%)
MP38-22	114	630	1.4	22.0625	16.7	0.0271	17.3	0.0043	4.7	0.27	27.9	1.3	27.2	4.7	-38.1	407.4	27.9	1.3	-73.3
MP38-8	190	1310	1.7	25.6452	36.6	0.0241	36.7	0.0045	2.9	0.08	28.9	0.8	24.2	8.8	-417.2	985.6	28.9	0.8	-6.9
MP38-6	1376	8960	1.8	22.2523	5.8	0.0283	7.2	0.0046	4.2	0.59	29.3	1.2	28.3	2.0	-58.9	141.8	29.3	1.2	-49.8
MP38-7	207	1620	1.6	23.3356	29.9	0.0271	29.9	0.0046	1.5	0.05	29.5	0.4	27.2	8.0	-176.1	759.8	29.5	0.4	-16.8
MP38-15	177	1320	0.9	26.9251	28.1	0.0237	28.2	0.0046	1.1	0.04	29.8	0.3	23.8	6.6	-546.3	768.6	29.8	0.3	-5.4
MP38-23	121	855	1.3	30.8379	43.3	0.0209	43.4	0.0047	2.7	0.06	30.1	0.8	21.0	9.0	-926.0	1312.2	30.1	0.8	-3.3
MP38-29	214	865	0.5	14.2124	18.5	0.0455	18.7	0.0047	2.4	0.13	30.2	0.7	45.2	8.3	938.9	382.9	30.2	0.7	3.2
MP38-14	1652	9325	2.1	21.4077	2.3	0.0303	2.6	0.0047	1.2	0.47	30.2	0.4	30.3	0.8	34.5	55.6	30.2	0.4	87.5
MP38-11	212	1430	1.2	22.3059	10.6	0.0291	10.7	0.0047	1.3	0.12	30.3	0.4	29.1	3.1	-64.8	259.2	30.3	0.4	-46.7
MP38-17	5419	20630	2.7	21.3298	1.7	0.0305	2.1	0.0047	1.3	0.62	30.3	0.4	30.5	0.6	43.2	39.5	30.3	0.4	70.2
MP38-1	667	5485	1.9	22.1516	4.6	0.0295	4.8	0.0047	1.3	0.28	30.5	0.4	29.5	1.4	-47.9	112.3	30.5	0.4	-63.6
MP38-9	313	1180	0.5	19.7965	31.7	0.0330	31.7	0.0047	0.7	0.02	30.5	0.2	33.0	10.3	218.7	750.9	30.5	0.2	13.9
MP38-18	214	1630	1.1	25.2455	33.6	0.0259	33.6	0.0047	1.7	0.05	30.5	0.5	26.0	8.6	-376.2	892.4	30.5	0.5	-8.1
MP38-10	203	1025	0.7	20.0067	22.1	0.0328	22.8	0.0048	5.5	0.24	30.6	1.7	32.8	7.3	194.2	519.9	30.6	1.7	15.7
MP38-3	1568	8515	1.9	20.5530	7.5	0.0320	7.8	0.0048	2.1	0.26	30.7	0.6	32.0	2.4	131.2	176.5	30.7	0.6	23.4
MP38-19	731	5195	1.3	23.2495	12.1	0.0283	12.2	0.0048	0.8	0.07	30.7	0.3	28.4	3.4	-166.9	302.8	30.7	0.3	-18.4
MP38-13	3081	17665	4.0	21.4121	1.8	0.0309	2.1	0.0048	1.1	0.52	30.8	0.3	30.9	0.6	34.0	42.5	30.8	0.3	90.6
MP38-12	985	6090	1.1	21.6747	3.2	0.0306	3.6	0.0048	1.6	0.44	30.9	0.5	30.6	1.1	4.7	76.8	30.9	0.5	651.1
MP38-16	141	1175	1.3	20.0400	372.9	0.0332	372.9	0.0048	2.5	0.01	31.0	0.8	33.1	122.2	190.4	0.0	31.0	0.8	16.3
MP38-28	1525	7955	1.7	21.7980	4.7	0.0306	4.7	0.0048	0.5	0.11	31.1	0.2	30.6	1.4	-8.9	112.5	31.1	0.2	-350.4
MP38-26	1608	4185	0.4	20.2201	11.3	0.0330	11.4	0.0048	1.5	0.13	31.2	0.5	33.0	3.7	169.5	264.2	31.2	0.5	18.4
MP38-27	232	1355	0.8	22.2340	56.4	0.0302	56.6	0.0049	4.6	0.08	31.3	1.4	30.2	16.8	-56.9	1485.1	31.3	1.4	-54.9
MP38-4	1018	6355	1.7	21.5485	3.4	0.0311	3.7	0.0049	1.4	0.37	31.3	0.4	31.1	1.1	18.8	82.4	31.3	0.4	166.2
MP38-24	148	720	1.0	22.8331	19.8	0.0296	20.1	0.0049	3.1	0.15	31.5	1.0	29.6	5.9	-122.1	493.0	31.5	1.0	-25.8
MP38-21	1948	13900	4.7	21.5541	3.7	0.0315	3.9	0.0049	1.2	0.31	31.7	0.4	31.5	1.2	18.2	89.7	31.7	0.4	173.9
MP38-25	1203	6385	1.3	21.5722	3.9	0.0316	4.0	0.0049	1.0	0.25	31.8	0.3	31.6	1.2	16.2	93.5	31.8	0.3	196.7
MP38-30	1099	2245	1.6	14.9121	11.2	0.0483	11.3	0.0052	0.8	0.07	33.6	0.3	47.9	5.3	839.6	234.5	33.6	0.3	4.0

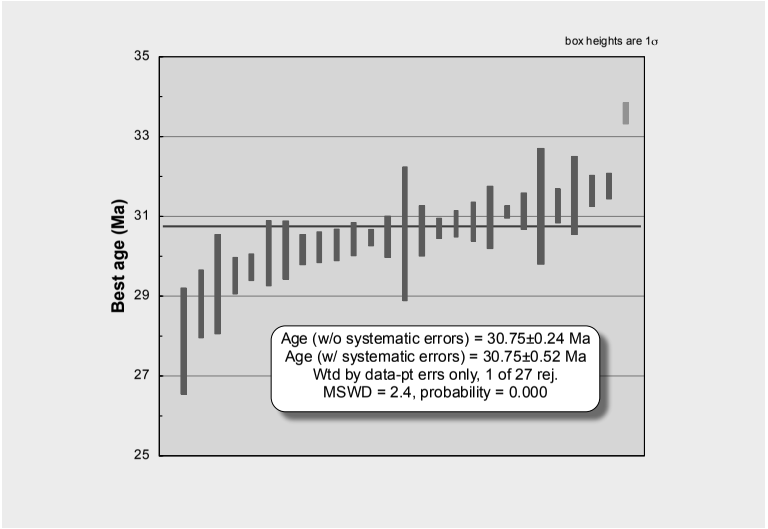

APPENDIX 2.3.

MT. AETNA AR/AR DATA TABLES, IDEOGRAMS, AND AGE SPECTRA

Appendix 2.3 contains the data tables and supporting figures for all the Ar/Ar analyses conducted as part of this study. Tables 2.3.1, 2.3.2, and 2.3.3 contain the analytical data for the laser-fusion analyses, biotite step-heat analyses, and K-feldspar step-heat analyses, respectively. Footnotes at the bottom of each table contain addition information regarding sample preparation and irradiation, age calculations, instrumentation, and analytical parameters. Figures 2.3.1, 2.3.2, and 2.3.3 display the laser-fusion ideograms, biotite age spectra, and K-feldspar age spectra, respectively.

Table 2.3.1 - Mt. Aetna laser-fusion $^{40}Ar/^{39}Ar$ analytical data.

	ID	$^{40}Ar/^{39}Ar$	$^{37}Ar/^{39}Ar$	$^{36}Ar/^{39}Ar$ (x 10^{-3})	$^{39}Ar_K$ (x 10^{-15} mol)	K/Ca	$^{40}Ar^*$ (%)	Age (Ma)	±1σ (Ma)
	MP-15, Sanidine, J=0.0020186±0.05%, D=1.0014±0.001, NM-220E, Lab#=58049								
	22	10.65	0.0178	1.687	1.651	28.6	95.3	37.09	0.14
	15	10.40	0.0203	0.8478	4.855	25.1	97.6	37.11	0.08
	01	10.26	0.0175	0.3039	5.029	29.1	99.1	37.15	0.07
	10	10.33	0.0177	0.5431	4.842	28.8	98.5	37.18	0.07
	19	10.32	0.0192	0.4892	6.816	26.6	98.6	37.19	0.06
	08	10.32	0.0196	0.4748	11.073	26.1	98.7	37.21	0.06
	28	10.49	0.0189	1.019	6.234	27.0	97.1	37.23	0.07
	06	10.44	0.0179	0.8282	6.941	28.5	97.7	37.26	0.07
	12	10.37	0.0185	0.5960	5.263	27.5	98.3	37.27	0.07
	04	10.36	0.0186	0.5281	4.989	27.4	98.5	37.31	0.07
	14	10.34	0.0208	0.4562	6.926	24.5	98.7	37.31	0.06
	11	10.33	0.0182	0.3854	8.568	28.1	98.9	37.32	0.06
	03	10.41	0.0181	0.6535	2.390	28.2	98.2	37.32	0.11
	24	10.38	0.0186	0.5709	7.111	27.4	98.4	37.33	0.06
	16	10.43	0.0201	0.7203	5.238	25.4	98.0	37.33	0.07
	27	10.36	0.0184	0.4955	7.189	27.8	98.6	37.33	0.06
	21	10.37	0.0206	0.4955	7.105	24.8	98.6	37.37	0.06
	09	10.35	0.0189	0.4271	6.391	27.0	98.8	37.37	0.07
	07	10.35	0.0190	0.3775	6.920	26.9	98.9	37.41	0.06
	30	10.57	0.0193	1.135	3.549	26.4	96.8	37.42	0.09
	31	10.52	0.0192	0.9347	7.029	26.6	97.4	37.42	0.07
	26	10.32	0.0189	0.2497	7.833	27.0	99.3	37.44	0.06
	17	10.39	0.0193	0.4711	6.342	26.5	98.7	37.46	0.06
	18	10.46	0.0179	0.7200	7.117	28.6	98.0	37.46	0.06
	13	10.44	0.0214	0.6420	3.576	23.9	98.2	37.47	0.09
	02	10.34	0.0190	0.2767	10.381	26.8	99.2	37.49	0.05
	05	10.39	0.0191	0.4156	8.302	26.7	98.8	37.52	0.06
	29	10.42	0.0193	0.5045	4.958	26.4	98.6	37.54	0.07
X	23	12.32	0.0179	6.831	0.619	28.4	83.6	37.64	0.41
X	25	10.73	0.0186	1.379	3.904	27.5	96.2	37.70	0.08
X	20	10.61	0.0194	0.9471	4.443	26.3	97.4	37.76	0.08
	Mean age ± 2σ	n=28	MSWD=3.03		26.9	±2.7		37.34	0.06
	NM-531, Sanidine, J=0.0016137±0.06%, D=1.005±0.001, NM-233G, Lab#=59577								
	12	12.91	0.0170	0.8561	2.149	30.0	98.1	36.99	0.09
	07	12.76	0.0177	0.2442	3.510	28.9	99.4	37.06	0.07
	14	12.99	0.0179	0.9973	8.770	28.4	97.7	37.09	0.05
	09	12.74	0.0182	0.1550	4.588	28.1	99.7	37.09	0.06
X	02	13.88	0.0161	4.002	5.285	31.6	91.5	37.10	0.07
	10	12.79	0.0181	0.3185	6.551	28.1	99.3	37.10	0.06
	06	12.83	0.0187	0.3776	5.837	27.3	99.1	37.18	0.06
	11	12.81	0.0168	0.2486	7.672	30.4	99.4	37.20	0.05
	05	12.77	0.0175	0.0906	9.726	29.2	99.8	37.23	0.05
X	13	13.79	0.0165	3.562	3.306	30.9	92.4	37.23	0.09
	01	12.78	0.0186	0.1064	6.720	27.4	99.8	37.26	0.05
	03	12.77	0.0173	0.0788	9.605	29.5	99.8	37.26	0.05
	08	13.03	0.0173	0.9311	3.500	29.5	97.9	37.27	0.07
	15	12.81	0.0173	0.0977	5.491	29.5	99.8	37.33	0.05
	04	12.91	0.0186	0.4356	4.475	27.4	99.0	37.33	0.07
	Mean age ± 2σ	n=13	MSWD=2.79		28.8	±2.1		37.20	0.07
	NM-1152, Sanidine, J=0.001612±0.06%, D=1.005±0.001, NM-233G, Lab#=59578								
	05	12.78	0.0171	0.3235	1.702	29.9	99.3	37.03	0.08

	09	12.73	0.0178	0.1321	8.982	28.7	99.7	37.04	0.05
	06	12.79	0.0203	0.2534	5.101	25.1	99.4	37.10	0.06
X	04	15.42	0.0176	9.120	4.214	28.9	82.5	37.13	0.09
	03	12.77	0.0180	0.1220	7.707	28.3	99.7	37.17	0.05
X	08	13.71	0.0184	3.291	4.882	27.8	92.9	37.17	0.07
	14	12.90	0.0167	0.5306	6.643	30.5	98.8	37.18	0.06
	01	12.85	0.0184	0.3036	2.628	27.7	99.3	37.26	0.07
	12	12.79	0.0166	0.0742	3.914	30.7	99.8	37.27	0.06
	15	12.79	0.0172	0.0472	3.488	29.7	99.9	37.29	0.06
	11	12.83	0.0176	0.1465	5.147	28.9	99.7	37.31	0.06
	02	12.81	0.0177	0.0851	6.569	28.9	99.8	37.32	0.05
	07	12.92	0.0209	0.4294	3.762	24.5	99.0	37.35	0.06
	13	12.83	0.0177	0.0609	3.855	28.9	99.9	37.39	0.06
	10	13.25	0.0184	1.454	3.596	27.7	96.8	37.42	0.07
	Mean age ± 2σ	n=13	MSWD=4.36		28.4	±3.7		37.24	0.08
	NM-1307, Sanidine, J=0.0016085±0.06%, D=1.005±0.001, NM-233G, Lab#=59579								
X	07	12.66	1.942	1.221	0.203	0.26	98.4	36.34	0.52
X	02	12.72	2.298	1.495	0.257	0.22	98.0	36.38	0.42
	01	12.67	0.0189	0.0557	1.834	27.0	99.9	36.86	0.08
	03	12.74	0.0175	0.2375	1.446	29.2	99.5	36.91	0.09
	09	12.73	0.0178	0.0516	1.955	28.6	99.9	37.03	0.08
	15	12.77	0.0192	0.0540	2.227	26.6	99.9	37.14	0.07
	11	12.84	0.0213	0.2429	1.799	23.9	99.5	37.19	0.08
	05	12.80	0.0171	0.0905	2.848	29.8	99.8	37.19	0.07
X	08	12.85	2.047	0.8502	0.229	0.25	99.4	37.25	0.48
	13	12.82	0.0175	0.0947	2.185	29.2	99.8	37.27	0.08
	14	12.82	0.0184	-0.0042	3.492	27.8	100.0	37.36	0.07
	12	12.85	0.0185	0.0060	2.071	27.5	100.0	37.41	0.07
	04	12.86	0.0181	0.0228	2.934	28.2	100.0	37.42	0.07
	10	12.88	0.0176	0.1046	2.842	29.0	99.8	37.44	0.07
X	06	13.01	3.598	1.266	0.154	0.14	99.4	37.76	0.67
	Mean age ± 2σ	n=11	MSWD=6.76		27.9	±3.3		37.23	0.12
	NM-1416, Sanidine, J=0.001605±0.05%, D=1.005±0.001, NM-233G, Lab#=59580								
	03	12.80	0.0187	0.2600	1.313	27.3	99.4	36.98	0.11
	14	12.86	0.0215	0.4503	1.832	23.7	99.0	36.99	0.09
	10	12.85	0.0192	0.3870	1.655	26.6	99.1	37.00	0.09
	01	12.81	0.0175	0.2161	1.544	29.1	99.5	37.03	0.09
	05	12.87	0.0181	0.4388	2.399	28.2	99.0	37.04	0.07
	08	12.80	0.0182	0.1776	1.444	28.1	99.6	37.05	0.10
	09	12.86	0.0191	0.2812	1.597	26.7	99.4	37.14	0.09
	06	12.98	0.0189	0.5507	1.145	27.0	98.8	37.25	0.11
	07	12.97	0.0192	0.3968	2.503	26.6	99.1	37.36	0.08
X	15	13.58	0.0188	1.198	0.938	27.1	97.4	38.43	0.16
X	02	22.01	0.0892	4.817	0.524	5.7	93.6	59.49	0.26
X	13	55.32	0.0195	3.061	1.380	26.1	98.4	153.25	0.27
X	16	86.99	0.0138	2.545	1.796	37.0	99.1	237.27	0.36
X	11	107.9	0.0134	2.177	1.702	38.1	99.4	290.66	0.44
X	04	142.5	0.0126	2.008	1.543	40.5	99.6	375.52	0.55
	Mean age ± 2σ	n=9	MSWD=2.36		27.0	±3.0		37.10	0.10
	MP-30, Sanidine, J=0.0020172±0.05%, D=1.0014±0.001, NM-220E, Lab#=58055								
	08	9.426	0.0057	0.4451	4.888	89.7	98.6	33.97	0.07
	04	9.677	0.0062	1.177	3.518	82.5	96.4	34.10	0.08
	13	9.535	0.0064	0.6914	4.587	79.1	97.9	34.10	0.07
	24	9.703	0.0060	1.239	3.581	84.4	96.2	34.12	0.09
	09	9.443	0.0056	0.3515	6.530	91.2	98.9	34.13	0.06
	27	9.443	0.0057	0.3387	7.716	89.8	98.9	34.14	0.05
	30	9.463	0.0059	0.3959	7.173	85.9	98.8	34.15	0.06
	03	9.542	0.0065	0.6558	7.667	79.0	98.0	34.16	0.06

	15	9.562	0.0054	0.7106	5.370	93.9	97.8	34.18	0.07
X	22	9.962	0.0066	2.052	4.211	77.1	93.9	34.19	0.08
	18	9.564	0.0059	0.6936	5.817	86.5	97.9	34.20	0.07
	20	9.518	0.0065	0.5240	9.153	78.9	98.4	34.22	0.05
	17	9.528	0.0075	0.5528	5.247	68.5	98.3	34.22	0.06
	26	9.472	0.0060	0.3441	10.252	84.6	98.9	34.24	0.05
X	25	12.13	0.0061	9.329	5.036	84.0	77.3	34.26	0.12
	19	9.522	0.0123	0.4870	7.316	41.6	98.5	34.27	0.06
	06	9.494	0.0056	0.3630	8.077	91.3	98.9	34.30	0.06
	07	9.529	0.0058	0.4706	5.498	87.6	98.5	34.31	0.06
	12	9.507	0.0062	0.3932	6.660	81.7	98.8	34.32	0.06
	28	9.585	0.0060	0.6244	7.588	85.1	98.1	34.35	0.06
	02	9.712	0.0064	1.054	4.307	80.3	96.8	34.35	0.08
	23	9.711	0.0063	1.002	8.757	80.4	97.0	34.41	0.06
	21	9.511	0.0064	0.3215	7.353	79.8	99.0	34.41	0.06
	16	9.824	0.0059	1.371	4.497	87.0	95.9	34.42	0.08
	05	9.652	0.0062	0.7678	3.993	82.8	97.7	34.44	0.08
	01	9.555	0.0064	0.4326	7.952	79.7	98.7	34.45	0.06
	29	9.671	0.0058	0.8023	4.548	88.2	97.6	34.47	0.08
	11	9.528	0.0055	0.3017	8.752	93.1	99.1	34.49	0.05
	14	9.683	0.0067	0.7956	3.194	76.6	97.6	34.52	0.09
	10	9.635	0.0051	0.5865	3.619	100.5	98.2	34.57	0.09
	Mean age ± 2σ	n=28	MSWD=4.82			83.2 ±20.7		34.28	0.06

MP-31, Sanidine, J=0.0020145±0.05%, D=1.0014±0.001, NM-220E, Lab#=58052

X	18	9.507	0.0051	0.6462	0.000	99.4	98.0	34.00	0.06
X	15	9.509	0.0053	0.6395	0.000	95.8	98.0	34.01	0.10
X	19	9.491	0.0058	0.5691	0.000	88.5	98.2	34.03	0.05
	13	9.477	0.0072	0.4678	0.000	70.6	98.5	34.08	0.06
	25	9.609	0.0065	0.8940	0.000	78.0	97.3	34.11	0.08
	17	9.461	0.0057	0.3829	0.000	90.0	98.8	34.11	0.05
	09	9.479	0.0056	0.4128	0.000	91.9	98.7	34.15	0.07
	02	9.470	0.0065	0.3676	0.000	78.1	98.9	34.17	0.06
	29	9.509	0.0071	0.4942	0.000	72.1	98.5	34.17	0.06
	20	9.626	0.0064	0.8641	0.000	79.6	97.4	34.20	0.07
	23	9.578	0.0067	0.6939	0.000	75.8	97.9	34.21	0.07
	28	9.510	0.0056	0.4447	0.000	90.8	98.6	34.23	0.06
	30	9.476	0.0066	0.3254	0.000	77.5	99.0	34.23	0.05
	07	9.502	0.0073	0.3935	0.000	69.5	98.8	34.25	0.05
	27	9.621	0.0067	0.7834	0.000	76.3	97.6	34.27	0.07
	22	9.570	0.0058	0.6015	0.000	88.7	98.1	34.28	0.06
	08	9.506	0.0062	0.3812	0.000	82.2	98.8	34.28	0.06
	01	9.533	0.0061	0.4709	0.000	83.0	98.5	34.28	0.06
	11	9.570	0.0066	0.5870	0.000	77.5	98.2	34.29	0.07
	26	9.560	0.0061	0.5371	0.000	84.2	98.3	34.31	0.06
	16	9.517	0.0062	0.3878	0.000	82.3	98.8	34.31	0.06
	24	9.577	0.0049	0.5739	0.000	104.1	98.2	34.33	0.08
	06	9.666	0.0062	0.8568	0.000	82.9	97.4	34.35	0.07
	21	9.557	0.0075	0.4808	0.000	68.3	98.5	34.36	0.05
	04	9.647	0.0067	0.7638	0.000	75.6	97.7	34.38	0.07
	05	9.507	0.0070	0.2774	0.000	72.7	99.1	34.40	0.06
	12	9.608	0.0061	0.6001	0.000	83.5	98.2	34.41	0.06
	14	9.559	0.0056	0.4218	0.000	90.5	98.7	34.43	0.06
	03	9.510	0.0058	0.2397	0.000	88.6	99.3	34.45	0.05
X	10	9.525	0.0057	0.2253	0.000	89.2	99.3	34.52	0.05
	Mean age ± 2σ	n=30	MSWD=2.94			82.9 ±17.8		34.28	0.06

MP-36, Sanidine, J=0.0022572±0.05%, D=1.005±0.001, NM-227A, Lab#=59199

X	15	9.513	0.0066	4.165	3.468	77.4	87.1	33.87	0.10
	14	8.688	0.0068	1.113	6.840	74.9	96.2	34.18	0.06
	05	8.536	0.0066	0.5818	4.185	77.8	98.0	34.20	0.07

	09	8.501	0.0062	0.4606	4.857	82.5	98.4	34.20	0.06
	06	8.465	0.0073	0.3359	7.605	70.3	98.8	34.20	0.05
X	10	9.047	0.0056	2.289	11.588	90.5	92.5	34.22	0.06
	11	8.624	0.0084	0.8422	9.224	61.1	97.1	34.24	0.05
	07	8.606	0.0070	0.7747	3.382	73.2	97.3	34.25	0.08
X	01	8.983	0.0067	2.044	7.132	75.7	93.3	34.26	0.06
	04	8.704	0.0058	1.059	5.030	88.7	96.4	34.31	0.07
X	08	9.407	0.0077	3.432	9.147	66.6	89.2	34.32	0.07
	02	8.760	0.0074	1.203	5.279	69.3	95.9	34.36	0.07
X	03	9.607	0.0086	4.069	4.012	59.1	87.5	34.36	0.09
X	13	9.294	0.0068	2.990	6.345	74.5	90.5	34.39	0.07
X	12	10.15	0.0084	5.873	3.932	60.8	82.9	34.42	0.10
	Mean age ± 2σ	n=8	MSWD=0.95		74.7	±16.9		34.24	0.05

MP-32, Biotite, J=0.0023828±0.07%, D=1.006±0.001, NM-227L, Lab#=59269

06	9.006	0.0332	3.678	0.000	15.3	88.0	34.19	0.18
14	8.785	0.0420	2.896	0.000	12.2	90.3	34.24	0.24
07	8.400	0.0255	1.535	0.000	20.0	94.6	34.31	0.10
13	9.060	0.0166	3.735	0.000	30.8	87.8	34.34	0.18
16	8.537	0.0092	1.911	0.000	55.2	93.4	34.41	0.16
12	8.448	0.0176	1.594	0.000	29.0	94.4	34.43	0.12
15	8.770	0.0225	2.634	0.000	22.6	91.1	34.50	0.18
11	8.545	0.0350	1.834	0.000	14.6	93.7	34.55	0.15
09	8.504	0.0294	1.677	0.000	17.3	94.2	34.58	0.10
05	9.385	0.0258	4.631	0.000	19.8	85.4	34.60	0.25
04	8.551	0.0041	1.794	0.000	124.8	93.8	34.62	0.15
08	9.329	0.0078	4.405	0.000	65.4	86.0	34.64	0.22
03	8.745	0.0095	2.308	0.000	54.0	92.2	34.80	0.27
10	8.678	0.0186	2.072	0.000	27.5	93.0	34.81	0.12
02	9.043	0.0238	3.140	0.000	21.5	89.8	35.03	0.16
Mean age ± 2σ	n=15	MSWD=2.07		35.3	±59.3		34.53	0.12

Notes:
x (or i) symbol preceding sample ID denotes analyses excluded from plateau (or isochron) age calculations.
Isotopic ratios corrected for blank, radioactive decay, and mass discrimination, not corrected for interfering reactions.
Errors quoted for individual analyses include analytical error only, without interfering reaction or J uncertainties.

Age calculations:
Ages calculated relative to FC-2 Fish Canyon Tuff sanidine interlaboratory standard (28.201 Ma, Kuiper et al, 2008).
Mean age is weighted mean age of Taylor (1982). Mean age error is weighted error of the mean (Taylor, 1982), multiplied by the root of the MSWD where MSWD>1, and also incorporates uncertainty in J factors and irradiation correction uncertainties.
MSWD values are calculated for n-1 degrees of freedom for plateau age.
Isochron ages, $^{40}Ar/^{36}Ar_i$ and MSWD values calculated from regression results obtained by the methods of York (1969).
Decay constants and isotopic abundances after Min et al., (2000).
All errors reported at ±2σ, unless otherwise noted.

Sample preparation and irradiation:
Sanidine and biotite separates prepared using crushing, dilute HF acid treatment, Franz magnetic separator, and hand-picking techniques.
Samples were loaded into machined Al discs and irradiated in 4 separate positions (NM-220E, NM-227A and L, and NM-233G) for 7 to 9 hours at , Nuclear Science Center, College Station, TX.
Neutron flux monitor Fish Canyon Tuff sanidine (FC-2).

Instrumentation:
Mass Analyzer Products 215-50 mass spectrometer on line with automated all-metal extraction system.
Samples were fused using a CO2 laser (heating duration 30 seconds).
Reactive gases removed during laser analysis by reaction with 2 SAES GP-50 getters, 1 operated at ~450°C and 1 at 20°C. Gas also exposed to a W filament operated at ~2000°C.

Analytical parameters:

Electron multiplier sensitivity ranged from 2.91 x 10^{-17} moles /pA to 5.26 x 10^{-17} moles /pA.

Total system blank and background for the laser averaged 476, 7.24, 1.61, 3.05, 17.1 x 10^{-18} moles at masses 40,39,38,37 and 36 respectively

J-factors determined to a precision of ± 0.1% by CO_2 laser-fusion of 6 single crystals from each of 10 radial positions around the irradiation tray.

Correction factors for interfering nuclear reactions were determined using K-glass and CaF_2 and are as follows:

$(^{39}Ar/^{37}Ar)_{Ca}$ = 0.00068 ± 2e-05

$(^{36}Ar/^{37}Ar)_{Ca}$ = 0.00028 ± 1e-05

$(^{38}Ar/^{39}Ar)_{K}$ = 0.013 ± 5e-04

$(^{40}Ar/^{39}Ar)_{K}$ = 0 ± 4e-04

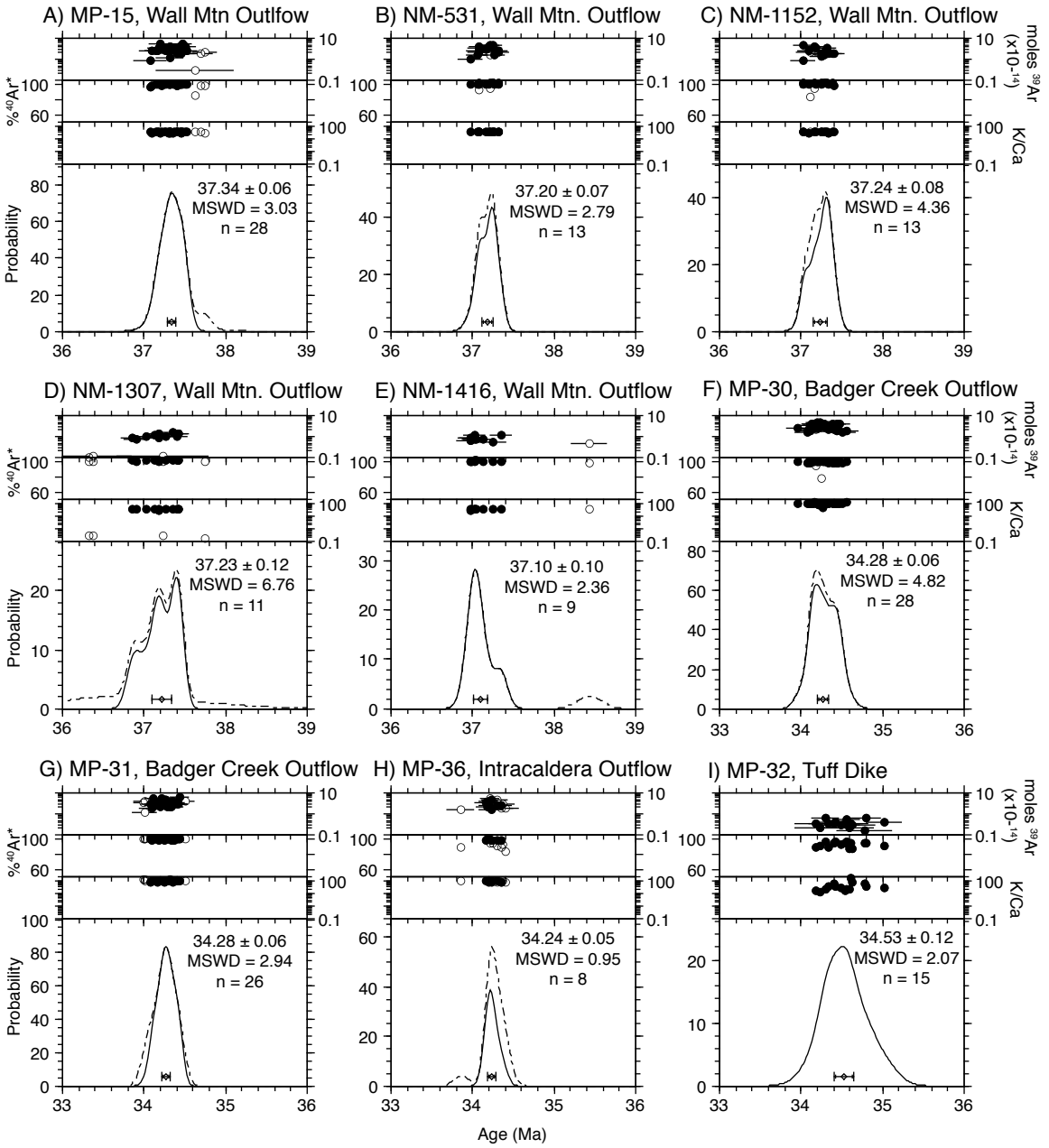

Figure 2.3.1 - Sanidine and biotite laser-fusion ideograms. Auxiliary plots include moles ^{39}Ar, K/Ca, and radiogenic yield (%^{40}Ar*). All errors are reported at 2σ and do not include error in decay constant.

Table 2.3.2 - Mt. Aetna biotite $^{40}Ar/^{39}Ar$ analytical data.

	ID	Power (Watts)	$^{40}Ar/^{39}Ar$	$^{37}Ar/^{39}Ar$	$^{36}Ar/^{39}Ar$ (x 10^{-3})	$^{39}Ar_K$ (x 10^{-15} mol)	K/Ca	$^{40}Ar^*$ (%)	^{39}Ar (%)	Age (Ma)	±1σ (Ma)
	MP-02, Biotite, 7.58 mg, J=0.0018969±0.07%, D=1.0014±0.001, NM-220A, Lab#=58000-01										
X	A	650	192.1	3.731	625.9	0.669	0.14	3.9	0.3	25.60	4.42
X	B	750	54.86	5.328	155.7	0.723	0.096	16.9	0.6	32.11	1.93
X	C	850	19.04	0.1603	28.92	5.85	3.2	55.2	3.3	36.09	0.36
X	D	920	11.81	0.0135	3.870	19.92	37.8	90.3	12.3	36.64	0.09
X	E	1000	11.04	0.0123	1.281	29.47	41.5	96.6	25.7	36.63	0.07
X	F	1075	10.67	0.0156	0.7226	39.07	32.6	98.0	43.4	35.93	0.07
X	G	1110	10.15	0.0171	-0.8702	24.27	29.8	102.6	54.4	35.76	0.08
X	H	1180	10.51	0.0532	0.8408	22.13	9.6	97.7	64.4	35.28	0.09
X	I	1210	10.52	0.0637	0.8502	26.10	8.0	97.7	76.2	35.32	0.08
X	J	1250	10.67	0.0646	1.440	36.15	7.9	96.1	92.6	35.23	0.07
X	K	1300	11.08	0.0501	2.716	14.37	10.2	92.8	99.1	35.32	0.12
X	L	1680	147.9	0.2408	467.3	1.949	2.1	6.6	100.0	33.69	2.87
	Integrated age ± 2σ		n=12			220.7	7.3	K2O=5.89%		35.72	0.16
	Plateau ± 2σ	no plateau	n=0	MSWD=0.00		0.000	0.000±0.000		0.0	0.00	0.00
	Isochron±2σ	steps A-L	n=12	MSWD=38.24			$^{40}Ar/^{36}Ar$=	295.0±2.4		35.80	0.08
	MP-03, Biotite, 8.72 mg, J=0.0018967±0.07%, D=1.0014±0.001, NM-220A, Lab#=58001-01										
X	A	650	156.7	0.5897	527.5	0.892	0.87	0.6	0.4	3.19	4.02
X	B	750	54.55	0.4414	159.7	1.206	1.2	13.5	0.8	25.44	1.60
X	C	850	18.13	0.0313	27.46	11.17	16.3	55.2	5.4	34.42	0.25
	D	920	11.25	0.0135	2.942	16.31	37.7	92.3	12.0	35.65	0.09
	E	1000	10.78	0.0161	1.256	24.77	31.6	96.6	22.0	35.75	0.07
	F	1075	10.93	0.0309	1.633	29.38	16.5	95.6	33.8	35.90	0.07
	G	1110	10.81	0.0450	1.195	23.72	11.3	96.8	43.4	35.93	0.08
	H	1180	10.78	0.1119	1.262	21.51	4.6	96.6	52.1	35.79	0.08
	I	1210	10.74	0.1159	1.291	22.54	4.4	96.6	61.2	35.62	0.08
X	J	1250	10.54	0.0734	0.7402	55.5	7.0	98.0	83.6	35.49	0.05
X	K	1300	10.66	0.0246	1.195	38.69	20.7	96.7	99.3	35.41	0.07
X	L	1680	188.3	0.2273	605.0	1.809	2.2	5.1	100.0	32.84	3.54
	Integrated age ± 2σ		n=12			247.5	8.7	K2O=5.75%		35.41	0.17
	Plateau ± 2σ	steps D-I	n=6	MSWD=2.48		138.2	17.0 ±28.1		55.9	35.78	0.11
	Isochron±2σ	steps A-L	n=12	MSWD=10.93			$^{40}Ar/^{36}Ar$=	285.8±2.2		35.70	0.07
	MP-04, Biotite, 8.75 mg, J=0.0018963±0.07%, D=1.0014±0.001, NM-220A, Lab#=58002-01										
X	A	650	84.20	0.0374	265.7	2.146	13.6	6.7	0.8	19.61	1.77
X	B	750	19.57	0.0147	25.60	7.04	34.8	61.3	3.5	41.17	0.32
X	C	850	13.53	0.0065	5.439	25.33	78.6	88.1	13.1	40.89	0.10
X	D	920	12.11	0.0082	2.485	19.01	62.0	93.9	20.3	39.04	0.11
X	E	1000	11.65	0.0076	1.513	26.35	66.8	96.2	30.2	38.46	0.08
X	F	1075	12.01	0.0126	2.346	35.35	40.5	94.2	43.6	38.85	0.07
X	G	1110	12.61	0.0387	2.547	16.48	13.2	94.1	49.8	40.68	0.10
X	H	1180	11.36	0.0511	1.783	39.78	10.0	95.4	64.9	37.22	0.07
X	I	1210	10.83	0.0418	1.532	36.96	12.2	95.9	78.9	35.66	0.07
X	J	1250	10.64	0.0596	1.367	43.00	8.6	96.3	95.2	35.17	0.07
X	K	1300	10.90	0.0234	2.230	12.15	21.8	94.0	99.8	35.17	0.14
X	L	1680	533.7	0.5389	1782.5	0.635	0.95	1.3	100.0	24.27	10.07
	Integrated age ± 2σ		n=12			264.2	15.8	K2O=6.12%		37.54	0.17
	Plateau ± 2σ	no plateau	n=0	MSWD=0.00		0.000	0.000±0.000		0.0	0.00	0.00
	Isochron±2σ	steps A-L	n=12	MSWD=511.21			$^{40}Ar/^{36}Ar$=	314.8±2.6		37.58	0.08
	MP-05, Biotite, 9.39 mg, J=0.0018958±0.07%, D=1.0014±0.001, NM-220A, Lab#=58003-01										
X	A	650	102.7	0.1883	337.7	1.802	2.7	2.8	0.7	10.10	2.24
X	B	750	28.74	0.0379	67.37	2.674	13.4	30.7	1.7	30.37	0.69

X	C	850	13.15	0.0082	9.975	25.04	62.1	77.6	10.9	35.06	0.11
X	D	920	10.97	0.0051	1.694	31.12	100.6	95.5	22.4	35.96	0.07
X	E	1000	11.04	0.0102	1.669	34.05	50.0	95.6	35.0	36.22	0.07
X	F	1075	11.11	0.0317	1.705	33.12	16.1	95.5	47.3	36.44	0.07
X	G	1110	10.79	0.0302	1.164	22.29	16.9	96.8	55.5	35.87	0.08
X	H	1180	10.63	0.0408	0.8120	47.08	12.5	97.8	72.9	35.67	0.06
X	I	1210	10.82	0.0828	1.559	34.29	6.2	95.8	85.6	35.59	0.07
X	J	1250	10.67	0.1179	1.241	28.15	4.3	96.7	96.0	35.43	0.07
X	K	1300	11.25	0.0382	3.213	9.74	13.4	91.6	99.6	35.37	0.15
X	L	1680	334.8	0.3221	1101.9	1.029	1.6	2.8	100.0	31.69	6.20
	Integrated age ± 2σ			n=12		270.4	11.8	K2O=5.83%		35.54	0.16
	Plateau ± 2σ	no plateau		n=0	MSWD=0.00	0.000	0.000±0.000		0.0	0.00	0.00
	Isochron±2σ	steps A-L		n=12	MSWD=29.11		$^{40}Ar/^{36}Ar$=	283.4±2.2		35.89	0.07

MP-07, Biotite, 8.6 mg, J=0.0018948±0.07%, D=1.0014±0.001, NM-220A, Lab#=58004-01

X	A	650	128.5	0.4420	422.1	1.593	1.2	2.9	0.6	13.10	2.45
X	B	750	32.84	0.0686	79.09	3.102	7.4	28.8	1.9	32.53	0.72
X	C	850	13.18	0.0128	10.07	24.55	39.9	77.4	11.8	35.02	0.13
X	D	920	10.78	0.0091	1.502	20.28	55.8	95.9	19.9	35.49	0.08
X	E	1000	10.97	0.0168	1.801	24.38	30.4	95.2	29.7	35.84	0.08
X	F	1075	11.03	0.0406	1.755	26.55	12.6	95.3	40.4	36.08	0.07
X	G	1110	10.72	0.0565	1.235	20.20	9.0	96.6	48.5	35.56	0.08
	H	1180	10.50	0.0735	0.8077	42.63	6.9	97.8	65.7	35.24	0.06
	I	1210	10.59	0.1008	1.120	35.51	5.1	97.0	80.0	35.25	0.07
	J	1250	10.60	0.0978	1.200	37.90	5.2	96.7	95.2	35.19	0.07
	K	1300	11.46	0.0374	4.012	10.24	13.7	89.7	99.4	35.28	0.15
X	L	1680	232.5	0.1572	740.0	1.587	3.2	6.0	100.0	47.42	3.90
	Integrated age ± 2σ			n=12		248.5	8.4	K2O=5.86%		35.31	0.17
	Plateau ± 2σ	steps H-K		n=4	MSWD=0.17	126.3	6.4 ±8.1		50.8	35.23	0.09
	Isochron±2σ	steps A-L		n=12	MSWD=24.28		$^{40}Ar/^{36}Ar$=	290.5±2.0		35.50	0.07

MP-08, Biotite, 11.14 mg, J=0.0018943±0.07%, D=1.0014±0.001, NM-220A, Lab#=58005-01

X	A	650	79.52	0.1353	260.5	5.031	3.8	3.2	1.6	8.80	1.36
X	B	750	20.44	0.0279	41.02	11.96	18.3	40.7	5.4	28.60	0.29
X	C	850	12.92	0.0097	8.658	39.14	52.7	80.2	17.9	35.55	0.10
X	D	920	12.07	0.0080	4.968	41.89	64.1	87.8	31.2	36.36	0.08
X	E	1000	11.86	0.0138	4.427	33.46	36.9	89.0	41.9	36.21	0.08
X	F	1075	12.37	0.0321	5.411	32.83	15.9	87.1	52.3	36.97	0.09
X	G	1110	11.42	0.0484	2.811	20.76	10.5	92.8	59.0	36.34	0.10
X	H	1180	11.27	0.0960	2.631	27.05	5.3	93.2	67.6	36.01	0.08
X	I	1210	10.85	0.0913	1.560	43.42	5.6	95.8	81.4	35.67	0.06
X	J	1250	10.60	0.1090	0.9705	43.90	4.7	97.4	95.4	35.43	0.06
X	K	1300	10.98	0.0429	2.151	13.22	11.9	94.2	99.6	35.49	0.13
X	L	1680	291.5	0.2169	949.9	1.278	2.4	3.7	100.0	37.19	4.92
	Integrated age ± 2σ			n=12		313.9	9.7	K2O=5.71%		35.28	0.19
	Plateau ± 2σ	no plateau		n=0	MSWD=0.00	0.000	0.000±0.000		0.0	0.00	0.00
	Isochron±2σ	steps A-L		n=12	MSWD=97.10		$^{40}Ar/^{36}Ar$=	278.3±1.8		36.11	0.08

MP-10, Biotite, 10.71 mg, J=0.001894±0.07%, D=1.0014±0.001, NM-220A, Lab#=58006-01

X	A	650	73.28	0.3009	240.1	2.149	1.7	3.2	0.7	8.17	1.63
X	B	750	31.71	0.0649	74.83	4.383	7.9	30.3	2.2	32.96	0.67
X	C	850	13.44	0.0148	11.40	27.14	34.5	74.9	11.1	34.55	0.11
X	D	920	11.33	0.0122	3.359	27.64	41.9	91.3	20.3	35.48	0.08
X	E	1000	11.00	0.0201	1.983	31.02	25.3	94.7	30.5	35.72	0.07
X	F	1075	11.24	0.0444	2.197	30.00	11.5	94.3	40.4	36.33	0.07
X	G	1110	10.98	0.0727	1.595	21.35	7.0	95.8	47.5	36.08	0.08
X	H	1180	10.63	0.1190	0.8229	31.32	4.3	97.8	57.8	35.68	0.07
X	I	1210	10.59	0.1048	0.8746	40.26	4.9	97.7	71.1	35.48	0.06
X	J	1250	10.54	0.0775	0.7583	59.3	6.6	97.9	90.7	35.40	0.06
X	K	1300	10.90	0.0260	1.785	25.49	19.6	95.2	99.1	35.61	0.09
X	L	1680	153.1	0.1048	484.2	2.603	4.9	6.6	100.0	34.47	2.84

	Integrated age ± 2σ		n=12		302.7	8.3	K2O=5.73%		35.33	0.16
	Plateau ± 2σ	no plateau	n=0	MSWD=0.00	0.0	0.0 ±0.0		0.0	0.00	0.00
	Isochron±2σ	steps A-L	n=12	MSWD=37.30		$^{40}Ar/^{36}Ar$=	281.3±2.1		35.73	0.07
	MP-12, Biotite, 9.73 mg, J=0.0018939±0.07%, D=1.0014±0.001, NM-220A, Lab#=58007-01									
X	A	650	142.5	0.2515	475.3	2.058	2.0	1.5	0.7	7.19	2.77
X	B	750	24.83	0.0346	58.30	6.29	14.7	30.6	2.9	26.15	0.47
X	C	850	12.18	0.0078	10.25	38.13	65.5	75.1	16.1	31.42	0.10
X	D	920	10.48	0.0073	3.880	34.33	70.0	89.1	28.0	32.04	0.07
X	E	1000	10.82	0.0137	4.984	36.01	37.2	86.4	40.5	32.09	0.08
X	F	1075	10.13	0.0299	2.660	36.62	17.1	92.3	53.1	32.10	0.07
X	G	1110	9.770	0.0442	1.992	20.75	11.5	94.0	60.3	31.54	0.09
X	H	1180	9.540	0.0671	1.261	41.35	7.6	96.2	74.6	31.50	0.06
X	I	1210	9.639	0.1079	1.492	33.62	4.7	95.5	86.3	31.61	0.07
X	J	1250	9.694	0.1950	1.324	29.38	2.6	96.1	96.5	32.00	0.07
X	K	1300	10.72	0.1359	5.470	8.90	3.8	85.0	99.5	31.32	0.18
X	L	1680	292.0	0.1893	953.9	1.338	2.7	3.5	100.0	34.67	5.10
	Integrated age ± 2σ		n=12		288.8	8.5	K2O=6.02%		31.49	0.18
	Plateau ± 2σ	no plateau	n=0	MSWD=0.00	0.000	0.000±0.000		0.0	0.00	0.00
	Isochron±2σ	steps A-L	n=12	MSWD=25.38		$^{40}Ar/^{36}Ar$=	286.5±2.0		31.86	0.07
	MP-13, Biotite, 11.01 mg, J=0.001894±0.08%, D=1.0014±0.001, NM-220A, Lab#=58008-01									
X	A	650	72.61	0.1187	236.4	4.161	4.3	3.8	1.6	9.51	1.31
X	B	750	19.07	0.0190	36.36	10.07	26.9	43.6	5.5	28.62	0.29
X	C	850	12.16	0.0061	7.102	41.61	83.9	82.7	21.6	34.53	0.09
X	E	1000	11.59	0.0119	4.511	39.14	42.8	88.5	36.6	35.18	0.08
X	F	1075	11.40	0.0283	3.440	42.22	18.1	91.1	52.5	35.63	0.07
X	G	1110	10.82	0.0764	2.115	19.08	6.7	94.3	59.7	35.01	0.09
X	H	1180	10.63	0.0734	1.536	36.52	6.9	95.8	73.3	34.92	0.07
X	I	1210	10.46	0.0988	1.015	32.13	5.2	97.2	85.1	34.88	0.06
X	J	1250	10.38	0.1874	0.7323	30.32	2.7	98.1	96.2	34.92	0.07
X	K	1300	10.78	0.1017	2.104	9.27	5.0	94.3	99.6	34.89	0.16
X	L	1680	241.8	0.3288	784.1	1.110	1.6	4.2	100.0	34.82	4.59
	Integrated age ± 2σ		n=11		265.6	8.0	K2O=4.89%		34.37	0.18
	Plateau ± 2σ	no plateau	n=0	MSWD=0.00	0.000	0.000±0.000		0.0	0.00	0.00
	Isochron±2σ	steps A-L	n=11	MSWD=64.53		$^{40}Ar/^{36}Ar$=	275.0±2.0		35.17	0.08
	MP-15, Biotite, 8.8 mg, J=0.0018942±0.09%, D=1.0014±0.001, NM-220A, Lab#=58009-01									
X	A	650	320.7	0.0810	1071.6	0.587	6.3	1.3	0.2	13.97	6.67
	B	750	65.71	0.0551	187.1	0.726	9.3	15.9	0.5	35.81	2.15
	C	850	25.07	0.0532	47.02	2.015	9.6	44.6	1.3	38.34	0.65
	D	920	15.33	0.0248	14.82	4.703	20.6	71.4	3.3	37.55	0.28
	E	1000	12.47	0.0152	5.016	13.50	33.5	88.1	8.7	37.69	0.12
	F	1075	11.62	0.0114	2.255	19.70	44.8	94.3	16.6	37.55	0.08
	G	1110	11.52	0.0110	1.979	17.12	46.6	94.9	23.5	37.52	0.10
	H	1180	11.74	0.0465	2.776	19.91	11.0	93.0	31.4	37.47	0.09
	I	1210	12.20	0.1334	4.294	20.08	3.8	89.7	39.4	37.52	0.10
	J	1250	11.77	0.0870	2.847	63.4	5.9	92.9	64.1	37.49	0.07
	K	1300	11.35	0.0137	1.421	92.3	37.3	96.3	99.5	37.48	0.05
	L	1680	248.0	0.2108	797.1	1.165	2.4	5.0	100.0	42.69	4.27
	M	1500	629.3	0.3465	2048.8	0.076	1.5	3.8	100.0	81.15	24.20
	Integrated age ± 2σ		n=13		255.3	11.2	K2O=5.88%		37.49	0.18
	Plateau ± 2σ	steps B-M	n=12	MSWD=0.91	254.7	25.0 ±34.2		99.8	37.51	0.09
	Isochron±2σ	steps A-M	n=13	MSWD=2.01		$^{40}Ar/^{36}Ar$=	295.1±2.1		37.52	0.09
	MP-15-HF, Biotite, 5.77 mg, J=0.001897±0.08%, D=1.0014±0.001, NM-220A, Lab#=58015-01									
X	A	650	75.52	0.0864	235.0	0.704	5.9	8.0	0.4	20.95	2.93
X	B	750	14.49	0.0277	11.44	0.698	18.5	76.7	0.8	38.16	1.63
X	C	850	12.55	0.0438	5.551	1.521	11.7	87.0	1.7	37.47	0.90
X	D	920	10.41	0.0233	-2.7406	2.913	21.9	107.8	3.5	38.54	0.45

X	E	1000	11.18	0.0094	0.7452	12.89	54.1	98.0	11.1	37.63	0.13
	F	1075	10.89	0.0035	0.1217	26.28	147.4	99.7	26.6	37.29	0.08
	G	1110	10.69	0.0036	-0.4694	18.28	142.4	101.3	37.3	37.18	0.10
	H	1180	10.98	0.0243	0.3604	15.84	21.0	99.1	46.5	37.36	0.13
	I	1210	10.81	0.1204	-0.4084	9.35	4.2	101.2	51.9	37.56	0.19
	J	1250	11.21	0.0632	1.333	35.33	8.1	96.5	72.1	37.17	0.08
	K	1300	11.01	0.0024	0.5748	47.59	209.4	98.5	98.8	37.23	0.07
	L	1680	91.88	0.0066	278.4	2.108	77.2	10.4	100.0	33.00	2.22
	Integrated age ± 2σ			n=12		173.5	20.3		K2O=6.09%	37.19	0.15
	Plateau ± 2σ	steps F-L		n=7	MSWD=1.50	154.8	111.5 ±161.7		89.2	37.24	0.11
	Isochron±2σ	steps A-L		n=12	MSWD=3.58		$^{40}Ar/^{36}Ar$=	286.6±3.8		37.30	0.09

MP-22, Biotite, 9.49 mg, J=0.0018946±0.09%, D=1.0014±0.001, NM-220A, Lab#=58010-01

X	A	750	15.00	0.0251	23.90	6.15	20.3	52.9	2.3	27.28	0.35
X	B	850	9.815	0.0062	3.273	38.54	82.5	90.1	16.9	30.40	0.07
X	C	920	9.271	0.0053	0.9119	34.98	96.5	97.1	30.1	30.92	0.06
X	D	1000	9.530	0.0099	1.346	37.86	51.4	95.8	44.1	31.37	0.06
X	E	1075	9.384	0.0134	1.012	41.36	38.1	96.8	59.4	31.21	0.06
X	F	1110	9.163	0.0140	0.5404	30.26	36.3	98.3	70.4	30.93	0.05
X	G	1180	9.087	0.0284	0.4385	39.80	18.0	98.6	84.8	30.78	0.05
X	H	1210	9.047	0.1124	0.3686	22.58	4.5	98.9	92.9	30.74	0.07
X	I	1250	9.143	0.4403	0.9090	13.25	1.2	97.5	97.6	30.62	0.10
X	J	1300	9.994	0.3418	4.292	6.03	1.5	87.6	99.8	30.08	0.24
X	K	1680	415.3	0.2783	1378.4	0.677	1.8	1.9	100.0	27.50	7.79
	Integrated age ± 2σ			n=11		271.5	10.1		K2O=5.80%	30.80	0.12
	Plateau ± 2σ	no plateau		n=0	MSWD=0.00	0.000	0.000±0.000		0.0	0.00	0.00
	Isochron±2σ	steps A-K		n=11	MSWD=30.11		$^{40}Ar/^{36}Ar$=	289.2±3.0		30.92	0.07

MP-24, Biotite, 9.24 mg, J=0.0018951±0.09%, D=1.0014±0.001, NM-220A, Lab#=58011-01

X	A	650	117.3	0.1652	383.6	1.257	3.1	3.4	0.5	13.80	2.71
X	B	750	34.56	0.0249	87.76	2.560	20.5	25.0	1.4	29.67	0.90
X	C	850	13.53	0.0101	11.31	20.71	50.4	75.3	9.3	34.97	0.14
X	D	920	11.00	0.0059	2.062	22.59	87.0	94.5	17.8	35.66	0.08
X	E	1000	11.01	0.0087	1.820	27.81	58.6	95.1	28.2	35.96	0.07
X	F	1075	11.06	0.0169	1.807	34.03	30.2	95.2	40.8	36.15	0.07
	G	1110	10.71	0.0221	1.017	22.86	23.1	97.2	49.2	35.73	0.07
	H	1180	10.53	0.0464	0.5926	37.06	11.0	98.4	62.7	35.55	0.06
	I	1210	10.51	0.0640	0.5911	43.54	8.0	98.4	78.5	35.51	0.06
	J	1250	10.49	0.0776	0.5416	47.48	6.6	98.5	95.4	35.49	0.06
	K	1300	11.50	0.0393	3.637	11.24	13.0	90.7	99.4	35.79	0.15
	L	1680	209.7	0.0980	676.3	1.628	5.2	4.7	100.0	33.66	3.43
	Integrated age ± 2σ			n=12		272.8	13.0		K2O=5.98%	35.47	0.16
	Plateau ± 2σ	steps G-L		n=6	MSWD=2.16	163.8	10.7 ±13.0		60.1	35.56	0.11
	Isochron±2σ	steps A-L		n=12	MSWD=16.78		$^{40}Ar/^{36}Ar$=	287.7±2.1		35.70	0.08

MP-25, Biotite, 11.21 mg, J=0.0018961±0.09%, D=1.0014±0.001, NM-220A, Lab#=58012-01

X	A	650	97.75	0.2458	324.9	1.587	2.1	1.8	0.5	6.05	2.08
X	B	750	31.26	0.0590	81.11	3.038	8.6	23.3	1.4	25.12	0.70
X	C	850	13.49	0.0113	11.95	23.72	45.0	73.8	8.6	34.23	0.13
X	D	920	11.06	0.0084	2.262	26.70	60.6	94.0	16.7	35.68	0.08
X	E	1000	11.06	0.0117	1.931	42.85	43.6	94.9	29.7	36.03	0.07
X	F	1075	11.16	0.0232	1.903	47.47	22.0	95.0	44.2	36.40	0.06
X	G	1110	10.82	0.0279	1.154	26.96	18.3	96.9	52.3	35.98	0.07
X	H	1180	10.65	0.0558	1.023	35.63	9.1	97.2	63.2	35.57	0.06
X	I	1210	10.55	0.0831	0.7087	50.02	6.1	98.1	78.4	35.53	0.06
X	J	1250	10.55	0.0843	0.7034	58.7	6.1	98.1	96.2	35.53	0.06
X	K	1300	11.66	0.0318	4.472	12.00	16.1	88.7	99.8	35.52	0.17
X	L	1680	639.9	0.1728	2122.4	0.569	3.0	2.0	100.0	43.64	11.44
	Integrated age ± 2σ			n=12		329.2	11.2		K2O=5.95%	35.46	0.16
	Plateau ± 2σ	no plateau		n=0	MSWD=0.00	0.000	0.000±0.000		0.0	0.00	0.00

	Isochron±2σ	steps A-L	n=12	MSWD=51.66		$^{40}Ar/^{36}Ar$=	279.8±2.0		35.83	0.08
	MP-30, Biotite, 9.71 mg, J=0.0018966±0.09%, D=1.0014±0.001, NM-220A, Lab#=58013-01									
X	A	650	22.31	0.0201	57.03	29.17	25.3	24.4	14.1	18.82	0.32
X	B	750	25.85	0.0160	49.49	27.00	31.8	43.4	26.9	38.53	0.30
X	C	850	25.34	0.0131	42.91	29.32	39.0	49.9	40.8	43.41	0.26
X	D	920	22.42	0.0134	33.02	17.09	38.2	56.5	48.8	43.40	0.25
X	E	1000	25.70	0.0177	42.30	20.21	28.8	51.3	58.3	45.23	0.27
X	F	1075	23.09	0.0186	36.08	25.17	27.5	53.8	69.9	42.62	0.26
X	G	1110	25.11	0.0297	42.64	17.99	17.2	49.8	78.2	42.90	0.28
X	H	1180	19.82	0.0898	25.99	13.26	5.7	61.3	84.3	41.65	0.26
X	I	1210	15.86	0.1224	14.46	14.68	4.2	73.1	91.0	39.78	0.18
X	J	1250	12.90	0.2327	7.208	16.57	2.2	83.6	98.5	37.05	0.15
X	K	1300	11.20	0.2812	0.5435	2.794	1.8	98.8	99.8	37.97	0.64
X	L	1680	551.2	0.1753	1821.0	0.531	2.9	2.4	100.0	45.05	9.83
	Integrated age ± 2σ		n=12			213.8	10.2	K2O=4.46%		38.55	0.43
	Plateau ± 2σ	no plateau	n=0	MSWD=0.00		0.000	0.000±0.000		0.0	0.00	0.00
	Isochron±2σ	steps A-L	n=12	MSWD=486.12			$^{40}Ar/^{36}Ar$=	310.3±2.2		38.45	0.25
	MP-31, Biotite, 7.32 mg, J=0.0019269±0.13%, D=1.0014±0.001, NM-220B, Lab#=58016-01									
X	A	650	72.39	0.0272	226.4	18.73	18.7	7.6	10.0	19.21	1.05
X	B	750	24.53	0.0242	52.42	23.35	21.0	36.8	22.5	31.60	0.30
X	C	850	18.64	0.0124	27.01	26.61	41.1	57.2	36.5	37.20	0.21
X	D	920	15.27	0.0099	15.67	23.08	51.6	69.7	48.5	37.11	0.16
X	E	1000	19.39	0.0146	28.87	23.69	34.9	56.0	60.8	37.89	0.23
X	F	1075	19.45	0.0193	28.77	23.73	26.5	56.3	73.0	38.20	0.21
X	G	1110	19.84	0.0231	29.98	14.25	22.1	55.3	80.3	38.29	0.26
X	H	1180	16.47	0.0467	18.84	16.78	10.9	66.2	88.8	38.03	0.19
X	I	1210	12.91	0.1349	8.703	11.88	3.8	80.2	94.8	36.11	0.18
X	J	1250	11.24	0.3369	3.229	8.73	1.5	91.8	99.2	36.00	0.16
X	K	1300	8.449	0.5228	-7.5357	1.472	0.98	126.9	99.9	37.41	1.16
X	L	1680	947.7	0.4075	3163.8	0.179	1.3	1.4	100.0	44.75	22.24
	Integrated age ± 2σ		n=12			192.5	11.0	K2O=5.24%		35.01	0.49
	Plateau ± 2σ	steps C-F	n=4	MSWD=0.00		0.0	0.0 ±0.0		0.0	0.00	0.00
	Isochron±2σ	steps C-F	n=4	MSWD=4.21			$^{40}Ar/^{36}Ar$=	312.3±9.7		36.15	0.81
	MP-32, Biotite, 4.81 mg, J=0.0023828±0.07%, D=1.006±0.001, NM-227L, Lab#=59269-01									
X	A	2	58.17	0.0519	60.40	1.379	9.8	69.3	0.5	167.91	0.74
X	B	3	70.69	0.0098	8.687	6.15	52.3	96.4	2.6	275.33	0.44
X	C	4	23.14	0.0069	3.844	10.98	73.8	95.1	6.4	93.49	0.17
X	D	5	21.53	0.0066	2.774	9.47	77.4	96.2	9.7	88.12	0.15
X	E	6	17.99	0.0161	1.585	36.56	31.8	97.4	23.0	74.86	0.11
X	F	8	13.78	0.0212	1.365	39.44	24.0	97.1	38.2	57.41	0.09
X	G	10	12.81	0.0263	1.186	32.82	19.4	97.3	51.5	53.53	0.08
X	H	13	9.954	0.0241	1.402	35.35	21.1	95.9	66.8	41.11	0.06
X	I	16	11.15	0.0238	1.985	24.63	21.5	94.8	77.9	45.49	0.08
X	J	18	13.00	0.0264	2.625	15.87	19.3	94.0	85.3	52.52	0.10
X	K	30	9.985	0.0254	2.693	30.17	20.1	92.0	100.0	39.62	0.08
	Integrated age ± 2σ		n=11			242.8	23.9	K2O=8.14%		62.37	0.17
	Plateau ± 2σ	no plateau	n=0	MSWD=0.00		0.000	0.000±0.000		0.0	0.00	0.00
	Isochron±2σ	steps A-K	n=11	√MSWD=1841.03			$^{40}Ar/^{36}Ar$=	8176.2±223.2		-1.96	0.04
	MP-37, Biotite, 4.5 mg, J=0.0023831±0.08%, D=1.006±0.001, NM-227L, Lab#=59270-01									
X	A	1	167.9	-0.5409	385.4	0.010	-	32.1	0.0	221.24	50.01
X	B	1	59.72	0.0154	197.0	0.291	33.2	2.5	0.1	6.53	3.08
X	C	2	20.70	0.0125	56.69	2.695	40.9	19.0	1.0	17.10	0.61
X	D	3	9.153	0.0042	9.587	14.71	120.3	69.0	6.0	27.32	0.12
X	E	4	7.837	0.0034	3.531	26.94	151.3	86.7	15.4	29.36	0.07
X	F	5	7.665	0.0037	2.963	21.22	138.4	88.6	23.0	29.34	0.07
	G	6	7.526	0.0103	2.330	52.4	49.8	90.9	43.1	29.55	0.05
	H	8	7.405	0.0191	1.801	44.6	26.8	92.8	61.4	29.70	0.05

	I	10	7.374	0.0249	1.811	26.35	20.5	92.8	72.9	29.56	0.06
	J	13	7.413	0.0301	1.819	21.40	16.9	92.8	82.6	29.72	0.07
	K	16	7.534	0.0295	2.172	11.84	17.3	91.5	88.1	29.79	0.08
	L	18	7.559	0.0431	2.475	8.31	11.8	90.4	92.0	29.52	0.09
	M	30	7.732	0.0469	2.913	10.80	10.9	88.9	97.2	29.70	0.09
	N	35	7.307	0.0466	1.382	5.64	11.0	94.5	100.0	29.82	0.11
	Integrated age ± 2σ			n=14		247.2	28.5	K2O=8.85%		29.29	0.11
	Plateau ± 2σ	steps G-N		n=8	MSWD=2.27	181.3	28.6	±25.9	73.4	29.65	0.09
	Isochron±2σ	steps A-N		n=14	MSWD=14.31		$^{40}Ar/^{36}Ar$=	247.8±3.2		30.04	0.07
	MP-38, Biotite, 4.3 mg, J=0.0023834±0.08%, D=1.006±0.001, NM-227L, Lab#=59271-01										
X	A	1	-1.2316	0.2698	63.08	-0.008	1.9	1599.4	0.0	-88.77	49.15
X	B	1	23.50	0.0867	61.47	0.083	5.9	22.7	0.0	23.12	5.64
X	C	2	17.27	0.0429	44.74	0.575	11.9	23.4	0.2	17.57	1.18
X	D	3	11.51	0.0094	17.04	4.37	54.1	56.2	1.8	27.99	0.26
X	E	4	8.686	0.0037	6.363	14.33	137.2	78.3	6.9	29.41	0.10
	F	5	8.049	0.0027	3.825	15.28	189.9	85.9	12.4	29.90	0.09
	G	6	7.712	0.0080	2.486	46.0	63.6	90.5	30.0	30.15	0.05
	H	8	7.601	0.0202	2.221	42.22	25.2	91.4	47.3	30.02	0.06
	I	10	7.506	0.0276	1.847	30.73	18.5	92.7	60.7	30.08	0.05
	J	13	7.490	0.0383	1.856	27.45	13.3	92.7	73.2	30.01	0.06
	K	16	7.562	0.0450	2.011	20.10	11.3	92.2	82.8	30.12	0.06
	L	18	7.626	0.0308	2.233	11.97	16.5	91.4	88.7	30.11	0.08
X	M	30	8.001	0.0453	3.711	14.43	11.3	86.3	95.9	29.85	0.08
X	N	35	7.358	0.0478	1.521	8.06	10.7	93.9	100.0	29.87	0.08
	Integrated age ± 2σ			n=14		235.6	21.5	K2O=8.83%		29.94	0.11
	Plateau ± 2σ	steps F-L		n=7	MSWD=1.52	193.8	42.6	±129.9	82.2	30.07	0.08
	Isochron±2σ	steps A-N		n=14	MSWD=5.02		$^{40}Ar/^{36}Ar$=	258.7±5.1		30.40	0.09

Notes:
x (or i) symbol preceding sample ID denotes analyses excluded from plateau (or isochron) age calculations.
Isotopic ratios corrected for blank, radioactive decay, and mass discrimination, not corrected for interfering reactions.
Errors quoted for individual analyses include analytical error only, without interfering reaction or J uncertainties.

Age calculations:
Ages calculated relative to FC-2 Fish Canyon Tuff sanidine interlaboratory standard (28.201 Ma, Kuiper et al, 2008).
Integrated age calculated by summing isotopic measurements of all steps.
Integrated age error calculated by quadratically combining errors of isotopic measurements of all steps.
Plateau age or preferred age calculated for the indicated steps by weighting each step by the inverse of the variance.
Plateau age error is inverse-variance-weighted mean error (Taylor, 1982) times root MSWD where MSWD>1.
MSWD values are calculated for n-1 degrees of freedom for plateau age.
Isochron ages, $^{40}Ar/^{36}Ar_i$ and MSWD values calculated from regression results obtained by the methods of York (1969).
Decay constants and isotopic abundances after Min et al. (2000).
Weight percent K_2O calculated from ^{39}Ar signal, sample weight, and instrument sensitivity.
All errors reported at ±2s, unless otherwise noted.

Sample preparation and irradiation:
Biotite separates prepared using crushing, dilute HCl acid treatment, Franz magnetic separator, and hand-picking techniques.
Samples were loaded into machined Al discs and irradiated in 3 separate positions (NM-220A and B and NM-227L) for 10 hours at Nuclear Science Center, College Station, TX or the Triga Reactor
Neutron flux monitor Fish Canyon Tuff sanidine (FC-2).

Instrumentation:
Mass Analyzer Products 215-50 mass spectrometer on line with automated all-metal extraction system.
Samples were step-heated using a Mo double-vacuum resistance furnace (heating duration 10 minutes), or CO2 laser (heating duration 1 minutes).
Reactive gases removed during furnace (laser) analysis by reaction with 3 (2) SAES GP-50 getters, 2 (1) operated at ~450°C and 1 at 20°C. Gas also exposed to a W filament operated at ~2000°C.

Analytical parameters:

Electron multiplier sensitivity ranged from 5.16 x 10^{-17} moles/pA to 6.26 x 10^{-17} moles /pA.

Total system blank and background for the furnace averaged 596, 3.49, .679, 2.28, 8.75 x 10^{-18} moles.
at masses 40, 39, 38, 37, and 36 respectively

Total system blank and background for the laser averaged 193, 5.67, 0.366, 0.963, 4.30 x 10^{-18} moles.
at masses 40, 39, 38, 37, and 36 respectively

J-factors determined to a precision of ± 0.1% by CO_2 laser-fusion of 6 single crystals from each of 10 radial positions around the irradiation tray.

Correction factors for interfering nuclear reactions were determined using K-glass and CaF_2 and are as follows:

$(^{39}Ar/^{37}Ar)_{Ca}$ = 0.00068 ± 2e-05

$(^{36}Ar/^{37}Ar)_{Ca}$ = 0.00028 ± 1e-05

$(^{38}Ar/^{39}Ar)_{K}$ = 0.013 ± 5e-4

$(^{40}Ar/^{39}Ar)_{K}$ = 0 ± 4e-4

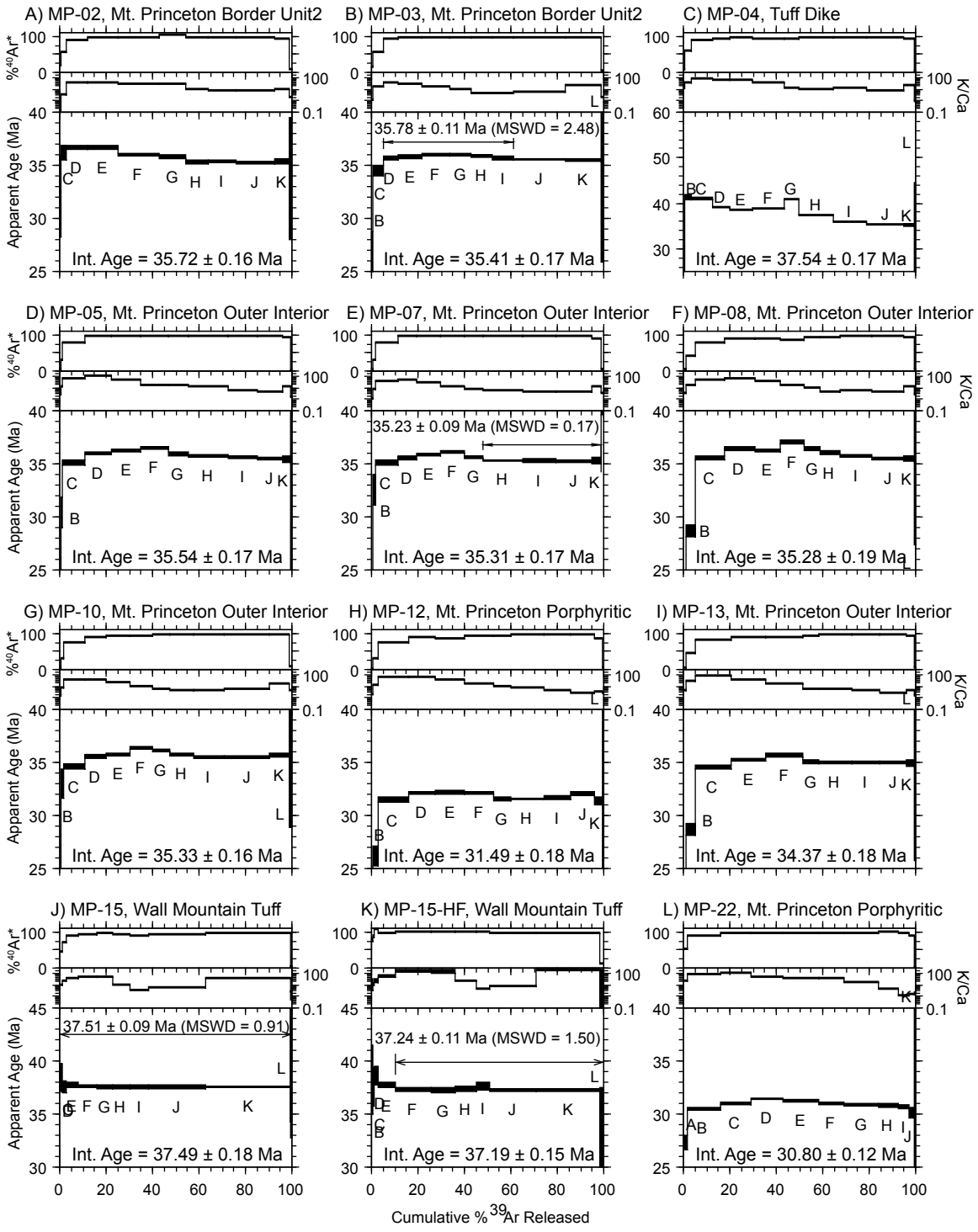

Figure 2.3.2 - Age spectra and K/Ca and radiogenic yield (%40Ar*) auxiliary plots for the Mt. Aetna caldera complex biotite. All errors are reported at 2σ and do not include error in decay constant.

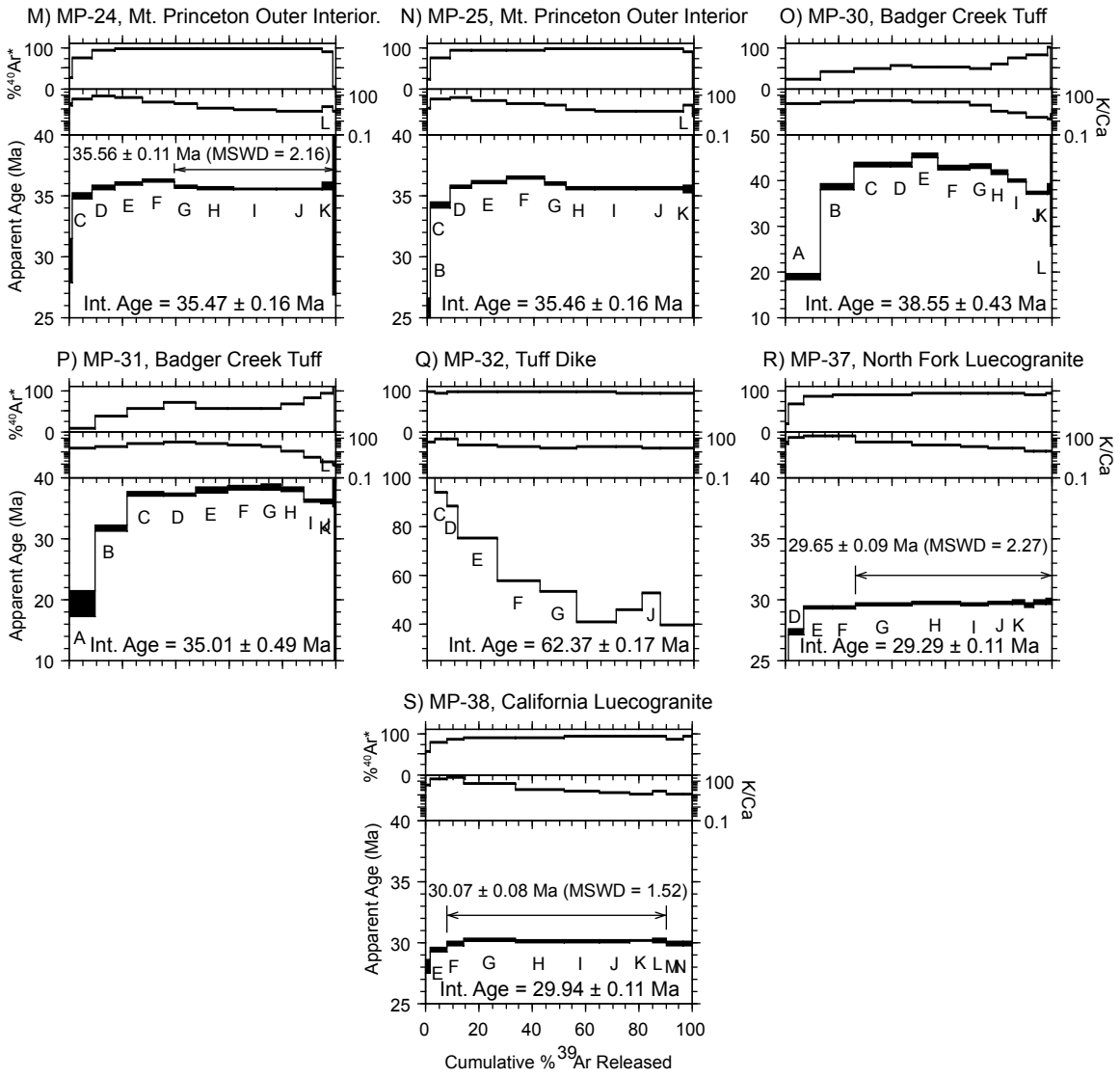

Figure 2.3.2 continued

Table 2.3.3 - K-feldpsar $^{40}Ar/^{39}Ar$ analytical data.

	ID	Power (°C)	$^{40}Ar/^{39}Ar$	$^{37}Ar/^{39}Ar$	$^{36}Ar/^{39}Ar$ (x 10^{-3})	$^{39}Ar_K$ (x 10^{-15} mol)	K/Ca	$^{40}Ar^*$ (%)	^{39}Ar (%)	Age (Ma)	±1σ (Ma)
	MP-05, K-Feldspar, 17.19 mg, J=0.0019532±0.05%, D=1.0014±0.001, NM-220C, Lab#=58028-01										
X	A	530	1065.2	0.0481	3572.1	0.67	10.6	0.9	0.1	33.96	16.76
X	B	530	208.1	-0.0239	673.3	0.72	-	4.4	0.2	32.45	4.77
X	C	580	129.6	-0.0304	403.8	0.98	-	7.9	0.4	36.24	2.92
X	D	580	60.75	-0.0145	174.8	1.46	-	14.9	0.6	32.15	1.55
X	E	580	46.14	0.0119	123.0	1.94	43.0	21.2	0.9	34.61	1.00
X	F	630	60.27	0.0045	174.6	1.42	114.2	14.4	1.2	30.72	1.62
X	G	630	28.09	-0.0096	61.13	2.32	-	35.7	1.5	35.48	0.76
X	H	630	26.37	0.0200	55.52	3.00	25.5	37.8	2.0	35.27	0.69
X	I	680	42.73	-0.0027	109.9	2.10	-	24.0	2.4	36.24	0.95
X	J	680	19.67	0.0269	33.00	3.13	19.0	50.4	2.9	35.11	0.47
X	K	680	19.46	0.0039	32.59	4.25	129.3	50.5	3.5	34.78	0.39
X	L	730	21.80	0.0124	39.51	2.53	41.2	46.4	4.0	35.80	0.62
X	M	730	16.04	0.0098	20.74	4.17	51.9	61.8	4.6	35.07	0.33
X	N	780	17.04	0.0030	23.53	4.66	169.6	59.2	5.4	35.68	0.35
X	O	780	14.60	0.0135	15.40	6.58	37.7	68.8	6.4	35.56	0.25
X	P	830	13.94	0.0113	13.74	6.40	45.1	70.9	7.5	34.95	0.22
X	Q	830	12.07	0.0073	7.252	8.3	69.5	82.2	8.8	35.12	0.16
X	R	880	12.87	0.0104	9.484	7.4	49.1	78.2	10.0	35.62	0.21
X	S	880	11.69	0.0073	5.880	9.5	69.6	85.1	11.5	35.22	0.15
X	T	930	14.22	0.0078	14.41	8.1	65.7	70.0	12.8	35.24	0.21
X	U	930	13.10	0.0087	10.71	10.3	58.7	75.8	14.5	35.14	0.17
X	V	980	19.95	0.0121	34.35	8.9	42.3	49.1	15.9	34.67	0.31
X	W	980	17.40	0.0074	25.55	11.7	69.1	56.6	17.8	34.86	0.26
X	X	1030	29.29	0.0041	65.53	11.2	125.9	33.9	19.6	35.11	0.43
X	Y	1030	22.35	0.0030	42.47	14.3	171.0	43.8	21.9	34.66	0.29
X	Z	1080	34.56	0.0017	83.91	15.2	294.6	28.2	24.4	34.55	0.51
X	AA	1080	22.25	0.0067	42.42	18.7	75.9	43.6	27.4	34.36	0.28
X	AB	1130	27.92	0.0061	60.77	23.5	83.2	35.6	31.2	35.23	0.34
X	AC	1130	19.96	0.0111	34.25	24.5	46.1	49.3	35.2	34.80	0.25
X	AD	1180	19.12	0.0098	32.41	27.6	51.8	49.9	39.6	33.78	0.24
X	AE	1180	19.08	0.0074	31.22	52.9	68.5	51.6	48.1	34.86	0.19
X	AF	1180	17.08	0.0071	24.59	62.4	71.9	57.4	58.2	34.72	0.16
X	AG	1180	15.83	0.0073	19.75	71.8	70.3	63.1	69.8	35.34	0.15
X	AH	1280	13.32	0.0062	11.39	82.8	82.0	74.7	83.1	35.22	0.10
X	AI	1330	13.94	0.0074	13.27	72.4	69.1	71.9	94.8	35.46	0.11
X	AJ	1400	15.13	0.0103	17.00	14.9	49.5	66.8	97.2	35.75	0.18
X	AK	1750	19.76	0.0117	32.11	17.3	43.8	52.0	100.0	36.33	0.25
	Integrated age ± 2σ			n=37		619.9	68.5	K2O=7.09%		35.06	0.34
	Plateau ± 2σ	no plateau		n=0	MSWD=0.00	0.000	0.000±0.000		0.0	0.00	0.00
	Isochron±2σ	steps A-AK		n=37	MSWD=3.24		$^{40}Ar/^{36}Ar$=	293.5±1.2		35.32	0.12
	MP-08, K-Feldspar, 17.71 mg, J=0.0019508±0.06%, D=1.0014±0.001, NM-220C, Lab#=58031-01										
X	A	530	845.9	0.0468	2772.9	0.595	10.9	3.1	0.1	92.17	14.32
X	B	530	150.4	0.0311	476.9	0.73	16.4	6.3	0.2	33.60	3.50
X	C	580	98.06	0.0515	287.1	0.89	9.9	13.5	0.3	46.63	2.79
X	D	580	46.45	0.0433	124.7	1.23	11.8	20.7	0.5	33.94	1.48
X	E	580	35.30	0.0249	84.41	1.57	20.5	29.3	0.7	36.57	1.02
X	F	630	46.71	0.0043	119.2	1.11	119.1	24.6	0.8	40.56	1.43
X	G	630	21.95	0.0221	39.24	1.82	23.1	47.2	1.1	36.59	0.73
X	H	630	20.42	0.0172	34.51	2.50	29.6	50.0	1.4	36.11	0.60
X	I	680	33.46	0.0434	77.30	2.07	11.8	31.7	1.7	37.50	0.90
X	J	680	16.42	0.0328	20.49	3.15	15.6	63.1	2.1	36.62	0.41
X	K	680	15.17	0.0299	16.49	4.37	17.1	67.9	2.7	36.39	0.32
X	L	730	17.39	0.0401	23.86	2.95	12.7	59.5	3.1	36.54	0.50
X	M	730	13.05	0.0234	9.995	4.76	21.8	77.4	3.8	35.67	0.26

X	N	780	17.92	0.0283	26.02	6.34	18.0	57.1	4.6	36.16	0.30
X	O	780	11.92	0.0227	6.468	8.8	22.5	84.0	5.8	35.35	0.15
X	P	830	12.49	0.0212	8.429	8.5	24.1	80.0	7.0	35.32	0.19
X	Q	830	11.04	0.0225	3.733	11.1	22.7	90.0	8.5	35.12	0.12
X	R	880	11.92	0.0206	6.309	9.9	24.7	84.4	9.9	35.54	0.14
X	S	930	13.95	0.0161	12.98	16.1	31.8	72.5	12.0	35.74	0.15
X	T	980	12.61	0.0157	8.982	17.2	32.5	78.9	14.4	35.17	0.13
X	U	1030	13.91	0.0133	13.26	20.6	38.3	71.8	17.2	35.31	0.15
X	V	1080	14.65	0.0099	16.09	20.6	51.4	67.5	20.0	34.98	0.16
X	W	1130	17.78	0.0153	26.54	28.1	33.4	55.9	23.8	35.13	0.20
X	X	1130	18.17	0.0117	28.22	29.5	43.8	54.1	27.8	34.75	0.20
	Y	1180	19.39	0.0167	31.86	29.2	30.5	51.4	31.8	35.24	0.22
	Z	1180	18.70	0.0131	29.46	50.7	39.0	53.4	38.7	35.32	0.19
	AA	1220	16.18	0.0100	20.84	25.4	51.2	61.9	42.2	35.39	0.17
	AB	1250	14.30	0.0083	14.50	56.9	61.4	70.0	49.9	35.40	0.12
	AC	1280	13.73	0.0063	12.30	113.5	80.4	73.5	65.4	35.67	0.10
	AD	1310	14.43	0.0062	14.49	122.7	83.0	70.3	82.1	35.84	0.11
X	AE	1350	16.09	0.0099	19.67	61.1	51.6	63.9	90.4	36.30	0.14
X	AF	1450	18.02	0.0139	25.48	14.2	36.7	58.2	92.4	37.03	0.23
X	AG	1750	17.86	0.0110	25.20	56.1	46.5	58.3	100.0	36.79	0.16
	Integrated age ± 2σ			n=33		734.1	44.6	K2O=8.16%		35.76	0.26
	Plateau ± 2σ steps Y-AD			n=6	MSWD=2.75	398.4	67.7 ±42.9		54.3	35.57	0.19
	Isochron±2σ steps A-AG			n=33	MSWD=6.97		$^{40}Ar/^{36}Ar$=	301.3±1.6		35.28	0.12

MP-09, K-Feldspar, 14.81 mg, J=0.0019514±0.06%, D=1.0014±0.001, NM-220C, Lab#=58032-01

X	A	530	830.9	-0.0280	1741.0	0.97	-	38.1	0.1	880.27	7.65
X	B	530	88.40	0.0176	235.8	0.81	28.9	21.2	0.3	65.65	2.44
X	C	580	50.92	-0.0377	104.4	1.10	-	39.4	0.4	70.22	1.42
X	D	580	28.84	-0.0731	55.89	0.85	-	42.7	0.6	43.45	1.30
X	E	580	24.36	0.0264	46.02	1.73	19.4	44.2	0.8	38.01	0.85
X	F	630	30.27	0.0742	45.57	1.57	6.9	55.5	1.1	59.07	0.87
X	G	630	17.61	0.0602	25.01	2.03	8.5	58.0	1.4	36.12	0.65
X	H	630	16.72	0.0479	25.20	2.57	10.7	55.5	1.8	32.80	0.52
X	I	680	22.50	0.0547	31.61	1.77	9.3	58.5	2.1	46.39	0.74
X	J	680	13.43	0.0391	13.02	2.61	13.1	71.3	2.5	33.87	0.45
X	K	680	12.80	0.0367	11.86	3.52	13.9	72.6	3.0	32.88	0.33
X	L	730	16.16	0.0220	16.85	2.19	23.2	69.2	3.4	39.49	0.54
X	M	730	11.48	0.0231	5.594	3.59	22.0	85.6	3.9	34.73	0.29
X	N	780	18.07	0.0057	22.66	5.39	89.6	62.9	4.7	40.14	0.33
X	O	780	10.63	0.0036	3.491	6.8	141.9	90.3	5.8	33.94	0.17
X	P	830	11.17	0.0052	4.362	6.33	99.0	88.5	6.8	34.93	0.18
X	Q	830	10.47	-0.0025	2.567	8.8	-	92.7	8.1	34.31	0.14
X	R	880	11.94	-0.0069	6.100	8.7	-	84.9	9.5	35.82	0.17
X	S	880	10.09	-0.0018	1.394	11.9	-	95.9	11.3	34.20	0.11
X	T	930	11.22	0.0007	4.085	10.4	694.6	89.2	12.9	35.39	0.12
X	U	930	10.16	0.0020	1.497	14.0	253.9	95.6	15.1	34.35	0.10
X	V	980	11.01	0.0028	4.065	11.7	182.8	89.1	16.9	34.66	0.12
X	W	980	10.22	0.0039	1.959	16.1	129.6	94.3	19.4	34.10	0.11
X	X	1030	11.23	0.0011	5.067	12.0	454.6	86.7	21.2	34.42	0.13
X	Y	1030	10.70	0.0051	3.579	14.8	99.3	90.1	23.5	34.08	0.12
X	Z	1080	12.27	-0.0053	8.272	11.2	-	80.1	25.2	34.72	0.16
X	AA	1080	11.59	0.0021	5.664	16.1	243.3	85.6	27.7	35.06	0.12
X	AB	1130	13.63	0.0018	11.21	12.8	283.7	75.7	29.7	36.46	0.15
X	AC	1130	11.84	0.0014	5.834	16.2	354.6	85.4	32.2	35.75	0.13
X	AD	1180	12.69	0.0023	7.366	8.8	221.5	82.8	33.6	37.15	0.18
X	AE	1180	12.83	0.0022	7.443	18.0	228.5	82.9	36.4	37.57	0.14
X	AF	1180	13.10	0.0040	7.406	20.4	126.3	83.3	39.5	38.55	0.13
X	AG	1180	13.27	0.0025	7.506	10.3	207.6	83.3	41.1	39.01	0.15
X	AH	1280	12.82	0.0045	5.023	99.8	114.0	88.4	56.5	40.02	0.08
X	AI	1330	13.58	0.0056	7.189	157.6	91.2	84.3	80.9	40.42	0.09
X	AJ	1380	13.77	0.0056	7.848	53.7	90.4	83.2	89.2	40.43	0.10
X	AK	1550	15.13	0.0057	10.58	46.1	89.2	79.3	96.3	42.36	0.12
X	AL	1750	15.06	0.0051	11.87	24.0	99.8	76.7	100.0	40.76	0.14

	Integrated age ± 2σ		n=38		647.2	104.5	K2O=8.60%		40.02	0.18
	Plateau ± 2σ	no plateau	n=0	MSWD=0.00	0.000	0.000±0.000		0.0	0.00	0.00
	Isochron±2σ	steps A-AL	n=38	MSWD=178.09		$^{40}Ar/^{36}Ar$=	459.8±3.3		33.99	0.10
	MP-10, K-Feldspar, 16.62 mg, J=0.0019536±0.07%, D=1.0014±0.001, NM-220C, Lab#=58034-01									
X	A	530	185.3	0.0459	420.3	1.56	11.1	33.0	0.3	206.33	2.87
X	B	530	28.35	0.0288	60.44	1.34	17.7	37.0	0.5	37.10	1.10
X	C	580	31.12	0.0351	42.45	2.42	14.5	59.7	0.9	65.26	0.68
X	D	580	12.99	0.0336	14.37	2.15	15.2	67.3	1.2	30.97	0.46
X	E	630	21.61	0.0641	22.04	4.32	8.0	69.9	2.0	53.20	0.35
X	F	630	10.66	0.0765	7.618	3.06	6.7	78.9	2.5	29.82	0.35
X	G	680	14.69	0.0659	13.22	4.22	7.7	73.4	3.2	38.17	0.29
X	H	680	9.576	0.0451	4.362	3.83	11.3	86.6	3.8	29.38	0.23
X	I	730	10.61	0.0309	5.330	4.14	16.5	85.2	4.5	32.00	0.23
X	J	730	8.998	0.0319	2.713	4.58	16.0	91.1	5.2	29.05	0.22
X	K	780	9.150	0.0197	2.705	4.15	25.9	91.3	5.9	29.59	0.19
X	L	780	8.741	0.0270	2.043	4.60	18.9	93.1	6.7	28.84	0.21
X	M	830	9.068	0.0262	2.545	3.70	19.5	91.7	7.3	29.47	0.27
X	N	830	8.842	0.0218	1.832	3.88	23.4	93.9	7.9	29.42	0.24
X	O	880	9.456	0.0187	3.291	2.95	27.3	89.7	8.4	30.06	0.30
X	P	880	9.015	0.0281	2.388	3.48	18.2	92.2	9.0	29.45	0.24
X	Q	930	9.951	0.0445	5.163	2.93	11.5	84.7	9.5	29.86	0.34
X	R	930	9.474	0.0127	3.757	3.83	40.2	88.3	10.1	29.64	0.26
X	S	980	11.02	0.0241	8.346	3.76	21.1	77.6	10.8	30.31	0.27
X	T	980	10.25	0.0058	5.814	5.48	87.7	83.2	11.7	30.23	0.21
X	U	1030	12.03	0.0149	10.76	6.29	34.3	73.6	12.7	31.36	0.22
X	V	1030	11.23	0.0084	7.493	10.5	61.0	80.3	14.4	31.92	0.13
X	W	1080	12.30	0.0178	10.91	13.3	28.7	73.8	16.6	32.13	0.15
X	X	1080	11.26	0.0130	7.333	15.7	39.3	80.8	19.2	32.21	0.11
X	Y	1130	12.04	0.0136	9.421	15.7	37.6	76.9	21.8	32.76	0.13
X	Z	1130	11.74	0.0127	8.432	27.1	40.1	78.8	26.3	32.74	0.12
X	AA	1180	11.52	0.0147	7.900	22.0	34.7	79.7	30.0	32.51	0.12
X	AB	1180	10.86	0.0111	5.676	55.4	45.8	84.5	39.2	32.50	0.09
X	AC	1180	10.43	0.0082	4.353	64.8	62.3	87.7	49.9	32.39	0.08
	AD	1280	10.44	0.0063	3.465	177.8	80.9	90.2	79.4	33.35	0.06
	AE	1330	10.51	0.0077	3.603	66.0	66.0	89.9	90.3	33.43	0.09
	AF	1380	10.70	0.0208	4.310	10.1	24.5	88.1	92.0	33.37	0.13
	AG	1550	10.53	0.0139	4.001	18.2	36.7	88.8	95.0	33.09	0.11
	AH	1750	11.00	0.0094	5.362	30.3	54.1	85.6	100.0	33.33	0.09
	Integrated age ± 2σ		n=34		603.4	41.7	K2O=7.14%		33.42	0.14
	Plateau ± 2σ	steps AD-AH	n=5	MSWD=1.66	302.3	70.4 ±45.0		50.1	33.33	0.11
	Isochron±2σ	steps A-AH	n=34	MSWD=117.58		$^{40}Ar/^{36}Ar$=	436.6±4.3		30.11	0.11
	MP-12, K-Feldspar, 15.56 mg, J=0.0019548±0.06%, D=1.0014±0.001, NM-220C, Lab#=58036-01									
X	A	530	217.5	-0.0006	624.5	1.37	-	15.2	0.2	114.29	3.78
X	B	530	29.69	0.0010	79.36	2.73	532.1	21.0	0.6	22.16	0.71
X	C	580	15.45	0.0166	29.30	3.26	30.8	43.9	1.0	24.11	0.42
X	D	580	10.54	0.0119	14.91	4.21	42.8	58.2	1.6	21.78	0.33
X	E	580	9.678	0.0097	11.75	5.12	52.5	64.1	2.3	22.04	0.23
X	F	630	9.964	0.0266	10.15	3.73	19.2	69.9	2.8	24.73	0.28
X	G	630	8.095	0.0073	5.008	5.95	69.4	81.7	3.7	23.48	0.17
X	H	680	9.188	0.0190	7.127	7.2	26.9	77.1	4.7	25.14	0.15
X	I	680	7.698	0.0115	3.045	9.3	44.2	88.3	6.0	24.13	0.11
X	J	680	7.699	0.0081	2.490	10.8	62.9	90.4	7.5	24.71	0.10
X	K	730	8.130	0.0094	3.113	6.03	54.4	88.7	8.3	25.59	0.15
X	L	730	7.477	0.0122	1.360	9.3	41.9	94.6	9.6	25.11	0.10
X	M	780	7.890	0.0059	2.191	9.6	86.8	91.8	10.9	25.70	0.11
X	N	780	7.517	0.0052	0.9242	13.3	98.5	96.4	12.8	25.71	0.08
X	O	830	7.804	0.0054	1.566	12.5	94.0	94.1	14.5	26.05	0.09
X	P	830	7.583	0.0010	0.7160	15.0	520.0	97.2	16.6	26.15	0.07
X	Q	880	8.154	0.0046	2.200	16.5	112.1	92.0	18.9	26.62	0.08
X	R	880	7.847	0.0019	1.289	16.1	262.7	95.1	21.1	26.49	0.07

X	S	930	8.644	0.0033	3.792	11.3	154.7	87.0	22.7	26.69	0.11
X	T	930	8.453	0.0058	2.983	12.6	88.3	89.6	24.4	26.86	0.11
X	U	980	10.13	0.0065	8.777	10.1	78.0	74.4	25.8	26.75	0.13
X	V	980	9.638	0.0050	7.324	12.6	103.0	77.5	27.6	26.52	0.13
X	W	1030	11.99	0.0057	15.11	11.9	89.7	62.7	29.2	26.68	0.19
X	X	1030	11.07	0.0031	11.88	17.1	164.9	68.3	31.6	26.83	0.16
X	Y	1080	12.83	0.0056	17.88	19.7	90.9	58.8	34.4	26.78	0.18
X	Z	1080	11.60	0.0075	13.35	27.4	67.9	66.0	38.2	27.15	0.13
X	AA	1130	12.30	0.0057	15.65	32.9	89.4	62.4	42.7	27.23	0.13
X	AB	1130	11.21	0.0077	11.72	40.0	66.1	69.1	48.3	27.48	0.11
X	AC	1180	10.59	0.0079	9.377	20.9	64.9	73.8	51.2	27.73	0.13
X	AD	1180	10.21	0.0077	7.839	39.3	66.0	77.3	56.6	27.99	0.10
X	AE	1180	9.871	0.0056	6.536	42.8	90.6	80.4	62.6	28.16	0.08
X	AF	1180	9.982	0.0053	6.551	43.3	97.0	80.6	68.6	28.54	0.08
X	AG	1280	10.58	0.0034	7.612	69.9	150.2	78.7	78.3	29.52	0.08
X	AH	1330	10.57	0.0027	7.226	116.2	185.7	79.8	94.5	29.90	0.07
X	AI	1380	10.88	0.0066	7.977	20.4	77.5	78.3	97.3	30.20	0.12
X	AJ	1450	11.76	0.0239	9.900	2.47	21.4	75.1	97.6	31.31	0.36
X	AK	1550	11.81	0.0095	9.520	6.19	53.6	76.2	98.5	31.87	0.19
X	AL	1750	13.05	0.0118	13.20	10.8	43.1	70.1	100.0	32.41	0.19
	Integrated age ± 2σ			n=38		719.8	88.3	K2O=9.09%		27.99	0.14
	Plateau ± 2σ	no plateau		n=0	MSWD=0.00	0.000	0.000±0.000		0.0	0.00	0.00
	Isochron±2σ	steps A-AL		n=38	MSWD=184.34		$^{40}Ar/^{36}Ar$=	353.2±2.3		26.02	0.07

MP-13, K-Feldspar, 14.88 mg, J=0.0019825±0.07%, D=1.0014±0.001, NM-220D, Lab#=58038-01

X	A	530	383.6	-0.0028	1053.6	0.86	-	18.8	0.1	245.21	5.77
X	B	530	48.77	0.0020	137.5	0.95	250.5	16.7	0.3	29.25	1.73
X	C	580	30.47	-0.0034	69.69	1.14	-	32.4	0.4	35.46	1.33
X	D	580	17.59	0.0189	33.00	1.64	27.0	44.5	0.6	28.20	0.68
X	E	580	15.73	-0.0003	25.80	2.09	-	51.5	0.9	29.15	0.54
X	F	630	16.08	0.0468	23.53	1.55	10.9	56.7	1.1	32.78	0.79
X	G	630	12.21	0.0293	12.39	2.62	17.4	70.0	1.5	30.75	0.40
X	H	630	11.87	0.0122	11.00	3.54	41.9	72.6	2.0	30.99	0.34
X	I	680	14.01	0.0383	14.89	2.33	13.3	68.6	2.3	34.50	0.48
X	J	680	10.90	0.0205	5.995	3.89	24.9	83.7	2.9	32.79	0.27
X	K	680	10.68	0.0132	5.408	5.57	38.6	85.0	3.6	32.64	0.19
X	M	730	10.21	0.0291	3.626	3.95	17.5	89.5	4.2	32.85	0.31
X	N	780	11.70	0.0082	7.690	5.46	62.2	80.6	5.0	33.87	0.26
X	O	780	10.07	0.0104	2.861	10.9	48.9	91.6	6.5	33.15	0.13
X	P	830	10.22	0.0167	3.280	9.3	30.6	90.5	7.8	33.25	0.14
X	Q	830	9.574	0.0109	1.435	11.5	47.0	95.6	9.4	32.88	0.11
X	R	880	10.19	0.0076	2.869	9.5	66.7	91.7	10.7	33.56	0.14
X	S	880	9.590	0.0083	1.351	11.6	61.3	95.8	12.3	33.02	0.10
X	T	930	10.25	0.0094	3.455	8.8	54.1	90.0	13.5	33.17	0.15
X	U	930	9.896	0.0105	2.147	10.4	48.5	93.6	15.0	33.27	0.12
X	V	980	11.48	0.0092	7.658	8.3	55.6	80.3	16.1	33.10	0.18
X	W	980	10.36	0.0061	4.077	9.7	83.3	88.4	17.5	32.88	0.16
X	X	1030	12.81	0.0057	12.44	8.6	90.0	71.3	18.7	32.82	0.18
X	Y	1030	11.33	0.0078	7.087	10.4	65.5	81.5	20.1	33.19	0.15
X	Z	1080	14.37	0.0080	17.56	10.9	63.7	63.9	21.6	33.01	0.24
X	AA	1080	12.60	0.0110	11.31	14.0	46.2	73.5	23.6	33.25	0.14
X	AB	1130	15.07	0.0079	20.00	18.5	64.8	60.8	26.2	32.91	0.19
X	AC	1130	13.24	0.0067	13.86	23.7	76.0	69.1	29.5	32.86	0.15
X	AD	1180	13.88	0.0085	15.25	36.1	60.1	67.5	34.5	33.67	0.14
X	AE	1180	13.01	0.0093	12.31	55.7	55.1	72.0	42.3	33.67	0.13
X	AF	1180	11.89	0.0090	8.575	52.1	56.9	78.7	49.5	33.62	0.09
X	AG	1280	11.19	0.0051	5.726	93.0	99.6	84.9	62.5	34.10	0.07
X	AH	1330	11.73	0.0034	6.868	154.7	151.7	82.7	84.0	34.84	0.08
X	AI	1380	12.50	0.0046	9.317	56.3	110.7	78.0	91.8	34.98	0.10
X	AJ	1450	12.86	0.0191	10.57	9.8	26.7	75.7	93.2	34.97	0.19
X	AK	1550	12.53	0.0062	9.564	24.7	82.0	77.4	96.6	34.84	0.12
X	AL	1750	13.20	0.0046	11.28	24.2	112.0	74.7	100.0	35.42	0.14
	Integrated age ± 2σ			n=37		718.2	70.7	K2O=9.35%		34.23	0.17

	Plateau ± 2σ	no plateau	n=0	MSWD=0.00	0.000	0.000±0.000		0.0	0.00	0.00
	Isochron±2σ	steps A-AL	n=37	MSWD=48.00		$^{40}Ar/^{36}Ar$=	327.4±2.4		32.89	0.09
	MP-21, K-Feldspar, 16.3 mg, J=0.0019797±0.05%, D=1.0014±0.001, NM-220D, Lab#=58042-01									
X	A	530	199.1	0.0213	457.5	0.325	23.9	32.1	0.0	218.06	5.17
X	B	530	34.91	-0.0668	90.60	0.287	-	23.3	0.1	29.18	3.36
X	C	580	21.09	-0.1052	31.77	0.378	-	55.4	0.1	41.84	2.38
X	D	580	14.27	0.0618	21.57	0.517	8.3	55.3	0.2	28.37	1.62
X	E	580	14.29	-0.0510	20.70	0.69	-	57.1	0.3	29.34	1.30
X	F	630	15.08	0.0537	15.25	0.542	9.5	70.1	0.4	37.89	1.43
X	G	630	10.57	0.0486	7.809	0.87	10.5	78.2	0.5	29.69	0.88
X	H	630	10.85	0.0243	7.758	1.47	21.0	78.9	0.8	30.71	0.57
X	I	680	12.27	0.0196	6.099	1.12	26.0	85.3	0.9	37.51	0.70
X	J	680	9.223	0.0002	3.117	1.79	######	90.0	1.2	29.80	0.45
X	K	730	10.21	0.0186	2.911	2.39	27.4	91.6	1.6	33.54	0.38
X	L	730	8.868	0.0292	1.679	3.13	17.5	94.4	2.0	30.06	0.25
X	M	730	9.019	0.0229	2.270	3.83	22.3	92.6	2.6	29.98	0.24
X	N	780	8.772	0.0010	0.6533	2.21	518.4	97.8	2.9	30.79	0.33
X	O	780	9.681	0.0078	3.492	4.59	65.1	89.3	3.6	31.04	0.21
X	P	830	8.708	0.0114	0.4618	3.99	44.8	98.4	4.2	30.77	0.19
X	Q	830	8.833	0.0182	0.6969	6.59	28.1	97.7	5.2	30.97	0.15
X	R	880	8.655	0.0116	0.2887	5.53	44.1	99.0	6.0	30.76	0.17
X	S	930	8.917	0.0119	0.5612	8.0	43.0	98.1	7.2	31.41	0.12
X	T	980	8.817	0.0060	0.5380	15.7	85.7	98.2	9.6	31.08	0.08
X	U	1030	8.975	0.0060	0.8817	18.6	84.9	97.1	12.3	31.28	0.08
X	V	1050	9.143	0.0077	0.9068	16.1	66.4	97.1	14.7	31.85	0.09
X	W	1080	9.312	0.0063	1.367	17.3	81.4	95.7	17.3	31.96	0.08
X	X	1100	9.414	0.0064	1.346	16.6	80.3	95.8	19.8	32.35	0.09
X	Y	1130	9.726	0.0065	1.794	19.9	78.5	94.5	22.8	32.99	0.09
X	Z	1180	10.17	0.0076	2.444	28.3	66.9	92.9	27.0	33.89	0.08
X	AA	1180	10.19	0.0071	2.022	59.6	71.8	94.1	35.9	34.40	0.06
X	AB	1180	9.992	0.0065	1.513	70.6	78.4	95.5	46.5	34.23	0.06
X	AC	1280	10.01	0.0059	1.132	155.7	86.4	96.7	69.8	34.69	0.05
X	AD	1330	9.784	0.0069	0.6338	142.6	74.4	98.1	91.1	34.42	0.05
X	AE	1380	9.951	0.0066	1.183	27.9	77.6	96.5	95.3	34.43	0.08
X	AF	1550	10.57	0.0097	3.145	11.6	52.6	91.2	97.0	34.58	0.11
X	AG	1750	11.13	0.0060	4.715	20.0	84.7	87.5	100.0	34.91	0.11
	Integrated age ± 2σ		n=33			668.8	71.9	K2O=7.96%		33.93	0.09
	Plateau ± 2σ	no plateau	n=0	MSWD=0.00	0.0	0.0 ±0.0		0.0		0.00	0.00
	Isochron±2σ	steps A-AG	n=33	MSWD=123.08		$^{40}Ar/^{36}Ar$=	473.4±8.3		32.80	0.07
	MP-23, K-Feldspar, 16.12 mg, J=0.0023609±0.04%, D=1.006±0.001, NM-227J, Lab#=59254-01									
X	A	700	13.47	0.0037	15.67	0.085	137.1	65.6	0.0	37.78	10.64
X	B	540	160.2	0.0054	433.2	6.17	93.7	20.1	0.8	133.89	2.57
X	C	540	15.11	0.0046	34.65	5.06	111.7	32.2	1.4	20.89	0.45
X	D	590	11.10	0.0047	19.63	7.19	107.8	47.7	2.3	22.73	0.33
X	E	590	8.699	0.0059	12.79	9.04	86.3	56.5	3.4	21.10	0.22
X	F	640	8.523	0.0092	9.902	11.3	55.5	65.6	4.8	23.99	0.20
X	G	640	7.428	0.0073	7.271	14.3	69.9	71.0	6.5	22.64	0.13
X	H	690	7.572	0.0093	6.502	16.3	55.1	74.6	8.5	24.22	0.12
X	I	690	6.901	0.0072	4.206	21.5	70.7	82.0	11.0	24.25	0.09
X	J	740	7.001	0.0066	4.221	23.5	77.4	82.2	13.7	24.66	0.09
X	K	740	6.615	0.0054	2.672	30.2	94.0	88.1	17.1	24.96	0.07
X	L	790	6.722	0.0052	2.807	28.3	98.0	87.7	20.2	25.25	0.07
X	M	790	6.556	0.0046	2.041	36.4	111.7	90.8	24.1	25.51	0.07
X	N	840	6.837	0.0048	2.821	32.0	106.5	87.8	27.4	25.72	0.08
X	O	840	6.693	0.0040	2.241	38.7	128.2	90.1	31.3	25.84	0.07
X	P	890	6.976	0.0044	3.067	31.0	115.5	87.0	34.4	26.00	0.08
X	Q	890	6.771	0.0038	2.224	40.4	133.2	90.3	38.2	26.19	0.07
X	R	940	7.061	0.0040	3.064	34.9	129.0	87.2	41.4	26.37	0.07
X	S	940	6.912	0.0033	2.487	42.9	154.7	89.4	45.3	26.46	0.06
X	T	990	7.352	0.0034	3.812	34.1	149.7	84.7	48.2	26.67	0.08

X	U	990	7.180	0.0036	3.336	40.4	141.7	86.3	51.6	26.53	0.07
X	V	1040	7.790	0.0034	5.230	31.5	150.9	80.1	54.2	26.75	0.10
X	W	1040	7.532	0.0029	4.204	40.2	175.6	83.5	57.5	26.94	0.08
X	X	1090	8.177	0.0049	5.961	33.2	103.6	78.4	60.0	27.47	0.09
X	Y	1090	7.784	0.0051	4.697	40.3	99.7	82.2	63.1	27.39	0.08
X	Z	1140	8.382	0.0073	6.614	27.7	70.0	76.7	65.2	27.53	0.12
X	AA	1190	8.362	0.0114	5.938	51.6	44.7	79.0	68.9	28.30	0.09
X	AB	1190	8.461	0.0071	5.448	90.7	71.7	81.0	75.1	29.33	0.08
X	AC	1190	8.661	0.0028	5.774	98.3	182.0	80.3	81.4	29.77	0.08
X	AD	1190	8.736	0.0013	5.861	100.3	390.7	80.2	87.5	29.98	0.09
X	AE	1290	8.659	0.0006	5.430	107.8	812.9	81.4	93.6	30.19	0.07
X	AF	1340	9.168	0.0007	7.230	44.7	727.2	76.7	96.0	30.10	0.10
X	AG	1390	10.07	0.0010	11.09	15.2	492.8	67.4	96.8	29.07	0.18
X	AH	1590	9.184	0.0010	7.405	48.1	530.1	76.1	99.3	29.94	0.09
X	AI	1740	11.21	0.0015	14.69	13.0	342.9	61.2	100.0	29.39	0.19
	Integrated age ± 2σ			n=35		1246.4	126.0	K2O=12.58%		28.18	0.13
	Plateau ± 2σ	no plateau		n=0	MSWD=0.00	0.000	0.000±0.000		0.0	0.00	0.00
	Isochron±2σ	steps A-AI		n=35	MSWD=299.44		$^{40}Ar/^{36}Ar$=	395.1±2.8		25.12	0.06

MP-24, K-Feldspar, 16.4 mg, J=0.0019817±0.06%, D=1.0014±0.001, NM-220D, Lab#=58044-01

X	A	530	546.9	0.0484	1811.9	0.77	10.6	2.1	0.1	41.06	9.84
X	B	530	83.43	0.0914	254.7	0.73	5.6	9.8	0.2	29.41	3.02
X	C	580	41.53	0.0113	105.0	1.04	45.0	25.3	0.4	37.70	1.57
X	D	580	26.03	0.0373	57.43	1.42	13.7	34.8	0.6	32.56	0.95
X	E	580	23.02	0.0204	42.37	1.78	25.0	45.6	0.8	37.68	0.83
X	F	630	21.41	0.0318	39.22	1.44	16.1	45.9	1.0	35.27	0.79
X	G	630	15.81	0.0346	20.28	2.22	14.7	62.1	1.3	35.23	0.54
X	H	680	18.43	0.0033	28.43	3.34	154.6	54.4	1.8	36.00	0.46
X	I	680	12.73	0.0163	9.442	4.29	31.3	78.1	2.4	35.68	0.32
X	J	680	12.52	0.0175	9.099	5.51	29.2	78.5	3.2	35.29	0.23
X	K	730	12.55	0.0188	7.818	3.26	27.2	81.6	3.6	36.73	0.33
X	L	730	11.09	0.0134	3.942	5.40	38.1	89.5	4.4	35.63	0.19
X	M	780	11.71	0.0179	6.335	6.26	28.4	84.0	5.3	35.30	0.19
X	N	780	10.48	0.0126	2.263	8.6	40.4	93.6	6.5	35.23	0.12
X	O	830	11.43	0.0083	5.306	9.0	61.7	86.3	7.8	35.39	0.14
X	P	830	10.16	0.0128	1.177	11.5	40.0	96.6	9.4	35.21	0.10
X	Q	880	10.59	0.0056	2.635	10.3	91.4	92.6	10.8	35.21	0.12
X	R	880	10.07	0.0125	0.7855	12.7	40.9	97.7	12.6	35.31	0.09
X	S	930	10.26	0.0075	1.508	10.5	68.2	95.7	14.1	35.23	0.11
X	T	930	10.06	0.0069	0.8042	14.1	73.6	97.6	16.1	35.26	0.08
X	U	980	10.40	0.0097	1.964	11.5	52.4	94.4	17.7	35.23	0.10
X	V	980	10.22	0.0110	1.337	15.5	46.2	96.1	19.9	35.28	0.10
X	W	1030	10.81	0.0115	3.245	12.3	44.3	91.1	21.6	35.37	0.11
X	X	1030	10.59	0.0063	2.621	16.9	81.3	92.7	24.0	35.23	0.10
X	Y	1080	11.71	0.0095	6.573	13.4	53.7	83.4	25.8	35.06	0.14
X	Z	1080	11.07	0.0109	4.552	18.0	47.0	87.8	28.4	34.91	0.11
	AA	1130	12.84	0.0078	10.50	16.4	65.0	75.8	30.7	34.95	0.15
	AB	1130	11.83	0.0121	6.869	20.4	42.2	82.8	33.6	35.19	0.11
	AC	1180	12.57	0.0119	9.117	22.7	43.0	78.6	36.7	35.43	0.13
	AD	1180	12.43	0.0088	9.073	50.7	58.1	78.4	43.9	35.01	0.12
	AE	1180	12.15	0.0076	8.006	56.0	67.0	80.5	51.7	35.13	0.10
	AF	1280	11.41	0.0051	5.356	135.0	100.6	86.1	70.7	35.28	0.07
	AG	1330	11.62	0.0051	5.943	124.2	99.3	84.9	88.2	35.42	0.07
	AH	1380	11.90	0.0048	6.900	34.9	105.7	82.8	93.1	35.38	0.10
	AI	1450	12.54	0.0092	9.077	9.0	55.3	78.6	94.4	35.38	0.17
X	AJ	1550	12.91	0.0095	9.997	21.3	53.7	77.1	97.4	35.72	0.13
X	AK	1750	13.00	0.0051	10.59	18.7	100.1	75.9	100.0	35.43	0.14
	Integrated age ± 2σ			n=37		711.1	63.5	K2O=8.40%		35.29	0.16
	Plateau ± 2σ	steps AA-AI		n=9	MSWD=2.29	469.4	84.6 ±49.8		66.0	35.27	0.11
	Isochron±2σ	steps A-AK		n=37	MSWD=2.68		$^{40}Ar/^{36}Ar$=	296.8±2.1		35.26	0.07

MP-25, K-Feldspar, 15.8 mg, J=0.0019835±0.07%, D=1.0014±0.001, NM-220D, Lab#=58046-01

X	A	530	382.7	0.0403	1255.7	0.542	12.7	3.1	0.1	41.95	8.19
X	B	530	70.19	0.0782	208.1	0.477	6.5	12.4	0.2	31.25	3.04
X	C	580	36.10	0.0260	87.16	0.67	19.6	28.6	0.3	37.16	1.63
X	D	580	22.87	0.0166	46.03	0.88	30.8	40.5	0.4	33.31	1.22
X	E	630	24.24	-0.0295	48.96	1.34	-	40.3	0.6	35.12	0.83
X	F	630	14.85	0.0216	18.24	1.72	23.6	63.7	0.9	33.98	0.59
X	G	680	17.81	0.0010	26.38	2.29	514.6	56.2	1.2	35.97	0.52
X	H	680	12.70	0.0235	9.136	2.85	21.7	78.7	1.7	35.94	0.34
	I	730	14.09	0.0149	15.08	3.39	34.2	68.4	2.2	34.62	0.33
	J	730	11.32	0.0228	5.494	4.21	22.4	85.7	2.8	34.84	0.25
	K	780	12.10	0.0084	7.818	4.60	61.0	80.9	3.5	35.17	0.24
	L	780	10.61	0.0044	2.838	6.00	117.1	92.1	4.5	35.12	0.19
	M	830	11.00	0.0055	3.986	6.19	93.1	89.3	5.4	35.27	0.17
	N	830	10.20	0.0081	1.268	8.0	63.1	96.3	6.7	35.31	0.13
	O	880	10.45	0.0006	2.122	7.5	865.5	94.0	7.8	35.30	0.14
	P	880	10.06	0.0062	1.155	9.9	82.4	96.6	9.3	34.93	0.10
	Q	930	10.10	0.0016	1.299	8.8	312.4	96.2	10.7	34.92	0.11
	R	980	10.28	0.0056	1.622	14.3	91.5	95.3	12.9	35.20	0.09
	S	1010	10.24	0.0045	1.594	14.4	114.5	95.4	15.1	35.10	0.10
	T	1040	10.39	0.0044	2.146	14.8	114.7	93.9	17.4	35.06	0.10
	U	1080	10.78	0.0031	3.457	17.3	164.5	90.5	20.1	35.07	0.11
	V	1110	11.10	0.0041	4.561	17.2	123.6	87.8	22.7	35.03	0.13
	W	1130	11.45	0.0093	5.811	15.6	54.7	85.0	25.1	34.96	0.13
	X	1150	12.02	0.0089	7.584	16.0	57.2	81.3	27.6	35.12	0.12
	Y	1180	12.83	0.0079	10.34	21.3	64.8	76.2	30.9	35.12	0.14
	Z	1180	13.13	0.0058	11.39	50.4	88.0	74.3	38.7	35.08	0.14
	AA	1180	13.12	0.0045	11.39	14.0	113.5	74.3	40.9	35.04	0.17
	AB	1230	12.40	0.0057	9.036	41.9	89.8	78.5	47.3	34.97	0.11
	AC	1280	12.16	0.0044	7.863	161.3	116.8	80.9	72.2	35.33	0.09
X	AD	1330	11.91	0.0054	6.973	99.2	95.1	82.7	87.6	35.39	0.08
X	AE	1380	11.42	0.0043	5.429	35.3	119.3	85.9	93.0	35.26	0.10
X	AF	1750	13.34	0.0048	11.52	45.3	105.3	74.4	100.0	35.67	0.12
	Integrated age ± 2σ			n=32		647.4	93.4	K2O=7.93%		35.24	0.16
	Plateau ± 2σ	steps I-AC		n=21	MSWD=1.29	456.8	117.5	±354.9	70.6	35.10	0.08
	Isochron±2σ	steps A-AF		n=32	MSWD=2.36		$^{40}Ar/^{36}Ar$=	297.9±2.4		35.12	0.08

MP-37, K-Feldspar, 18.76 mg, J=0.0023619±0.05%, D=1.006±0.001, NM-227J, Lab#=59255-01

X	A	700	-81.6523	4.621	-436.1575	0.001	0.11	-58.3	0.0	195.74	563.99
X	B	540	92.13	0.0040	276.3	10.7	128.8	11.4	1.1	44.70	1.62
X	C	540	17.68	0.0030	41.18	8.92	167.8	31.1	2.0	23.62	0.39
X	D	590	10.11	0.0039	15.06	11.2	129.5	55.9	3.2	24.27	0.21
X	E	590	8.380	0.0042	8.657	14.1	120.2	69.4	4.6	24.96	0.15
X	F	640	7.760	0.0050	6.022	15.9	103.0	77.0	6.2	25.63	0.12
X	G	640	7.272	0.0039	4.175	20.4	130.0	83.0	8.2	25.88	0.10
X	H	690	7.141	0.0054	3.182	21.6	93.8	86.8	10.3	26.57	0.09
X	I	690	6.900	0.0039	2.024	28.3	130.6	91.3	12.9	27.00	0.07
X	J	740	6.963	0.0034	1.997	29.5	149.0	91.5	15.7	27.30	0.07
X	K	740	6.734	0.0026	1.054	39.7	195.8	95.4	19.3	27.52	0.05
X	L	790	6.756	0.0028	1.072	38.6	179.6	95.3	22.7	27.59	0.06
X	M	790	6.713	0.0024	0.6985	50.0	210.1	96.9	27.0	27.87	0.05
X	N	840	6.770	0.0023	0.9106	45.4	217.3	96.0	30.7	27.85	0.05
X	O	840	6.685	0.0024	0.5943	57.2	213.5	97.4	35.3	27.89	0.05
X	P	890	6.822	0.0025	1.068	47.8	200.3	95.4	39.0	27.87	0.05
X	Q	890	6.756	0.0022	0.7536	60.6	233.4	96.7	43.5	27.99	0.05
X	R	940	7.001	0.0022	1.539	50.6	228.9	93.5	47.1	28.05	0.06
X	S	940	6.915	0.0022	1.208	64.1	233.0	94.8	51.6	28.10	0.05
X	T	990	7.321	0.0024	2.509	48.2	215.1	89.9	54.8	28.19	0.07
X	U	990	7.198	0.0023	2.130	56.7	225.0	91.2	58.5	28.14	0.06
X	V	1040	7.644	0.0024	3.691	41.5	209.8	85.7	61.1	28.07	0.07
X	W	1040	7.458	0.0029	3.047	50.3	177.3	87.9	64.2	28.09	0.06
X	X	1090	8.096	0.0053	4.962	39.1	95.9	81.9	66.5	28.40	0.08
X	Y	1090	7.899	0.0053	4.082	46.0	96.4	84.7	69.2	28.67	0.07
X	Z	1140	8.425	0.0082	5.721	30.7	62.3	79.9	70.9	28.85	0.10

X	AA	1190	8.916	0.0090	7.236	63.6	56.6	76.0	74.4	29.03	0.09
X	AB	1190	9.131	0.0032	7.463	120.5	160.3	75.8	80.8	29.66	0.08
X	AC	1190	9.350	0.0011	7.608	122.0	445.4	75.9	86.8	30.41	0.08
X	AD	1190	9.455	0.0007	7.469	113.7	765.2	76.6	92.1	31.03	0.08
X	AE	1290	9.321	0.0005	6.454	98.2	943.8	79.5	96.4	31.74	0.08
X	AF	1340	9.788	0.0005	7.806	36.2	936.3	76.4	97.9	32.02	0.11
X	AG	1390	9.995	0.0037	7.512	8.75	138.3	77.8	98.3	33.27	0.19
X	AH	1590	9.887	0.0005	8.213	30.4	######	75.4	99.6	31.93	0.11
X	AI	1740	10.36	0.0001	9.753	10.6	######	72.1	100.0	32.00	0.17
	Integrated age ± 2σ			n=35		1531.0	184.3	K2O=13.27%		29.02	0.13
	Plateau ± 2σ	no plateau		n=0	MSWD=0.00	0.000	0.000±0.000		0.0	0.00	0.00
	Isochron±2σ	steps A-AI		n=35	MSWD=229.64		$^{40}Ar/^{36}Ar$=	352.7±1.9		27.60	0.04

MP-38, K-Feldspar, 17.78 mg, J=0.002363±0.04%, D=1.006±0.001, NM-227J, Lab#=59256-01

X	A	540	61.69	0.0056	180.9	12.9	90.7	13.3	8.4	35.26	1.06
X	B	540	11.14	0.0049	21.02	9.08	103.8	44.2	13.6	21.14	0.25
X	C	590	7.785	0.0053	8.959	12.7	95.6	66.0	20.0	22.05	0.16
X	D	590	6.951	0.0055	5.719	14.7	93.3	75.7	26.5	22.58	0.11
X	E	640	6.497	0.0056	4.086	17.8	91.3	81.4	33.2	22.70	0.09
X	F	640	6.225	0.0065	2.645	21.8	78.7	87.4	40.1	23.36	0.07
X	G	690	6.217	0.0078	2.237	23.8	65.4	89.4	46.3	23.83	0.08
X	H	690	5.978	0.0063	1.404	29.7	81.6	93.1	52.8	23.87	0.06
X	I	740	6.002	0.0068	1.405	31.2	75.5	93.1	58.2	23.97	0.06
X	J	740	5.897	0.0051	0.9318	38.4	99.6	95.3	63.7	24.12	0.05
X	K	790	5.942	0.0054	0.8386	36.2	93.9	95.8	68.0	24.42	0.05
X	L	790	5.933	0.0045	0.6844	42.7	112.4	96.6	72.1	24.58	0.05
X	M	840	6.031	0.0049	0.8819	36.7	103.8	95.7	75.0	24.75	0.05
X	N	840	6.053	0.0048	0.7136	41.9	107.2	96.5	77.9	25.06	0.05
X	O	890	6.263	0.0055	1.151	32.6	92.2	94.6	79.8	25.40	0.06
X	P	890	6.248	0.0047	1.080	37.8	109.2	94.9	81.8	25.42	0.05
X	Q	940	6.664	0.0056	2.277	29.2	90.5	89.9	83.2	25.69	0.07
X	R	940	6.590	0.0050	2.120	34.4	102.8	90.5	84.6	25.58	0.06
X	S	990	7.302	0.0046	4.579	27.0	110.1	81.5	85.7	25.51	0.08
X	T	990	7.157	0.0037	4.067	33.6	138.0	83.2	86.8	25.54	0.08
X	U	1040	8.066	0.0043	7.152	28.2	119.8	73.8	87.8	25.53	0.10
X	V	1040	7.698	0.0040	5.603	36.1	126.7	78.5	88.8	25.91	0.09
X	W	1090	8.438	0.0052	7.895	32.2	98.4	72.3	89.7	26.18	0.11
X	X	1090	7.821	0.0051	5.464	40.4	100.6	79.3	90.7	26.61	0.08
X	Y	1140	8.379	0.0084	7.458	30.5	61.0	73.7	91.4	26.48	0.10
X	Z	1190	8.627	0.0101	7.966	69.0	50.7	72.7	92.8	26.89	0.09
X	AA	1190	8.529	0.0037	7.491	133.6	137.8	74.0	95.1	27.08	0.08
X	AB	1190	8.502	0.0016	6.984	142.6	321.6	75.7	96.9	27.60	0.07
X	AC	1190	8.439	0.0011	6.431	130.2	461.9	77.5	98.3	28.02	0.07
X	AD	1190	8.473	0.0012	6.158	92.2	429.8	78.5	99.1	28.51	0.07
X	AE	1290	8.142	0.0006	4.641	46.9	839.4	83.1	99.5	29.01	0.08
X	AF	1340	8.657	0.0007	6.427	29.0	735.2	78.0	99.7	28.96	0.10
X	AG	1390	8.682	0.0007	6.689	8.14	756.8	77.2	99.7	28.74	0.16
X	AH	1590	8.778	0.0014	6.840	23.6	374.2	76.9	99.9	28.95	0.12
X	AI	1740	9.620	0.0013	8.847	12.2	398.5	72.8	100.0	30.01	0.17
	Integrated age ± 2σ			n=35		1419.2	127.9	K2O=12.97%		26.45	0.12
	Plateau ± 2σ	no plateau		n=0	MSWD=0.00	0.000	0.000±0.000		0.0	0.00	0.00
	Isochron±2σ	steps A-AI		n=35	MSWD=287.67		$^{40}Ar/^{36}Ar$=	374.8±2.1		24.41	0.04

Notes:
x (or i) symbol preceding sample ID denotes analyses excluded from plateau (or isochron) age calculations.
Isotopic ratios corrected for blank, radioactive decay, and mass discrimination, not corrected for interfering reactions.
Errors quoted for individual analyses include analytical error only, without interfering reaction or J uncertainties.

Age calculations:

Ages calculated relative to FC-2 Fish Canyon Tuff sanidine interlaboratory standard (28.201 Ma, Kuiper et al, 2008).
Integrated age calculated by summing isotopic measurements of all steps.
Integrated age error calculated by quadratically combining errors of isotopic measurements of all steps.
Plateau age or preferred age calculated for the indicated steps by weighting each step by the inverse of the variance.
Plateau age error is inverse-variance-weighted mean error (Taylor, 1982) times root MSWD where MSWD>1.
MSWD values are calculated for n-1 degrees of freedom for plateau age.
Isochron ages, $^{40}Ar/^{36}Ar_I$ and MSWD values calculated from regression results obtained by the methods of York (1969).
Decay constants and isotopic abundances after Min et al. (2000).
Weight percent K_2O calculated from ^{39}Ar signal, sample weight, and instrument sensitivity.
All errors reported at ±2s, unless otherwise noted.

Sample preparation and irradiation:

K-feldspar separates were prepared using crushing, Franz magnetic separator, heavy liquids
and hand-picking techniques.
Samples were loaded into machined Al discs and irradiated in 3 separate positions (NM-220C and D, and NM-227J)
for 10 hours at Nuclear Science Center, College Station, TX or the Triga Reactor
Neutron flux monitor Fish Canyon Tuff sanidine (FC-2).

Instrumentation:

Mass Analyzer Products 215-50 mass spectrometer on line with automated all-metal extraction system.
Samples were step-heated using a Mo double-vacuum resistance furnace (heating duration 10 minutes),
or CO2 laser (heating duration 2 minutes).
Reactive gases removed during furnace (laser) analysis by reaction with 3 (2) SAES GP-50 getters, 2 (1) operated
at ~450°C and 1 at 20°C. Gas also exposed to a W filament operated at ~2000°C.

Analytical parameters:

Electron multiplier sensitivity ranged from 6.99 x 10^{-17} moles/pA to 1.11 x 10^{-16} moles /pA.
Total system blank and background for the furnace averaged 1883, 20.3, 4.4, 9.3, 57.4 x 10^{-18} moles.
at masses 40, 39, 38, 37, and 36 respectively
J-factors determined to a precision of ± 0.1% by CO_2 laser-fusion of 6 single crystals from each of 10 radial positions
around the irradiation tray.
Correction factors for interfering nuclear reactions were determined using K-glass and CaF_2 and are as follows:

$(^{39}Ar/^{37}Ar)_{Ca}$ = 0.00068 ± 2e-05
$(^{36}Ar/^{37}Ar)_{Ca}$ = 0.00028 ± 1e-05
$(^{38}Ar/^{39}Ar)_{K}$ = 0.013 ± 5e-4
$(^{40}Ar/^{39}Ar)_{K}$ = 0 ± 4e-4

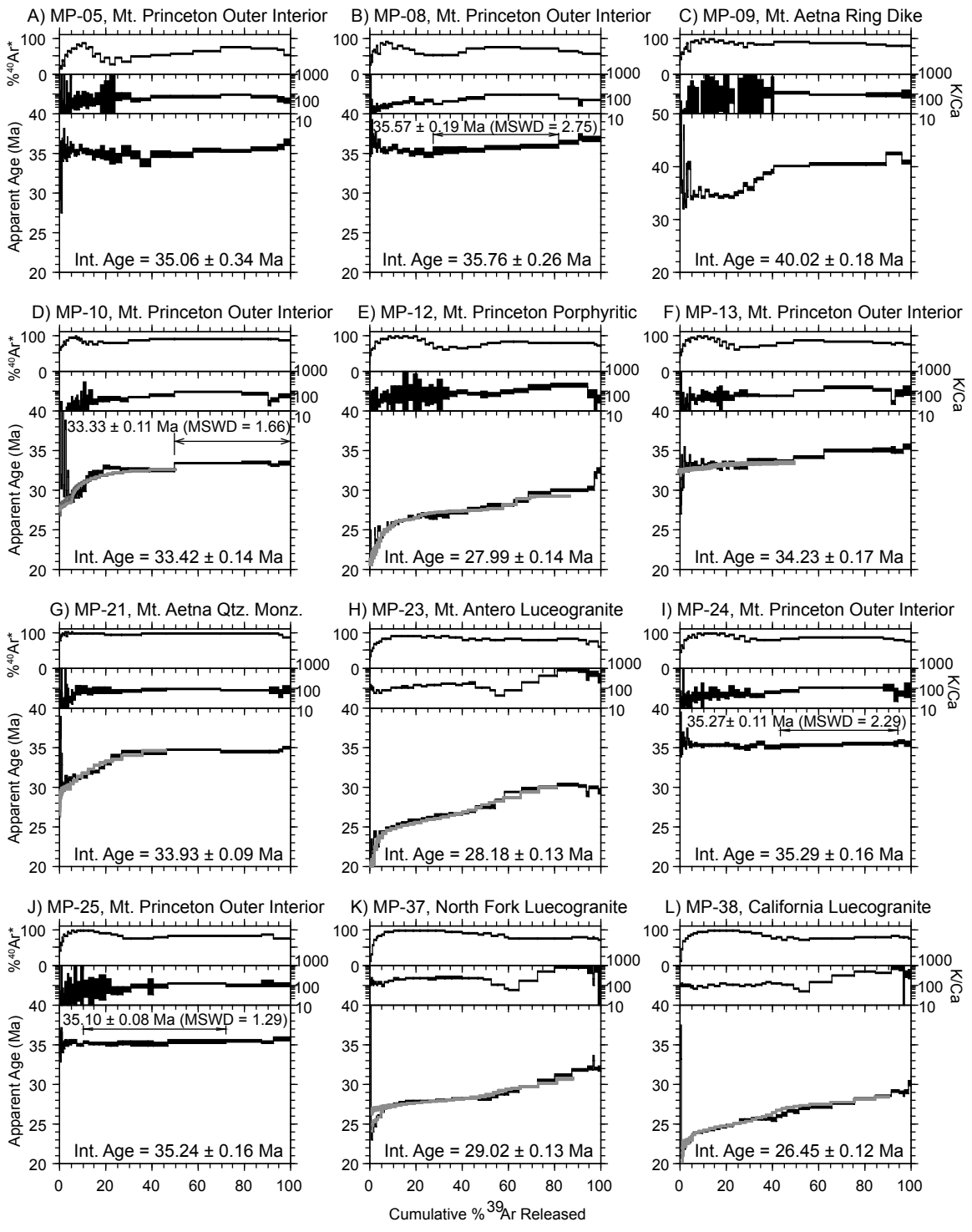

Figure 2.3.3 - K-feldspar age spectra and K/Ca and radiogenic yield (%^{40}Ar*) auxiliary plots. All errors are reported at 2σ and do not include error in decay constant. Modeled age spectra used to model MDD cooling histories are shown in gray.

APPENDIX 2.4.

SUPPLEMENTAL MDD PLOTS FOR THE MT. AETNA CALDERA COMPLEX K-FELDSPAR

Appendix 2.4 contains Arrhenius and log (r/r_o) plots used for MDD thermal modeling of K-feldspars from the Mt. Aetna caldera complex. Modeled age spectra and thermal histories are located within the main body of the text. All MDD thermal histories were modeled using algorithms developed by Lovera et al. (1989, 1991). Arrhenius plots are constructed using the heating schedule and the fraction of the $^{39}Ar_K$ released for each step. Log (r/r_o) plots are constructed by fitting an Arrhenius reference line (r_o) to the data points on the Arrhenius plot, calculating the deviation of the Arrhenius trend from r_o, and comparing that to the cumulative $^{39}Ar_K$ released. Black lines are the actual data and gray lines are the modeled data.

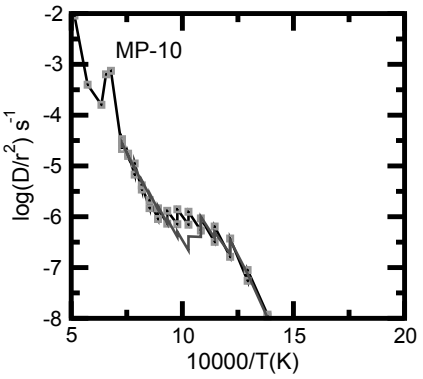
MP-10
log(D/r^2) s^{-1}
10000/T(K)

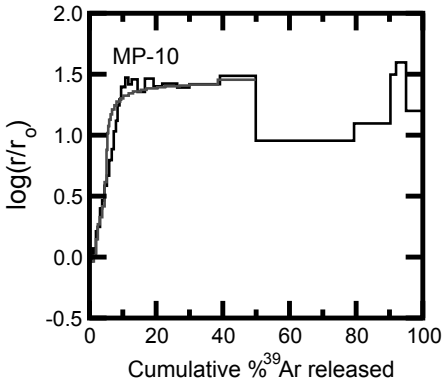
MP-10
log(r/r$_o$)
Cumulative %^{39}Ar released

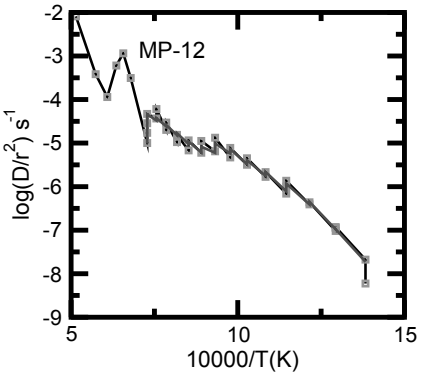
MP-12
log(D/r^2) s^{-1}
10000/T(K)

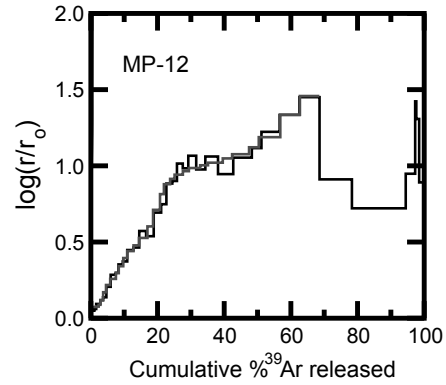
MP-12
log(r/r$_o$)
Cumulative %^{39}Ar released

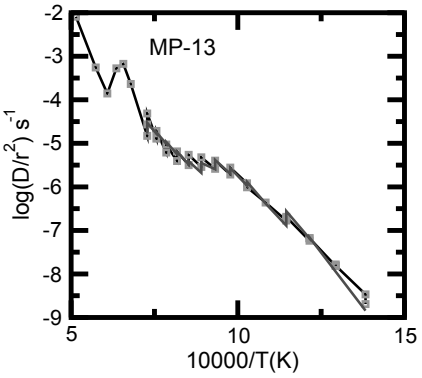
MP-13
log(D/r^2) s^{-1}
10000/T(K)

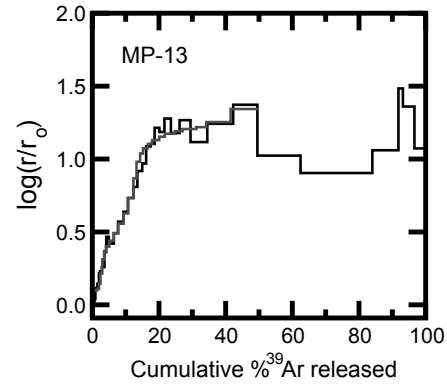
MP-13
log(r/r$_o$)
Cumulative %^{39}Ar released

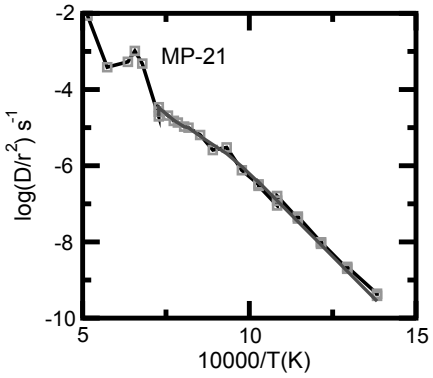
MP-21
log(D/r^2) s^{-1}
10000/T(K)

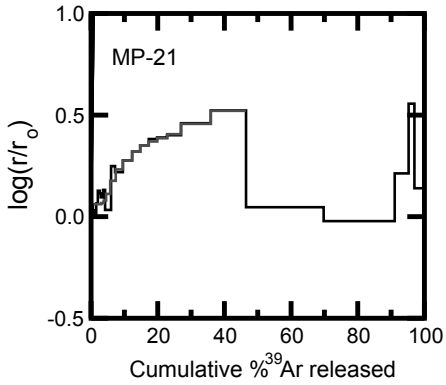
MP-21
log(r/r$_o$)
Cumulative %^{39}Ar released

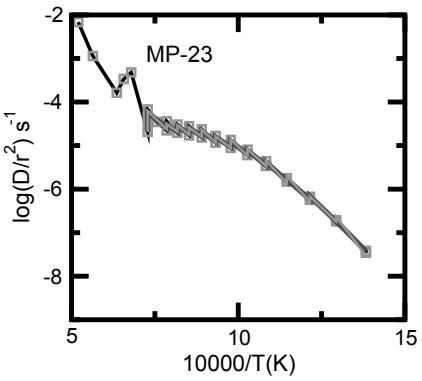
MP-23
log(D/r^2) s^{-1}
10000/T(K)

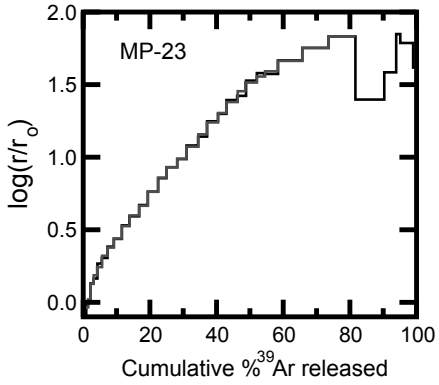
MP-23
log(r/r$_o$)
Cumulative %^{39}Ar released

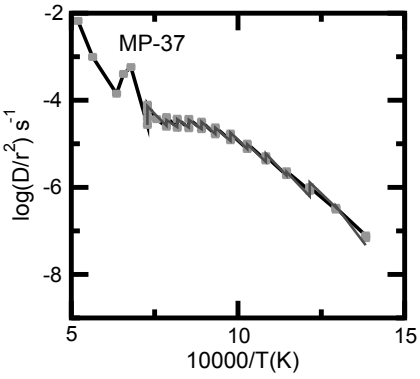
MP-37
log(D/r^2) s^{-1}
10000/T(K)

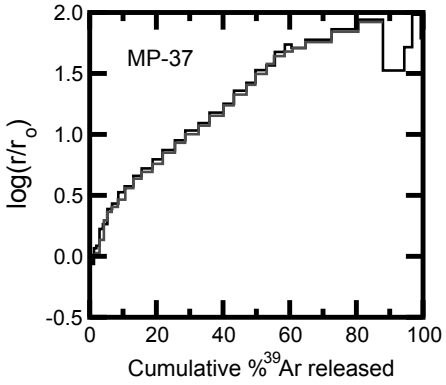
MP-37
log(r/r$_o$)
Cumulative %^{39}Ar released

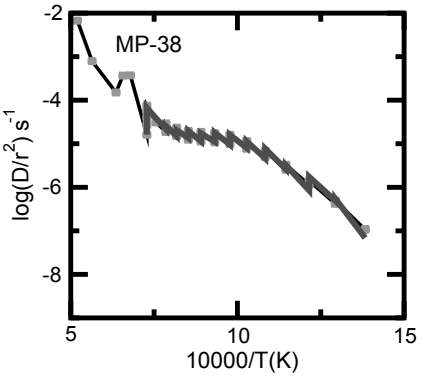
MP-38
log(D/r^2) s^{-1}
10000/T(K)

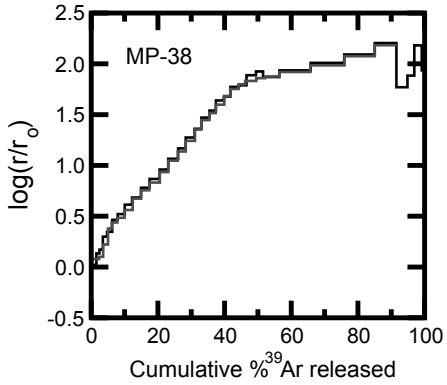
MP-38
log(r/r$_o$)
Cumulative %^{39}Ar released

APPENDIX 3.1.

LOCATION OF THE DATED ORGAN CALDERA COMPLEX SAMPLES

Sample	Map Unit	Easting[1]	Northing[1]
ORGAN-2	Squaw Mountain Tuff	350844	3573782
ORGAN-4	Squaw Mountain Tuff	348650	3574050
ORGAN-6	Rhyolitic West-side Lava	348148	3574225
ORGAN-7	Dacitic West-side Lava	347717	3575183
ORGAN-8	Dacitic West-side Lava	347595	3575216
ORGAN-9	Sugarloaf Peak Qtz. Monz.	352552	3581838
ORGAN-10	Equigranular ONP[2] Syenite	351675	3581925
ORGAN-11	Dacitic West-side Lava	347203	3576560
ORGAN-12	Rhyolitic West Side Lava	346786	3576524
ORGAN-13	Sugarloaf Peak Qtz. Monz.	352496	3588559
ORGAN-14	Cueva Tuff	349632	3566265
ORGAN-17	Cueva Tuff	349527	3566305
ORGAN-18	Cueva Tuff	349569	3566400
ORGAN-21	Baylor Peak Rhyolite Porphyry	351649	3584902
ORGAN-22	Aplite Dike in Sugarloaf Peak Qtz. Monz.	351988	3583565
ORGAN-24	Sugarloaf Peak Qtz. Monz.	353281	3580893
ORGAN-25	Mafic enclaves in Sugarloaf Peak Qtz. Monz.	353588	3582243
ORGAN-27	Achenbach Park Tuff	349122	3567499
ORGAN-28	Achenbach Park Tuff	349081	3568132
ORGAN-30	Orejon Andesite	352773	3578860
ORGAN-31	Equigranular ONP Qtz. Syenite	352965	3579133
ORGAN-32	Orejon Andesite	352993	3578934
ORGAN-33	Orejon Andesite	352836	3578746
ORGAN-35	ONP Alkali Feldspar Granite	354872	3570437
ORGAN-36	Equigranular ONP Syenite	358711	3575725
ORGAN-37	Granite of Granite Peak	357049	3576416
ORGAN-41	ONP Alkali Feldspar Granite	355614	3574574
ORGAN-42	Precambrian Granite	361778	3577873
ORGAN-43	ONP Monzodiorite	356012	3579598
ORGAN-45	ONP Monzodiorite	356294	3580066
ORGAN-46	Inequigranular ONP Syenite	360051	3577609
ORGAN-47	ONP Monzodiorite	358645	3577945

1 - Section 13S; NAD 27
2 – ONP (Organ Needle Pluton)

APPENDIX 3.2.

ORGAN CALDERA U/PB DATA TABLES AND *TuffZirc* PLOTS

Appendix 3.2 contains the LA-ICP-MS U/Pb zircon data tables and *TuffZirc* plots (Ludwig, 2003; Ludwid and Mundil, 2002;). The *TuffZirc* ages were calculated from single grain ages using methods and algorithms of *Isoplot 3.70* (Ludwig, 2003). All uncertainties of individual analyses are reported at the 1-sigma level and include only analytical errors. *TuffZirc* ages are reported at the 2-sigma level. U concentration and U/Th are calibrated relative to the Sri Lanka zircon standard and are accurate to ~20%. Common Pb correction is from ^{204}Pb, with composition interpreted from Stacey and Kramers (1975) and uncertainties of 1.0 for ^{206}Pb/ ^{204}Pb, 0.3 for ^{207}Pb/ ^{204}Pb, and 2.0 for ^{208}Pb/ ^{204}Pb. U/Pb ages and ^{206}Pb/ ^{207}Pb fractionation is calibrated relative to fragments of a large Sri Lanka zircon of 564±4 Ma (2σ). U decay constants and composition are as follows: ^{238}U = 9.8485 x 10 -10, ^{235}U = 1.55125 x 10 -10, ^{238}U/ ^{235}U = 137.88. For a more comprehensive description of LA-ICP-MS U-Pb zircon analytical procedures see Gehrels et al. (2008) and the Arizona Laserchron website (https://sites.google.com/a/laserchron.org/laserchron/home/).

ORGAN-9, Sugarloaf Peak qtz. Monz.																		
							Isotope ratios					Apparent ages (Ma)						
Analysis	U	206Pb	U/Th	206Pb*	±	207Pb*	±	206Pb*	±	error	206Pb*	±	207Pb*	±	206Pb*	±	Best age	±
	(ppm)	204Pb		207Pb*	(%)	235U*	(%)	238U	(%)	corr.	238U*	(Ma)	235U	(Ma)	207Pb*	(Ma)	(Ma)	(Ma)
ORGAN-9-5C	99	134	0.9	25.0119	172.0	0.0276	173.1	0.0050	19.0	0.11	32.2	6.1	27.7	47.3	-352.2	0.0	32.2	6.1
ORGAN-9-3R	103	4724	1.1	12.8285	33.5	0.0542	36.5	0.0050	14.5	0.40	32.4	4.7	53.5	19.0	1145.7	684.7	32.4	4.7
ORGAN-9-22R	132	3094	1.0	12.5111	39.4	0.0557	40.9	0.0051	11.0	0.27	32.5	3.6	55.0	21.9	1195.2	808.6	32.5	3.6
ORGAN-9-21R	144	2013	1.0	16.8011	33.2	0.0418	35.7	0.0051	13.2	0.37	32.7	4.3	41.6	14.5	586.2	738.9	32.7	4.3
ORGAN-9-20R	77	1664	0.8	18.6623	162.1	0.0376	162.9	0.0051	16.1	0.10	32.7	5.2	37.5	60.1	353.6	1270.4	32.7	5.2
ORGAN-9-12R	178	2798	1.1	19.1595	46.4	0.0372	47.5	0.0052	10.0	0.21	33.3	3.3	37.1	17.3	293.9	1115.5	33.3	3.3
ORGAN-9-23R	258	4267	1.1	25.4246	44.7	0.0283	45.8	0.0052	9.9	0.22	33.5	3.3	28.3	12.8	-394.6	1216.2	33.5	3.3
ORGAN-9-16R	164	3460	0.9	22.5594	54.9	0.0320	56.3	0.0052	12.3	0.22	33.7	4.1	32.0	17.7	-92.5	1449.8	33.7	4.1
ORGAN-9-2R	131	2444	1.1	14.7376	52.4	0.0491	53.1	0.0053	8.1	0.15	33.8	2.7	48.7	25.2	864.1	1171.1	33.8	2.7
ORGAN-9-24R	147	4953	1.1	10.2679	116.5	0.0705	117.2	0.0053	12.2	0.10	33.8	4.1	69.2	78.5	1574.7	28.5	33.8	4.1
ORGAN-9-26R	198	7979	0.9	34.2620	68.4	0.0212	68.7	0.0053	6.1	0.09	33.8	2.0	21.3	14.5	-1244.1	738.2	33.8	2.0
ORGAN-9-5R	176	5798	0.8	20.5293	57.8	0.0356	58.1	0.0053	5.8	0.10	34.1	2.0	35.5	20.3	134.0	1478.2	34.1	2.0
ORGAN-9-6C	168	5677	1.0	4.3967	595.5	0.1665	595.7	0.0053	13.1	0.02	34.1	4.5	156.4	1276.4	3034.1	450.8	34.1	4.5
ORGAN-9-2C	187	1971	0.7	18.2982	47.7	0.0401	48.1	0.0053	6.5	0.14	34.2	2.2	39.9	18.8	397.9	1130.6	34.2	2.2
ORGAN-9-14R	203	2898	1.0	21.8879	30.8	0.0336	31.7	0.0053	7.7	0.24	34.3	2.6	33.5	10.5	-18.8	759.7	34.3	2.6
ORGAN-9-16C	455	6899	0.6	23.7930	23.6	0.0309	24.4	0.0053	6.2	0.25	34.3	2.1	30.9	7.4	-224.8	600.5	34.3	2.1
ORGAN-9-6R	150	2649	1.1	17.7998	106.9	0.0415	107.4	0.0054	10.2	0.10	34.4	3.5	41.2	43.4	459.5	738.1	34.4	3.5
ORGAN-9-13R	196	4858	1.0	22.2338	62.3	0.0332	62.8	0.0054	8.1	0.13	34.5	2.8	33.2	20.5	-56.9	1677.4	34.5	2.8
ORGAN-9-9C	732	19214	0.4	21.2842	12.7	0.0350	12.8	0.0054	1.9	0.15	34.7	0.7	34.9	4.4	48.4	303.6	34.7	0.7
ORGAN-9-1C	268	5808	0.9	28.5956	50.3	0.0261	50.7	0.0054	6.4	0.13	34.8	2.2	26.2	13.1	-711.0	1478.3	34.8	2.2
ORGAN-9-19R	184	5419	1.0	22.8902	32.8	0.0326	34.2	0.0054	9.9	0.29	34.8	3.5	32.6	11.0	-128.3	828.6	34.8	3.5
ORGAN-9-12C	131	2762	1.1	20.0385	54.7	0.0375	55.2	0.0055	7.5	0.14	35.0	2.6	37.4	20.3	190.5	1372.4	35.0	2.6
ORGAN-9-10C	189	3759	1.0	29.5440	65.5	0.0255	66.0	0.0055	8.2	0.12	35.1	2.9	25.5	16.6	-802.7	2062.5	35.1	2.9
ORGAN-9-8R	62	911	1.0	0.2711	3620.2	2.7790	3620.3	0.0055	19.2	0.01	35.1	6.7	1349.9	#NUM!	#VALUE!	804.2	35.1	6.7
ORGAN-9-25R	195	3003	1.0	16.9842	32.7	0.0446	33.3	0.0055	6.1	0.18	35.3	2.1	44.3	14.4	562.6	731.1	35.3	2.1
ORGAN-9-1R	138	4192	0.9	22.3671	53.9	0.0341	54.9	0.0055	10.2	0.19	35.6	3.6	34.0	18.4	-71.5	1413.9	35.6	3.6
ORGAN-9-4R	187	2169	1.1	17.1932	39.3	0.0449	40.6	0.0056	10.3	0.25	36.0	3.7	44.6	17.7	535.9	891.7	36.0	3.7
ORGAN-9-11C	223	2005	0.8	17.4224	30.6	0.0444	31.9	0.0056	8.9	0.28	36.1	3.2	44.1	13.8	506.8	688.3	36.1	3.2
ORGAN-9-15R	182	916	0.9	18.2730	38.8	0.0429	41.0	0.0057	13.4	0.33	36.6	4.9	42.7	17.1	401.0	900.5	36.6	4.9

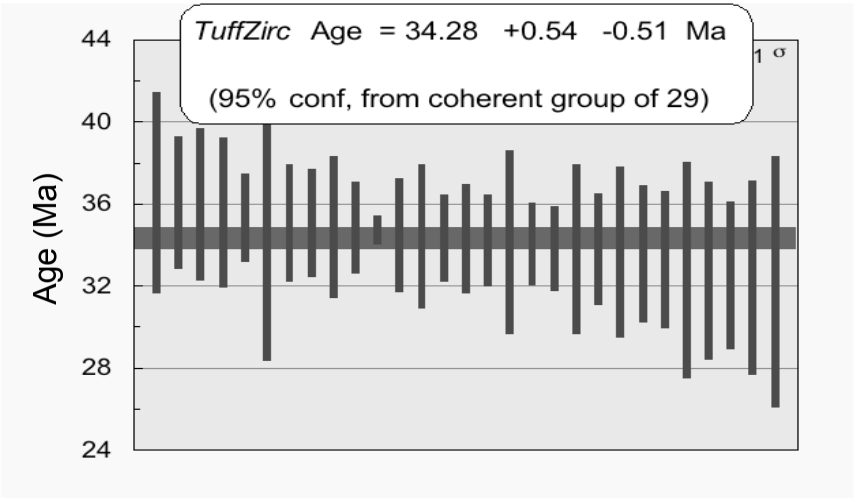

ORGAN-10, Equigranular ONP syenite							Isotope ratios						Apparent ages (Ma)						
Analysis	U	206Pb	U/Th	206Pb*	±	207Pb*	±	206Pb*	±	error	206Pb*	±	207Pb*	±	206Pb*	±	Best age	±
	(ppm)	204Pb		207Pb*	(%)	235U*	(%)	238U	(%)	corr.	238U*	(Ma)	235U	(Ma)	207Pb*	(Ma)	(Ma)	(Ma)
ORGAN-10-13C	167	587	0.6	9.9310	36.1	0.0652	40.6	0.0047	18.5	0.46	30.2	5.6	64.2	25.2	1636.9	694.9	30.2	5.6
ORGAN-10-10R	97	2176	0.6	6.8515	99.2	0.0998	101.4	0.0050	21.1	0.21	31.9	6.7	96.6	93.7	2299.0	#VALUE!	31.9	6.7
ORGAN-10-16R	59	785	0.8	6.5286	77.4	0.1101	80.4	0.0052	21.7	0.27	33.5	7.3	106.1	81.2	2381.6	672.7	33.5	7.3
ORGAN-10-5C	64	1484	0.6	7.0637	204.3	0.1021	205.5	0.0052	22.4	0.11	33.6	7.5	98.7	195.7	2246.5	12.5	33.6	7.5
ORGAN-10-6C	186	3400	0.4	21.2640	46.7	0.0346	47.9	0.0053	10.6	0.22	34.3	3.6	34.5	16.3	50.7	1174.2	34.3	3.6
ORGAN-10-18R	114	1978	0.7	8.7520	258.2	0.0854	258.4	0.0054	11.1	0.04	34.9	3.8	83.2	209.4	1868.2	487.0	34.9	3.8
ORGAN-10-1C	118	3228	0.7	27.9833	73.1	0.0268	73.9	0.0054	10.3	0.14	34.9	3.6	26.8	19.5	-651.1	2319.5	34.9	3.6
ORGAN-10-2R	153	172	0.8	14.7462	53.5	0.0508	56.8	0.0054	19.2	0.34	35.0	6.7	50.3	27.9	862.9	1199.1	35.0	6.7
ORGAN-10-13R	206	6739	0.5	20.2919	32.7	0.0371	32.9	0.0055	3.3	0.10	35.1	1.2	37.0	11.9	161.2	783.6	35.1	1.2
ORGAN-10-9C	139	2050	0.7	9.0802	191.9	0.0833	192.6	0.0055	15.4	0.08	35.3	5.4	81.2	151.4	1801.5	252.4	35.3	5.4
ORGAN-10-12C	121	2375	0.7	13.0470	119.2	0.0589	119.8	0.0056	12.2	0.10	35.8	4.4	58.1	67.8	1112.0	355.6	35.8	4.4
ORGAN-10-7C	100	2634	0.6	8.9508	140.7	0.0879	141.8	0.0057	18.2	0.13	36.7	6.7	85.5	116.9	1827.6	9.9	36.7	6.7
ORGAN-10-11R	91	2803	0.7	12.2702	165.3	0.0652	166.5	0.0058	20.3	0.12	37.3	7.6	64.1	103.8	1233.5	543.1	37.3	7.6
ORGAN-10-17R	96	800	0.6	36.8525	58.5	0.0225	59.7	0.0060	11.8	0.20	38.7	4.5	22.6	13.4	-1478.7	394.0	38.7	4.5

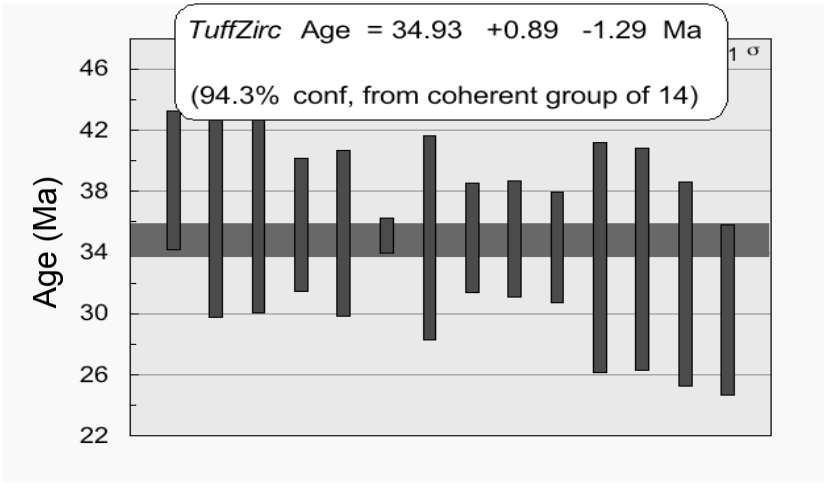

ORGAN-13, Sugarloaf Peak qtz. Monz																		
						Isotope ratios						Apparent ages (Ma)						
Analysis	U	206Pb	U/Th	206Pb*	±	207Pb*	±	206Pb*	±	error	206Pb*	±	207Pb*	±	206Pb*	±	Best age	±
	(ppm)	204Pb		207Pb*	(%)	235U*	(%)	238U	(%)	corr.	238U*	(Ma)	235U	(Ma)	207Pb*	(Ma)	(Ma)	(Ma)
ORGAN-13-16R	107	615	1.4	18.8800	54.6	0.0374	55.6	0.0051	10.4	0.19	32.9	3.4	37.3	20.3	327.3	1336.3	32.9	3.4
ORGAN-13-9R	395	6987	0.6	21.8746	25.3	0.0327	25.5	0.0052	3.2	0.13	33.4	1.1	32.7	8.2	-17.4	619.7	33.4	1.1
ORGAN-13-14R	286	4132	1.0	27.3029	50.4	0.0269	50.6	0.0053	4.9	0.10	34.3	1.7	27.0	13.5	-584.0	1444.3	34.3	1.7
ORGAN-13-13R	134	2500	1.0	21.1486	38.7	0.0348	40.6	0.0053	12.2	0.30	34.3	4.2	34.7	13.9	63.6	954.1	34.3	4.2
ORGAN-13-7R	132	2082	1.5	-2.3966	1974.4	-0.3071	1974.4	0.0053	13.0	0.01	34.3	4.5	-372.5	#NUM!	0.0	1095.5	34.3	4.5
ORGAN-13-2C	159	7252	1.0	19.3331	26.2	0.0383	26.5	0.0054	4.6	0.17	34.6	1.6	38.2	10.0	273.2	608.5	34.6	1.6
ORGAN-13-18R	402	4661	0.9	28.7722	18.5	0.0259	18.8	0.0054	3.0	0.16	34.7	1.1	25.9	4.8	-728.1	520.9	34.7	1.1
ORGAN-13-1C	1143	17519	0.4	20.8288	5.5	0.0358	5.7	0.0054	1.6	0.28	34.7	0.6	35.7	2.0	99.8	130.0	34.7	0.6
ORGAN-13-4R	313	5433	1.1	26.2342	29.2	0.0285	29.5	0.0054	4.0	0.14	34.8	1.4	28.5	8.3	-477.0	788.1	34.8	1.4
ORGAN-13-6R	211	13614	1.0	14.4905	34.4	0.0517	35.0	0.0054	6.6	0.19	34.9	2.3	51.2	17.5	899.0	731.1	34.9	2.3
ORGAN-13-20R	532	7130	0.7	20.6575	16.6	0.0363	17.1	0.0054	4.3	0.25	35.0	1.5	36.2	6.1	119.3	393.5	35.0	1.5
ORGAN-13-25R	445	8770	0.6	23.8287	32.7	0.0315	33.5	0.0054	7.2	0.22	35.0	2.5	31.5	10.4	-228.5	842.7	35.0	2.5
ORGAN-13-22R	444	10794	0.9	25.7675	30.4	0.0292	30.7	0.0055	4.2	0.14	35.1	1.5	29.3	8.9	-429.6	813.8	35.1	1.5
ORGAN-13-1R	342	7426	0.9	23.8539	41.1	0.0317	42.3	0.0055	10.1	0.24	35.3	3.5	31.7	13.2	-231.2	1074.3	35.3	3.5
ORGAN-13-3R	263	1073	1.0	13.1843	38.8	0.0574	39.1	0.0055	4.4	0.11	35.3	1.5	56.7	21.5	1091.0	808.8	35.3	1.5
ORGAN-13-5R	696	14425	0.3	20.0898	10.5	0.0377	10.9	0.0055	3.0	0.28	35.3	1.1	37.6	4.0	184.5	245.3	35.3	1.1
ORGAN-13-19R	502	9070	0.6	25.7504	16.4	0.0294	16.8	0.0055	3.6	0.21	35.3	1.3	29.5	4.9	-427.9	432.9	35.3	1.3
ORGAN-13-10R	289	8426	1.0	16.1738	11.0	0.0471	12.1	0.0055	5.0	0.41	35.5	1.8	46.7	5.5	668.2	236.3	35.5	1.8
ORGAN-13-11R	250	3452	1.2	24.6041	44.6	0.0310	44.8	0.0055	4.4	0.10	35.5	1.6	31.0	13.7	-309.9	1193.1	35.5	1.6
ORGAN-13-4C	334	3735	1.0	28.3100	41.2	0.0270	41.4	0.0056	4.5	0.11	35.7	1.6	27.1	11.1	-683.1	1180.2	35.7	1.6
ORGAN-13-3C	873	28375	0.4	22.3332	10.6	0.0343	10.8	0.0056	2.0	0.18	35.7	0.7	34.3	3.6	-67.8	260.4	35.7	0.7
ORGAN-13-8R	193	2624	1.1	21.2987	41.8	0.0362	42.5	0.0056	7.6	0.18	35.9	2.7	36.1	15.1	46.8	1040.8	35.9	2.7
ORGAN-13-17R	212	4146	1.1	23.6815	33.5	0.0327	33.8	0.0056	4.4	0.13	36.1	1.6	32.6	10.9	-212.9	862.4	36.1	1.6
ORGAN-13-12R	210	4284	1.0	18.6363	40.8	0.0416	41.7	0.0056	8.3	0.20	36.2	3.0	41.4	16.9	356.7	959.4	36.2	3.0
ORGAN-13-20C	275	2887	0.8	17.1834	38.7	0.0456	39.3	0.0057	7.1	0.18	36.5	2.6	45.3	17.4	537.2	877.4	36.5	2.6
ORGAN-13-2R	266	1155	0.8	26.0404	61.5	0.0301	62.3	0.0057	10.1	0.16	36.6	3.7	30.1	18.5	-457.4	1779.7	36.6	3.7
ORGAN-13-17C	227	402	0.8	20.6214	29.9	0.0382	31.3	0.0057	9.0	0.29	36.7	3.3	38.1	11.7	123.4	719.2	36.7	3.3
ORGAN-13-21R	211	3300	1.0	14.3013	129.4	0.0557	129.7	0.0058	9.6	0.07	37.1	3.5	55.0	69.6	926.1	554.8	37.1	3.5
ORGAN-13-23R	238	4610	0.8	33.5914	42.2	0.0237	42.6	0.0058	5.2	0.12	37.1	1.9	23.8	10.0	-1182.6	1353.4	37.1	1.9
ORGAN-13-24R	231	5656	0.8	17.9660	31.7	0.0454	33.1	0.0059	9.5	0.29	38.0	3.6	45.1	14.6	438.8	723.0	38.0	3.6

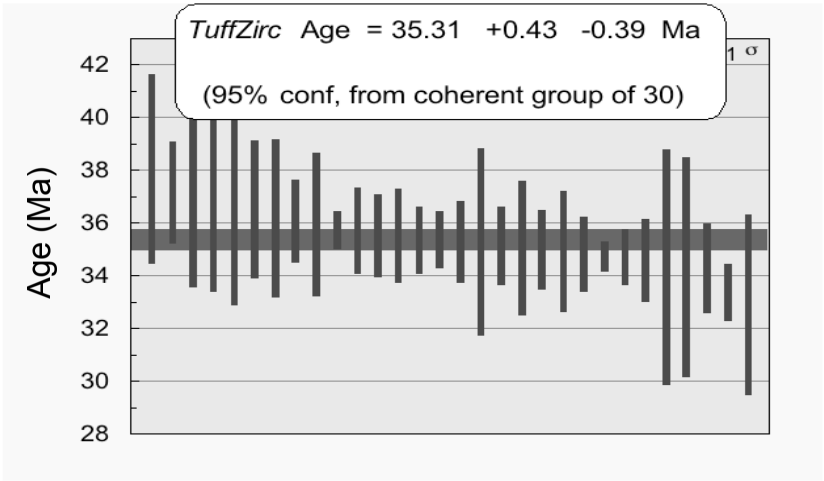

ORGAN-37, Granite of Granite Peak																			
							Isotope ratios					Apparent ages (Ma)							
Analysis	U	206Pb	U/Th	206Pb*	±	207Pb*	±	206Pb*	±	error	206Pb*	±	207Pb*	±	206Pb*	±	Best age	±
	(ppm)	204Pb		207Pb*	(%)	235U*	(%)	238U	(%)	corr.	238U*	(Ma)	235U	(Ma)	207Pb*	(Ma)	(Ma)	(Ma)
ORGAN-37-1R	157	3080	1.0	16.5163	23.8	0.0454	26.5	0.0054	11.6	0.44	34.9	4.1	45.1	11.7	623.1	521.0	34.9	4.1
ORGAN-37-3C	133	2525	0.6	22.3017	31.5	0.0340	33.0	0.0055	9.7	0.29	35.4	3.4	34.0	11.0	-64.3	786.2	35.4	3.4
ORGAN-37-4C	177	1182	0.7	6.5106	340.7	0.1134	340.9	0.0054	9.4	0.03	34.4	3.2	109.0	367.7	2386.3	360.3	34.4	3.2
ORGAN-37-4R	587	12339	0.5	21.5331	11.2	0.0351	12.0	0.0055	4.5	0.37	35.2	1.6	35.0	4.1	20.5	268.8	35.2	1.6
ORGAN-37-5R	95	4699	1.0	4.7496	474.8	0.1752	475.0	0.0060	14.8	0.03	38.8	5.7	163.9	897.0	2909.7	291.8	38.8	5.7
ORGAN-37-6R	172	3893	0.6	25.3073	36.1	0.0308	38.5	0.0057	13.3	0.35	36.4	4.8	30.8	11.7	-382.6	964.9	36.4	4.8
ORGAN-37-7C	280	2102	0.6	26.6479	59.5	0.0283	59.6	0.0055	4.4	0.07	35.2	1.5	28.4	16.7	-518.6	1728.6	35.2	1.5
ORGAN-37-7R	199	4130	1.1	18.0976	37.4	0.0410	38.5	0.0054	9.1	0.24	34.6	3.2	40.8	15.4	422.6	861.6	34.6	3.2
ORGAN-37-8R	137	3178	1.0	-4.5808	1001.5	-0.1587	1001.5	0.0053	8.7	0.01	33.9	2.9	-175.4	#NUM!	0.0	936.5	33.9	2.9
ORGAN-37-9R	282	8606	0.5	29.8258	49.4	0.0252	49.9	0.0055	6.7	0.14	35.1	2.4	25.3	12.5	-829.7	1487.8	35.1	2.4
ORGAN-37-10R	255	4632	0.4	24.0365	44.0	0.0314	44.9	0.0055	8.9	0.20	35.2	3.1	31.4	13.9	-250.5	1163.4	35.2	3.1
ORGAN-37-11R	93	2220	0.9	6.8153	151.2	0.1147	151.5	0.0057	8.8	0.06	36.5	3.2	110.3	159.6	2308.1	272.4	36.5	3.2
ORGAN-37-12R	233	3490	0.5	21.5579	25.5	0.0369	26.7	0.0058	7.9	0.30	37.1	2.9	36.8	9.6	17.7	621.3	37.1	2.9
ORGAN-37-13C	340	8598	2.0	24.4484	31.6	0.0306	32.2	0.0054	6.0	0.19	34.8	2.1	30.6	9.7	-293.6	823.4	34.8	2.1
ORGAN-37-15R	135	3342	0.7	6.2205	370.8	0.1166	371.0	0.0053	13.9	0.04	33.8	4.7	112.0	415.0	2463.6	388.8	33.8	4.7
ORGAN-37-16R	189	8368	0.7	22.8355	35.9	0.0328	37.1	0.0054	9.3	0.25	35.0	3.2	32.8	12.0	-122.4	912.4	35.0	3.2
ORGAN-37-19R	110	3461	0.9	22.0799	75.5	0.0347	76.3	0.0056	10.9	0.14	35.7	3.9	34.6	26.0	-40.0	2173.2	35.7	3.9
ORGAN-37-21R	176	2564	1.1	12.7784	272.6	0.0592	272.7	0.0055	8.5	0.03	35.3	3.0	58.4	156.0	1153.4	1213.2	35.3	3.0
ORGAN-37-22R	99	2400	0.6	10.0382	151.2	0.0744	151.6	0.0054	11.9	0.08	34.8	4.1	72.8	107.0	1617.0	186.4	34.8	4.1
ORGAN-37-23R	278	6635	0.8	20.6326	30.4	0.0384	30.8	0.0057	4.5	0.15	36.9	1.7	38.2	11.5	122.1	732.2	36.9	1.7
ORGAN-37-23C	506	15379	0.6	22.9749	14.3	0.0335	14.6	0.0056	3.1	0.21	35.9	1.1	33.5	4.8	-137.4	354.8	35.9	1.1
ORGAN-37-25R	169	2580	1.0	30.6321	44.7	0.0248	45.3	0.0055	7.5	0.16	35.4	2.6	24.9	11.1	-906.5	1352.8	35.4	2.6
ORGAN-37-28R	85	2205	0.7	18.7611	126.3	0.0418	127.0	0.0057	13.0	0.10	36.5	4.7	41.6	51.7	341.7	987.7	36.5	4.7
ORGAN-37-29R	389	6658	0.5	24.9662	38.7	0.0308	38.9	0.0056	4.2	0.11	35.8	1.5	30.8	11.8	-347.4	1030.7	35.8	1.5

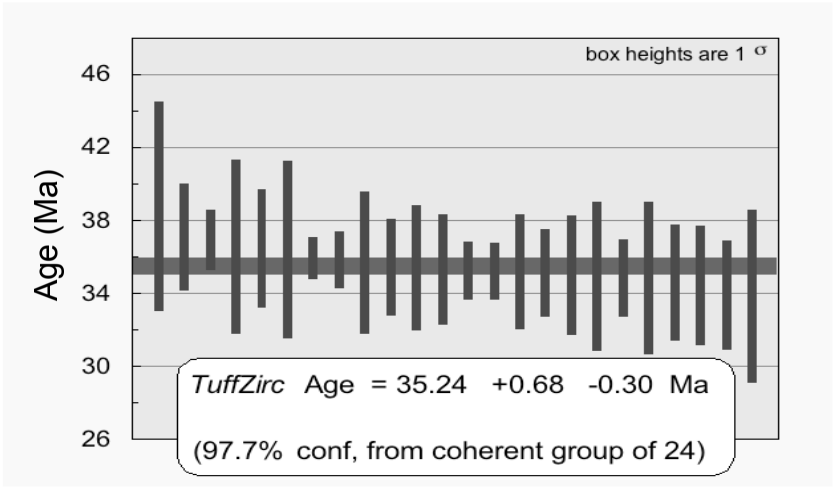

ORGAN-41, ONP alkali feldspar granite																		
						Isotope ratios						Apparent ages (Ma)						
Analysis	U	206Pb	U/Th	206Pb*	±	207Pb*	±	206Pb*	±	error	206Pb*	±	207Pb*	±	206Pb*	±	Best age	±
	(ppm)	204Pb		207Pb*	(%)	235U*	(%)	238U	(%)	corr.	238U*	(Ma)	235U	(Ma)	207Pb*	(Ma)	(Ma)	(Ma)
ORGAN-41-27C	171	1012	1.0	19.5801	51.2	0.0363	54.4	0.0052	18.2	0.34	33.2	6.0	36.2	19.4	244.1	1258.7	33.2	6.0
ORGAN-41-3C	231	1843	1.1	14.1218	39.1	0.0522	41.5	0.0053	14.1	0.34	34.4	4.8	51.7	20.9	952.0	830.7	34.4	4.8
ORGAN-41-6C	247	3957	0.9	32.0477	46.9	0.0234	47.1	0.0054	3.6	0.08	35.0	1.3	23.5	10.9	-1039.7	1469.4	35.0	1.3
ORGAN-41-5R	286	6150	0.7	24.2762	18.5	0.0309	20.1	0.0054	7.8	0.39	35.0	2.7	30.9	6.1	-275.6	473.7	35.0	2.7
ORGAN-41-2C	284	1466	1.1	26.4091	33.6	0.0288	34.2	0.0055	6.0	0.17	35.5	2.1	28.9	9.7	-494.6	915.7	35.5	2.1
ORGAN-41-10R	173	4825	1.1	17.3768	61.6	0.0440	62.1	0.0055	7.4	0.12	35.6	2.6	43.7	26.5	512.6	1502.7	35.6	2.6
ORGAN-41-22C	233	1001	1.0	18.7198	30.9	0.0409	32.9	0.0055	11.1	0.34	35.7	4.0	40.7	13.1	346.7	715.2	35.7	4.0
ORGAN-41-14R	174	4242	1.3	18.8855	45.2	0.0405	46.2	0.0056	9.7	0.21	35.7	3.4	40.4	18.3	326.7	1078.5	35.7	3.4
ORGAN-41-25R	260	5902	1.2	19.6425	23.0	0.0390	26.2	0.0056	12.6	0.48	35.8	4.5	38.9	10.0	236.8	537.2	35.8	4.5
ORGAN-41-23R	226	4843	1.1	15.4642	38.7	0.0498	40.5	0.0056	11.9	0.29	35.9	4.2	49.3	19.5	763.5	846.2	35.9	4.2
ORGAN-41-7C	267	5627	1.0	21.2184	34.1	0.0364	34.5	0.0056	5.2	0.15	36.0	1.9	36.3	12.3	55.8	835.9	36.0	1.9
ORGAN-41-21R	200	5484	1.2	12.8974	122.0	0.0599	122.3	0.0056	9.0	0.07	36.0	3.2	59.1	70.3	1135.0	357.0	36.0	3.2
ORGAN-41-10C	436	11376	0.7	19.7793	15.9	0.0392	16.3	0.0056	3.4	0.21	36.1	1.2	39.0	6.2	220.7	370.7	36.1	1.2
ORGAN-41-17R	166	4441	1.2	40.4907	178.6	0.0191	178.9	0.0056	10.8	0.06	36.1	3.9	19.3	34.1	-1802.2	0.0	36.1	3.9
ORGAN-41-3R	352	7557	1.2	20.0280	24.9	0.0390	25.2	0.0057	4.3	0.17	36.4	1.5	38.9	9.6	191.8	586.5	36.4	1.5
ORGAN-41-19R	248	4874	1.2	18.2925	39.4	0.0428	40.1	0.0057	7.6	0.19	36.5	2.8	42.5	16.7	398.6	915.0	36.5	2.8
ORGAN-41-23C	356	3281	0.7	18.9642	20.2	0.0413	20.8	0.0057	5.0	0.24	36.5	1.8	41.1	8.4	317.2	463.2	36.5	1.8
ORGAN-41-1R	207	3824	1.1	31.1637	76.8	0.0251	77.3	0.0057	8.1	0.10	36.5	3.0	25.2	19.2	-956.8	2648.7	36.5	3.0
ORGAN-41-12R	254	3776	0.8	17.8255	51.8	0.0443	52.0	0.0057	5.0	0.10	36.8	1.8	44.0	22.4	456.3	1230.1	36.8	1.8
ORGAN-41-9C	274	4714	0.7	32.6622	31.4	0.0242	32.2	0.0057	7.2	0.22	36.9	2.6	24.3	7.7	-1096.8	970.7	36.9	2.6
ORGAN-41-13R	261	6708	1.4	21.5712	32.1	0.0367	32.6	0.0057	6.1	0.19	36.9	2.3	36.6	11.7	16.3	787.9	36.9	2.3
ORGAN-41-4C	217	1521	0.9	22.3017	40.4	0.0355	40.8	0.0057	5.2	0.13	36.9	1.9	35.4	14.2	-64.3	1023.2	36.9	1.9
ORGAN-41-18C	264	11597	0.8	21.1431	34.7	0.0375	35.0	0.0057	4.4	0.13	37.0	1.6	37.4	12.8	64.3	848.9	37.0	1.6
ORGAN-41-9R	344	3654	0.6	18.3936	25.7	0.0431	26.4	0.0058	5.8	0.22	37.0	2.1	42.9	11.1	386.3	587.0	37.0	2.1
ORGAN-41-8R	174	5892	1.1	17.7953	29.3	0.0447	29.9	0.0058	5.7	0.19	37.1	2.1	44.4	13.0	460.1	663.8	37.1	2.1
ORGAN-41-20C	255	6348	1.2	15.9782	38.9	0.0499	39.5	0.0058	6.4	0.16	37.1	2.4	49.4	19.0	694.2	861.3	37.1	2.4
ORGAN-41-15R	155	2546	1.1	9.1712	338.5	0.0872	338.6	0.0058	8.9	0.03	37.3	3.3	84.9	282.8	1783.4	888.8	37.3	3.3
ORGAN-41-19C	235	4342	1.2	-8.9632	654.8	-0.0898	654.9	0.0058	12.5	0.02	37.5	4.7	-95.5	-780.0	0.0	1305.7	37.5	4.7
ORGAN-41-12C	312	10191	0.6	17.5413	23.1	0.0459	24.7	0.0058	8.7	0.35	37.5	3.3	45.6	11.0	491.9	515.8	37.5	3.3
ORGAN-41-24R	216	798	1.0	31.1166	46.9	0.0259	48.3	0.0059	11.3	0.23	37.6	4.2	26.0	12.4	-952.3	1442.1	37.6	4.2
ORGAN-41-16R	149	3233	0.9	22.1565	32.8	0.0366	34.7	0.0059	11.0	0.32	37.8	4.2	36.5	12.4	-48.4	818.2	37.8	4.2
ORGAN-41-1C	242	5562	0.8	23.1085	52.6	0.0354	53.3	0.0059	8.6	0.16	38.2	3.3	35.4	18.5	-151.8	1394.8	38.2	3.3
ORGAN-41-20R	240	4749	1.1	25.5478	49.2	0.0326	50.0	0.0060	9.0	0.18	38.8	3.5	32.6	16.0	-407.2	1358.0	38.8	3.5
ORGAN-41-4C	299	6065	1.1	10.5066	4.3	0.5441	18.4	0.0415	17.9	0.97	261.9	46.0	441.1	66.1	1531.6	80.8	261.9	46.0

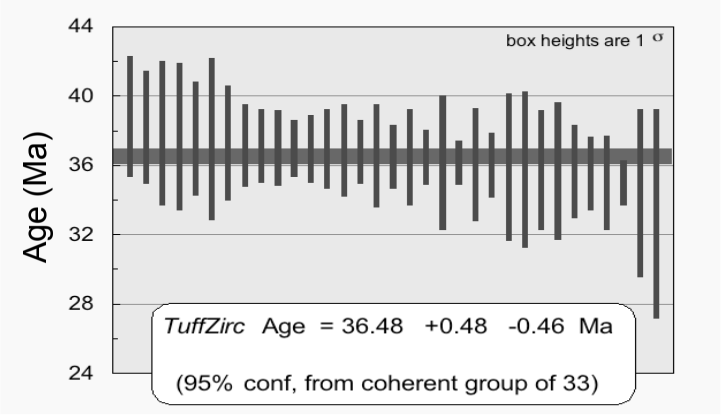

ORGAN-45, ONP monzodiorite																		
						Isotope ratios						Apparent ages (Ma)						
Analysis	U	206Pb	U/Th	206Pb*	±	207Pb*	±	206Pb*	±	error	206Pb*	±	207Pb*	±	206Pb*	±	Best age	±
	(ppm)	204Pb		207Pb*	(%)	235U*	(%)	238U	(%)	corr.	238U*	(Ma)	235U	(Ma)	207Pb*	(Ma)	(Ma)	(Ma)
ORGAN-45-1R	349	4318	1.1	23.6649	22.1	0.0341	23.1	0.0058	7.0	0.30	37.6	2.6	34.0	7.7	-211.2	559.5	37.6	2.6
ORGAN-45-3C	458	5005	1.0	18.0988	8.4	0.0419	9.5	0.0055	4.5	0.47	35.4	1.6	41.7	3.9	422.4	187.4	35.4	1.6
ORGAN-45-3R	183	2663	1.8	7.9589	1160.3	0.0956	1160.4	0.0055	5.3	0.00	35.5	1.9	92.7	#NUM!	2037.9	0.0	35.5	1.9
ORGAN-45-4C	439	6985	0.9	30.5674	28.2	0.0252	28.5	0.0056	3.9	0.14	35.9	1.4	25.3	7.1	-900.4	831.6	35.9	1.4
ORGAN-45-4R	265	3450	1.3	19.7565	26.4	0.0407	27.0	0.0058	5.7	0.21	37.5	2.1	40.5	10.7	223.4	618.8	37.5	2.1
ORGAN-45-5C	344	6225	1.1	22.0891	35.7	0.0346	35.9	0.0055	3.3	0.09	35.6	1.2	34.5	12.2	-41.0	892.9	35.6	1.2
ORGAN-45-5R	268	7959	1.3	26.0228	30.6	0.0292	31.2	0.0055	6.4	0.20	35.4	2.2	29.2	9.0	-455.6	821.7	35.4	2.2
ORGAN-45-6R	468	15175	1.1	24.5795	27.0	0.0314	27.2	0.0056	3.4	0.13	36.0	1.2	31.4	8.4	-307.3	702.4	36.0	1.2
ORGAN-45-7R	331	9034	1.3	20.0824	29.0	0.0384	29.4	0.0056	4.8	0.16	36.0	1.7	38.3	11.0	185.4	688.1	36.0	1.7
ORGAN-45-9R	638	14410	0.9	20.5544	12.2	0.0372	12.4	0.0055	1.9	0.16	35.6	0.7	37.1	4.5	131.1	288.3	35.6	0.7
ORGAN-45-10R	443	17570	0.9	24.5847	28.8	0.0313	29.0	0.0056	3.2	0.11	35.9	1.1	31.3	8.9	-307.9	749.8	35.9	1.1
ORGAN-45-11C	329	7052	0.9	19.7488	16.6	0.0404	18.6	0.0058	8.3	0.45	37.2	3.1	40.2	7.3	224.3	386.3	37.2	3.1
ORGAN-45-11R	354	5704	1.2	23.7819	31.5	0.0329	32.0	0.0057	5.6	0.17	36.5	2.0	32.9	10.4	-223.6	810.3	36.5	2.0
ORGAN-45-13C	399	6195	1.0	19.1127	20.6	0.0408	20.8	0.0056	3.3	0.16	36.3	1.2	40.6	8.3	299.5	473.1	36.3	1.2
ORGAN-45-13R	207	5553	1.4	19.3537	40.9	0.0418	41.6	0.0059	7.8	0.19	37.7	2.9	41.6	16.9	270.8	974.3	37.7	2.9
ORGAN-45-14R	350	6507	1.3	23.6947	33.4	0.0334	34.0	0.0057	6.1	0.18	36.8	2.3	33.3	11.1	-214.3	859.6	36.8	2.3
ORGAN-45-15R	507	32018	1.1	20.1493	14.3	0.0384	14.6	0.0056	3.1	0.21	36.1	1.1	38.3	5.5	177.7	334.5	36.1	1.1
ORGAN-45-16C	612	12368	0.9	20.9819	22.6	0.0375	22.9	0.0057	3.7	0.16	36.7	1.4	37.4	8.4	82.4	542.8	36.7	1.4
ORGAN-45-16R	400	9281	1.1	31.7978	22.3	0.0251	22.5	0.0058	2.7	0.12	37.2	1.0	25.2	5.6	-1016.3	669.6	37.2	1.0
ORGAN-45-17R	344	10268	0.9	20.4226	26.6	0.0358	29.2	0.0053	11.9	0.41	34.1	4.0	35.7	10.2	146.2	634.2	34.1	4.0
ORGAN-45-17C	297	5863	1.1	25.4351	28.2	0.0305	30.8	0.0056	12.4	0.40	36.2	4.5	30.5	9.3	-395.7	748.1	36.2	4.5
ORGAN-45-18C	305	3753	0.9	21.6390	25.9	0.0364	26.4	0.0057	5.2	0.20	36.7	1.9	36.3	9.4	8.8	632.7	36.7	1.9
ORGAN-45-18R	347	2805	1.0	19.4621	27.9	0.0415	28.2	0.0059	4.1	0.15	37.7	1.5	41.3	11.4	258.0	652.3	37.7	1.5
ORGAN-45-19C	349	4570	1.0	21.1707	32.4	0.0377	34.2	0.0058	11.0	0.32	37.2	4.1	37.6	12.6	61.1	789.3	37.2	4.1
ORGAN-45-20R	298	2463	1.3	23.4755	40.5	0.0322	41.2	0.0055	7.7	0.19	35.3	2.7	32.2	13.1	-191.1	1049.8	35.3	2.7
ORGAN-45-22C	353	6135	1.0	20.3815	33.2	0.0366	33.8	0.0054	6.4	0.19	34.7	2.2	36.5	12.1	150.9	796.5	34.7	2.2
ORGAN-45-22R	484	8522	1.2	24.1019	20.0	0.0322	20.7	0.0056	5.3	0.25	36.2	1.9	32.2	6.6	-257.3	511.9	36.2	1.9
ORGAN-45-23R	172	3570	1.5	14.5385	175.3	0.0532	175.6	0.0056	8.9	0.05	36.0	3.2	52.6	90.2	892.2	880.7	36.0	3.2

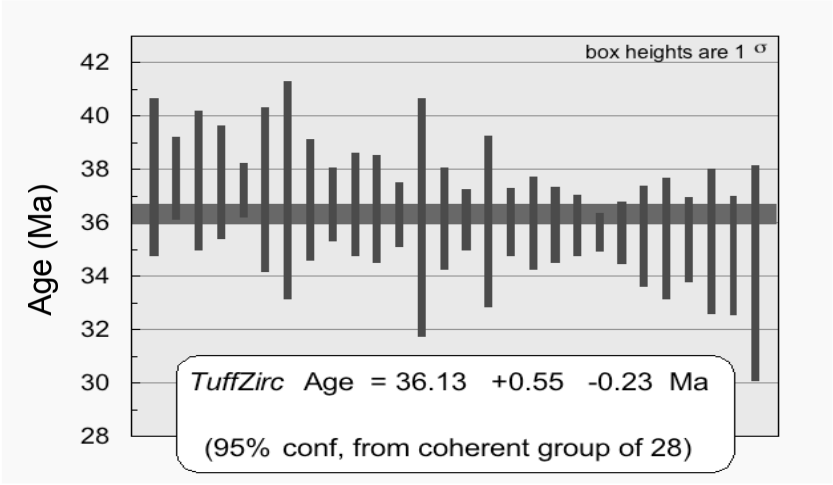

ORGAN-46, Inequigranular ONP syenite																			
							Isotope ratios					Apparent ages (Ma)							
Analysis	U	206Pb	U/Th	206Pb*	±	207Pb*	±	206Pb*	±	error	206Pb*	±	207Pb*	±	206Pb*	±	Best age	±
	(ppm)	204Pb		207Pb*	(%)	235U*	(%)	238U	(%)	corr.	238U*	(Ma)	235U	(Ma)	207Pb*	(Ma)	(Ma)	(Ma)
ORGAN-46-1C	379	8367	1.0	25.0289	39.1	0.0301	39.3	0.0055	4.0	0.10	35.2	1.4	30.1	11.7	-353.9	1043.6	35.2	1.4
ORGAN-46-1R	273	4856	2.0	79.4327	103.9	0.0094	104.0	0.0054	4.5	0.04	34.8	1.6	9.5	9.8	0.0	0.0	34.8	1.6
ORGAN-46-2R	176	2590	1.2	24.9326	45.9	0.0299	46.5	0.0054	7.8	0.17	34.8	2.7	29.9	13.7	-344.0	1239.6	34.8	2.7
ORGAN-46-3C	256	3737	0.7	22.8558	44.6	0.0332	44.9	0.0055	4.7	0.11	35.4	1.7	33.2	14.7	-124.6	1153.3	35.4	1.7
ORGAN-46-3R	200	4728	1.2	1.7805	1593.8	0.4337	1593.8	0.0056	4.7	0.00	36.0	1.7	365.8	#NUM!	0.0	430.7	36.0	1.7
ORGAN-46-4C	184	3763	1.0	34.9683	59.3	0.0213	60.5	0.0054	11.8	0.20	34.8	4.1	21.4	12.8	-1308.5	2040.0	34.8	4.1
ORGAN-46-5R	180	2753	0.6	11.7518	135.8	0.0648	136.0	0.0055	7.6	0.06	35.5	2.7	63.8	84.3	1317.7	312.1	35.5	2.7
ORGAN-46-6C	190	3520	0.9	7.7333	482.8	0.0950	483.0	0.0053	13.8	0.03	34.2	4.7	92.1	453.2	2088.6	1101.9	34.2	4.7
ORGAN-46-6R	125	1855	1.2	19.3681	38.9	0.0381	39.9	0.0053	9.0	0.23	34.4	3.1	37.9	14.9	269.1	923.5	34.4	3.1
ORGAN-46-8C	199	2633	0.9	33.2006	29.0	0.0237	31.3	0.0057	11.7	0.37	36.6	4.3	23.7	7.3	-1146.6	903.8	36.6	4.3
ORGAN-46-8R	139	6528	1.1	11.8160	218.7	0.0652	218.9	0.0056	10.5	0.05	35.9	3.8	64.1	136.9	1307.1	775.2	35.9	3.8
ORGAN-46-9C	116	2686	0.7	15.4807	39.8	0.0500	41.7	0.0056	12.5	0.30	36.1	4.5	49.5	20.1	761.2	872.0	36.1	4.5
ORGAN-46-9R	116	2179	0.8	22.7322	123.9	0.0317	124.6	0.0052	13.6	0.11	33.6	4.5	31.7	38.9	-111.2	1357.1	33.6	4.5
ORGAN-46-10C	153	3213	0.9	0.6740	2712.5	1.1097	2712.6	0.0054	9.9	0.00	34.9	3.4	758.0	#NUM!	0.0	159.1	34.9	3.4
ORGAN-46-11C	227	11514	0.9	22.5835	57.6	0.0330	58.3	0.0054	9.1	0.16	34.8	3.2	33.0	18.9	-95.1	1533.3	34.8	3.2
ORGAN-46-11R	1438	30671	1.9	21.4686	6.9	0.0356	7.3	0.0055	2.3	0.31	35.6	0.8	35.5	2.6	27.7	166.6	35.6	0.8
ORGAN-46-12C	195	4920	2.1	26.3559	56.5	0.0296	56.9	0.0057	7.2	0.13	36.4	2.6	29.6	16.6	-489.2	1616.2	36.4	2.6
ORGAN-46-13R	300	5986	1.4	20.7140	35.8	0.0389	36.7	0.0058	8.3	0.23	37.5	3.1	38.7	13.9	112.9	869.0	37.5	3.1
ORGAN-46-15R	275	3766	1.4	31.7630	35.9	0.0246	36.3	0.0057	5.5	0.15	36.4	2.0	24.6	8.8	-1013.0	1094.6	36.4	2.0
ORGAN-46-19R	99	1620	0.7	20.6828	73.0	0.0376	73.4	0.0056	7.4	0.10	36.2	2.7	37.4	27.0	116.4	2012.6	36.2	2.7
ORGAN-46-20C	100	2890	0.8	8.7747	84.1	0.0866	85.4	0.0055	14.4	0.17	35.4	5.1	84.3	69.2	1863.5	335.1	35.4	5.1
ORGAN-46-21C	164	2079	0.8	7.6934	341.6	0.1000	341.7	0.0056	7.9	0.02	35.9	2.8	96.8	326.2	2097.7	608.9	35.9	2.8
ORGAN-46-22C	504	9867	1.3	21.7724	16.4	0.0350	16.5	0.0055	2.0	0.12	35.5	0.7	34.9	5.7	-6.0	398.3	35.5	0.7
ORGAN-46-23R	182	3606	0.8	32.8891	73.5	0.0238	74.0	0.0057	7.9	0.11	36.5	2.9	23.9	17.5	-1117.9	2571.3	36.5	2.9
ORGAN-46-24R	265	6784	1.4	28.1103	28.9	0.0269	30.9	0.0055	10.9	0.35	35.3	3.8	27.0	8.2	-663.6	810.6	35.3	3.8
ORGAN-46-24C	316	8165	1.0	28.0157	28.5	0.0284	28.8	0.0058	4.3	0.15	37.1	1.6	28.5	8.1	-654.3	796.9	37.1	1.6
ORGAN-46-26R	103	2520	0.9	18.3149	71.9	0.0441	72.9	0.0059	11.8	0.16	37.6	4.4	43.8	31.3	395.9	1884.2	37.6	4.4

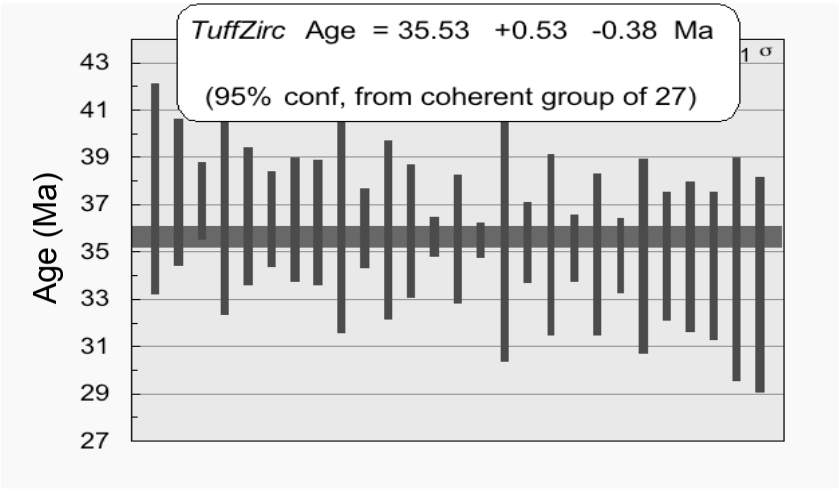

APPENDIX 3.3.

ORGAN CALDERA AR/AR DATA TABLES, IDEOGRAMS, AND AGE SPECTRA

Appendix 3.3 contains the data tables and supporting figures for all the Ar/Ar analyses conducted as part of this study. Tables 3.3.1, 3.3.2, and 3.3.3 contain the analytical data for the sanidine single-crystal laser-fusion analyses, biotite, plagioclase, hornblende, and groundmass concentrate step-heat analyses, and K-feldspar step-heat analyses, respectively. Footnotes at the bottom of each table contain addition information regarding sample preparation and irradiation, age calculations, instrumentation, and analytical parameters. Figures 3.3.1, 3.3.2, and 3.3.3 display the laser-fusion ideograms, biotite, plagioclase, hornblende, and groundmass spectra age spectra, and K-feldspar age spectra, respectively.

Table 3.3.1. Organ Caldera sanidine single-crystal laser-fusion $^{40}Ar/^{39}Ar$ analytical data.

	ID	$^{40}Ar/^{39}Ar$	$^{37}Ar/^{39}Ar$	$^{36}Ar/^{39}Ar$ (x 10^{-3})	$^{39}Ar_K$ (x 10^{-15} mol)	K/Ca	$^{40}Ar^*$ (%)	Age (Ma)	±1σ (Ma)
	ORGAN-2, Sanidine, J=0.0023237±0.05%, D=1.005±0.001, NM-227F, Lab#=59228								
	09	8.676	0.0358	0.6560	2.968	14.2	97.8	35.70	0.10
	10	8.942	0.0277	1.545	1.671	18.4	94.9	35.71	0.12
	05	8.675	0.0275	0.5594	1.856	18.6	98.1	35.81	0.10
	07	8.843	0.0269	1.080	3.326	18.9	96.4	35.87	0.08
	04	8.835	0.0258	1.050	4.703	19.8	96.5	35.87	0.07
	12	8.862	0.0300	1.135	3.363	17.0	96.2	35.88	0.09
	06	8.884	0.0274	1.210	4.265	18.6	96.0	35.88	0.08
	14	8.832	0.0272	1.015	2.984	18.8	96.6	35.90	0.09
	15	8.746	0.0307	0.7197	2.076	16.6	97.6	35.91	0.10
	11	8.680	0.0266	0.4328	2.409	19.2	98.6	35.99	0.09
	01	8.748	0.0251	0.6282	2.562	20.4	97.9	36.03	0.09
	03	8.932	0.0254	1.188	2.947	20.1	96.1	36.11	0.09
	02	8.943	0.0281	1.175	4.477	18.2	96.1	36.17	0.09
	08	8.910	0.0259	1.011	2.351	19.7	96.7	36.23	0.10
	13	8.789	0.0262	0.5450	2.243	19.5	98.2	36.31	0.09
	Mean age ± 2σ	n=15	MSWD=3.57			18.5 ±3.1		35.96	0.09
	ORGAN-4, Sanidine, J=0.0023243±0.04%, D=1.005±0.001, NM-227F, Lab#=59229								
	06	10.04	0.0215	5.318	2.533	23.7	84.4	35.66	0.11
x	04	10.98	0.0292	8.347	3.848	17.5	77.5	35.83	0.12
	13	10.57	0.0296	6.923	2.668	17.2	80.7	35.88	0.13
	01	9.038	0.0229	1.678	4.683	22.3	94.5	35.96	0.07
	02	9.147	0.0272	1.980	2.813	18.8	93.6	36.04	0.10
x	12	11.13	0.0435	8.694	2.942	11.7	76.9	36.06	0.14
	09	8.684	0.0253	0.3717	1.687	20.1	98.8	36.09	0.12
	15	8.899	0.0244	1.062	2.435	20.9	96.5	36.13	0.09
	11	8.777	0.0220	0.6399	2.996	23.2	97.9	36.15	0.09
	14	8.748	0.0235	0.5346	1.869	21.7	98.2	36.15	0.10
	05	8.779	0.0276	0.6379	2.142	18.5	97.9	36.16	0.09
	07	8.737	0.0234	0.4568	2.651	21.8	98.5	36.20	0.09
	03	8.959	0.0270	1.138	2.177	18.9	96.3	36.29	0.10
	08	8.770	0.0586	0.5003	3.897	8.7	98.4	36.30	0.08
	10	9.600	0.0484	3.250	3.201	10.5	90.0	36.37	0.10
	Mean age ± 2σ	n=13	MSWD=3.64			19.0 ±9.2		36.12	0.10
	ORGAN-6, Sanidine, J=0.0023241±0.04%, D=1.005±0.001, NM-227F, Lab#=59230								
	02	9.397	0.0942	3.274	1.174	5.4	89.8	35.51	0.17
	03	8.988	0.0760	1.845	1.119	6.7	94.0	35.56	0.16
	01	8.681	0.0748	0.8002	1.063	6.8	97.3	35.56	0.16
	15	8.714	0.0952	0.7784	1.029	5.4	97.4	35.74	0.17
	09	8.685	0.0956	0.6740	0.818	5.3	97.8	35.75	0.20
	13	8.693	0.0956	0.6767	1.101	5.3	97.8	35.77	0.16
	04	8.802	0.0965	1.040	0.853	5.3	96.6	35.78	0.20
	05	8.797	0.0899	0.9815	1.183	5.7	96.8	35.83	0.15
	12	9.067	0.0896	1.883	1.284	5.7	93.9	35.84	0.15
	08	8.823	0.0561	1.028	1.267	9.1	96.6	35.87	0.15
	07	8.585	0.0965	0.1910	0.626	5.3	99.4	35.92	0.26
	06	8.609	0.0940	0.2610	1.164	5.4	99.2	35.93	0.15
	10	8.787	0.0747	0.8567	1.018	6.8	97.2	35.94	0.17
	11	8.721	0.0591	0.6049	0.805	8.6	98.0	35.96	0.21
	14	8.716	0.0879	0.5742	0.866	5.8	98.1	35.99	0.19
	Mean age ± 2σ	n=15	MSWD=0.80			6.2 ±2.5		35.79	0.09

ORGAN-14, Sanidine, J=0.0023232±0.04%, D=1.005±0.001, NM-227F, Lab#=59231

x	10	12.70	0.0064	14.23	0.943	79.2	66.9	35.72	0.27
	04	9.270	0.0036	2.395	0.764	141.3	92.4	36.01	0.22
	13	10.73	0.0043	7.219	1.123	119.2	80.1	36.18	0.20
	05	9.128	0.0050	1.768	1.433	101.2	94.3	36.20	0.13
	15	8.881	0.0050	0.8559	1.386	101.7	97.2	36.29	0.13
x	14	11.10	0.0047	8.256	1.766	108.1	78.0	36.40	0.18
	02	9.009	0.0032	1.155	1.399	159.5	96.2	36.45	0.14
	07	9.722	0.0043	3.545	1.319	117.5	89.2	36.48	0.15
	01	9.310	0.0035	2.142	1.440	147.3	93.2	36.49	0.14
	09	10.68	0.0041	6.770	1.113	125.1	81.3	36.51	0.20
	08	9.633	0.0033	3.218	1.719	155.2	90.1	36.52	0.14
	03	9.171	0.0040	1.607	1.239	127.8	94.8	36.57	0.15
	06	9.127	0.0055	1.458	1.449	93.4	95.3	36.57	0.14
	12	9.388	0.0031	2.339	2.015	164.2	92.6	36.57	0.11
	11	9.379	0.0049	2.198	1.216	105.1	93.1	36.71	0.16
	Mean age ± 2σ	n=13	MSWD=1.39			127.6 ±48.0		36.45	0.10

ORGAN-17, Sanidine, J=0.002322±0.04%, D=1.005±0.001, NM-227F, Lab#=59232

	12	8.789	0.0035	0.5545	3.169	144.6	98.1	36.26	0.09
	15	8.915	0.0043	0.9592	2.826	118.2	96.8	36.29	0.09
x	14	10.93	0.0038	7.767	2.351	135.5	79.0	36.30	0.14
	02	9.597	0.0037	3.250	5.242	136.4	90.0	36.31	0.08
	08	8.921	0.0044	0.9387	3.139	116.9	96.9	36.33	0.09
	05	8.826	0.0031	0.5959	2.318	163.5	98.0	36.36	0.09
	06	8.890	0.0033	0.8112	2.894	152.6	97.3	36.36	0.09
	10	9.875	0.0033	4.113	2.347	152.3	87.7	36.40	0.12
	07	9.761	0.0034	3.723	4.290	150.0	88.7	36.41	0.09
x	13	11.36	0.0047	9.103	2.699	108.3	76.3	36.44	0.14
	03	9.053	0.0035	1.251	2.692	146.3	95.9	36.50	0.10
	01	8.873	0.0036	0.6376	2.766	142.1	97.9	36.51	0.09
x	04	12.77	0.0032	13.78	2.450	157.7	68.1	36.55	0.16
	11	8.991	0.0034	0.9432	6.648	149.3	96.9	36.62	0.06
	09	9.196	0.0039	1.595	2.149	131.9	94.9	36.67	0.10
	Mean age ± 2σ	n=12	MSWD=2.50			142.0 ±28.0		36.43	0.09

ORGAN-18, Sanidine, J=0.0023209±0.04%, D=1.005±0.001, NM-227F, Lab#=59233

10	8.729	0.0053	0.3018	2.018	96.1	99.0	36.30	0.10
11	9.055	0.0051	1.380	4.714	99.6	95.5	36.33	0.07
13	9.083	0.0041	1.453	2.065	124.4	95.3	36.36	0.10
15	8.693	0.0052	0.1262	2.275	97.5	99.6	36.37	0.09
01	8.940	0.0042	0.9286	2.745	120.3	96.9	36.41	0.09
08	8.760	0.0049	0.2921	3.473	105.1	99.0	36.44	0.08
09	8.787	0.0047	0.3656	6.339	109.2	98.8	36.46	0.06
14	8.714	0.0053	0.1036	2.008	96.1	99.7	36.49	0.10
02	8.857	0.0047	0.5755	4.285	108.1	98.1	36.50	0.07
07	8.740	0.0043	0.1711	5.787	119.4	99.4	36.51	0.06
06	8.713	0.0050	0.0785	5.431	101.6	99.7	36.51	0.06
04	8.709	0.0062	0.0623	2.109	82.1	99.8	36.52	0.10
12	8.729	0.0049	0.1211	2.262	105.2	99.6	36.52	0.09
03	8.776	0.0035	0.2690	6.080	145.8	99.1	36.54	0.06
Mean age ± 2σ	n=14	MSWD=0.92			107.9 ±31.2		36.46	0.05

ORGAN-27, Sanidine, J=0.0023203±0.05%, D=1.005±0.001, NM-227F, Lab#=59234

09	8.654	0.0409	0.3992	1.072	12.5	98.7	35.87	0.16
13	8.561	0.0403	0.0634	0.757	12.7	99.8	35.90	0.21
02	8.676	0.0445	0.3712	0.935	11.5	98.8	36.00	0.18
01	8.634	0.0471	0.2227	0.990	10.8	99.3	36.01	0.17
04	8.703	0.0487	0.4349	1.410	10.5	98.6	36.04	0.13
03	8.660	0.0432	0.2814	0.875	11.8	99.1	36.05	0.19
11	8.616	0.0422	0.1146	0.736	12.1	99.6	36.06	0.22

08	8.761	0.0425	0.5750	0.947	12.0	98.1	36.11	0.18
15	8.674	0.0420	0.1816	0.524	12.1	99.4	36.22	0.31
14	8.672	0.0476	0.1545	0.728	10.7	99.5	36.25	0.22
07	8.670	0.0492	0.1255	1.467	10.4	99.6	36.28	0.12
10	8.662	0.0451	0.0255	0.874	11.3	100.0	36.37	0.19
12	8.701	0.0411	0.1276	0.888	12.4	99.6	36.40	0.20
05	8.678	0.0395	-0.0708	0.882	12.9	100.3	36.55	0.19
06	8.746	0.0429	0.1401	0.956	11.9	99.6	36.58	0.18
Mean age ± 2σ	n=15	MSWD=1.51			11.7 ±1.6		36.17	0.12

ORGAN-28, Sanidine, J=0.0023205±0.04%, D=1.005±0.001, NM-227F, Lab#=59235

01	8.632	0.0415	0.2465	0.867	12.3	99.2	35.97	0.19
07	8.649	0.0407	0.2541	0.800	12.5	99.2	36.03	0.21
03	8.657	0.0411	0.2100	0.537	12.4	99.3	36.12	0.28
11	8.695	0.0462	0.2995	2.279	11.1	99.0	36.17	0.08
10	8.649	0.0316	0.1397	0.876	16.1	99.6	36.17	0.19
06	8.699	0.0530	0.3047	0.959	9.6	99.0	36.18	0.18
02	8.642	0.0473	0.0801	0.732	10.8	99.8	36.22	0.22
13	8.672	0.0398	0.1198	0.731	12.8	99.6	36.30	0.22
15	8.729	0.0481	0.2985	1.293	10.6	99.0	36.32	0.14
05	8.696	0.0400	0.1641	2.236	12.8	99.5	36.34	0.09
04	8.651	0.0362	-0.0121	0.856	14.1	100.1	36.37	0.19
09	8.664	0.0520	0.0272	0.879	9.8	100.0	36.38	0.19
08	8.634	0.0373	-0.0815	0.984	13.7	100.3	36.38	0.17
14	8.696	0.0392	0.1277	0.913	13.0	99.6	36.39	0.18
12	8.683	0.0450	-0.0687	0.717	11.3	100.3	36.58	0.22
Mean age ± 2σ	n=15	MSWD=0.71			12.2 ±3.4		36.26	0.09

Notes:
x (or i) symbol preceding sample ID denotes analyses excluded from plateau (or isochron) age calculations.
Isotopic ratios corrected for blank, radioactive decay, and mass discrimination, not corrected for interfering reactions.
Errors quoted for individual analyses include analytical error only, without interfering reaction or J uncertainties.

Age calculations:
Ages calculated relative to FC-2 Fish Canyon Tuff sanidine interlaboratory standard (28.201 Ma, Kuiper et al, 2008).
Mean age is weighted mean age of Taylor (1982). Mean age error is weighted error
of the mean (Taylor, 1982), multiplied by the root of the MSWD where MSWD>1, and also
incorporates uncertainty in J factors and irradiation correction uncertainties.
MSWD values are calculated for n-1 degrees of freedom for plateau age.
Isochron ages, $^{40}Ar/^{36}Ar_i$ and MSWD values calculated from regression results obtained by the methods of York (1969).
Decay constants and isotopic abundances after Min et al., (2000).
All errors reported at ±2σ, unless otherwise noted.

Sample preparation and irradiation:
Sanidine separates prepared using crushing, dilute HF acid treatment,
Franz magnetic separator, heavy density liquids, and hand-picking techniques.
Samples were loaded into machined Al discs and irradiated in NM-227F position for 10 hrs at the Triga Reactor
Neutron flux monitor Fish Canyon Tuff sanidine (FC-2).

Instrumentation:
Mass Analyzer Products 215-50 mass spectrometer on line with automated all-metal extraction system.
Samples were fused using a CO2 laser (heating duration 30 seconds).
Reactive gases removed during laser analysis by reaction with 2 SAES GP-50 getters, 1 operated
at ~450°C and 1 at 20°C. Gas also exposed to a W filament operated at ~2000°C.

Analytical parameters:
Electron multiplier sensitivity was 4.75 x 10^{-17} moles /pA.
Total system blank and background for the laser averaged 312, 4.48, 0.60, 2.45, 12.9 x 10^{-18} moles at masses
40,39,38,37 and 36 respectively
J-factors determined to a precision of ± 0.1% by CO_2 laser-fusion of 6 single crystals from each of 10 radial positions

around the irradiation tray.

Correction factors for interfering nuclear reactions were determined using K-glass and CaF_2 and are as follows:

$(^{39}Ar/^{37}Ar)_{Ca}$ = 0.00068 ± 2e-05

$(^{36}Ar/^{37}Ar)_{Ca}$ = 0.00028 ± 1e-05

$(^{38}Ar/^{39}Ar)_{K}$ = 0.013 ± 5e-04

$(^{40}Ar/^{39}Ar)_{K}$ = 0 ± 4e-04

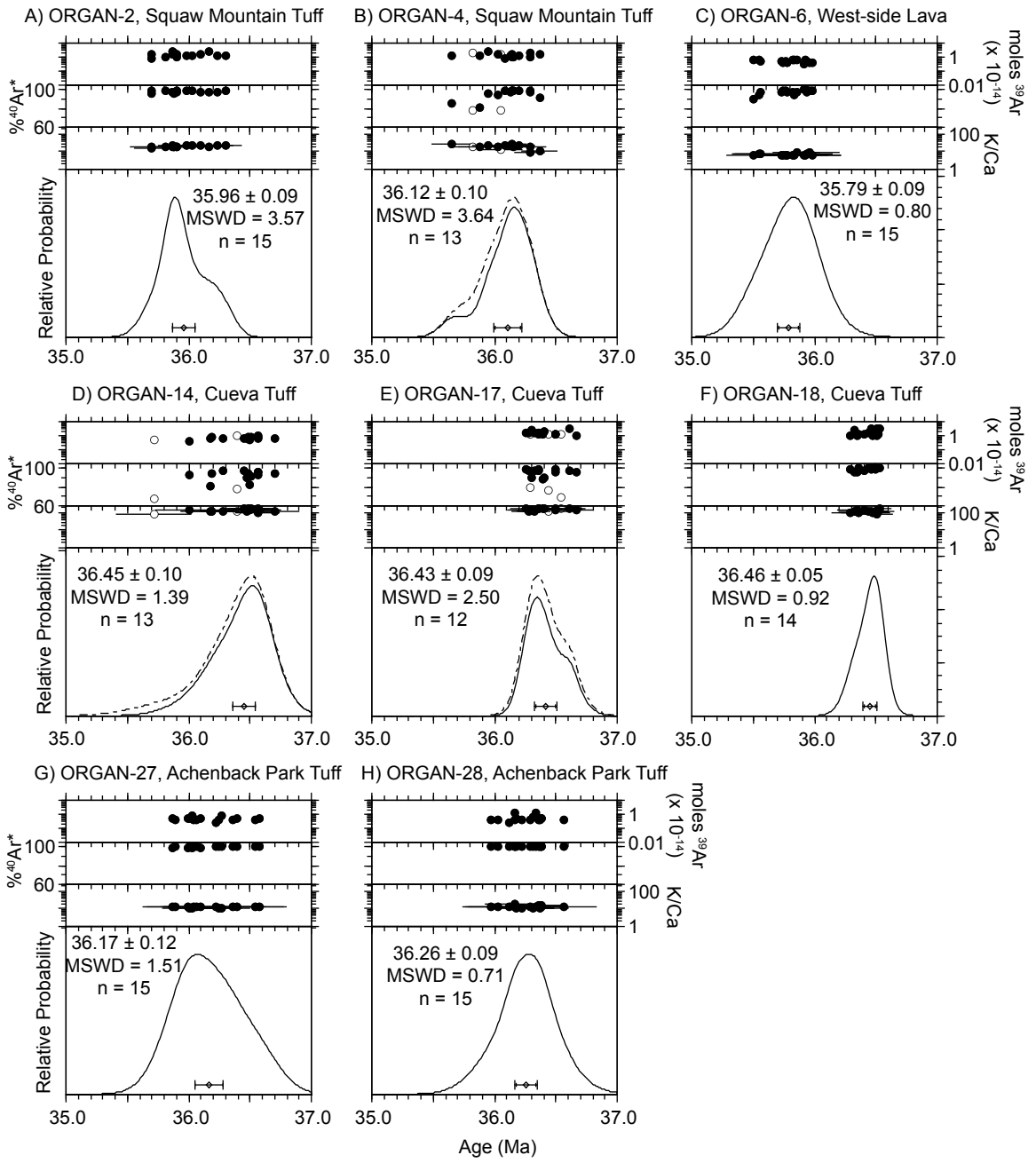

Figure 3.3.1 - Sanidine single-crystal laser-fusion ideograms. Auxiliary plots include moles ^{39}Ar, K/Ca, and radiogenic yield (%^{40}Ar*). All errors are reported at 2σ and do not include error in decay constant.

Table 3.3.2. Organ caldera bt., plag., hbl., and gmc. $^{40}Ar/^{39}Ar$ analytical data.

	ID	Power (Watts)	$^{40}Ar/^{39}Ar$	$^{37}Ar/^{39}Ar$	$^{36}Ar/^{39}Ar$ (x 10^{-3})	$^{39}Ar_K$ (x 10^{-15} mol)	K/Ca	$^{40}Ar^*$ (%)	^{39}Ar (%)	Age (Ma)	±1σ (Ma)
	ORGAN-7, Biotite, 4.45 mg, J=0.0023837±0.09%, D=1.006±0.001, NM-227L, Lab#=59272-01										
x	A	1	76.05	-0.0636	211.9	0.049	-	17.6	0.0	57.61	9.95
x	B	1	96.22	0.0312	293.9	0.132	16.4	9.7	0.1	40.47	5.46
x	C	2	28.88	0.0381	80.58	0.635	13.4	17.5	0.4	21.95	1.38
x	D	3	11.89	0.0247	15.12	1.39	20.7	62.4	1.2	32.09	0.50
x	E	4	9.440	0.0155	4.766	4.04	32.9	85.1	3.4	34.68	0.19
x	F	5	9.026	0.0105	2.732	4.15	48.5	91.1	5.6	35.48	0.16
x	G	6	9.122	0.0283	2.753	26.4	18.0	91.1	19.8	35.87	0.07
	H	8	8.894	0.0628	2.081	27.2	8.1	93.1	34.4	35.76	0.07
	I	10	8.844	0.0629	1.892	25.0	8.1	93.7	47.9	35.78	0.07
	J	13	8.918	0.0321	2.206	23.3	15.9	92.7	60.5	35.69	0.07
	K	16	8.880	0.0199	2.052	25.9	25.7	93.2	74.4	35.72	0.07
	L	18	8.864	0.0084	2.039	13.7	60.6	93.2	81.8	35.66	0.08
	M	30	8.980	0.0101	2.511	22.0	50.7	91.7	93.7	35.56	0.07
	N	35	8.723	0.0116	1.636	11.8	44.1	94.5	100.0	35.57	0.08
	Integrated age ± 2σ			n=14		185.7	16.0		K2O=6.73%	35.62	0.12
	Plateau ± 2σ	steps H-N		n=7	MSWD=1.37	148.9	26.4 ±42.7		80.2	35.68	0.09
	Isochron±2σ	steps A-N		n=14	MSWD=12.26		$^{40}Ar/^{36}Ar$=	276.5±5.1		35.85	0.09
	ORGAN-8, Biotite, 4.3 mg, J=0.0023843±0.09%, D=1.006±0.001, NM-227L, Lab#=59273-01										
x	A	1	-185.6122	0.2772	-798.1338	-0.004	1.8	-27.1	0.0	207.16	108.13
x	B	1	125.6	0.2014	439.9	0.140	2.5	-3.5	0.1	-19.39	6.49
x	C	2	81.52	0.1851	266.4	0.399	2.8	3.5	0.4	12.27	2.75
x	D	3	21.81	0.1359	51.13	0.742	3.8	30.7	1.0	29.03	0.87
x	E	4	10.91	0.1006	11.98	1.30	5.1	67.6	2.0	31.91	0.50
x	F	5	9.232	0.0802	3.407	1.08	6.4	89.2	2.8	35.54	0.41
x	G	6	8.977	0.0651	2.463	10.0	7.8	92.0	10.6	35.64	0.08
x	H	8	8.779	0.0554	1.529	13.0	9.2	94.9	20.7	35.97	0.07
	I	10	8.724	0.0487	1.463	13.1	10.5	95.1	30.9	35.82	0.07
	J	13	8.649	0.0305	1.264	19.3	16.7	95.7	46.0	35.74	0.07
	K	16	8.702	0.0295	1.357	17.3	17.3	95.4	59.5	35.85	0.07
	L	18	8.710	0.0209	1.527	12.4	24.4	94.8	69.2	35.66	0.08
	M	30	8.736	0.0190	1.539	22.8	26.9	94.8	87.0	35.76	0.06
	N	35	8.632	0.0093	1.182	16.8	55.1	96.0	100.0	35.76	0.07
	Integrated age ± 2σ			n=14		128.4	15.0		K2O=4.81%	35.56	0.13
	Plateau ± 2σ	steps I-N		n=6	MSWD=0.79	101.8	25.5 ±31.6		79.3	35.77	0.08
	Isochron±2σ	steps A-N		n=14	MSWD=4.70		$^{40}Ar/^{36}Ar$=	269.4±3.2		35.94	0.08
	ORGAN-9, Biotite, 4.55 mg, J=0.0023845±0.08%, D=1.006±0.001, NM-227L, Lab#=59274-01										
x	A	1	73.21	0.4813	384.8	0.007	1.1	-55.3	0.0	-185.78	63.23
x	B	1	25.06	0.0686	81.14	0.418	7.4	4.3	0.2	4.73	1.72
x	C	2	19.13	0.0268	53.15	3.10	19.1	17.9	1.5	14.84	0.50
x	D	3	12.87	0.0111	21.09	9.25	46.0	51.6	5.3	28.72	0.21
x	E	4	10.30	0.0079	9.397	18.1	64.2	73.0	12.9	32.49	0.11
x	F	5	9.449	0.0082	5.979	15.2	62.5	81.3	19.2	33.19	0.09
	G	6	9.188	0.0211	4.840	49.3	24.2	84.4	39.9	33.52	0.07
	H	8	8.825	0.0356	3.617	43.9	14.3	87.9	58.2	33.52	0.06
	I	10	8.525	0.0477	2.441	35.4	10.7	91.6	73.0	33.73	0.06
x	J	13	8.502	0.0595	2.249	30.6	8.6	92.2	85.8	33.88	0.06
x	K	16	8.633	0.0563	2.899	15.0	9.1	90.1	92.1	33.61	0.08
x	L	18	9.089	0.0472	4.638	6.09	10.8	85.0	94.6	33.36	0.12
x	M	30	9.169	0.0449	5.007	12.9	11.4	83.9	100.0	33.24	0.10
	Integrated age ± 2σ			n=13		239.2	14.7		K2O=8.47%	33.00	0.14
	Plateau ± 2σ	steps G-I		n=3	MSWD=3.62	128.6	17.1 ±14.0		53.8	33.60	0.15

	Isochron±2σ	steps A-M	n=13	MSWD=19.89		$^{40}Ar/^{36}Ar$=	223.5±2.5		34.72	0.09
	ORGAN-12, Biotite, 5.08 mg, J=0.0023846±0.08%, D=1.006±0.001, NM-227L, Lab#=59275-01									
x	A	1	101.6	0.2017	323.9	0.064	2.5	5.8	0.0	25.54	9.59
x	B	1	90.74	0.1805	308.0	0.583	2.8	-0.3	0.5	-1.08	3.29
x	C	2	55.47	0.1197	178.5	0.924	4.3	4.9	1.1	11.90	1.91
x	D	3	12.83	0.0851	22.67	1.32	6.0	47.8	2.0	26.55	0.56
x	E	4	8.894	0.1398	5.743	1.78	3.6	81.0	3.3	31.16	0.30
x	F	5	8.953	0.1608	2.793	1.10	3.2	90.9	4.1	35.16	0.47
x	G	6	9.021	0.1233	2.027	10.7	4.1	93.5	11.6	36.40	0.08
x	H	8	8.859	0.1026	1.576	16.7	5.0	94.8	23.3	36.27	0.08
	I	10	8.693	0.0718	1.332	20.4	7.1	95.5	37.7	35.86	0.07
	J	13	8.647	0.0657	1.242	22.6	7.8	95.8	53.6	35.78	0.06
	K	16	8.608	0.0398	1.031	20.8	12.8	96.5	68.2	35.86	0.06
	L	18	8.610	0.0216	1.091	16.9	23.6	96.3	80.1	35.79	0.07
	M	30	8.630	0.0187	1.309	17.7	27.3	95.5	92.5	35.60	0.07
	N	35	8.657	0.0160	1.265	10.7	32.0	95.7	100.0	35.77	0.08
	Integrated age ± 2σ		n=14			142.3	8.6	K2O=4.51%		35.43	0.14
	Plateau ± 2σ	steps I-N	n=6	MSWD=1.87		109.1	16.6 ±21.2		76.7	35.78	0.09
	Isochron±2σ	steps A-N	n=14	MSWD=42.23		$^{40}Ar/^{36}Ar$=	264.1±3.0			36.03	0.07
	ORGAN-13, Biotite, 4.78 mg, J=0.0023845±0.07%, D=1.006±0.001, NM-227L, Lab#=59276-01									
x	A	1	-46.5673	0.1675	-237.1100	-0.008	3.0	-50.5	0.0	99.83	55.11
x	B	1	66.22	0.4160	226.5	0.082	1.2	-1.0	0.0	-2.97	7.52
x	C	2	21.16	0.2609	56.21	0.752	2.0	21.6	0.3	19.81	1.08
x	D	3	11.94	0.0365	15.41	5.98	14.0	61.9	2.7	31.94	0.18
	E	4	8.975	0.0145	4.257	14.5	35.1	86.0	8.3	33.35	0.09
	F	5	8.254	0.0115	1.649	13.8	44.3	94.1	13.7	33.56	0.08
	G	6	8.003	0.0291	0.8113	53.2	17.5	97.0	34.5	33.55	0.05
	H	8	7.877	0.0466	0.4564	59.2	10.9	98.3	57.7	33.47	0.05
	I	10	7.857	0.0429	0.3359	39.8	11.9	98.8	73.2	33.53	0.05
	J	13	7.834	0.0388	0.3232	33.9	13.1	98.8	86.5	33.45	0.05
	K	16	7.847	0.0502	0.4172	17.2	10.2	98.5	93.2	33.39	0.07
x	L	18	7.816	0.0438	0.5956	6.94	11.6	97.8	95.9	33.03	0.09
x	M	30	7.875	0.0367	0.6314	7.89	13.9	97.7	99.0	33.23	0.10
x	N	35	8.010	0.0292	1.183	2.57	17.5	95.7	100.0	33.11	0.20
	Integrated age ± 2σ		n=14			255.7	13.5	K2O=8.62%		33.37	0.10
	Plateau ± 2σ	steps E-K	n=7	MSWD=1.44		231.5	16.4 ±27.2		90.5	33.48	0.07
	Isochron±2σ	steps A-N	n=14	MSWD=10.01		$^{40}Ar/^{36}Ar$=	266.9±4.0			33.53	0.06
	ORGAN-24, Biotite, 4.54 mg, J=0.0023842±0.05%, D=1.006±0.001, NM-227L, Lab#=59277-01									
x	A	1	-6.1815	1.127	63.29	-0.006	0.45	400.5	0.0	-111.64	76.14
x	B	1	73.12	0.2929	237.6	0.068	1.7	4.0	0.0	12.74	7.75
x	C	2	23.21	0.2067	55.75	0.688	2.5	29.1	0.3	29.21	1.34
x	D	3	11.20	0.0478	12.00	4.63	10.7	68.4	2.2	33.09	0.21
	E	4	8.739	0.0100	2.415	14.0	51.3	91.8	8.0	34.66	0.08
	F	5	8.278	0.0065	0.9172	15.0	78.0	96.7	14.2	34.58	0.07
	G	6	8.181	0.0185	0.4304	55.2	27.6	98.5	37.1	34.79	0.05
	H	8	8.093	0.0444	0.2466	51.9	11.5	99.2	58.6	34.65	0.05
	I	10	8.099	0.0522	0.2623	36.5	9.8	99.1	73.7	34.66	0.05
	J	13	8.100	0.0635	0.3002	29.3	8.0	99.0	85.9	34.62	0.05
	K	16	8.108	0.0883	0.3321	13.9	5.8	98.9	91.7	34.62	0.07
	L	18	8.147	0.0929	0.5063	6.75	5.5	98.3	94.5	34.57	0.09
x	M	30	8.119	0.0596	0.5067	10.5	8.6	98.2	98.8	34.44	0.07
x	N	35	8.380	0.0600	1.598	2.87	8.5	94.4	100.0	34.17	0.19
	Integrated age ± 2σ		n=14			241.2	11.9	K2O=8.56%		34.61	0.09
	Plateau ± 2σ	steps E-L	n=8	MSWD=1.50		222.4	21.2 ±53.2		92.2	34.66	0.06
	Isochron±2σ	steps A-N	n=14	MSWD=3.29		$^{40}Ar/^{36}Ar$=	271.0±5.6			34.69	0.05
	ORGAN-25, Biotite, 4.94 mg, J=0.0023839±0.05%, D=1.006±0.001, NM-227L, Lab#=59278-01									
x	A	1	16.93	0.0450	58.41	0.033	11.3	-2.0	0.0	-1.47	12.03

x	B	1	24.86	0.0368	81.50	1.12	13.9	3.1	0.4	3.35	1.06
x	C	2	21.08	0.0174	61.13	6.26	29.2	14.3	2.9	13.08	0.47
x	D	3	13.85	0.0071	25.67	17.1	71.4	45.2	9.5	27.11	0.21
x	E	4	10.98	0.0055	12.25	31.8	93.0	67.0	21.8	31.81	0.11
x	F	5	10.34	0.0052	9.425	26.0	98.0	73.1	31.9	32.65	0.11
	G	6	10.23	0.0103	8.562	63.4	49.4	75.3	56.5	33.27	0.09
	H	8	10.39	0.0205	8.760	45.6	24.9	75.1	74.1	33.70	0.09
	I	10	10.19	0.0354	8.246	26.0	14.4	76.1	84.2	33.48	0.10
	J	13	9.920	0.0601	7.426	21.6	8.5	77.9	92.6	33.39	0.10
x	K	16	9.583	0.0804	5.972	10.6	6.3	81.6	96.6	33.79	0.10
x	L	18	9.977	0.0737	7.541	2.67	6.9	77.7	97.7	33.49	0.25
x	M	30	9.803	0.0835	6.670	4.56	6.1	80.0	99.4	33.85	0.17
x	N	35	10.15	0.0810	7.466	1.43	6.3	78.3	100.0	34.34	0.42
	Integrated age ± 2σ			n=14		258.1	22.2		K2O=8.42%	32.15	0.19
	Plateau ± 2σ	steps G-J		n=4	MSWD=3.75	156.6	30.8	±36.1	60.7	33.46	0.19
	Isochron±2σ	steps A-N		n=14	MSWD=9.31		$^{40}Ar/^{36}Ar$=	208.1±2.2		36.42	0.12
	ORGAN-31, Biotite, 8.51 mg, J=0.0023836±0.06%, D=1.006±0.001, NM-227L, Lab#=59279-02										
x	A	650	60.25	0.0463	193.0	0.78	11.0	5.3	0.4	13.95	1.78
x	B	750	21.86	0.0132	49.29	1.65	38.7	33.4	1.1	31.52	0.65
x	C	850	13.08	0.0043	17.44	10.1	119.5	60.6	5.7	34.22	0.18
	D	920	10.82	0.0033	9.249	11.3	156.2	74.7	10.9	34.93	0.14
	E	1000	10.58	0.0041	8.151	12.7	123.4	77.2	16.7	35.27	0.13
	F	1075	10.28	0.0050	7.048	17.4	101.6	79.7	24.6	35.39	0.10
	G	1110	9.400	0.0049	4.100	17.3	105.0	87.1	32.5	35.35	0.09
	H	1180	9.078	0.0295	3.186	30.8	17.3	89.7	46.5	35.13	0.07
	I	1210	8.688	0.0355	1.813	44.0	14.4	93.9	66.5	35.20	0.06
	J	1250	8.434	0.0232	1.026	47.3	22.0	96.4	88.1	35.11	0.05
x	K	1300	8.314	0.0035	0.6684	19.5	143.8	97.6	97.0	35.04	0.06
x	L	1720	8.780	0.0069	1.940	6.7	74.3	93.5	100.0	35.43	0.12
	Integrated age ± 2σ			n=12		219.6	27.7		K2O=4.16%	35.03	0.13
	Plateau ± 2σ	steps D-J		n=7	MSWD=2.33	180.8	50.4	±116.4	82.3	35.19	0.10
	Isochron±2σ	steps A-L		n=12	MSWD=11.07		$^{40}Ar/^{36}Ar$=	281.6±2.6		35.32	0.07
	Organ-35, Biotite, 5.47 mg, J=0.0016057±0.15%, D=1.002±0.001, NM-236D, Lab#=59745-01										
x	A	2	191.2	0.0503	633.6	0.380	10.2	2.1	0.3	11.73	3.66
x	B	3	51.48	0.0184	155.6	1.02	27.8	10.7	0.9	16.07	1.08
x	C	4	34.84	0.0079	91.62	1.39	64.7	22.3	1.9	22.67	0.64
x	D	5	20.76	0.0024	34.59	1.21	209.3	50.7	2.7	30.69	0.34
x	E	6	18.59	0.0015	22.95	2.90	333.5	63.5	4.7	34.36	0.21
	F	8	16.57	0.0011	14.02	10.5	469.7	75.0	11.7	36.13	0.12
	G	10	14.14	0.0007	5.840	12.7	699.4	87.8	20.3	36.11	0.08
	H	13	13.64	0.0002	4.032	23.3	2117.9	91.3	36.0	36.21	0.07
	I	16	13.34	0.0004	3.091	25.0	######	93.2	52.9	36.13	0.07
	J	18	13.41	0.0002	3.234	15.3	######	92.9	63.2	36.22	0.07
	K	30	13.29	0.0000	2.944	37.8	#######	93.5	88.7	36.10	0.06
	L	35	13.63	0.0004	3.948	16.7	######	91.4	100.0	36.25	0.07
	Integrated age ± 2σ			n=12		148.3	742.0		K2O=6.49%	35.75	0.17
	Plateau ± 2σ	steps F-L		n=7	MSWD=0.78	141.4	4243.7	±7690.0	95.3	36.17	0.12
	Isochron±2σ	steps A-L		n=12	MSWD=36.76		$^{40}Ar/^{36}Ar$=	264.0±2.1		36.52	0.12
	Organ-36, Biotite, 5.11 mg, J=0.0016086±0.16%, D=1.002±0.001, NM-236D, Lab#=59746-01										
x	A	2	639.5	0.0898	2151.5	0.050	5.7	0.6	0.0	10.82	17.26
x	B	3	251.8	0.1150	854.3	0.175	4.4	-0.2	0.2	-1.78	5.34
x	C	4	102.8	0.0947	332.4	0.372	5.4	4.4	0.5	13.39	2.65
x	D	5	56.48	0.0530	163.8	0.328	9.6	14.3	0.8	23.65	1.95
x	E	6	38.89	0.0256	99.42	1.45	19.9	24.4	2.1	27.77	0.65
x	F	8	17.92	0.0100	20.10	11.2	51.0	66.8	11.8	34.90	0.15
	G	10	13.81	0.0119	4.890	14.5	42.9	89.5	24.4	36.04	0.08
	H	13	13.40	0.0155	3.573	18.0	32.9	92.1	40.1	35.98	0.07
	I	16	13.31	0.0193	3.024	17.1	26.4	93.3	54.9	36.17	0.07

	J	18	13.17	0.0282	2.938	12.6	18.1	93.4	65.9	35.85	0.07
	K	30	13.07	0.0580	2.528	23.5	8.8	94.3	86.3	35.91	0.06
	L	35	13.22	0.0386	2.996	15.8	13.2	93.3	100.0	35.94	0.07
	Integrated age ± 2σ			n=12		115.2	17.6		K2O=5.38%	35.60	0.18
	Plateau ± 2σ	steps G-L		n=6	MSWD=2.35	101.6	22.7	±25.7	88.2	35.98	0.14
	Isochron±2σ	steps A-L		n=12	MSWD=8.32		$^{40}Ar/^{36}Ar$=	276.7±2.1		36.14	0.13
	Organ-37, Biotite, 5.8 mg, J=0.0016102±0.16%, D=1.002±0.001, NM-236D, Lab#=59747-01										
x	A	2	136.6	0.0517	452.7	0.264	9.9	2.1	0.2	8.24	3.29
x	B	3	50.65	0.0470	163.1	0.693	10.8	4.8	0.7	7.16	1.14
x	C	4	41.96	0.0287	125.9	0.90	17.8	11.3	1.4	13.98	0.96
x	D	5	30.79	0.0191	79.10	0.714	26.7	24.1	1.9	21.71	0.84
x	E	6	20.11	0.0109	32.68	2.56	46.9	52.0	3.7	30.53	0.26
x	F	8	15.16	0.0056	10.72	17.2	90.6	79.1	16.3	34.98	0.10
	G	10	13.95	0.0049	6.190	16.9	103.9	86.9	28.6	35.37	0.08
	H	13	13.92	0.0069	5.985	17.8	73.5	87.3	41.6	35.43	0.08
	I	16	13.54	0.0125	4.648	18.2	40.9	89.9	54.9	35.48	0.07
	J	18	13.46	0.0242	4.405	13.8	21.1	90.3	65.0	35.46	0.08
	K	30	13.20	0.0437	3.617	29.7	11.7	91.9	86.6	35.40	0.06
	L	35	13.18	0.0288	3.594	18.3	17.7	92.0	100.0	35.34	0.07
	Integrated age ± 2σ			n=12		137.1	25.0		K2O=5.64%	34.86	0.17
	Plateau ± 2σ	steps G-L		n=6	MSWD=0.54	114.8	41.6	±73.3	83.7	35.41	0.13
	Isochron±2σ	steps A-L		n=12	MSWD=31.54		$^{40}Ar/^{36}Ar$=	248.1±2.2		36.06	0.13
	Organ-41, Biotite, 5.13 mg, J=0.0016114±0.15%, D=1.002±0.001, NM-236D, Lab#=59748-01										
x	A	2	146.4	0.1102	479.4	0.148	4.6	3.2	0.1	13.91	4.19
x	B	3	57.30	0.0370	161.6	0.412	13.8	16.7	0.3	27.95	1.68
x	C	4	22.25	0.0101	35.69	2.58	50.7	52.6	1.9	34.16	0.31
	D	5	16.27	0.0053	13.25	4.68	96.4	75.9	4.8	36.06	0.17
	E	6	14.51	0.0034	6.903	13.3	152.3	85.9	13.0	36.39	0.09
	F	8	13.42	0.0049	3.371	28.5	104.4	92.6	30.6	36.26	0.06
	G	10	13.20	0.0112	2.695	16.3	45.5	94.0	40.6	36.20	0.07
	H	13	13.37	0.0423	3.184	21.1	12.1	93.0	53.6	36.30	0.06
	I	16	13.32	0.0670	3.117	20.8	7.6	93.1	66.4	36.20	0.07
	J	18	13.37	0.0539	3.292	13.1	9.5	92.8	74.5	36.18	0.08
	K	30	13.32	0.0472	3.013	31.8	10.8	93.3	94.1	36.29	0.06
	L	35	14.11	0.0269	5.756	9.7	19.0	88.0	100.0	36.23	0.09
	Integrated age ± 2σ			n=12		162.4	15.9		K2O=7.55%	36.18	0.16
	Plateau ± 2σ	steps D-L		n=9	MSWD=0.79	159.3	45.6	±107.2	98.1	36.25	0.12
	Isochron±2σ	steps A-L		n=12	MSWD=2.15		$^{40}Ar/^{36}Ar$=	279.4±3.5		36.42	0.13
	Organ-42, Biotite, 5.01 mg, J=0.0016122±0.14%, D=1.002±0.001, NM-236D, Lab#=59749-02										
x	A	2	85.57	0.0306	280.1	0.465	16.7	3.3	0.2	8.20	1.83
x	B	3	49.20	0.0151	157.0	1.11	33.8	5.7	0.7	8.21	0.91
x	C	4	23.89	0.0079	52.21	3.40	64.3	35.4	2.3	24.78	0.32
x	D	5	17.05	0.0066	19.70	4.26	77.5	65.8	4.3	32.82	0.19
x	E	6	14.36	0.0051	7.879	14.3	100.5	83.8	11.1	35.16	0.09
	F	8	13.36	0.0053	3.314	40.3	97.0	92.7	30.0	36.16	0.06
	G	10	13.33	0.0046	3.329	30.2	111.1	92.6	44.3	36.06	0.06
	H	13	13.26	0.0097	2.875	37.4	52.7	93.6	61.8	36.24	0.06
x	I	16	13.26	0.0159	2.525	31.7	32.1	94.4	76.8	36.55	0.06
x	J	18	13.21	0.0205	2.463	15.4	24.8	94.5	84.0	36.46	0.07
x	K	30	13.26	0.0291	2.414	24.6	17.5	94.6	95.6	36.64	0.06
x	L	35	13.29	0.0271	2.736	9.3	18.8	93.9	100.0	36.45	0.08
	Integrated age ± 2σ			n=12		212.4	40.7		K2O=10.10%	35.78	0.15
	Plateau ± 2σ	steps F-H		n=3	MSWD=2.26	107.9	85.6	±60.9	50.8	36.16	0.15
	Isochron±2σ	steps A-L		n=12	MSWD=36.99		$^{40}Ar/^{36}Ar$=	235.8±2.0		36.80	0.11
	Organ-43, Biotite, 5.21 mg, J=0.0016128±0.14%, D=1.002±0.001, NM-236D, Lab#=59750-01										
x	A	2	155.2	0.1347	524.6	0.124	3.8	0.1	0.1	0.54	5.06

x	B	3	70.27	0.0520	225.5	0.432	9.8	5.2	0.3	10.71	2.12
x	C	4	50.64	0.0474	152.9	0.694	10.8	10.8	0.7	16.10	1.24
x	D	5	35.12	0.0376	87.24	0.629	13.6	26.6	1.1	27.36	0.87
x	E	6	24.27	0.0300	45.87	2.34	17.0	44.2	2.5	31.36	0.35
x	F	8	14.80	0.0192	9.329	12.6	26.6	81.4	9.9	35.21	0.10
	G	10	13.09	0.0197	3.106	15.0	25.8	93.0	18.8	35.58	0.07
	H	13	12.78	0.0264	2.324	21.5	19.3	94.7	31.6	35.35	0.07
	I	16	12.65	0.0370	1.843	27.4	13.8	95.7	47.7	35.39	0.05
	J	18	12.56	0.0426	1.527	22.5	12.0	96.5	61.0	35.39	0.06
	K	30	12.47	0.0518	1.200	44.8	9.9	97.2	87.5	35.42	0.05
	L	35	12.67	0.0578	1.906	21.1	8.8	95.6	100.0	35.39	0.06
	Integrated age ± 2σ			n=12		169.2	12.7	K2O=7.74%		35.14	0.15
	Plateau ± 2σ	steps G-L		n=6	MSWD=1.39	152.4	13.6 ±13.0		90.1	35.42	0.12
	Isochron±2σ	steps A-L		n=12	MSWD=8.10		$^{40}Ar/^{36}Ar$=	263.7±2.4		35.61	0.11

Organ-45, Biotite, 4.91 mg, J=0.0016126±0.15%, D=1.002±0.001, NM-236D, Lab#=59751-01

X	A	2	75.62	0.0307	232.7	0.261	16.6	9.1	0.2	20.11	2.91
X	B	3	54.40	0.0242	165.9	0.587	21.1	9.9	0.7	15.79	1.31
X	C	4	33.68	0.0124	91.33	1.17	41.2	19.9	1.6	19.65	0.71
X	D	6	17.19	0.0058	22.63	4.67	87.8	61.1	5.3	30.72	0.23
X	E	8	13.42	0.0046	5.386	20.5	111.4	88.2	21.5	34.56	0.07
X	F	10	12.99	0.0067	3.549	18.3	75.7	91.9	36.0	34.89	0.07
X	G	13	12.81	0.0133	3.003	19.6	38.3	93.1	51.4	34.84	0.06
X	H	16	12.64	0.0191	1.883	19.1	26.7	95.6	66.5	35.31	0.06
X	I	18	12.62	0.0260	1.757	12.3	19.6	95.9	76.3	35.37	0.08
X	J	30	12.58	0.0298	1.725	24.0	17.1	96.0	95.3	35.28	0.06
X	K	35	13.55	0.0404	4.591	5.99	12.6	90.0	100.0	35.65	0.11
	Integrated age ± 2σ			n=11		126.3	29.5	K2O=6.13%		34.63	0.16
	Plateau ± 2σ	no plateau		n=0	MSWD=0.00	0.000	0.000±0.000		0.0	0.00	0.00
	Isochron±2σ	steps A-K		n=11	MSWD=26.34		$^{40}Ar/^{36}Ar$=	246.6±2.8		35.48	0.12

Organ-46, Biotite, 5.09 mg, J=0.0016118±0.16%, D=1.002±0.001, NM-236D, Lab#=59752-01

x	A	2	70.25	0.0206	229.2	0.498	24.7	3.6	0.4	7.38	2.25
x	B	3	33.95	0.0133	102.7	0.90	38.2	10.5	1.2	10.53	0.84
x	C	4	26.96	0.0088	69.90	1.63	58.1	23.4	2.7	18.48	0.49
x	D	5	22.27	0.0072	43.52	1.68	70.8	42.2	4.1	27.53	0.43
x	E	6	18.65	0.0052	25.33	5.47	98.5	59.8	9.0	32.61	0.20
x	F	8	14.85	0.0035	9.035	22.0	146.3	82.0	28.3	35.56	0.09
	G	10	14.28	0.0034	6.636	18.9	148.6	86.3	45.0	35.96	0.08
	H	13	14.50	0.0060	7.644	18.0	85.6	84.4	60.8	35.74	0.08
	I	16	14.26	0.0057	6.791	13.8	90.1	85.9	72.9	35.79	0.09
	J	18	13.94	0.0063	5.882	8.31	81.4	87.5	80.2	35.62	0.10
	K	30	13.46	0.0149	4.121	15.7	34.2	91.0	94.0	35.74	0.08
	L	35	13.20	0.0092	3.245	6.78	55.6	92.7	100.0	35.73	0.09
	Integrated age ± 2σ			n=12		113.8	77.1	K2O=5.33%		34.90	0.19
	Plateau ± 2σ	steps G-L		n=6	MSWD=1.57	81.6	88.2 ±77.4		71.7	35.77	0.14
	Isochron±2σ	steps A-L		n=12	MSWD=46.05		$^{40}Ar/^{36}Ar$=	225.8±2.3		36.97	0.14

Organ-47, Biotite, 5.11 mg, J=0.0016104±0.16%, D=1.002±0.001, NM-236D, Lab#=59753-01

x	A	2	70.21	0.0313	225.7	0.301	16.3	5.0	0.2	10.30	2.51
x	B	3	33.26	0.0361	100.1	0.92	14.1	11.1	0.6	10.83	0.68
x	C	4	23.45	0.0117	49.49	2.12	43.4	37.6	1.8	25.81	0.35
x	D	5	15.30	0.0049	13.53	3.06	104.5	73.9	3.4	32.99	0.20
x	E	6	14.19	0.0042	7.557	9.5	122.2	84.3	8.4	34.88	0.10
	F	8	12.99	0.0031	2.263	37.0	166.8	94.9	28.0	35.94	0.06
	G	10	12.79	0.0045	1.458	31.1	112.3	96.7	44.4	36.07	0.06
	H	13	12.72	0.0087	1.347	30.5	58.9	96.9	60.5	35.96	0.05
	I	16	12.67	0.0147	1.207	27.5	34.7	97.2	75.0	35.91	0.05
	J	18	12.63	0.0206	1.152	14.5	24.7	97.3	82.7	35.84	0.06
	K	30	12.63	0.0193	1.114	23.5	26.5	97.4	95.1	35.89	0.06
x	L	35	12.59	0.0153	1.084	9.2	33.5	97.5	100.0	35.79	0.07

	Integrated age ± 2σ		n=12		189.1	49.8	K2O=8.83%		35.56	0.15
	Plateau ± 2σ	steps F-K	n=6	MSWD=1.67	164.0	81.6 ±114.8		86.7	35.94	0.13
	Isochron±2σ	steps A-L	n=12	MSWD=23.61		$^{40}Ar/^{36}Ar$=	224.6±2.5		36.21	0.12
	ORGAN-8, Plagioclase, 10.12 mg, J=0.0023824±0.06%, D=1.005±0.001, NM-227L, Lab#=59282-01									
x	A	3	131.8	1.469	438.5	0.527	0.35	1.8	1.4	10.30	6.73
x	B	5	33.33	1.864	94.71	1.89	0.27	16.5	6.2	23.89	4.55
x	C	10	10.17	4.802	8.923	3.28	0.11	78.0	14.7	34.36	0.44
	D	15	8.639	5.162	2.586	6.63	0.099	96.1	31.8	35.94	0.19
	E	20	9.345	5.503	4.936	8.63	0.093	89.3	54.0	36.12	0.28
	F	25	9.272	5.765	4.829	6.49	0.089	89.7	70.7	36.04	0.20
	G	30	9.379	6.022	4.789	3.68	0.085	90.2	80.2	36.65	0.28
	H	33	9.533	6.300	5.531	2.57	0.081	88.3	86.8	36.47	0.32
	I	35	10.73	6.211	9.452	1.44	0.082	78.7	90.5	36.61	0.54
	J	40	11.47	6.576	12.37	1.60	0.078	72.8	94.7	36.21	0.52
	K	45	9.692	6.842	6.004	1.30	0.075	87.5	98.0	36.76	0.57
x	L	50	9.550	6.574	3.093	0.766	0.078	96.1	100.0	39.74	0.90
	Integrated age ± 2σ		n=12		38.8	0.094	K2O=0.62%		35.17	0.63
	Plateau ± 2σ	steps D-K	n=8	MSWD=1.05	32.3	0.089±0.016		83.3	36.19	0.21
	Isochron±2σ	steps A-L	n=12	MSWD=4.95		$^{40}Ar/^{36}Ar$=	283.0±6.6		36.29	0.18
	ORGAN-7, Hornblende, 13.3 mg, J=0.0023832±0.06%, D=1.005±0.001, NM-227L, Lab#=59280-01									
x	A	3	798.2	1.069	2643.1	0.170	0.48	2.2	0.3	73.97	17.26
x	B	3	205.8	0.8495	681.2	0.116	0.60	2.2	0.5	19.77	9.38
x	C	4	238.4	1.543	766.7	0.066	0.33	5.0	0.6	51.38	15.81
x	D	4	437.9	0.3250	1432.3	0.036	1.6	3.4	0.7	62.92	29.80
x	E	5	145.7	1.480	396.4	0.024	0.34	19.7	0.7	121.13	28.87
x	F	6	113.2	0.1795	378.6	0.039	2.8	1.2	0.8	5.74	21.16
x	G	8	32.18	0.5052	67.84	0.050	1.0	37.8	0.9	52.35	12.73
x	H	10	28.70	0.7152	80.21	0.064	0.71	17.6	1.0	21.92	9.56
x	I	13	28.22	0.6186	62.21	0.110	0.82	35.0	1.2	42.62	5.69
x	J	18	16.74	2.025	22.60	0.226	0.25	61.1	1.6	44.14	2.89
x	K	25	12.47	4.531	17.01	1.71	0.11	62.7	4.5	33.88	0.51
	L	30	10.08	4.875	7.375	5.07	0.10	82.4	13.3	35.98	0.24
	N	33	9.393	4.417	5.345	5.97	0.12	87.1	23.7	35.43	0.41
	O	35	9.584	6.784	5.849	6.16	0.075	87.9	34.4	36.51	0.32
	P	40	9.073	5.506	4.297	9.5	0.093	91.1	50.9	35.80	0.33
	Q	0	9.999	4.911	6.548	7.79	0.10	84.8	64.4	36.69	0.39
	R	45	8.968	5.549	3.792	10.8	0.092	92.7	83.1	36.00	0.27
	S	60	9.238	6.607	4.610	9.7	0.077	91.2	100.0	36.53	0.30
	Integrated age ± 2σ		n=18		57.6	0.093	K2O=0.70%		36.24	0.44
	Plateau ± 2σ	steps L-S	n=7	MSWD=1.62	55.0	0.093±0.030		95.5	36.13	0.30
	Isochron±2σ	steps A-S	n=18	MSWD=3.97		$^{40}Ar/^{36}Ar$=	297.4±2.6		36.04	0.20
	ORGAN-8, Hornblende, 13.35 mg, J=0.0023827±0.06%, D=1.005±0.001, NM-227L, Lab#=59281-01									
x	A	3	389.8	2.891	1335.2	0.274	0.18	-1.1	0.5	-19.61	9.76
x	B	5	155.8	2.687	527.5	0.290	0.19	0.1	1.0	0.65	5.63
x	C	10	20.86	3.015	56.27	0.192	0.17	21.5	1.3	19.48	3.51
x	D	15	13.70	1.953	18.22	0.446	0.26	61.9	2.0	36.66	1.35
x	E	20	10.54	4.152	8.466	1.70	0.12	79.6	4.9	36.28	0.42
x	F	25	8.761	4.790	3.151	6.24	0.11	94.0	15.6	35.64	0.18
	G	30	8.962	6.439	3.482	10.0	0.079	94.5	32.5	36.71	0.26
	H	33	8.846	4.941	2.848	5.35	0.10	95.2	41.6	36.44	0.19
	I	35	8.869	5.041	3.169	7.24	0.10	94.2	54.0	36.17	0.17
	J	40	8.863	5.593	3.265	12.1	0.091	94.4	74.5	36.23	0.21
	K	45	8.652	5.110	2.614	10.9	0.100	96.0	93.0	35.97	0.23
x	L	50	8.739	5.076	2.306	4.14	0.10	97.1	100.0	36.72	0.22
	Integrated age ± 2σ		n=12		58.8	0.096	K2O=0.71%		35.75	0.36
	Plateau ± 2σ	steps G-K	n=5	MSWD=1.45	45.5	0.094±0.020		77.4	36.28	0.23
	Isochron±2σ	steps A-L	n=12	MSWD=6.31		$^{40}Ar/^{36}Ar$=	283.9±2.7		36.28	0.12

Organ-36, Hornblende, 13.32 mg, J=0.0016033±0.13%, D=1.002±0.001, NM-236D, Lab#=59742-01

X	A	2	7066.6	2.402	24168.5	0.019	0.21	-1.1	0.1	-234.92	133.26
X	B	3	2874.0	1.922	9493.3	0.053	0.27	2.4	0.2	192.16	43.26
X	C	4	1030.7	1.767	3335.4	0.067	0.29	4.4	0.4	128.44	19.06
X	D	4	714.8	1.184	2244.2	0.065	0.43	7.2	0.6	145.99	14.05
X	E	5	632.4	0.9638	1889.5	0.064	0.53	11.7	0.8	205.91	13.41
X	F	6	465.4	0.5811	1390.2	0.169	0.88	11.7	1.3	153.76	7.73
X	G	8	133.2	0.4297	373.5	0.945	1.2	17.2	4.2	65.91	1.93
X	H	10	34.99	1.927	70.24	1.56	0.26	41.1	8.9	41.81	0.65
X	I	13	21.94	4.537	27.93	3.68	0.11	64.1	20.1	40.95	0.26
X	J	18	22.47	6.658	29.93	6.19	0.077	63.1	38.9	41.36	0.31
X	K	25	19.86	4.681	22.54	8.27	0.11	68.5	64.0	39.60	0.23
X	L	30	19.11	4.882	20.55	6.12	0.10	70.4	82.6	39.17	0.20
X	M	35	19.70	4.669	20.88	5.72	0.11	70.7	100.0	40.52	0.24
	Integrated age ± 2σ			n=13		32.9	0.11	K2O=0.59%		42.46	0.74
	Plateau ± 2σ	no plateau		n=0	MSWD=0.00	0.000	0.000±0.000		0.0	0.00	0.00
	Isochron±2σ	steps A-M		n=13	MSWD=28.50		$^{40}Ar/^{36}Ar$=	310.3±1.5		39.21	0.25

Organ-46, Hornblende, 12.91 mg, J=0.0016035±0.14%, D=1.002±0.001, NM-236D, Lab#=59779-01

X	A	2	4921.0	3.897	11688.1	0.026	0.13	29.8	0.1	2218.27	86.26
X	B	3	2818.0	2.481	5960.5	0.053	0.21	37.5	0.2	1816.56	45.72
X	C	4	1662.1	1.801	2500.2	0.053	0.28	55.6	0.4	1664.49	34.91
X	D	4	997.1	0.2234	1290.1	0.055	2.3	61.8	0.6	1257.69	26.51
X	E	5	587.2	0.3927	815.4	0.067	1.3	59.0	0.8	808.72	17.36
X	F	6	450.5	0.5196	665.8	0.131	0.98	56.3	1.1	625.16	8.05
X	G	8	149.3	2.619	278.6	0.623	0.19	45.0	3.0	187.58	2.08
X	H	10	44.46	5.630	48.59	1.95	0.091	68.8	8.8	87.94	0.54
X	I	13	34.05	6.544	24.28	5.54	0.078	80.5	25.2	79.12	0.30
X	J	18	29.48	6.528	20.92	7.72	0.078	80.9	48.1	68.99	0.26
X	K	25	27.14	6.704	18.83	7.44	0.076	81.6	70.1	64.15	0.27
X	L	30	30.35	6.832	22.91	4.83	0.075	79.6	84.4	69.88	0.32
X	M	35	26.57	7.045	18.30	5.26	0.072	81.9	100.0	63.06	0.28
	Integrated age ± 2σ			n=13		33.8	0.078	K2O=0.63%		90.90	0.68
	Plateau ± 2σ	no plateau		n=0	MSWD=0.00	0.000	0.000±0.000		0.0	0.00	0.00
	Isochron±2σ	steps A-M		n=13	MSWD=498.56		$^{40}Ar/^{36}Ar$=	564.8±3.5		54.09	0.40

Organ-47, Hornblende, 12.81 mg, J=0.0016043±0.15%, D=1.002±0.001, NM-236D, Lab#=59743-01

X	A	2	1873.6	2.160	5980.1	0.032	0.24	5.7	0.1	289.52	35.31
X	B	3	755.4	1.047	1897.9	0.116	0.49	25.8	0.4	497.82	11.64
X	C	4	549.4	0.9376	1096.7	0.117	0.54	41.0	0.8	565.29	9.01
X	D	4	279.9	0.4846	513.1	0.149	1.1	45.8	1.2	342.71	5.89
X	E	5	166.2	0.2559	317.1	0.194	2.0	43.6	1.7	201.40	3.74
X	F	6	91.65	0.1701	160.7	0.592	3.0	48.2	3.4	125.34	1.44
X	G	8	42.04	0.4380	60.46	2.28	1.2	57.6	9.9	69.76	0.49
X	H	10	27.39	3.890	29.98	2.74	0.13	68.9	17.8	54.70	0.34
X	I	13	22.62	7.186	20.28	5.93	0.071	76.2	34.7	50.17	0.29
X	J	18	19.21	7.641	13.31	8.85	0.067	82.9	60.0	46.42	0.22
X	K	25	23.35	7.465	18.98	7.16	0.068	78.7	80.4	53.45	0.25
X	L	30	20.04	6.851	15.22	4.30	0.074	80.5	92.7	46.96	0.33
X	M	35	20.19	7.061	15.55	2.57	0.072	80.2	100.0	47.17	0.28
	Integrated age ± 2σ			n=13		35.0	0.080	K2O=0.65%		58.28	0.52
	Plateau ± 2σ	no plateau		n=0	MSWD=0.00	0.000	0.000±0.000		0.0	0.00	0.00
	Isochron±2σ	steps A-M		n=13	MSWD=236.59		$^{40}Ar/^{36}Ar$=	436.9±3.0		43.39	0.31

ORGAN-11, gmc, 28.58 mg, J=0.0023622±0.05%, D=1.005±0.001, NM-227K, Lab#=59267-01

x	A	550	217.5	0.3594	716.0	2.86	1.4	2.7	0.9	25.37	3.90
x	B	625	35.68	0.3008	102.2	4.51	1.7	15.4	2.4	23.63	0.78
x	C	700	11.59	0.3337	11.73	7.7	1.5	70.3	4.8	34.89	0.17
x	D	750	9.854	0.3030	4.469	3.86	1.7	86.8	6.0	36.61	0.21
x	E	800	9.309	0.3349	2.371	22.6	1.5	92.8	13.2	36.93	0.08

x	F	875	8.941	0.3456	1.481	38.6	1.5	95.4	25.6	36.49	0.06
	G	975	8.968	0.2894	1.707	69.4	1.8	94.6	47.7	36.30	0.06
	H	1075	9.394	0.2338	3.208	74.6	2.2	90.1	71.5	36.21	0.06
	I	1250	10.51	0.2602	6.887	41.2	2.0	80.8	84.6	36.33	0.09
x	J	1700	12.75	0.5311	14.25	48.2	0.96	67.3	100.0	36.71	0.13
	Integrated age ± 2σ			n=10		313.6	1.6	K2O=1.78%		36.10	0.21
	Plateau ± 2σ	steps G-I		n=3	MSWD=0.82	185.3	2.0 ±0.4		59.1	36.27	0.08
	Isochron±2σ	steps A-J		n=10	MSWD=36.82		$^{40}Ar/^{36}Ar$=	285.4±1.8		36.53	0.07
	ORGAN-30, gmc, 20.71 mg, J=0.0023666±0.06%, D=1.005±0.001, NM-227K, Lab#=59263-01										
X	A	3	435.4	0.9314	1351.6	0.97	0.55	8.3	0.2	150.20	7.42
X	B	5	72.23	0.6088	163.3	10.3	0.84	33.3	2.7	101.28	0.97
X	C	10	17.14	0.3515	14.11	55.2	1.5	75.8	16.1	55.44	0.14
X	D	15	12.21	0.2777	5.388	89.5	1.8	87.1	37.7	45.50	0.08
X	E	20	11.08	0.3486	4.469	93.2	1.5	88.3	60.2	41.88	0.07
X	F	25	9.702	0.2941	3.293	90.9	1.7	90.2	82.2	37.50	0.06
X	G	30	9.599	0.3119	3.608	42.5	1.6	89.2	92.5	36.67	0.07
X	H	33	10.28	0.4347	5.113	12.0	1.2	85.6	95.4	37.73	0.13
X	I	35	10.58	0.5528	6.105	6.43	0.92	83.4	97.0	37.81	0.19
X	J	40	10.59	0.6032	5.611	6.30	0.85	84.8	98.5	38.47	0.20
X	K	45	10.83	0.6370	5.919	4.14	0.80	84.3	99.5	39.12	0.26
X	L	50	10.66	0.6428	4.778	2.05	0.79	87.2	100.0	39.84	0.41
	Integrated age ± 2σ			n=12		413.6	1.5	K2O=3.24%		44.48	0.23
	Plateau ± 2σ	no plateau		n=0	MSWD=0.00	0.000	0.000±0.000		0.0	0.00	0.00
	Isochron±2σ	steps A-L		n=12	MSWD=1354.39		$^{40}Ar/^{36}Ar$=	434.7±2.7		38.00	0.10
	ORGAN-32, gmc, 21.6 mg, J=0.0023652±0.05%, D=1.005±0.001, NM-227K, Lab#=59264-01										
X	A	550	450.7	########	1495.7	1.02	-	-42.2	0.4	-336.13	32.55
X	B	625	40.73	-92.2771	117.3	2.97	-	-3.8	1.5	-6.37	2.53
X	C	700	16.59	-38.3397	34.73	9.8	-	19.0	5.1	13.22	1.03
X	D	750	9.384	-28.5441	7.554	6.6	-	51.0	7.5	20.18	0.79
X	E	800	8.942	-7.6414	4.178	19.8	-	79.1	14.8	30.18	0.25
X	F	875	8.546	0.4217	2.777	35.4	1.2	90.8	27.9	33.26	0.09
X	G	975	8.329	-6.5986	2.016	56.7	-	86.3	48.9	30.67	0.18
X	H	1075	8.872	0.1758	3.376	42.1	2.9	88.9	64.5	33.80	0.08
X	I	1250	9.170	-7.0085	4.559	55.4	-	79.0	84.9	30.90	0.20
X	J	1700	11.56	0.5623	11.51	40.8	0.91	71.0	100.0	35.16	0.14
	Integrated age ± 2σ			n=10		270.5	-0.053	K2O=2.03%		29.65	0.52
	Plateau ± 2σ	no plateau		n=0	MSWD=0.00	0.000	0.000±0.000		0.0	0.00	0.00
	Isochron±2σ	steps A-J		n=10	MSWD=677.80		$^{40}Ar/^{36}Ar$=	217.2±1.6		33.76	0.08
	ORGAN-33, gmc, 25.26 mg, J=0.0023624±0.05%, D=1.005±0.001, NM-227K, Lab#=59265-01										
X	A	550	171.0	0.1413	485.2	0.239	3.6	16.2	0.1	115.93	5.74
X	B	625	130.6	0.4850	372.3	1.37	1.1	15.8	0.6	87.20	2.55
X	C	700	27.07	0.4127	43.78	5.2	1.2	52.3	2.4	60.26	0.45
X	D	750	16.06	0.2935	14.53	4.26	1.7	73.4	3.9	50.28	0.27
X	E	800	14.01	0.2137	8.852	15.0	2.4	81.4	9.2	48.65	0.14
X	F	875	13.52	0.1849	6.756	20.7	2.8	85.3	16.5	49.20	0.11
X	G	975	12.95	0.2266	6.161	32.0	2.3	86.1	27.8	47.55	0.10
X	H	1075	10.64	0.2514	3.972	54.4	2.0	89.2	47.0	40.56	0.08
X	I	1250	9.188	0.1965	2.816	94.1	2.6	91.1	80.2	35.81	0.06
X	J	1700	10.99	0.4316	6.232	56.3	1.2	83.6	100.0	39.28	0.08
	Integrated age ± 2σ			n=10		283.6	1.9	K2O=1.83%		41.38	0.17
	Plateau ± 2σ	no plateau		n=0	MSWD=0.00	0.000	0.000±0.000		0.0	0.00	0.00
	Isochron±2σ	steps A-J		n=10	MSWD=1622.32		$^{40}Ar/^{36}Ar$=	479.0±3.9		37.24	0.12

Notes:
x (or i) symbol preceding sample ID denotes analyses excluded from plateau (or isochron) age calculations.

Isotopic ratios corrected for blank, radioactive decay, and mass discrimination, not corrected for interfering reactions.
Errors quoted for individual analyses include analytical error only, without interfering reaction or J uncertainties.

Age calculations:

Ages calculated relative to FC-2 Fish Canyon Tuff sanidine interlaboratory standard (28.201 Ma, Kuiper et al, 2008).
Integrated age calculated by summing isotopic measurements of all steps.
Integrated age error calculated by quadratically combining errors of isotopic measurements of all steps.
Plateau age or preferred age calculated for the indicated steps by weighting each step by the inverse of the variance.
Plateau age error is inverse-variance-weighted mean error (Taylor, 1982) times root MSWD where MSWD>1.
MSWD values are calculated for n-1 degrees of freedom for plateau age.
Isochron ages, $^{40}Ar/^{36}Ar_i$ and MSWD values calculated from regression results obtained by the methods of York (1969).
Decay constants and isotopic abundances after Min et al. (2000).
Weight percent K_2O calculated from ^{39}Ar signal, sample weight, and instrument sensitivity.
All errors reported at ±2s, unless otherwise noted.

Sample preparation and irradiation:

Biotite, plagioclase, hornblende, and concentrated groundmass separates prepared using crushing,
dilute HCl acid treatment, Franz magnetic separator, heavy liquids, and hand-picking techniques.
Samples were loaded into machined Al discs and irradiated in 3 separate positions (NM-227K and L and NM-236D)
for 10 hours (NM227) or 7 hours (NM236) at the Triga Reactor
Neutron flux monitor Fish Canyon Tuff sanidine (FC-2).

Instrumentation:

Mass Analyzer Products 215-50 mass spectrometer on line with automated all-metal extraction system.
Samples were step-heated using a Mo double-vacuum resistance furnace (heating duration 10 minutes),
or CO2 laser (heating duration 1 minutes).
Reactive gases removed during furnace (laser) analysis by reaction with 3 (2) SAES GP-50 getters, 2 (1) operated
at ~450°C and 1 at 20°C. Gas also exposed to a W filament operated at ~2000°C.

Analytical parameters:

Electron multiplier sensitivity ranged from 4.15 x 10^{-17} moles/pA to 5.05 x 10^{-17} moles /pA.
Total system blank and background for the laser averaged 1234, 18.2, 1.66, 6.06, 19.3 x 10^{-18} moles.
at masses 40, 39, 38, 37, and 36 respectively
J-factors determined to a precision of ± 0.1% by CO_2 laser-fusion of 6 single crystals from each of 10 radial positions
around the irradiation tray.
Correction factors for interfering nuclear reactions were determined using K-glass and CaF_2 and are as follows:

$(^{39}Ar/^{37}Ar)_{Ca}$ = 0.00068 ± 2e-05
$(^{36}Ar/^{37}Ar)_{Ca}$ = 0.00028 ± 1e-05
$(^{38}Ar/^{39}Ar)_{K}$ = 0.013 ± 5e-4
$(^{40}Ar/^{39}Ar)_{K}$ = 0 ± 4e-4

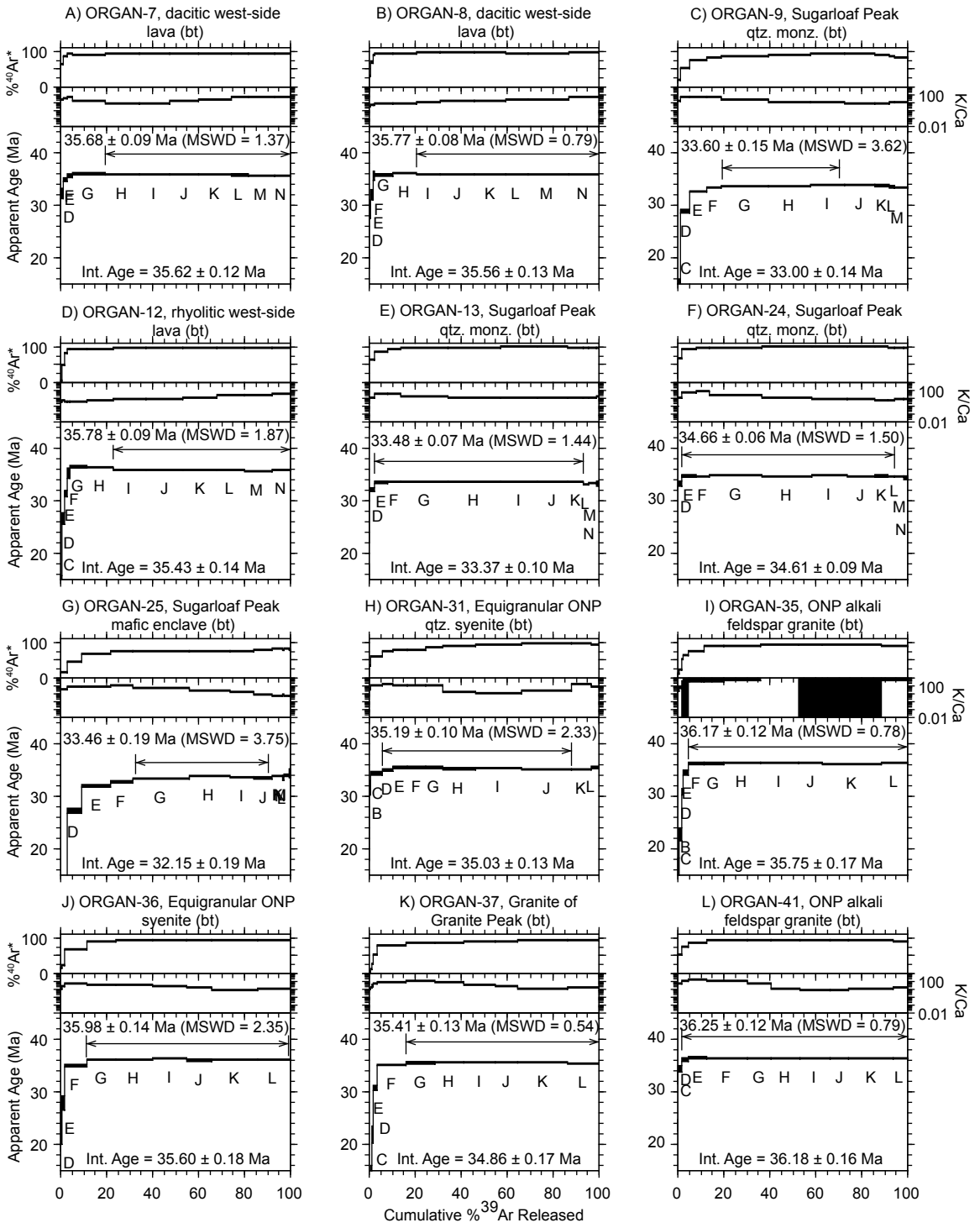

Figure 3.3.2 - Biotite, plagioclase, hornblende, and groundmass concentrate age spectra and K/Ca and radiogenic yield (%^{40}Ar*) auxiliary plots. All errors are reported at 2σ and do not include error in decay constant.

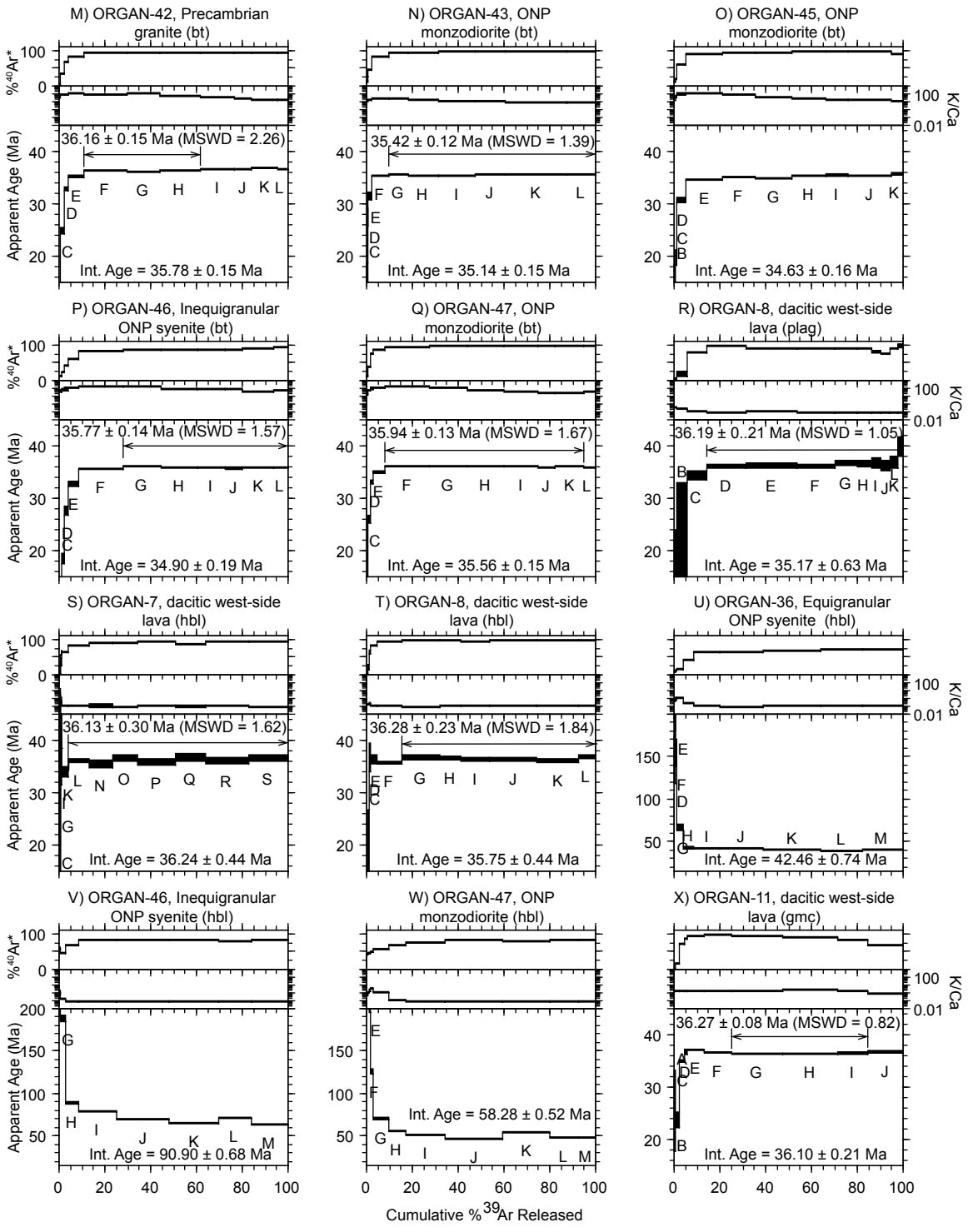

Figure 3.3.2 continued.

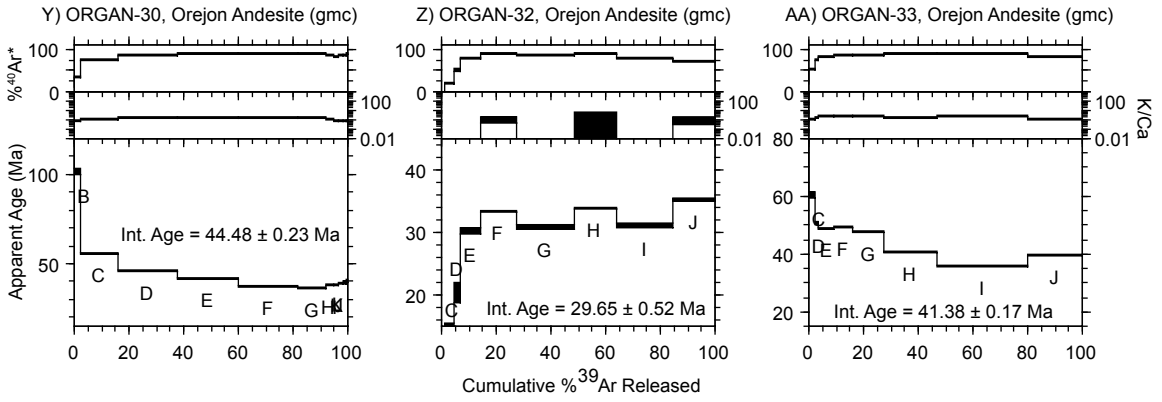

Figure 3.3.2 continued.

Table 3.3.3. Organ caldera K-feldspar $^{40}Ar/^{39}Ar$ analytical data

	ID	Power (T in °C)	$^{40}Ar/^{39}Ar$	$^{37}Ar/^{39}Ar$	$^{36}Ar/^{39}Ar$ (x 10^{-3})	$^{39}Ar_K$ (x 10^{-15} mol)	K/Ca	$^{40}Ar^*$ (%)	^{39}Ar (%)	Age (Ma)	±1σ (Ma)
	ORGAN-9, K-Feldspar, 17.88 mg, J=0.0023637±0.04%, D=1.006±0.001, NM-227J, Lab#=59257-01										
X	A	540	367.5	0.0442	1126.2	5.68	11.6	9.5	0.5	144.45	5.81
X	B	540	38.44	0.0370	103.0	3.72	13.8	20.8	0.8	34.29	0.97
X	C	590	24.66	0.0469	56.29	5.37	10.9	32.5	1.3	34.38	0.57
X	D	590	17.92	0.0537	34.86	6.06	9.5	42.5	1.9	32.65	0.42
X	E	640	24.24	0.0706	53.61	8.03	7.2	34.6	2.6	35.95	0.56
X	F	640	11.50	0.0713	13.17	9.59	7.2	66.2	3.5	32.62	0.21
X	G	690	16.83	0.0794	29.57	12.0	6.4	48.1	4.6	34.68	0.32
X	H	690	9.952	0.0680	7.954	15.2	7.5	76.4	5.9	32.58	0.14
X	I	740	12.18	0.0623	14.60	17.3	8.2	64.6	7.5	33.71	0.17
X	J	740	8.646	0.0505	3.448	21.3	10.1	88.3	9.4	32.68	0.09
X	K	790	11.25	0.0473	11.99	21.5	10.8	68.5	11.4	33.02	0.15
X	L	790	8.691	0.0364	3.510	25.2	14.0	88.1	13.6	32.79	0.09
X	M	840	11.51	0.0356	12.50	23.4	14.4	67.9	15.8	33.47	0.14
X	N	840	9.021	0.0272	4.735	26.3	18.7	84.5	18.1	32.65	0.10
X	O	890	13.12	0.0255	18.42	22.1	20.0	58.5	20.1	32.90	0.18
X	P	890	8.818	0.0226	4.152	24.5	22.5	86.1	22.3	32.52	0.10
X	Q	940	13.95	0.0209	21.21	21.0	24.4	55.1	24.2	32.93	0.20
X	R	940	9.725	0.0183	7.008	23.6	27.9	78.7	26.4	32.79	0.11
X	S	990	15.09	0.0185	24.78	21.9	27.6	51.5	28.3	33.27	0.23
X	T	990	11.72	0.0199	13.55	26.0	25.7	65.8	30.7	33.07	0.16
X	U	1040	16.50	0.0219	27.77	26.5	23.3	50.2	33.1	35.50	0.25
X	V	1040	13.78	0.0229	19.87	32.1	22.3	57.4	36.0	33.88	0.19
X	W	1090	16.57	0.0252	28.68	40.5	20.2	48.8	39.7	34.68	0.21
X	X	1090	15.27	0.0297	24.47	46.0	17.2	52.6	43.8	34.44	0.19
X	Y	1140	14.36	0.0345	20.84	48.0	14.8	57.1	48.2	35.11	0.17
X	Z	1190	12.25	0.0268	12.97	136.9	19.0	68.7	60.5	36.03	0.11
X	AA	1190	12.81	0.0169	14.49	204.9	30.2	66.6	79.0	36.49	0.12
X	AB	1190	14.50	0.0197	19.76	125.3	25.8	59.7	90.4	37.05	0.15
X	AC	1190	16.00	0.0289	24.29	61.0	17.6	55.1	95.9	37.73	0.19
X	AD	1190	17.77	0.0480	30.18	26.8	10.6	49.8	98.3	37.87	0.25
X	AE	1290	18.56	0.1425	31.86	2.76	3.6	49.3	98.6	39.18	0.58
X	AF	1340	33.70	0.2463	78.48	2.87	2.1	31.2	98.8	44.97	0.91
X	AG	1390	20.32	0.0773	34.30	2.63	6.6	50.1	99.1	43.54	0.60
X	AH	1590	19.42	0.0944	33.34	6.02	5.4	49.3	99.6	40.92	0.36
X	AI	1740	16.90	0.0288	28.19	4.43	17.7	50.7	100.0	36.70	0.39
	Integrated age ± 2σ			n=35		1106.2	17.2	K2O=10.05%		35.91	0.31
	Plateau ± 2σ	no plateau		n=0	MSWD=0.00	0.000	0.000±0.000		0.0	0.00	0.00
	Isochron±2σ	steps A-AI		n=35	MSWD=64.43		$^{40}Ar/^{36}Ar$=	326.0±1.4		32.34	0.10
	ORGAN-10, K-Feldspar, 17.31 mg, J=0.0023635±0.04%, D=1.006±0.001, NM-227J, Lab#=59258-01										
X	A	540	221.3	0.0359	670.5	2.44	14.2	10.5	0.4	97.57	4.29
X	B	540	28.30	0.0279	70.03	1.55	18.3	26.9	0.7	32.59	1.18
X	C	590	19.88	0.0371	40.29	1.94	13.7	40.1	1.0	34.16	0.80
X	D	590	15.36	0.0372	26.88	2.19	13.7	48.3	1.4	31.79	0.56
X	E	640	21.42	0.0392	45.54	2.79	13.0	37.2	1.8	34.10	0.77
X	F	640	11.76	0.0357	14.27	3.14	14.3	64.2	2.4	32.33	0.39
X	G	690	13.28	0.0386	18.74	3.79	13.2	58.3	3.0	33.18	0.45
X	H	690	9.463	0.0296	6.127	4.58	17.2	80.9	3.8	32.78	0.24
X	I	740	11.19	0.0310	11.12	5.29	16.5	70.6	4.7	33.86	0.28
X	J	740	8.560	0.0297	2.920	6.61	17.2	89.9	5.8	32.97	0.17
X	K	790	10.58	0.0323	9.741	6.80	15.8	72.8	6.9	33.00	0.22
X	L	790	8.261	0.0306	1.706	8.57	16.7	93.9	8.4	33.22	0.12
X	M	840	9.156	0.0317	4.786	8.37	16.1	84.6	9.8	33.16	0.15
X	N	840	8.270	0.0299	1.748	10.9	17.1	93.8	11.6	33.21	0.10
X	O	890	8.983	0.0301	4.176	9.82	16.9	86.3	13.3	33.19	0.15

X	P	890	8.410	0.0297	2.345	13.0	17.2	91.8	15.5	33.06	0.11
X	Q	940	9.834	0.0277	7.335	11.5	18.4	78.0	17.4	32.84	0.15
X	R	940	8.964	0.0281	4.162	15.2	18.2	86.3	20.0	33.13	0.12
X	S	990	10.87	0.0247	10.83	13.9	20.6	70.5	22.3	32.84	0.16
X	T	990	9.510	0.0273	5.864	17.3	18.7	81.8	25.2	33.31	0.13
X	U	1040	11.61	0.0245	13.54	17.8	20.8	65.5	28.2	32.57	0.17
X	V	1040	9.874	0.0265	7.629	19.8	19.3	77.2	31.6	32.64	0.14
X	W	1090	10.82	0.0260	10.92	26.2	19.6	70.2	36.0	32.54	0.14
X	X	1090	10.67	0.0270	10.39	31.2	18.9	71.2	41.2	32.56	0.13
X	Y	1140	9.873	0.0310	7.417	33.9	16.5	77.8	47.0	32.90	0.10
X	Z	1190	9.031	0.0286	3.736	122.1	17.9	87.8	67.5	33.95	0.06
X	AA	1190	9.197	0.0305	4.133	116.8	16.8	86.7	87.2	34.16	0.07
X	AB	1190	9.346	0.0351	4.441	45.5	14.5	86.0	94.9	34.40	0.08
X	AC	1190	9.879	0.0365	6.125	17.3	14.0	81.7	97.8	34.55	0.12
X	AD	1290	14.17	0.0364	12.36	2.08	14.0	74.2	98.2	44.94	0.54
X	AE	1340	22.08	0.0371	16.19	1.96	13.8	78.4	98.5	73.34	0.60
X	AF	1390	24.35	0.0415	15.19	1.27	12.3	81.6	98.7	83.98	0.83
X	AG	1590	17.94	0.0413	11.30	2.89	12.3	81.4	99.2	62.10	0.42
X	AH	1740	11.78	0.0239	9.040	4.68	21.3	77.3	100.0	38.97	0.28
	Integrated age ± 2σ			n=34		593.2	17.1	K2O=5.57%		34.28	0.17
	Plateau ± 2σ	no plateau		n=0	MSWD=0.00	0.000	0.000±0.000		0.0	0.00	0.00
	Isochron±2σ	steps A-AH		n=34	MSWD=379.36		$^{40}Ar/^{36}Ar$=	369.3±2.8		32.10	0.08

ORGAN-13, K-Feldspar, 18.18 mg, J=0.0023628±0.04%, D=1.006±0.001, NM-227J, Lab#=59259-01

X	A	540	380.9	0.0344	958.0	4.78	14.8	25.7	0.4	380.67	4.66
X	B	540	26.80	0.0345	51.73	2.88	14.8	43.0	0.6	49.10	0.69
X	C	590	23.04	0.0497	38.91	4.05	10.3	50.1	1.0	49.23	0.59
X	D	590	16.07	0.0753	20.88	4.92	6.8	61.6	1.4	42.31	0.44
X	E	640	21.91	0.0778	38.66	6.63	6.6	47.9	1.9	44.77	0.38
X	F	640	10.67	0.0598	8.307	8.02	8.5	77.0	2.6	35.15	0.20
X	G	690	14.23	0.0601	17.83	10.07	8.5	63.0	3.4	38.33	0.24
X	H	690	8.924	0.0388	3.774	12.8	13.1	87.5	4.5	33.44	0.13
X	I	740	10.68	0.0293	8.351	14.7	17.4	76.9	5.7	35.14	0.15
X	J	740	8.163	0.0204	1.810	18.7	25.0	93.5	7.2	32.66	0.09
X	K	790	9.801	0.0180	6.367	19.2	28.3	80.8	8.8	33.90	0.11
X	L	790	8.022	0.0122	1.153	23.4	42.0	95.8	10.7	32.89	0.07
X	M	840	9.582	0.0130	5.403	22.2	39.3	83.3	12.5	34.18	0.11
X	N	840	8.090	0.0098	1.555	25.3	51.8	94.3	14.6	32.67	0.08
X	O	890	10.80	0.0115	9.839	22.0	44.5	73.1	16.4	33.80	0.13
X	P	890	8.279	0.0090	2.063	24.4	56.8	92.6	18.4	32.84	0.08
X	Q	940	11.28	0.0125	11.31	21.9	40.7	70.3	20.2	33.97	0.15
X	R	940	8.569	0.0088	2.846	23.3	57.9	90.2	22.2	33.08	0.09
X	S	990	11.41	0.0116	11.72	20.8	44.0	69.6	23.9	34.01	0.16
X	T	990	9.242	0.0111	5.085	24.7	46.0	83.7	25.9	33.13	0.10
X	U	1040	11.75	0.0147	12.69	24.7	34.6	68.1	28.0	34.25	0.15
X	V	1040	10.29	0.0136	7.999	30.7	37.5	77.0	30.5	33.92	0.12
X	W	1090	12.07	0.0165	12.97	36.8	30.9	68.2	33.5	35.27	0.14
X	X	1090	11.25	0.0181	10.46	41.0	28.2	72.5	36.9	34.94	0.12
X	Y	1140	11.25	0.0203	9.644	42.2	25.1	74.7	40.4	35.94	0.12
X	Z	1190	10.12	0.0171	5.626	105.7	29.8	83.6	49.1	36.18	0.08
X	AA	1190	9.673	0.0094	3.631	192.2	54.0	88.9	64.9	36.79	0.07
X	AB	1190	9.630	0.0077	3.120	179.2	66.2	90.4	79.6	37.24	0.06
X	AC	1190	9.688	0.0090	3.239	127.1	56.6	90.1	90.1	37.34	0.07
X	AD	1190	9.822	0.0133	3.591	66.8	38.3	89.2	95.6	37.47	0.07
X	AE	1290	9.810	0.0198	2.927	17.2	25.8	91.2	97.0	38.25	0.11
X	AF	1340	10.29	0.0310	3.319	10.10	16.5	90.5	97.9	39.79	0.16
X	AG	1390	10.59	0.0195	3.772	5.73	26.2	89.5	98.3	40.48	0.20
X	AH	1590	10.92	0.0202	3.746	8.96	25.3	89.9	99.1	41.94	0.16
X	AI	1740	10.73	0.0260	5.766	11.2	19.6	84.1	100.0	38.60	0.17
	Integrated age ± 2σ			n=35		1214.2	35.1	K2O=10.86%		37.63	0.18
	Plateau ± 2σ	no plateau		n=0	MSWD=0.00	0.000	0.000±0.000		0.0	0.00	0.00
	Isochron±2σ	steps A-AI		n=35	MSWD=395.74		$^{40}Ar/^{36}Ar$=	372.6±2.1		34.12	0.06

ORGAN-21, K-Feldspar, 14.61 mg, J=0.0023617±0.05%, D=1.006±0.001, NM-227J, Lab#=59260-01

X	A	540	84.52	0.0427	239.5	1.56	11.9	16.3	0.3	58.51	2.25
X	B	540	14.05	0.0421	22.42	0.717	12.1	52.9	0.4	31.81	1.17
X	C	590	12.35	0.0809	17.81	0.963	6.3	57.4	0.5	30.36	1.04
X	D	590	10.76	0.0683	11.39	1.17	7.5	68.8	0.7	31.68	0.72
X	E	640	17.04	0.0415	33.64	1.68	12.3	41.6	1.0	30.40	0.76
X	F	640	9.125	0.0422	7.095	2.01	12.1	77.0	1.3	30.11	0.46
X	G	690	11.13	0.0317	12.47	2.80	16.1	66.9	1.7	31.88	0.45
X	H	690	8.432	0.0238	2.194	3.18	21.4	92.3	2.3	33.31	0.28
X	I	740	9.232	0.0279	4.294	4.35	18.3	86.3	3.0	34.08	0.24
X	J	740	8.368	0.0254	1.676	5.07	20.1	94.1	3.8	33.69	0.18
X	K	790	9.368	0.0271	4.836	5.88	18.8	84.8	4.7	33.97	0.20
X	L	790	8.256	0.0264	0.8131	7.63	19.3	97.1	5.9	34.29	0.13
X	M	840	8.616	0.0274	2.129	7.89	18.6	92.7	7.2	34.17	0.14
X	N	840	8.262	0.0253	0.7798	10.6	20.2	97.2	8.9	34.36	0.11
X	O	890	8.495	0.0240	1.555	9.62	21.3	94.6	10.4	34.38	0.12
X	P	890	8.283	0.0259	0.8232	13.3	19.7	97.1	12.6	34.40	0.09
X	Q	940	8.406	0.0235	1.201	11.4	21.7	95.8	14.4	34.45	0.11
X	R	940	8.291	0.0253	0.6539	15.8	20.2	97.7	16.9	34.64	0.09
X	S	990	8.450	0.0241	1.612	12.9	21.2	94.4	19.0	34.12	0.10
X	T	990	8.293	0.0242	0.8973	17.6	21.1	96.8	21.8	34.35	0.07
X	U	1040	8.524	0.0245	2.043	14.4	20.8	92.9	24.1	33.89	0.10
X	V	1040	8.351	0.0231	1.169	17.7	22.1	95.9	27.0	34.25	0.08
X	W	1090	8.446	0.0276	2.183	16.7	18.5	92.4	29.7	33.38	0.10
X	X	1090	8.410	0.0257	2.033	20.8	19.8	92.9	33.0	33.42	0.08
X	Y	1140	8.463	0.0252	1.887	26.3	20.2	93.4	37.2	33.83	0.08
X	Z	1190	8.248	0.0241	1.181	136.5	21.1	95.8	59.1	33.80	0.05
X	AA	1190	8.337	0.0240	1.238	127.1	21.2	95.6	79.5	34.11	0.05
X	AB	1190	8.298	0.0238	0.8682	59.9	21.4	96.9	89.1	34.40	0.06
X	AC	1190	8.365	0.0244	0.9343	26.9	20.9	96.7	93.4	34.61	0.07
X	AD	1290	8.235	0.0248	0.9283	4.91	20.5	96.7	94.2	34.06	0.19
X	AE	1340	8.304	0.0234	0.9460	6.35	21.8	96.7	95.2	34.33	0.16
X	AF	1390	8.324	0.0214	0.9910	6.10	23.8	96.5	96.2	34.36	0.16
X	AG	1590	8.465	0.0252	0.9903	13.0	20.3	96.6	98.3	34.96	0.10
X	AH	1740	9.121	0.0231	3.126	10.8	22.1	89.9	100.0	35.06	0.14
	Integrated age ± 2σ			n=34		623.6	20.6	K2O=6.94%		34.13	0.10
	Plateau ± 2σ	no plateau		n=0	MSWD=0.00	0.000	0.000±0.000		0.0	0.00	0.00
	Isochron±2σ	steps A-AH		n=34	MSWD=22.26		$^{40}Ar/^{36}Ar$=	304.7±3.9		34.10	0.05

ORGAN-22, K-Feldspar, 19.03 mg, J=0.0023606±0.04%, D=1.006±0.001, NM-227J, Lab#=59261-01

X	A	540	93.85	0.0108	294.1	11.9	47.1	7.4	0.8	29.75	1.72
X	B	540	16.87	0.0079	37.65	8.20	64.3	34.0	1.4	24.61	0.38
X	C	590	13.84	0.0079	31.51	14.5	64.2	32.7	2.4	19.43	2.88
X	D	590	9.411	0.0090	12.03	13.3	56.6	62.2	3.3	25.10	0.21
X	E	640	17.12	0.0082	37.97	16.0	62.5	34.4	4.4	25.29	0.31
X	F	640	7.342	0.0082	4.813	19.1	62.0	80.6	5.8	25.36	0.10
X	G	690	12.90	0.0100	22.87	19.9	51.2	47.6	7.1	26.30	0.21
X	H	690	7.171	0.0081	2.898	22.8	62.9	88.1	8.7	27.05	0.08
X	I	740	10.58	0.0086	13.43	21.8	59.6	62.5	10.2	28.33	0.14
X	J	740	8.343	0.0060	5.187	25.5	85.4	81.6	12.0	29.15	0.10
X	K	790	9.743	0.0060	8.948	23.1	85.3	72.8	13.6	30.38	0.12
X	L	790	7.818	0.0041	1.904	28.3	124.8	92.8	15.6	31.05	0.07
X	M	840	9.393	0.0041	6.980	26.8	125.2	78.0	17.4	31.36	0.11
X	N	840	8.016	0.0031	1.998	34.9	163.4	92.6	19.9	31.77	0.07
X	O	890	8.933	0.0035	4.752	31.5	147.5	84.3	22.0	32.20	0.09
X	P	890	8.005	0.0032	1.539	41.5	161.9	94.3	24.9	32.30	0.07
X	Q	940	9.196	0.0032	5.504	36.4	159.6	82.3	27.5	32.38	0.09
X	R	940	8.398	0.0026	2.744	48.0	194.7	90.3	30.8	32.45	0.07
X	S	990	9.509	0.0030	6.671	40.3	172.0	79.3	33.6	32.24	0.10
X	T	990	9.182	0.0028	5.618	52.1	179.6	81.9	37.2	32.18	0.08
X	U	1040	10.29	0.0047	9.538	44.4	107.8	72.6	40.3	31.96	0.11
X	V	1040	10.46	0.0043	9.989	54.6	119.0	71.8	44.1	32.13	0.11

X	W	1090	11.24	0.0061	13.06	45.1	83.3	65.6	47.2	31.57	0.13
X	X	1090	11.09	0.0056	12.45	51.2	91.5	66.8	50.8	31.70	0.13
X	Y	1140	10.70	0.0070	11.03	40.2	72.5	69.5	53.6	31.82	0.13
X	Z	1190	10.16	0.0042	9.234	82.7	122.3	73.1	59.3	31.81	0.09
X	AA	1190	11.66	0.0020	14.04	116.3	258.2	64.4	67.4	32.11	0.12
X	AB	1190	13.70	0.0013	21.04	114.4	382.9	54.6	75.3	31.99	0.15
X	AC	1190	15.06	0.0013	25.42	117.2	397.2	50.1	83.5	32.28	0.17
X	AD	1190	15.58	0.0013	26.87	106.4	404.1	49.0	90.9	32.70	0.18
X	AE	1290	15.35	0.0019	26.19	34.9	263.3	49.6	93.3	32.57	0.21
X	AF	1340	16.31	0.0014	29.54	31.8	377.0	46.5	95.5	32.43	0.25
X	AG	1390	15.57	0.0012	26.16	21.6	428.0	50.3	97.0	33.52	0.25
X	AH	1590	16.27	0.0019	28.20	24.6	268.1	48.8	98.7	33.95	0.23
X	AI	1740	16.53	0.0027	29.29	18.6	187.7	47.6	100.0	33.69	0.26
	Integrated age ± 2σ			n=35		1439.5	141.4	K2O=12.31%		31.46	0.24
	Plateau ± 2σ	no plateau		n=0	MSWD=0.00	0.000	0.000±0.000		0.0	0.00	0.00
	Isochron±2σ	steps A-AI		n=35	MSWD=300.91		$^{40}Ar/^{36}Ar$=	304.1±1.2		30.96	0.06

ORGAN-24, K-Feldspar, 59236 mg, J=0.0023214±0.04%, D=1.006±0.001, NM-227F, Lab#=59236-01

X	A	700	78.32	3.896	-34.8369	-0.002	0.13	113.6	0.0	344.39	478.56
X	B	540	318.8	0.0330	407.0	7.28	15.5	62.3	0.5	693.67	2.41
X	C	540	37.80	0.0317	43.74	1.45	16.1	65.8	0.6	102.73	0.97
X	D	590	28.87	0.0625	26.04	5.02	8.2	73.4	1.0	87.82	0.43
X	E	590	22.80	0.0570	18.35	5.13	9.0	76.2	1.4	72.38	0.39
X	F	640	23.21	0.0482	19.52	6.82	10.6	75.2	1.9	72.63	0.32
X	G	640	15.81	0.0386	8.929	8.7	13.2	83.3	2.5	55.11	0.20
X	H	690	15.92	0.0332	10.60	10.4	15.4	80.3	3.3	53.52	0.18
X	I	690	10.41	0.0209	3.871	13.4	24.4	89.0	4.2	38.90	0.11
X	J	740	11.24	0.0180	5.342	15.1	28.3	86.0	5.3	40.57	0.11
X	K	740	8.794	0.0121	2.086	19.6	42.2	93.0	6.8	34.39	0.08
X	L	790	10.53	0.0105	4.615	20.5	48.4	87.0	8.3	38.49	0.11
X	M	790	8.395	0.0069	1.263	25.3	73.5	95.6	10.2	33.73	0.07
X	N	840	10.27	0.0077	3.956	24.3	66.5	88.6	12.0	38.24	0.10
X	O	840	8.361	0.0056	1.167	28.7	90.7	95.9	14.2	33.71	0.07
X	P	890	10.31	0.0068	4.124	25.5	75.4	88.2	16.1	38.18	0.11
X	Q	890	8.531	0.0049	1.638	29.4	104.2	94.3	18.4	33.84	0.07
X	R	940	10.51	0.0066	4.942	25.7	76.7	86.1	20.4	38.02	0.09
X	S	940	8.736	0.0058	1.802	28.8	87.3	93.9	22.6	34.49	0.08
X	T	990	10.77	0.0081	5.384	24.4	63.2	85.2	24.5	38.54	0.11
X	U	990	9.792	0.0072	3.874	28.6	70.8	88.3	26.8	36.34	0.10
X	V	1040	11.86	0.0112	7.785	26.8	45.6	80.6	28.9	40.15	0.12
X	W	1040	11.34	0.0094	6.360	32.2	54.2	83.4	31.5	39.71	0.10
X	X	1090	13.17	0.0136	9.902	37.2	37.5	77.8	34.5	42.99	0.13
X	Y	1090	12.53	0.0158	8.983	43.4	32.3	78.8	38.0	41.46	0.11
X	Z	1140	12.48	0.0184	7.266	38.1	27.7	82.8	41.2	43.34	0.11
X	AA	1190	12.48	0.0157	4.020	105.4	32.5	90.5	50.0	47.32	0.08
X	AB	1190	13.08	0.0080	2.493	183.4	63.6	94.4	66.0	51.68	0.08
X	AC	1190	13.07	0.0059	2.369	153.2	86.1	94.6	80.0	51.78	0.08
X	AD	1190	13.05	0.0061	2.610	103.8	83.8	94.1	89.9	51.41	0.08
X	AE	1190	12.93	0.0080	2.879	56.0	64.0	93.4	95.3	50.60	0.08
X	AF	1290	12.81	0.0089	3.110	11.5	57.6	92.8	96.5	49.80	0.13
X	AG	1340	13.32	0.0117	4.132	6.75	43.7	90.8	97.1	50.68	0.17
X	AH	1390	13.52	0.0196	4.922	4.47	26.0	89.2	97.6	50.52	0.26
X	AI	1590	13.54	0.0096	3.216	20.6	53.3	93.0	99.6	52.70	0.11
X	AJ	1740	15.12	0.0061	8.027	4.09	84.3	84.3	100.0	53.36	0.25
	Integrated age ± 2σ			n=36		1181.1	47.9	K2O=0.00%		50.22	0.17
	Plateau ± 2σ	no plateau		n=0	MSWD=0.00	0.000	0.000±0.000		0.0	0.00	0.00
	Isochron±2σ	steps A-AJ		n=36	MSWD=2136.45		$^{40}Ar/^{36}Ar$=	1116.0±8.0		33.73	0.10

ORGAN-31, K-Feldspar, 17.88 mg, J=0.0023226±0.04%, D=1.006±0.001, NM-227F, Lab#=59237-01

X	A	700	23.40	-6.0396	117.5	-0.001	-	-50.5	0.0	-50.68	708.69
X	B	540	202.0	0.0193	649.7	3.50	26.4	4.9	0.4	41.92	3.64
X	C	540	38.85	0.0157	106.2	2.64	32.5	19.2	0.7	31.50	1.08

X	D	590	23.85	0.0192	55.12	3.33	26.6	31.7	1.1	31.84	0.73
X	E	590	17.50	0.0213	34.42	4.06	23.9	41.8	1.5	30.85	0.51
X	F	640	16.89	0.0265	31.42	4.58	19.2	45.0	2.1	32.00	0.42
X	G	640	12.53	0.0229	16.28	5.73	22.3	61.6	2.7	32.49	0.26
X	H	690	13.92	0.0276	20.62	6.24	18.5	56.2	3.4	32.93	0.34
X	I	690	10.19	0.0235	7.803	8.15	21.7	77.4	4.4	33.19	0.18
X	J	740	11.47	0.0241	12.06	8.67	21.2	68.9	5.4	33.28	0.24
X	K	740	9.191	0.0249	4.183	12.0	20.5	86.6	6.8	33.48	0.15
X	L	790	10.21	0.0237	7.087	12.6	21.5	79.5	8.2	34.13	0.15
X	M	790	8.911	0.0234	2.735	16.8	21.8	90.9	10.2	34.10	0.10
X	N	840	9.857	0.0242	5.969	15.6	21.1	82.1	12.0	34.05	0.12
X	O	840	8.819	0.0237	2.510	20.8	21.5	91.6	14.5	33.99	0.09
X	P	890	9.877	0.0243	5.867	18.1	21.0	82.5	16.7	34.27	0.12
X	Q	890	8.998	0.0237	2.898	23.6	21.5	90.5	19.5	34.26	0.09
X	R	940	10.44	0.0228	7.960	20.5	22.4	77.5	22.0	34.05	0.12
X	S	940	9.634	0.0245	5.123	25.7	20.8	84.3	25.2	34.17	0.11
X	T	990	11.97	0.0241	13.21	20.7	21.1	67.4	27.7	33.93	0.16
X	U	990	10.69	0.0235	8.862	25.0	21.7	75.5	30.9	33.98	0.13
X	V	1040	13.13	0.0213	17.23	20.1	24.0	61.2	33.4	33.82	0.17
X	W	1040	11.75	0.0224	12.52	23.1	22.7	68.5	36.4	33.87	0.14
X	X	1090	13.64	0.0214	19.36	21.7	23.8	58.0	39.2	33.32	0.19
X	Y	1090	13.28	0.0226	18.02	26.0	22.5	59.9	42.6	33.47	0.18
X	Z	1140	12.69	0.0225	15.39	33.7	22.7	64.2	47.0	34.25	0.17
X	AA	1190	11.10	0.0229	9.277	169.3	22.3	75.3	70.3	35.15	0.09
X	AB	1190	11.93	0.0236	12.15	115.9	21.6	69.9	87.3	35.08	0.11
X	AC	1190	12.36	0.0243	13.32	42.1	21.0	68.1	93.7	35.44	0.14
X	AD	1190	13.51	0.0232	16.90	15.2	21.9	63.0	96.0	35.83	0.20
X	AE	1190	14.58	0.0265	21.60	6.02	19.3	56.2	96.9	34.50	0.35
X	AF	1290	16.34	0.0105	28.10	1.05	48.7	49.1	97.1	33.80	1.17
X	AG	1740	14.80	0.0216	20.47	18.8	23.7	59.1	100.0	36.81	0.24
	Integrated age ± 2σ			n=33		751.0	22.0		K2O=6.95%	34.05	0.22
	Plateau ± 2σ	no plateau		n=0	MSWD=0.00	0.000	0.000±0.000		0.0	0.00	0.00
	Isochron±2σ	steps A-AG		n=33	MSWD=22.50		$^{40}Ar/^{36}Ar$=	297.2±1.7		34.18	0.09

Organ-36, K-Feldspar, 7.78 mg, J=0.0015943±0.05%, D=1.002±0.001, NM-236C, Lab#=59735-01

X	A	750	-119.5706	-1.6832	-763.9663	0.001	-	-88.7	0.0	285.57	462.76
X	B	500	601.2	0.0374	1740.2	0.579	13.6	14.5	0.2	237.64	7.64
X	C	500	103.7	0.1355	308.0	0.282	3.8	12.3	0.3	36.75	4.17
X	D	550	72.96	0.1431	167.2	0.468	3.6	32.3	0.5	67.48	2.05
X	E	550	30.42	0.1067	71.24	0.606	4.8	30.8	0.7	27.13	1.29
X	F	600	52.69	0.0971	109.4	0.828	5.3	38.7	1.0	58.53	1.73
X	G	600	18.14	0.0685	29.53	0.931	7.4	51.9	1.4	27.24	0.77
X	H	650	40.59	0.0900	79.23	1.354	5.7	42.3	1.9	49.44	0.98
X	I	650	14.87	0.0499	17.79	1.44	10.2	64.7	2.4	27.82	0.47
X	J	700	27.18	0.0857	42.57	1.76	6.0	53.7	3.0	42.13	0.64
X	K	700	12.86	0.0359	9.148	1.98	14.2	79.0	3.8	29.38	0.36
X	L	750	20.14	0.0411	24.26	2.26	12.4	64.4	4.6	37.46	0.43
X	M	750	11.98	0.0463	7.110	2.45	11.0	82.5	5.5	28.58	0.27
X	N	800	16.42	0.0625	16.37	2.31	8.2	70.6	6.4	33.48	0.39
X	O	800	11.66	0.0337	6.117	2.51	15.1	84.5	7.3	28.50	0.28
X	P	850	16.35	0.0250	18.45	2.15	20.4	66.6	8.1	31.51	0.40
X	Q	850	11.92	0.0457	6.375	2.18	11.2	84.2	8.9	29.05	0.28
X	R	900	19.15	0.0523	25.51	1.87	9.8	60.6	9.6	33.57	0.46
X	S	900	12.98	0.0419	8.909	1.94	12.2	79.7	10.3	29.93	0.36
X	T	950	20.99	0.0220	30.27	1.98	23.2	57.4	11.1	34.78	0.52
X	U	950	15.66	0.0310	16.07	2.31	16.5	69.7	12.0	31.54	0.37
X	V	1000	24.21	0.0217	38.51	2.90	23.5	53.0	13.1	37.04	0.39
X	W	1000	23.65	0.0189	39.18	3.70	26.9	51.0	14.5	34.86	0.40
X	X	1050	26.51	0.0164	43.61	5.45	31.2	51.4	16.5	39.30	0.45
X	Y	1050	22.07	0.0245	31.86	6.26	20.8	57.3	18.9	36.54	0.31
X	Z	1100	27.48	0.0166	44.76	11.90	30.7	51.9	23.5	41.12	0.31
X	AA	1100	25.10	0.0225	42.34	6.63	22.6	50.1	26.1	36.35	0.34
X	AB	1150	24.31	0.0245	34.77	61.2	20.8	57.7	50.5	40.50	0.19

X	AC	1150	20.74	0.0235	19.10	42.5	21.7	72.8	68.2	43.50	0.15
X	AD	1150	20.66	0.0183	11.90	33.8	27.9	83.0	82.9	49.34	0.12
X	AE	1200	22.23	0.0125	7.834	7.27	40.9	89.6	86.1	57.19	0.16
X	AF	1250	23.70	0.0098	7.993	20.1	52.0	90.0	95.0	61.20	0.14
X	AG	1350	26.22	0.0387	12.88	4.86	13.2	85.5	97.2	64.25	0.26
X	AH	1550	28.15	0.0348	18.69	6.07	14.7	80.4	100.0	64.84	0.27
X	AI	1170	42.35	1.159	103.7	0.020	0.44	27.8	100.0	34.07	22.92
	Integrated age ± 2σ			n=35		244.8	20.2	K2O=7.58%		44.18	0.30
	Plateau ± 2σ	no plateau		n=0	MSWD=0.00	0.000	0.000±0.000		0.0	0.00	0.00
	Isochron±2σ	steps A-AI		n=35	MSWD=1532.10		$^{40}Ar/^{36}Ar$=	403.3±3.1		43.87	0.15

Organ-37, K-Feldspar, 12.58 mg, J=0.0015936±0.06%, D=1.002±0.001, NM-236C, Lab#=59736-01

X	A	750	31.64	-0.9232	-6.5682	-0.022	-	105.9	0.0	95.13	24.80
X	B	500	377.6	0.0098	1115.9	2.31	52.1	12.7	0.3	134.43	4.48
X	C	500	71.60	0.0100	197.7	1.76	50.9	18.4	0.6	38.00	1.26
X	D	550	41.14	0.0055	96.93	2.82	93.6	30.4	1.0	36.06	0.75
X	E	550	26.03	0.0245	52.10	2.93	20.8	40.8	1.4	30.75	0.59
X	F	600	26.95	0.0242	51.39	4.03	21.1	43.7	1.9	33.99	0.56
X	G	600	15.88	0.0210	21.07	4.49	24.3	60.8	2.6	27.91	0.29
X	H	650	21.16	0.0310	31.80	5.86	16.5	55.6	3.4	33.97	0.29
X	I	650	13.04	0.0116	9.970	7.01	43.9	77.4	4.4	29.17	0.18
X	J	700	16.28	0.0168	17.77	8.05	30.4	67.7	5.5	31.87	0.22
X	K	700	12.12	0.0124	6.284	9.83	41.2	84.7	6.9	29.68	0.13
X	L	750	13.88	0.0097	10.37	10.48	52.8	77.9	8.4	31.26	0.14
X	M	750	11.62	0.0112	3.417	12.60	45.7	91.3	10.2	30.67	0.11
X	N	800	13.43	0.0070	8.637	11.50	72.8	81.0	11.9	31.45	0.13
X	O	800	11.62	0.0061	2.875	13.74	83.0	92.7	13.9	31.12	0.09
X	P	850	13.55	0.0114	8.652	11.76	44.6	81.1	15.6	31.77	0.13
X	Q	850	11.82	0.0113	3.599	13.19	45.1	91.0	17.5	31.08	0.09
X	R	900	14.68	0.0094	12.07	10.61	54.0	75.7	19.0	32.12	0.14
X	S	900	12.84	0.0120	6.730	12.22	42.7	84.5	20.8	31.35	0.13
X	T	950	16.98	0.0049	19.75	10.88	104.1	65.6	22.4	32.19	0.20
X	U	950	15.06	0.0062	14.12	13.39	82.2	72.3	24.4	31.47	0.15
X	V	1000	19.57	0.0044	28.03	13.38	114.8	57.7	26.4	32.60	0.20
X	W	1000	17.77	0.0060	22.18	17.0	84.9	63.1	28.9	32.41	0.18
X	X	1050	20.96	0.0078	31.37	18.6	65.5	55.8	31.7	33.77	0.22
X	Y	1050	18.97	0.0051	25.23	22.5	99.7	60.7	35.1	33.25	0.19
X	Z	1100	20.91	0.0106	30.44	26.7	48.1	57.0	39.2	34.40	0.20
X	AA	1100	20.02	0.0105	28.47	16.5	48.4	58.0	41.7	33.53	0.18
X	AB	1150	18.84	0.0114	22.79	50.8	44.8	64.2	49.6	34.96	0.14
X	AC	1150	16.88	0.0093	15.34	53.5	55.1	73.1	58.1	35.65	0.12
X	AD	1150	16.14	0.0049	12.56	59.4	104.3	77.0	67.7	35.88	0.10
X	AE	1200	15.83	0.0018	10.27	25.3	278.9	80.8	71.8	36.91	0.13
X	AF	1250	16.06	0.0009	11.23	89.8	588.4	79.3	86.8	36.77	0.09
X	AG	1350	16.52	0.0007	13.35	39.9	754.4	76.1	93.6	36.30	0.11
X	AH	1550	19.01	0.0026	20.89	33.8	197.5	67.5	99.4	37.02	0.15
X	AJ	1650	25.79	0.0146	44.70	3.33	34.9	48.8	100.0	36.30	0.43
	Integrated age ± 2σ			n=35		639.8	73.2	K2O=12.26%		34.31	0.22
	Plateau ± 2σ	no plateau		n=0	MSWD=0.00	0.000	0.000±0.000		0.0	0.00	0.00
	Isochron±2σ	steps A-AJ		n=35	MSWD=218.64		$^{40}Ar/^{36}Ar$=	339.6±1.8		31.80	0.09

Organ-41, K-Feldspar, 10.95 mg, J=0.001594±0.06%, D=1.002±0.001, NM-236C, Lab#=59737-01

X	A	750	-72.9664	10.61	-73.9689	0.003	0.048	68.9	0.0	-154.02	211.76
X	B	500	366.1	0.0184	1188.8	1.53	27.7	4.0	0.4	42.66	5.04
X	C	500	69.33	0.0029	204.7	1.270	176.5	12.7	0.8	25.56	1.66
X	D	550	29.18	0.0105	65.78	1.60	48.7	33.4	1.3	28.17	0.92
X	E	550	21.30	0.0170	42.18	2.37	30.0	41.5	1.9	25.57	0.59
X	F	600	20.14	0.0181	34.10	3.46	28.1	50.0	2.9	29.11	0.44
X	G	600	13.85	0.0276	13.33	4.26	18.5	71.6	4.2	28.66	0.26
X	H	650	13.38	0.0243	8.587	4.97	21.0	81.0	5.6	31.34	0.21
X	I	650	12.60	0.0197	5.209	6.20	25.9	87.8	7.4	31.96	0.15
X	J	700	13.18	0.0234	5.668	5.60	21.8	87.3	9.0	33.24	0.17

X	K	700	12.32	0.0192	2.860	6.36	26.6	93.1	10.9	33.15	0.14
X	L	750	12.56	0.0264	3.477	5.43	19.4	91.8	12.5	33.34	0.15
X	M	750	12.30	0.0203	2.176	5.36	25.1	94.8	14.1	33.68	0.16
X	N	800	12.58	0.0321	2.483	3.94	15.9	94.2	15.2	34.23	0.19
X	O	800	12.55	0.0242	2.614	4.00	21.1	93.9	16.4	34.03	0.19
X	P	850	12.95	0.0326	3.810	2.79	15.7	91.3	17.2	34.17	0.27
X	Q	850	12.67	0.0339	3.155	2.72	15.0	92.7	18.0	33.91	0.24
X	R	900	13.26	0.0454	4.940	1.83	11.2	89.0	18.6	34.10	0.41
X	S	900	13.08	0.0216	5.392	1.84	23.6	87.8	19.1	33.19	0.41
X	T	950	15.21	0.0291	11.71	1.238	17.5	77.3	19.5	33.96	0.56
X	U	950	14.44	0.0184	10.69	1.403	27.7	78.1	19.9	32.61	0.50
X	V	1000	16.86	0.0291	16.15	1.173	17.5	71.7	20.3	34.91	0.66
X	W	1000	15.79	0.0112	12.84	1.61	45.4	76.0	20.8	34.66	0.54
X	X	1050	17.39	0.0422	18.26	1.71	12.1	69.0	21.3	34.66	0.54
X	Y	1050	15.97	0.0196	14.28	2.30	26.0	73.6	22.0	33.95	0.38
X	Z	1100	14.90	0.0276	7.845	7.44	18.5	84.4	24.2	36.33	0.16
X	AA	1100	14.85	0.0200	8.215	4.51	25.4	83.7	25.6	35.87	0.26
X	AB	1150	15.61	0.0259	11.36	65.7	19.7	78.5	45.9	35.39	0.10
X	AC	1150	16.98	0.0232	16.81	71.2	22.0	70.7	69.0	34.71	0.11
X	AD	1150	17.84	0.0262	19.39	49.0	19.5	67.9	85.6	34.98	0.13
X	AE	1200	16.64	0.0348	14.96	7.48	14.7	73.4	88.2	35.30	0.18
X	AF	1250	17.31	0.0324	15.18	14.4	15.8	74.1	93.2	37.02	0.15
X	AG	1350	19.35	0.0436	23.26	3.89	11.7	64.5	94.6	36.03	0.35
X	AH	1550	20.49	0.0250	27.45	13.61	20.4	60.4	99.4	35.76	0.20
X	AI	1650	34.85	0.0052	74.60	1.69	97.3	36.7	100.0	36.96	0.71
	Integrated age ± 2σ			n=35		313.9	20.1	K2O=6.91%		34.13	0.22
	Plateau ± 2σ	no plateau		n=0	MSWD=0.00	0.000	0.000±0.000		0.0	0.00	0.00
	Isochron±2σ	steps A-AI		n=35	MSWD=63.97		$^{40}Ar/^{36}Ar$=	306.9±2.1		33.98	0.11

Organ-42, K-Feldspar, 9.81 mg, J=0.0015953±0.06%, D=1.002±0.001, NM-236C, Lab#=59738-06

X	A	750	224.0	-21.8047	-273.8774	-0.001	-	135.3	0.0	713.10	508.26
X	B	500	1531.3	-0.0024	625.1	1.49	-	87.9	0.3	2099.22	10.27
X	C	500	162.9	-0.0056	102.0	1.191	-	81.5	0.5	351.68	1.74
X	D	550	102.1	0.0236	46.34	1.86	21.6	86.6	0.8	241.52	1.01
X	E	550	52.03	0.0107	25.66	2.54	47.8	85.4	1.2	125.37	0.53
X	F	600	77.31	0.0108	32.66	3.79	47.3	87.5	1.8	187.61	0.65
X	G	600	25.62	0.0091	10.49	4.36	55.8	87.9	2.6	64.57	0.26
X	H	650	50.87	0.0150	18.15	5.92	34.1	89.5	3.6	128.27	0.40
X	I	650	14.66	0.0187	4.705	6.45	27.3	90.5	4.7	38.31	0.16
X	J	700	29.76	0.0137	10.45	7.71	37.1	89.6	6.0	76.24	0.23
X	K	700	10.91	0.0134	2.768	8.58	37.9	92.5	7.5	29.21	0.10
X	L	750	18.66	0.0098	5.137	9.05	52.3	91.9	9.1	49.36	0.15
X	M	750	10.07	0.0097	2.048	10.93	52.8	94.0	11.0	27.41	0.10
X	N	800	15.64	0.0111	4.287	10.04	45.8	91.9	12.7	41.46	0.12
X	O	800	9.194	0.0067	1.974	10.94	76.3	93.7	14.6	24.95	0.09
X	P	850	12.01	0.0112	3.511	8.89	45.4	91.4	16.2	31.75	0.13
X	Q	850	9.329	0.0085	1.590	9.40	60.0	95.0	17.8	25.66	0.09
X	R	900	13.23	0.0140	4.338	7.01	36.5	90.3	19.1	34.54	0.16
X	S	900	11.00	0.0172	3.054	8.03	29.7	91.8	20.5	29.24	0.13
X	T	950	18.86	0.0140	9.115	6.80	36.5	85.7	21.7	46.57	0.20
X	U	950	17.32	0.0078	6.360	8.46	65.8	89.1	23.2	44.52	0.17
X	V	1000	32.90	0.0086	14.99	8.43	59.4	86.5	24.7	81.27	0.25
X	W	1000	31.61	0.0054	12.46	11.77	94.2	88.3	26.8	79.75	0.22
X	X	1050	46.42	0.0055	18.66	13.33	92.3	88.1	29.2	115.69	0.31
X	Y	1050	39.78	0.0064	13.89	19.4	79.3	89.7	32.8	101.30	0.21
X	Z	1100	46.27	0.0046	15.17	24.2	111.3	90.3	37.2	118.09	0.25
X	AA	1100	35.90	0.0066	11.53	15.9	77.7	90.5	40.2	92.48	0.20
X	AB	1150	35.78	0.0058	9.157	58.4	87.9	92.4	51.1	94.09	0.19
X	AC	1150	28.21	0.0031	4.811	40.0	163.6	95.0	58.8	76.58	0.15
X	AD	1150	31.71	0.0017	3.969	36.9	305.5	96.3	66.0	87.03	0.16
X	AE	1200	43.17	0.0028	4.839	9.99	183.5	96.7	67.9	117.98	0.28
X	AF	1250	48.13	0.0009	4.967	64.0	582.5	97.0	80.7	131.42	0.24
X	AG	1350	46.97	0.0001	5.104	70.3	######	96.8	95.1	128.14	0.24

X	AH	1550	35.80	0.0019	7.928	22.2	263.4	93.5	99.8	95.15	0.24
X	AI	1650	61.49	0.0618	112.3	0.938	8.3	46.0	100.0	80.86	1.58
	Integrated age ± 2σ			n=35		529.3	95.5	K2O=12.99%		102.29	0.30
	Plateau ± 2σ	no plateau		n=0	MSWD=0.00	0.000	0.000±0.000		0.0	0.00	0.00
	Isochron±2σ	steps A-AI		n=35	MSWD=1656.26		$^{40}Ar/^{36}Ar$=	5633.1±65.8		2.95	0.03

Organ-46, K-Feldspar, 13.52 mg, J=0.0015969±0.06%, D=1.002±0.001, NM-236C, Lab#=59739-01

X	A	750	179.9	-1.1269	1023.8	-0.002	-	-68.3	0.0	-399.16	806.58
X	B	500	1385.6	0.0075	1363.3	2.07	67.6	70.9	0.3	1727.38	6.30
X	C	500	147.5	0.0070	192.8	2.24	73.3	61.4	0.7	247.17	1.43
X	D	550	119.7	0.0241	105.3	3.61	21.2	74.0	1.2	242.22	1.02
X	E	550	51.14	0.0338	53.44	4.24	15.1	69.1	1.9	100.49	0.62
X	F	600	76.22	0.0353	51.60	5.25	14.5	80.0	2.7	170.07	0.71
X	G	600	25.91	0.0403	21.95	5.80	12.7	75.0	3.7	55.90	0.30
X	H	650	52.51	0.0403	36.06	7.75	12.7	79.7	4.9	118.42	0.42
X	I	650	16.03	0.0273	9.677	8.60	18.7	82.2	6.3	38.07	0.18
X	J	700	30.87	0.0265	19.55	10.40	19.3	81.3	7.9	71.90	0.23
X	K	700	12.91	0.0195	4.833	11.93	26.2	88.9	9.8	33.24	0.12
X	L	750	21.87	0.0186	12.14	13.23	27.4	83.6	12.0	52.65	0.16
X	M	750	10.80	0.0154	3.007	14.9	33.0	91.8	14.4	28.72	0.10
X	N	800	16.23	0.0151	8.248	13.71	33.9	85.0	16.6	39.86	0.13
X	O	800	10.31	0.0179	2.707	15.5	28.5	92.3	19.2	27.58	0.08
X	P	850	15.31	0.0246	9.114	12.92	20.8	82.4	21.3	36.48	0.14
X	Q	850	11.17	0.0215	3.735	13.94	23.8	90.1	23.6	29.15	0.10
X	R	900	19.39	0.0237	14.70	11.46	21.6	77.6	25.5	43.44	0.17
X	S	900	14.42	0.0175	7.813	12.95	29.2	84.0	27.7	35.05	0.12
X	T	950	27.78	0.0166	25.83	11.91	30.8	72.5	29.7	57.94	0.26
X	U	950	22.05	0.0140	16.52	14.6	36.3	77.9	32.1	49.49	0.17
X	V	1000	37.60	0.0119	33.85	14.6	42.8	73.4	34.6	78.93	0.30
X	W	1000	30.04	0.0129	22.41	18.4	39.7	78.0	37.8	67.19	0.20
X	X	1050	41.27	0.0116	32.09	20.4	44.0	77.0	41.3	90.61	0.29
X	Y	1050	32.73	0.0086	23.24	23.7	59.6	79.0	45.4	74.04	0.22
X	Z	1100	42.57	0.0146	29.17	27.8	35.0	79.8	50.2	96.62	0.25
X	AA	1100	32.93	0.0204	27.43	15.7	25.1	75.4	53.0	71.15	0.25
X	AB	1150	36.39	0.0254	24.24	44.4	20.1	80.3	60.9	83.47	0.21
X	AC	1150	32.92	0.0236	17.33	38.3	21.7	84.4	67.9	79.50	0.18
X	AD	1200	39.72	0.0133	11.15	25.8	38.3	91.7	72.6	103.47	0.22
X	AE	1250	41.52	0.0067	8.997	81.3	76.4	93.6	87.9	110.19	0.20
X	AF	1650	41.86	0.0120	12.98	63.0	42.6	90.8	100.0	107.88	0.20
	Integrated age ± 2σ			n=32		570.5	30.8	K2O=10.15%		89.18	0.35
	Plateau ± 2σ	no plateau		n=0	MSWD=0.00	0.000	0.000±0.000		0.0	0.00	0.00
	Isochron±2σ	steps A-AF		n=32	MSWD=3202.78		$^{40}Ar/^{36}Ar$=	1851.4±11.3		16.21	0.10

Notes:
x (or i) symbol preceding sample ID denotes analyses excluded from plateau (or isochron) age calculations.
Isotopic ratios corrected for blank, radioactive decay, and mass discrimination, not corrected for interfering reactions.
Errors quoted for individual analyses include analytical error only, without interfering reaction or J uncertainties.

Age calculations:
Ages calculated relative to FC-2 Fish Canyon Tuff sanidine interlaboratory standard (28.201 Ma, Kuiper et al, 2008).
Integrated age calculated by summing isotopic measurements of all steps.
Integrated age error calculated by quadratically combining errors of isotopic measurements of all steps.
Plateau age or preferred age calculated for the indicated steps by weighting each step by the inverse of the variance.
Plateau age error is inverse-variance-weighted mean error (Taylor, 1982) times root MSWD where MSWD>1.
MSWD values are calculated for n-1 degrees of freedom for plateau age.
Isochron ages, $^{40}Ar/^{36}Ar_i$ and MSWD values calculated from regression results obtained by the methods of York (1969).
Decay constants and isotopic abundances after Min et al. (2000).
Weight percent K_2O calculated from ^{39}Ar signal, sample weight, and instrument sensitivity.
All errors reported at ±2s, unless otherwise noted.

Sample preparation and irradiation:

K-feldspar separates were prepared using crushing, Franz magnetic separator, heavy liquids and hand-picking techniques.
Samples were loaded into machined Al discs and irradiated in 3 separate positions (NM-227F and J, and NM-236C) for 10 hours (NM227) or 7 hours (NM236) at the Triga Reactor
Neutron flux monitor Fish Canyon Tuff sanidine (FC-2).

Instrumentation:
Mass Analyzer Products 215-50 mass spectrometer on line with automated all-metal extraction system.
Samples were step-heated using a Mo double-vacuum resistance furnace (heating duration 10 minutes), or CO2 laser (heating duration 2 minutes).
Reactive gases removed during furnace (laser) analysis by reaction with 3 (2) SAES GP-50 getters, 2 (1) operated at ~450°C and 1 at 20°C. Gas also exposed to a W filament operated at ~2000°C.

Analytical parameters:
Electron multiplier sensitivity ranged from 9.87 x 10^{-17} moles/pA to 1.1 x 10^{-16} moles /pA.
Total system blank and background for the furnace averaged 813, 5.6, 1.16, 4.71, 25.5 x 10^{-18} moles.
at masses 40, 39, 38, 37, and 36 respectively
J-factors determined to a precision of ± 0.1% by CO_2 laser-fusion of 6 single crystals from each of 10 radial positions around the irradiation tray.
Correction factors for interfering nuclear reactions were determined using K-glass and CaF_2 and are as follows:

$(^{39}Ar/^{37}Ar)_{Ca}$ = 0.00068 ± 2e-05
$(^{36}Ar/^{37}Ar)_{Ca}$ = 0.00028 ± 1e-05
$(^{38}Ar/^{39}Ar)_{K}$ = 0.013 ± 5e-4
$(^{40}Ar/^{39}Ar)_{K}$ = 0 ± 4e-4

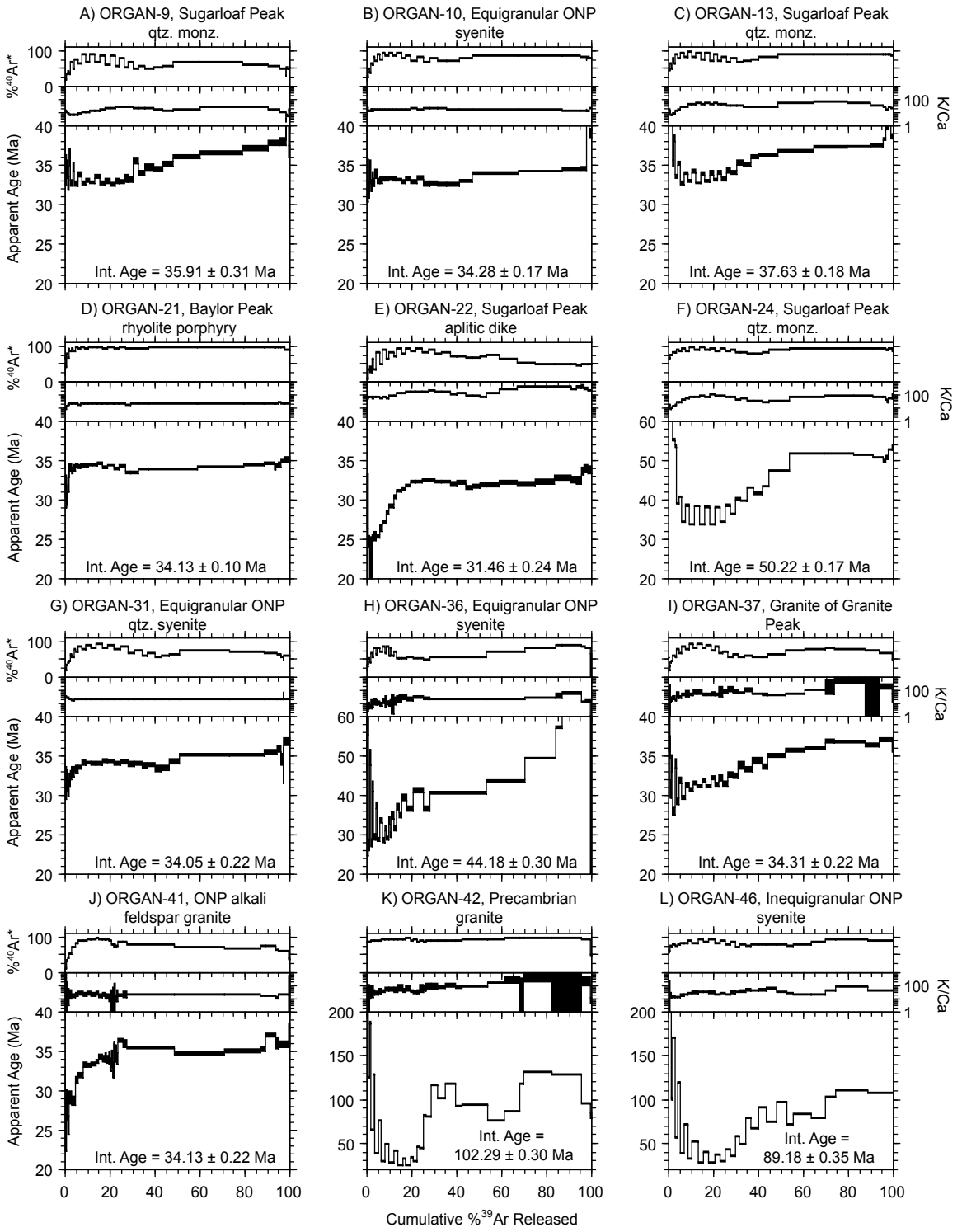

Figure 3.3.3 - K-feldspar age spectra and K/Ca and radiogenic yield (%^{40}Ar*) auxiliary plots. All errors are reported at 2σ and do not include error in decay constant.

APPENDIX 3.4.

SUPPLEMENTAL MDD PLOTS FOR ORGAN CALDERA COMPLEX K-FELDSPAR

Appendix 3.4 contains Arrhenius and log (r/r_o) plots used for MDD thermal modeling of K-feldspars from the Organ caldera complex. Modeled age spectra and thermal histories are located within the main body of the text. All MDD thermal histories were modeled using algorithms developed by Lovera et al. (1989, 1991). Arrhenius plots are constructed using the heating schedule and the fraction of the $^{39}Ar_K$ released for each step. Log (r/r_o) plots are constructed by fitting an Arrhenius reference line (r_o) to the data points on the Arrhenius plot, calculating the deviation of the Arrhenius trend from r_o, and comparing that to the cumulative $^{39}Ar_K$ released. Black lines are the measured data and gray lines are the modeled data.

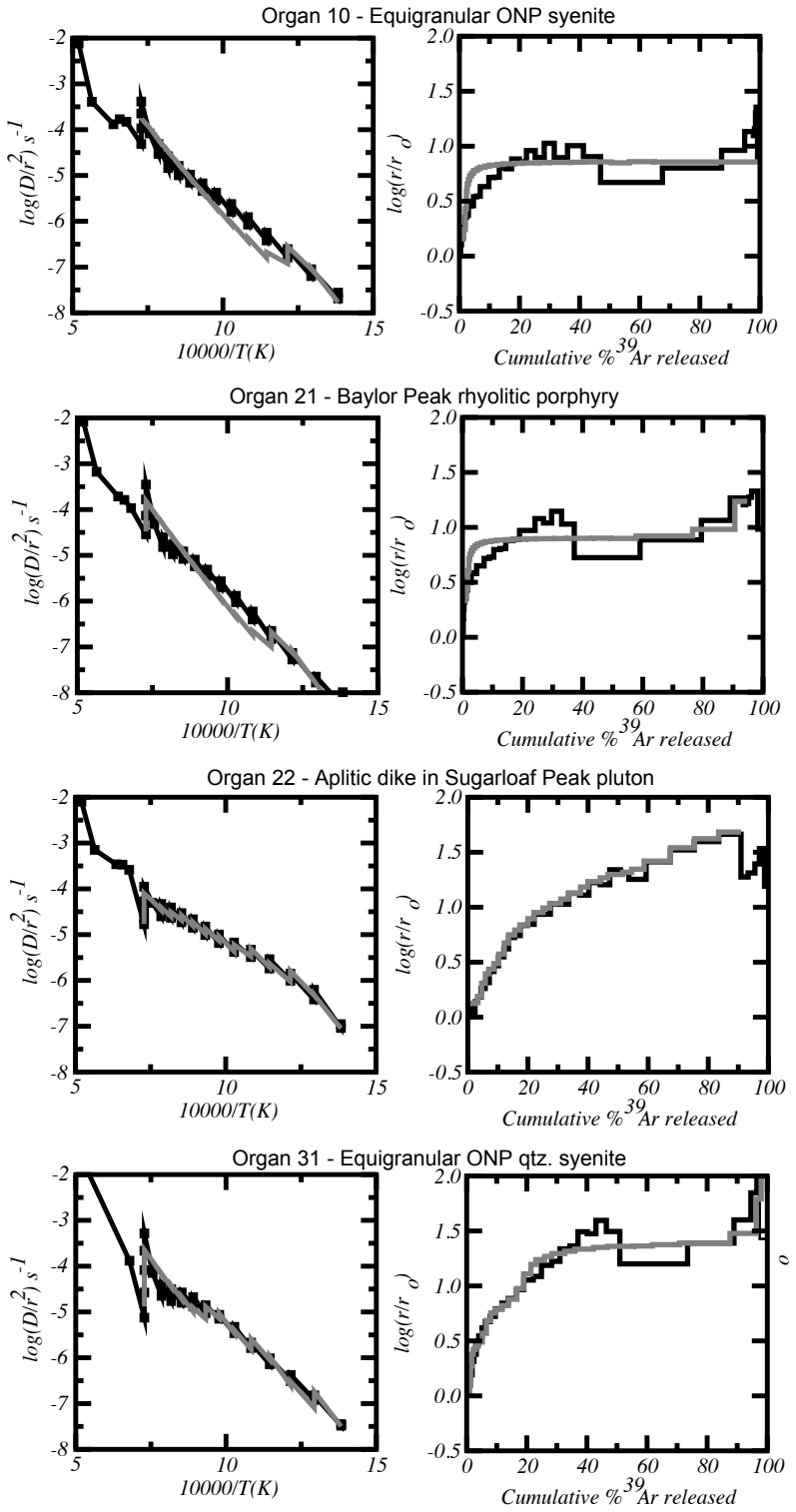
Organ 10 - Equigranular ONP syenite
log(D/r2) s-1
10000/T(K)
log(r/ro)
Cumulative %39Ar released
Organ 21 - Baylor Peak rhyolitic porphyry
log(D/r2) s-1
10000/T(K)
log(r/ro)
Cumulative %39Ar released
Organ 22 - Aplitic dike in Sugarloaf Peak pluton
log(D/r2) s-1
10000/T(K)
log(r/ro)
Cumulative %39Ar released
Organ 31 - Equigranular ONP qtz. syenite
log(D/r2) s-1
10000/T(K)
log(r/ro)
Cumulative %39Ar released

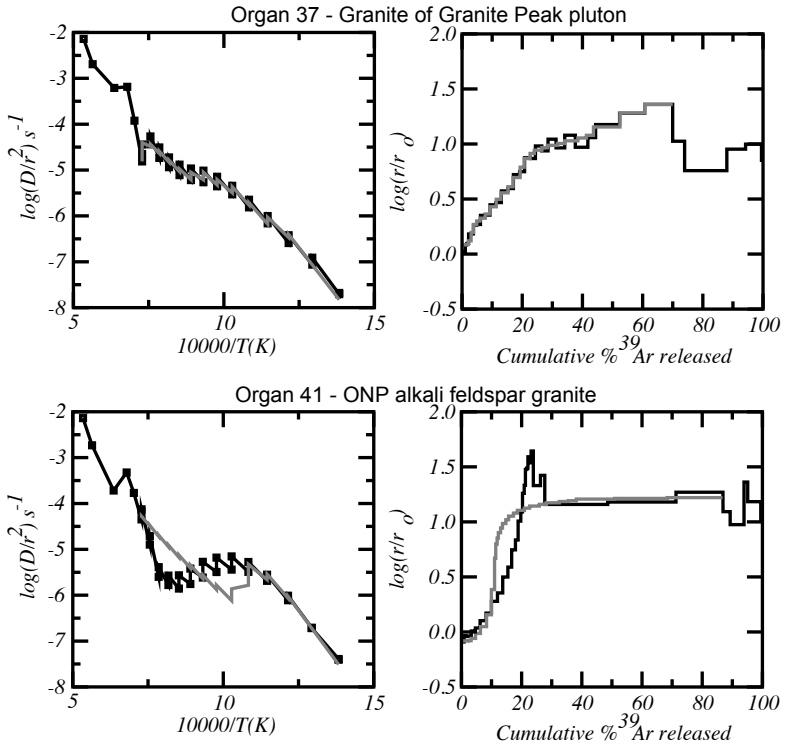
Organ 37 - Granite of Granite Peak pluton
log(D/r2) s-1
10000/T(K)
log(r/rd)
Cumulative %39Ar released
Organ 41 - ONP alkali feldspar granite
log(D/r2) s-1
10000/T(K)
log(r/rd)
Cumulative %39Ar released